frontiers | Research Topics

Fighting microbial biofilms: novel therapeutics and antibiofilm strategies

Edited by
Maria Gabriela Paraje, Fernando Gomes Souza Jr and Jordi Morató

Published in
Frontiers in Cellular and Infection Microbiology

ISSN 1664-8714
ISBN 978-2-8325-6830-9
DOI 10.3389/978-2-8325-6830-9

Generative AI statement
Any alternative text (Alt text) provided alongside figures in the articles in this ebook has been generated by Frontiers with the support of artificial intelligence and reasonable efforts have been made to ensure accuracy, including review by the authors wherever possible. If you identify any issues, please contact us.

About Frontiers

Frontiers is more than just an open access publisher of scholarly articles: it is a pioneering approach to the world of academia, radically improving the way scholarly research is managed. The grand vision of Frontiers is a world where all people have an equal opportunity to seek, share and generate knowledge. Frontiers provides immediate and permanent online open access to all its publications, but this alone is not enough to realize our grand goals.

Frontiers journal series

The Frontiers journal series is a multi-tier and interdisciplinary set of open-access, online journals, promising a paradigm shift from the current review, selection and dissemination processes in academic publishing. All Frontiers journals are driven by researchers for researchers; therefore, they constitute a service to the scholarly community. At the same time, the *Frontiers journal series* operates on a revolutionary invention, the tiered publishing system, initially addressing specific communities of scholars, and gradually climbing up to broader public understanding, thus serving the interests of the lay society, too.

Dedication to quality

Each Frontiers article is a landmark of the highest quality, thanks to genuinely collaborative interactions between authors and review editors, who include some of the world's best academicians. Research must be certified by peers before entering a stream of knowledge that may eventually reach the public - and shape society; therefore, Frontiers only applies the most rigorous and unbiased reviews. Frontiers revolutionizes research publishing by freely delivering the most outstanding research, evaluated with no bias from both the academic and social point of view. By applying the most advanced information technologies, Frontiers is catapulting scholarly publishing into a new generation.

What are Frontiers Research Topics?

Frontiers Research Topics are very popular trademarks of the *Frontiers journals series*: they are collections of at least ten articles, all centered on a particular subject. With their unique mix of varied contributions from Original Research to Review Articles, Frontiers Research Topics unify the most influential researchers, the latest key findings and historical advances in a hot research area.

Find out more on how to host your own Frontiers Research Topic or contribute to one as an author by contacting the Frontiers editorial office: frontiersin.org/about/contact

Fighting microbial biofilms: novel therapeutics and antibiofilm strategies

Topic editors

Maria Gabriela Paraje — National University of Cordoba, Argentina

Fernando Gomes Souza Jr — Federal University of Rio de Janeiro, Brazil

Jordi Morató — UNESCO Chair on Sustainability, Spain

Citation

Paraje, M. G., Gomes Souza Jr, F., Morató, J., eds. (2025). *Fighting microbial biofilms: novel therapeutics and antibiofilm strategies*. Lausanne: Frontiers Media SA. doi: 10.3389/978-2-8325-6830-9

Table of contents

frontiers | Frontiers in Cellular and Infection Microbiology

TYPE Editorial
PUBLISHED 28 August 2025
DOI 10.3389/fcimb.2025.1680391

OPEN ACCESS

EDITED AND REVIEWED BY
Yousef Abu Kwaik,
University of Louisville, United States

*CORRESPONDENCE
María Gabriela Paraje
gparaje@unc.edu.ar;
gabrielaparaje@gmail.com

RECEIVED 05 August 2025
ACCEPTED 19 August 2025
PUBLISHED 28 August 2025

CITATION
Paraje MG, Morató J and Gomes de Souza F Jr. (2025) Editorial: Fighting microbial biofilms: novel therapeutics and antibiofilm strategies.
Front. Cell. Infect. Microbiol. 15:1680391.
doi: 10.3389/fcimb.2025.1680391

Editorial: Fighting microbial biofilms: novel therapeutics and antibiofilm strategies

María Gabriela Paraje[1,2]*, Jordi Morató[3] and Fernando Gomes de Souza Jr.[4,5]

[1]Cátedra de Microbiología, Facultad de Ciencias Exactas, Físicas y Naturales, Universidad Nacional de Córdoba, Córdoba, Argentina, [2]Instituto Multidisciplinario de Biología Vegetal (IMBIV), Consejo Nacional de Investigaciones Científicas y Técnicas (CONICET), Córdoba, Argentina, [3]United Nations Educational, Scientific and Cultural Organization (UNESCO) Chair on Sustainability, Universitat Politècnica de Catalunya, Barcelona, Spain, [4]Federal University of Rio de Janeiro, Rio de Janeiro, Brazil, [5]College of Engineering and Computing, Florida International University, Miami, FL, United States

KEYWORDS

microbial biofilms, innovations, associated infections, biofilm, antibiofilm, novel therapeutic agent

Editorial on the Research Topic
Fighting microbial biofilms: novel therapeutics and antibiofilm strategies

Biofilms present researchers with a range of challenges and opportunities, particularly due to their complex architecture, persistence and resistance to conventional treatments, and pivotal role in chronic infections (Almatroudi, 2024; Coenye et al., 2024; Paraje, 2018). In recent years, numerous antibiofilm compounds and alternative strategies have been identified, aimed at preventing biofilm formation or promoting biofilm dispersal to eradicate mature communities (Zhao et al., 2023). The articles compiled in this Research Topic address these pressing issues by focusing on the development of novel therapeutics, innovative techniques, and safe, effective alternative approaches, reflecting the rapidly evolving landscape of this critical field. The Research Topic also underscores the importance of interdisciplinary collaboration. By bridging diverse scientific disciplines—including microbiology, nanotechnology, pharmacology, and clinical medicine—these contributions offer a comprehensive and contemporary perspective on biofilm research, while proposing novel therapeutic avenues to tackle the global challenge of biofilm-associated infections (Paraje, 2023; Da Silva et al., 2024). Altogether, this Research Topic compiles state-of-the-art investigations into biofilm formation, maturation, and disruption, providing a forward-looking overview of both current challenges and future opportunities in the field.

This Research Topic opens with an insightful Mini Review by Grooters et al., who explore emerging interventions—including ultraviolet radiation, antimicrobial peptide design, phage therapy, and immunotherapy—as promising tools to combat and control pathogenic biofilms. The authors emphasize that contemporary medicine is engaged in a microbial arms race, a mounting global challenge that demands innovative strategies extending beyond conventional antibiotic therapies. Their review provides a compelling

overview of alternative approaches that could reshape the future of biofilm management and antimicrobial resistance control. Despite years of effort to develop new antibiotics for eradicating multidrug-resistant and multi-virulent microbial infections, treatment failures and poor clinical outcomes remain common. Recognizing the pressing need for novel anti-virulence strategies, Bakeer et al. employed phenotypic assays, molecular docking, and genetic analyses to assess the anti-virulence potential of coumarin, simvastatin, and ibuprofen. These results highlight the promising role of ibuprofen as an adjuvant therapy, with the potential to enhance the efficacy of existing antibiotics against highly resistant and virulent *Staphylococcus aureus* infections, representing a valuable contribution to the ongoing search for alternative therapeutic approaches.

An additional innovative strategy for eradicating staphylococcal biofilms is presented by Grooters et al., who developed a localized drug delivery system using antibiotic-impregnated blood clots. Using murine blood clots to enhance antibiotic penetration in coagulase-negative staphylococci biofilms, their approach improved biofilm clearance in a preclinical model and highlights the need for further research into clot-biofilm interactions and their clinical potential in managing persistent infections. Furthermore, Gustafson et al. propose a novel therapeutic approach targeting a *Pseudomonas aeruginosa* biofilm-like structure using intrapleural enzyme-based therapy combined with antibiotic washes. This case demonstrates the clinical significance of biofilms in chronic and persistent infections and illustrates the potential of localized, enzyme-assisted interventions as valuable adjuncts to standard treatment protocols in complex post-surgical scenarios. The development of quorum-sensing (QS)-targeted therapies represents a promising adjunct to conventional antibiotic regimens in the fight against resistant bacterial pathogens. In this context, Pan et al. propose an innovative strategy to combat *P. aeruginosa* by targeting QS, a key regulator of virulence. Their approach combines QS inhibition with reduced antibiotic doses to control infection and limit resistance. Of seven synthesized cinnamoyl hydroxamates, two showed strong potential as QS inhibitors, supporting the integration of anti-virulence therapies with existing antimicrobial protocols.

The potential of the novel anti-biofilm peptide CRAMP - 34 in targeting biofilms offers a compelling alternative to conventional disruption strategies, shifting the focus toward inducing biofilm disassembly from within. In their study, Liu et al. demonstrated that CRAMP - 34 enhances the motility of *Acinetobacter lwoffii* biofilm-associated cells, promoting biofilm dispersion and effective eradication. These findings position CRAMP - 34 as a promising next-generation biofilm-eradicating agent and highlight bacterial motility as a valuable therapeutic target in anti-biofilm research.

Natural compounds in combination therapies are increasingly recognized as promising tools to combat resistant biofilm-forming pathogens. In this context, Paramanya et al. investigated the effects of apocarotenoids, particularly crocetin, on *Staphylococcal* strains. The study suggests that crocetin holds strong potential as an adjunct to conventional antibiotic, as it helps reduce biofilm formation and enhances the effectiveness of standard treatments against clinically relevant pathogens.

A critical aspect of biofilm research is the accurate assessment of biofilm viability, which is essential for evaluating both biofilm formation and the efficacy of antibacterial treatments. Tchatchiashvili et al. explore an alternative staining method using calcein acetoxymethyl and TMA-DPH, a membrane probe that assesses residual biofilm biomass. This novel viability assay is presented as a promising and reliable alternative to traditional SYTO9/PI staining, providing enhanced consistency and sensitivity across various bacterial species.

In a significant step towards innovative biofilm treatment strategies, iminosugars have emerged as a distinctive class of compounds with promising biofilm-inhibitory properties. In this context, Kozień et al. employed an *in vivo* wound infection mouse model to evaluate the efficacy of PDIA, a synthetic iminosugar, in treating biofilm-associated skin infections caused by *S. aureus* and *P. aeruginosa*. The findings identify PDIA as a promising candidate for treating biofilm-associated skin infections, and underscore the therapeutic potential of iminosugars in chronic and drug-resistant infections.

Further emphasizing the growing importance of nanotechnology in antimicrobial research, the contribution by López Venditti et al. provides valuable insights into the antimicrobial and antibiofilm potential of biogenic zinc nanoparticles (ZnNPs). Through a comparative analysis, the authors demonstrate the effectiveness of these green-synthesized ZnNPs against both planktonic and biofilm-forming states of various pathogenic microorganisms. This study reinforces the application of nanomaterials as sustainable and multifunctional agents to combat biofilm-associated infections, a matter of particular importance in the context of global health.

Judan Cruz et al. explore *Aeromonas* isolates treated with a panel of phytochemicals, providing valuable insights into environmental microbiology and public health. Their findings highlight the promising potential of phytochemicals as antibiofilm agents in environmental biotechnology and advanced wastewater treatment technologies.

Finally, Mayorga-Ramos et al. provide a comprehensive review of bacteriophage-based strategies for biofilm control, highlighting the potential of phages and their proteins to disrupt established biofilms. Their review emphasizes the versatility of phages as targeted, adaptable tools for use in clinical, industrial, and environmental settings.

In conclusion, the twelve articles published in the Research Topic "Fighting Microbial Biofilms: Novel Therapeutics and Antibiofilm Strategies" underscore the dynamic and rapidly advancing landscape of biofilm research. Collectively, these contributions shed light on significant progress in our understanding of how biofilms can be effectively targeted and disrupted through innovative antibiofilm agents and therapeutic strategies that act upon critical stages of biofilm development.

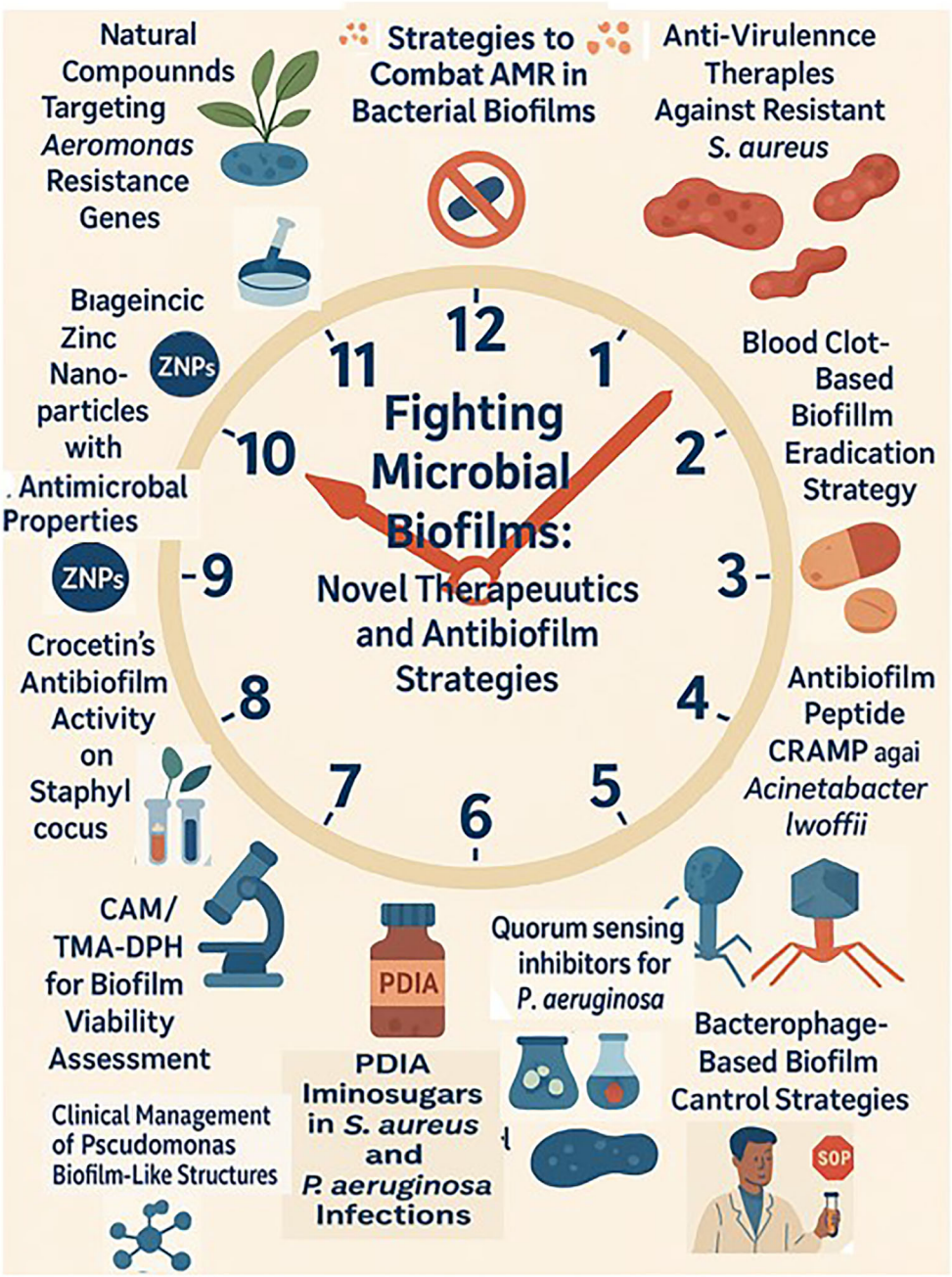

FIGURE 1
Overview of innovative strategies targeting biofilms and antimicrobial resistance. This figure illustrates the diversity of approaches explored across 12 research articles addressing the global threat of biofilm-associated infections and antimicrobial resistance (AMR).

The Topic Editors extend their sincere gratitude to all contributing authors for their high-quality work and to the reviewers and editors whose thoughtful feedback and scientific rigor greatly enhanced the content of this Research Topic. Their commitment and expertise were instrumental in bringing this Research Topic to fruition. We are equally thankful to our readers for their engagement and enthusiasm for this important and evolving field. It is our hope that this Research Topic will inspire interdisciplinary collaboration and innovation in the development of effective, targeted, and sustainable strategies to combat biofilms and their impact on human, animal, and environmental health, in alignment with the One Health approach.

Author contributions

MP: Conceptualization, Project administration, Writing – original draft, Writing – review & editing, Investigation, Validation, Visualization. JM: Writing – review & editing. FG: Writing – original draft, Writing – review & editing.

Acknowledgments

MP is a member of the Scientific and Technological Researcher Career (CIC – CONICET). Likewise, MP wishes to thank FG and JM for their valuable contributions and for accepting to collaborate on this Research Topic in *Frontiers*, as well as for their expertise throughout the editorial process. The authors gratefully acknowledge Arch. María Agustina Farchetto for designing Figure 1.

Conflict of interest

The authors declare that the research was conducted in the absence of any commercial or financial relationships that could be construed as a potential conflict of interest.

The author(s) declared that they were an editorial board member of Frontiers, at the time of submission. This had no impact on the peer review process and the final decision.

Generative AI statement

The author(s) declare that no Generative AI was used in the creation of this manuscript.

Any alternative text (alt text) provided alongside figures in this article has been generated by Frontiers with the support of artificial intelligence and reasonable efforts have been made to ensure accuracy, including review by the authors wherever possible. If you identify any issues, please contact us.

Publisher's note

References

Almatroudi, A. (2024). Investigating biofilms: advanced methods for comprehending microbial behavior and antibiotic resistance. *Front. Biosci. (Landmark Ed).* 29 (4), 133. doi: 10.31083/j.fbl2904133

Coenye, T., Ahonen, M., Anderson, S., Cámara, M., Chundi, P., Fields, M., et al. (2024). Global challenges and microbial biofilms: Identification of priority questions in biofilm research, innovation and policy. *Biofilm* 8, 100210. doi: 10.1016/j.bioflm.2024.100210

Da Silva, M. A., Andrada, K. F. C., Torales, M. M., Hughes, I. M., Pez, P., García-Martínez, J. C., et al. (2024). Synergistic activity of gold nanoparticles with amphotericin B on persister cells of *Candida tropicalis* biofilms. *J. Nanobiotechnology* 22, 1–12. doi: 10.1186/S12951-024-02415-6/FIGURES/6

Paraje, M. G. (2018). Persist and triumph: persistent cells in microbial biofilm. *Rev. Argent Microbiol.* 50, 231–233. doi: 10.1016/j.ram.2018.07.001

Paraje, M. G. (2023). From the magic bullet to nanotechnology: nanoantimicrobials as therapeutics to fight multidrug-resistant microorganisms. *Rev. Argent Microbiol.* 55, 204, 205. doi: 10.1016/j.ram.2023.08.001

Zhao, A., Sun, J., and Liu, Y. (2023). Understanding bacterial biofilms: From definition to treatment strategies. *Front. Cell. Infect. Microbiol.* 13. doi: 10.3389/fcimb.2023.1137947

frontiers | Frontiers in Cellular and Infection Microbiology

TYPE Mini Review
PUBLISHED 19 January 2024
DOI 10.3389/fcimb.2024.1352273

OPEN ACCESS

EDITED BY
Jordi Morató,
UNESCO Chair on Sustainability, Spain

REVIEWED BY
Tahereh Navidifar,
Shoushtar, Iran

*CORRESPONDENCE
Yong Li
yong.li@wmed.edu

RECEIVED 07 December 2023
ACCEPTED 04 January 2024
PUBLISHED 19 January 2024

CITATION
Grooters KE, Ku JC, Richter DM, Krinock MJ, Minor A, Li P, Kim A, Sawyer R and Li Y (2024) Strategies for combating antibiotic resistance in bacterial biofilms.
Front. Cell. Infect. Microbiol. 14:1352273.
doi: 10.3389/fcimb.2024.1352273

Strategies for combating antibiotic resistance in bacterial biofilms

Kayla E. Grooters[1], Jennifer C. Ku[1], David M. Richter[1], Matthew J. Krinock[1], Ashley Minor[1], Patrick Li[2,3], Audrey Kim[1], Robert Sawyer[4] and Yong Li[3]*

[1]Department of Medicine, Western Michigan University Homer Stryker M.D. School of Medicine, Kalamazoo, MI, United States, [2]University of Michigan, Ann Arbor, MI, United States, [3]Division of Biomedical Engineering, Department of Orthopedic Surgery, Western Michigan University Homer Stryker M.D. School of Medicine, Kalamazoo, MI, United States, [4]Department of Surgery, Western Michigan University Homer Stryker M.D. School of Medicine, Kalamazoo, MI, United States

Biofilms, which are complexes of microorganisms that adhere to surfaces and secrete protective extracellular matrices, wield substantial influence across diverse domains such as medicine, industry, and environmental science. Despite ongoing challenges posed by biofilms in clinical medicine, research in this field remains dynamic and indeterminate. This article provides a contemporary assessment of biofilms and their treatment, with a focus on recent advances, to chronicle the evolving landscape of biofilm research.

KEYWORDS

biofilm, infection, bacteriophage, antibiotic resistance, treatment

1 Introduction

A biofilm is an immobile, three-dimensional matrix of microscopic organisms that have aggregated onto a surface to form a colony (Sharma et al., 2019). The organisms secrete adhesive proteins and extracellular matrix which help cement the cells to a surface and protect the colony from decussation, environmental hazards, host defenses, and antimicrobial compounds (Jacqueline and Caillon, 2014). One of the key issues with using antibiotics to treat biofilms is achieving the required minimum inhibitory concentration (MIC) of drug at the infection site. The MIC for a biofilm can be between 100-800x greater than the MIC for planktonic cells (Jacqueline and Caillon, 2014). In addition, singular bacteria within biofilms that have been exposed to high concentrations of antibiotics can persist and reestablish a more resistant biofilm, a phenomenon known as recalcitrance (Ciofu et al., 2022). Consequentially, biofilms are frequently refractory to antibiotic treatment and, thus, may require surgical intervention. However, surgery may still prove ineffective, resulting in significant morbidity and mortality, with biofilms implicated in over 500,000 deaths per year in the United States alone (Charani and Holmes, 2019).

Biofilms are known to occur in every human organ system, ranging from the respiratory and digestive tracts to the heart, eyes, and ears (Perry and Tan, 2023). Indeed, biofilms have been implicated in 65% of all bacterial infections (Jamal et al., 2018) and nearly 80% of chronic wounds (Malone et al., 2017). Interestingly, the incidence of biofilm-associated infections is on the rise (Cámara et al., 2022). Many such biofilms exhibit resistance to typical antibiotics and, thus, delay healing time and may require invasive interventions to resolve infection (Metcalf and Bowler, 2013). Furthermore, biofilms present important challenges for the design and use of invasive medical products and prosthetics. For example, biofilms are frequently implicated in catheter-associated infections (Gominet et al., 2017), where they complicate decontamination and treatment of the infection (Ielapi et al., 2020). Biofilms present similar complications in other life-saving interventions, such as endotracheal intubation (Diaconu et al., 2018). Importantly, biofilms commonly affect implanted devices—such as prosthetic joints and pacemakers—and are frequently refractory to pharmacological treatment, ultimately requiring removal of the device (Santos et al., 2011; Tande and Patel, 2014). As a result, recent analyses have estimated the global impact of biofilms to be upwards of $280 billion (Cámara et al., 2022).

Given such significant human and financial costs, there is an increasingly urgent need to develop novel strategies for the clinical management of biofilms. In this review, we focus on the formation and structure of biofilms, the mechanisms of antibiotic resistance within these systems, and highlight emerging non-antibiotic mechanisms of biofilm control.

2 Formation of bacterial biofilms

Biofilm formation is initiated by a complex series of environmental and genetic triggers, primarily involved in stress responses. External factors such as pH, temperature, nutrient availability, and environmental hazards all play a role in causing a planktonic microorganism to shift into an adherent state (Rather et al., 2021). The first step of biofilm formation is reversible adherence, where microorganisms use attachment devices, such as flagella, pili, and fimbriae, to glue themselves to an available substrate. During this stage, the microorganisms are free to abandon their attachment site and return to planktonic life or commit to irreversible attachment (Toyofuku et al., 2016). During irreversible attachment, the microorganisms upregulate various adhesion molecules and glycoproteins. From here, cells undergo division and microcolony formation. Bacteria in the colony communicate through quorum sensing, a process dependent on the synthesis, detection, and regulation of autoinducing molecules (Figure 1). This communication directs the rate of cell division and production of extracellular polymeric substance (Asma et al., 2022)—which accounts for over 90% of the dry mass of mature biofilms (Toyofuku et al., 2016).

2.1 Environmental control

Specifically, a biofilm's extracellular polymeric substance (EPS) matrix, which is composed of proteins, polysaccharides, extracellular DNA, and lipids, allows it to withstand challenges like fluid shear and mechanical pressure. While increased EPS production can only be speculated for environmental challenges like fluid shear, it was found that in staphylococcal biofilms, increased mechanical pressure stimulated the EPS of the biofilm to produce more polysaccharides (Hou et al., 2018). Further, hypoxic conditions may foster formation of bacterial biofilms—particularly for those involving *Staphylococcus aureus*. In the case of *S. aureus* CIP 53.154, hypoxia results in a 21-fold increase in biofilm production, associated with concomitant downregulation of *lexA*—a stress-response-related gene—indicating the hypoxic conditions were favorable for growth (Lamret et al., 2021). Similarly, Aristotelous (2022) found biofilms were unable to thrive in well-oxygenated environments, likely due to enhanced phagocytosis by neutrophils; however, under hypoxic conditions, biofilm-secreted virulence factors decreased the effectiveness of neutrophil phagocytosis and promoted bacterial persistence (Aristotelous, 2022). These studies illustrate how harsh environments—e.g.,

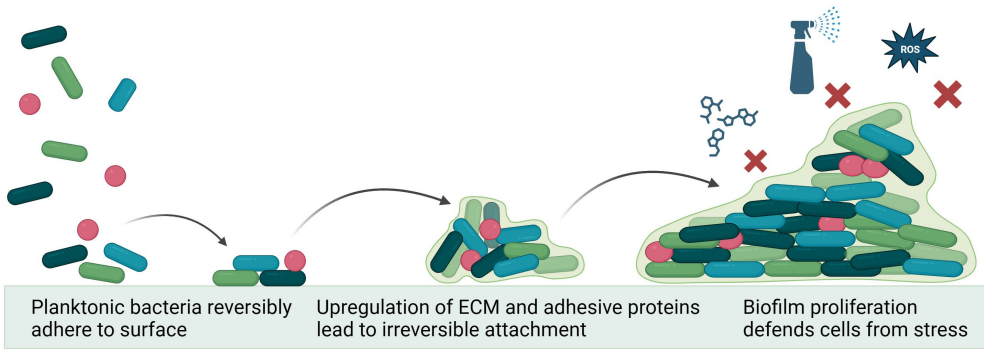

FIGURE 1
Mechanism of biofilm formation. Environmental conditions lead planktonic bacteria to utilize adhesion machinery to attach to a surface. Quorum sensing between colony members drives upregulation of extracellular matrix formation and changes in metabolic function, irreversibly cementing biofilm to surface and protecting the colony from environmental hazards (e.g., antiseptics, reactive oxygen species (ROS) and antibiotics. Figure made using Biorender.com.

those with fluid shear, mechanical pressure, and hypoxia—are quite habitable environments for many forms of biofilms.

3 Current management and treatment of biofilm infections

The cohesion of microorganisms leading to biofilm formation autonomously generates an extracellular matrix, establishing environments that promote bacterial tolerance and resistance to antibiotics through diverse mechanisms contingent upon factors, such as biofilm composition and prevailing growth conditions. Although many studies have studied drug penetration through the biofilm barrier, the underlying mechanisms remain inconclusive. Thus, understanding the mechanisms underlying biofilms' contribution to antibiotic tolerance and resistance is crucial for devising innovative strategies to combat these infections.

3.1 Structure: density and penetration

The efficacy of biofilm treatment is linked to the ability of the antimicrobial agent to penetrate the heterogenous biofilm structure. It has been shown that the capacity of the drug to penetrate the biofilm is highly dependent upon biofilm structure, bacteria genus and strain, and selected antibiotic (Singh et al., 2016). Extracellular DNA, a constituent of the structural framework of the biofilm, has been demonstrated to induce antibiotic resistance (Panlilio and Rice, 2021). Furthermore, the resistance of biofilms to antibiotics is significantly influenced by the bacterial exopolysaccharide (EPS) matrix, a key component in biofilm formation and maintenance (Liu et al., 2017). The production of EPS serves as an adaptive mechanism, with bacteria synthesizing them under stressful conditions, including exposure to antibiotics (Vazquez-Rodriguez et al., 2018). The reduced penetration through the EPS matrix constitutes a mechanism through which biofilms resist antibiotics (Yasir et al., 2018). Factors affecting antibiotic penetration include increased biofilm thickness, drug diffusion efficacy, and the concentration and duration of the administered antibiotic (Hall and Mah, 2017). Additionally, the slow or incomplete diffusion of antibiotics can trap them within the biofilm, resulting in their inactivation by extracellular matrix enzymes (Pinto et al., 2020).

3.2 The metabolic environment within biofilms

The heterogeneity bacterial population observed in biofilms gives rise to metabolically distinct microcolonies. Various mechanisms have been postulated to explain the observed heterogeneity in biofilms. According to the zone model, each bacterium responds to its microenvironment, leading to diverse physiological states within the same biofilm (Kirketerp-Møller et al., 2020). Differences in physiological activity have been shown to be due to differences in pH, hydrogen peroxide, and noncellular materials (Jang et al., 2016; Wu et al., 2018; Ghosh et al., 2019). It has been shown that the deepest layers of the biofilm are exposed to more nutrient-depleted conditions when compared to upper layers of the biofilm due to diffusion barrier and consumption of nutrients carried out by cells in the periphery of the biofilm (Liu et al., 2015). These nutrient-deficient zones have also been identified as a primary source of resistance in bacteria (Liu et al., 2022). Furthermore, nutrient-deficient zones promote the emergence of persister cells, dormant cells that exhibit slow growth and resistance to antibiotics (Olsen, 2015; Miyaue et al., 2018). Therefore, the existence of diverse zones results in a myriad of genotypes and phenotypes coexisting within a local environment. This phenomenon accounts for the emergence of unique metabolic pathways that contribute to drug resistance.

3.3 Efflux pumps

Efflux pumps have conventionally been associated with multidrug resistance due to their capability to extrude diverse antibiotics from bacteria (Nishino et al., 2021). Moreover, these pumps are known to play a crucial role in biofilm formation—particularly in the context of biofilm-associated drug assistance. The physiological heterogeneity within biofilms explains the observed patterns of efflux pump gene expression. For instance, Babin et al. noted the upregulation of specific antibiotic resistance pumps in the upper region of biofilms, while downregulation or no change was observed in the middle of the biofilm (Babin et al., 2017). In the case of *Pseudomonas aeruginosa*, it has been demonstrated that hypoxia enhances antibiotic resistance by altering the composition of multidrug efflux pumps (Schaible et al., 2012). Furthermore, efflux pump inhibitors have been shown to block the antibiotic tolerance of biofilms and completely abolish biofilm formation (Kvist et al., 2008; Zimmermann et al., 2019).

3.4 Quorum sensing

Biofilm formation is partly regulated by quorum sensing (QS), a mechanism through which bacteria employ signaling molecules to enhance communication and survival (Preda and Săndulescu, 2019). QS has been demonstrated to directly impact the regulation of biofilm resistance to antibiotics; specifically, QS regulates expression of various efflux pumps, subsequently influencing the QS system itself (Wang et al., 2019). Further, QS plays a critical role in formation of both gram-positive and -negative biofilms, albeit through slightly different mechanisms. While gram-negative bacteria employ acyl-homoserine lactones within their QS system, gram-positive bacteria employ larger oligopeptides. Both molecules, however, contribute to biofilm formation, thereby hindering antibiotic penetration (An et al., 2019; Gimza et al., 2019).

4 Clinical management of biofilms

The mechanical barrier assembled by biofilms shield constituent microorganisms from antimicrobial agents, thereby presenting significant issues for the clinical management of biofilms. Presently, biofilm management relies on antimicrobial agents and surgical debridement; however, inconsistent treatment outcomes persist. Thus, research in this field is essential to advance the strategies for eradicating biofilms.

4.1 Antibacterial therapies

The heterogeneity of biofilm formation presents a significant challenge in biofilm management. While cells within biofilms exhibit a much higher minimum inhibitory concentration of antibiotics, topical administration allows for delivery of elevated antibiotic concentrations to target biolfilms (Overhage et al., 2008; Yang et al., 2017). Antimicrobial agents have shown high efficacy against biofilm-associated bacteria. However, due to antibiotic resistance, combination therapy emerged as a therapeutic strategy for treating biofilm infections. Combining antibiotics with other agents, such as N-acetylcysteine and recombinant deoxyribonuclease I, has been shown to significantly reduce biofilms (Belfield et al., 2017). Furthermore, certain agents, including catechin, protocatechuic, and vanillic acids, exhibit synergistic effects when combined with antibiotics, inhibiting bacterial adhesion and, thus, biofilm formation (Bernal-Mercado et al., 2020). However, the eradication of biofilms using traditional antibiotic therapy remains challenging, as the large doses required to reach a concentration sufficient to eliminate biofilms frequently cause detrimental side effects to the patient (Ciofu et al., 2017).

4.2 Surgical debridement

The current best treatment to eradicate biofilms involves surgical debridement (Rodríguez-Merchán et al., 2021). This type of debridement uses sharp instruments to remove non-viable and possibly viable tissue surrounding a wound and requires properly trained medical providers and pain control options (Tran et al., 2023). Surgical debridement allows the wound to be more receptive to antibiotic therapies which increases the likelihood of eradicating the biofilm from the wound (Ousey and Ovens, 2023). While this form of debridement is the standard care for many open wound infections, it is unlikely that complete removal of the biofilm will occur, and new strategies including using surgical debridement with meshed skin graft simultaneously may have better outcomes related to healing and infection rates (Namgoong et al., 2020).

4.3 Alternative treatments

Due to the challenges seen with treatments with antibiotics, both as standalone and in combination, research has explored alternative approaches for biofilm eradication. More recently, quaternary ammonium compounds have exhibited high potency and a broad spectrum of activity for biofilm elimination; however, certain analogs have raised concerns regarding toxicity (Saverina et al., 2023). Elevated concentrations of antimicrobial lipids have also been shown potential in eradicating biofilms. In a related study, lipid-coated hybrid nanoparticles were utilized to enhance biofilm penetration for antibiotic treatment (Lee et al., 2022). Additionally, secondary metabolites, such as phenazines and quinolines, have demonstrated complete eradication of certain biofilms with the added benefits of low toxicity; however, it is worth noting that these metabolites have been found to trigger formation of biofilm, dependent on species and strain (Huigens, 2018). For antibiotic resistant biofilms that are challenging to treat, anticancer drugs, such as mitomycin C and cisplatin, have been successfully used as therapies, though clinical toxicity remains a concern (Wakharde et al., 2018). A deeper understanding of these alternative treatments holds potential to pave way for the development of new antibiotics and agents for effective biofilm treatment.

5 Novel strategies for eradication

Given the challenges biofilms pose to conventional treatment strategies, there is increasing interest in exploring novel therapeutic therapies. Such strategies aim to exploit various aspects of biofilm—such as the extracellular matrix—without relying on the metabolism of the cells themselves. These techniques are being investigated both for the prevention of biofilm formation on biotic and abiotic surfaces, as well as for the treatment of active infections.

5.1 Light-based strategies

The use of Ultraviolet Light as an anti-bacterial and anti-biofilm therapy is promising as UV light non-specifically targets DNA and RNA to assist in elimination of bacteria regardless of antibiotic resistance (Conner-Kerr et al., 1998). It plays a role in synthesis of cyclobutene pyrimidine dimers that disrupt cell growth and proliferation. The power of antibacterial photodynamic therapy (APDT) can be enhanced further through the use of photosensitizer molecules (PS), such as phenothiaziniums, tetrapyrroles, hypericin, and curcumin. Irradiation causes the electrons within a PS to enter higher energy orbitals. Upon return to ground state, these electrons can react with organic compounds inside cells, leading to free radical generation. These free radicals cause oxidative damage to the cell, promoting apoptosis (Ghorbani et al., 2018). It is unlikely that development of resistance to APDT would occur due to the non-specific nature of the target. Clinical application of this anti-bacterial method is limited to surface infections or medical device sterilization due to the difficulty of delivery and limited penetration of light through host-tissue (Argyraki et al., 2018). In addition, UV light is potentially carcinogenic to host-tissue, but has been shown to cause minimal damage when used at appropriate fluences (Barnes et al., 2018). More targeted treatment strategies utilizing light-based technology such as photodynamic therapy can further reduce host-tissue damage (Yin et al., 2013).

5.2 Antimicrobial peptides

Antimicrobial peptides (AMPs) have gained increasing attention due to their ability to decrease cell adhesion and reduce the thickness of a broad spectrum of biofilms (Shahrour et al., 2019). AMPs can be classified based on their secondary structure as either α-helical, β-sheet, loop, and extended peptides. To date, α-helical AMPs—such as Magainin-2 and LL-3—are the most well studied. The cationic amphipathic structure of these AMPs allows them to interact with negatively charged bacterial membranes, causing membrane lysis or invasion to carry out non-membranolytic mechanisms (Di Somma et al., 2020). AMPs exhibit additional antimicrobial activity as a result of non-membranolytic mechanisms, which are particularly useful in disruption genes or proteins that are essential for biofilm formation, function, and virulence (Luo and Song, 2021; Castillo-Juárez et al., 2022). There has been recent interest in isolating particular AMPs from plant essential oils. Eugenol derivatives from clove, bay, and pimento berry oils have been found to inhibit *Escherichia coli* O157: H7 biofilm formation by downregulating attachment proteins (Kim et al., 2016). Unfortunately, like antibiotics, AMPs are susceptible to intrinsic and acquired AMP resistance via various mechanisms, such as a more positively charged lipid membranes or efflux pumps—which may perpetuate selection for multi-drug resistant pathogens (Andersson et al., 2016).

5.3 Bacteriophage therapy

Additionally, bacteriophage therapy shows great promise as a specific, targeted option for treatment of biofilms, given their inherent antibacterial activity and minimal adverse effects. Bacteriophages are viruses that follow a lytic life cycle and infect specific strains of bacterial species, making them useful for targeting specific bacterial infections. Their lytic life cycle allows bacteriophages to replicate and spread through many bacteria, efficiently clearing infections. More importantly, the selective targeting of bacteria by bacteriophages spares human cells, thus, resulting in relatively few documented adverse events (Cesta et al., 2020). Due to coevolution with biofilm producing bacteria, bacteriophages have developed the ability to infect and lyse bacteria within biofilms through enzyme mediated degradation of biofilm ECM and can even infect cells during dormancy, causing lysis upon metabolic reactivation (Doub, 2020). Though bacteriophage resistance poses a challenge for therapy, bacteriophage "cocktails"—specific for multiple strains of a bacteria species—can be administered to reduce rates of resistance as well as help ensure the infecting pathogen is covered (Clarke et al., 2020). Furthermore, combination of phages and antibiotics has yielded promising results, even against multidrug-resistant biofilms (Akturk et al., 2019). In particular, pre-treatment of biofilms with phages has been shown to enhance the effects of antibiotics. (Townsend et al., 2020). Moreover, genetically engineered phages have also demonstrated the capacity of biofilm degradation and inhibitory effects (Li et al., 2020).

5.4 Immunotherapy

Several immunotherapeutic options have been explored with vaccination strategies and monoclonal antibodies being potential options. In the case of *S. aureus*, significant efforts have been made to develop a vaccine, but factors such as a lack of understanding of conserved antigens between strains and the need to account for both planktonic and biofilm components to fully eliminate infection have made a vaccine elusive (Bhattacharya et al., 2015). Monoclonal antibodies have had similar complications as preclinical and clinical trials fail to mitigate infection via passive immunity, however, application of monoclonal antibodies conjugated to antibiotics could provide another avenue for exploration as a way to concentrate antibiotics to the site of infection and increase their effectiveness (Speziale and Pietrocola, 2021).

6 Conclusion

As the average age of the US population increases, and the capacity of biomedical technology expands, so does the rate of hospitalization and surgical intervention (Pallin et al., 2014). Between 2005 and 2030, the number of total knee and total hip arthroplasties are predicted to increase by 174% (Antonelli and Chen, 2019). The number of artificial heart valve implantations is increasing by 5-7% every year (Saksena et al., 2019). These numbers only scratch the surface. Without urgent intervention, we can anticipate the rate of biofilm infections and antibiotic resistance to likewise multiply. Modern medicine is facing a microbial arms race, one which will require novel approaches, beyond conventional antibiotic therapy, to win. Inventions such as UV radiation, antimicrobial peptide design, phage therapy, and immunotherapy offer some possibilities to combat and control pathogenic biofilms and deserve further clinical investigation. Moreso, both public and private sector health entities would be wise to invest in both technology and training for clinicians involving biofilms. We are currently 20 years into the advent of antimicrobial stewardship programs and have deepened our understanding of microbial resistance and control (Charani and Holmes, 2019). By expanding these programs to explore biofilm regulation and resistance, medicine can enter the next generation of antimicrobial dominion to the benefit of patients worldwide.

Author contributions

KG: Conceptualization, Investigation, Supervision, Writing – original draft, Writing – review & editing. JK: Conceptualization, Investigation, Writing – original draft, Writing – review & editing. DR: Conceptualization, Investigation, Writing – original draft, Writing – review & editing. MK: Conceptualization, Investigation, Writing – original draft, Writing – review & editing. AM: Conceptualization, Investigation, Writing – original draft, Writing – review & editing. PL: Writing – review & editing. AK: Writing –

original draft. RS: Supervision, Writing – review & editing. YL: Conceptualization, Supervision, Writing – review & editing.

Funding

The author(s) declare that no financial support was received for the research, authorship, and/or publication of this article.

Acknowledgments

We want to acknowledge Dr. Hang Lin, PhD for his continued support of our research endeavors.

Conflict of interest

YL is an executive editor for Journal of Cellular Biochemistry.

The remaining authors declare that the research was conducted in the absence of any commercial or financial relationships that could be construed as a potential conflict of interest.

Publisher's note

References

Akturk, E., Oliveira, H., Santos, S. B., Costa, S., Kuyumcu, S., Melo, L. D. R., et al. (2019). Synergistic action of phage and antibiotics: parameters to enhance the killing efficacy against mono and dual-species biofilms. *Antibiotics* 8, 103. doi: 10.3390/antibiotics8030103

An, S.-Q., Murtagh, J., Twomey, K. B., Gupta, M. K., O'Sullivan, T. P., Ingram, R., et al. (2019). Modulation of antibiotic sensitivity and biofilm formation in Pseudomonas aeruginosa by interspecies signal analogues. *Nat. Commun.* 10, 2334. doi: 10.1038/s41467-019-10271-4

Andersson, D. I., Hughes, D., and Kubicek-Sutherland, J. Z. (2016). Mechanisms and consequences of bacterial resistance to antimicrobial peptides. *Drug Resist. Update* 26, 43–57. doi: 10.1016/J.DRUP.2016.04.002

Antonelli, B., and Chen, A. F. (2019). Reducing the risk of infection after total joint arthroplasty: preoperative optimization. *Arthroplasty* 1, 4. doi: 10.1186/s42836-019-0003-7

Argyraki, A., Markvart, M., Stavnsbjerg, C., Kragh, K. N., Ou, Y., Bjørndal, L., et al. (2018). UV light assisted antibiotics for eradication of *in vitro* biofilms. *Sci. Rep.* 8. doi: 10.1038/S41598-018-34340-8

Aristotelous, A. C. (2022). Biofilm neutrophils interactions under hypoxia: A mathematical modeling study. *Math. Biosci.* 352, 108893. doi: 10.1016/j.mbs.2022.108893

Asma, S. T., Imre, K., Morar, A., Herman, V., Acaroz, U., Mukhtar, H., et al. (2022). An overview of biofilm formation-combating strategies and mechanisms of action of antibiofilm agents. *Life (Basel).* 12. doi: 10.3390/life12081110

Babin, B. M., Atangcho, L., van Eldijk, M. B., Sweredoski, M. J., Moradian, A., Hess, S., et al. (2017). Selective proteomic analysis of antibiotic-tolerant cellular subpopulations in *pseudomonas aeruginosa* biofilms. *mBio* 8. doi: 10.1128/mBio.01593-17

Barnes, J. L., Zubair, M., John, K., Poirier, M. C., and Martin, F. L. (2018). Carcinogens and DNA damage. *Biochem. Soc. Trans.* 46, 1213–1224. doi: 10.1042/BST20180519

Belfield, K., Bayston, R., Hajduk, N., Levell, G., Birchall, J. P., and Daniel, M. (2017). Evaluation of combinations of putative anti-biofilm agents and antibiotics to eradicate biofilms of Staphylococcus aureus and Pseudomonas aeruginosa. *J. Antimicrobial. Chemother.* 72, 2531–2538. doi: 10.1093/jac/dkx192

Bernal-Mercado, A. T., Gutierrez-Pacheco, M. M., Encinas-Basurto, D., Mata-Haro, V., Lopez-Zavala, A. A., Islas-Osuna, M. A., et al. (2020). Synergistic mode of action of catechin, vanillic and protocatechuic acids to inhibit the adhesion of uropathogenic *Escherichia coli* on silicone surfaces. *J. Appl. Microbiol.* 128, 387–400. doi: 10.1111/jam.14472

Bhattacharya, M., Wozniak, D. J., Stoodley, P., and Hall-Stoodley, L. (2015). Prevention and treatment of Staphylococcus aureus biofilms. *Expert Rev. Anti Infect. Ther.* 13, 1499–1516. doi: 10.1586/14787210.2015.1100533

Cámara, M., Green, W., MacPhee, C. E., Rakowska, P. D., Raval, R., Richardson, M. C., et al. (2022). Economic significance of biofilms: a multidisciplinary and cross-sectoral challenge. *NPJ Biofilms. Microbiomes.* 8, 42. doi: 10.1038/s41522-022-00306-y

Castillo-Juárez, I., Blancas-Luciano, B. E., García-Contreras, R., and Fernández-Presas, A. M. (2022). Antimicrobial peptides properties beyond growth inhibition and bacterial killing. *PeerJ* 10. doi: 10.7717/PEERJ.12667

Cesta, N., Di Luca, M., Corbellino, M., Tavio, M., Galli, M., and Andreoni, M. (2020). Bacteriophage therapy: an overview and the position of Italian Society of Infectious and Tropical Diseases. *Infez. Med.* 28, 322–331.

Charani, E., and Holmes, A. (2019). Antibiotic stewardship—Twenty years in the making. *Antibiotics* 8, 7. doi: 10.3390/antibiotics8010007

Ciofu, O., Moser, C., Jensen, P.Ø., and Høiby, N. (2022). Tolerance and resistance of microbial biofilms. *Nat. Rev. Microbiol.* 20, 621–635. doi: 10.1038/s41579-022-00682-4

Ciofu, O., Rojo-Molinero, E., Macià, M. D., and Oliver, A. (2017). Antibiotic treatment of biofilm infections. *APMIS* 125, 304–319. doi: 10.1111/apm.12673

Clarke, A. L., De Soir, S., and Jones, J. D. (2020). The safety and efficacy of phage therapy for bone and joint infections: A systematic review. *Antibiot. (Basel).* 9, 1–11. doi: 10.3390/ANTIBIOTICS9110795

Conner-Kerr, T. A., Sullivan, P. K., Gaillard, J., Franklin, M. E., and Jones, R. M. (1998). The effects of ultraviolet radiation on antibiotic-resistant bacteria *in vitro*. *Ostomy. Wound Manage.* 44, 50–56.

Diaconu, O., Siriopol, I., Poloşanu, L. I., and Grigoraş, I. (2018). Endotracheal tube biofilm and its impact on the pathogenesis of ventilator-associated pneumonia. *J. Crit. Care Med.* 4, 50–55. doi: 10.2478/jccm-2018-0011

Di Somma, A., Moretta, A., Canè, C., Cirillo, A., and Duilio, A. (2020). Antimicrobial and antibiofilm peptides. *Biomolecules* 10. doi: 10.3390/BIOM10040652

Doub, J. B. (2020). Bacteriophage therapy for clinical biofilm infections: parameters that influence treatment protocols and current treatment approaches. *Antibiot. (Basel).* 9, 1–12. doi: 10.3390/ANTIBIOTICS9110799

Ghorbani, J., Rahban, D., Aghamiri, S., Teymouri, A., and Bahador, A. (2018). Photosensitizers in antibacterial photodynamic therapy: an overview. *Laser. Ther.* 27, 293–302. doi: 10.5978/islsm.27_18-RA-01

Ghosh, R., Barman, S., and Mandal, N. C. (2019). Phosphate deficiency induced biofilm formation of Burkholderia on insoluble phosphate granules plays a pivotal role for maximum release of soluble phosphate. *Sci. Rep.* 9, 5477. doi: 10.1038/s41598-019-41726-9

Gimza, B. D., Larias, M. I., Budny, B. G., and Shaw, L. N. (2019). Mapping the global network of extracellular protease regulation in staphylococcus aureus. *mSphere* 4. doi: 10.1128/mSphere.00676-19

Gominet, M., Compain, F., Beloin, C., and Lebeaux, D. (2017). Central venous catheters and biofilms: where do we stand in 2017? *APMIS* 125, 365–375. doi: 10.1111/apm.12665

Hall, C. W., and Mah, T.-F. (2017). Molecular mechanisms of biofilm-based antibiotic resistance and tolerance in pathogenic bacteria. *FEMS Microbiol. Rev.* 41, 276–301. doi: 10.1093/femsre/fux010

Hou, J., Veeregowda, D. H., van de Belt-Gritter, B., Busscher, H. J., and van der Mei, H. C. (2018). Extracellular Polymeric Matrix Production and Relaxation under Fluid Shear and Mechanical Pressure in Staphylococcus aureus Biofilms. *Appl. Environ. Microbiol.* 84. doi: 10.1128/AEM.01516-17

Huigens, R. W. (2018). The path to new halogenated quinolines with enhanced activities against staphylococcus epidermidis. *Microbiol. Insights* 11, 1178636118808532. doi: 10.1177/1178636118808532

Ielapi, N., Nicoletti, E., Lorè, C., Guasticchi, G., Avenoso, T., Barbetta, A., et al. (2020). The role of biofilm in central venous catheter related bloodstream infections: evidence-based nursing and review of the literature. *Rev. Recent Clin. Trials.* 15, 22–27. doi: 10.2174/1574887114666191018144739

Jacqueline, C., and Caillon, J. (2014). Impact of bacterial biofilm on the treatment of prosthetic joint infections. *J. Antimicrobial. Chemother.* 69, i37–i40. doi: 10.1093/jac/dku254

Jamal, M., Ahmad, W., Andleeb, S., Jalil, F., Imran, M., Nawaz, M. A., et al. (2018). Bacterial biofilm and associated infections. *J. Chin. Med. Assoc.* 81, 7–11. doi: 10.1016/j.jcma.2017.07.012

Jang, I.-A., Kim, J., and Park, W. (2016). Endogenous hydrogen peroxide increases biofilm formation by inducing exopolysaccharide production in Acinetobacter oleivorans DR1. *Sci. Rep.* 6, 21121. doi: 10.1038/srep21121

Kim, Y.-G., Lee, J.-H., Gwon, G., Kim, S.-I., Park, J. G., and Lee, J. (2016). Essential oils and eugenols inhibit biofilm formation and the virulence of escherichia coli O157: H7. *Sci. Rep.* 6, 36377. doi: 10.1038/srep36377

Kirketerp-Møller, K., Stewart, P. S., and Bjarnsholt, T. (2020). The zone model: A conceptual model for understanding the microenvironment of chronic wound infection. *Wound Repair Regener.* 28, 593–599. doi: 10.1111/wrr.12841

Kvist, M., Hancock, V., and Klemm, P. (2008). Inactivation of efflux pumps abolishes bacterial biofilm formation. *Appl. Environ. Microbiol.* 74, 7376–7382. doi: 10.1128/AEM.01310-08

Lamret, F., Varin-Simon, J., Velard, F., Terryn, C., Mongaret, C., Colin, M., et al. (2021). Staphylococcus aureus strain-dependent biofilm formation in bone-like environment. *Front. Microbiol.* 12. doi: 10.3389/fmicb.2021.714994

Lee, H. W., Kharel, S., and Loo, S. C. J. (2022). Lipid-coated hybrid nanoparticles for enhanced bacterial biofilm penetration and antibiofilm efficacy. *ACS Omega.* 7, 35814–35824. doi: 10.1021/acsomega.2c04008

Li, M., Shi, D., Li, Y., Xiao, Y., Chen, M., Chen, L., et al. (2020). Recombination of T4-like Phages and Its Activity against Pathogenic Escherichia coli in Planktonic and Biofilm Forms. *Virol. Sin.* 35, 651–661. doi: 10.1007/s12250-020-00233-2

Liu, S., Chen, L., Wang, L., Zhou, B., Ye, D., Zheng, X., et al. (2022). Cluster differences in antibiotic resistance, biofilm formation, mobility, and virulence of clinical enterobacter cloacae complex. *Front. Microbiol.* 13. doi: 10.3389/fmicb.2022.814831

Liu, J., Prindle, A., Humphries, J., Gabalda-Sagarra, M., Asally, M., Lee, D. D., et al. (2015). Metabolic co-dependence gives rise to collective oscillations within biofilms. *Nature* 523, 550–554. doi: 10.1038/nature14660

Liu, J., Zhang, J., Guo, L., Zhao, W., Hu, X., and Wei, X. (2017). Inactivation of a putative efflux pump (LmrB) in *Streptococcus mutans* results in altered biofilm structure and increased exopolysaccharide synthesis: implications for biofilm resistance. *Biofouling* 33, 481–493. doi: 10.1080/08927014.2017.1323206

Luo, Y., and Song, Y. (2021). Mechanism of antimicrobial peptides: antimicrobial, anti-inflammatory and antibiofilm activities. *Int. J. Mol. Sci.* 22. doi: 10.3390/IJMS222111401

Malone, M., Bjarnsholt, T., McBain, A. J., James, G. A., Stoodley, P., Leaper, D., et al. (2017). The prevalence of biofilms in chronic wounds: a systematic review and meta-analysis of published data. *J. Wound Care* 26, 20–25. doi: 10.12968/jowc.2017.26.1.20

Metcalf, D., and Bowler, P. (2013). Biofilm delays wound healing: A review of the evidence. *Burns. Trauma* 1, 5. doi: 10.4103/2321-3868.113329

Miyaue, S., Suzuki, E., Komiyama, Y., Kondo, Y., Morikawa, M., and Maeda, S. (2018). Bacterial memory of persisters: bacterial persister cells can retain their phenotype for days or weeks after withdrawal from colony–biofilm culture. *Front. Microbiol.* 9. doi: 10.3389/fmicb.2018.01396

Namgoong, S., Jung, S.-Y., Han, S.-K., Kim, A.-R., and Dhong, E.-S. (2020). Clinical experience with surgical debridement and simultaneous meshed skin grafts in treating biofilm-associated infection: an exploratory retrospective pilot study. *J. Plast. Surg. Handb. Surg.* 54, 47–54. doi: 10.1080/2000656X.2019.1673170

Nishino, K., Yamasaki, S., Nakashima, R., Zwama, M., and Hayashi-Nishino, M. (2021). Function and inhibitory mechanisms of multidrug efflux pumps. *Front. Microbiol.* 12. doi: 10.3389/fmicb.2021.737288

Olsen, I. (2015). Biofilm-specific antibiotic tolerance and resistance. *Eur. J. Clin. Microbiol. Infect. Dis.* 34, 877–886. doi: 10.1007/s10096-015-2323-z

Ousey, K., and Ovens, L. (2023). Comparing methods of debridement for removing biofilm in hard-to-heal wounds. *J. Wound Care* 32, S4–S10. doi: 10.12968/jowc.2023.32.Sup3b.S4

Overhage, J., Campisano, A., Bains, M., Torfs, E. C. W., Rehm, B. H. A., and Hancock, R. E. W. (2008). Human host defense peptide LL-37 prevents bacterial biofilm formation. *Infect. Immun.* 76, 4176–4182. doi: 10.1128/IAI.00318-08

Pallin, D. J., Espinola, J. A., and Camargo, C. A. (2014). US population aging and demand for inpatient services. *J. Hosp. Med.* 9, 193–196. doi: 10.1002/jhm.2145

Panlilio, H., and Rice, C. V. (2021). The role of extracellular DNA in the formation, architecture, stability, and treatment of bacterial biofilms. *Biotechnol. Bioeng.* 118, 2129–2141. doi: 10.1002/bit.27760

Perry, E. K., and Tan, M.-W. (2023). Bacterial biofilms in the human body: prevalence and impacts on health and disease. *Front. Cell Infect. Microbiol.* 13. doi: 10.3389/fcimb.2023.1237164

Pinto, R. M., Soares, F. A., Reis, S., Nunes, C., and Van Dijck, P. (2020). Innovative strategies toward the disassembly of the EPS matrix in bacterial biofilms. *Front. Microbiol.* 11. doi: 10.3389/fmicb.2020.00952

Preda, V. G., and Săndulescu, O. (2019). Communication is the key: biofilms, quorum sensing, formation and prevention. *Discoveries. (Craiova).* 7, e100. doi: 10.15190/d.2019.13

Rather, M. A., Gupta, K., and Mandal, M. (2021). Microbial biofilm: formation, architecture, antibiotic resistance, and control strategies. *Braz. J. Microbiol.* 52, 1701–1718. doi: 10.1007/s42770-021-00624-x

Rodríguez-Merchán, E. C., Davidson, D. J., and Liddle, A. D. (2021). Recent strategies to combat infections from biofilm-forming bacteria on orthopaedic implants. *Int. J. Mol. Sci.* 22, 10243. doi: 10.3390/ijms221910243

Saksena, D., Mishra, Y. K., Muralidharan, S., Kanhere, V., Srivastava, P., and Srivastava, C. P. (2019). Follow-up and management of valvular heart disease patients with prosthetic valve: a clinical practice guideline for Indian scenario. *Indian J. Thorac. Cardiovasc. Surg.* 35, 3–44. doi: 10.1007/s12055-019-00789-z

Santos, A. P. A., Watanabe, E., and de Andrade, D. (2011). Biofilme em marca-passo artificial: ficção ou realidade? *Arq. Bras. Cardiol.* 97, e113–e120. doi: 10.1590/S0066-782X2011001400018

Saverina, E. A., Frolov, N. A., Kamanina, O. A., Arlyapov, V. A., Vereshchagin, A. N., and Ananikov, V. P. (2023). From antibacterial to antibiofilm targeting: an emerging paradigm shift in the development of quaternary ammonium compounds (QACs). *ACS Infect. Dis.* 9, 394–422. doi: 10.1021/acsinfecdis.2c00469

Schaible, B., Taylor, C. T., and Schaffer, K. (2012). Hypoxia Increases Antibiotic Resistance in Pseudomonas aeruginosa through Altering the Composition of Multidrug Efflux Pumps. *Antimicrob. Agents Chemother.* 56, 2114–2118. doi: 10.1128/AAC.05574-11

Shahrour, H., Ferrer-Espada, R., Dandache, I., Bárcena-Varela, S., Sánchez-Gómez, S., Chokr, A., et al. (2019). *AMPs as anti-biofilm agents for human therapy and prophylaxis*. (Singapore: Springer), 257–279. doi: 10.1007/978-981-13-3588-4_14

Sharma, D., Misba, L., and Khan, A. U. (2019). Antibiotics versus biofilm: an emerging battleground in microbial communities. *Antimicrob. Resist. Infect. Control.* 8, 76. doi: 10.1186/s13756-019-0533-3

Singh, R., Sahore, S., Kaur, P., Rani, A., and Ray, P. (2016). Penetration barrier contributes to bacterial biofilm-associated resistance against only select antibiotics, and exhibits genus-, strain- and antibiotic-specific differences. *Pathog. Dis.* 74, ftw056. doi: 10.1093/femspd/ftw056

Speziale, P., and Pietrocola, G. (2021). Monoclonal antibodies targeting surface-exposed and secreted proteins from staphylococci. *Vaccines (Basel).* 9. doi: 10.3390/VACCINES9050459

Tande, A. J., and Patel, R. (2014). Prosthetic joint infection. *Clin. Microbiol. Rev.* 27, 302–345. doi: 10.1128/CMR.00111-13

Townsend, E. M., Moat, J., and Jameson, E. (2020). CAUTI's next top model - Model dependent Klebsiella biofilm inhibition by bacteriophages and antimicrobials. *Biofilm* 2, 100038. doi: 10.1016/j.bioflm.2020.100038

Toyofuku, M., Inaba, T., Kiyokawa, T., Obana, N., Yawata, Y., and Nomura, N. (2016). Environmental factors that shape biofilm formation. *Biosci. Biotechnol. Biochem.* 80, 7–12. doi: 10.1080/09168451.2015.1058701

Tran, D. L., Huang, R.-W., Chiu, E. S., Rajhathy, E. M., Gregory, J. H., Ayello, E. A., et al. (2023). Debridement: technical considerations and treatment options for the interprofessional team. *Adv. Skin. Wound Care* 36, 180–187. doi: 10.1097/01.ASW.0000920660.07232.f7

Vazquez-Rodriguez, A., Vasto-Anzaldo, X. G., Barboza Perez, D., Vázquez-Garza, E., Chapoy-Villanueva, H., García-Rivas, G., et al. (2018). Microbial Competition of Rhodotorula mucilaginosa UANL-001L and E. coli increase biosynthesis of Non-Toxic Exopolysaccharide with Applications as a Wide-Spectrum Antimicrobial. *Sci. Rep.* 8, 798. doi: 10.1038/s41598-017-17908-8

Wakharde, A. A., Halbandge, S. D., Phule, D. B., and Karuppayil, S. M. (2018). Anticancer drugs as antibiofilm agents in *candida albicans*: potential targets. *Assay. Drug Dev. Technol.* 16, 232–246. doi: 10.1089/adt.2017.826

Wang, Y., Liu, B., Grenier, D., and Yi, L. (2019). Regulatory mechanisms of the luxS/AI-2 system and bacterial resistance. *Antimicrob. Agents Chemother.* 63. doi: 10.1128/AAC.01186-19

Wu, Y., Klapper, I., and Stewart, P. S. (2018). Hypoxia arising from concerted oxygen consumption by neutrophils and microorganisms in biofilms. *Pathog. Dis.* 76. doi: 10.1093/femspd/fty043

Yang, B., Lei, Z., Zhao, Y., Ahmed, S., Wang, C., Zhang, S., et al. (2017). Combination susceptibility testing of common antimicrobials *in vitro* and the effects of sub-MIC of antimicrobials on staphylococcus aureus biofilm formation. *Front. Microbiol.* 8. doi: 10.3389/fmicb.2017.02125

Yasir, M., Willcox, M. D. P., and Dutta, D. (2018). Action of antimicrobial peptides against bacterial biofilms. *Mater. (Basel).* 11. doi: 10.3390/ma11122468

Yin, R., Dai, T., Avci, P., Jorge, A. E. S., De Melo, W. C. M. A., Vecchio, D., et al. (2013). Light based anti-infectives: ultraviolet C irradiation, photodynamic therapy, blue light, and beyond. *Curr. Opin. Pharmacol.* 13, 731–762. doi: 10.1016/J.COPH.2013.08.009

Zimmermann, S., Klinger-Strobel, M., Bohnert, J. A., Wendler, S., Rödel, J., Pletz, M. W., et al. (2019). Clinically approved drugs inhibit the staphylococcus aureus multidrug norA efflux pump and reduce biofilm formation. *Front. Microbiol.* 10. doi: 10.3389/fmicb.2019.02762

frontiers | Frontiers in Cellular and Infection Microbiology

TYPE Original Research
PUBLISHED 13 May 2024
DOI 10.3389/fcimb.2024.1404960

OPEN ACCESS

EDITED BY
Maria Gabriela Paraje,
National University of Cordoba, Argentina

REVIEWED BY
Juan Pablo Caeiro,
National University of Cordoba, Argentina
Jose Baronetti,
Instituto Multidisciplinario de Biologia Vegetal (IMBIV), Argentina

*CORRESPONDENCE
Jintae Lee
jtlee@ynu.ac.kr

RECEIVED 22 March 2024
ACCEPTED 26 April 2024
PUBLISHED 13 May 2024

CITATION
Paramanya S, Lee J-H and Lee J (2024) Antibiofilm activity of carotenoid crocetin against Staphylococcal strains.
Front. Cell. Infect. Microbiol. 14:1404960.
doi: 10.3389/fcimb.2024.1404960

Antibiofilm activity of carotenoid crocetin against Staphylococcal strains

Saurav Paramanya, Jin-Hyung Lee and Jintae Lee*

School of Chemical Engineering, Yeungnam University, Gyeongsan, Republic of Korea

Staphylococcus aureus and *Staphylococcus epidermidis* stand as notorious threats to human beings owing to the myriad of infections they cause. The bacteria readily form biofilms that help in withstanding the effects of antibiotics and the immune system. Intending to combat the biofilm formation and reduce the virulence of the pathogens, we investigated the effects of carotenoids, crocetin, and crocin, on four Staphylococcal strains. Crocetin was found to be the most effective as it diminished the biofilm formation of *S. aureus* ATCC 6538 significantly at 50 µg/mL without exhibiting bactericidal effect (MIC >800 µg/mL) and also inhibited the formation of biofilm by MSSA 25923 and *S. epidermidis* at a concentration as low as 2 µg/mL, and that by methicillin-resistant *S. aureus* MW2 at 100 µg/mL. It displayed minimal to no antibiofilm efficacy on the Gram-negative strains *Escherichia coli* O157:H7 and *Pseudomonas aeruginosa* as well as a fungal strain of *Candida albicans*. It could also curb the formation of fibrils, which partly contributes to the biofilm formation in *S. epidermidis*. Additionally, the ADME analysis of crocetin proclaims how relatively non-toxic the chemical is. Also, crocetin displayed synergistic antibiofilm characteristics in combination with tobramycin. The presence of a polyene chain with carboxylic acid groups at its ends is hypothesized to contribute to the strong antibiofilm characteristics of crocetin. These findings suggest that using apocarotenoids, particularly crocetin might help curb the biofilm formation by *S. aureus* and *S. epidermidis*.

KEYWORDS

antibiofilm, crocetin, fibrils, Staphylococcus aureus, Staphylococcus epidermidis

1 Introduction

Biofilms are a complex matrix of microorganisms adhering to biotic or abiotic surfaces, typically forming an amalgamation of polysaccharides, proteins, and organic components, prevalent in diverse environments such as clinical and industrial settings, food processing facilities, and drinking water distribution systems (Bazargani and Rohloff, 2016; Khan et al., 2020). Such biofilms pose a grave threat to humans owing to the exacerbated resistance to antimicrobials and host defenses (Gebreyohannes et al., 2019), thus increasing the susceptibility to chronic infections.

Staphylococcus aureus is a prevalent human pathogen capable of causing a range of infectious diseases, including skin and soft tissue infections, endocarditis, osteomyelitis, and severe pneumonia leading to fatalities (Guo et al., 2020). The bacterium employs a complex network to orchestrate the synthesis of virulence factors like hemolysins, enterotoxins, and immune-evasive staphyloxanthin. These factors contribute to various life-threatening infections such as bacteremia, pulmonary infections, gastroenteritis, and toxic shock syndrome (Valliammai et al., 2020; Park et al., 2023). The strain's propensity to form biofilms on damaged tissues and medical implants contributes to its development of antibiotic resistance and virulence (Moormeier and Bayles, 2017). Since the introduction of penicillin in the 1940s and methicillin in the 1950s to the present (Nandhini et al., 2022), *Staphylococcus aureus* has adapted rapidly by becoming resistant to each new type of drug. The ability to combat the effect of drugs led it to become the main cause of community-acquired and nosocomial infections resulting in high morbidity and mortality rates (Tong et al., 2015).

Staphylococcus epidermidis is the most frequently encountered Coagulase-negative staphylococci (CoNS) implicated in clinical diseases (Argemi et al., 2019).

CoNS can lead to severe infections affecting various areas such as the bloodstream, skin, soft tissues, urinary tract, prosthetic joints, and vascular grafts, with *S. epidermidis* particularly implicated in catheter-related urinary tract infections (Michels et al., 2021; Rubini et al., 2021). Prolonged intensive care practices have led to a quintessential commensal organism like *S. epidermidis* inducing a multitude of infections by evading the host's defense mechanisms and developing resistance to multiple drugs (Kleinschmidt et al., 2015).

A class of isoprenoid derivatives called carotenoids are biosynthesized by microorganisms, fungi, algae, and plants which serve as effective free-radical scavengers (Mohd Hatta et al., 2023). These carotenoids find their way into animals through fruits and vegetables wherein they undergo oxidative cleavage for the retinal formation and activation of the transcriptional system. The cleavage process results in products, including apocarotenoids, recognized for their biological activity as anticancer agents and cell modulators (Kim et al., 2014). One such apocarotenoid, crocetin, found in saffron, is renowned for its wide range of biological activities in addition to its high therapeutic index (Gupta, 2019). Although saffron possesses a plethora of medicinal benefits owing to the presence of active ingredients and found enormous usage in ancient times, there are no studies regarding the antibiofilm characteristics of crocetin or the other active ingredients (Carradori et al., 2016; Butnariu et al., 2022). The anticancerous property of crocetin has been studied extensively (Colapietro et al., 2019), but there was a need for its antibiofilm property to be assessed to help combat the drug resistance by the pathogens.

The following study was conducted to find a compound that could hinder the formation of biofilm and toxin production by *S. aureus* and *S. epidermidis* without decimating the bacterium. The two most active ingredients of saffron, crocetin and crocin were used to assess their antibiofilm attributes against *S. aureus* and *S. epidermidis*. Crocetin and crocin share structural resemblances with fatty acids. Similar to fatty acids, crocetin possesses a long alkyl chain terminated by carboxylic acid groups at its ends, while crocin differs in its end groups, containing gentiobiose instead. Fatty acids are recognized as established antibiofilm agents, effectively curbing the growth and formation of biofilms across various pathogens (Kumar et al., 2020). Due to the high resemblance of crocetin to fatty acids and its superior activity compared to crocin, it was taken into account for the further investigation of its activity against the other four *Staphylococcus* strains, *Staphylococcus aureus* ATCC 6538, *Staphylococcus aureus* ATCC 25923, *Staphylococcus epidermidis* ATCC 14990, and a methicillin-resistant *Staphylococcus aureus* (MRSA MW2). Live imaging microscopy, scanning electron microscopy, lipase activity, hemolysis, EPS production, metabolic activity, and hydrophobicity assays were committed to evaluate the biofilm-inhibiting and toxin-inhibiting activity of crocetin against the aforementioned strains. Furthermore, ADME analysis was simulated to analyze the toxicity of crocetin and crocin.

2 Materials and methods

2.1 Bacterial strains, culture media, chemicals, and growth analysis

The strains used for the experiments were two methicillin-sensitive *S. aureus* strains (ATCC 6538 and ATCC 25923), a methicillin-resistant *S. aureus* strain (MW2), an *S. epidermidis* strain (ATCC 14990), a fungal strain of *C. albicans* DAY185, an enterohaemorrhagic *E. coli* O157:H7 strain, and a *P. aeruginosa* PAO1 strain. Colonies of MSSA ATCC 6538, MSSA ATCC 25923, *S. epidermidis* ATCC 14990, *E. coli* O157:H7, and *P. aeruginosa* PAO1 were inoculated in Luria-Bertani (LB) medium at 37 °C while MRSA MW2 was cultivated in LB medium containing 0.2% of glucose under the same condition. The fungal strain, *C. albicans* DAY185 was inoculated in Potato Dextrose Broth (PDB) at 37 °C. *V. parahaemolyticus* was cultured in mLB (mineral Luria-Bertani) medium viz. LB medium supplemented with 3% (w/v) NaCl. The test compounds, crocetin, crocin, and tobramycin along with crystal violet were procured from Sigma-Aldrich (St Louis, MO, USA). Crocetin and crocin were dissolved in Dimethyl Sulfoxide (DMSO) while tobramycin was dissolved in distilled water, and 0.1% of DMSO was used as control as it doesn't serve as a suitable medium for bacterial growth and biofilm formation. The growth of the bacterium was assessed by forming Colony Forming Units (CFU) on 90 mm petri plates after incubating the MSSA ATCC 6538 in LB medium with or without crocetin or crocin or a combination of tobramycin and crocetin or crocin at 37 °C for 24 hrs.

2.2 Crystal-violet biofilm assay

The test compounds' effect on the biofilm formation was assessed by a crystal-violet biofilm assay as previously reported (Jeon et al., 2024). The cells of *S. aureus* and *S. epidermidis* (~10^7 CFU/mL) were inoculated in LB medium and crocetin or crocin

were added at 0, 5, 10, 20, 50, and 100 µg/mL to the wells of the 96-well plates. To assess the effect of combination of tobramycin with either crocetin or crocin, a crystal violet assay was performed following the methodology reported previously (Park et al., 2022) wherein *S. aureus* cells (~10^7 CFU/mL) were inoculated in LB medium, and a fixed concentration of tobramycin at 2 µg/mL was added to 96-well plates, along with varying concentrations of crocetin or crocin (0, 20, and 50 µg/mL). The plates were then incubated at 37°C for 24 hrs without agitation. The planktonic cells were discarded by washing the plates well with distilled water three times. The biofilm cells were stained with 0.1% (w/v) of crystal violet for 20 mins. and then washed using distilled water thrice. The stained biofilm cells were dissolved using 95% ethanol with vigorous shaking. The absorbances were read at 570 nm using a Multiskan plate reader (Thermo Fisher Scientific, Waltham, MA, USA). The results of biofilm formation were derived from three independent cultures, each having six replicate wells.

2.3 Dispersal assay

The biofilm dispersal assay was conducted to evaluate how crocetin affects *S. aureus* and *S. epidermidis* using the method previously reported (Sathiyamoorthi et al., 2024). After allowing biofilms to form for 24 hrs at 37°C and the above biofilm assay in the section 2.2 was performed.

2.4 Microscopic observations of biofilms

The *S. aureus* and *S. epidermidis* biofilms were formed in 96-well plates as discussed earlier (2.2) in the presence or absence of crocetin (0, 5, 10, 20, 50, and 100 µg/mL) at 37 °C for 24 hrs and the plates were washed thrice with distilled water to discard the planktonic cells followed by staining with 0.1% (w/v) crystal violet and subsequent washing of the stain. The stained biofilms were observed under the iRiS^{TM} Digital Cell Imaging System (Logos Biosystems, Anyang, Korea). ImageJ (https://imagej.nih.gov/ij/index.html) was then employed to generate color-coded 3D biofilm images.

Additionally, the biofilm reduction by crocetin was observed by SEM, as previously reported. *S. aureus* ATCC 6538 and *S. epidermidis* cells (~10^7 CFU/mL) were inoculated in fresh LB medium with or without crocetin (0, 5, 10, 20, 50, and 100 µg/mL) in a 96-well plate. Each well was equipped with a piece of nylon membrane (~ 0.16 cm^2) and subsequently, the cells were incubated for 24 h at 37°C without agitation. Biofilms established on the membranes were then fixed with a 1:1 concoction of glutaraldehyde (2.5%) and formaldehyde (2%) for 24 hrs, followed by dehydration with ethanol (50, 70, 90, 95, and 99%) sequentially. Utilizing a critical point dryer (HCP-2, Hitachi, Tokyo, Japan), the nylon membranes were subjected to drying and was proceeded by the metal coating using Precision Etching Coating System (Gatan, Inc., Pleasanton, USA) with subsequent observation using S-4800 (Hitachi, Tokyo, Japan), a field emission scanning electron microscope.

2.5 Hemolytic activity assay

A hemolytic activity assay was carried out using sheep blood cells (MB Cell, South Korea) as described previously (Kim et al., 2018). The cells of *S. aureus* (~2×10^7 CFU/mL) were suspended in 2 mL of LB medium and were cultivated using 0, 20, and 50 µg/mL of crocetin with vigorous shaking at 250 rpm for 24 hrs. Fresh sheep blood was subjected to centrifugation at 3,000 × g for 2 mins., and the red blood cells were collected and then cleaned three times with PBS followed by their resuspension in PBS buffer (3.3%). The cell culture of *S. aureus* (600 µL) was then added to 2 mL of red blood cells and the sample was subjected to 1 hour of shaking at 250 rpm at 37 °C. The mixtures underwent centrifugation for 10 mins. at 16,600 × g, and the absorbances of supernatants were gauged at 543 nm.

2.6 Exopolysaccharide production assay

An assay was performed to estimate the production of exopolysaccharides as previously described (Ahmed et al., 2022). Briefly, *S. epidermidis* was incubated with or without crocetin at 5, 10, and 20 µg/mL in LB with shaking at 250 rpm for 24 h at 37°C. The tubes underwent centrifugation at 10,000 rpm for 10 mins. and the resulting supernatants were combined with chilled ethanol in a ratio of 1:3 and allowed to stand undisturbed at 4°C overnight. The suspension was centrifuged at 10,000 rpm for 5 mins. to collect the EPS precipitates followed by subsequent solubilizing in 200 µL of water. A phenol-sulfuric acid mixture was prepared in the ratio of 1:5 and added to the 200 µL samples, followed by incubation at room temperature for 30 minutes, and then left undisturbed for an additional 20 minutes before measuring the absorbances at 490 nm.

2.7 Biofilm cell viability assay

The metabolic viabilities of the cells in the biofilms of *S. epidermidis* was estimated using Triphenyl tetrazolium chloride (TTC) assay as described earlier (Faleye et al., 2023) with slight modifications. Briefly, cells of *S. epidermidis* were grown in LB medium overnight and the 1:100 dilution of the same was treated with crocetin at 0, 2, 5, 10, and 20 µg/mL in a 96-well plate. TTC dye was introduced into each well to achieve a final concentration of 0.05% w/v, followed by incubation of the plate at 37°C for 24 hrs. The plate was washed with distilled water to remove the non-adherent cells, and the formazan production by TTC was solubilized in methanol. The absorbance of each well was measured at 500 nm using a Multiskan EX microplate reader. The metabolic viabilities of biofilm cells were quantified and expressed as a percentage of absorbance relative to untreated controls.

2.8 Lipase production assay

The effect of crocetin on *S. aureus* was quantified by an extracellular lipase production assay wherein the cells of *S. aureus* (~2×10^7 CFU/mL) were incubated in 2 mL of LB medium at 37 °C

for 20 hrs with constant shaking in the absence or presence of crocetin (0, 20, and 50 µg/mL) as reported earlier (Kim et al., 2022). To summarize, culture supernatants (0.1 mL) were homogenized with 0.9 mL of substrate solution which comprised of 10% of buffer A containing 3 mg/mL of p-nitrophenyl palmitate in isopropyl alcohol and 90% of buffer B containing 1 mg/mL of gum arabic and 2 mg/mL sodium deoxycholate in 50 mM Na_2PO_4 buffer, followed by heating at 40°C for 30 mins. 1 M Na_2CO_3 was added to cease the reactions and the reaction supernatants' absorbances were quantified at 405 nm.

2.9 Hydrophobicity assay

A hydrophobicity assay was carried out as described previously (Lee et al., 2016). *S. aureus* and *S. epidermidis* cells were incubated overnight in LB medium at 37 °C and were garnered after centrifuging them at 7,000×g for 5 mins. The garnered cells were mixed with 2 mL of PBS and 300 µL of hexadecane followed by a vortexing of 4 mins. The sample containing tubes was allowed to rest for 30 mins. for the phases to separate. The aqueous phases were used to measure the absorbances at OD_{600}. Cell surface hydrophobicity (H%) was expressed by measuring the reduction in optical density (OD) of the aqueous phase and calculated using the equation H% = [(ODo - OD)/ODo] × 100, where ODo represents the initial OD before extraction with hexadecane, and OD represents the OD after extraction.

2.10 Evaluation of absorption, distribution, metabolism, and excretion properties

ADME software was accessed to appraise the drug-like properties of crocetin and crocin. The online web servers (https://preadmet.qsarhub.com/), (https://www.molinspiration.com), and GUSAR (https://www.way2drug.com/) were accessed on 10th November, 2023.

2.11 Statistical analysis

The statistical analysis was conducted using one-way ANOVA followed by Dunnett's test in SPSS version 23 (SPSS Inc., Chicago, IL, USA). Mean values accompanied by standard deviations were reported, with significance considered at p-values below 0.05.

3 Results

3.1 Antibiofilm activities of the apocarotenoids against *S. aureus* and *S. epidermidis*

The apocarotenoids, namely, crocetin and crocin were tested at concentrations up to 100 µg/mL for *S. aureus* ATCC 6538 and MRSA MW2, and 50 µg/mL for *S. aureus* ATCC 25923 and *S. epidermidis* to assess their antibiofilm efficiencies against the aforementioned pathogens. Only crocetin showed a significant effect on the biofilm formation while crocin remained ineffective (Figures 1B, 2D–F). Crocetin could inhibit the biofilm growth by *S. epidermidis* and *S. aureus* ATCC 25923 by 52% and 55% respectively at a concentration of 2 µg/mL (Figures 2A, C) while in the case of *S. aureus* ATCC 6538, a reduction of 67% was observed at a higher concentration of 50 µg/mL (Figure 1A). A reduction of 55% in biofilm formation was observed in MRSA MW2 at a high concentration of 100 µg/mL (Figure 2B). The effect of crocetin on the cell growth of *S. aureus* ATCC 6538 was observed by performing colony forming unit (CFU) assay wherein a delay in the growth of planktonic cells was observed starting from the lowest tested concentration, 20 µg/mL until 400 µg/mL; however, at 800 µg/mL, the compound started exhibiting bacteriostatic effect (Figure 1C). CFU assay of the same bacterium using crocin showed no significant effect on the cell growth of the pathogen even at high concentrations (Figure 1D). These results suggest that crocetin dwindles the biofilm formation without exhibiting a significant effect on the planktonic cell growth. On the other hand, the dispersal assay showed that mature biofilms of *S. aureus* and *S. epidermidis* were not affected when treated with crocetin at concentrations of 20 and 50 µg/mL (Supplementary Figures 3A, B), which confirmed that biofilm dispersal is much difficult than biofilm inhibition.

3.2 Antibiofilm characteristics of crocetin on other microbes

The biofilm assay was further performed on other pathogens, namely, *C. albicans* DAY185, a fungal strain, as well as two Gram-negative strains: *E. coli* O157:H7 and *P. aeruginosa* PAO1. While the fungal strain (*C. albicans* DAY185) and Gram-negative strain of *E. coli* O157:H7 were scarcely affected at the same concentrations (Figures 3A, B), crocetin, unlike the other pathogens listed above, did not affect *P. aeruginosa* PAO1 biofilm development (Figure 3C).

3.3 Synergistic antibiofilm characteristics of the combination of tobramycin with crocetin

The biofilm assay was conducted on *S. aureus* to evaluate the effect of combining tobramycin with either crocetin or crocin. The CFU results demonstrate a slight reduction of less than 10-fold in the colonies formed by *S. aureus* when treated with tobramycin alone, with no significant change observed in the presence of crocetin alone. Combining 10 µg/mL of tobramycin with 20 µg/mL of crocetin resulted in approximately a 1000-fold reduction, while the reduction increased to around 10,000-fold with 50 µg/mL of crocetin and the same concentration of tobramycin (Figure 4A). The biofilm assay revealed that tobramycin alone at a concentration of 2 µg/mL reduced biofilm growth by 19%, while crocetin alone at 20 µg/mL decreased it by 48%. However, when crocetin was combined with 2 µg/mL of tobramycin at concentrations of 20

10.3389/fcimb.2024.1404960

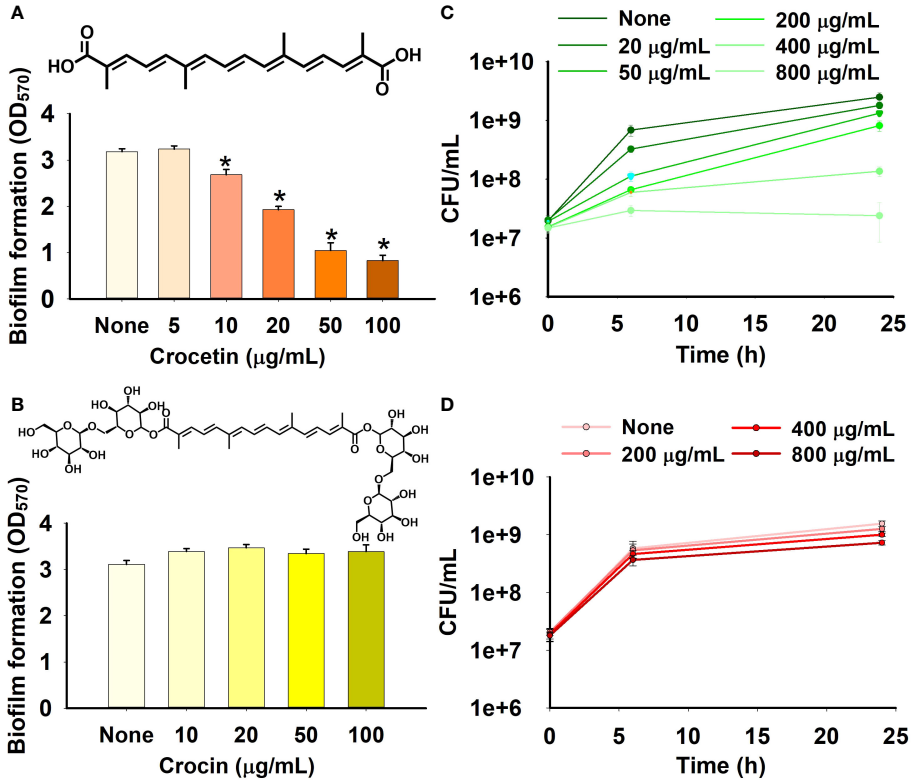

FIGURE 1
Effect of crocetin and crocin on biofilm formation and cell growth. Biofilm formation by *S. aureus* ATCC 6538 in the presence of crocetin **(A)**, crocin **(B)**. *S. aureus* cell growth in the presence of crocetin **(C)**, and crocin **(D)**. *p<0.05 *vs* untreated controls (None).

and 50 μg/mL, the reduction in biofilm growth was notably higher at 83% and 97%, respectively. (Figure 4B). Nonetheless, the combination of tobramycin with crocin did not impact CFU or biofilm growth by *S. aureus* (Figures 4C, D).

3.4 Microscopic findings of crocetin's effect on *S. aureus* and *S. epidermidis*

The biofilms formed by the bacteria were observed by live-imaging microscopy and SEM. 3D color images that were obtained through live-imaging microscopy showed blue or bluish-cyan for 'None' indicating strong high biofilms (Figures 5A, 6A, Supplementary Figure 1). At concentrations of 50 and 100 μg/mL (for *S. aureus* ATCC 6538) and 10 and 20 μg/mL (*S. aureus* ATCC 25923 and *S. epidermidis*), red color with patches of yellow exhibited scarcely to no biofilm formation owing to crocetin's antibiofilm attributes (Figures 5A, 6A, Supplementary Figure 1). The SEM images were found to be following the results of the biofilm assay. The cell growth could be seen decreasing in a dose-dependent manner owing to the decrease in biofilm formation without imparting any changes to the morphology of the bacterial cells (Figures 5B, 6B). Furthermore, fibril production by *S. epidermidis* decreased in a dose-dependent manner, with untreated sample demonstrating significant fibrils in their respective images. The reduction in fibrils, which play a role in the formation of biofilms in *S. epidermidis*, could be correlated with a significant reduction in its biofilms. Presumably, crocetin curtails biofilm development by targeting the fibril growth in *S. epidermidis*. This concludes that crocetin is capable of inhibiting the biofilm formation of the bacteria in question without affecting their cell morphology.

3.5 Effect of crocetin on *S. aureus'* hemolytic activity, hydrophobicity, and lipase production

A myriad of virulence factors is produced by *S. aureus* which includes hemolysin, and extracellular lipase which called for the need to investigate the effect of crocetin on them. Crocetin up to 50 μg/mL showed ineffectiveness in hindering lipase production by the bacterium (Supplementary Figure 2A), preventing hemolysis of sheep red blood cells (RBCs) (Supplementary Figure 2B), and did not enhance bacterial affinity towards the aqueous phase in the hydrophobicity assay against *S. aureus* (Supplementary Figure 2C).

3.6 Effect of crocetin on *S epidermidis'* EPS production, metabolic activity, and hydrophobicity

Crocetin up to 20 μg/mL was found ineffective in preventing EPS production by *S. epidermidis* cells (Supplementary Figure 2D), had no impact on the metabolic activity of biofilm cells

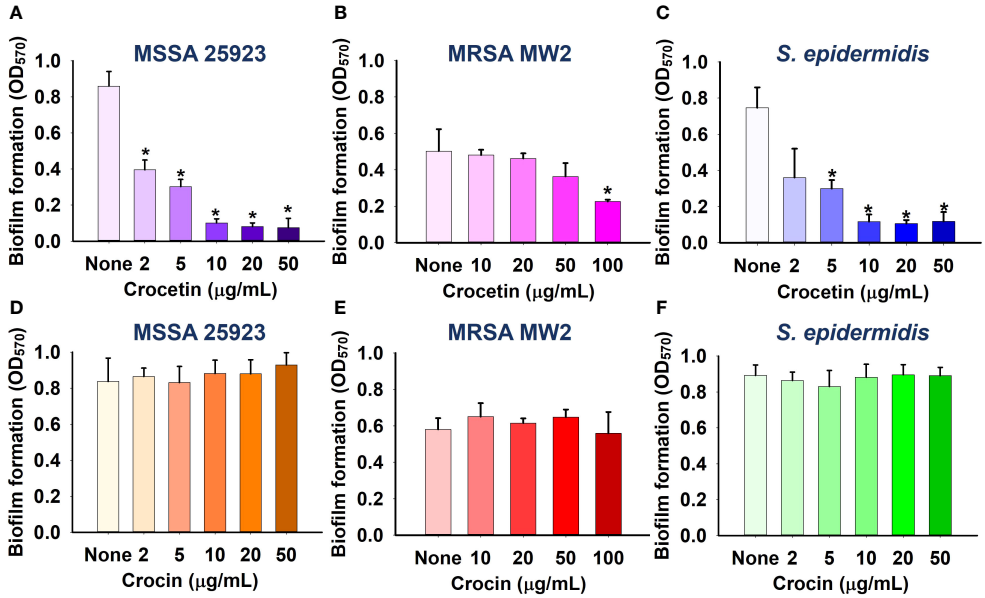

FIGURE 2
Effect of crocetin on biofilm formation by *S. aureus* ATCC 25923 **(A)**, MRSA MW2 **(B)**, and *S. epidermidis* **(C)**, and effect of crocin on biofilm formation by *S. aureus* ATCC 25923 **(D)**, MRSA MW2 **(E)**, and *S. epidermidis* **(F)**. *$p<0.05$ *vs* untreated controls (None).

(Supplementary Figure 2E), and did not alter the bacterium's hydrophobicity (Supplementary Figure 2F).

3.7 Crocetin and crocin ADME profiling

Crocetin and crocin ADME profiles found that the former violated one and the latter three of Lipinski's five rules, with both compounds having miLogP<5. The skin permeability of both substances was adequate, but they differed significantly in terms of human intestine absorption, which was high for crocetin (>95%), but severely low for crocin (1%). Crocetin was discovered to have no fish toxicity, however, crocin demonstrated a high toxicity for the same. Both compounds were found to induce carcinogenic properties in mice. The molecular volume, a determining factor for the transport characteristics of compounds, was found to be higher in crocin compared to crocetin. This difference could elucidate the superior absorption of crocetin over crocin, which eventually metabolizes into crocetin and glucuronide conjugates. Another significant factor influencing transport characteristics, the Total Polar Surface Area (TPSA), was found to exceed the ideal score of 140 Å in the case of crocin, while it was almost half the ideal score in the case of crocetin. This further attests the superior absorptivity of crocetin compared to crocin. The observation that the two compounds in question are environmentally non-toxic suggests their potential as green alternatives. Table 1 contains an in-depth breakdown of ADME parameters.

4 Discussion

This study reveals that the saffron-derived crocetin exerts substantial antibiofilm effects on *S. aureus* and *S. epidermidis* strains without exhibiting any bactericidal effects. The non-

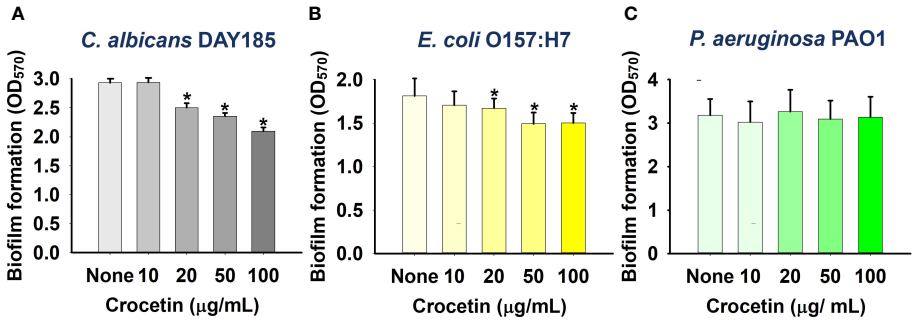

FIGURE 3
Effect of crocetin on biofilm formation by *C. albicans* DAY185 **(A)**, *E. coli* O157:H7 **(B)**, and *P. aeruginosa* PAO1 **(C)**. *p<0.05 *vs* untreated controls (None).

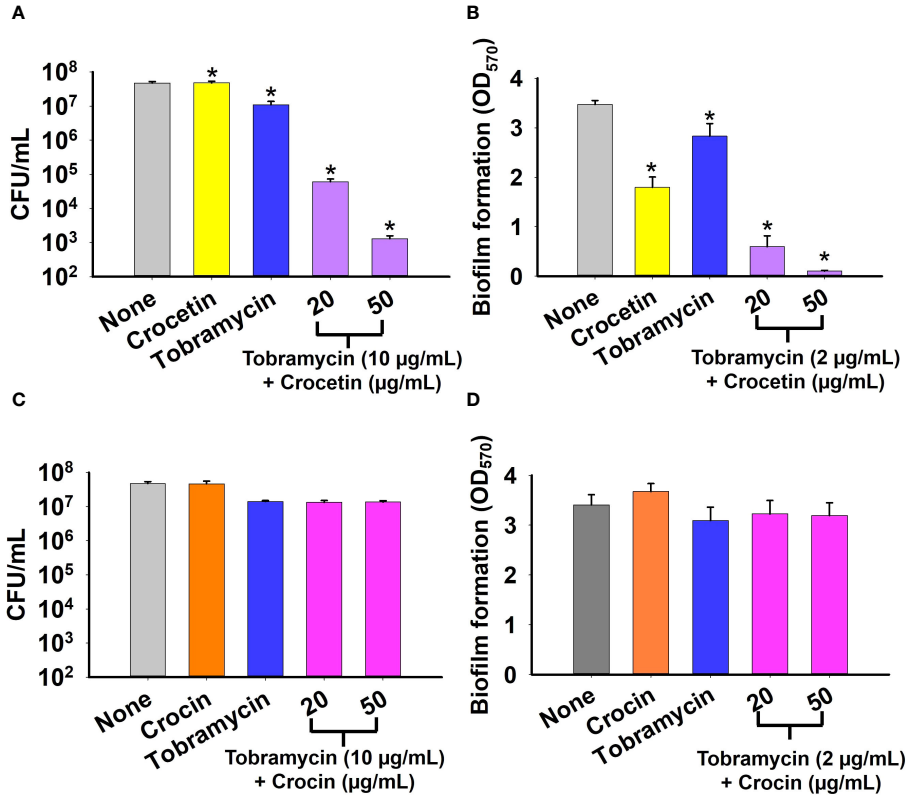

FIGURE 4
Effect of combination of tobramycin with crocetin or crocin on cell survival and biofilm formation. *S. aureus* cell survival in the presence of tobramycin and crocetin **(A)**, and tobramycin and crocin **(C)**. Biofilm formation by *S. aureus* ATCC 6538 in the presence of tobramycin and crocetin **(B)**, and tobramycin and crocin **(D)**. *p<0.05 *vs* untreated controls (None).

toxicity of crocetin along with crocin has also been established by the ADME profiles of the same.

Saffron has widely been used as an effective treatment in ancient India and China and is known to possess a plethora of active components including crocetin and crocin, and extensive research has suggested its potential efficacy in addressing various health conditions, including diabetes mellitus, cancers, Alzheimer's disease, and numerous other ailments (Razak et al., 2017). *S. aureus* biofilms have been associated with chronic wound infections as well as a common skin disorder, acne vulgaris, which is primarily caused by *P. acnes* but exacerbated by the presence of *S. aureus* biofilms (Archer et al., 2011; Tyner and Patel, 2016). Thus, the inhibitory effect of crocetin on *S. aureus* biofilms holds promise in aiding the treatment of such conditions.

Our research highlights that crocetin, our test compound, notably reduces biofilm formation only in Gram-positive strains, showing minimal to no effect on Gram-negative bacteria and the fungal strain, *Candida albicans* (Figures 1–3). Gram-negative bacteria possess an outer membrane that sets them apart from Gram-positive bacteria, rendering them more resistant to antibiotics (Bann et al., 2021). While this membrane permits the passage of smaller molecules, bacteria can modify it by altering its hydrophobic properties or through mutations in porins, conferring resistance to several antibiotics, including β-lactams (Breijyeh et al., 2020). Thus, enhancing compound penetration through this outer membrane is crucial for antibiotic efficacy (Miller, 2016). It is hypothesized that crocetin's limited penetration through the outer membrane of Gram-negative bacteria accounts for its reduced effectiveness against them. Similarly, the unique composition of fungal cell membranes compared to bacterial ones requires specific antifungal binding to fungal membrane components for optimal penetration and efficacy (Osset-Trénor et al., 2023). Antifungals typically act by creating pores in the fungal membrane to facilitate the passage of smaller molecules or by targeting genes and enzymes essential for membrane function (Costa-de-Oliveira and Rodrigues, 2020). Crocetin might not achieve these actions at a sufficient level, explaining its diminished effectiveness against fungi.

Our study demonstrates the presence of fibrils dispersed throughout the biofilms of *S. epidermidis*, which are recognized contributors to the pathogen's biofilm-forming ability (Figure 6). In the mature biofilms of *S. epidermidis*, amyloid fibrils are formed by accumulated-associated protein (aap) and small basic protein (sbp). The A domain of the aap facilitates adhesion to unconditioned biomaterial, while sbp contributes to the integrity of both protein and polysaccharide biofilm matrices (Foster, 2020). There are reports indicating the presence of fibrils as localized tufts on *S. epidermidis* cells, which impact the cell surface hydrophobicity and, to some extent, the biofilm-forming ability, although not significantly (Banner et al., 2007). Another study involving the same strain suggests that Aap plays a role in skin colonization by

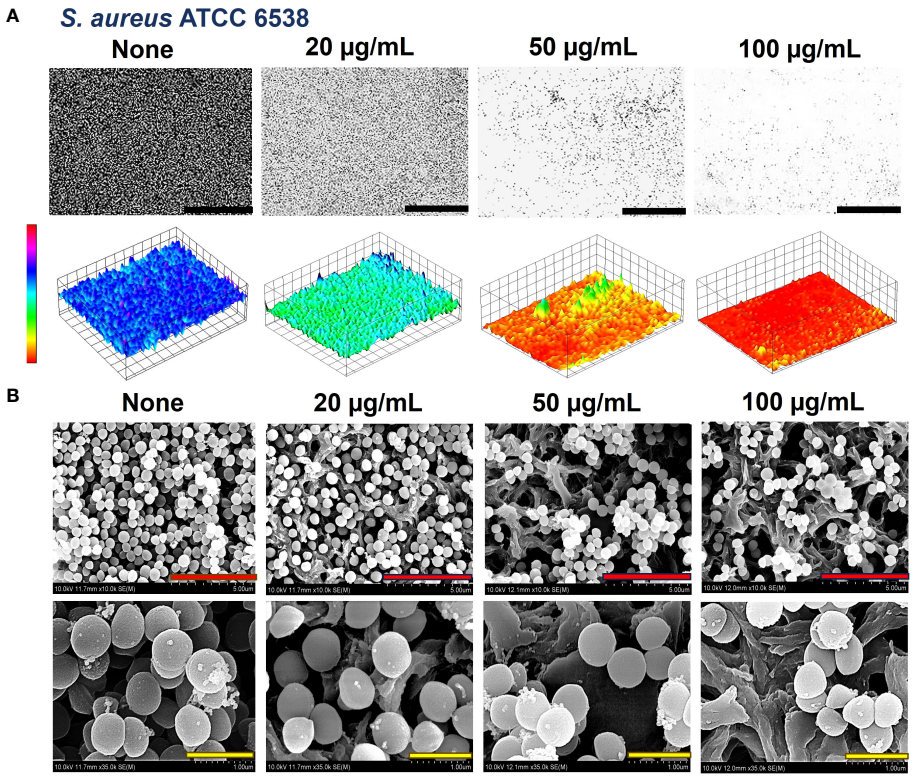

FIGURE 5
Antibiofilm effect of crocetin on *S. aureus*. Constructed color-coded 3D images of *S. aureus* ATCC 6538 in the presence of crocetin **(A)** and corresponding SEM images **(B)**. 50, 5, and 1 µm are represented by black, red, and yellow scale bars respectively.

mediating adhesion to corneocytes (Macintosh et al., 2009). A recent study indicates that Sbp has the ability to form functional amyloid fibrils, elucidating its function as a scaffolding protein in *S. epidermidis* biofilm formation (Wang et al., 2018). Interestingly, the biofilms of *S. aureus* did not display the presence of such fibrils (Figure 5). It's hypothesized that crocetin encumbers the biofilm development of the tested strains in the same manner. We suggest the elucidation of the upregulation and downregulation patterns of genes associated with biofilm formation in both *S. aureus* and *S. epidermidis*. The mounting evidence indicates that changes in gene expression during initial bacterial adherence and intercellular adhesion (biofilm formation) offer propitious avenues for novel therapeutic interventions targeting *S. aureus* and *S. epidermidis* biofilm formation, presenting potentially advantageous alternatives to existing treatments.

Carotenoids are characterized by their chemical structure, which in turn dictates their potential biological functions. They are capable of absorbing surplus energy from the other molecules owing to their polyene backbone having a distinct arrangement of single and double bonds while the particular end groups can affect their polarity (Zeb and Mehmood, 2004).

Numerous phytochemicals, including carotenoids, have been reported to demonstrate antibiofilm and antimicrobial properties (Kim et al., 2024). Astaxanthin, an algae-derived carotenoid has been reported to dwindle the biofilm growth in *S. aureus* by mitigating its adherence to the surface and in *S. epidermidis* by expressing a bactericidal effect (Weintraub et al., 2017; Haasbroek et al., 2022). Additionally, a research investigation explores the antibiofilm characteristic of zeaxanthin, which disrupts the quorum sensing (QS) systems and inhibits biofilm formation in *P. aeruginosa* (Gökalsın et al., 2017). A related investigation involving lutein on the identical strain highlights the compound's capacity to impede biofilm formation by degrading extracellular polymeric substances (EPS), which provide stability to the biofilms (Sampathkumar et al., 2019). The structural resemblances of these carotenoids to crocetin (Figure 7) suggest that the polyene backbone could play a role in influencing their antibiofilm properties.

Crocetin, categorized as a lipophilic carotenoid, contrasts with crocin, which serves as the hydrophilic diester of crocetin combined with gentiobiose (Zhao et al., 2021). While crocetin demonstrated robust antibiofilm activity against staphylococcal strains and exhibited antibacterial effects at relatively high concentrations, crocin, on the other hand, proved ineffective in displaying antibiofilm or antibacterial properties (Figures 1, 2). It's intriguing that despite sharing the polyene backbone characteristic with crocetin and other carotenoids discussed above (Figures 1B, 7), crocin was incompetent in controlling the biofilm formation and growth. This is an implication of the end groups playing an equally consequential role in controlling the antibiofilm characteristics of the carotenoids. Perhaps, the gentiobiose substitution in crocetin to form crocin denigrates its antibiofilm property. The unbound carboxylic acid groups in crocetin promote an increase in its acidity and stabilization through conjugation, unlike

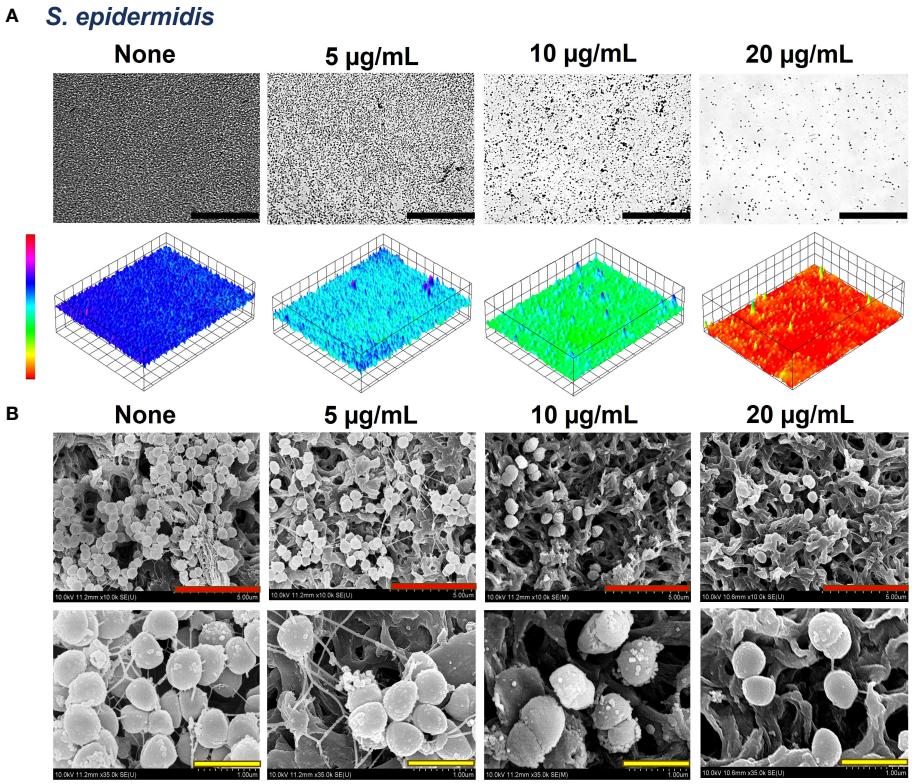

FIGURE 6
Antibiofilm effects of crocetin on *S. epidermidis*. Constructed color-coded 3D images of *S. epidermidis* in the presence of crocetin **(A)** and corresponding SEM images **(B)**. 50, 5, and 1 µm are represented by black, red, and yellow scale bars respectively. .

TABLE 1 ADME (absorption, distribution, metabolism, and excretion) profiles of crocetin and crocin.

Property	Crocetin	Crocin
Lipinski rule of five	Violated	Violated
Lead like violations	1	2
Lipinski rule of five violations	0	3
Plasma protein binding	94.835851	26.980257
Blood brain barrier permeability	1.08903	0.0274059
Skin permeability	-0.954783	-2.32731
Human intestinal absorption	96.707985	0.164266
Caco2	21.1005	12.2488
Mouse carcinogenicity	Positive	Positive
Acute fish toxicity (medaka)	0.00111522	78.6123
Acute fish toxicity (minnow)	0.00155463	96.7506
In vitro hERG inhibition	Medium risk	Ambiguous
miLogP	4.63	-1.45
Mol volume	324.80	861.10
TPSA	74.60	381.97
GPCR ligand	0.13	-3.49
Ion channel modulator	0.19	-3.67
Kinase inhibitor	-0.01	-3.66
Nuclear receptor ligand	0.68	-3.62
Protein inhibitor	-0.04	-3.18
Enzyme inhibitor	0.40	-3.48
Rat IP LD50 classification	Nontoxic in AD	Nontoxic in AD
Rat IV LD50 classification	Class 5 in AD	Nontoxic in AD
Rat oral LD50 classification	Nontoxic in AD	Class 5 out of AD
Rat SC LD50 classification	Class 5 in AD	Nontoxic in AD

(Continued)

TABLE 1 Continued

crocin, where the gentiobiose residues do not participate in conjugation (Akhtari et al., 2013). This attribute might potentially enhance the antibiofilm properties of crocetin and analogous compounds. It's been previously reported that the combination of tobramycin with myristoleic acid effectively suppresses the CFU count and inhibits biofilm formation by *S. aureus* (Park et al., 2022). Our research findings demonstrate analogous outcomes when tobramycin is

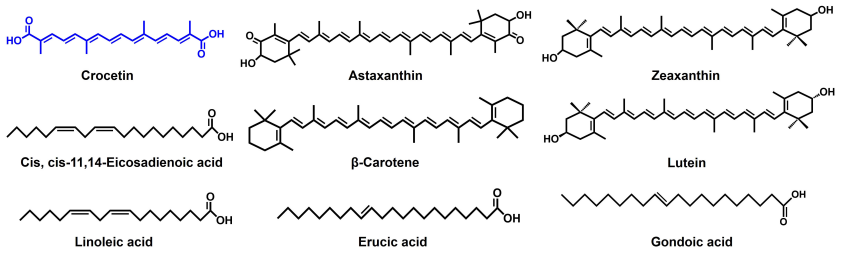

FIGURE 7
Structures of compounds reported to have antibiofilm activity.

employed concurrently with crocetin on the same strain. Fatty acids, particularly at high concentrations, exhibit antimicrobial activities by potentially altering cell membrane permeability, disrupting membranes, and causing leakage of intracellular metabolites, while another study found that the combined antibiofilm effect of lauric acid with gentamicin and streptomycin was linked to its surfactant properties, aiding in the penetration of the biofilm matrix (Desbois and Smith, 2010; Hess et al., 2014). Because crocetin shares structural similarities with fatty acids, we hypothesize that it works on *S. aureus* in a manner similar to that of fatty acids. However, the mechanism by which crocetin curtails the formation and growth of staphylococcal biofilms remains ambiguous, underscoring the necessity to comprehend its interaction with bacterial cells and the biofilm matrix. Thus, we suggest delineating the mechanism of action of crocetin on the biofilms of *S. aureus* and *S. epidermidis* which can provide a better understanding of the efficacy of the compound in question.

The oral intake of crocetin has been linked to its swift absorption into the bloodstream in the case of both mice and humans (Asai et al., 2005; Umigai et al., 2011). In mice, crocetin persists either as an intact free form or as its glucuronide conjugates, while crocin, following oral administration, hydrolyzes into crocetin either before or after intestinal absorption (Zhang et al., 2017).

The compounds under investigation demonstrated antidepressant effects in mice, with crocetin proving to be more effective than crocin (Amin et al., 2015). Following its daily oral administration, crocetin has been observed to improve physical performance in humans, particularly among men, during tests that induce fatigue (Mizuma et al., 2009). These findings suggest that orally incorporating crocetin offers multiple benefits and may also serve as a promising mode of administration for treating biofilm-associated infections caused by *S. aureus* and *S. epidermidis*. Moreover, our ADME results (Table 1) showcase that crocetin is environmentally innocuous and exhibits substantial skin permeability, attesting its potential for dermal administration in treating topical biofilm-associated infections caused by the mentioned strains.

Crocetin was identified as a potent antibiofilm agent against the tested strains and its inhibitory potential was found to be enhanced through synergistic administration with an aminoglycoside for treating staphylococcal infections. When utilized alongside a low dosage of tobramycin, it has the potential to markedly reduce both colony formation and biofilm development by *S. aureus*, rendering it a promising candidate for inclusion in treatment regimens (Figures 4A, B). While the mechanism of action remains unclear, this aspect has the potential to revolutionize the medical field, especially considering the significant challenges posed by antimicrobial resistance.

Data availability statement

The original contributions presented in the study are included in the article/Supplementary Material. Further inquiries can be directed to the corresponding author.

Author contributions

SP: Investigation, Methodology, Software, Validation, Writing – original draft, Writing – review & editing. J-HL: Conceptualization, Funding acquisition, Methodology, Project administration, Resources, Supervision, Validation, Writing – original draft, Writing – review & editing. JL: Conceptualization, Funding acquisition, Project administration, Writing – original draft, Writing – review & editing.

Funding

The author(s) declare financial support was received for the research, authorship, and/or publication of this article. This research was supported by the Basic Science Research Program of the National Research Foundation of Korea (NRF) funded by the Ministry of Education (2021R1I1A3A04037486 to J-HL) and by grants from the NRF funded by the Korean government (MSIT) (2021R1A2C1008368 to JL).

Conflict of interest

The authors declare that the research was conducted in the absence of any commercial or financial relationships that could be construed as a potential conflict of interest.

Publisher's note

All claims expressed in this article are solely those of the authors and do not necessarily represent those of their affiliated

organizations, or those of the publisher, the editors and the reviewers. Any product that may be evaluated in this article, or claim that may be made by its manufacturer, is not guaranteed or endorsed by the publisher.

Supplementary material

The Supplementary Material for this article can be found online at: https://www.frontiersin.org/articles/10.3389/fcimb.2024.1404960/full#supplementary-material

References

Ahmed, B., Jailani, A., Lee, J.-H., and Lee, J. (2022). Inhibition of growth, biofilm formation, virulence, and surface attachment of *Agrobacterium tumefaciens* by cinnamaldehyde derivatives. *Front. Microbiol.* 13. doi: 10.3389/fmicb.2022.1001865

Akhtari, K., Hassanzadeh, K., Fakhraei, B., Fakhraei, N., Hassanzadeh, H., and Zarei, S. A. (2013). A density functional theory study of the reactivity descriptors and antioxidant behavior of crocin. *Comput. Theor. Chem.* 1013, 123–129. doi: 10.1016/j.comptc.2013.03.015

Amin, B., Nakhsaz, A., and Hosseinzadeh, H. (2015). Evaluation of the antidepressant-like effects of acute and sub-acute administration of crocin and crocetin in mice. *Avicenna J. Phytomed.* 5, 458.

Archer, N. K., Mazaitis, M. J., Costerton, J. W., Leid, J. G., Powers, M. E., and Shirtliff, M. E. (2011). *Staphylococcus aureus* biofilms: properties, regulation, and roles in human disease. *Virulence* 2, 445–459. doi: 10.4161/viru.2.5.17724

Argemi, X., Hansmann, Y., Prola, K., and Prévost, G. (2019). Coagulase-negative staphylococci pathogenomics. *Int. J. Mol. Sci.* 20, 1215. doi: 10.3390/ijms20051215

Asai, A., Nakano, T., Takahashi, M., and Nagao, A. (2005). Orally administered crocetin and crocins are absorbed into blood plasma as crocetin and its glucuronide conjugates in mice. *J. Agric. Food Chem.* 53, 7302–7306. doi: 10.1021/jf0509355

Bann, S. J., Ballantine, R. D., and Cochrane, S. A. (2021). The tridecaptins: non-ribosomal peptides that selectively target Gram-negative bacteria. *RSC Med. Chem.* 12, 538–551. doi: 10.1039/D0MD00413H

Banner, M. A., Cunniffe, J. G., Macintosh, R. L., Foster, T. J., Rohde, H., Mack, D., et al. (2007). Localized tufts of fibrils on *Staphylococcus epidermidis* NCTC 11047 are comprised of the accumulation-associated protein. *J. Bacteriol.* 189, 2793–2804. doi: 10.1128/JB.00952-06

Bazargani, M. M., and Rohloff, J. (2016). Antibiofilm activity of essential oils and plant extracts against *Staphylococcus aureus* and *Escherichia coli* biofilms. *Food control* 61, 156–164. doi: 10.1016/j.foodcont.2015.09.036

Breijyeh, Z., Jubeh, B., and Karaman, R. (2020). Resistance of gram-negative bacteria to current antibacterial agents and approaches to resolve it. *Mol.* 25, 1340. doi: 10.3390/molecules25061340

Butnariu, M., Quispe, C., Herrera-Bravo, J., Sharifi-Rad, J., Singh, L., Aborehab, N. M., et al. (2022). The pharmacological activities of *Crocus sativus* L.: a review based on the mechanisms and therapeutic opportunities of its phytoconstituents. *Oxid. Med. Cell. Longev.* 2022, 1–29. doi: 10.1155/2022/8214821

Carradori, S., Chimenti, P., Fazzari, M., Granese, A., and Angiolella, L. (2016). Antimicrobial activity, synergism and inhibition of germ tube formation by *Crocus sativus*-derived compounds against *Candida* spp. *J. Enzyme Inhib. Med. Chem.* 31, 189–193. doi: 10.1080/14756366.2016.1180596

Colapietro, A., Mancini, A., D'Alessandro, A. M., and Festuccia, C. (2019). Crocetin and crocin from saffron in cancer chemotherapy and chemoprevention. *Anti-Cancer Agents Med. Chem.* 19, 38–47. doi: 10.2174/1871520619666181231112453

Costa-de-Oliveira, S., and Rodrigues, A. G. (2020). *Candida albicans* antifungal resistance and tolerance in bloodstream infections: The triad yeast-host-antifungal. *Microorganisms* 8, 154. doi: 10.3390/microorganisms8020154

Desbois, A. P., and Smith, V. J. (2010). Antibacterial free fatty acids: activities, mechanisms of action and biotechnological potential. *Appl. Microbiol. Biotechnol.* 85, 1629–1642. doi: 10.1007/s00253-009-2355-3

Faleye, O. S., Lee, J.-H., and Lee, J. (2023). Selected flavonoids exhibit antibiofilm and antibacterial effects against *Vibrio* by disrupting membrane integrity, virulence and metabolic activities. *Biofilm* 6, 100165. doi: 10.1016/j.bioflm.2023.100165

Foster, T. J. (2020). Surface proteins of *Staphylococcus epidermidis*. *Front. Microbiol.* 11. doi: 10.3389/fmicb.2020.01829

Gebreyohannes, G., Nyerere, A., Bii, C., and Sbhatu, D. B. (2019). Challenges of intervention, treatment, and antibiotic resistance of biofilm-forming microorganisms. *Heliyon* 5, 1–7. doi: 10.1016/j.heliyon.2019.e02192

Gökalsın, B., Aksoydan, B., Erman, B., and Sesal, N. C. (2017). Reducing virulence and biofilm of *Pseudomonas aeruginosa* by potential quorum sensing inhibitor carotenoid: zeaxanthin. *Microb. Ecol.* 74, 466–473. doi: 10.1007/s00248-017-0949-3

Guo, Y., Song, G., Sun, M., Wang, J., and Wang, Y. (2020). Prevalence and therapies of antibiotic-resistance in *Staphylococcus aureus*. *Front. Cell. Infect. Microbiol.* 10. doi: 10.3389/fcimb.2020.00107

Gupta, S. K. (2019). A review on therapeutic potentials of crocetin-A carotenoid derived from saffron. *Curr. Res. Pharm. Sci.* 9 (4), 54–62. doi: 10.24092/CRPS.2019.090401

Haasbroek, K., Yagi, M., and Yonei, Y. (2022). *Staphylococcus aureus* biofilm inhibiting activity of advanced glycation endproduct crosslink breaking and glycation inhibiting compounds. *Antibiotics* 11, 1412. doi: 10.3390/antibiotics11101412

Hess, D. J., Henry-Stanley, M. J., and Wells, C. L. (2014). Antibacterial synergy of glycerol monolaurate and aminoglycosides in *Staphylococcus aureus* biofilms. *Antimicrob. Agents Chemother.* 58, 6970–6973. doi: 10.1128/AAC.03672-14

Jeon, H., Boya, B. R., Gyuwon, K., Lee, J.-H., and Lee, J. (2024). Inhibitory effects of bromoindoles on *Escherichia coli* O157:H7 biofilms. *Biotechnol. Bioprocess Eng.* 1–10. doi: 10.1007/s12257-024-00097-3

Khan, F., Pham, D. T. N., Oloketuyi, S. F., Manivasagan, P., Oh, J., and Kim, Y.-M. (2020). Chitosan and their derivatives: Antibiofilm drugs against pathogenic bacteria. *Colloids Surf. B: Biointerfaces* 185, 110627. doi: 10.1016/j.colsurfb.2019.110627

Kim, Y.-G., Lee, J.-H., Kim, S.-H., Park, S.-Y., Kim, Y.-J., Ryu, C.-M., et al. (2024). Inhibition of biofilm Formation in *Cutibacterium acnes*, *Staphylococcus aureus*, and *Candida albicans* by the phytopigment shikonin. *Int. J. Mol. Sci.* 25, 2426. doi: 10.3390/ijms25042426

Kim, S. H., Lee, J. M., Kim, S. C., Park, C. B., and Lee, P. C. (2014). Proposed cytotoxic mechanisms of the saffron carotenoids crocin and crocetin on cancer cell lines. *Biochem. Cell Biol.* 92, 105–111. doi: 10.1139/bcb-2013-0091

Kim, S., Lee, J.-H., Kim, Y.-G., Tan, Y., and Lee, J. (2022). Hydroquinones inhibit biofilm formation and virulence factor production in *Staphylococcus aureus*. *Int. J. Mol. Sci.* 23, 10683. doi: 10.3390/ijms231810683

Kim, Y.-G., Lee, J.-H., Raorane, C. J., Oh, S. T., Park, J. G., and Lee, J. (2018). Herring oil and omega fatty acids inhibit Staphylococcus aureus biofilm formation and virulence. *Front. Microbiol.* 9. doi: 10.3389/fmicb.2018.01241

Kleinschmidt, S., Huygens, F., Faoagali, J., Rathnayake, I. U., and Hafner, L. M. (2015). *Staphylococcus epidermidis* as a cause of bacteremia. *Future Microbiol.* 10, 1859–1879. doi: 10.2217/fmb.15.98

Kumar, P., Lee, J.-H., Beyenal, H., and Lee, J. (2020). Fatty acids as antibiofilm and antivirulence agents. *Trends Microbiol.* 28, 753–768. doi: 10.1016/j.tim.2020.03.014

Lee, J.-H., Kim, Y.-G., Lee, K., Kim, C.-J., Park, D.-J., Ju, Y., et al. (2016). Streptomyces-derived actinomycin D inhibits biofilm formation by *Staphylococcus aureus* and its hemolytic activity. *Biofouling* 32, 45–56. doi: 10.1080/08927014.2015.1125888

Macintosh, R. L., Brittan, J. L., Bhattacharya, R., Jenkinson, H. F., Derrick, J., Upton, M., et al. (2009). The terminal A domain of the fibrillar accumulation-associated protein (Aap) of *Staphylococcus epidermidis* mediates adhesion to human corneocytes. *J. Bacteriol.* 191, 7007–7016. doi: 10.1128/JB.00764-09

Michels, R., Last, K., Becker, S. L., and Papan, C. (2021). Update on coagulase-negative staphylococci—what the clinician should know. *Microorganisms* 9, 830. doi: 10.3390/microorganisms9040830

Miller, S. I. (2016). Antibiotic resistance and regulation of the gram-negative bacterial outer membrane barrier by host innate immune molecules. *MBio* 7, 10–1128. doi: 10.1128/mBio.01541-16

Mizuma, H., Tanaka, M., Nozaki, S., Mizuno, K., Tahara, T., Ataka, S., et al. (2009). Daily oral administration of crocetin attenuates physical fatigue in human subjects. *Nutr. Res.* 29, 145–150. doi: 10.1016/j.nutres.2009.02.003

Mohd Hatta, F. A., Othman, R., Ali, Q. A., Hassan, N., and Ramya, R. (2023). Carotenoids composition, antioxidant and antimicrobial capacities of *Crocus sativus* L. stigma. *Food Res.* 7, 337–343. doi: 10.26656/fr.2017.7(4).390

Moormeier, D. E., and Bayles, K. W. (2017). *Staphylococcus aureus* biofilm: a complex developmental organism. *Mol. Microbiol.* 104, 365–376. doi: 10.1111/mmi.13634

Nandhini, P., Kumar, P., Mickymaray, S., Alothaim, A. S., Somasundaram, J., and Rajan, M. (2022). Recent developments in methicillin-resistant *Staphylococcus aureus* (MRSA) treatment: A review. *Antibiotics* 11, 606. doi: 10.3390/antibiotics11050606

Osset-Trénor, P., Pascual-Ahuir, A., and Proft, M. (2023). Fungal drug response and antimicrobial resistance. *J. Fungi* 9, 565. doi: 10.3390/jof9050565

Park, S., Lee, J.-H., Kim, Y.-G., Hu, L., and Lee, J. (2022). Fatty acids as aminoglycoside antibiotic adjuvants against *Staphylococcus aureus*. *Front. Microbiol.* 13. doi: 10.3389/fmicb.2022.876932

Park, I., Lee, J.-H., Ma, J. Y., Tan, Y., and Lee, J. (2023). Antivirulence activities of retinoic acids against *Staphylococcus aureus*. *Front. Microbiol.* 14. doi: 10.3389/fmicb.2023.1224085

Razak, S. I. A., Anwar Hamzah, M. S., Yee, F. C., Kadir, M. R. A., and Nayan, N. H. M. (2017). A review on medicinal properties of saffron toward major diseases. *J. Herbs Spices Med. Plants.* 23, 98–116. doi: 10.1080/10496475.2016.1272522

Rubini, D., Hari, B. N. V., and Nithyanand, P. (2021). Chitosan coated catheters alleviates mixed species biofilms of *Staphylococcus epidermidis* and *Candida albicans*. *Carbohydr. Polym.* 252, 117192. doi: 10.1016/j.carbpol.2020.117192

Sampathkumar, S. J., Srivastava, P., Ramachandran, S., Sivashanmugam, K., and Gothandam, K. M. (2019). Lutein: A potential antibiofilm and antiquorum sensing molecule from green microalga *Chlorella pyrenoidosa*. *Microb. Pathog.* 135, 103658. doi: 10.1016/j.micpath.2019.103658

Sathiyamoorthi, E., Lee, J.-H., and Lee, J. (2024). Antibacterial and antibiofilm activity of halogenated phenylboronic acids against *Vibrio parahaemolyticus* and *Vibrio harveyi*. *Front. Cell. Infect. Microbiol.* 14, 1340910. doi: 10.3389/fcimb.2024.1340910

Tong, S. Y. C., Davis, J. S., Eichenberger, E., Holland, T. L., and Fowler, J. V. G. (2015). Staphylococcus aureus infections: epidemiology, pathophysiology, clinical manifestations, and management. *Clin. Microbiol. Rev.* 28, 603–661. doi: 10.1128/CMR.00134-14

Tyner, H., and Patel, R. (2016). *Propionibacterium acnes* biofilm–A sanctuary for *Staphylococcus aureus*? *Anaerobe* 40, 63–67. doi: 10.1016/j.anaerobe.2016.05.014

Umigai, N., Murakami, K., Ulit, M. V., Antonio, L. S., Shirotori, M., Morikawa, H., et al. (2011). The pharmacokinetic profile of crocetin in healthy adult human volunteers after a single oral administration. *Phytomedicine* 18, 575–578. doi: 10.1016/j.phymed.2010.10.019

Valliammai, A., Selvaraj, A., Yuvashree, U., Aravindraja, C., and Karutha Pandian, S. (2020). sarA-dependent antibiofilm activity of thymol enhances the antibacterial efficacy of rifampicin against *Staphylococcus aureus*. *Front. Microbiol.* 11. doi: 10.3389/fmicb.2020.01744

Wang, Y., Jiang, J., Gao, Y., Sun, Y., Dai, J., Wu, Y., et al. (2018). *Staphylococcus epidermidis* small basic protein (Sbp) forms amyloid fibrils, consistent with its function as a scaffolding protein in biofilms. *J. Biol. Chem.* 293, 14296–14311. doi: 10.1074/jbc.RA118.002448

Weintraub, S., Shpigel, T., Harris, L. G., Schuster, R., Lewis, E. C., and Lewitus, D. Y. (2017). Astaxanthin-based polymers as new antimicrobial compounds. *Polym. Chem.* 8, 4182–4189. doi: 10.1039/C7PY00663B

Zeb, A., and Mehmood, S. (2004). Carotenoids contents from various sources and their potential health applications. *Pak. J. Nutr.* 3, 199–204. doi: 10.3923/pjn.2004.199.204

Zhang, Y., Fei, F., Zhen, L., Zhu, X., Wang, J., Li, S., et al. (2017). Sensitive analysis and simultaneous assessment of pharmacokinetic properties of crocin and crocetin after oral administration in rats. *J. Chromatogr. B* 1044, 1–7. doi: 10.1016/j.jchromb.2016.12.003

Zhao, C., Kam, H.-T., Chen, Y., Gong, G., Hoi, M. P.-M., Skalicka-Woźniak, K., et al. (2021). Crocetin and its glycoside crocin, two bioactive constituents from *Crocus sativus* L.(saffron), differentially inhibit angiogenesis by inhibiting endothelial cytoskeleton organization and cell migration through VEGFR2/SRC/FAK and VEGFR2/MEK/ERK signaling pathways. *Front. Pharmacol.* 12. doi: 10.3389/fphar.2021.675359

frontiers | Frontiers in Cellular and Infection Microbiology

TYPE Original Research
PUBLISHED 31 July 2024
DOI 10.3389/fcimb.2024.1395577

OPEN ACCESS

EDITED BY
Maria Gabriela Paraje,
National University of Cordoba, Argentina

REVIEWED BY
Antonella Migliaccio,
University of Naples Federico II, Italy
Mariana Claudia Allievi,
University of Buenos Aires, Argentina
Natalia Guiñazu,
National University of Comahue, Argentina

*CORRESPONDENCE
Aleksandra Polichtaleksandra.policht@uj.edu.pl

RECEIVED 04 March 2024
ACCEPTED 11 July 2024
PUBLISHED 31 July 2024

CITATION
Kozień Ł, Polichtal A, Heczko P, Arent Z, Bracha U, Pardyak L, Pietsch-Fulbiszewska A, Gallienne E, Piwowar P, Okoń K, Tomusiak-Plebanek A and Strus M (2024) PDIA iminosugar influence on subcutaneous *Staphylococcus aureus* and *Pseudomonas aeruginosa* infections in mice. *Front. Cell. Infect. Microbiol.* 14:1395577. doi: 10.3389/fcimb.2024.1395577

PDIA iminosugar influence on subcutaneous *Staphylococcus aureus* and *Pseudomonas aeruginosa* infections in mice

Łucja Kozień[1], Aleksandra Polichtal*, Piotr Heczko[1], Zbigniew Arent[2], Urszula Bracha[2], Laura Pardyak[2], Agnieszka Pietsch-Fulbiszewska[2], Estelle Gallienne[3], Piotr Piwowar[4], Krzysztof Okoń[1], Anna Tomusiak-Plebanek[5] and Magdalena Strus[1]

[1]Department of Bacteriology, Ecology of Microbes and Parasitology, Faculty of Medicine, Jagiellonian University Medical College, Krakow, Poland, [2]Center of Experimental and Innovative Medicine, University Centre of Veterinary Medicine JU-UA, University of Agriculture in Krakow, Krakow, Poland, [3]Institut de Chimie Organique et Analytique (ICOA), UMR 7311, Université d'Orléans & CNRS, Orléans, France, [4]Faculty of Electrical Engineering, Automatics, Computer Science and Biomedical Engineering, AGH University of Science and Technology, Kraków, Poland, [5]Department of Bacteriology, Ecology of Microbes and Parasitology, Faculty of Medicine, Jagiellonian University Medical College, Kraków, Poland

Introduction: Biofilm-associated infections persist as a therapeutic challenge in contemporary medicine. The efficacy of antibiotic therapies is ineffective in numerous instances, necessitating a heightened focus on exploring novel anti-biofilm medical strategies. Among these, iminosugars emerge as a distinctive class of compounds displaying promising biofilm inhibition properties.

Methods: This study employs an *in vivo* wound infection mouse model to evaluate the effectiveness of PDIA in treating biofilm-associated skin wound infections caused by *Staphylococcus aureus* and *Pseudomonas aeruginosa*. Dermic wounds in mice were infected with biofilm-forming strains, specifically *S. aureus* 48 and *P. aeruginosa* 5, which were isolated from patients with diabetic foot, and are well-known for their strong biofilm formation. The subsequent analysis included clinical, microbiological, and histopathological parameters. Furthermore, an exploration into the susceptibility of the infectious strains to hydrogen peroxide was conducted, acknowledging its potential presence during induced inflammation in mouse dermal wounds within an *in vivo* model.

Results: The findings revealed the efficacy of PDIA iminosugar against the *S. aureus* strain, evidenced by a reduction in bacterial numbers within the wound and the inflammatory focus.

Discussion: This study suggests that PDIA iminosugar emerges as an active and potentially effective antibiofilm agent, positioning it as a viable treatment option for staphylococcal infections.

KEYWORDS

antibiofilm drug, wound infection, *Staphylococcus* infection, *Pseudomonas* infection, PDIA iminosugar

1 Introduction

Due to its multifaceted resistance to multiple drugs, biofilm formation presents a considerable and persistent threat in human bacterial and mycotic infections, contributing to chronic infections that are challenging to treat. Therefore, research on novel strategies to prevent and/or treat pathogen biofilm formation is one of the most expanding fields in experimental medicine. Among the most challenging objectives, developing a viable technique that selectively targets adhesive properties without compromising bacterial viability is imperative (Srinivasan et al., 2021). Furthermore, bacteria and yeasts produce biofilms on different indwelling medical devices such as implants, vascular grafts, heart valves, intrauterine devices, pacemakers, prosthetic joints, catheters, sutures, and contact lenses (Kannappan et al., 2017).

Staphylococcus aureus and *Pseudomonas aeruginosa* are among the most prevalently defined etiological agents causing a range of severe nosocomial, chronic, antibiotic-resistant, and biofilm-associated infections (Mulcahy et al., 2014; Cheung et al., 2021). They exhibit diverse virulence factors encompassing the synthesis of pathogenic toxins (both proteinaceous and non-proteinaceous molecules) along with genetic determinants facilitating their adept colonization and sustained persistence within a host organism (Tolker-Nielsen, 2014; Graf et al., 2019). Among countless defensive strategies various bacteria employ to counter unfavorable external conditions, forming a biofilm stands out as a particularly efficacious protective mechanism (Dos Santos et al., 2018). The strain-dependent nature of the bacteria in question significantly influences the multiplicity of virulent factors and pathogenicity. For instance, amidst tissue inflammation, phagocytic cells of the immune system, including neutrophils, undergo a respiratory burst upon encountering antigens from infectious microorganisms. This event culminates in the release of reactive bactericidal products stemming from aerobic metabolism, such as singlet oxygen (1O2) or hydrogen peroxide (H_2O_2) (Clark, 1999). Certain bacteria, such as *P. aeruginosa* and *S. aureus*, can mitigate the harmful impacts of H_2O_2 generated by host cells. In addition to biofilm formation, bacteria employ a mechanism to shield themselves from oxidative stress by producing a diverse array of enzymes, including catalase, superoxide dismutase (SOD), and reductases. However, this capability is strain-dependent (Allaoui et al., 2009). Consequently, strains capable of biofilm production yet failing to initiate its formation prior to the onset of host inflammation may encounter challenges in survival and may be hindered in their ability to instigate a severe infection.

Amidst the manifold therapeutic strategies recently documented for biofilm inhibition encompassing diverse mechanisms and categorized into various classes as outlined by (Srinivasan et al., 2021), only the dissolution of exopolysaccharide (EPS) structures within the biofilm is explicitly highlighted. Notably, a specific class of iminosugars can inhibit biofilm synthesis, potentially through interaction with the glucosyltransferase enzyme involved in EPS synthesis (Ren et al., 2016). The prototype of this group was already described in 2008 by Islam as an anti-adherence activity of mulberry leaves. The active substance appeared to be 1-deoxynojirimycin, which inhibited EPS production by *Streptococcus mutans* (Islam et al., 2008). Our group described several synthetic iminosugar derivatives actively inhibiting early biofilm formation by *P. aeruginosa* but not influencing bacterial reproduction (Strus et al., 2016). More recently, except for its anti-biofilm activity, N-nonyloxypentyl-L-DNJ iminosugar enantiomer was reported to be a molecule displaying high antibacterial properties against *S. aureus* (De Gregorio et al., 2020). Last year, we published a paper on beta-1-C-propyl-1,4-dideoxy-1,4-imino-L-arabinitol (PDIA iminosugar) which inhibited early biofilm production of *Enterobacter* spp., *P. aeruginosa*, *Enterococcus* spp. and *S. aureus* at 8 and 24 h, and *Klebsiella* spp., *Acinetobacter* spp. and *S. epidermidis* in 24 h. In addition, we found that the same iminosugar inhibited mature biofilm formation of *P. aeruginosa* in 32 h and of *Acinetobacter* spp., *S. aureus*, and *S. epidermidis* at 48 h. PDIA at a concentration of 0.9 mM caused no growth inhibition of the tested bacteria (Kozień et al., 2022).

The current investigation sought to assess the *in vivo* effectiveness of PDIA in an animal model simulating experimental subcutaneous wound infection induced by *S. aureus* and *P. aeruginosa*. Additionally, endeavors were made to observe distinct trajectories of local inflammatory processes provoked by *S. aureus* and *P. aeruginosa* within tissues during experimental skin infections. Moreover, the infectious strains' susceptibility to H_2O_2 was assessed to outline potential environmental factors encountered in the *in vivo* investigation.

2 Materials and methods

2.1 Bacterial strains and growth conditions

Two bacterial strains (*S. aureus* 48 and *P. aeruginosa* 5) were deliberately chosen based on their demonstrated high biofilm-forming proficiency and the biofilm susceptibility to the inhibitory properties of PDIA iminosugar (Kozień et al., 2022). Both strains are integral components of the bacterial strains' repository at the Department of Microbiology, Jagiellonian University Medical College, originating from patients afflicted with diabetic foot infections (*P. aeruginosa* 5) and chronic otitis media (*S. aureus* 48). The taxonomic identities of these strains were verified through mass spectrometry (MALDI-TOF MS Biotyper, Bruker Scientific LLC, Billerica, MA, USA) following the manufacturer's guidelines.

To initiate bacterial cultures, an inoculum was generated by subjecting glass beads coated with bacteria from cryogenically preserved pure cultures to incubation in 10 mL of Tryptic Soy Broth (TSB) (Beckton Dickinson, Franklin Lakes, NJ, USA) at 37°C for 24 hours. Subsequently, to ensure strain purity, 10 µL aliquots of the cultures were streaked onto Columbia Agar (Biomaxima, Poland) and incubated similarly. This process was iterated three times to attain bacterial populations of heightened viability.

For further experimentation, a single colony from 24-hour pure culture plates was introduced into 10 mL of TSB broth using a sterile loop, thoroughly mixed, and incubated at 37°C for 24 h. Post-incubation, a serial dilution methodology in TSB broth generated a bacterial suspension of a 1.0 x 10^5 colony-forming units of bacteria

per milliliter (CFU/mL) density (Sutton, 2011). These meticulously prepared suspensions of 1.0 x 10^5 CFU/mL density were utilized in subsequent stages of the experimental protocol.

2.2 Iminosugar

The iminosugar derivative under investigation (PDIA, beta-1-C-propyl-1,4-dideoxy-1,4-imino-L-arabinitol) was synthesized at the Institute of Organic and Analytical Chemistry, University of Orleans and CNRS, France. Our preceding study presented its chemical structure (Kozień et al., 2022). In the experiments, a solution of iminosugar at a concentration of 1 mM was employed. This concentration was chosen based on previous *in vitro* experiments, described by Kozień et al. (2022), in which 0.9 mM concentration appeared to be effective. Thus, the dose of 1 mM was used locally *in vivo*. To obtain this concentration, PDIA was dissolved in DMSO (Sigma Aldrich, USA) to a concentration of 100 mM. Next, to reduce the DMSO toxicity, it was diluted in sterile water reaching the final concentration of 1mM PDIA in 1% DMSO.

2.3 Animals

All experiments with animals were performed following the Guide for the Care and Use of Laboratory Animals published by the US National Institutes of Health and have received approval under resolution 6/2022 from the Second Local Institutional Animal Care and Use Committee (IACUC) in Kraków.

Six groups of male and female BALB/C mice (Animal Facility of Clinical Immunology and Transplantation Department of the Pediatrics Institute in the Jagiellonian University Medical College) aged 6-10 weeks were employed. Mice were divided into following groups: procedure control (9 mice); iminosugar control (8 mice); *S. aureus* 48 (SA 48) infection (10 mice); SA 48 infection with iminosugar (8 mice); *P. aeruginosa* 5 (PAR 5) infection (8 mice) and PAR 5 infection with iminosugar (8 mice).

2.4 Experimental wound infection

The model of subcutaneous infection was modified as previously described (Liu et al., 2019). Following the induction of general anesthesia via an intraperitoneal administration of a combined dose of ketamine (Vetaketam, VET-ARGO, Poland) and xylazine (Vetaxyl, VET-ARGO, Poland) at 50 mg/kg (ketamine) and 5 mg/kg (xylazine), a 10-millimeter incision was meticulously made on the dorsal region of each mouse subject. Subsequently, the skin was delicately dissected to create a subcutaneous pouch. The resultant wounds were then deliberately subjected to infection with designated bacterial strains or left uninfected, serving as the control groups.

Distinct bacterial strains were employed for the infected cohorts. In the instances of the infected groups, a 50 µl suspension of the selected bacterial strains (boasting a density of 1 x 10^5 CFU/mL) was meticulously introduced into the formed subcutaneous pouch. To gauge the *in vivo* efficacy of the PDIA iminosugar being tested on the two infection groups (each with distinct strains), a 500 µl solution of 1 mM iminosugar was systematically injected into the subcutaneous pouch containing the bacterial suspension. The control group of animals received the same volume of sterile saline. Subcutaneous meloxicam (Melovem, Dopharma B.V., The Netherlands) was administered as an analgesic at 5 mg/kg.

The groups were arranged and divided, as shown in Table 1.

After bacterial inoculation and iminosugar injection, each wound was carefully sutured, and the animals were maintained for three additional days under conditions consistent with those during the adaptation period. Throughout this interval, comprehensive clinical assessments were conducted, including meticulous evaluations of wound healing and the systematic monitoring of edema, redness, and exudate appearance, strictly adhering to the procedures delineated in section 2.5. Following a three-day interval, euthanasia of the mice was carried out through the dislodgement of the cervical vertebrae after anesthesia induction via isoflurane (Isotek, Laboratorios Karizoo S.A., Spain) administered at a dosage of 1000 mg/g (Marquardt et al., 2018). Subsequently, a necropsy was conducted, during which tissues and organs were harvested for microbiological and histopathological examinations.

2.5 Clinical evaluation scale

The assessment of wound healing throughout the 3-day experimental period involved the application of a clinical evaluation scale. The surgical wound was appraised through a modified version of the NERDS and STONEES scales, initially designed for evaluating wound infections in human subjects (Woo and Sibbald, 2009). Particular attention was directed towards four discernible parameters — healing, exudate, edema, and redness —

TABLE 1 Experimental groups.

Group name	Number of mice in the group (n)	Infectious strain	Procedure
Control	9	–	subcutaneous incision
Control + I	8	–	subcutaneous incision + PDIA iminosugar
SA48	10	*S. aureus* 48	subcutaneous incision + *S. aureus*
SA48 + I	8	*S. aureus* 48	subcutaneous incision + *S. aureus* + PDIA iminosugar
PAR5	8	*P. aeruginosa* 5	subcutaneous incision + *P. aeruginosa*
PAR5 + I	8	*P. aeruginosa* 5	subcutaneous incision + *P. aeruginosa* + PDIA iminosugar

Control: procedure control (subcutaneous incision alone), Control + I: iminosugar control (subcutaneous incision with insertion of PDIA iminosugar), SA 48: control of S. aureus infection (subcutaneous incision with insertion of S. aureus strain 48), SA48 + I: S. aureus infection with iminosugar (subcutaneous incision with insertion of S. aureus strain 48 and PDIA iminosugar), PAR5: control of P. aeruginosa infection (subcutaneous incision with insertion of P. aeruginosa strain 5) and PAR 5 + I: P. aeruginosa infection with iminosugar (subcutaneous incision with insertion of P. aeruginosa strain 5 and PDIA iminosugar).

each exhibiting varying degrees of intensity. The observations were systematically categorized utilizing the ensuing scale:

- **Healing:** 0 - indicative of normal healing, 1 - indicative of wound dehiscence
- **Exudate:** 0 - representing a dry wound, 1 - signifying a moist wound with slight exudate, 2 - indicative of a moist wound with abundant exudate
- **Edema:** 0 - suggesting an absence of edema, 1 - denoting a significant level of edema, 2 - representing a substantial presence of edema
- **Redness:** 0 - indicative of the absence of redness, 1 - denoting the presence of redness

2.6 Microbiological analysis

On day three, the specimens obtained from each mouse during the post-surgery necropsy comprised wound swabs, intracardial blood samples (ranging in volumes from 300 to 1000 µl), and spleens. After collection, the wound swabs, blood samples, and spleens were immersed in 5, 0.5, and 1.5 milliliters of TSB broth. The spleens underwent homogenization using a sterile mortar. Following meticulous mixing, NaCl-based decimal serial dilutions were prepared, and the samples were quantitatively inoculated onto the respective agar media: Columbia Agar (BioMaxima, Poland), MacConkey Agar (BioMaxima, Poland), and Sabouraud Dextrose Agar (BioMaxima, Poland). The inoculated agar plates were then incubated at **37°C** for **24** h (Lagier et al., 2015).

2.6.1 Isolation of *S. aureus* 48 and *P. aeruginosa* 5 strains from mouse specimens based on drug resistance profiles

During microbiological testing, our paramount objective was to detect *S. aureus* 48 and *P. aeruginosa* 5 strains within the infection groups' wounds. To attain this goal, we executed a comparative scrutiny of the drug susceptibility profiles characterizing the subjected strains. Colonies of *Staphylococcus* spp. were cultured on Columbia medium, while those of *Pseudomonas* spp. were cultivated on MacConkey medium. Subsequently, colonies were sub-cultured onto agar plate sectors and incubated at 37°C for 24 h. Following incubation, a 0.5 McFarland saline suspension was crafted from each sector and introduced into Mueller-Hinton II Broth (Biomaxima, Poland) via a sterile swab. Antibiotic discs (OXOID, UK), precisely detailed in Tables 2, 3, were affixed to the surfaces of the pre-inoculated plates of Mueller-Hinton II Agar (Biomaxima, Poland) and subjected again to a 24 h incubation period at 37°C. After incubation periods, the measured growth inhibition zones (in millimeters) facilitated the derivation of drug resistance patterns. Establishing the identity of isolates from wounds necessitated a thorough juxtaposition of the acquired drug resistance profiles with the reference test strains, as delineated in Tables 2, 3. This methodical comparative analysis facilitated the accurate discernment of the isolates correlated with the specified test strains and has already been used in our other study (Tomusiak-Plebanek et al., 2018).

TABLE 2 Drug resistance patterns of *S. aureus* 48 strain.

Strain tested	The size of the inhibition zone [mm] for individual antibiotics				
	FOX (30µg)	DA (2 µg)	E (15 µg)	CN (10 µg)	SXT (25 µg)
S. aureus 48	R	R	R	21	30

R, Resistance; FOX, Cefoxitin; DA, Clindamycin; E, Erythromycin; CN, Gentamycin; SXT, Sulfamethoxazole/Trimethoprim.

2.7 Histological analysis

Tissue sections encompassing the epidermis, dermis, and panniculus carnosus muscle were procured from each mouse subject for subsequent histopathological scrutiny. These tissue samples were placed in tubes containing 10% formalin (Chempur, Poland). Post-fixation, the skin tissues underwent processing in a state-of-the-art tissue processor (Thermo Shandon Limited EXCELSIOR AS, UK) and were embedded in paraffin (Thermo Shandon Limited HISTOSTAR, UK). The resultant paraffin blocks were precision-cut into 3-µm sections using a microtome (LEICA Histocore AUTOCUT, Germany) and stained with hematoxylin and eosin (SAKURA PRISMA E2S, Netherlands), followed by cover-slipping with a film (SAKURA FILM COVERSLIPPER, Netherlands). Histologic evaluation was undertaken by a certified histopathologist utilizing an Olympus BX53 microscope, with observations made under magnifications of up to 400 x. The structural attributes of the specimens were methodically described, encompassing considerations of tissue composition, inflammatory intensity, the constitution of inflammatory infiltrate, the presence of granulation tissue, and any indications of ulceration. The quantification of neutrophilic infiltrate, chronic inflammatory cells, and granulation tissue was categorized on a scale of 0 to 3 (Klopfleisch, 2013) where:

- 0 - absence of the given feature
- 1 - mild intensity
- 2 - moderate intensity
- 3 - severe intensity

The cumulative parameters for each mouse subject were aggregated and subjected to rigorous statistical analysis.

TABLE 3 Drug resistance patterns of *P. aeruginosa* 5 strain.

Strain tested	The size of the inhibition zone [mm] for individual antibiotics				
	IMP (10 µg)	ATM (30 µg)	CIP (5 µg)	TOB (10 µg)	CAZ (10 µg)
P. aeruginosa 5	25	23	31	21	19

IMP, Imipenem; ATM, Aztreonam; CIP, Ciprofloxacin; TOB, Tobramycin; CAZ, Ceftazidime.

2.8 Hydrogen peroxide's *in vitro* effect on *S. aureus* 48 and *P. aeruginosa* 5 strains

To ascertain the potential impact of H_2O_2 on pathogenic strains of *S. aureus* 48 and *P. aeruginosa* 5 under *in vivo* conditions, an empirical investigation was conducted to scrutinize the time-based dynamics of the test bacteria population in the presence of H_2O_2. The experiment was conducted based on our previously described procedure, incorporating certain modifications (Strus et al., 2006). Sequential dilutions of 3% H_2O_2 (APTEO, Poland) in aseptic distilled water were prepared, yielding final concentrations spanning from 110 mM to 0.6 mM. *S. aureus* 48 and *P. aeruginosa* 5 strain cultivation adhered to the methodology expounded in Section 2.1.

A singular colony from 24 h pure culture plates was introduced into 10 mL of TSB broth via a sterile loop, comprehensively mixed, and subjected to a 24 h incubation at 37°C.

Following incubation, a serial dilution approach in TSB broth solution was employed to generate a bacterial suspension with a density of 1.0 x 10^5 CFU/mL, mirroring conditions analogous to *in vivo* scenarios. These suspensions served as the foundation for subsequent experimental phases.

The experimentation transpired within sterile glass tubes. Extracting 700 µl from 1.0 x 10^5 CFU/mL bacterial suspensions, each sample was enriched with 100 µl of the relevant H_2O_2 concentration, ensuring a final sample volume encompassing H_2O_2 concentrations ranging from 0.6 mM to 110 mM. Nine concentrations were systematically examined for each strain. The control cohort incorporated an equivalent volume of bacterial culture, supplemented with 100 µl of distilled water. The assays were performed in duplicate.

Both the test and control tubes underwent a 6 h incubation period at 37°C. At intervals of 0, 1, 4, and 6 h, 100 µl from each suspension was harvested, subjected to serial dilutions on tryptone soy agar (TSA, Biomaxima, Poland), and incubated again at 37°C for 24 h to ascertain bacterial quantification.

2.9 Statistical analysis

The statistical analysis was executed within the R environment (R Core Team, 2019), leveraging non-parametric tests due to the failure to meet assumptions requisite for parametric tests. Specifically, the Wilcoxon rank sum test was employed to evaluate disparities in medians between groups. P values ≤0.05 were considered statistically significant. The graphical representation of the findings was crafted utilizing the OriginLab software (OriginPro 2021).

3 Results

The comparison among distinct groups of animals was conducted through three autonomous assays: clinical observations, quantification of inoculated bacteria in dissected tissues, and microscopic scrutiny of tissue alterations.

3.1 Clinical observations

No fatalities among the mice were documented in any experimental group. Examination of the data gleaned from clinical observations conducted on infected, treated, and control animals revealed discrepant outcomes. The detailed results can be referenced in the Supplementary Materials (Supplementary Figure 1).

3.2 Microbiology

Bacteria numbers representative of the test strains in animal tissues obtained from mouse wound swabs 72 h after wound formation/infection are outlined in Table 4. Notably, no bacterial presence was detected in blood or spleen samples collected from the mice. The comparison of the resistance patterns of the wound isolates with the injected bacteria confirmed that they were identical as judged on their resistance patterns.

The application of the PDIA iminosugar exhibited a noteworthy impact, significantly inhibiting the proliferation of the *S. aureus* 48 strain in mice tissues (p=0.0411) over three days (72 h) compared to control conditions. The comprehensive results are visually presented in Figure 1. Notably, such inhibitory effects were not evident in the groups of mice infected with *P. aeruginosa* 5. Furthermore, in contrast to the groups infected with *P. aeruginosa* 5, those infected with *S. aureus* 48 demonstrated a markedly elevated bacterial number.

3.3 Histopathology

The observations regarding the quantities of *S. aureus* bacteria in infected mice were corroborated through histopathological examination. Significant differences were identified concerning the reduction in tissue granulation (p=3.3908 x 10^{-5}) and the decrease in neutrophil inflammatory cell accumulation within tissues (p=0.0011). These findings are visually depicted in Figures 2, 3.

No comprehensible association was identified within groups afflicted with *Pseudomonas* infection. Statistically noteworthy distinctions were manifested in tissue granulation (p=0.0359) and the aggregation of inflammatory neutrophil cells (p=0.0262) within the *S. aureus* 48 group when juxtaposed against the control group. These disparities substantiate staphylococcal infections' considerably more severe trajectory than *Pseudomonas* infections, where such distinctions remained elusive.

The utilized iminosugar concentration exhibited a potential mitigating effect on the inflammatory response within subcutaneous pocket tissues, as evidenced by the diminished tissue granulation in the iminosugar-treated control group relative to the iminosugar-free control group (p=0.0107).

Clinical observations of both control and test subjects failed to yield conclusive data, perhaps attributed to the employed technique, wherein a significant portion of the inflammatory process was concealed within the pockets beneath the animals' skin.

10.3389/fcimb.2024.1395577

TABLE 4 The number of bacteria in animal tissues at 72 hours of the experiment in Control groups and groups infected with *Staphylococcus aureus* 48 and *Pseudomonas aeruginosa* 5.

Group name	Control	Control + I	SA 48	SA 48 + I	PAR 5	PAR 5 +I
Mouse number	The number of bacteria present in wound swabs collected from mice [CFU/mL]		The number of inoculated *Staphylococcus aureus* 48 bacteria in wound swabs collected from mice [CFU/mL]		The number of inoculated *Pseudomonas aeruginosa* 5 bacteria in wound swabs collected from mice [CFU/mL]	
1	ND	ND	4.20E+04	3.50E+04	1.50E+01	1.00E+01
2	ND	ND	3.00E+04	6.00E+04	2.50E+01	ND
3	ND	ND	2.00E+04	1.50E+04	ND	ND
4	ND	ND	6.00E+05	5.55E+04	3.00E+02	1.50E+01
5	ND	ND	4.00E+05	1.00E+04	ND	ND
6	ND	ND	6.00E+03	1.00E+03	ND	1.25E+03
7	ND	ND	1.60E+04	5.00E+00	2.00E+01	ND
8	ND	ND	1.00E+04	1.00E+02	ND	1.50E+02
9	ND		4.00E+04			
10			4.00E+04			
average	**ND**	**ND**	**1.20E+05**	**2.21E+04**	**4.50E+01**	**1.78E+02**
SD			**2.05E+05**	**2.48E+04**	**1.40E+02**	**5.99E+02**
$p < 0.05$			**0.0411**			

ND, not detectable.
The bold values indicate the means obtained from the analysis of all examined mice in respective groups, along with standard deviations.

3.4 Hydrogen peroxide impact on *S. aureus* 48 and *P. aeruginosa* 5

The precise viable bacterial counts of *S. aureus* 48 and *P. aeruginosa* 5 following exposure to varying concentrations of H_2O_2 (110 mM, 55 mM, 27.65 mM, 14 mM, 6.8 mM, 3.5 mM, 1.8 mM, 0.88 mM, and 0.59 mM) at designated time points (0 h, 1 h, 4 h and 6 h) are detailed in the Supplementary Materials.

S. aureus 48 demonstrated high resistance to high concentrations of H_2O_2, as illustrated in Figure 4. After 6 h of exposure, an decrease in the bacterial population of *S. aureus* 48 was noted at the following concentrations of H_2O_2: 6.8 mM, 3.5 mM, 1.8 mM, 0.88 mM, and 0.59 mM.

In contrast to *S. aureus* 48, *P. aeruginosa* 5 exhibited markedly diminished resistance to elevated concentrations of H_2O_2. Figure 5 illustrates the population dynamics of *P. aeruginosa* 5 following a 6 h exposure to H_2O_2 concentrations of 1.8 mM, 0.88 mM, and 0.59 mM. Notably, it is observed that *S. aureus* 48 demonstrated growth under identical experimental conditions, extending to H_2O_2 concentrations of 6.8 mM and 3.5 mM.

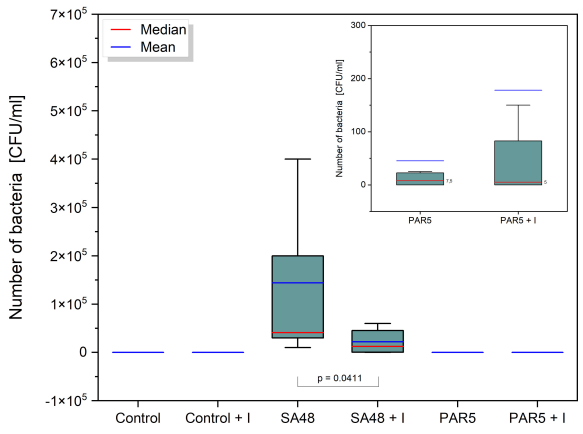

FIGURE 1
Box plot showing the distribution [CFU/mL] of *S. aureus 48* bacteria in the SA 48 and SA 48 + I groups, and *P. aeruginosa 5* bacteria in the PAR5 and PAR 5 + I groups, extracted from wound swabs taken from mice 72 h after wound formation/infection. The graph indicates statistical significance obtained after comparing all results.

4 Discussion

While numerous publications have explored biofilm inhibitors, only a limited number have investigated the efficacy of anti-biofilm structures in *in vitro* studies. Recently, a surge in studies has been reported, employing diverse experimental designs and host organisms ranging from the nematode *Caenorhabditis elegans* to rodents (O'Loughlin et al., 2013; Luo et al., 2017; Jordan et al., 2022).

Experiments conducted on nematodes offer insight into fundamental relationships, specifically their survival in the presence of bacterial pathogens with or without an antibiofilm compound treatment. Despite claims of relevance to bacterial proliferation in the nematode gut (Utari and Quax, 2013; Luo

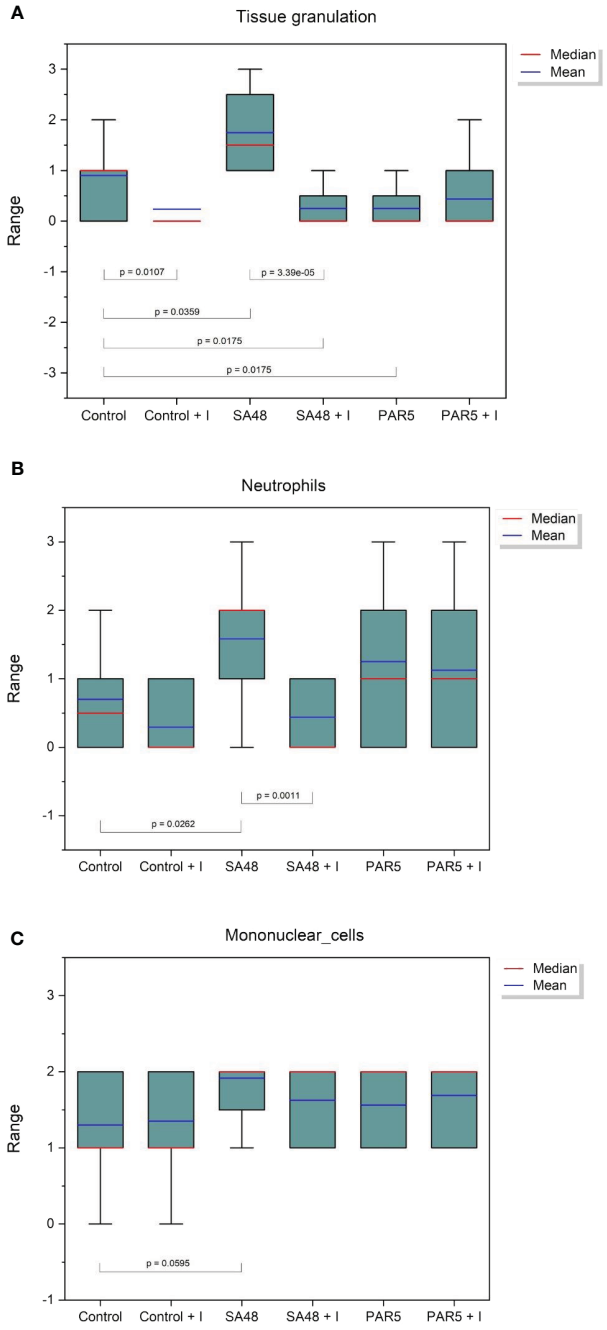

FIGURE 2
Box plot showing the distribution of histopathological findings for: **(A)** Tissue granulation, **(B)** Neutrophil inflammatory cells, and **(C)** Mononuclear cells for each study group. Statistical significance is indicated on the graph.

et al., 2017), this model is somewhat distant from the complex *in vivo* conditions encountered in infected wounds.

Contrastingly, investigations involving mouse subjects afford a more comprehensive exploration, encompassing not only the assessment of post-bacterial load morbidity in animals but also the scrutiny of tissue healing following the administration of antibiofilm drugs (Fitzgerald et al., 2017; Choi et al., 2020; Silveira et al., 2021; Farshadzadeh et al., 2022). Notably, investigations employing catheters as subcutaneous implants and inducing *S. aureus* infections have revealed elevated CFU counts in subjects with catheters, concomitant with a concurrent diminishment in tissue pathology. This observed phenomenon is ascribed to the catheter's role in constraining the dissemination of bacteria through the adjacent tissues (Jordan et al., 2022).

In vivo models for staphylococcal infections originating from the deployment of medical devices facilitate the investigation of biofilm development across varied materials and in unique infection scenarios, encompassing conditions such as prosthetic joint infections or catheter-related infections (Carli et al., 2017).

We employed a straightforward experimental model wherein an early biofilm formation inhibitor was introduced into subcutaneous skin pouches already harboring infections initiated by either *S. aureus* or *P. aeruginosa*, known for their heightened biofilm production. This model offers a streamlined interpretation as it involves only two variables: bacterial multiplication coupled with biofilm formation and the efficacy of the biofilm inhibitor. Burkatovskaya et al. (2008) undertook analogous experiments using an *in vivo* mouse wound infection model, infiltrating chitosan acetate into a wound dressing (Burkatovskaya et al., 2008). Despite the bandage application leading to enhanced wound healing, challenges arose, such as mice dislodging the bandages or encountering difficulties during the experiment's initial stages of bandage removal.

Our *in vivo* model exhibited no discernible morbidity in mice, suggesting a localized infection. It is crucial to emphasize that PDIA does not impact bacterial multiplication but selectively hinders biofilm production. The comparison of staphylococcal multiplication in the wound with clinical symptoms and histology may indicate that the bacteria, although multiply in the wound, are unable to build biofilm and are more readily ingested by the accumulated phagocytic cells. Introducing a foreign body into a wound inevitably complicates the experimental course of infection (particularly with *S. aureus*), elevating bacterial virulence and multiplication rates (Carli et al., 2017; Jordan et al., 2022). Despite the absence of significant differences in clinical observations, the relatively short experimental duration (72 h) might have influenced the outcomes. Notably, even under heightened bacterial doses causing substantial stress to the mice, no fatalities occurred in any of the study groups. In a related study, Lu et al. investigated a mouse wound infection model, exploring the impact of varying inoculum concentrations of infectious *S. aureus* over a two-day infection period, encompassing bacterial growth and subclinical effects. Results revealed diminished bacterial numbers at the minimum concentration of 10^6 CFU/mL, accompanied by a broader spectrum of infection signs. Conversely, administering a higher quantity of bacteria (specifically 10^7 CFU/mL) led to a noteworthy enhancement in the consistency of subclinical effects (Lu et al., 2014). The primary focus, therefore, centered on microbiological and histopathological parameters, enabling a comprehensive analysis of tissue dynamics (Versey et al., 2021).

Thus, our findings on *S. aureus* 48 suggest a tangible impact of PDIA on the organization and structure of *S. aureus* 48 populations within the wound. This effect may exhibit synergy with the actions of certain antibiotics, particularly those impeding cell wall synthesis. Instances of favorable interactions between biofilm inhibitors and

10.3389/fcimb.2024.1395577

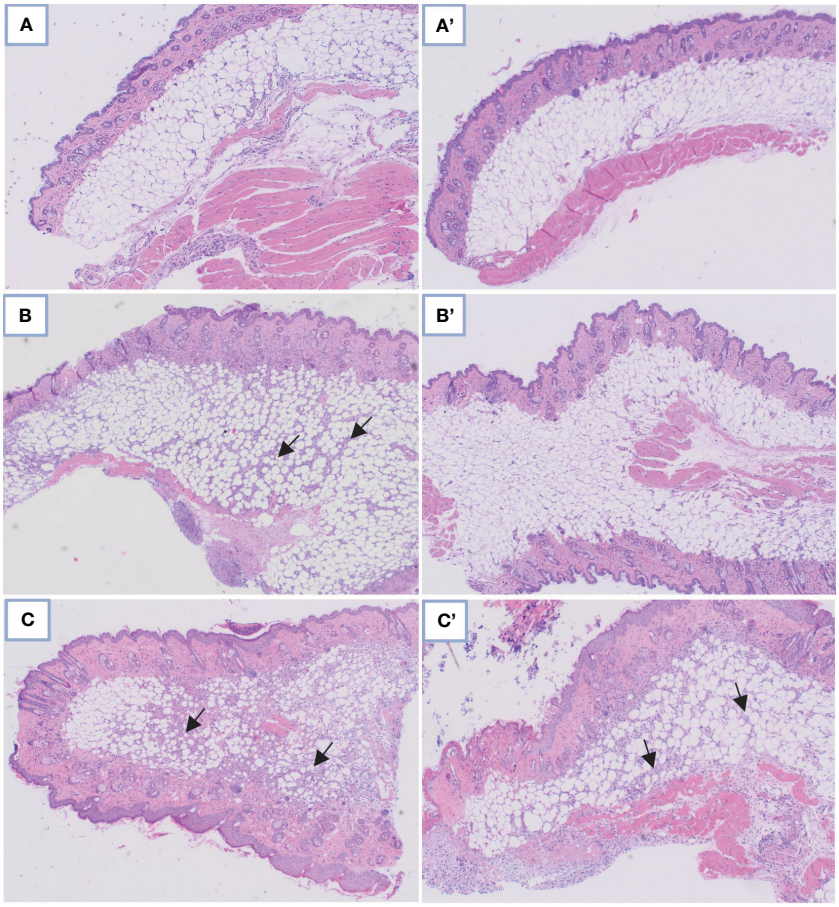

FIGURE 3
Comparison of microscopic images in control skin tissue: **(A)** Without and A' with PDIA iminosugar administration; in the *S. aureus*-infected skin tissue: **(B)** Without and B' with PDIA iminosugar administration; in the *P. aeruginosa*-infected skin tissue: **(C)** Without and C' with PDIA iminosugar administration. Histopathology was performed using an upright microscope at 400× magnification. The black arrows indicate an inflammatory focus exacerbation.

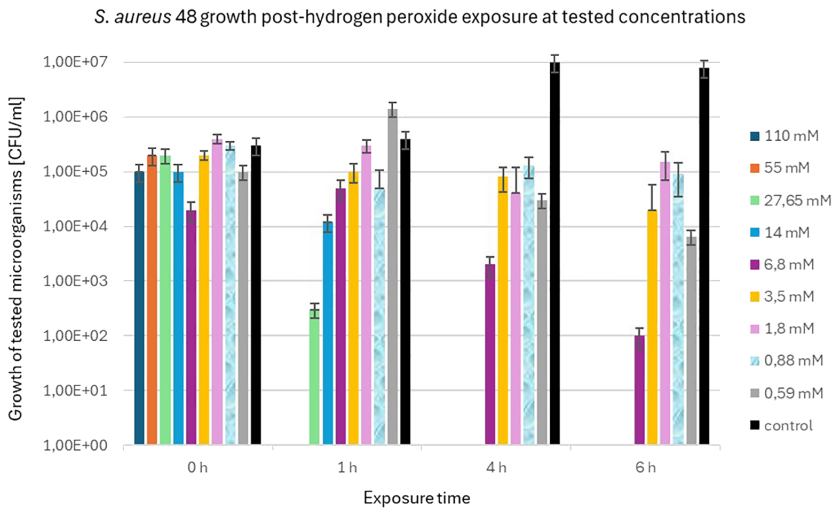

FIGURE 4
Population counts [CFU/mL] of *S. aureus* 48 during 6-hour exposures to different H_2O_2 concentrations versus unexposed controls.

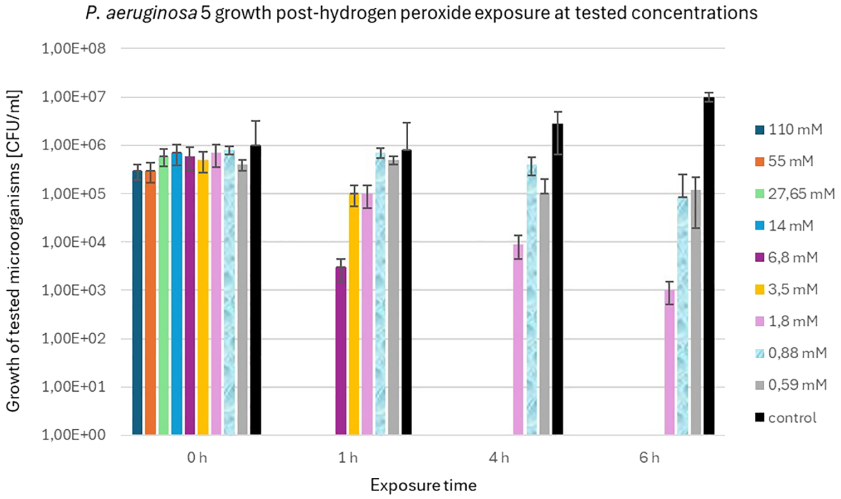

FIGURE 5
Population counts [CFU/mL] of *P. aeruginosa* 5 during 6-hour exposures to different H_2O_2 concentrations versus unexposed controls.

antibiotics are documented in the literature (Pletzer et al., 2016; Roy et al., 2018; Silveira et al., 2021), and are supported by *in vitro* studies (Cirioni et al., 2006; Donelli et al., 2007; Kaplan et al., 2012; Ma et al., 2017; Pletzer et al., 2018). These interactions are worthy of being investigated in future studies on PDIA.

Tissue granulation found in biofilm infections can indicate ongoing acute inflammation, often accompanied by infiltrating inflammatory cells (neutrophils). Pro-inflammatory molecules secreted by neutrophils can lead to the destruction of host cells (Gajula et al., 2020; Versey et al., 2021; Murphy et al., 2023).

Furthermore, biofilm-associated wound infections involving *S. aureus* induce abnormalities in the collagen composition of granulation tissue, thereby resulting in compromised biomechanical properties of the wound tissue (Gurjala et al., 2011; Roy et al., 2020). The outcomes of our investigation substantiate this postulate; the extent of tissue granulation within the *Staphylococcus*-infected group (*S. aureus* 48 group) exhibited the highest magnitude, whereas the administration of PDIA iminosugar significantly attenuated this histopathological parameter (*S. aureus* 48 + I group). Analogously, a parallel deduction can be drawn for neutrophil infiltration, with PDIA iminosugar prominently diminishing the levels thereof in the context of staphylococcal infection. Comparable findings were elucidated by Zaleski et al. (2006) in examining the impact of hyaluronic acid-binding peptides on staphylococcal infection in mouse wounds. Despite manifesting no antimicrobial efficacy *in vitro*, specific peptides demonstrated noteworthy *in vivo* effectiveness by diminishing bacterial burden and ameliorating inflammation in mouse wounds (Zaleski et al., 2006).

Zaleski et al. investigated whether the hyaluronic acid-binding peptide PEP35, which exhibited the most efficacious *in vivo* response against staphylococcal infection in mouse wounds, could modulate the host inflammatory response *in vivo*. The investigation showcased the immunomodulatory prowess of PEP35, evident in the augmentation of CXC cytokine production, attracting neutrophils to the infection site (Zaleski et al., 2006). Furthermore, the brief half-life of PEP35 precluded a protracted inflammatory response that might result in tissue damage (Lee et al., 2010).

In addition to mitigating bacterial numbers and ameliorating histopathological parameters during staphylococcal infection in murine wounds, as observed with the tested PDIA iminosugar, it also demonstrated a reduction in inflammation in the non-infected wound itself, as evidenced by the tissue granulation results in the control groups (Control vs. Control + I). Thus, PDIA iminosugar exerts an antibiofilm effect and potentially possesses immunomodulatory properties. Further exploration of this aspect would be advantageous in subsequent research endeavors.

In the context of wounds afflicted with *Pseudomonas* infection, a discernible impediment to the healing process is evident, as documented by other researchers (Zhao et al., 2010; Seth et al., 2012; Watters et al., 2013). Our investigation, however, did not reveal indications of an augmented inflammatory response or a significant microbial burden in the groups infected with *P. aeruginosa* 5. The inefficacy of the inhibitor in *P. aeruginosa* mice infection remains a perplexing observation, especially considering the pronounced *in vitro* efficacy of the PDIA iminosugar (Kozień et al., 2022). In contrast to *S. aureus*, the employed *P. aeruginosa* strain might have been ineffectual in establishing and perpetuating the infection within the wound, or perhaps the infectious dose employed was insufficient.

To offer a plausible elucidation, experiments were conducted to juxtapose the *in vitro* effects of H_2O_2, serving as an exemplar of an inflammatory oxygen burst, on the bacteria utilized in the *in vivo* studies. The findings indicated that *P. aeruginosa* 5 exhibited greater susceptibility to the adverse effects of H_2O_2 than *S. aureus* 48. This susceptibility may be contingent upon the specific strain. The amelioration of oxidative stress in *P. aeruginosa* is contingent upon the expression of genes such as superoxide dismutase (SOD), catalase (KatA, and KatB) (Hassett et al., 1999). Conversely, in the case of *S. aureus*, the PerR regulator members, alkyl hydroperoxide reductase (AhpC), and KatA are the pertinent factors (Cosgrove

et al., 2007). These observations explicate the histopathological disparities observed between staphylococcal and *Pseudomonas* infections in the mice under examination. The *Pseudomonas* strain was probably effectively eliminated from the inflamed tissue through reactive oxygen species formed during tissue inflammation (Winterbourn et al., 2016).

As evinced above, the PDIA biofilm inhibitor manifests *in vivo* efficacy in a wound infection model in mice with *S. aureus*, thereby prompting the initiation of more sophisticated experiments, including those involving foreign bodies in conjunction with selectively chosen antibiotics.

Data availability statement

The original contributions presented in the study are included in the article/Supplementary Material. Further inquiries can be directed to the corresponding author.

Ethics statement

The animal study was approved by Second Local Institutional Animal Care and Use Committee (IACUC) in Kraków. The study was conducted in accordance with the local legislation and institutional requirements.

Author contributions

ŁK: Data curation, Investigation, Methodology, Project administration, Validation, Writing – original draft, Writing – review & editing. AP: Data curation, Investigation, Writing – review & editing. PH: Conceptualization, Funding acquisition, Supervision, Writing – original draft. ZA: Investigation, Methodology, Resources, Writing – review & editing. UB: Investigation, Writing – review & editing. LP: Investigation, Writing – review & editing. AP-F: Investigation, Writing – review & editing. EG: Resources, Writing – review & editing. PP: Formal analysis, Writing – review & editing. KO: Investigation, Writing – review & editing. AT-P: Methodology, Writing – review & editing, Data curation, Formal analysis. MS: Conceptualization, Methodology, Supervision, Writing – review & editing.

Funding

The author(s) declare financial support was received for the research, authorship, and/or publication of this article. This research was funded by the Polish National Science Centre, grant number 2018/31/B/NZ6/02443 and N N401 547040.

Conflict of interest

The authors declare that the research was conducted in the absence of any commercial or financial relationships that could be construed as a potential conflict of interest.

Publisher's note

Supplementary material

The Supplementary Material for this article can be found online at: https://www.frontiersin.org/articles/10.3389/fcimb.2024.1395577/full#supplementary-material

SUPPLEMENTARY FIGURE 1
Box plot showing the distribution of clinical observations (wound healing, edema, redness, exudate) conducted on infected, treated, and control animals. The graph indicates statistical significance obtained after comparing all results.

References

Allaoui, A., Botteaux, A., Dumont, J. E., Hoste, C., and De Deken, X. (2009). Dual oxidases and hydrogen peroxide in a complex dialogue between host mucosae and bacteria. *Trends Mol. Med.* 15, 571–579. doi: 10.1016/j.molmed.2009.10.003

Burkatovskaya, M., Castano, A. P., Demidova-Rice, T. N., Tegos, G. P., and Hamblin, M. R. (2008). Effect of chitosan acetate bandage on wound healing in infected and noninfected wounds in mice. *Wound Repair Regen.* 16, 425–431. doi: 10.1111/j.1524-475X.2008.00382.x

Carli, A. V., Bhimani, S., Xu, Y., Shirley, M. B., De Mesy Bentley, K. L., Ross, F. P., et al. (2017). Quantification of peri-implant bacterial load and in *vivo* biofilm formation in an innovative, clinically representative mouse model of periprosthetic joint infection. *J. Bone Joint Surg. Am.* 99, e25. doi: 10.2106/JBJS.16.00815

Cheung, G. Y. C., Bae, J. S., and Otto, M. (2021). Pathogenicity and virulence of *Staphylococcus aureus*. *Virulence* 12, 547–569. doi: 10.1080/21505594.2021.1878688

Choi, M., Hasan, N., Cao, J., Lee, J., Hlaing, S. P., and Yoo, J. W. (2020). Chitosan-based nitric oxide-releasing dressing for anti-biofilm and in *vivo* healing activities in MRSA biofilm-infected wounds. *Int. J. Biol. Macromol.* 142, 680–692. doi: 10.1016/j.ijbiomac.2019.10.009

Cirioni, O., Giacometti, A., Ghiselli, R., Kamysz, W., Orlando, F., Mocchegiani, F., et al. (2006). Citropin 1.1-treated central venous catheters improve the efficacy of hydrophobic antibiotics in the treatment of experimental staphylococcal catheter-related infection. *Peptides (N.Y.)* 27, 1210–1216. doi: 10.1016/j.peptides.2005.10.007

Clark, R. A. (1999). Activation of the neutrophil respiratory burst oxidase. *J. Infect. Dis.* 179, 309–317. doi: 10.1086/513849

Cosgrove, K., Coutts, G., Jonsson, I. M., Tarkowski, A., Kokai-Kun, J. F., Mond, J. J., et al. (2007). Catalase (KatA) and alkyl hydroperoxide reductase (AhpC) have compensatory roles in peroxide stress resistance and are required for survival, persistence, and nasal colonization in *Staphylococcus aureus*. *J. Bacteriol.* 189, 1025–1035. doi: 10.1128/JB.01524-06

De Gregorio, E., Esposito, A., Vollaro, A., De Fenza, M., D'alonzo, D., Migliaccio, A., et al. (2020). N-nonyloxypentyl-l-deoxynojirimycin inhibits growth, biofilm formation

and virulence factors expression of *Staphylococcus aureus*. *Antibiotics* 9, 362. doi: 10.3390/antibiotics9060362

Donelli, G., Francolini, I., Romoli, D., Guaglianone, E., Piozzi, A., Ragunath, C., et al. (2007). Synergistic activity of dispersin B and cefamandole nafate in inhibition of staphylococcal biofilm growth on polyurethanes. *Antimicrob. Agents Chemother.* 51, 2733–2740. doi: 10.1128/AAC.01249-06

Dos Santos, A. L. S., Galdino, A. C. M., de Mello, T. P., Ramos, L., de, S., Branquinha, M. H., et al. (2018). What are the advantages of living in a community? A microbial biofilm perspective! *Mem. Inst. Oswaldo Cruz* 113, e180212. doi: 10.1590/0074-02760180212

Farshadzadeh, Z., Pourhajibagher, M., Taheri, B., Ekrami, A., Modarressi, M. H., Azimzadeh, M., et al. (2022). Antimicrobial and anti-biofilm potencies of dermcidin-derived peptide DCD-1L against *Acinetobacter baumannii*: an in *vivo* wound healing model. *BMC Microbiol.* 22, 25. doi: 10.1186/s12866-022-02439-8

Fitzgerald, D. J., Renick, P. J., Forrest, E. C., Tetens, S. P., Earnest, D. N., McMillan, J., et al. (2017). Cadexomer iodine provides superior efficacy against bacterial wound biofilms in *vitro* and in *vivo*. *Wound Repair Regen.* 25, 13–24. doi: 10.1111/wrr.12497

Gajula, B., Munnamgi, S., and Basu, S. (2020). How bacterial biofilms affect chronic wound healing: a narrative review. *Int. J. Surg.* 3, e16. doi: 10.1097/GH9.0000000000000016

Graf, A. C., Leonard, A., Schäuble, M., Rieckmann, L. M., Hoyer, J., Maass, S., et al. (2019). Virulence factors produced by *Staphylococcus aureus* biofilms have a moonlighting function contributing to biofilm integrity. *Mol. Cell. Proteomics* 18, 1036–1053. doi: 10.1074/mcp.RA118.001120

Gurjala, A. N., Geringer, M. R., Seth, A. K., Hong, S. J., Smeltzer, M. S., Galiano, R. D., et al. (2011). Development of a novel, highly quantitative in *vivo* model for the study of biofilm-impaired cutaneous wound healing. *Wound Repair Regen.* 19, 400–410. doi: 10.1111/j.1524-475X.2011.00690.x

Hassett, D. J., Ma, J. F., Elkins, J. G., McDermott, T. R., Ochsner, U. A., West, S. E. H., et al. (1999). Quorum sensing in *Pseudomonas aeruginosa* controls expression of catalase and superoxide dismutase genes and mediates biofilm susceptibility to hydrogen peroxide. *Mol. Microbiol.* 34, 1082–1093. doi: 10.1046/j.1365-2958.1999.01672.x

Islam, B., Khan, S. N., Haque, I., Alam, M., Mushfiq, M., and Khan, A. U. (2008). Novel anti-adherence activity of mulberry leaves: Inhibition of *Streptococcus mutans* biofilm by 1-deoxynojirimycin isolated from *Morus alba*. *J. Antimicrob. Chemother.* 62, 751–757. doi: 10.1093/jac/dkn253

Jordan, S. C., Hall, P. R., and Daly, S. M. (2022). Nonconformity of biofilm formation in *vivo* and in *vitro* based on *Staphylococcus aureus* accessory gene regulator status. *Sci. Rep.* 12, 1251. doi: 10.1038/s41598-022-05382-w

Kannappan, A., Sivaranjani, M., Srinivasan, R., Rathna, J., Pandian, S. K., and Ravi, A. V. (2017). Inhibitory efficacy of geraniol on biofilm formation and development of adaptive resistance in *Staphylococcus epidermidis* RP62A. *J. Med. Microbiol.* 66, 1506–1515. doi: 10.1099/jmm.0.000570

Kaplan, J. B., Lovetri, K., Cardona, S. T., Madhyastha, S., Sadovskaya, I., Jabbouri, S., et al. (2012). Recombinant human DNase I decreases biofilm and increases antimicrobial susceptibility in staphylococci. *J. Antibiot.* 65, 73–77. doi: 10.1038/ja.2011.113

Klopfleisch, R. (2013). Multiparametric and semiquantitative scoring systems for the evaluation of mouse model histopathology – a systematic review. *BMC Vet. Res.* 9, 123. doi: 10.1186/1746-6148-9-123

Kozień, Ł., Gallienne, E., Martin, O., Front, S., Strus, M., and Heczko, P. (2022). PDIA, an iminosugar compound with a wide biofilm inhibitory spectrum covering both Gram-positive and Gram-negative human bacterial pathogens. *Microorganisms* 10, 1222. doi: 10.3390/microorganisms10061222

Lagier, J. C., Edouard, S., Pagnier, I., Mediannikov, O., Drancourt, M., and Raoult, D. (2015). Current and past strategies for bacterial culture in clinical microbiology. *Clin. Microbiol. Rev.* 28, 208–236. doi: 10.1128/CMR.00110-14

Lee, J. C., Greenwich, J. L., Zhanel, G. G., Han, X., Cumming, A., Saward, L., et al. (2010). Modulation of the local neutrophil response by a novel hyaluronic acid-binding peptide reduces bacterial burden during staphylococcal wound infection. *Infect. Immun.* 78, 4176–4186. doi: 10.1128/IAI.01364-09

Liu, Y. H., Wu, P. H., Kang, C. C., Tsai, Y. S., Chou, C. K., Liang, C. T., et al. (2019). Group A *Streptococcus* subcutaneous infection-induced central nervous system inflammation is attenuated by blocking peripheral TNF. *Front. Microbiol.* 10. doi: 10.3389/fmicb.2019.00265

Lu, C. W., Lin, T. Y., Shieh, J. S., Wang, M. J., and Chiu, K. M. (2014). Antimicrobial effect of continuous lidocaine infusion in a *Staphylococcus aureus*-induced wound infection in a mouse model. *Ann. Plast. Surg.* 73, 598–601. doi: 10.1097/SAP.0b013e318276d8e7

Luo, J., Dong, B., Wang, K., Cai, S., Liu, T., Cheng, X., et al. (2017). Baicalin inhibits biofilm formation, attenuates the quorum sensing-controlled virulence and enhances *Pseudomonas aeruginosa* clearance in a mouse peritoneal implant infection model. *PloS One* 12, e0176883. doi: 10.1371/journal.pone.0176883

Ma, Z., Han, J., Chang, B., Gao, L., Lu, Z., Lu, F., et al. (2017). Membrane-active amphipathic peptide WRL3 with in *vitro* antibiofilm capability and in *vivo* efficacy in treating methicillin-resistant *Staphylococcus aureus* burn wound infections. *ACS Infect. Dis.* 3, 820–832. doi: 10.1021/acsinfecdis.7b00100

Marquardt, N., Feja, M., Hünigen, H., Plendl, J., Menken, L., Fink, H., et al. (2018). Euthanasia of laboratory mice: Are isoflurane and sevoflurane real alternatives to carbon dioxide? *PloS One* 13, e0203793. doi: 10.1371/journal.pone.0203793

Mulcahy, L. R., Isabella, V. M., and Lewis, K. (2014). *Pseudomonas aeruginosa* biofilms in disease. *Microb. Ecol.* 68, 1–12. doi: 10.1007/s00248-013-0297-x

Murphy, C. A., Bowler, P. G., and Chowdhury, M. F. (2023). Granulitis: defining a common, biofilm-induced, hyperinflammatory wound pathology. *J. Wound Care* 32, 22–28. doi: 10.12968/jowc.2023.32.1.22

O'Loughlin, C. T., Miller, L. C., Siryaporn, A., Drescher, K., Semmelhack, M. F., and Bassler, B. L. (2013). A quorum-sensing inhibitor blocks *Pseudomonas aeruginosa* virulence and biofilm formation. *Proc. Natl. Acad. Sci. U.S.A.* 110, 17981–17986. doi: 10.1073/pnas.1316981110

Pletzer, D., Coleman, S. R., and Hancock, R. E. W. (2016). Anti-biofilm peptides as a new weapon in antimicrobial warfare. *Curr. Opin. Microbiol.* 33, 35–40. doi: 10.1016/j.mib.2016.05.016

Pletzer, D., Mansour, S. C., and Hancock, R. E. W. (2018). Synergy between conventional antibiotics and anti-biofilm peptides in a murine, sub-cutaneous abscess model caused by recalcitrant ESKAPE pathogens. *PloS Pathog.* 14, e1007084. doi: 10.1371/journal.ppat.1007084

R Core Team (2019). *R A Language and Environment for Statistical Computing*. Vienna, Austria: R Foundation for Statistical Computing.

Ren, Z., Cui, T., Zeng, J., Chen, L., Zhang, W., Xu, X., et al. (2016). Molecule targeting glucosyltransferase inhibits *Streptococcus mutans* biofilm formation and virulence. *Antimicrob. Agents Chemother.* 60, 126–135. doi: 10.1128/AAC.00919-15

Roy, R., Tiwari, M., Donelli, G., and Tiwari, V. (2018). Strategies for combating bacterial biofilms: A focus on anti-biofilm agents and their mechanisms of action. *Virulence* 9, 522–554. doi: 10.1080/21505594.2017.1313372

Roy, S., Santra, S., Das, A., Dixith, S., Sinha, M., Ghatak, S., et al. (2020). *Staphylococcus aureus* biofilm infection compromises wound healing by causing deficiencies in granulation tissue collagen. *Ann. Surg.* 271, 1174–1185. doi: 10.1097/SLA.0000000000003053

Seth, A. K., Geringer, M. R., Gurjala, A. N., Hong, S. J., Galiano, R. D., Leung, K. P., et al. (2012). Treatment of *Pseudomonas aeruginosa* biofilm-infected wounds with clinical wound care strategies: A quantitative study using an in *vivo* rabbit ear model. *Plast. Reconstr. Surg.* 129, 262e–274e. doi: 10.1097/PRS.0b013e31823aeb3b

Silveira, G. G. O. S., Torres, M. D. T., Ribeiro, C. F. A., Meneguetti, B. T., Carvalho, C. M. E., de la Fuente-Nunez, C., et al. (2021). Antibiofilm peptides: relevant preclinical animal infection models and translational potential. *ACS Pharmacol. Transl. Sci.* 4, 55–73. doi: 10.1021/acsptsci.0c00191

Srinivasan, R., Santhakumari, S., Poonguzhali, P., Geetha, M., Dyavaiah, M., and Xiangmin, L. (2021). Bacterial biofilm inhibition: a focused review on recent therapeutic strategies for combating the biofilm mediated infections. *Front. Microbiol.* 12, 676458. doi: 10.3389/fmicb.2021.676458

Strus, M., Brzychczy-Włoch, M., Gosiewski, T., Kochan, P., and Heczko, P. B. (2006). The in *vitro* effect of hydrogen peroxide on vaginal microbial communities. *FEMS Immunol. Med. Microbiol.* 48, 56–63. doi: 10.1111/fim.2006.48.issue-1

Strus, M., Mikołajczyk, D., Machul, A., Heczko, P. B., Chronowska, A., Stochel, G., et al. (2016). Effects of the selected iminosugar derivatives on *Pseudomonas aeruginosa* biofilm formation. *Microb. Drug Resist.* 22, 638–645. doi: 10.1089/mdr.2015.0231

Sutton, S. (2011). Accuracy of plate counts. *J. Valid. Technol.* 17, 42–46.

Tolker-Nielsen, T. (2014). *Pseudomonas aeruginosa* biofilm infections: from molecular biofilm biology to new treatment possibilities. *APMIS Suppl.* 138, 1–51. doi: 10.1111/apm.12335

Tomusiak-Plebanek, A., Heczko, P., Skowron, B., Baranowska, A., Okoń, K., Thor, P. J., et al. (2018). Lactobacilli with superoxide dismutase-like or catalase activity are more effective in alleviating inflammation in an inflammatory bowel disease mouse model. *Drug Des. Devel. Ther.* 12, 3221–3233. doi: 10.2147/DDDT.S164559

Utari, P. D., and Quax, W. J. (2013). *Caenorhabditis elegans* reveals novel *Pseudomonas aeruginosa* virulence mechanism. *Trends Microbiol.* 21, 313–315. doi: 10.1016/j.tim.2013.04.007

Versey, Z., da Cruz Nizer, W. S., Russell, E., Zigic, S., DeZeeuw, K. G., Marek, J. E., et al. (2021). Biofilm-innate immune interface: contribution to chronic wound formation. *Front. Immunol.* 12. doi: 10.3389/fimmu.2021.648554

Watters, C., Deleon, K., Trivedi, U., Griswold, J. A., Lyte, M., Hampel, K. J., et al. (2013). *Pseudomonas aeruginosa* biofilms perturb wound resolution and antibiotic tolerance in diabetic mice. *Med. Microbiol. Immunol.* 202, 131–141. doi: 10.1007/s00430-012-0277-7

Winterbourn, C. C., Kettle, A. J., and Hampton, M. B. (2016). Reactive oxygen species and neutrophil function. *Annu. Rev. Biochem.* 85, 765–792. doi: 10.1146/annurev-biochem-060815-014442

Woo, K., and Sibbald, R. G. (2009). A cross-sectional validation study of using NERDS and STONEES to assess bacterial burden. *Ostomy Wound Manage* 55, 40–48.

Zaleski, K. J., Kolodka, T., Cywes-Bentley, C., McLoughlin, R. M., Delaney, M. L., Charlton, B. T., et al. (2006). Hyaluronic acid binding peptides prevent experimental staphylococcal wound infection. *Antimicrob. Agents Chemother.* 50, 3856–3860. doi: 10.1128/AAC.00082-06

Zhao, G., Hochwalt, P. C., Usui, M. L., Underwood, R. A., Singh, P. K., James, G. A., et al. (2010). Delayed wound healing in diabetic (db/db) mice with *Pseudomonas aeruginosa* biofilm challenge: A model for the study of chronic wounds. *Wound Repair Regen.* 18, 467–477. doi: 10.1111/wrr.2010.18.issue-5

frontiers | Frontiers in Cellular and Infection Microbiology

TYPE Original Research
PUBLISHED 06 August 2024
DOI 10.3389/fcimb.2024.1424038

OPEN ACCESS

EDITED BY
Maria Gabriela Paraje,
National University of Cordoba, Argentina

REVIEWED BY
Sahana Vasudevan,
Institute for Stem Cell Science and Regenerative Medicine (inStem), India
Estela Galvan,
National Scientific and Technical Research Council (CONICET), Argentina

*CORRESPONDENCE
Ai-Qun Jia
aqjia@hainmc.edu.cn

RECEIVED 27 April 2024
ACCEPTED 18 July 2024
PUBLISHED 06 August 2024

CITATION
Pan D, Wu H, Li J-J, Wang B and Jia A-Q (2024) Two cinnamoyl hydroxamates as potential quorum sensing inhibitors against *Pseudomonas aeruginosa*. *Front. Cell. Infect. Microbiol.* 14:1424038. doi: 10.3389/fcimb.2024.1424038

Two cinnamoyl hydroxamates as potential quorum sensing inhibitors against *Pseudomonas aeruginosa*

Deng Pan[1,2], Hua Wu[1], Jun-Jian Li[2], Bo Wang[1] and Ai-Qun Jia[1*]

[1]Hainan General Hospital, Hainan Affiliated Hospital of Hainan Medical University, Haikou, China, [2]Key Laboratory of Tropical Biological Resources of Ministry of Education, School of Pharmaceutical Sciences, Hainan University, Haikou, China

Introduction: *Pseudomonas aeruginosa* is a ubiquitous pathogen that causes various infectious diseases through the regulation of quorum sensing (QS). The strategy of interfering with the QS systems of *P. aeruginosa*, coupled with a reduction in the dosage of conventional antibiotics, presents a potential solution to treating infection and mitigating antibiotic resistance. In this study, seven cinnamoyl hydroxamates were synthesized to evaluate their inhibitory effects on QS of *P. aeruginosa*. Among these cinnamic acid derivatives, we found cinnamoyl hydroxamic acid (CHA) and 3-methoxy-cinnamoyl hydroxamic acid (MCHA) were the two most effective candidates. Furtherly, the effect of CHA and MCHA on the production of virulence factors and biofilm of *P. aeruginosa* were evaluated. Ultimately, our study may offer promising potential for treating *P. aeruginosa* infections and reducing its virulence.

Methods: The disc diffusion test were conducted to evaluate inhibitory effects on QS of seven cinnamoyl hydroxamates. The influence of CHA and MCHA on the production of virulence and flagellar motility of *P. aeruginosa* was furtherly explored. Scanning electron microscopy (SEM) experiment were conducted to evaluate the suppression of CHA and MCHA on the formed biofilm of *P. aeruginosa*. RT-qPCR was used to detect rhlI, lasA, lasB, rhlA, rhlB, and oprL genes in *P. aeruginosa*. *In silico* docking study was performed to explore the molecular mechanism of CHA and MCHA. The synergistic effects of CHA with gentamicin were detected on biofilm cell dispersal.

Result: After treatment of CHA or MCHA, the production of multiple virulence factors, including pyocyanin, proteases, rhamnolipid, and siderophore, and swimming and swarming motilities in *P. aeruginosa* were inhibited significantly. And our results showed CHA and MCHA could eliminate the formed biofilm of *P. aeruginosa*. RT-qPCR revealed that CHA and MCHA inhibited the expression of QS related genes in *P. aeruginosa*. Molecular docking indicated that CHA and MCHA primarily inhibited the RhlI/R system in *P. aeruginosa* by competing with the cognate signaling molecule C4-HSL.Additionally, CHA exhibited potent synergistic effects with gentamicin on biofilm cell dispersal.

Discussion: *P. aeruginosa* is one of the most clinically and epidemiologically important bacteria and a primary cause of catheter-related urinary tract infections and ventilator-associated pneumonia. This study aims to explore whether cinnamoyl hydroxamates have inhibitory effects on QS. And our results indicate that CHA and MCHA, as two novel QSIs, offer promising potential for treating P. aeruginosa infections and reducing its virulence.

KEYWORDS

cinnamoyl hydroxamates, *Pseudomonas aeruginosa*, quorum sensing inhibitors, biofilms, gentamicin

1 Introduction

Pseudomonas aeruginosa, a highly opportunistic pathogen, with about an 8% detection rate in most Chinese hospitals, commonly colonizes immunocompromised hosts and mechanically ventilated patients (Liu et al., 2023). As a significant contributor to the high mortality rates associated with nosocomial and ventilator-associated pneumonia, *P. aeruginosa* is recognized as one of the most life-threatening bacteria by the World Health Organization (WHO) (Thi et al., 2020). Despite the use of antibiotics like gentamicin for treating infections caused by *P. aeruginosa*, the rampant misuse and overuse of these drugs are accelerating the global crisis of antimicrobial resistance (Mladenovic-Antic et al., 2016).

Quorum sensing (QS) represents a cell-cell communication mechanism found in bacteria that is mediated by cell density. Once the released extracellular signaling molecules reach a certain threshold, QS is triggered to regulate gene expression and several physiological processes, such as virulence factor synthesis, biofilm formation, and bacterial motility (Lee and Zhang, 2015). Therefore, interfering with bacterial QS systems offers a promising alternative strategy for fighting pathogens by attenuating QS-regulated virulence factors (Defoirdt, 2018). In *P. aeruginosa*, the *las*, *rhl*, and *pqs* systems constitute the three major QS pathways. Regulation of these systems is achieved through the action of two LuxR-type receptors (LasR and RhlR) and one LysR-type receptor (PqsR, also known as MvfR), each governing distinct subsets of virulence. The *las* system, positioned at the top of the QS hierarchy, controls the downstream QS systems in response to bacterial cell density (Soukarieh et al., 2018).

Cinnamoyl hydroxamic acid (CHA) is recognized for its role in hydroxamic acid-based histone deacetylase (HDAC) inhibition, and several cinnamoyl hydroxamates have been identified with anticancer properties (Zagni et al., 2019). Previous research conducted by our team revealed four cinnamic acid derivatives with potential QS inhibitor activities (Cheng et al., 2020; Pan et al., 2022; Zhou et al., 2022), which enlightened us to consider whether cinnamoyl hydroxamates also have inhibitory effects on QS because of the structural similarity and it was also known hydroxamates exhibited a range of bioactive effects (Yan et al., 2023). In this study, seven cinnamoyl hydroxamates were synthesized and their QS inhibitory activities against *P. aeruginosa* were evaluated. Notably, two cinnamoyl hydroxamates (CHA and methoxy-cinnamoyl hydroxamic acid (MCHA)) showed excellent QS inhibitory activity against *P. aeruginosa*. Furthermore, CHA exhibited robust synergistic potential in conjunction with gentamicin in inhibiting QS-regulated biofilm formation by *P. aeruginosa*. Our results confirmed that CHA and MCHA are effective QS inhibitors against *P. aeruginosa*, highlighting their potential in augmenting therapeutic strategies against infections caused by this pathogen.

2 Materials and methods

2.1 Bacterial strains, culture conditions, and reagents

P. aeruginosa PAO1 was a kind gift from Prof. Q. H. Gong (Ocean University of China, China). *Chromobacterium violaceum* ATCC 12472 was purchased from the Guangdong Microbial Culture Collection Center (Guangzhou, China). In general, the bacteria were cultured in Luria-Bertani (LB) broth (Hope Bio-Technology, Qingdao, China) under constant shaking (180 rpm) with aeration. Guided by QS inhibitor screening, seven cinnamoyl hydroxamates were identified and synthesized from cinnamic acid according to previous published methods (Usachova et al., 2010), followed by purification via column chromatography and characterization by ^{1}H-NMR spectroscopy (AVANCE NEO 400, Bruker BioSpin, Switzerland). More comprehensive details are provided in the Supporting Information. Prior to subsequent experiments, the seven cinnamoyl hydroxamates (a-g) were dissolved in dimethyl sulfoxide (DMSO) to a stock concentration of 100 mg/mL. Antibiotics (gentamicin, polymyxin B, and aztreonam) were purchased from Solarbio (Beijing, China) and dissolved in deionized water.

2.2 Screening of QS inhibitory activity by disc diffusion tests

C. violaceum ATCC 12472 was used as the indicator strain for the screening of QS inhibitors (Tang et al., 2020). The bacteria were cultured in LB medium (*C. violaceum* ATCC 12472 at 28°C; *P. aeruginosa* PAO1 at 37°C) with shaking at 180 rpm to the logarithmic growth phase, then diluted at a 1:100 ratio with LB solid medium and poured into Petri dishes (90 mm × 15 mm). Subsequently, sterile round filter papers (6 × 6 mm) impregnated with 4 μL of each cinnamoyl hydroxamate solution (100 mg/mL) were added to the dishes, followed by incubation at 28°C for 24 h, with DMSO used as the negative control.

2.3 Minimum inhibitory concentration determination and growth curve analysis

To measure the MICs of CHA, MCHA, gentamicin, polymyxin B, and aztreonam, standard broth microdilution was used according to the guidelines of the Clinical and Laboratory Standards Institute (CLSI, 2021). Briefly, 100 μL of cation-adjusted Mueller-Hinton Broth (MHB, Hope Bio-Technology, Qingdao, China) was added to each well of a 96-well polystyrene plate. Subsequently, CHA (0–1.2 mg/mL), MCHA (0–1.2 mg/mL), and antibiotics (0–64 μg/mL) were serially diluted 2-fold from top to bottom in the wells. Overnight-cultured PAO1 strains were diluted with MHB medium and 100 μL of diluted PAO1 strain was added to the plate to achieve a final bacterial concentration of approximately 5×10^5 colony-forming units (CFU)/mL. The plates were prepared in triplicate, then incubated at 37°C for 24 h. The MICs were determined as the lowest concentration of the test solution that inhibited the visible growth of the tested microorganism (Wiegand et al., 2008).

To assess the cytotoxic effects of CHA and MCHA and determine their appropriate sub-MICs for further study, growth curves of PAO1 were monitored in both the presence and absence of CHA and MCHA at specified concentrations. The experimental methods were similar to those used for MIC determination. Specifically, overnight-cultured PAO1 strains were diluted with MHB medium and placed into a 96-well plate. Solutions of CHA or MCHA at sub-MIC levels were added to the wells. The plates were then incubated at 37°C and growth curves were recorded at 620 nm using a microplate reader (Biotek Epoch2, USA) at 3-h intervals over a 24-h period.

2.4 Biofilm elimination assays of CHA and MCHA against PAO1

Overnight-cultured PAO1 strains were diluted with trypticase soy broth (TSB, Hope Bio-Technology, Qingdao, China) and added to a 96-well plate (200 μL per well), followed by incubation at 37°C for 24 h. After incubation, the plate was washed with sterile phosphate-buffered saline (PBS, pH = 7.3, 10 mM) to remove the medium and planktonic bacteria. Solutions of CHA or MCHA in TSB medium (200 μL) at designated concentrations were added to each well, and the plates were incubated at 37°C for 17 h. Finally, the plates were gently washed with PBS and the retained biofilms were quantified using crystal violet assay, with absorbance measured at 570 nm (Merritt et al., 2011).

2.5 Scanning electron microscopy

For the SEM experiments, overnight-cultured PAO1 strains were diluted with TSB and added to a 24-well plate (1 mL per well). Sterile coverslips (14 × 14 mm) were placed at the bottom of the plate, followed by culture at 37°C for 24 h. After incubation, the plates were washed with sterile PBS to remove the medium and planktonic bacteria. Solutions of CHA or MCHA in TSB (1 mL) at designated concentrations were added to each well, and the plates were incubated again at 37°C for 17 h. The non-adherent cells were then removed by washing the coverslips with PBS. Residual biofilms were fixed using 2.5% glutaraldehyde in a new 24-well plate at 4°C for 4 h, and the samples were dehydrated by increasing concentrations of ethanol (30%, 50%, 70%, 90%, 95%, and 100%, 10 min each). All samples were allowed to dry before SEM-based visualization (Hitachi, S-3000N, Japan) (Zhou et al., 2018a).

2.6 QS-regulated virulence factor assays

The pyocyanin quantification assay was performed as described previously (Essar et al., 1990). Briefly, overnight-cultured PAO1 strains were diluted with PDP medium (2% tryptone, 1% K_2SO_4, 0.14% $MgCl_2$, and 1% glycerol, Hope Bio-Technology, Qingdao, China) and incubated with CHA or MCHA at sub-MICs at 37°C and 180 rpm for 24 h. The known QS inhibitor hordenine (Hor, 1 mg/mL, dissolved in DMSO) was used as a positive control and DMSO was used as a negative control. After centrifugation (10 000 rpm, 4°C, 10 min), the PAO1 culture supernatant (5 mL) was extracted with 3 mL of chloroform, followed by the addition of 0.2 M HCl (1 mL) to the chloroform layer. The upper aqueous phase was then collected by centrifugation at 11 000 × *g* for 10 min and absorbance was measured at 520 nm using a microplate reader (Biotek Epoch2, USA).

Elastase quantitative analysis was performed following the previous methodology (Zeng et al., 2022), with minor modifications. Briefly, overnight-cultured PAO1 strains were diluted with TSB, and 2 mL of PAO1 cultures was incubated with CHA or MCHA at sub-MICs at 37°C, 180 rpm to the logarithmic growth phase. Hor (1 mg/mL) was used as a positive control and DMSO was used as a negative control. The bacterial cultures were subsequently centrifuged at 11 000 ×*g* for 10 min and the supernatants were collected by filtering through a 0.22-μm nylon filter. The subsequent experimental steps were performed according to the protocols provided with the elastase ELISA kit (Enzyme-linked Biotechnology, Shanghai, China).

Protease quantitative analysis was performed according to previously published research (Prithiviraj et al., 2005), with minor modifications. In brief, overnight-cultured PAO1 strains were diluted with TSB, with 1 mL of the bacterial cultures then transferred to a 12-well polystyrene plate and incubated with CHA or MCHA at sub-

MICs at 37°C and 180 rpm to the logarithmic growth phase. Hor (1 mg/mL) was used as a positive control and DMSO was used as a negative control. The bacterial cultures were then centrifuged at 11 000 ×*g* for 10 min and the supernatant was filtered through a 0.22-μm nylon filter. Sterile supernatant (150 μL) was added to 250 μL of 0.3% azocasein (w/v)-Tris/HCl solution (50 mM, pH 7.8). The azocasein-treated solutions were then incubated at 37°C for 3 h, after which the reaction was terminated by the addition of 1.2 mL trichloroacetic acid (10%, w/v) for 20 min. Following centrifugation at 11 000 × *g* for 10 min, the supernatant was added to 1 M equal volume of NaOH. Protease activities were determined by measuring absorbance at 440 nm with a microplate reader after CHA or MCHA treatment (Biotek Epoch2, USA).

The effects of CHA or MCHA on *P. aeruginosa* PAO1 rhamnolipids were analyzed using the concentrated H_2SO_4-orcinol approach (Grosso-Becerra et al., 2016). In brief, overnight-cultured PAO1 strains were diluted with protease peptone glucose ammonium salt medium (PPGAS, 20 mM NH_4C1, 20 mM KCl, 120 mM Tris-HCl, 0.5% glucose, 1% protease peptone, 1.6 mM $MgSO_4$, adjusted to pH 7.2) and incubated with CHA or MCHA at sub-MICs at 37°C and 180 rpm for 48 h. Hor (1 mg/mL) was used as a positive control and DMSO was used as a negative control. Subsequently, the bacterial cultures were centrifuged at 5 500 ×*g* for 10 min and the supernatants were collected. The supernatants were extracted twice with ethyl acetate, with the organic layers combined and evaporated to dryness at 25°C. The dry extract was resuspended in 500 μL of sterile distilled water, after which 100 μL of the sample was added to 0.19% orcinol in 53% H_2SO_4 (900 μL) and incubated in a water bath at 80°C for 30 min. After cooling to room temperature, the OD_{421} was measured.

Siderophore quantitative analysis was performed as described previously (Yin et al., 2022). Briefly, overnight-cultured PAO1 strains were first diluted with TSB, with 5 mL of these cultures then incubated with CHA or MCHA at sub-MICs at 37°C and 180 rpm to the logarithmic growth phase. Hor (1 mg/mL) was used as a positive control and DMSO was used as a negative control. The bacterial cultures were then centrifuged at 11 000 ×*g* for 10 min and the supernatants were collected using a 0.22-μm nylon filter. Subsequently, 3 mL of filtrate was mixed with an equal volume of chrome azurol S (CAS) test solution (Coolaber, Beijing, China), and incubated for 1 h in the dark at room temperature. After incubation, reaction solution absorbance was determined at 680 nm using a microplate reader (Biotek Epoch2, USA).

2.7 Flagellar motility assay of CHA or MCHA against *P. aeruginosa*

Swimming and swarming motilities were assessed as described previously (Rashid and Kornberg, 2000). Briefly, 2 μL of PAO1 grown in LB for 17 h was diluted in fresh sterile LB medium to obtain an OD_{620} of 0.5, then spotted onto the center of swimming plates (0.8% nutrient broth, 0.5% glucose, 0.3% agar) or swarming plates (0.8% nutrient broth, 0.5% glucose, 0.5% agar). The plates were supplemented with CHA or MCHA or not. After 17–24 h of static incubation at 37°C, swimming and swarming motilities were directly observed at the air-agar interface.

2.8 Real-time quantitative PCR

Overnight-cultured PAO1 strains diluted in LB medium with CHA (200 μg/mL) or MCHA (300 μg/mL) were incubated at 37°C and 180 rpm for 17 h. After washing the biofilm cells with PBS, the attached cells were scraped and collected in a microtube. Total RNA was extracted using a UNIQ-10 column Trizol total RNA extraction kit (Sangon Biotech, Shanghai, China) and extracted RNA purity was detected by electrophoresis. The samples were then reverse-transcribed to single-stranded complementary DNA (cDNA) in a 20-μL volume of the reaction mixture using Maxima Reverse Transcriptase (200 U, Thermo Fisher Scientific, Waltham, MA, USA). Then, RT-qPCR was performed in a 20-μL reaction volume, containing 10 μL of SYBR Green qPCR Master Mix (Sangon Biotech, Shanghai, China), 2 μL of template cDNA, 0.8 μL of each primer (Sangon Biotech, Shanghai, China), and 7.2 μL of DNase/RNase-free water. After that, 96-well plates with added samples were placed in an ABI Stepone plus fluorescence PCR instrument (ABI, Foster City, USA) for reaction. The qPCR conditions were 95°C for 3 min, followed by 45 cycles of 95°C for 5 s and 60°C for 30 s. Amplification of specific transcripts was confirmed by melting curve profiles generated at the end of the PCR program. Fold changes in expression versus control conditions were determined using the $2^{-\Delta\Delta Ct}$ method, with *rpsL* as a housekeeping gene (Grosso-Becerra et al., 2016) (see Supplementary Table S1 for primer sequences).

2.9 *In silico* docking study

Co-crystallized structures of LasR (PDB code: 2UV0) and PqsR (PDB code: 4JVD) were obtained from the Protein Data Bank (http://www.rcsb.org/pdb/) (Berman et al., 2000). Another structure of the homology RhlR model was downloaded from supporting information in a previously reported reference (Nam et al., 2020). As the crystal structure of LasR was a tetramer in 2UV0, one monomer was selected for docking calculation. Schrödinger software release 2017-1 (New York, USA) was used to carry out *in silico* calculations. Before docking calculations, several necessary structural preparations of the protein were required, including removal of dispensable water molecule removal, hydrogen addition, and minimization. All 3D ligand structures were prepared using the LigPrep module (LigPrep, Schrödinger, New York, USA), optimized through the OPLS3 force field (Harder et al., 2016). Glide XP (extra precision) in the Schrodinger suite was used for ligand docking. The binding energy of each ligand was calculated through the OPLS3 force field. Finally, the docking pose was optimized while the protein was kept fixed.

2.10 Checkerboard assays

The interactions between CHA or MCHA and antibiotics (gentamicin, polymyxin B, aztreonam) were examined against the

P. aeruginosa PAO1 strain using the broth microdilution checkerboard assay, with the fractional inhibitory concentration index (FICI) used to analyze the types of interactions between compounds (Ham et al., 2021). Briefly, CHA or MCHA and one antibiotic were diluted with MHB medium into a series of concentrations based on the MICs of CHA and MCHA. Similarly, overnight-grown bacterial colonies were also diluted with MHB to a final concentration of approximately 5×10^5 CFU/mL in each well. Results were observed after static incubation at 37°C for 24 h. All experiments were performed in triplicate. The FICIs were calculated using the equation: FICI = MIC (antibiotic combined with CHA or MCHA)/MIC (antibiotic alone) + MIC (CHA or MCHA combined with antibiotic)/MIC (CHA or MCHA alone), where FICI ≤ 0.5, 0.5 < FICI ≤ 4, and FICI > 4 mean synergistic, indifferent, and antagonistic effects, respectively (Zhou et al., 2018b).

2.11 Effects of CHA combined with gentamicin on PAO1 biofilm elimination

2.11.1 Crystal violet staining analysis

The methods employed were the same as those used for the biofilm elimination assay (Section 2.4). This experiment was performed with four distinct groups: DMSO negative control, 50 μg/mL CHA, 2 μg/mL gentamicin, and CHA (50 μg/mL) combined with gentamicin (2 μg/mL).

2.11.2 Quantification of CFU assay

Biofilms were grown as described in Section 2.4. Following a 24 h incubation period, plates were washed with sterile PBS to remove any remaining medium and planktonic bacteria. Subsequently, fresh sterilized TSB medium was used for dilution, to which was added either 50 μg/mL CHA, 2 μg/mL gentamicin, or a combination of both to a final volume of 200 μL per well, followed by incubation at 37°C for 17 h. DMSO was used as a negative control. After that, biofilm cells were detached by sonication at 300 W power and 40 kHz for 5 min. Sterile PBS was added, followed by vigorous mixing. The resulting solution was then serially diluted in a 10-fold gradient and plated onto LB agar plates. Colonies were counted and the CFU per biofilms were calculated.

2.12 SEM analysis

The procedures used to assess the morphology of biofilms after their elimination followed those described in Section 2.5, except for the division into four groups: DMSO as the negative control, 50 μg/mL CHA, 2 μg/mL gentamicin, and the combination of CHA (50 μg/mL) with gentamicin (2 μg/mL).

2.13 Statistical analysis

Data are presented as mean ± standard deviation (SD). Experiments were performed in triplicate and statistical analyses were executed using one-way analysis of variance (ANOVA) with Dunnett test or Student's *t*-test. Statistically significant values were defined as $P < 0.05$, < 0.01, or < 0.001. GraphPad Prism v8 (GraphPad Software Inc., San Diego, CA, USA) was used for all graphical and statistical evaluations.

3 Results

3.1 Assessment of QS inhibition by CHA and MCHA

The production of purple pigment (violacein) in *C. violaceum* ATCC 12472 is regulated by the QS systems. This result is a naturally occurring and readily observable phenotype, making it a commonly used indicator strain for QSI (McLean et al., 2004). In the present study, as illustrated in Figure 1A, the presence of CHA or MCHA resulted in the formation of a white and turbid zone around the filter paper discs, signifying a notable suppression of synthesis of both violacein in *C. violaceum* ATCC 12472 and pyocyanin in *P. aeruginosa* PAO1. In contrast, the other five cinnamoyl hydroxamates (c-g) exhibited minimal inhibitory effects (see Supporting Information). These findings confirm the QS inhibitory potential of both CHA and MCHA.

3.2 Susceptibility of PAO1 to CHA, MCHA, and antibiotics

The MICs of CHA, MCHA, gentamicin, polymyxin B, and aztreonam against *P. aeruginosa* PAO1, assessed using a broth microdilution assay, were 400 μg/mL, 600 μg/mL, 4 μg/mL, 4 μg/mL, and 4 μg/mL, respectively. Growth curve analysis indicated that CHA (50–200 μg/mL) and MCHA (75–300 μg/mL) did not inhibit *P. aeruginosa* growth (Figures 1B, C), although the growth rate of *P. aeruginosa* was slower than that in control group in the initial period. Subsequent experiments utilized sub-MICs for CHA (low-dose group (L-CHA): 50 μg/mL; middle-dose group (M-CHA): 100 μg/mL; high-dose group (H-CHA): 200 μg/mL) and MCHA (low-dose group (L-MCHA): 75 μg/mL; middle-dose group (M-MCHA): 150 μg/mL; high-dose group (H-MCHA): 300 μg/mL). The FICIs of all combinations exceeded 0.5, indicating that all compounds showed no synergistic or antagonistic interaction with the tested antibiotics against PAO1 planktonic cells (Supplementary Table S2).

3.3 Effects of CHA and MCHA on biofilms

The effects of CHA and MCHA on *P. aeruginosa* PAO1 formed biofilms in 96-well plates were evaluated using crystal violet staining. As shown in Figure 2A, *P. aeruginosa* PAO1 formed biofilms were significantly eliminated by CHA and MCHA in a dose-dependent manner. Compared to the control group, the reduction in formed biofilms reached 50% and 58% under CHA (200 μg/mL) and MCHA (300 μg/mL) treatment, respectively. SEM

10.3389/fcimb.2024.1424038

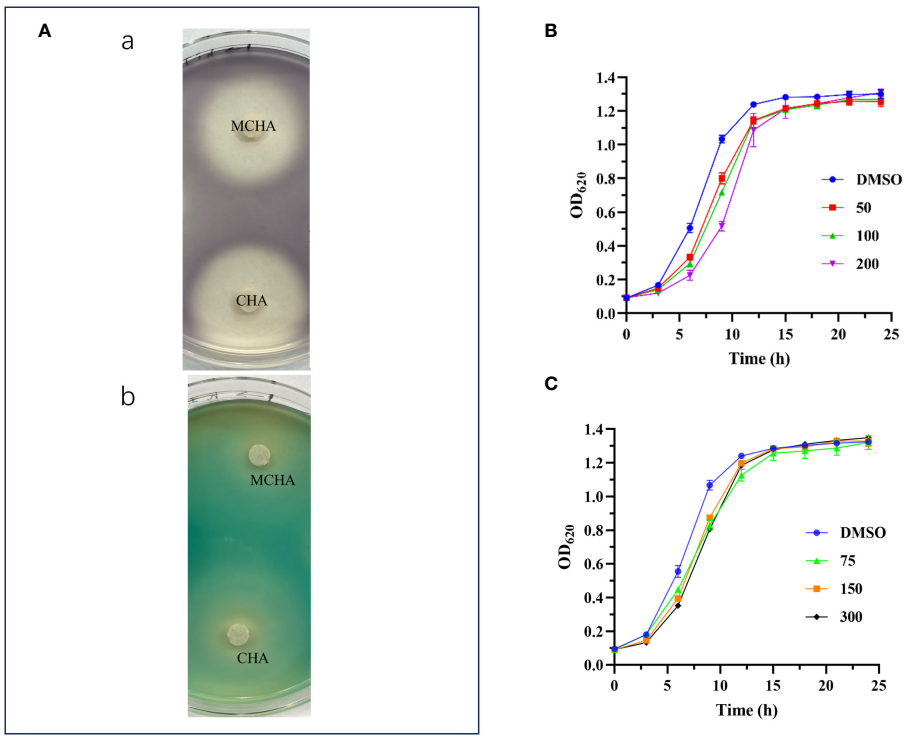

FIGURE 1
QS inhibitory activities of CHA and MCHA. **(A)** QS inhibitory activities of CHA and MCHA on a Petri dish against strains *C. violaceum* ATCC 12472 (a) and *P. aeruginosa* PAO1 (b). Growth curves of *P. aeruginosa* PAO1 treated with CHA **(B)** and MCHA **(C)** at sub-MICs, respectively.

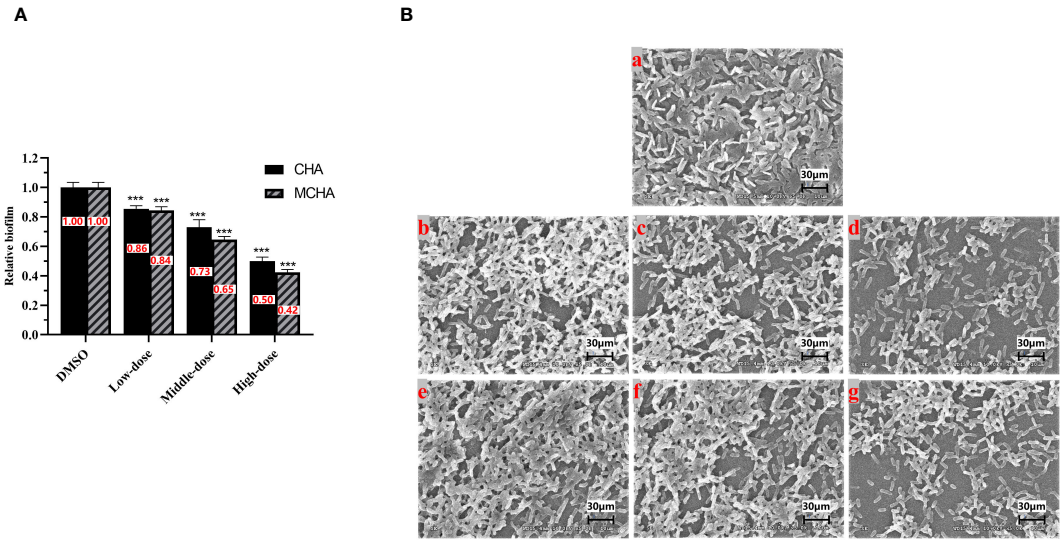

FIGURE 2
Effects of CHA and MCHA on *P. aeruginosa* PAO1 biofilm disruption. **(A)** Analysis of crystal violet staining assay with CHA and MCHA; **(B)** SEM images of formed *P. aeruginosa* biofilms treated with (a) DMSO, (b) 50, (c) 100, (d) 200 μg/mL CHA, or (e) 75, (f) 150, (g) 300 μg/mL MCHA, respectively. Data are presented as absorbance of mean ± SD of three independent experiments. ***$P < 0.001$ compared to DMSO control group by one-way ANOVA, n = 3. Low-dose group (CHA: 50 μg/mL; MCHA: 75 μg/mL); Middle-dose group (CHA: 100 μg/mL; MCHA: 150 μg/mL); High-dose group (CHA:200 μg/mL; MCHA: 300 μg/mL).

10.3389/fcimb.2024.1424038

analysis revealed CHA and MCHA treatments transformed *P. aeruginosa* PAO1 biofilms from dense to more porous and less compact structures, in line with crystal violet staining results, demonstrating concentration-dependent effects, while also obviously reducing extracellular secretion and bacterial aggregation (Figure 2B). These findings demonstrate that exposure to CHA and MCHA can significantly disrupt formed biofilms of *P. aeruginosa* PAO1.

3.4 Effects of CHA and MCHA on *P. aeruginosa* PAO1 virulence factors

The effects of CHA and MCHA on pyocyanin production by *P. aeruginosa* PAO1 were first examined. As shown in Figure 3A, CHA and MCHA exerted significant inhibitory effects on pyocyanin production. Compared to the control group, CHA (200 μg/mL) and MCHA (300 μg/mL) inhibited pyocyanin production by 95% and 92%, respectively, both exceeding that of the positive control Hor (47%).

Subsequently, the effects of CHA and MCHA on elastase and protease activities in *P. aeruginosa* PAO1 were determined. As shown in Figure 3B, elastase activity was inhibited by CHA and MCHA in a concentration-dependent manner. CHA at 50 μg/mL, 100 μg/mL, and 200 μg/mL achieved elastase inhibition rates of 25%, 33%, and 39%, respectively, while MCHA at 75 μg/mL, 150 μg/mL, and 300 μg/mL achieved elastase inhibition rates of 21%, 28%, and 32%, respectively, exceeding that of the positive control Hor (19%). In addition, while CHA and MCHA did not significantly affect protease activity at lower concentrations (Figure 3C), treatment with CHA at 200 μg/mL and MCHA at 300 μg/mL inhibited protease activity by 40% and 33%, respectively, surpassing that of Hor (27%).

The effects of CHA and MCHA on the production of rhamnolipid by *P. aeruginosa* PAO1 were also evaluated. As shown in Figure 3D, CHA at 200 μg/mL and MCHA at 300 μg/mL inhibited rhamnolipid production by 69% and 85%, respectively, both exceeding the inhibitory effects of Hor (35%).

The CAS assay, composed of chrome azurol sulphonate, hexadecyl-trimethyl-ammonium bromide (HDTMA), and iron ions, changes from blue to orange-yellow when siderophores from *P. aeruginosa* bind to iron ions, enabling siderophore detection. As shown in Figure 3E, CHA and MCHA significantly reduced siderophore production, with CHA at 200 μg/mL and MCHA at 300 μg/mL inhibiting siderophore activity by 51% and 55%, respectively, surpassing the 8% inhibition achieved by Hor.

3.5 Effects of CHA and MCHA on *P. aeruginosa* PAO1 motility

Enhanced motility facilitates bacterial infection of hosts. This study explored the effects of CHA and MCHA on *P. aeruginosa* PAO1 motility via swimming and swarming experiments. As shown in Figure 4, after treatment sub-MICs of CHA and MCHA, both the

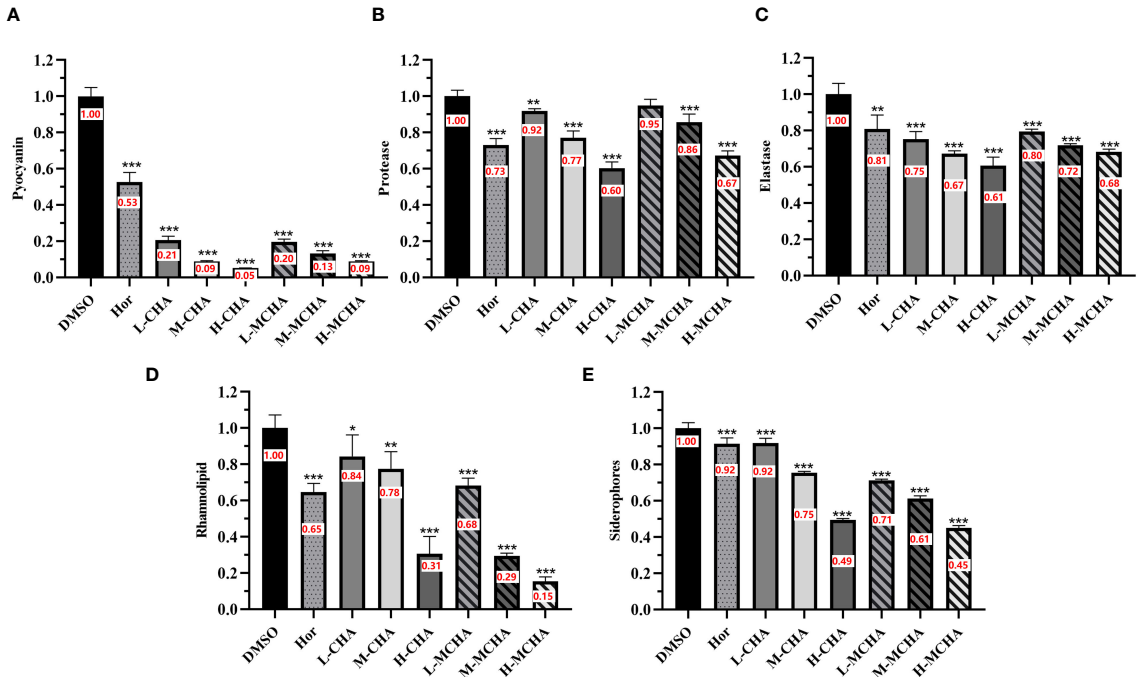

FIGURE 3
Inhibitory effects of CHA and MCHA on *P. aeruginosa* PAO1 virulence factors. **(A)** Pyocyanin; **(B)** Protease; **(C)** Elastase; **(D)** Rhamnolipid; **(E)** Siderophores Data are presented as absorbance of mean ± SD of three independent experiments. *$P < 0.05$, **$P < 0.01$, ***$P < 0.001$ compared to DMSO control group by one-way ANOVA, n = 3. L-CHA: CHA low-dose group (50 μg/mL); M-CHA: CHA middle-dose group (100 μg/mL); H-CHA: CHA high-dose group (200 μg/mL); L-MCHA: MCHA low-dose group (75 μg/mL); M-MCHA: MCHA middle-dose group (150 μg/mL); H-MCHA: MCHA high-dose group (300 μg/mL).

10.3389/fcimb.2024.1424038

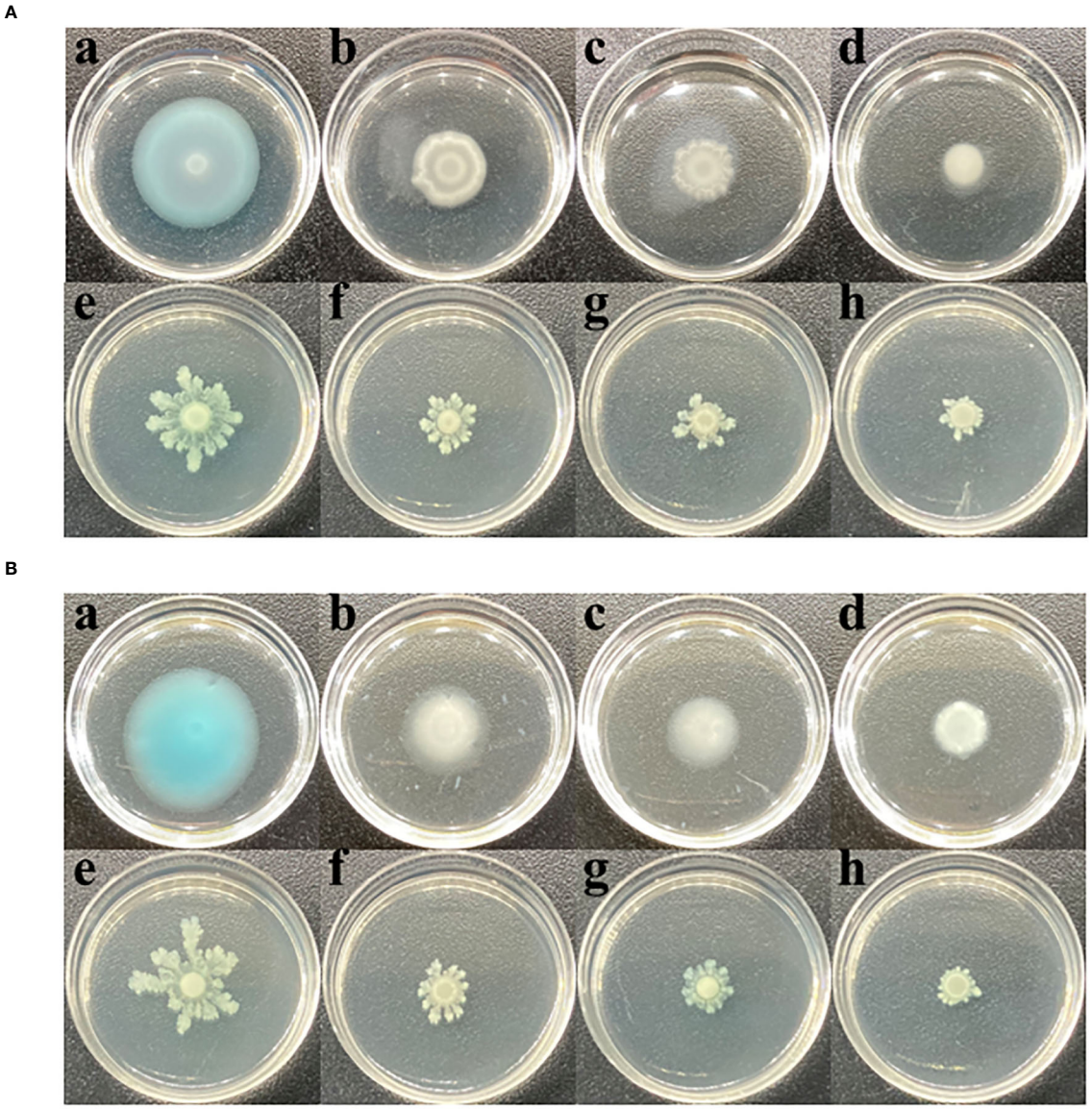

FIGURE 4
Effects of CHA and MCHA on swimming and swarming motilities of *P. aeruginosa* PAO1 at sub-MICs. **(A)** The effects of CHA on swimming (a. DMSO; b. CHA 50 μg/mL; c. CHA 100 μg/mL, d. CHA 200 μg/mL) and swarming (e. DMSO; f. CHA 50 μg/mL; g. CHA 100 μg/mL, h. CHA 200 μg/mL). **(B)** The effects of MCHA on swimming (a. DMSO; b. CHA 75 μg/mL; c. CHA 150 μg/mL, d. CHA 300 μg/mL) and swarming (e. DMSO; f. CHA 75 μg/mL; g. CHA 150 μg/mL, h. CHA 300 μg/mL).

swimming and swarming motilities of *P. aeruginosa* PAO1 were significantly suppressed. The diameter of the swimming diffusion zone decreased from 3.1 ± 0.2 cm in the untreated DMSO group to 1.8 ± 0.1 cm, 1.4 ± 0.1 cm, and 0.9 ± 0.1 cm in the 50 μg/mL, 100 μg/mL, and 200 μg/mL CHA-treated groups and to 1.9 ± 0.1 cm, 1.5 ± 0.1 cm, and 1.1 ± 0.1 cm in the 75 μg/mL, 150 μg/mL, and 300 μg/mL MCHA-treated groups, respectively.

3.6 Effects of CHA and MCHA on QS-related gene expression

To further investigate the mechanism by which CHA and MCHA inhibit the QS system, biofilm formation, and motility of *P. aeruginosa* PAO1, RT-qPCR was used to examine the gene expression changes. As shown in Figure 5, CHA (200 μg/mL) and MCHA (300 μg/mL) treatments reduced the expression of PAO1 QS-related genes to varying degrees. Notably, *lasR*, which encodes the transcriptional regulator protein LasR in the LasI/LasR system, was down-regulated by 62% (CHA) and 72% (MCHA); *rhl*R, encoding the transcriptional regulator protein RhlR in the RhlI/R system, was down-regulated by 73% (CHA) and 81% (MCHA); *rhl*I, a butyl-homoserine lactone (C4-HSL) synthase gene, was down-regulated by 80% (CHA) and 58% (MCHA); and *pqs*H, a 2-heptyl-3-hydroxy-4(1H)-quinolone synthase gene in the *pqs* system, was downregulated by 75% (CHA) and 50% (MCHA). Significant down-regulation was also observed in *P. aeruginosa* PAO1 virulence factor-related genes, with *lasA*, encoding protease LasA

10.3389/fcimb.2024.1424038

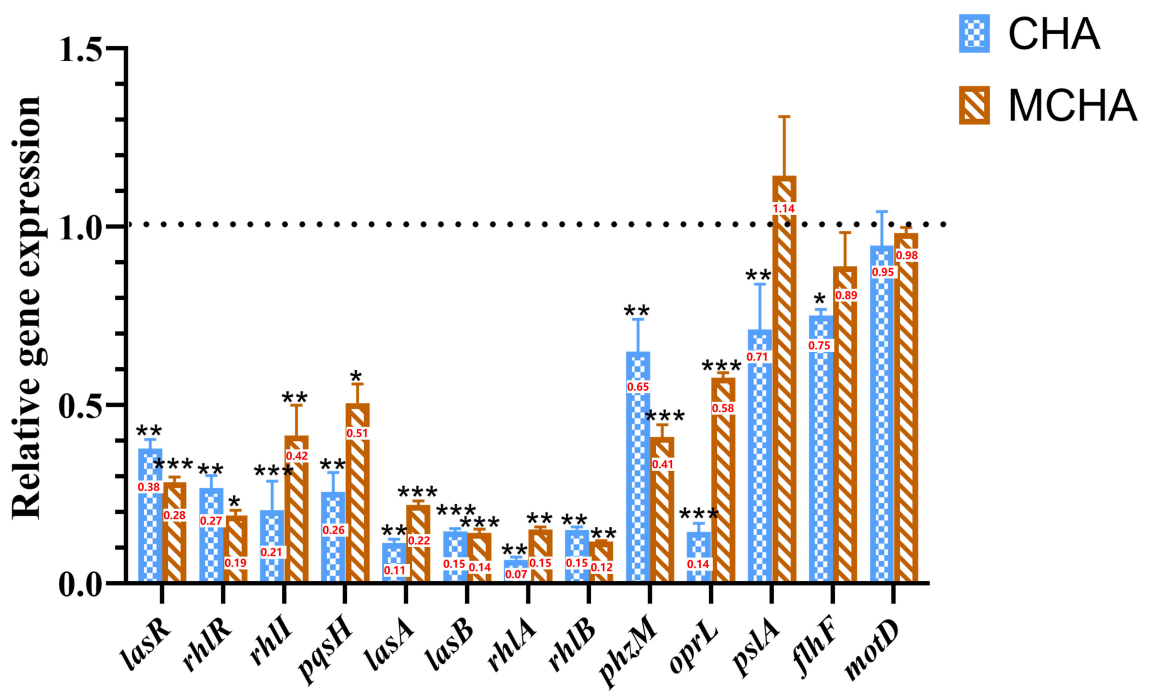

FIGURE 5
Effects of CHA and MCHA on QS and virulence-related genes in *P. aeruginosa* PAO1. Data are averages of the three experiments, expressed as multiple ± SD of gene expression level, n = 3. Data are presented as expression fold-changes of mean ± SD of three independent experiments. $^{*}P < 0.05$, $^{**}P < 0.01$, $^{***}P < 0.001$ compared to DMSO control group in *t*-test, n = 3.

synthesis, inhibited by 89% (CHA) and 78% (MCHA); *lasB*, encoding elastase LasB synthesis, inhibited by 86% (CHA and MCHA); *rhl*A and *rhl*B, rhamnolipid synthesis-related genes, inhibited by 93% and 85% (CHA) and by 85% and 88% (MCHA), respectively; and *phz*M, a pyocyanin synthesis-related gene, inhibited by 36% (CHA) and 59% (MCHA). Results also showed that CHA and MCHA exerted inhibitory effects on biofilm and motility-related genes, with *opr*L, encoding peptidoglycan-associated lipoprotein synthesis, inhibited by 86% (CHA) and 43% (MCHA); *psl*A, encoding biofilm formation proteins, inhibited by 30% (CHA); and *flh*F and *mot*D, encoding the flagellar biosynthesis regulator and flagellar motor protein, down-regulated by 25% (CHA) and 6% (CHA), respectively.

3.7 Docking simulations

Results showed that the interactions of CHA and MCHA with the LasR and PqsR proteins were weaker than those with their ligands N-3-oxododecanoyl homoserine lacton (3-oxo-C12-HSL) and 2-heptyl-3,4-dihydroxyquinoline (PQS, quinolone signal molecule), respectively (Figures 6, 7 and Table 1). Conversely, the binding energies of CHA and MCHA with the RhlR was -31.19, -31.58 kcal/mol, respectively. Both of them were lower than -26.80 kcal/mol, the binding energy of the signal molecule (C4-HSL) with the RhlR. This result indicated that the docking of CHA and MCHA with the RhlR protein was stronger than that of the C4-HSL ligand. These findings suggest that CHA and MCHA predominantly target the RhlI/R system to inhibit QS in *P. aeruginosa*, consistent with the RT-qPCR results.

3.8 Synergistic anti-biofilm activity of CHA in combination with gentamicin

Due to its lowest FICI value, gentamicin was selected to investigate its potential synergistic anti-biofilm effects with CHA on *P. aeruginosa* PAO1. Given that the optimal blood concentration of gentamicin is 4–8 μg/mL, and its MIC against *P. aeruginosa* PAO1 was determined to be 4 μg/mL, half the optimal blood concentration (2 μg/mL) was used for subsequent experiments. Biofilm formation significantly contributes to pathogenic resistance. Here, crystal violet staining (Figure 8A) revealed that 2 μg/mL gentamicin alone had negligible impact on *P. aeruginosa* PAO1 biofilm formation, while 50 μg/mL CHA independently reduced biofilm formation by 13%. Notably, when the same concentration of gentamicin (2 μg/mL) and CHA (50 μg/mL) were used together, the *P. aeruginosa* PAO1 biofilm clearance rate reached 76%. Furthermore, CFU analysis obtained similar results (Figure 8B), showing a 90.7% reduction in viable bacteria in the biofilms, suggesting that CHA enhanced the anti-biofilm effects of gentamicin on *P. aeruginosa* PAO1. Consistently, SEM analysis (Figure 8C) illustrated that the DMSO group biofilms were dense and thick, with the 2 μg/mL gentamicin and 50 μg/mL CHA treatments alone showing no significant effect on biofilm clearance. In contrast, the combined gentamicin and CHA group

10.3389/fcimb.2024.1424038

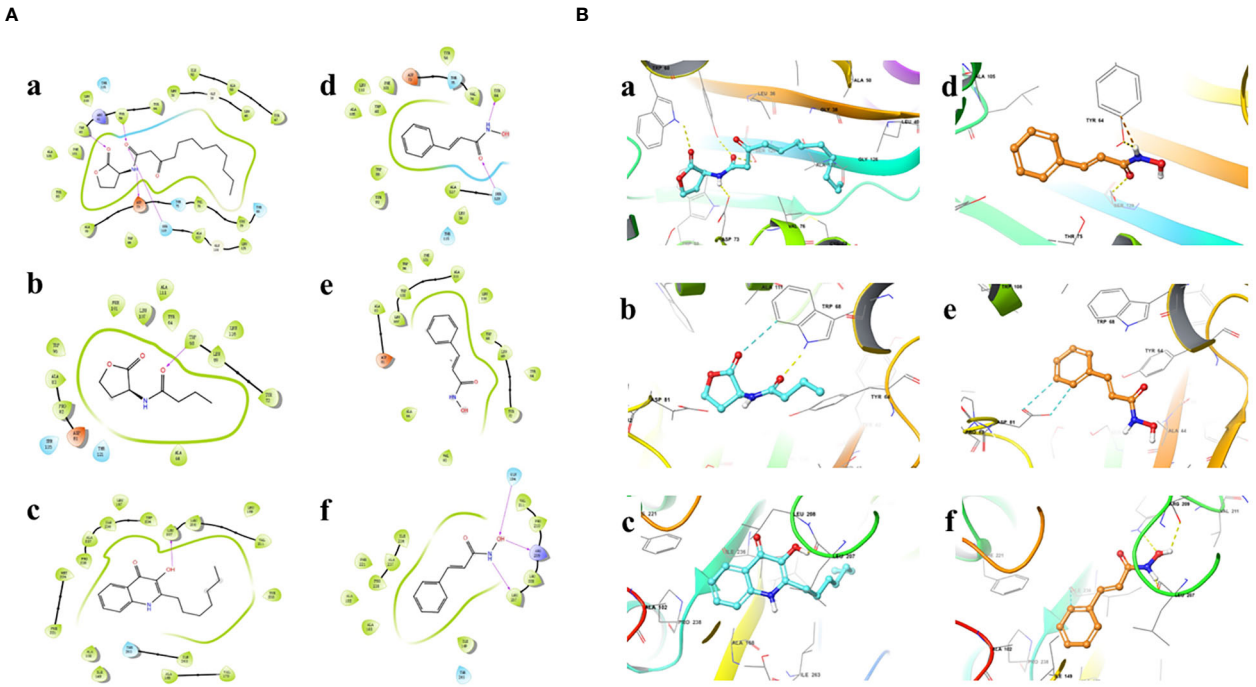

FIGURE 6
2D **(A)** and 3D **(B)** docking diagrams of receptor proteins LasR (a, d), RhlR (b, e), and PqsR (c, f) with 3-oxo-C12-HSL (a), C4-HSL (b), PQS (c), and CHA (d–f).

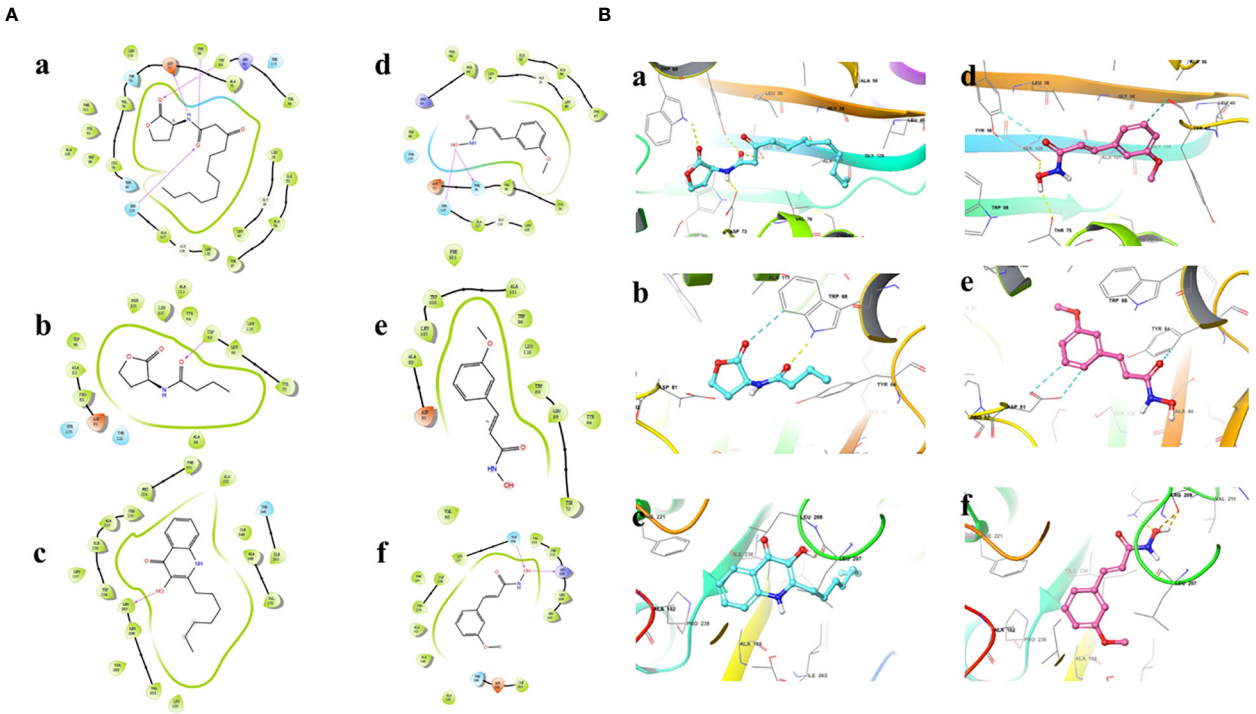

FIGURE 7
2D **(A)** and 3D **(B)** docking diagrams of receptor proteins LasR (a, d), RhlR (b, e) and PqsR (c, f) with 3-oxo-C12-HSL (a), C4-HSL (b), PQS (c), and MCHA (d–f).

TABLE 1 Binding energy of autoinducers, CHA, and MCHA to their target receptors and amino acid residues involved in their complex formation.

Receptors	Ligands	Hydrogen bonds	Aromatic H-Bond	Docking scores	ΔG(bind) kcal/mol
LasR	3-oxo-C12-HSL	Tyr56, Trp60, Asp73, Ser129	–	-9.631	-90.21
LasR	CHA	Tyr64, Ser129	–	-6.646	-42.47
LasR	MCHA	Thr75, Ser129	Tyr47, Tyr56	-6.906	-52.24
RhlR	C4-HSL	Trp68	Trp68	-5.327	-26.80
RhlR	CHA	–	Asp81	-6.426	-31.19
RhlR	MCHA	–	Asp81, Tyr64	-6.564	-31.58
PqsR	PQS	Leu207	–	-7.735	-51.38
PqsR	CHA	Gln194, Leu207, Arg209	–	-5.837	-35.89
PqsR	MCHA	Gln194, Arg209	–	-6.832	-36.86

showed a notable reduction in biofilms thinness and strength, allowing gentamicin more easily to penetrate and kill the bacteria, thus restoring the sensitivity of *P. aeruginosa* PAO1 to gentamicin.

4 Discussion

P. aeruginosa is one of the most clinically and epidemiologically important bacteria and a primary cause of catheter-related urinary tract infections and ventilator-associated pneumonia (Tenover et al., 2022). Of concern, its resistance to multiple antibiotics, such as tazobactam, carbapenems, fluoroquinolones, ceftazidime, aminoglycosides, and polymyxins, is increasing (de Lacerda Coriolano et al., 2021). Consequently, targeting QS has emerged as a new promising antibacterial strategy, which is capable of preventing the development of bacterial resistance and suppressing virulence factor production. In our previous works, we found four cinnamic acid derivatives exhibited inhibitory activities on QS (Cheng et al., 2020; Pan et al., 2022; Zhou et al., 2022). In this study, according to the drug-likeness analysis, a total of seven cinnamoyl hydroxamates were synthesized selectively. After QSI screenings against test strain ATCC 12472 and PAO1, CHA and MCHA showed excellent QS inhibitory effects against ATCC 12472 and PAO1, among which CHA showed more potent than MCHA bearing 3-methoxy. Unfortunately, four cinnamoyl hydroxamates bearing methoxy or hydroxy at *ortho*- or *para*-

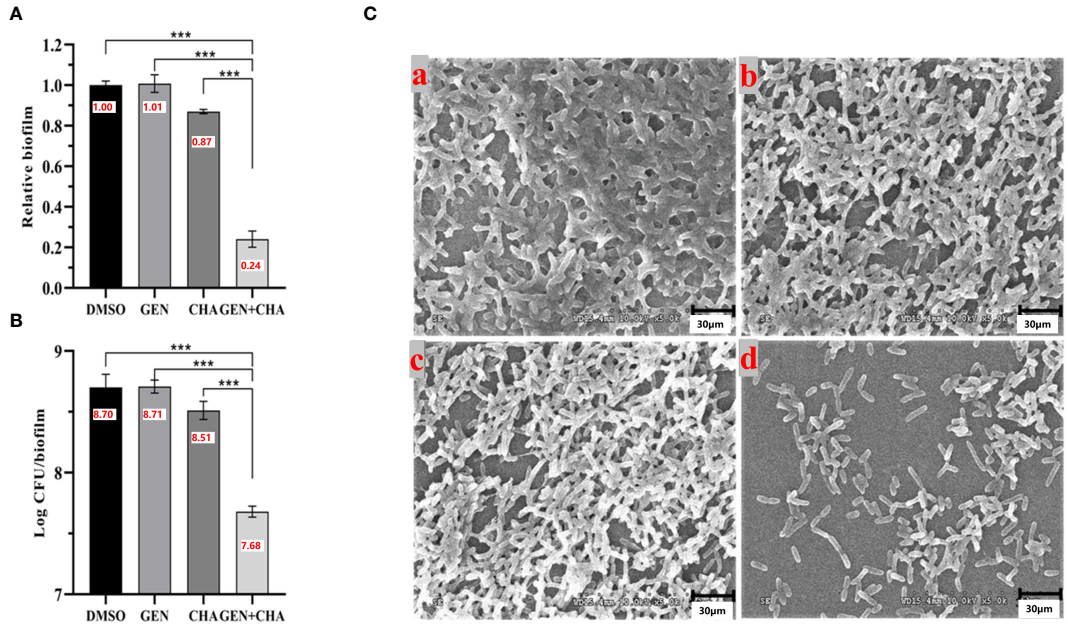

FIGURE 8
Destruction effects of CHA (50 μg/mL) and gentamicin (2 μg/mL) alone and in combination on *P. aeruginosa* PAO1 biofilms. **(A)** Crystal violet staining; **(B)** Log CFU/biofilms; **(C)** SEM images of formed biofilms of *P. aeruginosa* PAO1 treated with (a) DMSO, (b) 2 μg/mL gentamicin, (c) 50 μg/mL CHA, or (d) 2 μg/mL gentamicin and 50 μg/mL CHA, respectively. Data are presented as absorbance of mean ± SD of three independent experiments. ***$P < 0.001$ versus corresponding control by one-way ANOVA, n = 3.

position of phenyl showed weak or no QSI activities. Subsequently, two cinnamoyl hydroxamates bearing fluoro groups also showed no QSI activities against ATCC 12472 and PAO1.

Based on the above findings, we investigated the inhibitory effects of CHA and MCHA on the virulence factor production, motility, and biofilm formation in *P. aeruginosa* PAO1 at sub-MICs. The mechanisms by which CHA and MCHA impact QS systems were initially explored by detecting the mRNA levels of QS-related genes and conducting molecular docking analysis. Furthermore, the potential synergistic effects of combining CHA with gentamicin against PAO1 were investigated.

Many extracellular virulence factors in *P. aeruginosa*, such as pyocyanin, proteases, rhamnolipid, and siderophore, play crucial roles in its pathogenicity, invasive ability, and toxicity (Strateva and Mitov, 2011). Pyocyanin, a blue redox-active secondary metabolite regulated by the *rhl* QS system, inactivates catalase and modulates *L-glutathione* (GSH) redox cycling in lung cells. *In vivo* experiments have also indicated that the bacterial load of pyocyanin-deficient mutant strains is 1 000–10 000 lower than that of their respective wild-type counterparts (Lau et al., 2004; Morkunas et al., 2012). *P. aeruginosa* secretes multiple proteases, including elastase, which are under QS regulation and essential for survival within hosts. These proteases can damage host tissue and degrade host immunoglobulins (Pearson et al., 1997; Li and Lee, 2019; Aldawsari et al., 2021). Rhamnolipids, surfactant-active virulence factors in *P. aeruginosa*, facilitate immune cell and erythrocyte destruction, swarming and twitching motility, and biofilm formation (Laabei et al., 2014), with their production dependent on both the *rhl* system and *rhlAB* (encoding a rhamnosyltransferase) (Pearson et al., 1997). Siderophores are vital for acquiring iron, crucial for processes such as electron transport and DNA replication, and serve as key virulence factors in *P. aeruginosa*, significantly affecting biofilm formation and virulence (Jeong et al., 2023). Popat et al. (2017) reported that two major siderophores in *P. aeruginosa*, pyoverdine and pyochelin, are regulated by the *P. aeruginosa* QS quinolone signal molecule (PQS). Therefore, targeting virulence factor production offers a viable approach to combat *P. aeruginosa* infections. In this study, our results demonstrated that CHA and MCHA significantly inhibited pyocyanin, protease, elastase, rhamnolipid, and siderophore production, outperforming the efficacy of the positive control Hor. Notably, compared to the negative control, pyocyanin production was reduced to 5% after treatment with 200 μg/mL CHA or MCHA. These findings were supported by RT-qPCR analysis, showing significant down-regulation in the expression of genes regulating virulence factors (Ullah et al., 2017; Ahmed et al., 2019; Yang et al., 2021), including *phz*M (pyocyanin), *las*A (proteases), *las*B (elastase), *rhl*A/B (rhamnolipid), and *opr*l (outer membrane proteins) in *P. aeruginosa* PAO1 post-treatment with CHA or MCHA. These outcomes suggest that CHA and MCHA hold promise in attenuating the pathogenicity of *P. aeruginosa.*

Swimming and swarming motilities, regulated by the *las* and *rhl* QS systems in *P. aeruginosa* (Köhler et al., 2000; Sonbol et al., 2022), are important virulence traits. Swimming motility, driven by a single polar flagellum, is crucial for locating infection sites, while swarming motility, which relies on multiple flagella, plays an essential role in the early stage of biofilm establishment (Khan et al., 2020). In the current study, treatment with CHA and MCHA significantly reduced swimming and swarming motilities in *P. aeruginosa* PAO1 compared to the control group, suggesting that these compounds can effectively inhibit *P. aeruginosa* motility. These inhibitory effects were further confirmed by RT-qPCR analysis, which showed a decrease in the expression of motility-related genes *flh*F and *mot*D (Lee et al., 2011). Biofilms, complex structures composed of autogenic extracellular polymeric substances such as polysaccharides, extracellular DNA, proteins, and lipids, enable bacteria to survive adverse conditions, including antibiotic exposure and host immune responses (Vestby et al., 2020). Studies have shown that bacteria within biofilms exhibit resistance up to 1000 times greater than their planktonic counterparts. Known for its proficiency in forming biofilms, *P. aeruginosa* poses significant challenges in clinical environments due to this robust defense mechanism (Thi et al., 2020). In the present research, we found that both CHA and MCHA effectively eliminated formed biofilms in *P. aeruginosa*, by disrupting biofilm architecture, which leaded to a more dispersed and less cohesive structure. Additionally, treatment with CHA significantly reduced the expression of the *psl*A gene, which regulates the production of exopolysaccharides to provide structural support during the primary stage of biofilm formation (Colvin et al., 2012). The observed inhibitory effects on motility and biofilm formation suggest that CHA and MCHA may limit *P. aeruginosa* proliferation and reduce antibiotic resistance, highlighting their potential as candidate agents in treating *P. aeruginosa* infections.

QS is a communication system employed by bacterial populations to coordinate virulence gene expression, representing a promising new target for antimicrobial chemotherapy (Vattem et al., 2007). The pathogenicity of *P. aeruginosa* is mediated through its QS systems, notably the *las*, *rhl*, and *pqs* systems. Here, we explored the effects of CHA and MCHA on QS-regulated genes in *P. aeruginosa* PAO1, with RT-qPCR analysis revealing a marked down-regulation in the expression of QS-regulated genes *las*R, *rhl*R, *rhl*I, and *pqs*H following treatment. Among the QS systems, the *las* system is pivotal, orchestrating the activation of the *rhl* and *pqs* systems (Chadha et al., 2022). Notably, CHA and MCHA both induced the down-regulation of *lasR*. Ahmed et al. (2019) showed that *trans*-cinnamaldehyde effectively down-regulates *lasI* and *lasR* levels in *P. aeruginosa*, although the exact mechanism remains unclear. Maura et al. (2016) reported that PqsR controls *lasR* and *rhlR* expression during the early phases of bacterial growth, while RhlR suppresses (PqsR) the QS system during the late exponential and stationary phases. Ueda et al. (2009) also found that uracil can influence all three QS pathways in *P. aeruginosa*. We suspect that CHA and MCHA may influence the autoregulatory loops of the three QS systems or the uridine monophosphate (UMP) synthesis pathway, thereby reducing *lasR* levels. However, the specific mechanism needs to be explored in further studies.

Molecular docking calculations were performed to investigate the possible interactions between CHA or MCHA and receptors of QS signaling molecules in *P. aeruginosa* PAO1. The QS signaling molecules 3-oxo-C12-HSL, C4-HSL, and PQS, were docked against the LasR, RhlR, and PqsR receptors respectively (Kumar et al.,

2015). The *in silico* molecular docking results demonstrated that both CHA and MCHA could bind to LasR, RhlR, and PqsR, achieving high ligand-receptor docking scores with all three receptors. Notably, the CHA-RhlR and MCHA-RhlR complexes showed the highest docking scores, surpassing that of the natural autoinducer C4-HSL. Even though only aromatic and weaker H-bond interactions but no hydrogen bond was detected between CHA or MCHA with RhlR in *silico* docking analysis. We speculate the great matching degree between CHA or MCHA and RhlR might contribute lower binding energy between them. On the whole, these findings suggest that CHA and MCHA have the potential to act as potent inhibitors of LasR, RhlR, and PqsR, with particularly pronounced inhibitory effects against RhlR, potentially functioning as antagonists to these receptor signals.

Combinatorial therapies have garnered increasing attention due to their ability to target multiple therapeutic pathways (Vasudevan et al., 2018). Numerous QSIs have shown synergistic effects with antibiotics. For instance, Balaban et al. (2003) demonstrated that combining the RNAIII-inhibiting peptide (RIP) with conventional antibiotics completely eradicated *Staphylococcus epidermidis* infections *in vivo*. Roudashti et al. (2017) reported enhanced effectiveness of curcumin in combination with ceftazidime and ciprofloxacin against the QS system in *P. aeruginosa*. In our previous research, we highlighted the synergistic effects of various QSIs (Zhou et al., 2018b; Cheng et al., 2020; Pan et al., 2022; Xu et al., 2022). In this study, we found gentamicin (2 μg/mL) exhibited little effect on biofilms of *P. aeruginosa*, while CHA-alone (50 μg/mL) treatment only resulted in a slight decrease of biofilms. Nevertheless, it was notable that combinatorial administration of CHA (50 μg/mL) with gentamicin (2 μg/mL) significantly reduced biofilm formation and increased biofilm cell dispersal compared to individual treatments. Furthermore, CHA greatly enhanced the bactericidal effect of gentamicin on viable bacteria in the biofilms. These results suggest that CHA, acting as a QSI, may enhance the susceptibility of *P. aeruginosa* to gentamicin by disrupting its QS-regulated biofilms. Thus, combining CHA with gentamicin presents a promising alternative to current single-drug therapies. Our work would provide a new strategy for the prevention and treatment of *P. aeruginosa* in food, drinking water, public health, nosocomial infection and many other aspects. Unfortunately, for the clinical application of CHA and MCHA, much work remains to be performed in further study, such as their cytotoxicity in eukaryotic cells and the efficacy *in vivo*.

5 Conclusions

This study is the first to report the inhibitory effects of CHA and MCHA against the QS system in *P. aeruginosa*. Results showed CHA and MCHA inhibited the production of multiple virulence factors, including pyocyanin, proteases, rhamnolipid, and siderophore, and suppressed biofilm formation and swimming and swarming motilities in *P. aeruginosa*. Furthermore, CHA exhibited potent synergistic inhibitory effects with gentamicin on biofilm formation and biofilm cell dispersal. These results indicate that CHA and MCHA, as two novel QSIs, offer promising potential for treating *P. aeruginosa* infections and reducing its virulence.

Data availability statement

The original contributions presented in the study are included in the article/Supplementary Material. Further inquiries can be directed to the corresponding author.

Ethics statement

The manuscript presents research on animals that do not require ethical approval for their study.

Author contributions

DP: Data curation, Formal analysis, Investigation, Methodology, Software, Visualization, Writing – original draft, Writing – review & editing. HW: Investigation, Methodology, Software, Writing – review & editing. JL: Writing – original draft, Writing – review & editing. BW: Funding acquisition, Supervision, Writing – review & editing. AJ: Conceptualization, Funding acquisition, Investigation, Project administration, Resources, Supervision, Validation, Writing – review & editing.

Funding

The author(s) declare financial support was received for the research, authorship, and/or publication of this article. This work was supported by grants from the National Natural Science Foundation of China (82160664), Hainan Province Science and Technology Special Fund (ZDYF2024SHFZ103).

Conflict of interest

The authors declare that the research was conducted in the absence of any commercial or financial relationships that could be construed as a potential conflict of interest.

Publisher's note

Supplementary material

The Supplementary Material for this article can be found online at: https://www.frontiersin.org/articles/10.3389/fcimb.2024.1424038/full#supplementary-material

References

Ahmed, S. A. K. S., Rudden, M., Smyth, T. J., Dooley, J. S. G., Marchant, R., and Banat, I. M. (2019). Natural quorum sensing inhibitors effectively downregulate gene expression of *Pseudomonas aeruginosa* virulence factors. *Appl. Microbiol. Biot.* 103, 3521–3535. doi: 10.1007/s00253-019-09618-0

Aldawsari, M. F., Khafagy, E. S., Saqr, A. A., Alalaiwe, A., Abbas, H. A., Shaldam, M. A., et al. (2021). Tackling virulence of *Pseudomonas aeruginosa* by the natural furanone sotolon. *Antibiotics* 10, 871. doi: 10.3390/antibiotics10070871

Balaban, N., Giacometti, A., Cirioni, O., Gov, Y., Ghiselli, R., Mocchegiani, F., et al. (2003). Use of the quorum-sensing inhibitor rnaiii-inhibiting peptide to prevent biofilm formation *in vivo* by drug-resistant staphylococcus epidermidis. *J. Infect. Dis.* 187, 625–630. doi: 10.1086/345879

Berman, H. M., Westbrook, J., Feng, Z., Gilliland, G., Bhat, T. N., Weissig, H., et al. (2000). The protein data bank. *Nucleic Acids Res.* 28, 235–242. doi: 10.1093/nar/28.1.235

Chadha, J., Harjai, K., and Chhibber, S. (2022). Repurposing phytochemicals as anti-virulent agents to attenuate quorum sensing-regulated virulence factors and biofilm formation in *Pseudomonas aeruginosa*. *Microb. Biotechnol.* 15, 1695–1718. doi: 10.1111/1751-7915.13981

Cheng, W. J., Zhou, J. W., Zhang, P. P., Luo, H. Z., Tang, S., Li, J. J., et al. (2020). Quorum sensing inhibition and tobramycin acceleration in *Chromobacterium violaceum* by two natural cinnamic acid derivatives. *Appl. Microbiol. Biot.* 104, 5025–5037. doi: 10.1007/s00253-020-10593-0

CLSI. (2021). *Performance Standards for Antimicrobial Susceptibility Testing. 31st ed. CLSI supplement M100.* (Clinical and Laboratory Standards Institute).

Colvin, K. M., Irie, Y., Tart, C. S., Urbano, R., Whitney, J. C., Ryder, C., et al. (2012). The Pel and Psl polysaccharides provide *Pseudomonas aeruginosa* structural redundancy within the biofilm matrix. *Environ. Microbiol.* 14, 1913–1928. doi: 10.1111/j.1462-2920.2011.02657.x

Defoirdt, T. (2018). Quorum-sensing systems as targets for antivirulence therapy. *Trends. Microbiol.* 26, 313–328. doi: 10.1016/j.tim.2017.10.005

de Lacerda Coriolano, D., de Souza, J. B., Bueno, E. V., Medeiros, S. M. F. R. D. S., Cavalcanti, I. D. L., and Cavalcanti, I. M. F. (2021). Antibacterial and antibiofilm potential of silver nanoparticles against antibiotic-sensitive and multidrug-resistant *Pseudomonas aeruginosa* strains. *Braz. J. Microbiol.* 52, 267–278. doi: 10.1007/s42770-020-00406-x

Essar, D. W., Eberly, L., Hadero, A., and Crawford, I. P. (1990). Identification and characterization of genes for a second anthranilate synthase in *Pseudomonas aeruginosa*: interchangeability of the two anthranilate synthases and evolutionary implications. *J. Bacteriol.* 172, 884–900. doi: 10.1128/jb.172.2.884-900.1990

Grosso-Becerra, M. V., González-Valdez, A., Granados-Martínez, M. J., Morales, E., Servín-González, L., Méndez, J. L., et al. (2016). *Pseudomonas aeruginosa* ATCC 9027 is a non-virulent strain suitable for mono-rhamnolipids production. *Appl. Microbiol. Biot.* 100, 9995–10004. doi: 10.1007/s00253-016-7789-9

Ham, S. Y., Kim, H. S., Jo Min, J., Lee, J. H., Byun, Y., Ko, G. J., et al. (2021). Combined treatment of 6-Gingerol analog and tobramycin for inhibiting *Pseudomonas aeruginosa* infections. *Microbiol. Spectr.* 9, e00192–e00121. doi: 10.1128/Spectrum.00192-21

Harder, E., Damm, W., Maple, J., Wu, C., Reboul, M., Xiang, J. Y., et al. (2016). OPLS3: A force field providing broad coverage of drug-like small molecules and proteins. *J. Chem. Theory Comput.* 12, 281–296. doi: 10.1021/acs.jctc.5b00864

Jeong, G. J., Khan, F., Khan, S., Tabassum, N., Mehta, S., and Kim, Y. M. (2023). *Pseudomonas aeruginosa* virulence attenuation by inhibiting siderophore functions. *Appl. Microbiol. Biot.* 107, 1019–1038. doi: 10.1007/s00253-022-12347-6

Khan, F., Pham, D. T. N., Oloketuyi, S. F., and Kim, Y. M. (2020). Regulation and controlling the motility properties of *Pseudomonas aeruginosa*. *Appl. Microbiol. Biot.* 104, 33–49. doi: 10.1007/s00253-019-10201-w

Köhler, T., Curty Lasta, K., Barja, F., van Delden, C., and Pechère, J. C. (2000). Swarming of *Pseudomonas aeruginosa* is dependent on cell-to-cell signaling and requires flagella and pili. *J. Bacteriol.* 182, 5990–5996. doi: 10.1128/JB.182.21.5990-5996.2000

Kumar, L., Chhibber, S., Kumar, R., Kumar, M., and Harjai, K. (2015). Zingerone silences quorum sensing and attenuates virulence of *Pseudomonas aeruginosa*. *Fitoterapia* 102, 84–95. doi: 10.1016/j.fitote.2015.02.002

Laabei, M., Jamieson, W. D., Lewis, S. E., Diggle, S. P., and Jenkins, A. T. A. (2014). A new assay for rhamnolipid detection-important virulence factors of *Pseudomonas aeruginosa*. *Appl. Microbiol. Biot.* 98, 7199–7209. doi: 10.1007/s00253-014-5904-3

Lau, G. W., Hassett, D. J., Ran, H., and Kong, F. (2004). The role of pyocyanin in *Pseudomonas aeruginosa* infection. *Trends. Mol. Med.* 10, 599–606. doi: 10.1016/j.molmed.2004.10.002

Lee, J. H., Cho, M. H., and Lee, J. (2011). 3-Indolylacetonitrile decreases *Escherichia coli* O157:H7 biofilm formation and *Pseudomonas aeruginosa* virulence. *Environ. Microbiol.* 13, 62–73. doi: 10.1111/j.1462-2920.2010.02308.x

Lee, J., and Zhang, L. (2015). The hierarchy quorum sensing network in *Pseudomonas aeruginosa*. *Protein Cell* 6, 26–41. doi: 10.1007/s13238-014-0100-x

Li, X. H., and Lee, J. H. (2019). Quorum sensing-dependent post-secretional activation of extracellular proteases in *Pseudomonas aeruginosa*. *J. Biol. Chem.* 294, 19635–19644. doi: 10.1074/jbc.RA119.011047

Liu, Y. N., Zhang, Y. F., Xu, Q., Qiu, Y., Lu, Q. B., Wang, T., et al. (2023). Infection and co-infection patterns of community-acquired pneumonia in patients of different ages in China from 2009 to 2020: a national surveillance study. *Lancet Microbe* 4, e330–e339. doi: 10.1016/S2666-5247(23)00031-9

Maura, D., Hazan, R., Kitao, T., Ballok, A. E., and Rahme, L. G. (2016). Evidence for direct control of virulence and defense gene circuits by the *Pseudomonas aeruginosa* quorum sensing regulator, MvfR. *Sci. Rep.* 6, 34083. doi: 10.1038/srep34083

McLean, R. J. C., Pierson, L. S., and Fuqua, C. (2004). A simple screening protocol for the identification of quorum signal antagonists. *J. Microbiol. Meth.* 58, 351–360. doi: 10.1016/j.mimet.2004.04.016

Merritt, J. H., Kadouri, D. E., and O'Toole, G. A. (2011). Growing and analyzing static biofilms. *Curr. Protoc. Microbiol.* 22, 1B.1.1–1B.1.18. doi: 10.1002/9780471729259.mc01b01s22

Mladenovic-Antic, S., Kocic, B., Velickovic-Radovanovic, R., Dinic, M., Petrovic, J., Randjelovic, G., et al. (2016). Correlation between antimicrobial consumption and antimicrobial resistance of *Pseudomonas aeruginosa* in a hospital setting: a 10-year study. *J. Clin. Pharm. Ther.* 41, 532–537. doi: 10.1111/jcpt.12432

Morkunas, B., Galloway, W. R. J. D., Wright, M., Ibbeson, B. M., Hodgkinson, J. T., O'Connell, K. M. G., et al. (2012). Inhibition of the production of the *Pseudomonas aeruginosa* virulence factor pyocyanin in wild-type cells by quorum sensing autoinducer-mimics. *Org. Biomol. Chem.* 10, 8452–8464. doi: 10.1039/c2ob26501j

Nam, S., Ham, S. Y., Kwon, H., Kim, H. S., Moon, S., Lee, J. H., et al. (2020). Discovery and characterization of pure rhlr antagonists against *Pseudomonas aeruginosa* infections. *J. Med. Chem.* 63, 8388–8407. doi: 10.1021/acs.jmedchem.0c00630

Pan, D., Wang, X. Y., Zhou, J. W., Yang, L., Khan, A., Wei, D. Q., et al. (2022). Virulence and biofilm inhibition of 3-methoxycinnamic acid against Agrobacterium tumefaciens. *J. Appl. Microbiol.* 133, 3161–3175. doi: 10.1111/jam.15774

Pearson, J. P., Pesci, E. C., and Iglewski, B. H. (1997). Roles of *Pseudomonas aeruginosa* las and rhl quorum-sensing systems in control of elastase and rhamnolipid biosynthesis genes. *J. Bacteriol.* 179, 5756–5767. doi: 10.1128/jb.179.18.5756-5767.1997

Popat, R., Harrison, F., da Silva, A. C., Easton, S. A. S., McNally, L., Williams, P., et al. (2017). Environmental modification *via* a quorum sensing molecule influences the social landscape of siderophore production. *P. R. Soc B-Biol. Sci.* 284, 20170200. doi: 10.1098/rspb.2017.0200

Prithiviraj, B., Bais, H. P., Weir, T., Suresh, B., Najarro, E. H., Dayakar, B. V., et al. (2005). Down regulation of virulence factors of *Pseudomonas aeruginosa* by salicylic acid attenuates its virulence on *Arabidopsis thaliana* and *Caenorhabditis elegans*. *Infect. Immun.* 73, 5319–5328. doi: 10.1128/IAI.73.9.5319-5328.2005

Rashid, M. H., and Kornberg, A. (2000). Inorganic polyphosphate is needed for swimming, swarming, and twitching motilities of *Pseudomonas aeruginosa*. *Proc. Natl. Acad. Sci. U. S. A.* 97, 4885–4890. doi: 10.1073/pnas.060030097

Roudashti, S., Zeighami, H., Mirshahabi, H., Bahari, S., Soltani, A., and Haghi, F. (2017). Synergistic activity of sub-inhibitory concentrations of curcumin with ceftazidime and ciprofloxacin against *Pseudomonas aeruginosa* quorum sensing related genes and virulence traits. *World J. Microb. Biot.* 33, 50. doi: 10.1007/s11274-016-2195-0

Sonbol, F., El-Banna, T., Elgaml, A., Aboelsuod, K. M., and Microbiology, A. (2022). Impact of quorum sensing system on virulence factors production in *Pseudomonas aeruginosa*. *Pure. Appl. Microbio.* 16, 1226–1238. doi: 10.22207/JPAM

Soukarieh, F., Williams, P., Stocks, M. J., and Cámara, M. (2018). *Pseudomonas aeruginosa* quorum sensing systems as drug discovery targets: Current position and future perspectives. *J. Med. Chem.* 61, 10385–10402. doi: 10.1021/acs.jmedchem.8b00540

Strateva, T., and Mitov, I. (2011). Contribution of an arsenal of virulence factors to pathogenesis of *Pseudomonas aeruginosa* infections. *Ann. Microbiol.* 61, 717–732. doi: 10.1007/s13213-011-0273-y

Tang, J., Wang, W., and Chu, W. (2020). Antimicrobial and anti-quorum sensing activities of phlorotannins from seaweed (*Hizikia fusiforme*). *Front. Cell. Infect. Microbio.* 10, 586750. doi: 10.3389/fcimb.2020.586750

Tenover, F. C., Nicolau, D. P., and Gill, C. M. (2022). Carbapenemase-producing *Pseudomonas aeruginosa* –an emerging challenge. *Emerg. Microbes Infect.* 11, 811–814. doi: 10.1080/22221751.2022.2048972

Thi, M. T., Wibowo, D., and Rehm, B. H. A. (2020). *Pseudomonas aeruginosa* biofilms. *Int. J. Mol. Sci.* 21, 8671. doi: 10.3390/ijms21228671

Ueda, A., Attila, C., Whiteley, M., and Wood, T. K. (2009). Uracil influences quorum sensing and biofilm formation in *Pseudomonas aeruginosa* and fluorouracil is an antagonist. *Microb. Biotechnol.* 2, 62–74. doi: 10.1111/j.1751-7915.2008.00060.x

Ullah, W., Qasim, M., Rahman, H., Jie, Y., and Muhammad, N. (2017). Beta-lactamase-producing *Pseudomonas aeruginosa*: Phenotypic characteristics and

molecular identification of virulence genes. *J. Chin. Med. Assoc.* 80, 173–177. doi: 10.1016/j.jcma.2016.08.011

Usachova, N., Leitis, G., Jirgensons, A., and Kalvinsh, I. (2010). Synthesis of hydroxamic acids by activation of carboxylic acids with N,N′-carbonyldiimidazole: Exploring the Efficiency of the Method. *Synthetic Commun.* 40, 927–935. doi: 10.1080/00397910903026723

Vasudevan, S., Swamy, S. S., Kaur, G., Princy, S. A., and Balamurugan, P. (2018). Synergism between quorum sensing inhibitors and antibiotics: combating the antibiotic resistance crisis. *Biotechnol. Appl. Quorum Sens. Inhibitors*, 209–225. doi: 10.1007/978-981-10-9026-4_10

Vattem, D. A., Mihalik, K., Crixell, S. H., and McLean, R. J. C. (2007). Dietary phytochemicals as quorum sensing inhibitors. *Fitoterapia* 78, 302–310. doi: 10.1016/j.fitote.2007.03.009

Vestby, L. K., Grønseth, T., Simm, R., and Nesse, L. L. (2020). Bacterial biofilm and its role in the pathogenesis of disease. *Antibiotics* 9, 59. doi: 10.3390/antibiotics9020059

Wiegand, I., Hilpert, K., and Hancock, R. E. W. (2008). Agar and broth dilution methods to determine the minimal inhibitory concentration (MIC) of antimicrobial substances. *Nat. Protoc.* 3, 163–175. doi: 10.1038/nprot.2007.521

Xu, K. Z., Tan, X. J., Chang, Z. Y., Li, J. J., and Jia, A. Q. (2022). 2-tert-butyl-1,4-benzoquinone, a food additive oxidant, reduces virulence factors of *Chromobacterium violaceum*. *LWT* 163, 113569. doi: 10.1016/j.lwt.2022.113569

Yan, J., Yue, K., Fan, X., Xu, X., Wang, J., Qin, M., et al. (2023). Synthesis and bioactivity evaluation of ferrocene-based hydroxamic acids as selective histone deacetylase 6 inhibitors. *Eur. J. Med. Chem.* 246, 115004. doi: 10.1016/j.ejmech.2022.115004

Yang, D., Hao, S., Zhao, L., Shi, F., Ye, G., Zou, Y., et al. (2021). Paeonol attenuates quorum-sensing regulated virulence and biofilm formation in *Pseudomonas aeruginosa*. *Front. Microbiol.* 12, 692474. doi: 10.3389/fmicb.2021.692474

Yin, L., Shen, W., Liu, J. S., and Jia, A. Q. (2022). 2-Hydroxymethyl-1-methyl-5-nitroimidazole, one siderophore inhibitor, occludes quorum sensing in *Pseudomonas aeruginosa*. *Front. Cell Infect. Microbiol.* 12, 955952. doi: 10.3389/fcimb.2022.955952

Zagni, C., Citarella, A., Oussama, M., Rescifina, A., Maugeri, A., Navarra, M., et al. (2019). Hydroxamic acid-based histone deacetylase (hdac) inhibitors bearing a pyrazole scaffold and a cinnamoyl linker. *Int. J. Mol. Sci.* 20, 945. doi: 10.3390/ijms20040945

Zeng, Y. X., Liu, J. S., Wang, Y. J., Tang, S., Wang, D. Y., Deng, S. M., et al. (2022). Actinomycin D: a novel *Pseudomonas aeruginosa* quorum sensing inhibitor from the endophyte *Streptomyces cyaneochromogenes* RC1. *World J. Microb. Biot.* 38, 170. doi: 10.1007/s11274-022-03360-y

Zhou, J. W., Chen, T. T., Tan, X. J., Sheng, J. Y., and Jia, A. Q. (2018b). Can the quorum sensing inhibitor resveratrol function as an aminoglycoside antibiotic accelerant against *Pseudomonas aeruginosa*? *Int. J. Antimicrob. Agents* 52, 35–41. doi: 10.1016/j.ijantimicag.2018.03.002

Zhou, J. W., Ji, P. C., Jiang, H., Tan, X. J., and Jia, A. Q. (2022). Quorum sensing inhibition and metabolic intervention of 4-hydroxycinnamic acid against *Agrobacterium tumefaciens*. *Front. Microbiol.* 13, 83063. doi: 10.3389/fmicb.2022.830632

Zhou, J. W., Luo, H. Z., Jiang, H., Jian, T. K., Chen, Z. Q., and Jia, A. Q. (2018a). Hordenine: A novel quorum sensing inhibitor and antibiofilm agent against *Pseudomonas aeruginosa*. *J. Agric. Food Chem.* 66, 1620–1628. doi: 10.1021/acs.jafc.7b05035

frontiers | Frontiers in Cellular and Infection Microbiology

TYPE Original Research
PUBLISHED 15 August 2024
DOI 10.3389/fcimb.2024.1406429

OPEN ACCESS

EDITED BY
Maria Gabriela Paraje,
National University of Cordoba, Argentina

REVIEWED BY
Nora Lía Padola,
National University of Central Buenos Aires, Argentina
Alumine Fessia,
National University of Río Cuarto, Argentina

*CORRESPONDENCE
Hongwei Chen
dyxchw@swu.edu.cn
Hongzao Yang
yhz03008@swu.edu.cn

†These authors have contributed equally to this work

RECEIVED 25 March 2024
ACCEPTED 26 July 2024
PUBLISHED 15 August 2024

CITATION
Liu L, Li H, Ma C, Liu J, Zhang Y, Xu D, Xiong J, He Y, Yang H and Chen H (2024) Effect of anti-biofilm peptide *CRAMP-34* on the biofilms of *Acinetobacter lwoffii* derived from dairy cows.
Front. Cell. Infect. Microbiol. 14:1406429.
doi: 10.3389/fcimb.2024.1406429

Effect of anti-biofilm peptide *CRAMP-34* on the biofilms of *Acinetobacter lwoffii* derived from dairy cows

Lin Liu[1,2†], Hui Li[1,2,3†], Chengjun Ma[1,2], Jingjing Liu[1,2], Yang Zhang[2,4], Dengfeng Xu[2,4], Jing Xiong[2,4], Yuzhang He[1,3], Hongzao Yang[1,2,5*] and Hongwei Chen[1,2,3,5*]

[1]College of Veterinary Medicine, Southwest University, Chongqing, China, [2]National Center of Technology Innovation for Pigs, Chongqing, China, [3]Immunology Research Center, Medical Research Institute, Southwest University, Chongqing, China, [4]Chongqing Academy of Animal Sciences, Chongqing, China, [5]Traditional Chinese Veterinary Research Institute, Southwest University, Chongqing, China

Dairy mastitis is one of the most common diseases in dairy farming, and the formation of pathogenic bacteria biofilms may be an important reason why traditional antibiotic therapy fails to resolve some cases of dairy mastitis. We isolated and identified three strains of *A. lwoffii* were with strong biofilm forming ability from dairy cow mastitis samples from Chongqing dairy farms in China. In order to investigate the effect of novel anti-biofilm peptide CRAMP-34 on *A.lwoffii* biofilms, the anti-biofilm effect was evaluated by crystal violet staining, biofilms viable bacteria counting and confocal laser scanning microscopy (CLSM). In addition, transcriptome sequencing analysis, qRT-PCR and phenotypic verification were used to explore the mechanism of its action. The results showed that CRAMP-34 had a dose-dependent eradicating effect on *A. lwoffii* biofilms. Transcriptome sequencing analysis showed that 36 differentially expressed genes (11 up-regulated and 25 down-regulated) were detected after the intervention with the sub-inhibitory concentration of CRAMP-34. These differentially expressed genes may be related to enzyme synthesis, fimbriae, iron uptake system, capsular polysaccharide and other virulence factors through the functional analysis of differential genes. The results of subsequent bacterial motility and adhesion tests showed that the motility of *A.lwoffii* were enhanced after the intervention of CRAMP-34, but there was no significant change in adhesion. It was speculated that CRAMP-34 may promote the dispersion of biofilm bacteria by enhancing the motility of biofilm bacteria, thereby achieving the effect of eradicating biofilms. Therefore, these results, along with our other previous findings, suggest that CRAMP-34 holds promise as a new biofilm eradicator and deserves further research and development.

KEYWORDS

dairy mastitis, anti-biofilm peptide, *Acinetobacter lwoffii*, biofilms, transcriptomic

1 Introduction

Mastitis is a common disease with high incidence in dairy cows, which seriously affects the health and economic value of dairy cows and is generally caused by pathogenic microorganisms. The most-frequently isolated bacteria in milk samples were *Escherichia coli*, *Streptococcus* spp., and *Klebsiella* spp (Krebs et al., 2023). In recent years, the isolation rate of *Acinetobacter lwoffii* was high in some dairy farms in China (Cui et al., 2024), but it did not attract enough attention. However, *A. lwoffii* is an opportunistic pathogen in patients with impaired immune systems, and which strong biofilm forming ability (Regalado et al., 2009; Pour et al., 2011; Xu et al., 2013). The establishment of biofilms depends on the ability of bacteria to attach to bovine mammary epithelial cells, and mastitis bacteria growing on biofilms are more resistant to antimicrobials (Cerioli et al., 2018).The ability of pathogens to form biofilms in the mammary gland would be a potential source of persistent or chronic infections (Vasudevan et al., 2003). In addition, the ability to invade mammary epithelial cells and the survival of bacteria in the cells are also related to the pathogenesis of persistent mastitis (Cerioli et al., 2018).

Although antibiotics have played a role in the treatment of cow mastitis, the problem of antibiotic residues and drug resistance has been troubling clinical veterinarians (Liu et al., 2024). Antimicrobial peptides are known as new antibiotic substitutes and have attracted much attention (Xia et al., 2021), mainly because they have a low potential to induce *de novo* resistance and have favorable penetration and inhibition of biofilms (Li et al., 2023; Masihzadeh et al., 2023; Wongchai et al., 2024). Some antimicrobial peptides show excellent effects in anti-biofilms, which are also known as anti-biofilm peptides (de la Fuente-Nunez and Hancock, 2015; Ghoreishi et al., 2022). Our previous studies have shown that the murine antimicrobial peptide CRAMP-34 inhibits biofilm formation and eradicates the preformed biofilms of the biofilms model strain *Pseudomonas aeruginosa* PAO1 (Zhang et al., 2022; Wang et al., 2023). Our extensive experiments have confirmed that CRAMP-34 is an excellent anti-biofilm peptide, and it can also delay the development of other antibiotic (colistin and ciprofloxacin) resistance (Wang et al., 2023). However, whether CRAMP-34 has the same inhibitory effect on *A. lwoffii* biofilms is yet to be clarified.

In the current study, we observed the effect of CRAMP-34 on *A. lwoffii* biofilms with strong biofilm-forming ability isolated from milk samples by crystal violet (CV) staining, biofilm viable bacteria counting and confocal laser scanning microscopy (CLSM). In addition, transcriptome sequencing analysis, qRT-PCR and phenotypic verification were used to explore the mechanism of its action. This work has significant implications for developing new antibiotic alternatives, reducing bacterial resistance and maintaining animal health and food safety.

2 Materials and methods

2.1 Strains and growth conditions

Three strains of *A. lwoffii were* isolated from clinical samples of dairy cow mastitis, and mastitis milk samples were from three dairy farms including Liangjiang Dairy Farm of Chongqing Tianyou Zongheng Animal Husbandry Development Co., Ltd. Briefly, the bacteria from the cow mastitis samples were first isolated using a dilution coating, then, the isolated single colony bacteria were purified using the conventional repetitive streaking technique (Chen et al., 2023). Finally, the purified single colony bacteria were used the universal primers 27F (5 ‘ -AGAGTTTGAT CMTGGCTCAG-3 ′) and 1492R (5 ′ -TACGGYTACCTTGTTAC GACTT-3 ′) as primers for 16 S rDNA amplification (GenBank: PP783574.1), the amplified products were tested by agarose gel electrophoresis and sent to Beijing Qingke Biotechnology Co., Ltd. for strain identification (Zhang et al., 2024). The identified *A. lwoffii* was mixed evenly in 60% glycerol broth and stored in -80 °C. *A. lwoffii* were removed from -80°C, incubated overnight at 37°C on Luria-Bertani (LB) agar plates, individual colonies were picked and incubated at 37°C in LB nutrient broth to log growth phase, and resuspended to 1×10^5- 10^6 Colony-Forming Units (CFU)/mL as the test bacterial solution (Koti et al., 2024).

2.2 The antimicrobial resistance analysis of *A. lwoffii*

Seven common antimicrobials (ampicillin, cefquinime, tetracycline, amikacin, ciprofloxacin, kanamycin, and gentamicin) were selected for the antimicrobial resistance analysis of *A. lwoffii*, which were commonly used in the prevention and treatment of mastitis in dairy cows and effective against gram-negative bacteria. The minimum inhibitory concentration (MIC) value of different classes of antimicrobials was determined using the microbroth dilution method recommended by the Clinical and Laboratory Standards Institute 2017 (CLSI 2017). Briefly, the bacterial solution was incubated overnight until the logarithmic growth phase was reached, and the bacterial solution concentration was measured at a UV spectrophotometer at a wavelength of 600 nm at 1×10^5-10^6 CFU/mL, the drug serially diluted with LB broth was then added to the 96-well plate, and finally add the resuspended bacterial solution, while making a negative control of the broth and the drug, and incubate in a 37°C incubator for 16-18 h. *In vitro A. lwoffii* biofilms were performed in 96-well plates, 100 μL of resuspended bacterial solution was added to each well, and the lid was closed and incubated in a 37°C incubator for 24 h. Then each well was washed twice gently with PBS (pH=7.4), and added the medicine diluted in advance with LB broth (dilution range was 256 MIC-1/4 MIC) and incubated at 37°C for 3 h. The optimal action time of CRAMP-34 to clear the biofilms screened in the previous experiment, which is consistent with it here for easy control. The biomass of biofilms were assayed, as described previously with minor modifications (Ma et al., 2024). The supernatant was discarded, sterile phosphate-buffered saline (PBS) was added to wash 3 times, 100 μL of 99% methanol was added to each well for 10 min to fix, followed by air drying, 0.04% CV staining was added to each well for 20 min, then the CV was gently washed 3 times with sterile PBS after aspiration, and then 100 was added μL of 33% acetic acid solution was dissolved for 30 min, absorbance values were measured at optical density 590 nm (OD_{590} nm), and the experiment was replicated 3 times independently.

2.3 Analysis of CRAMP-34's ability to eradicate biofilms

CRAMP-34 (GLLRKGGEKIGEKLKKIGQKIKNFFQKL VPQPEQ) was tested for the effect of eradicating on biofilms using the positive peptide LL-37 and ciprofloxacin lactate as a control (CRAMP-34 and LL-37 were purchased from synthesized by ChinaPeptides Co., Ltd., Shanghai, China, and other antibacterial drugs were purchased from Shanghai Maclean's Biochemical Technology Co., Ltd., Shanghai Yuanye Biotechnology Co., Ltd., and Meilun Biotechnology Co., Ltd., respectively). The above prepared bacterial solution was added to a 96-well cell culture plate and incubated in a 37°C incubator for 24 h pre-biofilms. Afterwards, the plates were washed three times with PBS. Next, 100 μL of each concentration of CRAMP-34, LL-37, and ciprofloxacin diluted with broth were added to the plate and incubated at 37°C for 3 h (8 MIC-1/2 MIC, CRAMP-34: 31.2 μg/mL, 15.60 μg/mL, 7.80 μg/mL, 3.90 μg/mL, 1.95μg/mL, LL-37: 15.60 μg/mL, 7.80 μg/mL, 3.90 μg/mL, 1.95 μg/mL, 0.975 μg/mL. Ciprofloxacin: 2.00 μg/mL, 1.00 μg/mL, 0.50 μg/mL, 0.25 μg/mL, 0.125 μg/mL). The biomass of biofilms was determined by CV staining method, and trypticase soy agar plates (TSA) were used to count viable bacteria as previously described with minor modifications (Zhang et al., 2022; Wang et al., 2023). Briefly, CV (0.04%) was added in biofilms samples for 20 min, and washing with sterile PBS. Then, 33% acetic acid was used to dissolve the bound CV, and absorbance was measured at OD_{590} nm. Meanwhile, bacteria count assay was used to analyze the number of bacteria in biofilms, the mature biofilms were treated with the above drugs for 3 h, the supernatant was discarded, PBS buffer was washed 3 times, 100 μL of 0.1% Triton-100X was added, pipetting and mixing were mixed to fully dissolve the biofilms, and 20 μL was piped to the pre-added 180 according to the results of the pre-test, select an appropriate concentration gradient to draw 20 μL dropped on the plate, then set the plate upright for a few minutes, wait for the liquid to dry, and then placed it in a 37°C constant temperature incubator overnight to record the number of bacteria, and follow the principle of regular gradient reduction of each gradient (Zhang et al., 2022; Wang et al., 2023).

2.4 Confocal laser scanning microscopy to observe the structure of the biofilms

CLSM is used to observe the three-dimensional image (3D) structure of biofilms as described in previous studies with some modifications (Zhang et al., 2022). In this experiment, 100 μL of test bacterial solution (OD_{600} = 0.1, 1×10^5- 10^6 CFU/mL) was added to a detachable microplate plate, incubated at 37°C for 24 h, and the biofilms were treated with CRAMP-34 at 37°C for 3 h. The biofilms were rinsed with NaCl (0.9% wt/vol) and stained with the Filmtracer™ LIVE/DEAD™ Biofilm Viability Kit (L10316, Molecular Probes, Thermo Fisher Scientific) in the dark for 20 min. Biofilm samples were rinsed with sterile water and then treated with a CLSM (CLSM-800; Zeiss GmbH, Oberkochen, Germany) with Plan-Apochromat 63x/1.40 oil objective. Signals were recorded with the green channel (SYTO9, excitation wavelength 488 nm) and the red channel (PI, excitation wavelength 561 nm). Multiple images with different Z-stacks are superimposed to form a 3D. Images were acquired using ZEN (black version) software. Each experiment was repeated at least three times. BiofilmQ software was used to analyze the fluorescence intensity, number of biofilms, volume, substrate area, surface area and other parameters, and the removal effect of CRAMP-34 on *A. lwoffii* biofilms were comprehensively evaluated.

2.5 RNA-seq and qRT-PCR validation

As mentioned above, the three test groups were set up in six-well cell culture plates, the first group was preformed biofilms grown in LB broth, the second group was *A. lwoffii* grown in LB broth (planktonic bacteria), the third group was the biofilms of the preformed biofilms formed after 24 h of LB broth culture treated with 3 h treatment of CRAMP at 1/2 MIC (3.90 μg/mL) concentration. The biofilm samples were washed three times with the same volume of NaCl solution, and added the pre-cooled NaCl solution, scraping with a cell scraper, the planktonic bacteria and cell scraper scraping samples were snap frozen and stored in liquid nitrogen, collected samples from three independent replicates of each group, entrusted Beijing Ovisen Gene Technology Co., Ltd. to complete high-throughput sequencing. Expression levels of genes were analyzed using DESeq software. The threshold for gene expression was expressed as FPKM values (0.1 or 1), and only genes with FPKM> 1 were analyzed in this study. The Kyoto Encyclopedia of Genes and Genomes (KEGG) pathways and Gene Ontology (GO) analysis were performed for the different genes. 7 representative differential genes related to biofilm were selected for qRT-PCR verification using 16S rRNA as the internal reference gene. Primers for qRT-PCR were designed by Invitrogen Inc. (Carlsbad, CA, USA) and listed in Supplementary Materials (Supplementary Table S1). The RNA extraction and cDNA synthesis were performed using the method of Roudashti and Zhou et al. with some modifications (Roudashti et al., 2017; Zhou et al., 2018). Experiments were repeated at least three times. The relative expression levels of each target gene were detected by $2^{-\Delta\Delta Ct}$ method.

2.6 Effect of CRAMP-34 on motility and adhesion of *A. lwoffii*

Transcriptomic analysis found that the expression of some genes related to bacterial pili was up-regulated or down-regulated after the action of CRAMP-34, and the up-regulation or down-regulation of some other genes related to enzymes and proteins also indirectly affected the changes in bacterial motility. Therefore, the effect of CRAMP-34 on the motility and adhesion of bacteria was next verified.

The method of counting bacteria in the upper layer of the biofilms was as described earlier (Zhang et al., 2022; Wang et al., 2023). Here, we increase the bacterial count of the upper layer of

other concentrations of the drug that has been carried out to the control for bacterial number changes.

A.lwoffii is a type of flagellate-free bacteria whose movement is mainly achieved through the movement of fimbriae, so we verified its twitch movement on a motile agar plate. In the previous experiment, we explored that the most suitable agar concentration for *A. lwoffii* movement was with an agar concentration of 0.1% LB. As mentioned above, we collected the biofilm bacteria, and took 10 μL of vertical and gentle drops on the surface of the agar, and gently moved to a 37°C constant temperature incubator for 48 h when the bacterial solution was slightly volatile and dry and did not flow on the surface (Long et al., 2024).

We took the above-mentioned prepared and enriched biofilm bacteria, diluted them 100 times, and put 100 μL into a new sterile 96-well plate for the control group and the CRAMP-34 intervention group, respectively. Three biological replicates were set for each group. Then, the samples were covered with plastic wrap and cultured in a constant temperature incubator at 37 °C for 3-4 h. After the incubation, the waste liquid was removed, and samples were gently washed twice with PBS, then biofilms were dissolved with 0.1% Triton. Then the number of adherent bacteria was measured by plate colony counting method (Long et al., 2024).

2.7 Statistical analyses

Data were analyzed by GraphPad Prism 8.0 software. Student's t-tests were used to calculate the statistical significance. $P < 0.05$ was considered statistically significant.

3 Results

3.1 Isolation and identification of bacteria from bovine mastitis samples

All samples were isolated and purified to obtain 32 main pathogens, and the morphological characteristics of the pathogenic bacteria were observed (Supplementary Figure 1), and then 16S rDNA amplification was carried out and sent to Beijing Qingke Biotechnology Co., Ltd. for strain identification, and the results showed that there were 13 species of pathogenic bacteria, mainly *Staphylococcus aureus*, *Streptococcus*, *E. coli*, *P. aeruginosa*, *A. lwoffii*, etc. (Table 1).

TABLE 1 Species and proportion of main pathogens detected in bovine mastitis samples.

Species of pathogenic bacteria	Number of detected strains	Detection rate (%)
Staphylococcus aureus	5	15.63
Other staphylococci	2	6.25
Streptococcus	1	3.13
Escherichia coli	5	15.63
Klebsiella pneumoniae	4	12.5
Pseudomonas aeruginosa	3	9.38
Acinetobacter lwoffii	3	9.38
Bacillus cloacillus	3	9.38
Other bacteria	6	18.75

3.2 Antibiotic sensitivity analysis of *A. lwoffii*

Antibiotic sensitivity analysis of *A. lwoffii* planktonic cells were showed in Table 2. The results showed that *A. lwoffii* planktonic cells were sensitive to most of the selected antibiotics. However, it is worth noting that these antibiotics do not have a significant ability to eradicate the biofilms, even have the ability to promote the formation of the biofilms at certain concentrations (Figure 1).

3.3 CRAMP-34 has an eradicating effect on preformed biofilms of *A. lwoffii*

The results showed that the effect of CRAMP-34 on the preformed biofilms of *A. lwoffii* was time- and concentration-dependent, with the higher the concentration, the more significant the eradication effect (Figure 2). After 3 h of intervention with CRAMP-34, the inhibition rate reached a very significant state, and there was little difference compared with the intervention of 4 h or 5 h. So, 3 h was adopted as the optimal intervention time in follow-up studies. In addition, compared with the commonly used antibiotics ciprofloxacin and human AMP LL-37. The results showed that CRAMP-34 had a more significant antibiofilm effect on *A. lwoffii* biofilms, including biomass and viable bacteria of biofilms (Figure 3).

To observe the anti-biofilm activity of CRAMP-34, CLSM was applied after live (SYTO 9) and dead (PI) staining of *A. lwoffii* biofilms (Figures 4A–F). The results showed that at a concentration of 15.625 μg/mL, CRAMP-34 extremely decreased *A. lwoffii* biofilms with a reduction in the number, volume, and area of biofilms number (P <0.001), and the number, volume, and area of *A. lwoffii* biofilms were markedly decreased by CRAMP-34 at the concentration of 7.8125 μg/ml (P <0.05). There was no significant difference in red fluorescence between the two groups under the condition of 15.625 μg/mL, the basal surface of the biofilms was positively and significantly decreased (P <0.001), and there was no significant difference in the basal area of the biofilms after the intervention of 7.8125 μg/mL (Figures 4G–K).

3.4 Transcriptome analysis

The volcano map and Venn diagram were plotted according to the criteria for differential gene screening qvalue<0.05 (Figure 5). Compared with the planktonic *A. lwoffii*, there are 84 differentially expressed genes (66 up-regulated and 18 down-regulated) in the *A. loffii* biofilm group, which are mainly involved in the regulation of amino acid biosynthesis and metabolism, biological membrane composition and the composition of ionic transmembrane

10.3389/fcimb.2024.1406429

TABLE 2 Antibiotic sensitivity analysis of *A. lwoffii*.

The class of the drug	Drug concentration (μg/mL)	MIC(μg/mL)	Sensitivity
β-lactams	Ampicillin (256)	4-8	S
	Cefquinime (32)	0.063-0.132	S
	Ceftiofur (256)	1-2	S
	Meropenem (2)	0.008	S
Aminoglycosides	Streptomycin (2048)	32	S
	Kanamycin (32)	0.063-0.125	S
Ampramycin (32)	0.125-0.25	S	S
Gentamicin (16)	0.016	S	
Tetracyclines	Tetracycline (256)	2	S
Macrolides	Roxithromycin (2048)	8	S
	Azithromycin (256)	0.5-1	S
Amide alcohols	Florfenicol (2048)	16	I
other	Enrofloxacin (256)	1-2	S
	Ciprofloxacin (8)	0.25	S
	Polymyxin (32)	0.25	S
	Amika star (2)	0.031-0.063	S
	Rifampicin (2)	0.031-0.063	S

S, sensitive; I, intermediate; R, resistant.

transporter. The group of CRAMP-34 treated *A. lwoffii* biofilms had 36 differentially expressed genes compared to the untreated group (11 up-regulated and 25 down-regulated), which mainly affected RNA metabolism, polysaccharide biosynthesis, ion binding, transmembrane transporter activity. The histogram of GO enrichment and clustering heatmap of differentially expressed genes was showed in Supplementary Figures 2 and Figure 3. According to the analysis of differential genes, CRAMP-34 may play a role on eradicating the biofilms through the following pathways, including enzyme synthesis, pili, iron uptake system, capsular polysaccharides and other related virulence genes (Table 3). Some genes related to biofilm were selected for verification by fluorescence quantitative PCR, and the fluorescence quantification results were consistent with the omics results (Figure 6A).

3.5 Validation of motility related phenotypes of *A. lwoffii* by CRAMP-34

The results showed that under the intervention of high concentration of CRAMP-34, the number of live bacteria in the upper layer was smaller than that in the control group. The number of viable bacteria was more than 99% less than that in the control group at the concentration of 4 MIC (1.64 Log_{10} CFU/Well reduction). The number of viable bacteria decreased by 0.14 Log_{10} CFU/Well when the concentration of 2 MIC was applied, and the number of viable bacteria was almost unchanged at the concentration of 1 MIC (decreased by 0.03 Log_{10} CFU/Well). However, when the subinhibitory concentration interfered with the biofilms, the bacteria in the upper layer began to increase, increasing by 0.15 Log_{10} CFU/Well at both 1/2 MIC and 1/4 MIC concentrations (Figure 6B).

On the surface of the soft agar, the diameter of the convulsive movement of the bacteria reflects the strength of the bacterial motility after the drug intervention. The results showed that the diameter of bacterial movement after CRAMP-34 treatment was 1.76 times that of control group (P <0.01) (Figure 6C).

The adhesion of biofilm bacterial was reflected by the number of bacteria adhering to the 96-well plate over the same time period, and the results showed no significant difference in the adhesion of

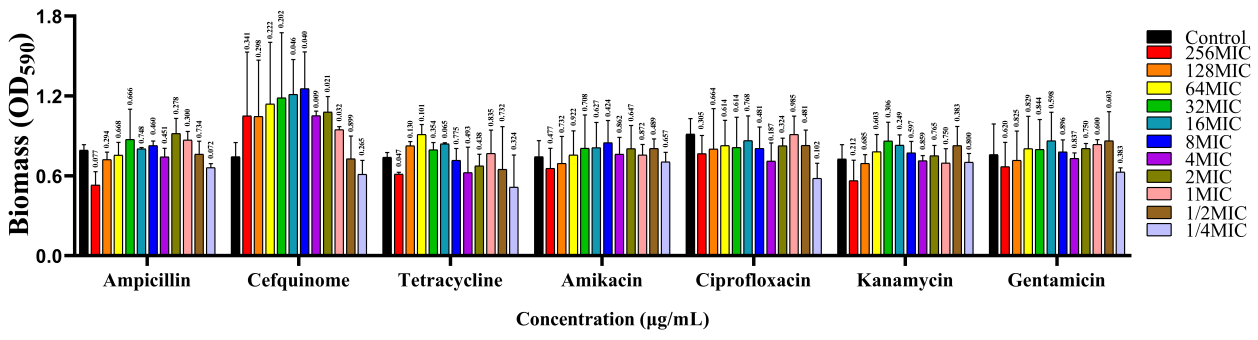

FIGURE 1
Analysis of antimicrobial resistance of *A. lwoffii* biofilm bacteria. 0, 1/4 MIC, 1/2 MIC, 1 MIC, 2 MIC, 4 MIC, 8 MIC (MIC, minimal inhibitory concentration), respectively, Ampicillin, cefquinime, tetracycline, amikacin, ciprofloxacin, kanamycin, and gentamicin at 16 MIC, 32 MIC, 64 MIC, 128 MIC, and 256 MIC were used to measure OD_{600nm} in *A. lwoffii* biofilms, and OD_{600nm} were used to quantify the biofilms using CV-0.04%. The trial was replicated three times independently. Student's t-tests were used to calculate the statistical significance. $P < 0.05$ was considered statistically significant.

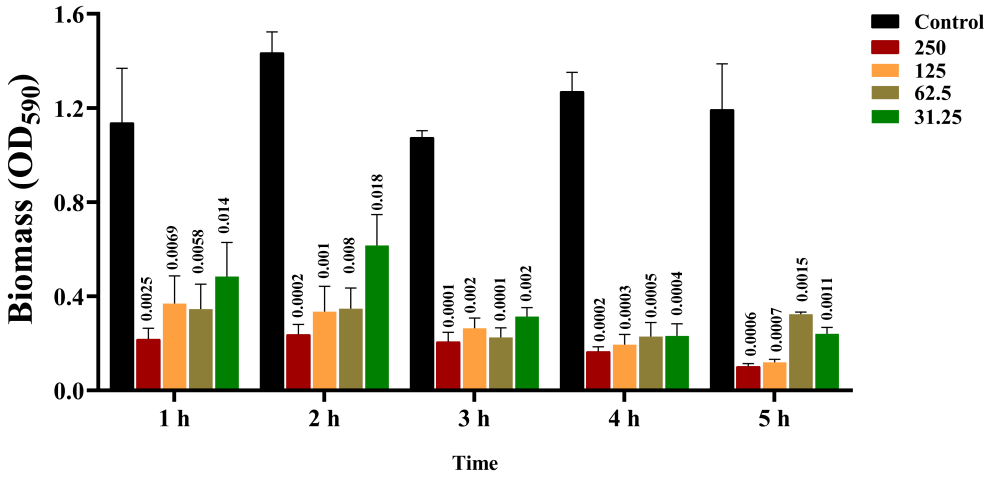

FIGURE 2
Screening results of CRAMP-34 with optimal action time. 0 μg/mL, 31.25 μg/mL, 62.5 μg/mL, 125 μg/were used at 1 h, 2 h, 3 h, 4 h, and 5 h, respectively. mL and 250 μg/mL of CRAMP-34 were treated with *A. lwoffii* biofilm and quantified using 0.04% crystal violet stainin (CV-0.04%). The trial was replicated 3 times independently. Student's t-tests were used to calculate the statistical significance. $P < 0.05$ was considered statistically significant.

biofilm bacterial after the application of CRAMP-34 compared to the control group ($P > 0.05$) (Figure 6D).

4 Discussion

The formation of biofilms by bacteria has led to the reduction or even ineffectiveness of traditional antibiotics against bacterial infections, which poses a serious challenge to the human and animal health industry (Rather et al., 2021). Bovine mastitis is the most influential disease in the dairy industry, but due to the irrational use of antibiotics in the breeding industry in the past, many dairy cow mastitis pathogens have developed drug resistance, making the recurrence of dairy cow mastitis incurable, and it is urgent to find drugs that can replace traditional antibiotics (El-Sayed and Kamel, 2021). In this study, we isolated and identified 13 pathogenic bacteria from 21 samples of dairy cow mastitis, mainly including *S. aureus*, *E. coli*, *Streptococcus*, *P. aeruginosa*, *A. lwoffii* and *Klebsiella pneumoniae*, indicating that a variety of conditionally pathogenic bacteria are becoming the main pathogens of mastitis in dairy cows. Biofilm bacterial infection leads to the development of various chronic infectious diseases (Zhang et al., 2021), biofilm infection plays a key role in mastitis in dairy cows, and continued treatment with conventional antibiotics is associated with an increased risk of drug resistance, which makes the clinical treatment of bovine mastitis a great challenge (Pedersen et al., 2021).

We identified the film-forming ability of the main pathogenic organisms by CV staining, and screened out 3 strains of *A. lwoffii* with strong biofilm-forming ability. At the same time, it was also found that the biofilm formation ability of *A. lwoffii* was the strongest among all isolates. It is important to note that *A. lwoffii*

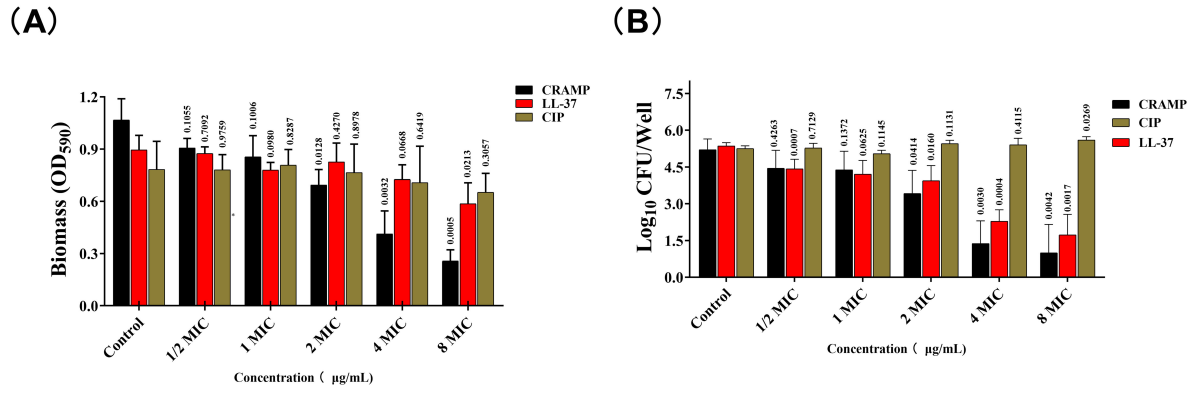

FIGURE 3
CRAMP-3 inhibits the biofilm activity of *A. lwoffii*. **(A)** Crystal violet staining (CV) was used to determine the biofilm of *A. lwoffii* treated with different concentrations (1/2 MIC-8MIC) of CRAMP-34, ciprofloxacin and LL-37. **(B)** Plate colony count (CC) was used to determine the number of viable biofilms of *A. lwoffii* treated with different concentrations (1/2 MIC-8 MIC) of CRAMP-34, ciprofloxacin, and LL-37. The test was repeated 3 times independently. Student's t-tests were used to calculate the statistical significance. $P < 0.05$ was considered statistically significant.

10.3389/fcimb.2024.1406429

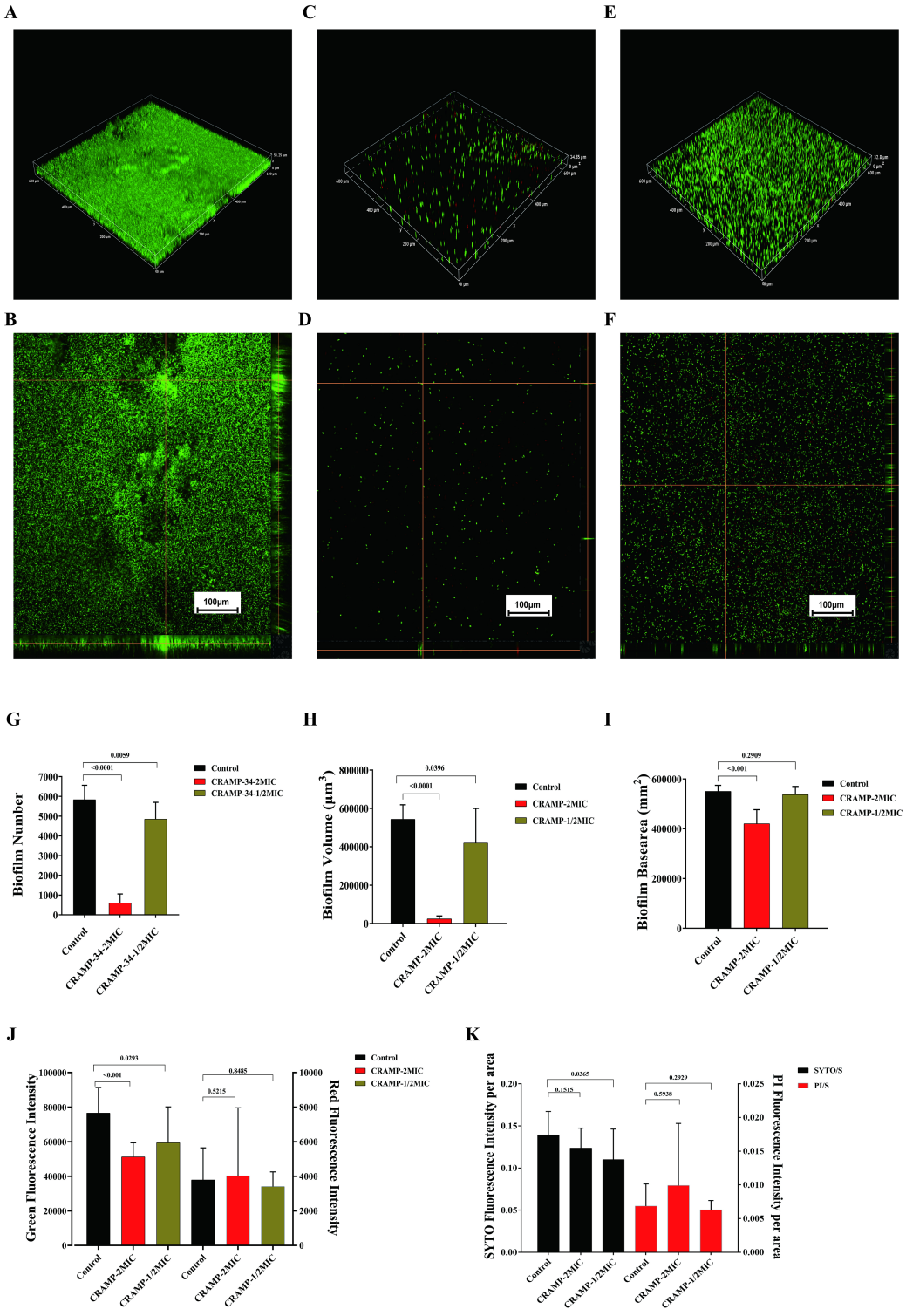

FIGURE 4
CLSM imaging of *A. lwoffii* before and after CRAMP-34 treatment. **(A, B)** 20× confocal laser scanning microscopy (CLSM) in three-dimensional image (3D) and orthogonal plots of the control group. **(C, D)** 20×CLSM 3D and orthogonal plots of CRAMP-34 treatment group at 2 MIC concentrations. **(E, F)** 3D and orthogonal plots of CRAMP-34 treatment group at 1/2 MIC concentrations of 20× CLSM. **(G)** Number of *A. lwoffii* biofilms treated with CRAMP-34 at 2 MIC and 1/2 MIC concentrations. **(H)** *A. lwoffii* biofilm volume after CRAMP-34 treatment with 2 MIC and 1/2 MIC concentrations. **(I)** Basal area of *A. lwoffii* biofilm after CRAMP-34 treatment with 2 MIC and 1/2 MIC concentrations. **(J)** Fluorescence intensity of *A. lwoffii* biofilm after treatment with cramp-34 at 2 mic and 1/2 mic concentrations. **(K)** Area ratio of *A. lwoffii* bioenvelope after CRAMP-34 treatment with 2 MIC and 1/2 MIC. The images were taken from three random shooting fields in three independent replicate experiments, and the fluorescence intensity, biofilm volume, and biofilm substrate area were analyzed and processed by the open-source software Biofilm Q. Statistical analysis was performed using Prism 8.0 software. One-way ANOVA and LSD multiple test were used to calculate the statistical significance.

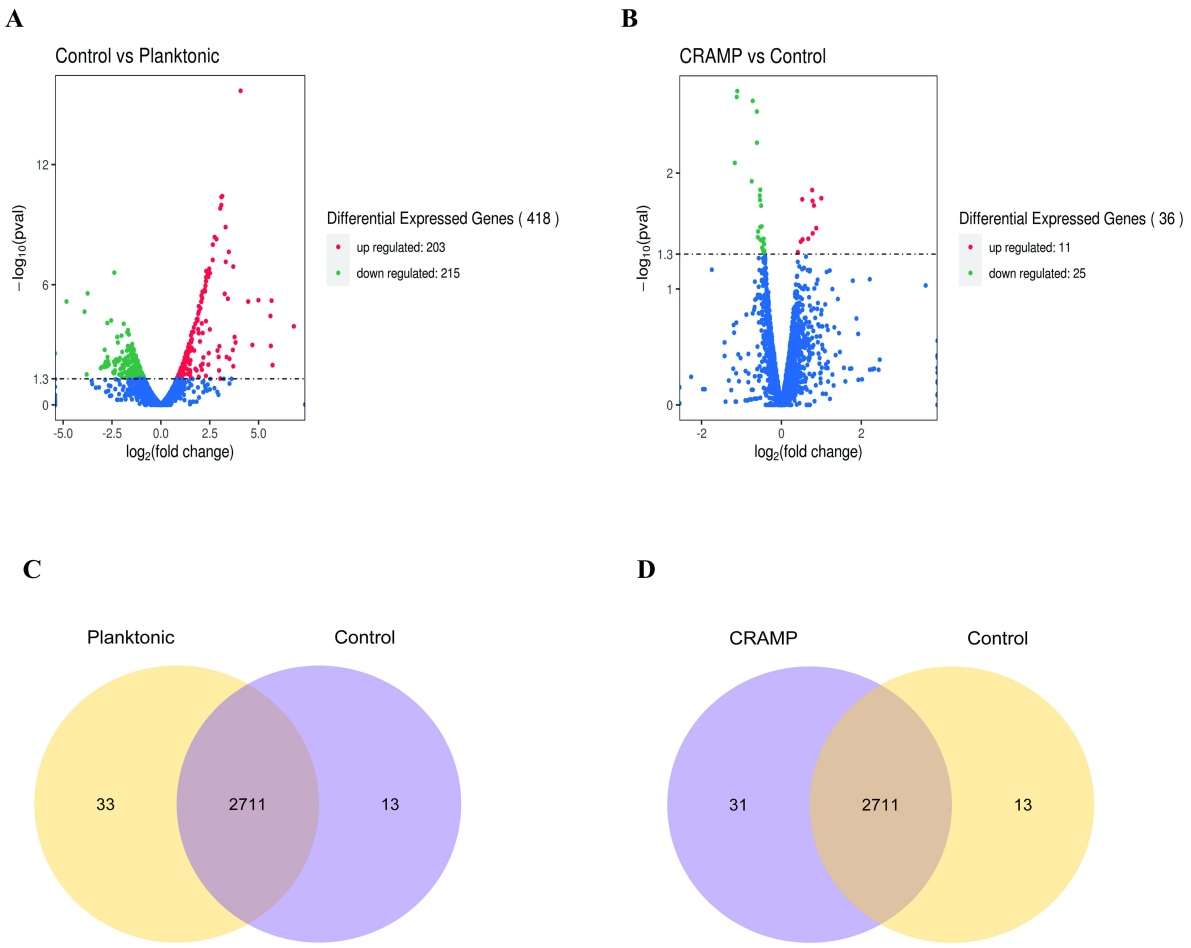

FIGURE 5
Differential genes in *A. lwoffii* biofilm before and after CRAMP-34 treatment. **(A)** Volcanic diagram of differential genes between *A. lwoffii* biofilm control group and plankton group. **(B)** Differential genes in *A lwoffii* biofilm before and after 1/2 MIC CRAMP-34 treatment. The red dots indicate genes whose expression is upregulated, the green dots indicate genes whose expression is downregulated, and the blue dots indicate genes whose expression has not changed significantly. **(C, D)** Venn diagram of association analysis of differentially expressed genes between groups.

belongs to the genus *Acinetobacter*, a ubiquitous conditionally pathogenic bacterium that is a normal microflora of the normal skin, oropharynx, and perineum (Ku et al., 2000), which is increasingly reported as a pathogen associated with nosocomial infections such as sepsis, pneumonia, meningitis, urinary tract infections, cutaneous, gastroenteritis, and wound infections (Rakitin et al., 2021). Studies have shown that *A. lwoffii* is a potentially drug-resistant flora, but there are few studies on the resistance mechanism of its bacterial biofilms (Elham and Fawzia, 2019). Subsequently, we selected drugs that are commonly used in clinical practice for the treatment of mastitis and effective against gram-negative bacteria, and carried out antimicrobial resistance analysis against the planktonic bacteria and biofilm bacteria of *A. lwoffii*. The results showed that planktonic *A. lwoffii* were sensitive to most antibiotics, but the higher concentration of some antibiotics not only can not eradicate the biofilms, in some concentrations even promote the formation of biofilms. It has been reported in the literature that antibiotics can stimulate and promote the formation of bacterial biofilms, and sub-inhibitory concentrations of antibiotics may even lead to the formation of thicker bacterial biofilms (Wu et al., 2014). In addition, it was reported that antimicrobial drugs may regulate the physiological state of bacteria by regulating the expression of genes, stimulate bacterial toxicity, and cause serious disease infections (Gao et al., 2022). These highlights the urgent need to develop alternatives to antibiotics to combat infections caused by bacterial biofilms.

At present, there are few studies on the mechanism of drug resistance of *A. lwoffii*, but it has aroused attention in the field of human medicine, and should be paid more attention to its harm in the field of veterinary medicine. In order to combat the harm of bacterial resistance, many researchers are committed to finding alternatives to traditional antibiotics, among which anti-biofilm peptides are an ideal alternative (Luo and Song, 2021). At present, the anti-biofilm peptide LL-37 discovered in human has been widely used in antimicrobial studies (Golla et al., 2020). In our previous research, we reported CRAMP-34 obtained by modifying murine anti-biofilm peptides has a strong ability to clear biofilm (Zhang et al., 2022). In this study, it was showed that CRAMP-34 was better than the positive peptide LL-37 in eradicating the preformed biofilms, while ciprofloxacin and gentamicin had

TABLE 3 Biofilm-related genes of differentially expressed.

Gene name	Gene ID	product	Log2FC
Translation of GTPases			
typA	ctg_00616_gene	GTP-binding protein TypA/BipA	-0.43194
lepA	ctg_00952_gene	Elongation factor 4	-0.42244
cysN	ctg_01982_gene	Sulfate adenylyltransferase subunit 1	-0.44659
Pimbima genes			
pilE	ctg_00334_gene	Fimbrial protein	-0.42754
Iron uptake system			
–	ctg_01636_gene	NADPH oxidoreductase	-1.1659
*desA*3_2	ctg_01635_gene	NADPH-dependent stearoyl-CoA 9-desaturase	-1.1178
*sodB*_1	ctg_01069_gene	Superoxide dismutase [Mn/Fe]	0.99968
Virulence-related genes			
*ptk*_2	ctg_00080_gene	Tyrosine-protein kinase ptk	-0.44302
deaD	ctg_00400_gene	ATP-dependent RNA helicase DeaD	-0.61323
putA	ctg_01526_gene	Bifunctional protein PutA	-0.455
pitA	ctg_02031_gene	Low-affinity inorganic phosphate transporter 1	-0.61193
other			
betB	01421	NAD/NADP-dependent betaine aldehyde dehydrogenase	2.881
otsB	02085	Trehalose-6-phosphate phosphatase	2.0008
yidC	02799	Membrane protein insertase YidC	-2.0796
rcsC-3	02286	Sensor histidine kinase RcsC	1.7063

almost no effect on the biofilms, which indicated that traditional antimicrobial drugs did have limitations in eradicating the preformed biofilms. Subsequently, after expanding the culture system in 6-well cell culture plates, it was found that CRAMP-34 still had a significant effect on clearing the biofilms even under the condition of sub-inhibitory concentration, indicating that CRAMP-34 had obvious ability to remove *A. lwoffii* biofilms in a certain concentration range. These results indicated that CRAMP-34 had a strong ability to eradicate *A. lwoffii* biofilms, and the eradication ability was concentration-dependent. The results of CLSM also showed that CRAMP-34 eradicated *A. lwoffii* biofilms mainly by reducing the number and volume of biofilms, but the relevant mechanism was still unclear. Considering the safety and efficacy of CRAMP-34, we chose a lower effective concentration to carry out a follow-up study, i.e., CRAMP-34 at 1/2 MIC.

In order to better explore the mechanism of eradicating biofilms by CRAMP-34, we investigated differentially expressed genes by transcriptome sequencing. By analyzing the transcriptome sequencing results, we found that compared with the control group, there were 84 differentially expressed genes in the planktonic cells group, which were mainly involved in the regulation of amino acid metabolism in biological processes and ion transmembrane transport in molecular functions. There were 36 significantly different genes in the sub-inhibitory concentration of CRAMP-34 intervention group, and the genes related to the biofilm were classified and sorted, and it was found that the sub-inhibitory concentration of CRAMP-34 mainly regulated the gene expression of enzyme synthesis, pili, iron uptake system, virulence genes and other pathways after intervening in the biofilm of *A. lwoffii*. Subsequently, through in-depth analysis of differential genes, we found a number of significantly differential genes that mainly regulate enzyme and protein synthesis, proteins are the bearers of functions in life activities, and their synthesis depends on several translational GTPases (trGTPases), and in this study, three down-regulated genes regulate the synthesis of this class of enzymes, namely the *typA* (BipA) protein regulated by *typA* genes elongation factor 4 regulated by the l*epA* gene and CysN (adenosyl transferase sulfate subunit 1) regulated by the *cysN* gene. According to Goh et al., BipA is an invert protease that is implicated in bacterial motility, cold shock, stress response, biofilm formation, and toxicity (Goh et al., 2021), BipA can regulate the formation of actin bases in host epithelial cells, flagellar-mediated motility and resistance to host defense mechanisms, suggesting that BipA in bacteria is not only a translating factor, but also a key factor in regulating stress adaptation and pathogenicity (DeLivron and Robinson, 2008). Studies have shown that the BipA protein increases virulence and decreases flagellar-mediated bacterial viability (Grant et al., 2003), and in the study of Eunsil Choi et al., BipA-deleted strains had high motility on plates (Choi and Hwang, 2018). Therefore, we hypothesized that the motility of *A. lwoffii* was also altered after the intervention of CRAMP-34, and our subsequent bacterial motility test also confirmed this hypothesis. In addition, BipA can directly or indirectly regulate the transcription of capsular or LPS-related genes (Choi et al., 2020), and among the differentially expressed genes we screened, ptk-2, which is associated with capsular polysaccharide production, was also significantly down-regulated (Hua et al., 2017), with capsular polysaccharides produced by bacteria that can push bacteria to more trophic and oxygen-rich places and kill competitors *ptk*-encoded tyrosine kinase can promote the synthesis of capsular polysaccharides (Hibbing et al., 2010), which produce adhesin and favor bacterial colonization (Zhu et al., 2022). In this study, *ptk*_2 down-regulation may indicate a decrease in capsular polysaccharide production, resulting in a reduction in the extracellular matrix, which is consistent with the results of our CV experiments treated with CRAMP-34. LepA, a ribosome-associated GTPs enzyme found in bacteria, mitochondria, and chloroplasts, is important for the stability and abundance of many membrane-associated proteins, including Mémpoin MspA, which is involved in nutrient absorption and is essential for drug sensitivity (Fishbein et al., 2020). Hanqing Liu et al. reported that LepA is a highly conserved protein that plays a crucial role in bacterial growth and functional protein synthesis under specific conditions, and is structurally similar to EF-G transferase (Liu et al., 2011). Studies have shown that knocking out the lepA gene can improve the survival rate of *E. coli* when treated with antimicrobial drugs (Li et al., 2014), and in our study, the lepA gene was down-regulated in the CRAMP-

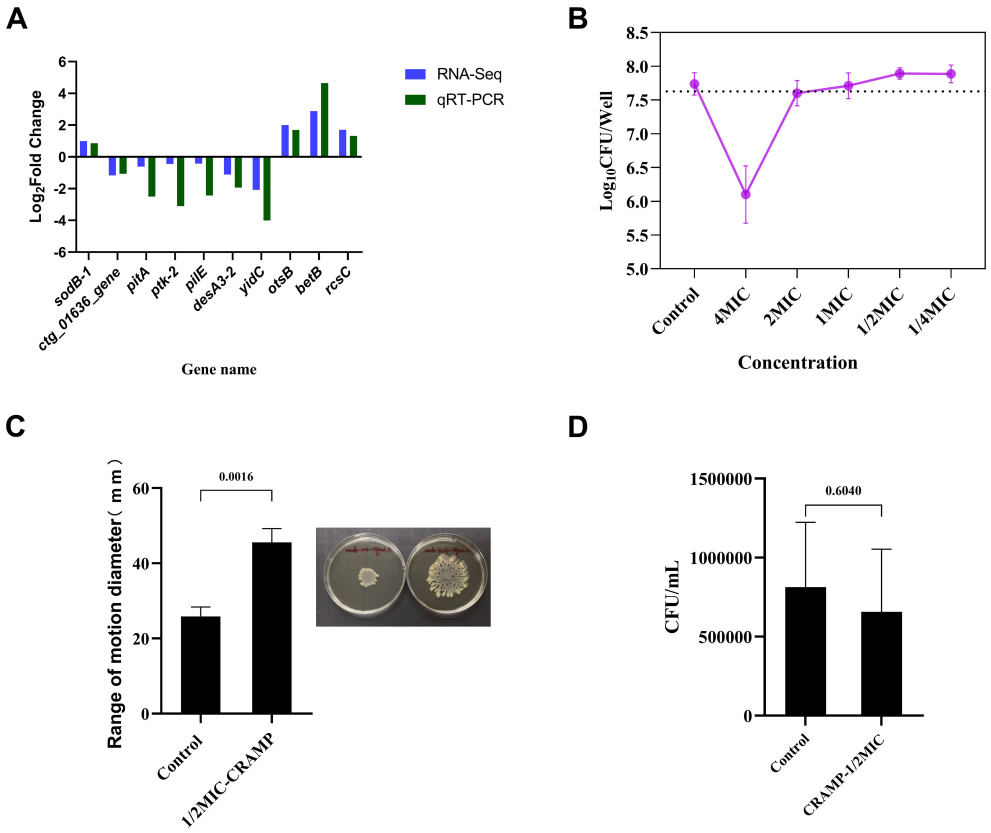

FIGURE 6
Validation of qRT-PCR and related phenotypic. **(A)** Validation of differentially expressed genes by qRT-PCR to demonstrate the reliability of transcriptome sequencing. Experiments were repeated at least 3 times independently. **(B)** Changes in the number of upper layer bacteria in culture system after the intervention of CRAMP-34 (1/4 MIC-4 MIC) on biofilm. **(C)** The change of movement diameter of biofilm bacteria after treatment with CRAMP-34. **(D)** Number of adhesion of *A lwoffii* on 96-well cell culture plates during the same period of time before and after CRAMP-34 treatment. The trial was replicated three times independently. Student's t-tests were used to calculate the statistical significance. $P < 0.05$ was considered statistically significant.

34 intervention group at subinhibitory concentrations, suggesting that the lepA gene may affect *A. lwoffii* resistance, but the mechanism of its influence needs to be further studied.

A. lwoffii is known to be a flagella-deficient bacterium that relies primarily on type IV pili-mediated twitching or surface-associated locomotion for locomotion. Type IV fimli have been reported in a variety of bacteria, which are associated with bacterial motility, bacterial-bacterial interactions, and bacterial attachment on biotic and abiotic surfaces (Denis et al., 2019). In addition, it has been reported in the literature that type IV fimbria can enhance virulence, promote biofilm formation, and promote horizontal gene transfer in different species of bacteria (Chlebek et al., 2021), and *P.aeruginosa* can rely on type IV pili to continuously extend, attach, and retract to pull itself for convulsive movement (Kuhn et al., 2021). In our study, the gene *pilE*, which is associated with type IV pili, was significantly down-regulated, and pilE can indirectly regulate bacterial motility by promoting the assembly of type IV pili (Nguyen et al., 2015), and the PilE protein can promote the adhesion of bacteria to host cells (Chen et al., 2020). The significant down-regulation of the *pilE* gene may be due to the bidirectional regulatory function of the gene, in which the bioenvelope bacteria are subjected to external stress during drug intervention, and in the face of dispersion pressure from the environment, the bacteria inversely regulate and activate the *pilE* gene of their fimbria in order to maintain their own homeostasis. In the study of Hu et al., the expression of pili can regulate iron homeostasis within bacteria (Hu et al., 2022). In this study, multiple iron-related genes were differentially expressed *desA*3_2, *sodB*_1, and *ctg*_01636_gene, *ctg*_01636_gene, because iron is an essential nutrient for the growth of bacterial pathogens, and iron plays a role in regulating microbial metabolism and physiology in proteins (Malmirchegini et al., 2014) (Malmirchegini et al., 2014). The changes in these genes suggest that CRAMP-34 may have affected the biofilm through iron uptake-related pathways.

Finally, the confirmatory test results of bacterial motility and adhesion showed that after the intervention of CRAMP-34 at sub-inhibitory concentration, the motility of *A. lwoffii* biofilm bacteria were significantly enhanced, the number of viable bacteria in the upper layer increased, and the diameter of the motile range increased by 1.76 times. It is speculated that CRAMP-34 may promote the transformation of biofilm bacteria into planktonic bacteria by increasing the motility of bacteria, leaving a central cavity of the biofilm, and eventually leading to the dispersion of the biofilm. However, the results of the biofilm bacterial adhesion test

showed that there was no significant change in the bacterial adhesion after the action of CRAMP-34, indicating that CRAMP-34 had no significant effect on the biofilm reformation ability of *A. lwoffii*. We reviewed the literature to analyze that the reason for the enhanced motility of bacteria may be due to the fact that BipA binds to ppGpp, which can directly control pilial biosynthesis and biofilm formation (Zheng et al., 2017). The ppGpp is an important second messenger in bacterial cells, which promotes bacterial adaptability and repair in adverse environments (Dalebroux et al., 2010), and it has a certain functional correlation with c-di-GMP, and low levels of c-di-GMP promote the diffusion of biofilms. In addition, the increase or decrease of the extracellular matrix, especially exopolysaccharides, is also an important reason for the change in motility. In our study, the gene PTK-2 encoding tyrosine kinase was significantly down-regulated, and tyrosine kinase promoted the synthesis of capsular polysaccharides, suggesting that the enhancement of motility of biofilm bacteria is likely to be directly related to capsular polysaccharides. The increased motility of bacteria leads to the transformation of biofilm bacteria into plankton, leaving a hollow biofilm, which leads to the dispersion of bacterial biofilm. However, the specific reasons why CRAMP-34 increases the movement of biofilm bacteria remain to be further investigated.

5 Conclusion

CRAMP-34 has the ability to eradicate *A. lwoffii* biofilms in a concentration-dependent manner, and the sub-inhibitory concentration of CRAMP-34 still has a significant eradicating ability, which mainly affects the gene expression of enzyme synthesis, fimbri, iron uptake system, virulence genes and other pathways. It was speculated that CRAMP-34 may promote the dispersion of biofilm bacteria by enhancing the motility of biofilm bacteria, thereby achieving the effect of eradicating biofilms.

Data availability statement

The original contributions presented in the study are included in the article/Supplementary Material. Further inquiries can be directed to the corresponding authors.

Author contributions

LL: Methodology, Validation, Visualization, Writing – original draft. HL: Conceptualization, Methodology, Visualization, Writing – original draft. CM: Methodology, Validation, Writing – original draft. JL: Methodology, Validation, Writing – review & editing. YZ: Resources, Visualization, Writing – review & editing. DX: Project administration, Resources, Visualization, Writing – review & editing. JX: Validation, Visualization, Writing – review & editing. YH: Conceptualization, Writing – review & editing. HY: Conceptualization, Data curation, Project administration, Supervision, Writing – review & editing. HC: Conceptualization, Funding acquisition, Methodology, Project administration, Supervision, Writing – review & editing.

Funding

The author(s) declare financial support was received for the research, authorship, and/or publication of this article. This research was funded by Chongqing Technical Innovation and Application Development Special General Project (CSTB2023TIAD-LDX0006), National Center of Technology Innovation for Pigs (NCTIP-XD/B12, NCTIP-XD/C17), The Project of Shandong Province on the Transformation of Scientific and Technological Achievements (2022LYXZ030), Science and Technology Plan Project of Yunnan Provincial Department of Science and Technology (202403AC100013) and Chongqing Natural Science Foundation (CSTB2024NSCQ-MSX0373).

Acknowledgments

We thank the Beijing Allwegene Technology Company Limited (Beijing, China) for helping draw pictures and analyze the omics data.

Conflict of interest

The authors declare that the research was conducted in the absence of any commercial or financial relationships that could be construed as a potential conflict of interest.

Publisher's note

Supplementary material

The Supplementary Material for this article can be found online at: https://www.frontiersin.org/articles/10.3389/fcimb.2024.1406429/full#supplementary-material

References

Cerioli, M. F., Moliva, M. V., Cariddi, L. N., and Reinoso, E. B. (2018). Effect of the essential oil of *Minthostachys verticillata* (griseb.) Epling and limonene on biofilm production in pathogens causing bovine mastitis. *Front. Vet. Sci.* 5. doi: 10.3389/fvets.2018.00146

Chen, X., Tang, B., Laborda, P., Zhao, Y., and Liu, F. (2023). First report of bacterial fruit blotch caused by *Kosakonia cowanii* on trichosanthis fructus in Jiangsu province, China. *Plant Dis.* 108 (3), 550–828. doi: 10.1094/PDIS-10-23-2048-PDN

Chen, Y., Yang, Z., Dong, Y., and Chen, Y. (2020). Recombinant pal/pile/flaa dna vaccine provides protective immunity against *Legionella pneumophila* in balb/c mice. *BMC Biotechnol.* 20, 28. doi: 10.1186/s12896-020-00620-3

Chlebek, J. L., Denise, R., Craig, L., and Dalia, A. B. (2021). Motor-independent retraction of type iv pili is governed by an inherent property of the pilus filament. *Proc. Natl. Acad. Sci. U. S. A.* 118. doi: 10.1073/pnas.2102780118

Choi, E., and Hwang, J. (2018). The gtpase bipa expressed at low temperature in *Escherichia coli* assists ribosome assembly and has chaperone-like activity. *J. Biol. Chem.* 293, 18404–18419. doi: 10.1074/jbc.RA118.002295

Choi, E., Jeon, H., Oh, C., and Hwang, J. (2020). Elucidation of a novel role of yebc in surface polysaccharides regulation of *Escherichia coli* bipa-deletion. *Front. Microbiol.* 11. doi: 10.3389/fmicb.2020.597515

Cui, Y., Song, K., Liu, X., Xu, H., Wang, X., Cheng, G., et al. (2024). Research on bacterial diversity and antibiotic resistance in the dairy farm environment in a part of Shandong province. *Animals* 14, 160. doi: 10.3390/ani14010160

Dalebroux, Z. D., Svensson, S. L., Gaynor, E. C., and Swanson, M. S. (2010). Ppgpp conjures bacterial virulence. *Microbiol. Mol. Biol. Rev.* 74, 171–199. doi: 10.1128/MMBR.00046-09

de la Fuente-Nunez, C., and Hancock, R. E. (2015). Using anti-biofilm peptides to treat antibiotic-resistant bacterial infections. *Postdoc J.* 3, 1–8. doi: 10.14304/SURYA.JPR.V3N2.1

DeLivron, M. A., and Robinson, V. L. (2008). *Salmonella enterica* serovar typhimurium bipa exhibits two distinct ribosome binding modes. *J. Bacteriol.* 190, 5944–5952. doi: 10.1128/JB.00763-08

Denis, K., Le Bris, M., Le Guennec, L., Barnier, J. P., Faure, C., Gouge, A., et al. (2019). Targeting type iv pili as an antivirulence strategy against invasive meningococcal disease. *Nat. Microbiol.* 4, 972–984. doi: 10.1038/s41564-019-0395-8

Elham, B., and Fawzia, A. (2019). Colistin resistance in *Acinetobacter baumannii* isolated from critically ill patients: clinical characteristics, antimicrobial susceptibility and outcome. *Afr. Health Sci.* 19, 2400–2406. doi: 10.4314/ahs.v19i3.13

El-Sayed, A., and Kamel, M. (2021). Bovine mastitis prevention and control in the post-antibiotic era. *Trop. Anim. Health Prod.* 53, 236. doi: 10.1007/s11250-021-02680-9

Fishbein, S., Tomasi, F. G., Wolf, I. D., Dulberger, C. L., Wang, A., Keshishian, H., et al. (2020). The conserved translation factor lepa is required for optimal synthesis of a porin family in *Mycobacterium smegmatis*. *J. Bacteriol.* 203. doi: 10.1128/JB.00604-20

Gao, P., Wei, Y., Wan, R. E., Wong, K. W., Iu, H., Tai, S., et al. (2022). Subinhibitory concentrations of antibiotics exacerbate staphylococcal infection by inducing bacterial virulence. *Microbiol. Spectr.* 10, e0064022. doi: 10.1128/spectrum.00640-22

Ghoreishi, F. S., Roghanian, R., and Emtiazi, G. (2022). Novel chronic wound healing by anti-biofilm peptides and protease. *Adv. Pharm. Bull.* 12, 424–436. doi: 10.34172/apb.2022.047

Goh, K. J., Ero, R., Yan, X. F., Park, J. E., Kundukad, B., Zheng, J., et al. (2021). Translational gtpase bipa is involved in the maturation of a large subunit of bacterial ribosome at suboptimal temperature. *Front. Microbiol.* 12. doi: 10.3389/fmicb.2021.686049

Golla, R. M., Mishra, B., Dang, X., Lakshmaiah, N. J., Li, A., Xu, L., et al. (2020). Resistome of *Staphylococcus aureus* in response to human cathelicidin ll-37 and its engineered antimicrobial peptides. *ACS Infect. Dis.* 6, 1866–1881. doi: 10.1021/acsinfecdis.0c00112

Grant, A. J., Farris, M., Alefounder, P., Williams, P. H., Woodward, M. J., and O'Connor, C. D. (2003). Co-ordination of pathogenicity island expression by the bipa gtpase in enteropathogenic *Escherichia coli* (EPEC). *Mol. Microbiol.* 48, 507–521. doi: 10.1046/j.1365-2958.2003.t01-1-03447.x

Hibbing, M. E., Fuqua, C., Parsek, M. R., and Peterson, S. B. (2010). Bacterial competition: surviving and thriving in the microbial jungle. *Nat. Rev. Microbiol.* 8, 15–25. doi: 10.1038/nrmicro2259

Hu, L. I., Stohl, E. A., and Seifert, H. S. (2022). The *Neisseria gonorrhoeae* type iv pilus promotes resistance to hydrogen peroxide- and ll-37-mediated killing by modulating the availability of intracellular, labile iron. *PloS Pathog.* 18, e1010561. doi: 10.1371/journal.ppat.1010561

Hua, X., Zhou, Z., Yang, Q., Shi, Q., Xu, Q., Wang, J., et al. (2017). Evolution of *Acinetobacter baumannii in vivo*: international clone ii, more resistance to ceftazidime, mutation in ptk. *Front. Microbiol.* 8. doi: 10.3389/fmicb.2017.01256

Koti, K., Rodas-Gonzalez, A., Nadon, C., McAllister, T., Yang, X., and Narvaez-Bravo, C. (2024). Evaluating disinfectant efficacy on mixed biofilms comprising shiga toxigenic *Escherichia coli*, lactic acid bacteria, and spoilage microorganisms. *Front. Microbiol.* 15. doi: 10.3389/fmicb.2024.1360645

Krebs, I., Zhang, Y., Wente, N., Leimbach, S., and Kromker, V. (2023). Bacteremia in severe mastitis of dairy cows. *Microorganisms* 11 (7), 1639. doi: 10.3390/microorganisms11071639

Ku, S. C., Hsueh, P. R., Yang, P. C., and Luh, K. T. (2000). Clinical and microbiological characteristics of bacteremia caused by *Acinetobacter lwoffii*. *Eur. J. Clin. Microbiol. Infect. Dis.* 19, 501–505. doi: 10.1007/s100960000315

Kuhn, M. J., Tala, L., Inclan, Y. F., Patino, R., Pierrat, X., Vos, I., et al. (2021). Mechanotaxis directs *Pseudomonas aeruginosa* twitching motility. *Proc. Natl. Acad. Sci. U. S. A.* 118. doi: 10.1073/pnas.2101759118

Li, L., Hong, Y., Luan, G., Mosel, M., Malik, M., Drlica, K., et al. (2014). Ribosomal elongation factor 4 promotes cell death associated with lethal stress. *Mbio* 5, e01708. doi: 10.1128/mBio.01708-14

Li, L., Li, J., Yu, X., Cao, R., Hong, M., Xu, Z., et al. (2023). Antimicrobial peptides fight against *Pseudomonas aeruginosa* at a sub-inhibitory concentration via anti-qs pathway. *Bioorganic Chem.* 141, 106922. doi: 10.1016/j.bioorg.2023.106922

Liu, H., Chen, C., Zhang, H., Kaur, J., Goldman, Y. E., and Cooperman, B. S. (2011). The conserved protein ef4 (lepa) modulates the elongation cycle of protein synthesis. *Proc. Natl. Acad. Sci. U. S. A.* 108, 16223–16228. doi: 10.1073/pnas.1103820108

Liu, G., Qin, P., Cheng, X., Wu, L., Zhao, W., and Gao, W. (2024). Evaluation of the mechanistic basis for the antibacterial activity of ursolic acid against *Staphylococcus aureus*. *Front. Microbiol.* 15. doi: 10.3389/fmicb.2024.1389242

Long, J., Yang, C., Liu, J., Ma, C., Jiao, M., Hu, H., et al. (2024). Tannic acid inhibits *Escherichia coli* biofilm formation and underlying molecular mechanisms: biofilm regulator csgd. *Biomed. Pharmacother.* 175, 116716. doi: 10.1016/j.biopha.2024.116716

Luo, Y., and Song, Y. (2021). Mechanism of antimicrobial peptides: antimicrobial, anti-inflammatory and antibiofilm activities. *Int. J. Mol. Sci.* 22 (21), 11401. doi: 10.3390/ijms222111401

Ma, C., Mei, C., Liu, J., Li, H., Jiao, M., Hu, H., et al. (2024). Effect of baicalin on eradicating biofilms of bovine milk derived *Acinetobacter lwoffii*. *BMC Vet. Res.* 20, 212. doi: 10.1186/s12917-024-04015-w

Malmirchegini, G. R., Sjodt, M., Shnitkind, S., Sawaya, M. R., Rosinski, J., Newton, S. M., et al. (2014). Novel mechanism of hemin capture by hbp2, the hemoglobin-binding hemophore from *Listeria monocytogenes*. *J. Biol. Chem.* 289, 34886–34899. doi: 10.1074/jbc.M114.583013

Masihzadeh, S., Amin, M., and Farshadzadeh, Z. (2023). *In vitro* and *in vivo* antibiofilm activity of the synthetic antimicrobial peptide wlbu2 against multiple drug resistant *Pseudomonas aeruginosa* strains. *BMC Microbiol.* 23, 131. doi: 10.1186/s12866-023-02886-x

Nguyen, Y., Harvey, H., Sugiman-Marangos, S., Bell, S. D., Buensuceso, R. N., Junop, M. S., et al. (2015). Structural and functional studies of the *Pseudomonas aeruginosa* minor pilin, pile. *J. Biol. Chem.* 290, 26856–26865. doi: 10.1074/jbc.M115.683334

Pedersen, R. R., Kromker, V., Bjarnsholt, T., Dahl-Pedersen, K., Buhl, R., and Jorgensen, E. (2021). Biofilm research in bovine mastitis. *Front. Vet. Sci.* 8. doi: 10.3389/fvets.2021.656810

Pour, N. K., Dusane, D. H., Dhakephalkar, P. K., Zamin, F. R., Zinjarde, S. S., and Chopade, B. A. (2011). Biofilm formation by *Acinetobacter baumannii* strains isolated from urinary tract infection and urinary catheters. *FEMS Immunol. Med. Microbiol.* 62, 328–338. doi: 10.1111/j.1574-695X.2011.00818.x

Rakitin, A. L., Ermakova, A. Y., Beletsky, A. V., Petrova, M., Mardanov, A. V., and Ravin, N. V. (2021). Genome analysis of *Acinetobacter lwoffii* strains isolated from permafrost soils aged from 15 thousand to 1.8 million years revealed their close relationships with present-day environmental and clinical isolates. *Biology-Basel* 10 (9), 871. doi: 10.3390/biology10090871

Rather, M. A., Gupta, K., and Mandal, M. (2021). Microbial biofilm: formation, architecture, antibiotic resistance, and control strategies. *Braz. J. Microbiol.* 52, 1701–1718. doi: 10.1007/s42770-021-00624-x

Regalado, N. G., Martin, G., and Antony, S. J. (2009). *Acinetobacter lwoffii*: bacteremia associated with acute gastroenteritis. *Travel Med. Infect. Dis.* 7, 316–317. doi: 10.1016/j.tmaid.2009.06.001

Roudashti, S., Zeighami, H., Mirshahabi, H., Bahari, S., Soltani, A., and Haghi, F. (2017). Synergistic activity of sub-inhibitory concentrations of curcumin with ceftazidime and ciprofloxacin against *Pseudomonas aeruginosa* quorum sensing related genes and virulence traits. *World J. Microbiol. Biotechnol.* 33, 50. doi: 10.1007/s11274-016-2195-0

Vasudevan, P., Nair, M. K., Annamalai, T., and Venkitanarayanan, K. S. (2003). Phenotypic and genotypic characterization of bovine mastitis isolates of *Staphylococcus aureus* for biofilm formation. *Vet. Microbiol.* 92, 179–185. doi: 10.1016/S0378-1135(02)00360-7

Wang, S., Ma, C., Long, J., Cheng, P., Zhang, Y., Peng, L., et al. (2023). Impact of cramp-34 on *Pseudomonas aeruginosa* biofilms and extracellular metabolites. *Front. Cell. Infect. Microbiol.* 13. doi: 10.3389/fcimb.2023.1295311

Wongchai, M., Wongkaewkhiaw, S., Kanthawong, S., Roytrakul, S., and Aunpad, R. (2024). Dual-function antimicrobial-antibiofilm peptide hybrid to tackle biofilm-

forming *Staphylococcus* epidermidis. *Ann. Clin. Microbiol. Antimicrob.* 23, 44. doi: 10.1186/s12941-024-00701-7

Wu, S., Li, X., Gunawardana, M., Maguire, K., Guerrero-Given, D., Schaudinn, C., et al. (2014). Beta- lactam antibiotics stimulate biofilm formation in non-typeable haemophilus influenzae by up-regulating carbohydrate metabolism. *PloS One* 9, e99204. doi: 10.1371/journal.pone.0099204

Xia, J., Ge, C., and Yao, H. (2021). Antimicrobial peptides from black soldier fly (*Hermetia illucens*) as potential antimicrobial factors representing an alternative to antibiotics in livestock farming. *Animals* 11 (7), 1937. doi: 10.3390/ani11071937

Xu, L., Lv, R., Wang, H., Hu, H., Zhao, X., Yang, R., et al. (2013). [Fitness costs of blandm-1 bearing plasmid pndm-bj01 in *Acinetobacter lwoffii*]. *Wei Sheng Wu Xue Bao.* 53, 99–104.

Zhang, Y., Cheng, P., Wang, S., Li, X., Peng, L., Fang, R., et al. (2022). *Pseudomonas aeruginosa* biofilm dispersion by the mouse antimicrobial peptide cramp. *Vet. Res.* 53, 80. doi: 10.1186/s13567-022-01097-y

Zhang, Y., He, X., Cheng, P., Li, X., Wang, S., Xiong, J., et al. (2021). Effects of a novel anti-biofilm peptide cramp combined with antibiotics on the formation of *Pseudomonas aeruginosa* biofilms. *Microb. Pathog.* 152, 104660. doi: 10.1016/j.micpath.2020.104660

Zhang, Y., Jiang, C., Li, Y., Sun, J., Chen, Z., Zhang, Q., et al. (2024). Screening, identification, and mechanism analysis of starch-degrading bacteria during curing process in tobacco leaf. *Front. Bioeng. Biotechnol.* 12. doi: 10.3389/fbioe.2024.1332113

Zheng, H., Singh, N., Shetye, G. S., Jin, Y., Li, D., and Luk, Y. Y. (2017). Synthetic analogs of rhamnolipids modulate structured biofilms formed by rhamnolipid-nonproducing mutant of *Pseudomonas aeruginosa*. *Bioorg. Med. Chem.* 25, 1830–1838. doi: 10.1016/j.bmc.2017.01.042

Zhou, J. W., Chen, T. T., Tan, X. J., Sheng, J. Y., and Jia, A. Q. (2018). Can the quorum sensing inhibitor resveratrol function as an aminoglycoside antibiotic accelerant against *Pseudomonas aeruginosa*? *Int. J. Antimicrob. Agents.* 52, 35–41. doi: 10.1016/j.ijantimicag.2018.03.002

Zhu, Y., Zhang, X., Wang, Y., Tao, Y., Shao, X., Li, Y., et al. (2022). Insight into carbapenem resistance and virulence of *Acinetobacter baumannii* from a children's medical centre in eastern China. *Ann. Clin. Microbiol. Antimicrob.* 21, 47. doi: 10.1186/s12941-022-00536-0

frontiers | Frontiers in Cellular and Infection Microbiology

TYPE Original Research
PUBLISHED 26 August 2024
DOI 10.3389/fcimb.2024.1403219

OPEN ACCESS

EDITED BY
Maria Gabriela Paraje,
National University of Cordoba, Argentina

REVIEWED BY
Sylwia Andrzejczuk,
Medical University of Lublin, Poland
Laura Decca,
Clínica Regional del Sud, Argentina

*CORRESPONDENCE
Mahmoud M. Bendary
M.pendary@pharm.psu.edu.eg

RECEIVED 19 March 2024
ACCEPTED 04 July 2024
PUBLISHED 26 August 2024

CITATION
Bakeer W, Gaafar M, El-Gendy AO, El Badry MA, Khalil MG, Mansour AT, Alharbi NK, Selim HMRM and Bendary MM (2024) Proven anti-virulence therapies in combating methicillin- and vancomycin-resistant *Staphylococcus aureus* infections. *Front. Cell. Infect. Microbiol.* 14:1403219. doi: 10.3389/fcimb.2024.1403219

Proven anti-virulence therapies in combating methicillin- and vancomycin-resistant *Staphylococcus aureus* infections

Walid Bakeer[1], Marwa Gaafar[1,2], Ahmed O. El-Gendy[1], Mohamed. A. El Badry[3], Mona G. Khalil[4], Abdallah Tageldein Mansour[5,6], Nada K. Alharbi[7], Heba M. R. M. Selim[8] and Mahmoud M. Bendary[9]*

[1]Department of Microbiology and Immunology, Faculty of Pharmacy, Beni-Suef University, Beni-Suef, Egypt, [2]Quality Control Specialist at Egyptian Drug Authority (EDA), Cairo, Egypt, [3]Department of Botany and Microbiology, Faculty of Sciences, Al- Azhar University, Cairo, Egypt, [4]Department of Pharmacology and Toxicology, Faculty of Pharmacy, Modern University for Technology and Information, Cairo, Egypt, [5]Department of Fish and Animal Production and Aquaculture, College of Agriculture and Food Sciences, King Faisal University, Al-Ahsa, Saudi Arabia, [6]Department of Fish and Animal Production, Faculty of Agriculture (Saba Basha), Alexandria University, Alexandria, Egypt, [7]Department of Biology, College of Science, Princess Nourah bint Abdulrahman University, Riyadh, Saudi Arabia, [8]Department of Pharmaceutical Sciences, College of Pharmacy, AlMaarefa University, Riyadh, Saudi Arabia, [9]Department of Microbiology and Immunology, Faculty of Pharmacy, Port Said University, Port Said, Egypt

Introduction: Despite years of efforts to develop new antibiotics for eradicating multidrug-resistant (MDR) and multi-virulent Methicillin-Resistant *Staphylococcus aureus* (MRSA) and Vancomycin-Resistant *Staphylococcus aureus* (VRSA) infections, treatment failures and poor prognoses in most cases have been common. Therefore, there is an urgent need for new therapeutic approaches targeting virulence arrays. Our aim is to discover new anti-virulence therapies targeting MRSA and VRSA virulence arrays.

Methodology: We employed phenotypic, molecular docking, and genetic studies to screen for anti-virulence activities among selected promising compounds: Coumarin, Simvastatin, and Ibuprofen.

Results: We found that nearly all detected MRSA and VRSA strains exhibited MDR and multi-virulent profiles. The molecular docking results aligned with the phenotypic and genetic assessments of virulence production. Biofilm and hemolysin productions were inhibited, and all virulence genes were downregulated upon treatment with sub-minimum inhibitory concentration (sub-MIC) of these promising compounds. Ibuprofen was the most active compound, exhibiting the highest inhibition and downregulation of virulence gene products. Moreover, *in vivo* and histopathological studies confirmed these results. Interestingly, we observed a significant decrease in wound area and improvements in re-epithelialization and tissue organization in the Ibuprofen and antimicrobial treated group compared with the group treated with antimicrobial alone. These findings support the idea that a combination of Ibuprofen and

antimicrobial drugs may offer a promising new therapy for MRSA and VRSA infections.

Conclusion: We hope that our findings can be implemented in clinical practice to assist physicians in making the most suitable treatment decisions.

KEYWORDS

anti-virulence, histopathological, molecular docking, coumarin, simvastatin, ibuprofen

Introduction

A key biological property of *Staphylococcus aureus* is its capacity to persist in various environments and on intact epithelia without being detected by the host. This silent presence allows *S. aureus* to spread easily and become a common part of the human microbiota (Taylor and Unakal, 2023). On the other hand, it is responsible for several diseases and a broad spectrum of potentially life-threatening infections, ranging from superficial skin abscesses to necrotizing tissue and pulmonary lesions, if it enters the bloodstream or internal tissues (Luzzago et al., 2014; Abd El-Hamid et al., 2022). Therefore, the relationship between *S. aureus* colonization, pathogenicity, and human diseases has been extensively studied (Hamdan-Partida et al., 2022). Furthermore, *S. aureus* is one of the most common human pathogens causing both community-acquired and nosocomial infections. It can produce different virulence factors that help in its adaptation and survival in various tissues and environmental conditions (Balasubramanian et al., 2017). Thus, recent clinical research has focused on the relationship between virulence arrays, pathogenicity, bacterial evolution, and host factors (Cheung et al., 2021). Several *S. aureus* virulence factors, including staphylokinase, leukocidin, invasive proteases, hemolysin, hyaluronidase, lipase, and nuclease, play important roles in colonization and pathogenicity, facilitating the initiation of the disease process, immune evasion, and host tissue destruction (Wieckowska-Szakiel et al., 2007).

Alarmingly, several life-threatening diseases have been associated with the multi-virulent strains of this pathogen. These strains create several public health crises, especially if they show resistance to available antimicrobial drugs. *S. aureus* can easily acquire resistance against all classes of antibiotics through targeted gene mutations or by horizontal transfer of resistance genes. The most notable example of these strains is methicillin-resistant *S. aureus* (MRSA), which is characterized by the presence of the *mecA* gene encoding penicillin-binding protein 2a. Originally a major cause of nosocomial infections, MRSA has now also become prevalent in community settings (Peacock and Paterson, 2015; Abd El-Hamid et al., 2023). Glycopeptides, particularly vancomycin, have been considered the most effective drugs against severe MRSA infections, as most MRSA strains are vancomycin-sensitive *S. aureus* (VSSA). However, there has been an alarming emergence of vancomycin-resistant *S. aureus* (VRSA), which may be attributed to the widespread use of vancomycin for the treatment of infections caused by MRSA (Cong et al., 2019; Rubinstein and Keynan, 2014).

In Egypt, the prevalence of MRSA has increased with significant variation across different regions and studies. A comprehensive meta-analysis of 64 studies revealed an overall MRSA prevalence of 63% among clinical isolates (Azzam et al., 2023). Recent data have indicated that the MRSA prevalence among clinical isolates ranges widely in this country, with rates between 50% and 82% in major cities such as Cairo and Alexandria and a lower rate of approximately 24% in Minia (Abouelfetouh, 2017). A study conducted in this area between 2005 and 2013 showed a significant rise in VRSA cases from 4.2% to 25.8% among hospital-associated infections (Saber et al., 2022). Another recent study has reported VRSA prevalence rates of 27.6% in dromedary camel isolates and 54.5% in human isolates (Al-Amery et al., 2019). These findings highlight a growing concern for antimicrobial resistance among the MRSA and VRSA isolates in the region. Therefore, the multidrug-resistant MRSA and VRSA strains have been implicated in serious problems and health crises throughout the world. This crisis has been compounded by the emergence of multi-virulent phenotypes.

In recent years, there has been an increase in resistance to available antimicrobial drugs, while antimicrobial development has lagged. Thus, the development and discovery of new drugs are urgently needed to overcome antimicrobial resistance, which has undermined the effectiveness of conventional antibiotics (Ghaly et al., 2020). In order to manage microbial infections, alternative anti-virulence therapies targeting virulence factors instead of microbial growth have been approved and have entered clinical trials by several health organizations worldwide (Dickey et al., 2017). It has been proven that virulence factors are involved in pathogenesis, while anti-virulence agents inhibit the production of disease-causing virulence factors, but are neither bactericidal nor bacteriostatic. Unlike antibiotics, which face problems related to the evolution and spread of resistance, the horizontal transfer of virulence genes cannot provide protection against anti-virulence therapies as they are correlated to single or very closely related species. Anti-virulence agents cannot be used as growth promoters in veterinary fields, in contrast to antibiotics, which is considered one of the major mechanisms responsible for antibiotic resistance. Furthermore, anti-virulence therapies have no effect on the normal

microbiota. Thus, the superinfection issues associated with the use of antibiotics are not involved during treatment with anti-virulence therapies (Dickey et al., 2017). These new strategies may assist in suppressing the production of key MRSA and VRSA toxins. In addition, they might be useful alone or in combination with other antibiotics to manage MRSA and VRSA infections and overcome the currently unmet problems related to biofilm-producing pathogens. Herein, we attempted to address the antimicrobial resistance crisis through the evaluation of the anti-virulence activities of some natural (coumarin) and synthetic (simvastatin and ibuprofen) compounds using different *in vitro*, *in vivo*, and molecular docking techniques.

Materials and methods

Characterization of MRSA and VRSA strains

During a 3-month period from January 2022 to April 2022, a total of 250 clinical specimens were collected from both inpatients and outpatients admitted to a general hospital in Cairo, Egypt. These specimens were recovered from different clinical sources, including blood, urine, pus, and wound swabs. All clinical specimens were collected aseptically following standard methodology according to instructions and guidelines (Cheesbrough, 2005). All the tested specimens were inoculated and enriched in both trypticase soy agar (TSA) and blood agar (BA) and then incubated at 37°C for 24 h (Hudzicki, 2016). The recovered *S. aureus* isolates were identified phenotypically based on standard procedures for the identification of bacterial pathogens according to the provided instructions and guidelines (Koneman et al., 2006; Cheesbrough, 2017). In addition, biochemical identification was conducted using API 20S. MRSA strains were identified using cefoxitin antibiotic disks (30 µg) on Mueller–Hinton agar plates through the Kirby–Bauer disc diffusion method, evaluated in accordance with the Clinical and Laboratory Standards Institute guidelines (CLSI, 2022). The minimum inhibitory concentration (MIC) breakpoints of oxacillin were also determined using the broth microdilution method in triplicate. Isolates were classified as MRSA if they exhibited a zone of inhibition ≤21 mm around the cefoxitin disk and had an MIC ≥4 µg/mL. In addition, the agar dilution assay was employed in triplicate to determine the MIC for the identification of VRSA strains according to CLSI (2022). In brief, Mueller–Hinton agar plates were prepared with vancomycin concentrations ranging from 0.5 to 64 µg/mL. Subsequently, 1–2 µL of the standardized bacterial suspensions (0.5 McFarland standard) was added to the surface of the agar plates, typically with 24–36 spots per plate. The inoculated plates were then incubated in an inverted position at 35°C for 18–24 h. The MIC denotes the minimum vancomycin concentration necessary to entirely halt visible growth of *S. aureus*. As per the CLSI guidelines (2022), isolates are categorized as VRSA if their MIC is ≥16 µg/mL. Additional confirmation tests to verify the MRSA and VRSA strains were performed in triplicate using the Biomerieux VITEK®2, an automated Identification/Antibiotic Susceptibility Testing (ID/AST) system. For more confirmation, the E-TEST procedure for the detection of VRSA strains was performed in trypticase as follows: firstly, a standardized inoculum of the bacterial strain was prepared by adjusting its turbidity to match the 0.5 McFarland standard. This inoculum was then evenly spread over a Mueller–Hinton agar plate using a sterile swab. After allowing the plate to dry for a few minutes, an E-TEST strip, which contains a gradient of vancomycin concentrations, was carefully placed on the agar surface. The plate was incubated at 35–37°C for 24 h. Following incubation, the MIC was determined by identifying the point at which the elliptical zone of inhibition intersects with the E-TEST strip. The MIC values were then interpreted to identify the resistant strains (Maharjan et al., 2021).

Screening of multiple drug-resistant MRSA and VRSA strains

The antimicrobial susceptibility testing of all identified isolates was conducted *in vitro* on 20 different commonly prescribed antimicrobial agents, covering various categories, therapeutic actions, and mechanisms of action. These antimicrobials included cefoxitin (FOX; 30 µg), benzylpenicillin (P; 10 U), amoxicillin/clavulanic acid (AMC; 20/10 µg), gentamicin (CN; 10 µg), clindamycin (DA; 2 µg), nitrofurantoin (NFT; 300 µg), linezolid (LZD; 30 µg), vancomycin (VA; 30 µg), teicoplanin (TEC; 30 µg), tetracycline (TET; 30 µg), erythromycin (E; 15 µg), doxycycline (DO; 30 µg), ciprofloxacin (CIP; 5 µg), levofloxacin (LEV; 5 µg), chloramphenicol (C; 30 µg), fusidic acid (FA; 10 µg), rifampicin (RD; 5 µg), cotrimoxazole (SXT; 25 µg), and pristinamycin (quinupristin/dalfopristin) (QD; 15 µg). This test was performed using the Kirby–Bauer disc diffusion method according to the criteria and guidelines of CLSI (2022). Isolates that showed resistance to at least one drug in three or more antimicrobial categories were identified as multidrug-resistant (MDR) (Magiorakos et al., 2012).

Phenotypic detection of some virulence factors of the identified MRSA and VRSA isolates

Quantitative determination of biofilm formation using the microtiter plate method

The microtiter plate (MTP) method was performed according to the standard procedures and instructions provided by Lade et al. (2019). In brief, biofilm production was assessed using the MTP method with crystal violet staining. Bacterial cultures were initially grown in 96-well plates, followed by washing to eliminate non-adherent cells after incubation. The residual biofilm was then stained with crystal violet and subsequently washed to remove surplus dye. To quantify the biofilm, the stained biofilm was dissolved using acetone, and its optical density was measured using a spectrophotometer. The experiment was conducted in triplicate using sterile trypticase soy broth (TSB) as a negative control, which was used as the cutoff point to quantify the biofilm formation ability [optical density cutoff (ODc) = average OD of the negative control + 3× standard deviation of the negative control]. The isolates were classified according to Stepanović et al. (2007) into the following

categories: strong biofilm producer (4 × ODc < OD), moderate biofilm producer (2 × ODc < OD ≤ 4 × ODc), weak biofilm producer (ODc < OD ≤ 2 × ODc), and no biofilm production (OD ≤ ODc).

Qualitative and quantitative detection of hemolysin production

A blood plate assay was used for the determination of both qualitative and quantitative hemolytic activity, which was performed three times to detect the average of measurements (Yigit and Aktas, 2009; Nouraei et al., 2020). The hemolysin-producing strain was characterized by the production of a clear zone. Hemolytic activity was determined in millimeters by measuring the diameter of the inoculate divided by the diameter of the clear zone around the inoculate. The precipitation zone was measured and expressed as a *Pz* value from 1 to 4 as follows: *Pz* 1 (negative) for no clearance, *Pz* 1+ (0.9–1) for mild, *Pz* 2+ for moderate (0.89–0.80), *Pz* 3+ (0.79–0.70) for strong, and *Pz* 4+ (≥0.69) for very strong hemolysin activity (Divyakolu et al., 2019; Almwafy et al., 2020).

Genotypic detection of some virulence factors of selected MRSA and VRSA strains

The MDR, hemolysin, and biofilm-producing MRSA and VRSA isolates were selected from the examined samples for further genotypic analysis. This molecular study examined 13 virulence genes, including five enterotoxin genes (*sea*, *seb*, *sec*, *sed*, and *see*), which were detected using multiplex PCR. In addition, three hemolysin genes (*hla*, *hlb*, and *hlg*), two intracellular adhesion toxin genes (*icaA* and *icaD*), one toxic shock syndrome toxin gene (*tst*), one exfoliative toxin B gene (*etb*), and one leukocidin gene (*lukED*) were investigated. All of these genes were detected with uniplex PCR. Negative controls (DNA extracted from the *Escherichia coli* reference strain ATCC 25922) and the positive control (DNA extracted from standard *S. aureus*, ATCC 33591) were used as controls for each PCR run. The standard strains were kindly provided by the Animal Production Research Institute in Dokki, Giza, Egypt. Electrophoresis of the amplified PCR products on an agarose gel (1.5%) stained with ethidium bromide (Sigma-Aldrich, St. Louis, MO, USA) allowed for their visualization under UV light. The primer sequences, annealing temperatures, and amplicon sizes are shown in Supplementary Table S1.

Assessment of anti-virulence compounds (coumarin, simvastatin, and ibuprofen) using molecular docking studies

Molecular docking analysis was used to evaluate the affinity scores of coumarin, simvastatin, and ibuprofen to specific virulence gene product targets *in vitro* and to predict any anti-virulence activity against virulence proteins. The virulence proteins included in the Protein Data Bank (PDB) were leukocidin, penicillin-binding protein (PBP), toxic shock syndrome toxin (TSST), enterotoxins, exfoliative toxin B, intracellular adhesive toxin A, and hemolysin. The sum of all interactions between the tested compounds and their target proteins was approximated with a docking score. The predicted top-ranking poses with the best scores were detected using the AutoDock Vina, GOLD, and MOE-Dock programs. GOLD and LeDock were able to identify the correct ligand binding poses. Both Glide (XP) and GOLD predicted the poses consistently with 90% accuracy (Wang et al., 2018).

Evaluation of the antimicrobial and anti-virulence activities of the selected compounds

The antimicrobial and anti-virulence effects of coumarin, simvastatin, and ibuprofen were evaluated against the three most highly multi-virulent MRSA/VRSA strains, as well as the standard *S. aureus* (ATCC 33591).

Determination of the MICs of the investigated compounds

For this evaluation, 100 µL of Mueller–Hinton broth medium was added to each well of a MTP. Subsequently, twofold serial dilutions of each drug were prepared in the respective wells of each row. Following this, a standardized suspension (100 µL) of the MRSA isolates (0.5 McFarland standard) was added to each well. During this analysis, two controls were utilized: a positive control (culture medium of the susceptible strain with the antimicrobial agent) and a negative control (culture medium without the antimicrobial agent). The final volume in each well of the MTP was 200 µL. The plates were sealed, placed in plastic bags, and incubated at 35°C for a total of 24 h. Absorbance was determined with an enzyme-linked immunosorbent assay (ELISA) reader at a wavelength equal to 630 nm (Flentie et al., 2019). The MIC was determined as the lowest concentration of the antimicrobial agent that entirely halted visible bacterial growth.

Evaluation of the anti-biofilm activities of coumarin, simvastatin, and ibuprofen

The biofilm-producing multi-virulent/MDR isolates were selected to examine the anti-biofilm activities of the compounds under investigation. Sub-MIC (half MIC value) concentrations of coumarin, simvastatin, and ibuprofen were employed to evaluate their anti-biofilm activities using the MTP method (Lade et al., 2019). The test was repeated three times, with both positive and negative controls included in each repetition.

Evaluation of the anti-hemolytic activities of coumarin, simvastatin, and ibuprofen

Blood samples (5 mL) from physiologically normal volunteers were centrifuged at 5,000 rpm for 10 min to separate plasma and erythrocytes. The supernatant was discarded, and the erythrocytes were collected and purified by washing three times using phosphate-buffered saline. Aliquots of 50 µL of erythrocytes were treated with 25 µL of sub-MIC (MIC = 0.5) of the tested compounds in a Falcon tube and incubated at room temperature for 60 min. The positive control, which was treated with Triton-X100 resulting in 100% hemolysis, and the negative control, an untreated tube, were both employed. The OD at 540 nm was measured using a UV spectrophotometer to reflect the degree of hemolysis (Yigit and Aktas, 2009; Afsar et al., 2016). The percentage of anti-hemolysis

was calculated using the following equation: % inhibition = 100 × (1 - OD sample) / OD of negative control.

Molecular detection of the anti-virulence activities of the investigated compounds using the real-time PCR method

RNA was extracted from the top three highly multi-virulent MRSA/VRSA strains along with the standard *S. aureus* (ATCC 33591) following the instructions provided in the RNeasy Mini Kit. The amplification conditions were set on a thermocycler, which included reverse transcription at 50°C for 30 min, initial denaturation at 94°C for 15 min, followed by 40 cycles of secondary denaturation at 94°C for 30 s, annealing at 57°C for 40 s, and extension at 72°C for 40 s. Subsequently, a dissociation curve was generated with denaturation at 94°C for 1 min, annealing at 57°C for 1 min, and a final denaturation at 94°C for 1 min. The amplification curves and the cycle threshold (Ct) values were determined using the Stratagene MX3005P software. To assess variations in the gene expression among the RNA samples, the Ct value of each sample was compared with that of the control group using the "ΔΔCT" method outlined by Yuan et al. (2006). Specifically, ΔΔCt was calculated as ΔCt reference – ΔCt target, where ΔCt (target) = Ct (control) – Ct (treatment) and ΔCt (reference) = Ct (control) – Ct (treatment). The dissociation curves were compared between different samples to eliminate false-positive results.

In vivo and histopathology studies

Animals

Adult male Wistar rats weighing 200–250 g were obtained from the animal facility at the National Research Centre (Giza, Egypt). They were maintained on a standard laboratory diet and provided unlimited access to tap water. The experimental animals were housed in a temperature-controlled room at 22–25°C with a 12-h light/dark cycle. Care for all animals adhered to ethical standards, and the study protocols followed institutional guidelines for the use of laboratory animals. The research was approved by the Ethics Committee for Animal Experimentation at the Faculty of Pharmacy, Port Said University (approval no. REC.PHARM.PSU.22–7), and complied with the Guide for the Care and Use of Laboratory Animals published by the US National Institutes of Health (NIH publication no. 85–23, revised 2011).

Experimental design

Four groups, each consisting of 15 rats, were classified as follows: group 1 (G1), which served as the negative control group (non-infected, untreated control group); group 2 (G2), the positive control group consisting of infected rats left untreated; and group 3 (G3) and group 4 (G4), which comprised challenged rats with the highest multi-virulent VRSA strain. G3 was treated topically with vancomycin, while G4 received a combination of vancomycin and the most potent anti-virulence compound. All rats underwent anesthesia using ketamine and xylazine before their back hair was shaved. Subsequently, a full-thickness wound was created using a 20-mm diameter biopsy puncher. Immediately after wound induction, 5 µL [1×10^5 colony forming unit per milliliter (CFU/ml)] of VRSA was applied to the wounds of rats in G2, G3, and G4. Following 24 h of bacterial inoculation, G3 and G4 commenced receiving topical application of vancomycin and the combination of vancomycin/the most potent anti-virulence compound on the wounds, respectively. The change in the wound healing area was monitored over a span of 3 weeks, with wound measurements taken using a caliper on days 3, 5, 10, 14, and 21 post-initial wounding. In addition, the total aerobic microbial count was assessed in all four groups on days 3, 5, 10, 14, and 21. Finally, the rats were euthanized and the skin tissue samples from the wound area dissected out for histopathological examination (Nagappa and Cheriyan, 2001).

Determination of *in vivo* antibacterial activity and wound healing ability of vancomycin/the most potent anti-virulence compound combination

An animal model experiment on wound healing was conducted to assess both the antibacterial efficacy and the healing potential of the combination of vancomycin/the most potent anti-virulence compound on infected skin wounds (Nagappa and Cheriyan, 2001; Van de Vyver et al., 2021). The percentage of wound healing area was calculated using the following equation: Wound area % = $(W_t/W_i) \times 100$, where, W_t is the wound area at a certain time point and W_i is the initial wound healing area.

Determination of the total aerobic microbial count

The total aerobic microbial count was assessed in the four groups on days 3, 10, and 14 using Dehydrated Plate Count Agar. The aseptic technique was employed, and the initial dilution was prepared from the sample to a 99-mL sterile saline blank, resulting in a 1/100 or 10^{-2} dilution. The CFU per milliliter or gram of the sample was determined by dividing the number of colonies by the dilution factor and then multiplying by the volume of specimen added to the liquefied agar. The CFU was calculated using the formula: Number of colonies (CFUs) = # of bacteria/mL dilution × amount plated.

Histopathological and healing score assessment

At the end of days 3, 5, 10, 14, and 21 post-initial wounding, the mice were euthanized and the skin tissue samples from the wound area were excised and placed in neutral buffered formalin (10%) for fixation. The samples were then processed in xylenes and alcohols before embedding in paraffin wax. Sections of 5 µm were sliced and subjected to hematoxylin and eosin (H&E) staining for examination under light microscopy (Bancroft and Gamble, 2008). An Olympus CX43 light microscope (Olympus, Tokyo, Japan) equipped with a

ToupTek camera (ToupTek, Hangzhou, China) was utilized to examine the tissue slides and to capture images. The histologic wound healing score (Abdellatif et al., 2021) was used to evaluate granulation tissue formation, re-epithelialization, inflammation, and angiogenesis at the wound site. The scoring criteria for re-epithelialization were as follows: 4 = Complete epidermal remodeling; 3 = Moderate epithelial proliferation; 2 = Incomplete epidermal organization; 1 = Poor epidermal organization; and 0 = Absence of epithelial proliferation. For the granulation tissue and collagen matrix organization, the scores were: 4 = Complete organized tissue; 3 = Thick granulation layer and well-formed collagen; 2 = Moderate remodeling; 1 = Thin immature and inflammatory tissue; and 0 = Immature granulation and inflammatory tissue. The degree of inflammation was assessed as follows: 4 = 13–15 inflammatory cells per histological field; 3 = 10–13 inflammatory cells per histological field; 2 = 7–10 inflammatory cells per histological field; 1 = 4–7 inflammatory cells per histological field; and 0 = 1–4 inflammatory cells per histological field. Angiogenesis was evaluated based on the number of vessels per site and associated features, with scores ranging from 4 = more than seven vessels per site arranged vertically toward the epithelial surface; 3 = five to six vessels per site, slight edema, and congestion; 2 = three to four vessels per site, moderate edema, and congestion; 1 = one to two vessels per site with edema, hemorrhage, and congestion; and 0 = absence of angiogenesis and presence of congestion, hemorrhage, and edema.

Statistical analysis

Qualitative data were presented as percentages and frequencies, while numerical data were expressed as mean, standard error, standard deviation, or median, with appropriate ranges. Analysis of variance (ANOVA) was conducted using a two-factor model without replication. Both categorical and numerical data analyses were performed using SPSS software (version 20; SPSS, Chicago, IL, USA). A p-value <0.05 was considered statistically significant. In addition, GraphPad Prism version 6 (GraphPad Software Inc., San Diego, CA, USA) and the R packages corrplot, heatmaply, ggpubr, and hmisc were employed for the construction of all heat maps in this study. Moreover, correlation coefficients (r values) were utilized to evaluate the associations between biofilm production and clinical samples, as well as the different strain types. Positive correlations were indicated by r values greater than 0, while negative correlations were observed when the r values were less than 0 (Elmanakhly et al., 2024).

Results

Prevalence of MRSA and VRSA isolates

Among the 250 clinical specimens, 62 isolates of *S. aureus* (24.8%) were confirmed using standard bacteriological methods and API 20S. These isolates were confirmed based on the genetic amplification of the specific 16S rRNA gene. Interestingly, 43.5% (27/62) of these isolates exhibited resistance to cefoxitin and oxacillin antibiotics and thus were classified as MRSA strains. On the other hand, 11.3% (7/62) of the detected *S. aureus* isolates were identified as VRSA strains based on broth microdilution and the Biomerieux VITEK®2 automated ID/AST system, with MIC breakpoints ≥16 μg/mL. Furthermore, the MIC values determined by the E-TEST were in agreement with those obtained using both the agar dilution method and the Biomerieux VITEK®2 automated ID/AST system, confirming seven VRSA strains with MIC values ≥16 μg/mL. It is worth noting that all VRSA strains also displayed resistance to cefoxitin and oxacillin antibiotics (seven VRSA out of 27 MRSA isolates). The majority of the MRSA and VRSA isolates were found in pus specimens; however, the urine and blood samples showed the lowest rates of infection with MRSA and VRSA isolates, respectively. Both MRSA and VRSA isolates were more prevalent among female samples compared with male samples.

Antimicrobial susceptibility profiles of the MRSA and VRSA isolates

Regrettably, all 27 MRSA isolates exhibited MDR patterns, indicating resistance to three or more antimicrobial classes, as depicted in Figure 1. These isolates demonstrated complete resistance to β-lactam antibiotics such as cefoxitin, penicillin G, and oxacillin, as well as β-lactams combined with β-lactamase inhibitors such as amoxicillin/clavulanic acid. As anticipated, the antimicrobial resistance patterns observed in the VRSA isolates were particularly alarming when compared with those of the VSSA isolates. Both VSSA and VRSA isolates exhibited high resistance rates to fusidic acid, gentamicin, and tetracycline; however, they demonstrated relatively lower resistance rates to nitrofurantoin and rifampicin. Fortunately, all of the VSSA strains and over 50% of the VRSA strains displayed sensitivity to pristinamycin (quinupristin/dalfopristin) and linezolid, as illustrated in Supplementary Figure S1.

Phenotypic identification of the hemolysin- and biofilm-producing MRSA and VRSA strains

All 27 MRSA isolates under investigation exhibited clear hemolytic zones on BA plates, indicating their capacity as hemolysin producers. Approximately 48.1% (13 out of 27) of the MRSA isolates were confirmed as biofilm producers using the MTP method (Supplementary Figures S1, S2). Among these 13 biofilm-producing MRSA isolates, six were VRSA isolates and seven were VSSA isolates (Supplementary Figure S1). Statistical analysis revealed that the source of the isolates could serve as a predictor of MRSA biofilm formation, as there was a significant association between the isolate source and biofilm formation. A strong positive

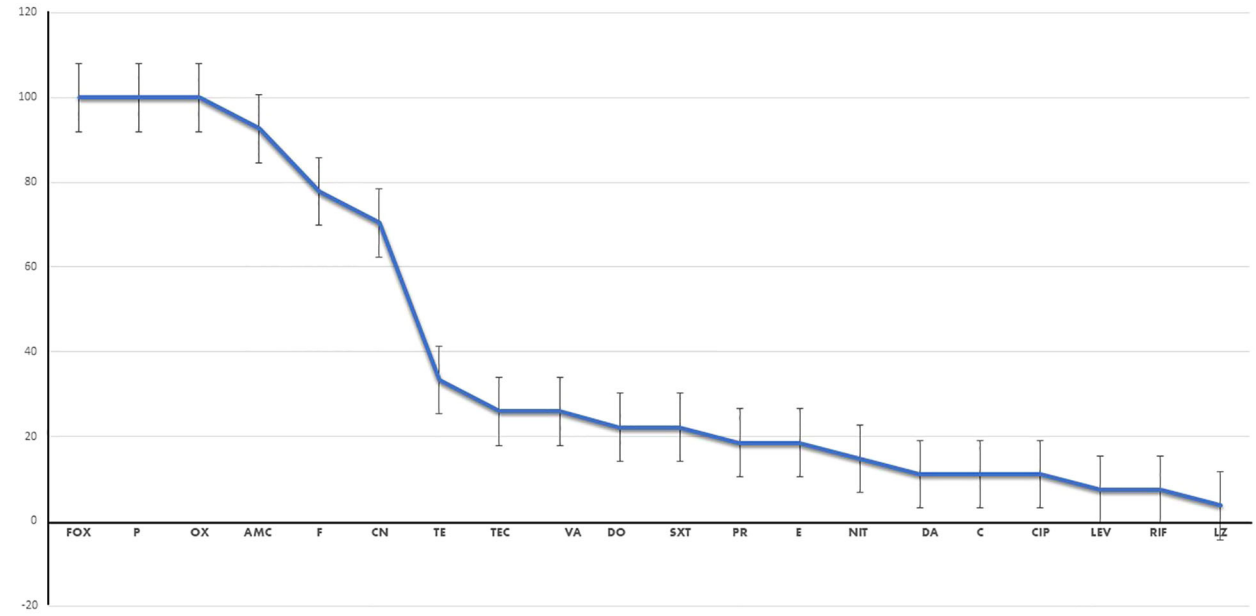

FIGURE 1
Percentage of resistance to each antimicrobial drug of the investigated isolates. *Fox*, cefoxitin; *P*, benzylpenicillin; *OX*, oxacillin; *AMC*, amoxicillin/clavulinic acid; *CN*, gentamicin; *E*, erythromycin; *DA*, clindamycin; *NFT*, nitrofurantoin; *LEZ*, linezolid; *VA*, vancomycin; *TEC*, teicoplanin; *TE*, tetracycline; *DC*, doxycycline; *CIP*, ciprofloxacin; *LEV*, levofloxacin; *C*, chloramphenicol; *FA*, fusidic acid; *RF*, rifampicin; *TMP/SXT*, cotrimoxazole; *QD*, pristinamycin (quinupristin/dalfopristin).

correlation was observed between biofilm production and both wound swab and urine samples, with a slightly weaker correlation for the pus samples ($r > 0$). However, a negative association was noted with the blood samples ($r < 0$). Similarly, biofilm production was consistently found among the VRSA strains ($r > 0$), while non-biofilm production was prevalent among the VSSA strains ($r < 0$), as shown in Supplementary Figure S3.

Molecular detection of virulence genes

Molecular analysis was conducted on 13 isolates, consisting of seven MRSA and six VRSA isolates, which were MDR, hemolysin, and biofilm producers, as illustrated in Figure 2. The virulence profiles of the examined isolates were striking, with all of them exhibiting multi-virulent profiles and harboring more than six virulence genes, with the exception of one isolate. The molecular analysis documented the presence of both the *icaD* and *seb* virulence genes in all the examined isolates (100%). Furthermore, all of the investigated isolates carried at least one of the hemolysin genes (i.e., *hla*, *hlb*, and *hlg*), with approximately 69.2% of these isolates possessing all three hemolysin genes; however, 92.3% of the tested isolates harbored *hla* or *hlb*, whereas *hlg* was detected in 84.6% of the investigated isolates.

Significantly, the *lukED*, *icaA*, and *tst* genes were detected in 92.3%, 76.9%, and 7.7% of the isolates in this study, respectively. The *seb*, *sed*, and *see* genes, on the other hand, were prevalent among the examined isolates at rates of 100%, 84.6%, and 69.2%, respectively. However, none of the examined isolates carried the *sec* and *sea* genes (Figure 2).

Molecular docking analysis of coumarin, simvastatin, and ibuprofen to predict their affinity scores for the MRSA virulence genes

The molecular docking results indicated that all tested compounds (i.e., coumarin, simvastatin, and ibuprofen) exhibited anti-virulence activities. Ibuprofen displayed the highest affinity for the targets leucocidin ED, exfoliative toxin B, intracellular adhesive toxin A, and hemolysin virulence proteins, with affinity scores of −6.2, −8.3, −15.38, and −12.90, respectively. In contrast, simvastatin showed greater affinity to PBP, TSST, and enterotoxin, with affinity scores of −7.5, −6.5, and −8.3, respectively. Conversely, coumarin exhibited lower affinity to all virulence factors, with affinity scores of −5.4, −6.5, −5, −7.5, −11.84, and −10.84. These docking results are detailed in Supplementary Table S2 and depicted in Figures 3, 4, and 5.

In vitro antibacterial and anti-virulence assays for the investigated compounds

Simvastatin demonstrated antibacterial effects at elevated concentrations against two MRSA strains and one VRSA strain (the top three most highly multi-virulent MRSA/VRSA strains), along with the standard *S. aureus* (ATCC 33591), with MICs ranging from 1,250 to 20,000 μg/mL. In addition, this drug exhibited relatively low anti-biofilm activities at sub-MIC values and had no effect on hemolysin production in all investigated isolates. On the other hand, coumarin showed antimicrobial

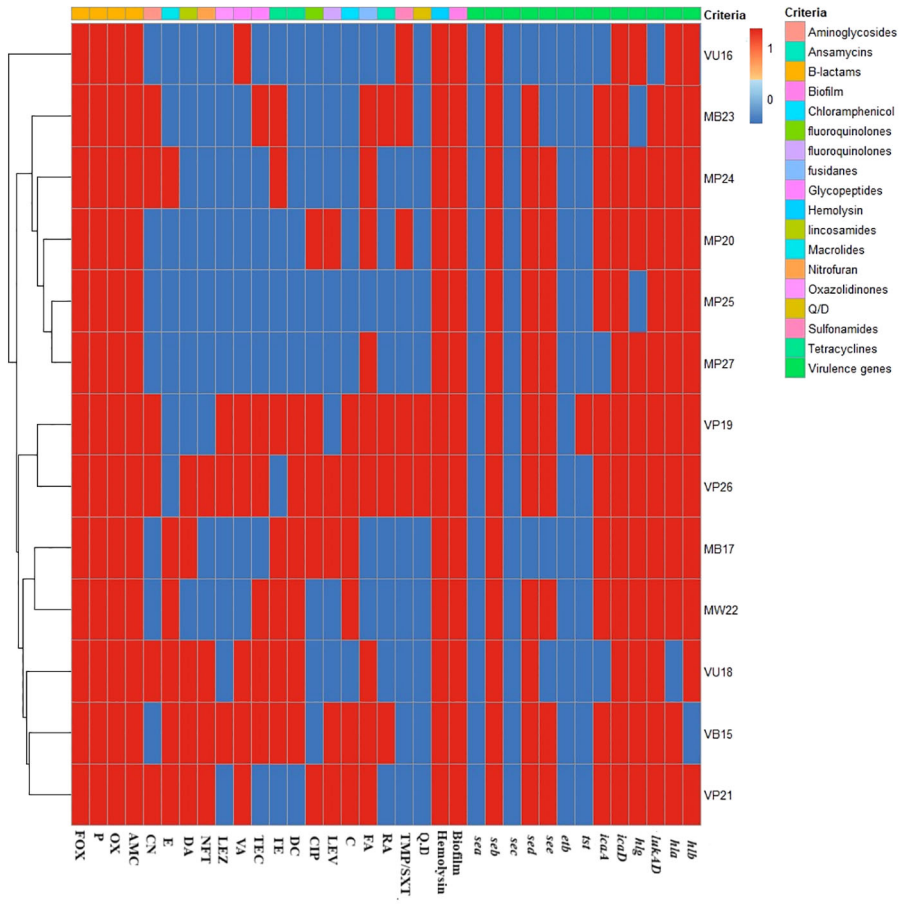

FIGURE 2
Heat map displaying the antimicrobial resistance and virulence gene profiles. For the isolate code, *M* and *V* represent the methicillin-resistant *Staphylococcus aureus* (MRSA) and vancomycin-resistant *S. aureus* (VRSA) strains, respectively. However, the *second letter* refer to the type of samples from which the isolate was recovered (i.e., *P*, pus; *B*, blood; *U*, urine; *W*, wound swab), and the *numerical values* refer to the order of recovery. The *red* and *blue colors* refer to the presence or the absence of resistance to each antimicrobial, biofilm, and hemolysin production, respectively. *Fox*, cefoxitin; *P*, benzylpenicillin; *OX*, oxacillin; *AMC*, amoxicillin/clavulinic acid; *CN*, gentamicin; *E*, erythromycin; *DA*, clindamycin; *NFT*, nitrofurantoin; *LEZ*, linezolid; *VA*, vancomycin; *TEC*, teicoplanin; *TE*, tetracycline; *DC*, doxycycline; *CIP*, ciprofloxacin; *LEV*, levofloxacin; *C*, chloramphenicol; *FA*, fusidic acid; *RF*, rifampicin; *TMP/SXT*, cotrimoxazole; *QD*, pristinamycin (quinupristin/dalfopristin). *sea*, *seb*, *sec*, *sed*, and *see* are the staphylococcal enterotoxins A, B, C, D, E genes; *hla*, *hlb*, and *hlg* are the hemolysin A, B, and G genes; *icaA* and *icaD* are the intracellular adhesive toxins A and D; *tst* is the toxic shock syndrome toxin gene; *etb* is the exfoliative toxin B gene; and *LukED* is the leukocidin gene.

activities, with MICs ranging from 0.763 to 390.6 µg/mL. Moreover, it displayed anti-biofilm and anti-hemolysis activities at sub-MIC values. As for ibuprofen, this drug demonstrated high antimicrobial activities at very low concentrations, with MIC values ranging from 0.24 to 0.10 µg/mL, and exhibited significant anti-biofilm and anti-hemolysis activities at sub-MIC values. Therefore, ibuprofen emerged as the most effective antimicrobial and anti-virulence compound against both MRSA and VRSA when compared with coumarin and simvastatin.

Assessment of anti-virulence activities through monitoring alterations in the expression of virulence genes

The expression levels of individual virulence genes were standardized using the corresponding bacterial housekeeping gene 16s rRNA. The fold changes in the expression of the virulence genes were assessed in VRSA and MRSA isolates treated with coumarin, simvastatin, and ibuprofen. The findings revealed that ibuprofen exhibited greater anti-virulence efficacy compared with coumarin and simvastatin, as evidenced by the downregulation of all the studied virulence genes upon ibuprofen treatment (Supplementary Figure S4).

Analysis of the effect of ibuprofen on wound healing through *in vivo* and histopathological examination

Total aerobic microbial count

Rats treated with vancomycin and the vancomycin/ibuprofen (the most potent anti-virulence drug) combination exhibited a significant decrease in the total microbial count by 95.69% and

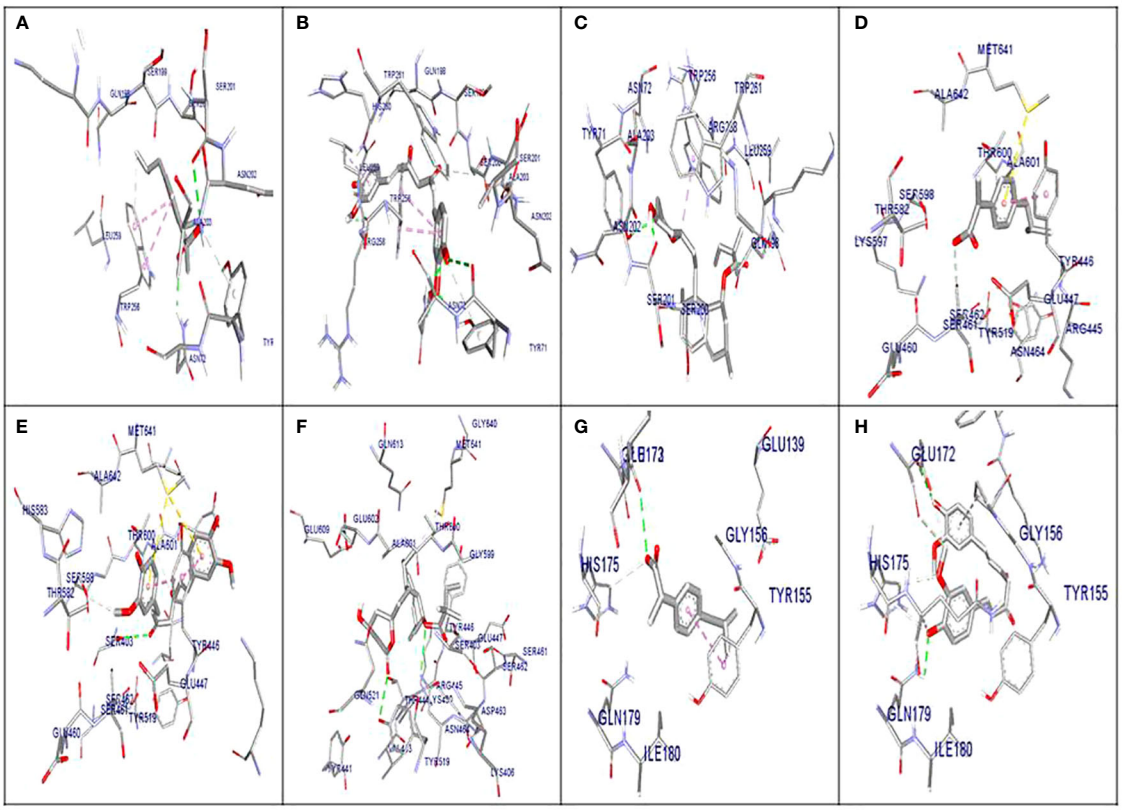

FIGURE 3
Molecular docking of the investigated compounds with the *lukED*, *pbp*, and *tst* virulence genes. **(A–C)** Three-dimensional visual representations of the drugs coumarin **(A)**, ibuprofen **(B)**, and simvastatin **(C)** showing bond formation and position in the active site of *lukED*. **(D–F)** Three-dimensional visual representations of the drugs coumarin **(D)**, ibuprofen **(E)**, and simvastatin **(F)** showing bond formation and position in the active site of *pbp*. **(G, H)** Three-dimensional visual representations of coumarin **(G)** and ibuprofen **(H)** showing bond formation and position in the active site of *tst*.

99.98%, respectively, compared with the infected, untreated group on day 3. Furthermore, on day 5, the total microbial count decreased in the vancomycin- and vancomycin/ibuprofen-treated groups by 99.99% and 99.96%, respectively. Similarly, on day 14, the treated groups showed a significant decrease in the microbial count by 99.89% and 99.99%, respectively. It is noteworthy that the vancomycin/ibuprofen-treated group displayed a significant decrease in the total microbial count compared with the vancomycin-treated group, as illustrated in Table 1.

Effect of vancomycin and the vancomycin/ibuprofen combination on wound healing in mice infected with VRSA

There was an insignificant decrease in the wound area percentage in the vancomycin-treated group on days 3, 5, and 10. In contrast, the vancomycin/ibuprofen-treated group exhibited a significant reduction in the wound area percentage on day 3 compared with the infected, untreated group (Figure 6). Moreover, there was a noteworthy decrease in the wound area percentage in the vancomycin-treated group by 18.34% and 12.5% on days 14 and 21, respectively, compared with the infected, untreated group. Notably, treatment with the vancomycin/ibuprofen combination significantly reduced the wound area percentage by 23.3% and 17.5% on days 14 and 21, respectively. It is worth mentioning that, on days 14 and 21, the vancomycin/ibuprofen group exhibited a significant decrease in the wound area percentage compared with the vancomycin-treated group (Figure 6).

Histopathology and healing score

On day 3, the histopathological images of the wound area across the different experimental groups exhibited similarities. A thick sero-cellular crust composed of necrotic tissue and inflammatory exudate covered the wound gap. Inflamed granulation tissue and hemorrhagic exudate were observed in some cases. The degree of inflammation appeared to decrease in G3 and G4 (Figures 7A-D). By day 5, G1 displayed a thick crust comprising necrotic tissue debris and infiltrating inflammatory cells, hindering re-epithelialization and granulation tissue formation. G2 exhibited intense infiltration of inflammatory cells at the wound site along with abundant necrotic tissue and bacterial clusters. Despite the presence of necrotic tissue in G3, inflammation was confined to the upper layer of the wound. In G4, granulation tissue formation was

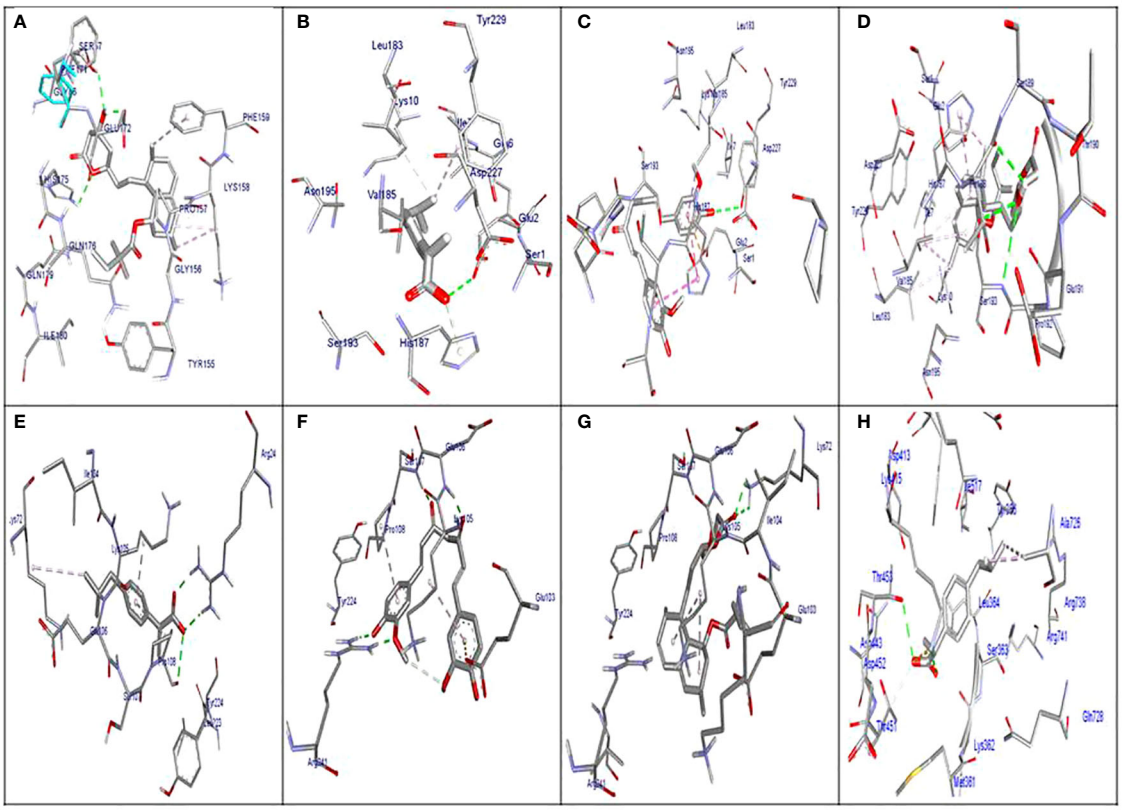

FIGURE 4
Molecular docking of the investigated compounds with the *tst*, *etb*, *ica*, and enterotoxin virulence genes. **(A)** Visual representation (3D and 2D) of simvastatin showing bond formation and position in the active site of *tst*. **(B–D)** Three-dimensional visual representations of coumarin **(B)**, ibuprofen **(C)**, and simvastatin **(D)** showing bond formation and position in the active site of enterotoxin. **(E, F)** Three-dimensional visual representations of coumarin **(E)** and ibuprofen **(F)** showing bond formation and position in the active site of *etb*. **(G)** Visual representation (3D and 2D) of simvastatin showing bond formation and position in the active site of *etb*. **(H)** Visual representation (3D and 2D) of coumarin showing bond formation and position in the active site of *icaA*.

evident, accompanied by numerous capillaries despite the pronounced inflammatory response (Figures 7E-H). On day 10, G1 presented with granulation tissue filling the wound gap along with significant inflammatory cell infiltration. Partial re-epithelialization was observed at the wound edges. G2 displayed a marked inflammatory cell infiltration and delayed re-epithelialization, with increased amounts of necrotic tissue in the wound gap. G3 exhibited partial re-epithelialization at the wound edges with granulation tissue filling the wound area, accompanied by moderate inflammatory cell infiltration. G4 showcased collagen-rich organized tissue filling the wound area, along with numerous newly formed blood vessels. Partial re-epithelialization was also noted, accompanied by mild inflammatory cell infiltration (Figures 8A-D).

On day 14, notable observations included delayed re-epithelialization in G1, with granulation tissue present and a marked infiltration of inflammatory cells filling the wound area. G2 displayed intense inflammation within the formed granulation tissue, coupled with delayed re-epithelialization and increased necrotic tissue debris. G3 exhibited significant improvement, with complete re-epithelialization and organized tissue filling the wound area, accompanied by mild inflammation. Similarly, G4 showed enhanced healing, with a wound surface fully covered by newly formed epithelium. Collagen-rich organized tissue filled the wound gap, showing minimal inflammation and numerous blood vessels (Figures 8E-H). Interestingly, by day 21, G1 demonstrated a granulation tissue core filling the wound gap, with delayed re-epithelialization and infiltration of inflammatory cells. The formed granulation tissue exhibited numerous dilated blood vessels and a marked inflammatory cell infiltration. G2 showed only partial re-epithelialization, while G3 displayed complete re-epithelialization, with the wound surface covered by newly formed epithelium. Organized tissue filled the wound gap, featuring numerous capillaries and minimal infiltration of inflammatory cells. G4 exhibited significant wound contraction and re-epithelialization, with the wound gap filled with collagen-rich organized tissue showing minimal inflammation. The wound surface was covered by hyperplastic newly formed epithelium (Figures 9A-D).

It is worth noting that the healing scores at different time intervals consistently showed superior healing criteria in G4, closely followed by G3. These groups demonstrated a notable reduction in inflammation during the initial stages of sacrifice compared with

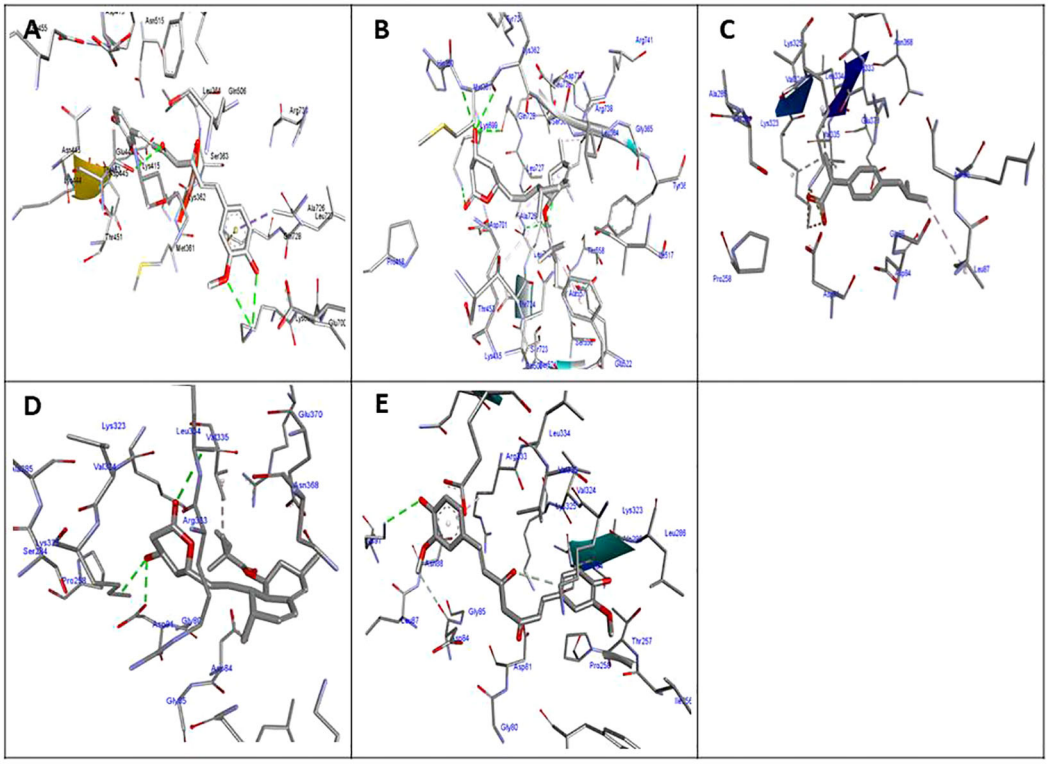

FIGURE 5
Molecular docking of the investigated compounds with the *icaA* and *hla* virulence genes. **(A, B)** Three-dimensional visual representations of ibuprofen **(A)** and simvastatin **(B)** showing bond formation and position in the active site of *icaA*. **(C–E)** Three-dimensional visual representations of coumarin **(C)**, ibuprofen **(D)**, and simvastatin **(E)** showing bond formation and position in the active site of *hla*.

the untreated groups (G1 and G2). Later on, G3 and G4 exhibited improved re-epithelialization and formation of organized tissue. In contrast, both untreated groups showed increased inflammation toward the end of the experiment.

Discussion

Serious complications from skin, soft tissue, bone, and lung infections, which contribute to increased morbidity and mortality globally, are often caused by MRSA strains. Unfortunately, the situation has worsened due to the widespread emergence of VRSA strains. Despite extensive efforts over the years to develop new antimicrobial drugs to combat MRSA and VRSA, treatment failures and poor prognoses remain common. Therefore, we aimed to address this crisis by investigating the anti-virulence activities of certain natural (coumarin) and synthetic (simvastatin and ibuprofen) compounds. Notably, the pathogenicity of *S. aureus* is attributed to its production of numerous virulence factors, including secreted toxin proteins (e.g., hemolysin), extracellular polysaccharides (e.g., intercellular adhesion), and other elements that facilitate infection processes (Karmakar et al., 2016).

Resistance to methicillin, macrolides, aminoglycosides, and lincosamides, as well as combinations of these antimicrobial drugs, has been frequently reported (Bendary et al., 2016a). *S. aureus* has developed resistance not only to methicillin but also to many commonly used antibiotics. As new antimicrobial drugs are introduced, it is likely that this highly adaptable pathogen will develop resistance to them as well. In this study, all of the detected MRSA strains exhibited MDR patterns, and the antimicrobial resistance patterns of the VRSA strains were particularly alarming. The widespread occurrence of the MDR strains in this study may be attributed to the overuse or misuse of various broad-spectrum antibiotics, particularly β-lactams such as penicillins and cephalosporins. This indiscriminate use leads to the

TABLE 1 Effect of vancomycin and the combination of vancomycin/ibuprofen on total microbial count.

Total microbial count (CFU/g tissue)			
	Day 3	Day 10	Day 14
Infected, untreated (positive control)	72×10^8 ± 30,000	10×10^6 ± 284.7	92×10^5 ± 233.3
Infected, vancomycin-treated group	31×10^7 ± 29667[a]	12.9×10^4 ± 100[a]	94×10^2 ± 16.7[a]
Infected, vancomycin/ibuprofen-treated group	98×10^4 ± 166.7[a,b]	10×10^2 ± 33.3[a,b]	66 ± 1.5[a,b]

Data are expressed as the mean ± SE, one-way ANOVA.
[a]Significant difference from the infected, untreated group.
[b]Significant difference from the infected, vancomycin-treated group.

10.3389/fcimb.2024.1403219

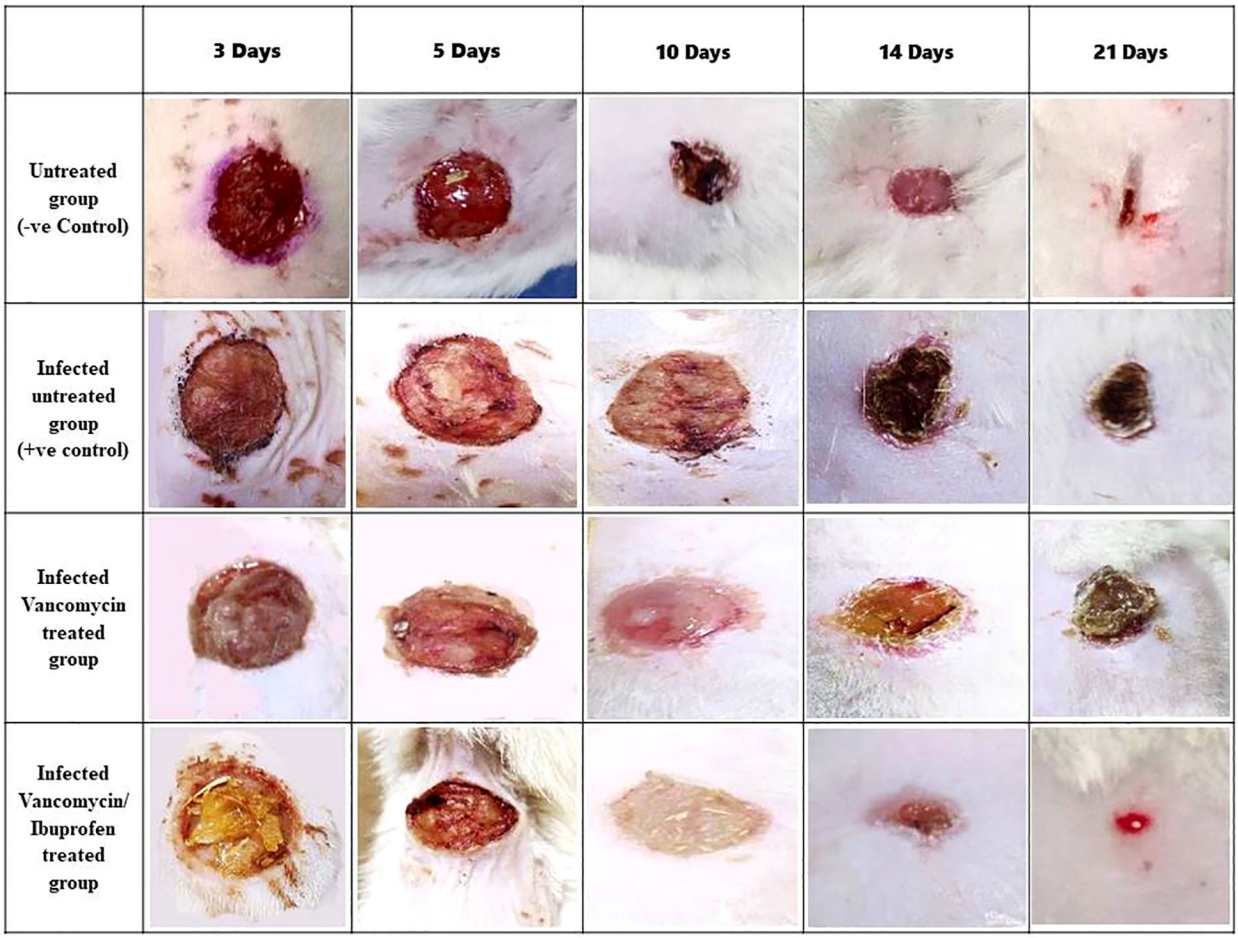

FIGURE 6
Wound area percentage during the healing process on days 3, 5, 10, 14, and 21. Data are expressed as the mean ± SEM, one-way ANOVA followed by the Tukey–Kramer multiple comparisons test. $p < 0.05$.

development of resistance and an increased risk of MRSA infection, corroborating findings from a previous study conducted in Iraq by Algammal et al. (2020).

Notably, infections caused by MDR–MRSA strains are often treated empirically with antibiotics that are ineffective against MRSA, which can exacerbate the antibiotic resistance (Romeo, 2008). Unfortunately, several studies have reported an increase in the prevalence of VRSA strains (Bendary et al., 2016b; Abd El-Aziz et al., 2018). Vancomycin is generally the drug of choice for the treatment of serious MRSA and MSSA infections. However, the irrational use of antibiotics has led to the emergence of VRSA strains (Khanam et al., 2016). Consequently, the MRSA and VRSA infections caused by MDR strains pose severe global health crises, making the development of novel antimicrobial drugs urgently necessary. To date, the development of new drugs with clear antibacterial mechanisms for MDR pathogens remains a significant challenge (Zhang et al., 2021).

The ability of staphylococci to produce biofilms is recognized as an important virulence trait (Vancraeynest et al., 2004). In this study, 48.1% of the MRSA isolates were confirmed to be biofilm producers using quantitative MTP methods, with genetic confirmation through the detection of the *icaD* and *icaA* genes. Another study reported a higher prevalence of biofilm-producing MRSA and VRSA strains (Saber et al., 2022). With regard to the hemolytic activity, 85.19% of the tested MRSA isolates in this study produced hemolysins, indicating significant hemolytic activity. In addition, most of the MRSA strains possessed hemolysin toxin-producing genes (Dunyach-Remy et al., 2016). Variations in biofilm and hemolysin production may be attributed to factors such as the geographical origin, the type of specimen, and genetic mutations of the *S. aureus* isolate. Environmental conditions, including the surface type (rough or smooth), surface charge, porosity, and growth medium, can also influence biofilm formation. These factors have been discussed in previous studies (Abdelraheem et al., 2021; Silva et al., 2021).

On the other hand, infections with MRSA strains are problematic due to the widespread presence of various clones carrying multiple antimicrobial resistance genes. The degree of microbial pathogenesis depends on the presence of virulence genes, and the absence of these genes is typically associated with non-pathogenic strains (Elsayed et al., 2022; Eibach et al., 2017).

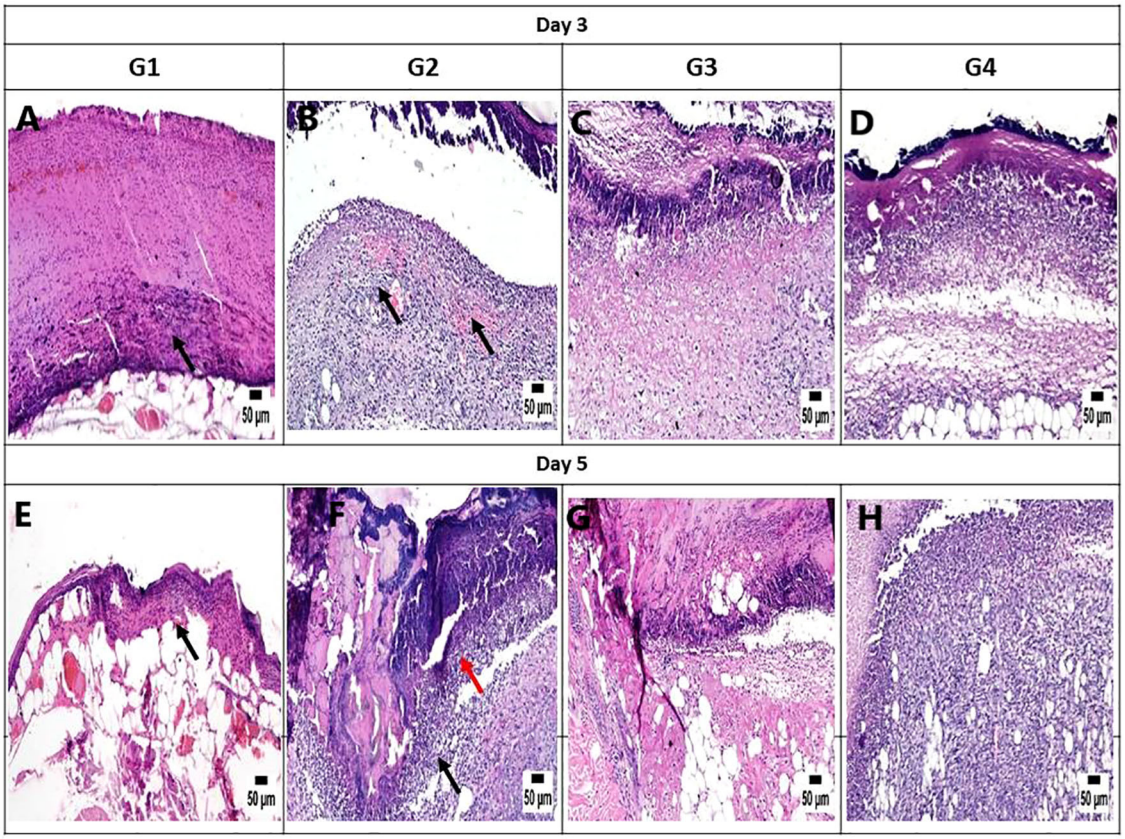

FIGURE 7
Photomicrograph of the mouse skin wound for the different groups after 3 and 5 days. **(A)** Photomicrograph of the skin in group 1 (G1) at 3 days, higher magnification showing necrotic tissue debris over the wound (*arrow*) (H&E). **(B)** Photomicrograph of the skin in G2 at 3 days showing intense inflammation and hemorrhage in the wound area (*arrow*) (H&E). **(C)** Photomicrograph of the skin in G3 at 3 days, higher magnification showing necrotic tissue in the wound area with mild inflammatory cell infiltration (H&E). **(D)** Photomicrograph of the skin in G4 at 3 days showing necrotic tissue in the wound area with mild inflammatory cell infiltration (H&E). **(E)** Photomicrograph of the skin in G1 at 5 days, higher magnification showing necrotic tissue debris over the wound (*arrow*) (H&E). **(F)** Photomicrograph of the skin in G2 at 5 days showing intense inflammation (*black arrow*) with the presence of bacterial colonies (*red arrow*) (H&E). **(G)** Photomicrograph of the skin in G3 at 5 days, higher magnification showing necrotic tissue in the wound area with mild inflammatory cell infiltration (H&E). **(H)** Photomicrograph of the skin in G4 at 5 days, higher magnification showing granulation tissue formation with inflammatory cell infiltration (H&E).

Unfortunately, the virulence profiles of the isolates investigated in this study were alarming, with all exhibiting multi-virulent profiles. The high frequency of certain virulence genes may indicate the emergence of multi-virulent isolates (Hoseini Alfatemi et al., 2014). Consequently, a new therapeutic strategy is needed to interfere with pathogen virulence arrays, preventing microbial pathogenesis without killing the microbes and, thus, applying less evolutionary pressure on resistance development. The discovery of new anti-virulence compounds is crucial for improving treatment success and prognosis in infectious diseases.

Molecular docking is a crucial tool for the development of new drugs. This technique models the interaction between a promising drug and its receptor at the atomic level, allowing researchers to understand fundamental biochemical processes and to assess the binding affinity with the target protein (McConkey et al., 2002). In this study, molecular docking analysis predicted the affinity scores of coumarin, simvastatin, and ibuprofen to specific virulence protein targets *in vitro*. The results demonstrated that all of these compounds have anti-virulence activities, with ibuprofen showing the highest affinity scores for most of the investigated virulence proteins. These anti-virulence compounds present a promising alternative therapy for effectively managing and treating infections with resistant MRSA strains. The molecular docking results were corroborated by phenotypic evaluations of the anti-biofilm and anti-hemolytic activities and were further confirmed genotypically using real-time PCR. All investigated virulence genes were downregulated upon treatment with these compounds, showing fold changes of less than 1, with the lowest levels of downregulation observed post-treatment with ibuprofen. These findings align with other studies suggesting that ibuprofen is a good candidate for repurposing as an antimicrobial agent (Obad et al., 2015; Oliveira et al., 2019). In addition, biofilm formation increased gradually with decreasing drug concentration, supporting previous research indicating that ibuprofen may be effective as an anti-biofilm agent and could be a viable alternative for the treatment of active and mature biofilms produced by *S. aureus* (Oliveira et al., 2019; Paes-Leme and da Silva, 2021).

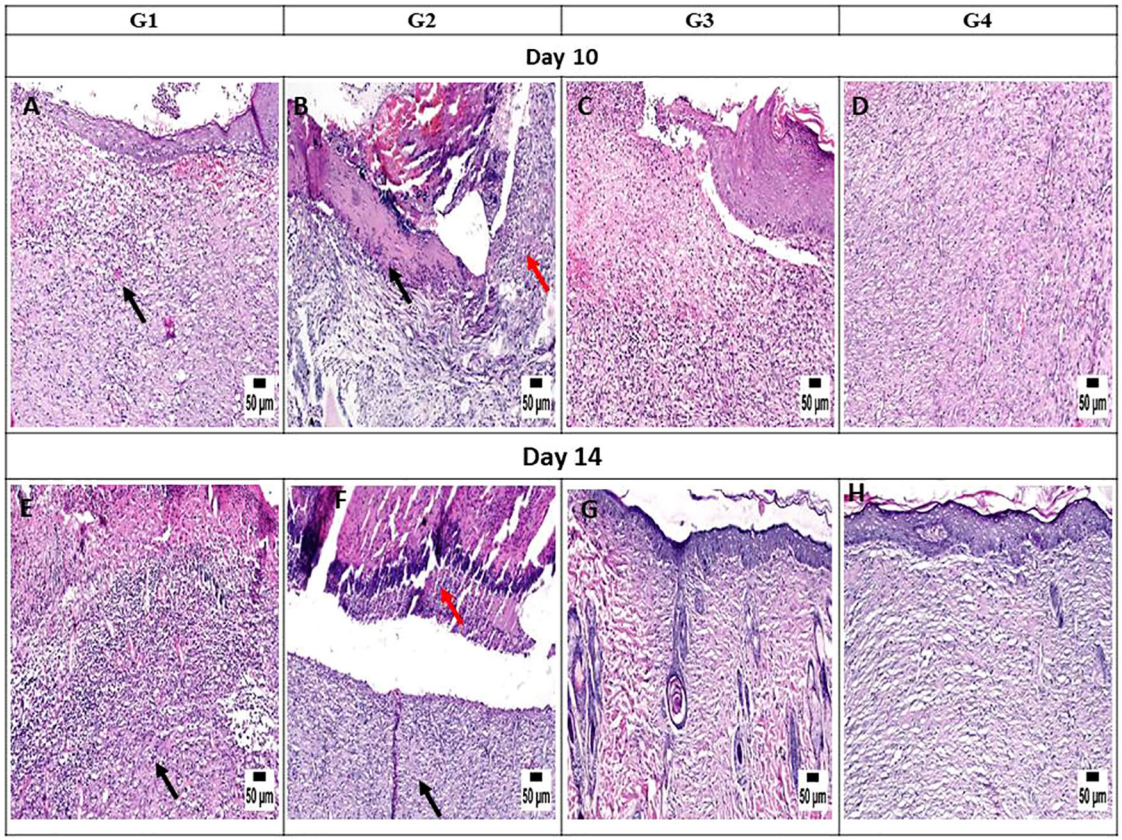

FIGURE 8
Photomicrograph of the mouse skin wound for the different groups after 10 and 14 days. **(A)** Photomicrograph of the skin in group 1 (G1) at 10 days, higher magnification showing inflamed granulation tissue filling the wound gap (*arrow*) with partial re-epithelization (H&E). **(B)** Photomicrograph of the skin in G2 at 10 days showing intense inflammation (*red arrow*) and necrotic tissue in the wound area (*black arrow*) (H&E). **(C)** Photomicrograph of the skin in G3 at 10 days, higher magnification showing granulation tissue in the wound area, inflammatory cell infiltration, and partial re-epithelization (H&E). **(D)** Photomicrograph of the skin in G4 at 10 days showing organized tissue filling the wound gap with mild inflammatory cell infiltration (H&E). **(E)** Photomicrograph of the skin in G1 at 14 days, higher magnification showing granulation tissue with inflammation (*arrow*) (H&E). **(F)** Photomicrograph of the skin in G2 at 14 days showing intense inflammation (*black arrow*) with the presence of necrotic debris (*red arrow*) (H&E). **(G)** Photomicrograph of the skin in G3 at 14 days, higher magnification showing organized tissue filling the wound area with re-epithelization (H&E). **(H)** Photomicrograph of the skin in G4 at 14 days, higher magnification showing organized tissue filling the wound area with complete re-epithelization (H&E).

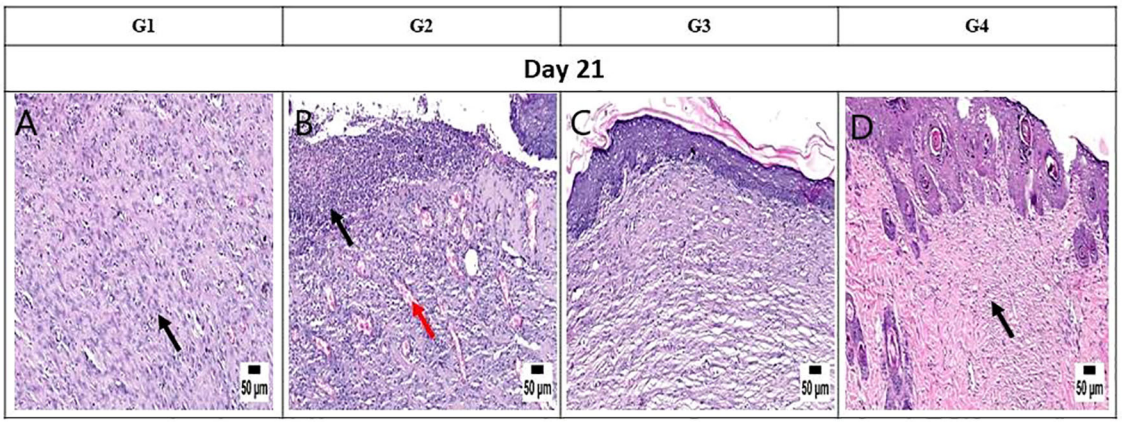

FIGURE 9
Photomicrograph of the mouse skin wound for the different groups after 21 days. **(A)** Photomicrograph of the skin in group 1 (G1) at 21 days, higher magnification showing granulation tissue filling the wound gap (*arrow*) with inflammatory cell infiltration (H&E). **(B)** Photomicrograph of the skin in G2 at 21 days, higher magnification showing intense inflammation (*arrow*) and numerous dilated vessels in the wound area (*red arrow*) (H&E). **(C)** Photomicrograph of the skin in G3 at 21 days, higher magnification showing complete re-epithelization and organized tissue filling the wound area (H&E). **(D)** Photomicrograph of the skin in G4 at 21 days, higher magnification showing collagen-rich organized tissue in the wound gap with complete re-epithelization (H&E).

Undeniably, wound infections caused by MRSA and VRSA strains are a significant global problem. Topical antibacterial and anti-inflammatory formulations can offer improved benefits for treating infected wounds. Previous studies have shown that local administration of ibuprofen provides a pronounced anti-inflammatory effect and reduces pain with smaller doses compared with oral administration. Consequently, the risk of side effects from local application is very low, making it much safer than oral ibuprofen (Sibbald et al., 2006). In addition, the potential antibacterial effect of ibuprofen has been observed in isolated bacterial strains (Al-Janabi, 2010).

Infected wound healing involves complex mechanisms, including the proliferative phase, hemostasis/inflammatory phase, and scar tissue remodeling, which cannot be fully replicated *in vitro* (Abbasi et al., 2022). Therefore, this *in vivo* study was designed to assess the combined effect of local ibuprofen and vancomycin on the treatment of wound infections and the improvement of wound healing. The study demonstrated that treating wound infections caused by VRSA strains with a combination of ibuprofen and vancomycin exhibited superior antibacterial activity compared with vancomycin alone. The combination effectively reduced the total microbial count of the wound over various time intervals (days 3, 5, 10, 14, and 21). In addition, this combination significantly decreased the wound area percentage, reflecting better wound healing, particularly on days 14 and 21. Notably, these results support the concept that the combination of ibuprofen/vancomycin may represent a promising new therapy for the treatment of wound infections and improvement of wound healing due to its superior antibacterial capacity and anti-inflammatory activity. Moreover, the mouse protection assay, which has been used in several studies, confirmed the antimicrobial and anti-virulence activities of some new drugs (Bourne et al., 1999; Hegazy et al., 2020).

In conclusion, MRSA and VRSA strains were frequently identified in several cases discussed in this report. This study confirmed resistance to last-resort anti-staphylococcal drugs such as linezolid and pristinamycin. Fortunately, the repurposing of simvastatin and ibuprofen (FDA-approved drugs) as new anti-virulence agents has shown promising potential without the need for extensive human trials. Interestingly, combining ibuprofen with other anti-staphylococcal drugs has been proven effective in treating MRSA and VRSA infections. These promising results, given the lack of novel antimicrobial drugs and the slow pace of new drug development, can be applied in clinical settings. Fortunately, no further safety evaluations or pharmacokinetic studies are required for these compounds to be used in different countries.

Data availability statement

The original contributions presented in the study are included in the article/Supplementary Material. Further inquiries can be directed to the corresponding author.

Ethics statement

Both ethical approvals and written informed consents to perform this report were necessary for both obtaining human samples and mice protection assays. Our report was done in accordance with to the guidelines of the Helsinki declaration for studies on human subjects. Before starting the work, the protocols of sample collection and in vivo mice protection assay were revised and approved by Faculty of Pharmacy Research Ethical Committee, Port-Said University (REC.PHARM.PSU) with the following Ethical approval number (REC.PHARM.PSU-2022–7). The informed consents for publication of the patients' clinical specimens were taken and a copy of the consent form is available for review by the Editor of this journal.

Author contributions

WB: Methodology, Supervision, Writing – review & editing. MG: Methodology, Writing – review & editing. AE-G: Supervision, Writing – review & editing. ME: Supervision, Writing – review & editing. MK: Supervision, Writing – review & editing. AM: Funding acquisition, Writing – review & editing. NA: Funding acquisition, Resources, Writing – original draft. HS: Writing – original draft, Conceptualization, Formal Analysis. MB: Methodology, Supervision, Writing – original draft, Writing – review & editing.

Funding

The author(s) declare that financial support was received for the research, authorship, and/or publication of this article. Princess Nourah bint Abdulrahman University Researchers Supporting Project number (PNURSP2024R153), Princess Nourah bint Abdulrahman University, Riyadh, Saudi Arabia. Deanship of Scientific Research, Vice Presidency for Graduate Studies and Scientific Research, King Faisal University, Saudi Arabia [GrantA176].

Acknowledgments

The authors gratefully acknowledge to Princess Nourah bint Abdulrahman University Researchers Supporting Project number (PNURSP2024R153), Princess Nourah bint Abdulrahman University, Riyadh, Saudi Arabia. Extended thank for supporting by Deanship of Scientific Research, Vice Presidency for Graduate Studies and Scientific Research, King Faisal University, Saudi Arabia [GrantA176].

Conflict of interest

The authors declare the research was conducted in the absence of any commercial or financial relationships that could be construed as a potential conflict of interest.

Publisher's note

All claims expressed in this article are solely those of the authors and do not necessarily represent those of their affiliated organizations, or those of the publisher, the editors and the reviewers. Any product that may be evaluated in this article, or claim that may be made by its manufacturer, is not guaranteed or endorsed by the publisher.

Supplementary material

The Supplementary Material for this article can be found online at: https://www.frontiersin.org/articles/10.3389/fcimb.2024.1403219/full#supplementary-material

References

Abbasi, K., Ashtiani, R. E., Abdolahi, M., Hosseini, M., Soufdoost, R. S., Alam, M., et al. (2022). Effect of collagen/ibuprofen hydrogel in wound healing: An in *vivo* study. *Adv. Materials Sci. Eng.* 2022, 1–7. doi: 10.1155/2022/xx

Abd El-Aziz, N. K., Abd El-Hamid, M. I., Bendary, M. M., El-Azazy, A. A., and Ammar, A. M. (2018). Existence of vancomycin resistance among methicillin-resistant S. aureus recovered from animal and human sources in Egypt. *Slovenian Veterinary Res.* 55, 221–230. doi: 10.26873/SVR-649-2018

Abd El-Hamid, M. I., El-Tarabili, R. M., Bahnass, M. M., Alshahrani, M. A., Saif, A., Alwutayd, K. M., et al. (2023). Partnering essential oils with antibiotics: proven therapies against bovine *Staphylococcus aureus* mastitis. *Front. Cell. infection Microbiol.* 13. doi: 10.3389/fcimb.2023.1265027

Abd El-Hamid, M. I., Sewid, A. H., Samir, M., Hegazy, W. A. H., Bahnass, M. M., Mosbah, R. A., et al. (2022). Clonal diversity and epidemiological characteristics of ST239-MRSA strains. *Front. Cell. Infection Microbiol.* 12. doi: 10.3389/fcimb.2022.782045

Abdellatif, M. M., Elakkad, Y. E., Elwakeel, A. A., Allam, R. M., and Mousa, M. R. (2021). Formulation and characterization of propolis and tea tree oil nanoemulsion loaded with clindamycin hydrochloride for wound healing: *In vitro* and *in vivo* wound healing assessment. *Saudi Pharm. J.* 29, 1238–1249. doi: 10.1016/j.jsps.2021.10.004

Abdelraheem, W. M., Abdelrahim, S. S., and Zaky, S. H. (2021). Phenotypic and genotypic detection of biofilm formation and methicillin resistance among *Staphylococcus aureus* isolates. *Clin. Microbiol. Infection* 2, 485–496. doi: 10.21608/mid.2021.80188.1163

Abouelfetouh, A. (2017). The status of methicillin resistance among Egyptian *Staphylococcus aureus* isolates: An overview. *Infect. Disord. Drug Targets* 17, 67–69. doi: 10.2174/1871526516666160802111200

Afsar, T., Razak, S., Khan, M. R., Mawash, S., Almajwal, A., Shabir, M., et al. (2016). Evaluation of antioxidant, anti-hemolytic and anticancer activity of various solvent extracts of Acacia hydaspica R. Parker aerial parts. *BMC complementary Altern. Med.* 16, 258. doi: 10.1186/s12906-016-1240-8

Al-Amery, K., Elhariri, M., Elsayed, A., El-Moghazy, G., Elhelw, R., El-Mahallawy, H., et al. (2019). Vancomycin-resistant *Staphylococcus aureus* isolated from camel meat and slaughterhouse workers in Egypt. *Antimicrobial. resistance infection control* 8, 129. doi: 10.1186/s13756-019-0585-4

Algammal, A. M., Hetta, H. F., Elkelish, A., Alkhalifah, D. H. H., Hozzein, W. N., Batiha, G. E., et al. (2020). Methicillin-resistant *Staphylococcus aureus* (MRSA): One health perspective approach to the bacterium epidemiology, virulence factors, antibiotic-resistance, and zoonotic impact. *Infection Drug Resistance* 13, 3255–3265. doi: 10.2147/IDR.S272733

Al-Janabi, A. A. (2010). *In vitro* Antibacterial activity of ibuprofen and acetaminophen. *J. Global Infect. Dis.* 2, 105–108. doi: 10.4103/0974-777X.62880

Almwafy, A. T., Barghoth, M. G., Desouky, S. E., and Roushdy, M. (2020). Preliminary characterization and identification of Gram-positive hemolysis bacteria. *Azzaytuna J. Pharm. Sci.* 62, 2020. doi: 10.21608/ajps.2020.118378

Azzam, A., Khaled, H., Mosa, M., Refaey, N., AlSaifi, M., Elsisi, S., et al. (2023). Epidemiology of clinically isolated methicillin-resistant *Staphylococcus aureus* (MRSA) and its susceptibility to linezolid and vancomycin in Egypt: a systematic review with meta-analysis. *BMC Infect. Dis.* 23, 263. doi: 10.1186/s12879-023-08202-2

Balasubramanian, D., Harper, L., Shopsin, B., and Torres, V. J. (2017). *Staphylococcus aureus* pathogenesis in diverse host environments. *Pathog. Dis.* 75, ftx005. doi: 10.1093/femspd/ftx005

Bancroft, J. D., and Gamble, M. (2008). **Theory and Practice of Histological Techniques** (*6th* ed.). Churchill Livingstone.

Bendary, M. M., Solyman, S. M., Azab, M. M., Mahmoud, N. F., and Hanora, A. M. (2016a). Characterization of Methicillin-Resistant *Staphylococcus aureus* isolated from human and animal samples in Egypt. *Cell. Mol. Biol.* 62, 94–100.

Bendary, M. M., Solyman, S. M., Azab, M. M., Mahmoud, N. F., and Hanora, A. M. (2016b). Genetic diversity of multidrug-resistant *Staphylococcus aureus* isolated from clinical and non-clinical samples in Egypt. *Cell. Mol. Biol.* 62, 55–61.

Bourne, K. Z., Bourne, N., Reising, S. F., and Stanberry, L. R. (1999). Plant products as topical microbicide candidates: assessment of *In vitro* and *In vivo* activity against herpes simplex virus type 2. *Antiviral Res.* 42, 219–226. doi: 10.1016/S0166-3542(99)00020-0

Cheesbrough, M. (2005). "Preface," in *In district laboratory practice in tropical countries (p. V)* (Cambridge, UK: Cambridge University Press). doi: 10.1017/CBO9780511581304.001

Cheesbrough, M. (2017). *Medical Laboratory Manual for Tropical Countries*. 255–275.

Cheung, G. Y. C., Bae, J. S., and Otto, M. (2021). Pathogenicity and virulence of *Staphylococcus aureus*. *Virulence* 12, 547–569. doi: 10.1080/21505594.2021.1878688

Clinical and Laboratory Standards Institute (CLSI) (2022). *Performance standards for antimicrobial susceptibility testing. Approved standard M100-S20* Vol. 32 (Wayne, Pa: National Committee for Clinical Laboratory Standards).

Cong, Y., Yang, S., and Rao, X. (2019). Vancomycin resistant *Staphylococcus aureus* infections: A review of case updating and clinical features. *J. Advanced Res.* 21, 169–176. doi: 10.1016/j.jare.2019.10.005

Dickey, S. W., Cheung, G. Y. C., and Otto, M. (2017). Different drugs for bad bugs: antivirulence strategies in the age of antibiotic resistance. *Nat. Rev. Drug Discovery* 16, 457–471. doi: 10.1038/nrd.2017.23

Divyakolu, S., Chikkala, R., and Ratnakar, K. S. (2019). Hemolysins of *Staphylococcus aureus*—An update on their biology, role in pathogenesis, and as targets for anti-virulence therapy. *Adv. Infect. Dis.* 9, 80–104.

Dunyach-Remy, C., Ngba Essebe, C., Sotto, A., and Lavigne, J. P. (2016). *Staphylococcus aureus* toxins and diabetic foot ulcers: role in pathogenesis and interest in diagnosis. *Toxins* 8, 209. doi: 10.3390/toxins8070209

Eibach, D., Nagel, M., Hogan, B., Azuure, C., Krumkamp, R., Dekker, D., et al. (2017). Nasal carriage of *Staphylococcus aureus* among children in the ashanti region of Ghana. *PloS One* 12, e0170320. doi: 10.1371/journal.pone.0170320

Elmanakhly, A. R., Safwat, N., Tohamy, S. T. K., Elsayed, K. M., ElSherif, H. M., Elsayed, M., et al. (2024). Comparative phenotypic and genotypic analysis of community-acquired and hospital-acquired intra-abdominal infections among liver transplanted patients. *J. Appl. Microbiol.* 135, lxae076. doi: 10.1093/jambio/lxae076

Elsayed, M. E., Abd El-Hamid, M. I., El-Gedawy, A., Bendary, M. M., ELTarabili, R.M., Alhomrani, M., et al. (2022). New Insights into Listeria monocytogenes Antimicrobial Resistance, Virulence Attributes and Their Prospective Correlation. *Antibiotics* (Basel, Switzerland), 11, 1447. doi: 10.3390/antibiotics11101447

Flentie, K., Spears, B. R., Chen, F., Purmort, N. B., DaPonte, K., Viveiros, E., et al. (2019). Microplate-based surface area assay for rapid phenotypic antibiotic susceptibility testing. *Sci. Rep.* 9, 237. doi: 10.1038/s41598-018-35916-0

Ghaly, M. F., Shaheen, A. A., Bouhy, A. M., and Bendary, M. M. (2020). Alternative therapy to manage otitis media caused by multidrug-resistant fungi. *Arch. Microbiol.* 202, 1231–1240. doi: 10.1007/s00203-020-01832-z

Hamdan-Partida, A., González-García, S., Martínez-Ruíz, F. J., Zavala-Sánchez, M.Á., Bustos-Hamdan, A., and Bustos-Martínez, J. (2022). Molecular characterization of *Staphylococcus aureus* strains isolated from mobile phones. *Microorganisms* 10, 669. doi: 10.3390/microorganisms10030669

Hegazy, W. A. H., Khayat, M. T., Ibrahim, T. S., Nassar, M. S., Bakhrebah, M. A., Abdulaal, W. H., et al. (2020). Repurposing anti-diabetic drugs to cripple quorum sensing in *Pseudomonas aeruginosa*. *Microorganisms* 8, 1285. doi: 10.3390/microorganisms8091285

Hoseini Alfatemi, S. M., Motamedifar, M., Hadi, N., and Sedigh Ebrahim Saraie, H. (2014). Analysis of virulence genes among methicillin-resistant *Staphylococcus aureus* (MRSA) strains. *Jundishapur J. Microbiol.* 7, e10741. doi: 10.5812/jjm.10741

Hudzicki, J. (2016). *Kirby-Bauer disk diffusion susceptibility test protocol* (Washington, DC, USA: American Society for Microbiology).

Karmakar, A., Dua, P., and Ghosh, C. (2016). Biochemical and molecular analysis of *Staphylococcus aureus* clinical isolates from hospitalized patients. *Can. J. Infect. Dis. Med. Microbiol.* 2016, 9041636. doi: 10.1155/2016/9041636

Khanam, S., Haq, J. A., Shamsuzzaman, S., Rahman, M. M., and Mamun, K. Z. (2016). Emergence of vancomycin-resistant *Staphylococcus aureus* during hospital admission at a tertiary care hospital in Bangladesh. *Bangladesh J. Infect. Dis.* 3, 11–16. doi: 10.3329/bjid.v3i1.28407

Koneman, E. W., Allen, S. D., and Janda, W. M. (2006). "The streptococcus-like bacteria," in *Color Atlas and Textbook of Diagnostic Microbiology*, *6th ed* (Philadelphia, PA: Lippincott Williams & Wilkins), 597–649.

Lade, H., Park, J. H., Chung, S. H., Kim, I. H., Kim, J. M., Joo, H. S., et al. (2019). Biofilm formation by *Staphylococcus aureus* clinical isolates is differentially affected by glucose and sodium chloride supplemented culture media. *J. Clin. Med.* 2, 1853. doi: 10.3390/jcm8111853

Luzzago, C., Locatelli, C., Franco, A., Scaccabarozzi, L., Gualdi, V., Viganò, R., et al. (2014). Clonal diversity, virulence-associated genes, and antimicrobial resistance profile of *Staphylococcus aureus* isolates from nasal cavities and soft tissue infections in wild ruminants in the Italian Alps. *Veterinary Microbiol.* 170, 157–161. doi: 10.1016/j.vetmic.2014.01.016

Magiorakos, A. P., Srinivasan, A., Carey, R. B., Carmeli, Y., Falagas, M. E., Giske, C. G., et al. (2012). Multidrug-resistant, extensively drug-resistant and pandrug-resistant bacteria: An international expert proposal for interim standard definitions for acquired resistance. *Clin. Microbiol. Infection* 18, 268–281. doi: 10.1111/j.1469-0691.2011.03570.x

Maharjan, M., Sah, A. K., Pyakurel, S., Thapa, S., Maharjan, S., Adhikari, N., et al. (2021). Molecular confirmation of vancomycin-resistant *Staphylococcus aureus* with *vanA* gene from a hospital in Kathmandu. *Int. J. Microbiol.* 2021, 3847347. doi: 10.1155/2021/3847347

McConkey, B. J., Sobolev, V., and Edelman, M. (2002). The performance of current methods in ligand-protein docking. *Curr. Sci.* 83, 845–855. doi: 10.1126/science.1079859

Nagappa, A. N., and Cheriyan, B. (2001). Wound healing activity of the aqueous extract of *Thespesia populnea* fruit. *Fitoterapia* 72, 503–506. doi: 10.1016/S0367-326X(01)00306-7

Nouraei, H., Sheykhi, S., ZareShahrabadi, Z., Khodadadi, H., Zomorodian, K., and Pakshir, K. (2020). Comparative analysis of virulence factors of homozygous and heterozygous strains of *Candida albicans* vaginal isolates. *Int. J. Microbiol.* 2020, 8889224. doi: 10.1155/2020/8889224

Obad, J., Šušković, J., and Kos, B. (2015). Antimicrobial activity of ibuprofen: New perspectives on an "old" non-antibiotic drug. *Eur. J. Pharm. Sci.* 71, 93–98. doi: 10.1016/j.ejps.2015.02.011

Oliveira, I. M., Borges, A., Borges, F., and Simões, M. (2019). Repurposing ibuprofen to control *Staphylococcus aureus* biofilms. *Eur. J. Medicinal Chem.* 166, 197–205. doi: 10.1016/j.ejmech.2019.01.046

Paes-Leme, R. C., and da Silva, R. V. (2021). Antimicrobial activity of non-steroidal anti-inflammatory drugs on biofilm: Current evidence and potential for drug repurposing. *Front. Microbiol.* 12. doi: 10.3389/fmicb.2021.707629

Peacock, S. J., and Paterson, G. K. (2015). Mechanisms of methicillin resistance in *Staphylococcus aureus*. *Annu. Rev. Biochem.* 84, 577–601. doi: 10.1146/annurev-biochem-060614-034516

Romeo, T. (2008). "Bacterial biofilms," in *Bacterial Biofilms*. Ed. T. Romeo (Berlin, Germany: Springer-Verlag Berlin Heidelberg), 207–223.

Rubinstein, E., and Keynan, Y. (2014). Vancomycin revisited - 60 years later. *Front. Public Health* 2, 217. doi: 10.3389/fpubh.2014.00217

Saber, T., Samir, M., El-Mekkawy, R. M., Ariny, E., El-Sayed, S. R., Enan, G., et al. (2022). Methicillin- and vancomycin-resistant *Staphylococcus aureus* from humans and ready-to-eat meat: Characterization of antimicrobial resistance and biofilm formation ability. *Front. Microbiol.* 12. doi: 10.3389/fmicb.2021.735494

Sibbald, R. G., Coutts, P., and Fierheller, M. (2006). "Improved persistent wound pain with a novel sustained release ibuprofen foam dressing," in *Symposium for Advanced Wound Care* (Poster 185, San Antonio, TX, USA).

Silva, V., Almeida, L., Gaio, V., Cerca, N., Manageiro, V., Caniça, M., et al. (2021). Biofilm formation of multidrug-resistant MRSA strains isolated from different types of human infections. *Pathog. (Basel Switzerland)* 10, 970. doi: 10.3390/pathogens10080970

Stepanović, S., Vuković, D., Hola, V., Di Bonaventura, G., Djukić, S., Cirković, I., et al. (2007). Quantification of biofilm in microtiter plates: Overview of testing conditions and practical recommendations for assessment of biofilm production by staphylococci. *APMIS Acta Pathologica Microbiologica Immunologica Scandinavica* 115, 891–899. doi: 10.1111/j.1600-0463.2007.apm_630.x

Taylor, T. A., and Unakal, C. G. (2023). *Staphylococcus aureus* infection. In *StatPearls* (USA: StatPearls Publishing).

Vancraeynest, D., Hermans, K., and Haesebrouck, F. (2004). Genotypic and phenotypic screening of high and low virulence *Staphylococcus aureus* isolates from rabbits for biofilm formation and MSCRAMMs. *Veterinary Microbiol.* 103, 241–247. doi: 10.1016/j.vetmic.2004.09.002

Van de Vyver, M., Boodhoo, K., Frazier, T., Hamel, K., Kopcewicz, M., Levi, B., et al. (2021). Histology scoring system for murine cutaneous wounds. *Stem Cells Dev.* 30, 1141–1152. doi: 10.1089/scd.2021.0124

Wang, C., Greene, D., Xiao, L., Qi, R., and Luo, R. (2018). Recent developments and applications of the MMPBSA method. *Front. Mol. Biosci.* 4, 87. doi: 10.3389/fmolb.2017.00087

Wieckowska-Szakiel, M., Sadowska, B., and Rózalska, B. (2007). Staphylokinase production by clinical *Staphylococcus aureus* strains. *Polish J. Microbiol.* 56, 97–102. doi: 10.33073/pjm-2007-015

Yigit, N., and Aktas, E. (2009). Comparison of the efficacy of different blood medium in determining the hemolytic activity of *Candida species*. *J. Mycologie Mèdicale* 19, 110–115. doi: 10.1016/j.mycmed.2009.03.005

Yuan, J. S., Reed, A., Chen, F., and Stewart, C. N. (2006). Statistical analysis of real-time PCR. *BMC Bioinf.* 7, 85. doi: 10.1186/1471-2105-7-85

Zhang, X., Zhang, Z., Shu, Q., Xu, C., Zheng, Q., Guo, Z., et al. (2021). Copper clusters: An effective antibacterial for eradicating multidrug-resistant bacterial infection *in vitro* and *in vivo*. *Advanced Funct. Materials* 31, 2008720. doi: 10.1002/adfm.202008720

frontiers | Frontiers in Cellular and Infection Microbiology

TYPE Mini Review
PUBLISHED 07 October 2024
DOI 10.3389/fcimb.2024.1428637

OPEN ACCESS

EDITED BY
Maria Gabriela Paraje,
National University of Cordoba, Argentina

REVIEWED BY
Marina Alejandra Golowczyc,
Independent Researcher, La Plata, Argentina
Ashish Patel,
Hemchandracharya North Gujarat University, India
İhsan Yaşa,
Ege University, Türkiye

*CORRESPONDENCE
Linda P. Guamán
linda.guaman@ute.edu.ec

RECEIVED 06 May 2024
ACCEPTED 29 July 2024
PUBLISHED 07 October 2024

CITATION
Mayorga-Ramos A, Carrera-Pacheco SE, Barba-Ostria C and Guamán LP (2024) Bacteriophage-mediated approaches for biofilm control.
Front. Cell. Infect. Microbiol. 14:1428637.
doi: 10.3389/fcimb.2024.1428637

Bacteriophage-mediated approaches for biofilm control

Arianna Mayorga-Ramos[1], Saskya E. Carrera-Pacheco[1], Carlos Barba-Ostria[2,3] and Linda P. Guamán[1]*

[1]Universidad UTE, Centro de Investigación Biomédica (CENBIO), Facultad de Ciencias de la Salud Eugenio Espejo, Quito, Ecuador, [2]Escuela de Medicina, Colegio de Ciencias de la Salud Quito, Universidad San Francisco de Quito USFQ, Quito, Ecuador, [3]Instituto de Microbiología, Universidad San Francisco de Quito USFQ, Quito, Ecuador

Biofilms are complex microbial communities in which planktonic and dormant bacteria are enveloped in extracellular polymeric substances (EPS) such as exopolysaccharides, proteins, lipids, and DNA. These multicellular structures present resistance to conventional antimicrobial treatments, including antibiotics. The formation of biofilms raises considerable concern in healthcare settings, biofilms can exacerbate infections in patients and compromise the integrity of medical devices employed during treatment. Similarly, certain bacterial species contribute to bulking, foaming, and biofilm development in water environments such as wastewater treatment plants, water reservoirs, and aquaculture facilities. Additionally, food production facilities provide ideal conditions for establishing bacterial biofilms, which can serve as reservoirs for foodborne pathogens. Efforts to combat antibiotic resistance involve exploring various strategies, including bacteriophage therapy. Research has been conducted on the effects of phages and their individual proteins to assess their potential for biofilm removal. However, challenges persist, prompting the examination of refined approaches such as drug-phage combination therapies, phage cocktails, and genetically modified phages for clinical applications. This review aims to highlight the progress regarding bacteriophage-based approaches for biofilm eradication in different settings.

KEYWORDS

bacteriophages, biofilms, antimicrobial design, antibiotic resistance, exopolysaccharide

1 Introduction

Biofilms are sophisticated microbial communities aggregated in a self-generated extracellular matrix, which anchors the cells together and facilitates communication and resource distribution among them (Penesyan et al., 2021). The architecture of biofilms endows them with distinct characteristics compared to planktonic (free-living) cells, including altered metabolism and enhanced resistance to external stressors (Lee et al., 2014; Yin et al., 2019).

The clinical significance of biofilms predominantly stems from their heightened resistance to antimicrobial agents, posing an enormous challenge in treating biofilm-associated infections (Schulze et al., 2021; Ali et al., 2023). Cells within biofilms exhibit antimicrobial resistance that can be up to a thousand times greater than that of planktonic cells (Mah and O'Toole, 2001; Sharma et al., 2019). Biofilms are implicated in a wide array of chronic infections and are responsible for the failure of numerous antimicrobial treatments, particularly in the context of medical device- and tissue-associated infections. The current treatment regimens, often relying on conventional antimicrobials, are increasingly proving inadequate in eradicating these resilient microbial communities (Usui et al., 2023).

Given the limitations of existing therapies and the escalating threat of multidrug-resistant microbes, there is an urgent need to develop novel anti-biofilm strategies. Innovative approaches, such as the use of antimicrobial peptides, nanotechnology, surface modifications of medical devices, and bacteriophage applications, are being explored to combat biofilm-associated infections (Yasir et al., 2018; Li et al., 2020; Mohanta et al., 2023; Kushwaha et al., 2024). Understanding the complex biology of biofilms and exploring bacteriophages as potential biocontrol agents are critical in addressing the biofilm-related challenges in medical and industrial environments. This review aims to provide a comprehensive overview of the basic biofilm biology, the resistance mechanisms within biofilms, and the emerging role of bacteriophages in biofilm control.

2 Biofilm formation

Biofilms, crucial in diverse environments, are complex microbial communities encapsulated in an extracellular polymeric substances (EPS) matrix (Li et al., 2022; Krishnan et al., 2023). Understanding each step of biofilm formation—from initial attachment through irreversible adhesion, microcolony formation, maturation, to dispersion—is crucial for developing effective eradication strategies. Each phase presents unique targets and mechanisms that can be disrupted to prevent biofilm formation or to dismantle existing biofilms. For instance, interventions at the initial attachment stage can prevent biofilm establishment, while strategies targeting biofilm maturation can disrupt the protective EPS matrix, enhancing the efficacy of antimicrobial agents. Therefore, detailed knowledge of these processes is essential for devising comprehensive and effective biofilm control measures, ultimately improving infection management and patient outcomes (Armbruster and Parsek, 2018; Nie et al., 2021).

1. Initial attachment: The initial phase involves microorganisms adhering to surfaces via physical forces (van der Waals forces, electrostatic attractions, hydrophobic effects). Bacterial appendages play a crucial role in surface movement, enabling the bacteria to explore and find optimal attachment sites. Additionally, pili, such as Type I and Type IV, facilitate adhesion by establishing strong interactions with the surface. These initial interactions are reversible, allowing the bacteria to detach and relocate if the conditions are unfavorable (Richter et al., 2017; Ramzan et al., 2022).
2. Irreversible attachment: The transition to irreversible attachment is marked by the production of EPS, which anchors the bacteria firmly to the surface. This EPS matrix not only strengthens adhesion but also forms a protective barrier that shields the microbial community from environmental stressors, including antimicrobial agents and components of the immune response. During this phase, these microorganisms can undergo significant genetic shifts, prioritizing the synthesis of EPS and reducing the expression of motility-related genes (Chávez-Jacobo et al., 2023; Guttenplan et al., 2010; Kim et al., 2023a).
3. Microcolony formation: As bacteria continue to produce EPS and proliferate, they form structured microcolonies, which are clusters of bacterial cells within the EPS matrix. This stage is characterized by spatial organization and differentiation within the biofilm, influenced by environmental gradients such as nutrient availability, oxygen concentration, and waste accumulation. Quorum sensing, a key cell-density signaling mechanism, is crucial in regulating gene expression associated with EPS production and biofilm maturation. This process ensures coordinated behavior among the bacterial population, facilitating efficient biofilm development (Zhang et al., 2018; Oyewole et al., 2022; Gulec and Eckford, 2023).
4. Biofilm maturation: In this phase, microcolonies merge, creating a layered, three-dimensional structure. EPS is crucial for structure and protection, creating diverse microenvironments within the biofilm. These niches allow for metabolic specialization among microbial populations. Additionally, the development of water channels, which occurs in this phase, is essential for nutrient distribution and waste removal, while quorum sensing ensures coordinated gene expression throughout the biofilm, regulating behaviors like virulence and resistance (Azulay et al., 2022; Xiu et al., 2022).
5. Dispersion: During this phase, cells detach from the mature biofilm to colonize new surfaces through passive mechanisms, such as fluid shear, and active, regulated processes initiated by environmental changes. Active dispersion involves the degradation of the EPS matrix, often facilitated by enzymes such as dispersin B, as well as phenotypic shifts that enable bacteria to revert to a planktonic, mobile phase (Rumbaugh and Sauer, 2020). Environmental triggers such as changes in nutrient levels or oxygen availability can initiate active dispersion, leading to the release of bacteria to colonize new environments. This process is crucial in clinical settings as it facilitates the spread of infections, particularly on medical devices, and contributes to the difficulty in treating biofilm-associated infections due to the rapid re-establishment of biofilms and increased resistance to antimicrobial agents (Werneburg et al., 2019).

Understanding these stages helps devise strategies to manage biofilm-related issues, emphasizing the dynamic nature of microbial communities and their interaction with environments. The study of biofilms bridges microbiology, molecular biology, and environmental sciences, offering insights into microbial behavior and potential control methods in medical and industrial contexts.

3 Bacteriophages-biofilm interaction in nature

The interactions between bacteriophages and biofilms are complex and rely on several factors determining biofilm destruction, coexistence, or limited phage efficacy in controlling biofilms.

The susceptibility of bacterial cells to phage infection can lead to the destruction of biofilms. When the biofilm is susceptible, bacteriophages attach to receptors on bacterial cells, inject their genetic material, and take over the bacterial machinery to replicate (Sutherland et al., 2004), leading to the lysis of infected cells and destroying the biofilm (Fernández et al., 2018; Papaianni et al., 2020). The availability of specific receptor sites on the biofilm bacteria's surface is crucial for phage attachment and infection (Uchiyama et al., 2014). The polysaccharide-degrading enzymes produced by bacteriophages weaken the biofilm structure, allowing phages to penetrate and disperse the biofilm, releasing individual bacteria, making them more susceptible to other antimicrobial agents (González et al., 2018; Chegini et al., 2020). Phages can also produce endolysins, which hydrolyze the peptidoglycan in bacterial cell walls from within, contributing to the release of newly formed viral particles (Abdelrahman et al., 2021).

The biofilm composition and structure affect both the coexistence of phages with bacteria and limit the effectiveness of phages in controlling biofilm formation. The biofilm's extracellular matrix, composed of polysaccharides, proteins, and DNA, can hinder phage diffusion and penetration, preventing them from reaching and killing biofilm bacteria (Limoli et al., 2015). In some cases, phages can promote biofilm formation and trigger specific responses in bacteria, increasing the adhesion, stability, and matrix production, allowing phages and bacteria to coexist within the biofilm (Secor et al., 2020). The presence, physiological state, and physical environment of different microorganisms (bacteria and fungi) influence phage accessibility to the biofilm (Bull et al., 2018; Ferriol-González and Domingo-Calap, 2020).

It is important to note that the interaction between phages and biofilms is still an active area of research. Further studies are needed to fully understand the complex dynamics between phages and biofilms in different environments and bacterial species.

3.1 Advantages and limitations of bacteriophages as antibacterial agents

Bacteriophages possess features such as self-replication within host bacteria, leading to increased concentrations in biofilms, and rapid replication, achieving high population densities swiftly (Talapko and Škrlec, 2020). They exhibit lytic activity against bacteria and produce enzymes that degrade the biofilm matrix, thereby enhancing biofilm penetration, infection, and elimination (Abedon, 2015). The continuous interactions between phages and hosts in biofilms drive evolutionary adaptations, potentially enhancing phage efficacy in disrupting biofilms (Talapko and Škrlec, 2020). All those characteristics, which are part of phages' lifestyle are advantageous to use them as antibacterial agents.

On the other hand, limitations include the high specificity of bacteriophages for their hosts and the development of phage resistance by biofilm bacteria (Talapko and Škrlec, 2020). Bacterial defense mechanisms within the biofilm, such as CRISPR-Cas systems, plasmids, genomic islands, modification and mutation of surface receptors, or production of substances that inhibit phage attachment, prevent bacteriophages from infecting and eliminating biofilm communities (Cady and O'Toole, 2011; Römling and Balsalobre, 2012; Hassan et al., 2021; Ngiam et al., 2022). In addition, the biofilm matrix acts as a physical barrier, hindering phage movement and penetration (Talapko and Škrlec, 2020; Hassan et al., 2021; Ngiam et al., 2022).

4 Phage penetration and innovative phage delivery systems

4.1 Penetration strategies

Bacteriophages have several strategies for penetrating biofilms, one of which involves the production of an enzyme called polysaccharide depolymerase. This enzyme can digest polysaccharide components of bacterial cell walls by identifying and binding to specific ligands on the bacterial surface, facilitating phage genome transfer (Knecht et al., 2019). Depolymerases are subdivided into several classifications according to their target in biofilms: capsular polysaccharides, lipopolysaccharides (LPS), O-polysaccharides or exopolysaccharides (Pires et al., 2016; Knecht et al., 2019). Based on their biochemical properties, depolymerases are classified into hydrolases and lyases. Phage hydrolases catalyze the breaking of chemical bonds with water, displaying activities such as sialidases, xylosidases, levanases, rhamnosidases, dextranases, and peptidases. Conversely, lyases catalyze the breaking of chemical bonds through mechanisms other than hydrolysis, encompassing hyaluronate, alginate, and pectin/pectate lyases (Pires et al., 2016; Knecht et al., 2019; Topka-Bielecka et al., 2021). These depolymerases exhibit high substrate specificity, playing a crucial role in the bacteriophage's ability to attach, invade, and ultimately destroy host bacteria (Yan et al., 2014).

Interestingly, bacteriophages have been genetically modified to express depolymerase during infection, enabling the simultaneous degradation of the bacterial cell wall and the biofilm matrix, thereby enhancing the chances of biofilm destruction (Lu and Collins, 2007). Furthermore, phages can produce endolysins, bactericidal proteins that hydrolyze bacterial cell walls, facilitating the release of

phage particles (Briers et al., 2009; Abdelrahman et al., 2021). These endolysins, in conjunction with proteins such as holin, breach the bacterial cytoplasmic membrane to access the peptidoglycan layer (Wang et al., 2000). Additionally, the protein spanin contributes to the degradation of the outer membrane in Gram-negative hosts, further aiding in the bacteriophage's infection process (Cahill and Young, 2019).

Phages can also switch between two life stages, lytic and lysogenic, contributing to their ability to penetrate and destroy the biofilm. During the lysogenic phase, the phage's DNA merges with the bacterium's genetic material, enabling the phage to penetrate and spread within the biofilm without destroying the host cells immediately (Weinbauer et al., 2003). This allows the phages to remain dormant until favorable conditions are present in the biofilm (Weinbauer et al., 2003). The control of the lytic and lysogenic phases involves various elements. Regulatory factors, including bacteriophage Lambda repressors CI and Cro, determine the lysogenic state; these elements were identified in previous studies (Carrasco et al., 2016; Lee et al., 2022). Other factors that can impact the lysogeny-lysis switch of phages are quorum sensing and the metabolic state of the host (Laganenka et al., 2019).

In clinical settings, an alternative to effectively reach and destroy biofilms is combining multiple bacteriophage mixtures with different host ranges into one solution. Bacteriophage cocktails can easily penetrate and destroy biofilms such as the ones from *Pseudomonas aeruginosa*, *Enterococcus faecalis*, and Methicillin-resistant *Staphylococcus aureus* (MRSA) (Hanlon, 2007; Kaur et al., 2016; Kwiatek et al., 2017; Khalifa et al., 2018). Another alternative is the phage-antibiotic synergy (PAS). In this approach, the phages can initiate biofilm breakdown, allowing antibiotics to penetrate more effectively and kill the bacteria more efficiently. Conversely, antibiotics can weaken the bacteria, making them more susceptible to phage infection (Morrisette et al., 2020). Other approaches involve using nanoparticles to improve phage penetration. For instance, a study by Quan et al. (2019) used magnetic nanoparticles to create artificial channels in infectious biofilms, improving the penetration and effectiveness of antimicrobial treatment. The experiment successfully demonstrated the creation of artificial channels in *S. aureus* biofilms, which significantly enhanced the penetration of the antibiotic gentamicin and the bacterial killing efficacy. This method offers a simple and effective way to eradicate infectious biofilms when combined with existing antibiotic therapies (Quan et al., 2019). The following sections provide more examples of these approaches.

Additionally, targeting ligands or antibodies can facilitate phages' penetration through the biofilm matrix, effectively reaching and infecting bacterial cells (Amankwah et al., 2021). Phages can also be genetically engineered to produce cell wall-degrading enzymes and display biofilm-specific peptides, thus allowing further binding and penetration of biofilms (Chegini et al., 2020; Zhao et al., 2023). Notably, the accessibility of phages to the biofilm can be affected by the types of microorganisms forming the structure, their physiological state, and the physical environment.

4.2 Nanoparticle-based delivery

Nanoparticle-based delivery systems have emerged as a promising strategy to enhance the efficacy of bacteriophage therapy in biofilm control by using the unique properties of nanoparticles to improve phage stability, targeting, and penetration into biofilms (Vera-González and Shukla, 2020). By combining bacteriophages with nanoparticles, natural compounds, and disinfectants, the destruction of biofilms can be more effective (Chegini et al., 2020). Various types of nanoparticles have been used to improve phage stability, targeting, and penetration into biofilms, including metallic (e.g., silver and gold nanoparticles) and polymeric (e.g., Poly Lactic-co-Glycolic Acid (PLGA) and chitosan) nanoparticles (Ahiwale et al., 2017; Abdelsattar et al., 2021).

Chitosan nanoparticles have several outstanding properties that make them useful in various biomedical applications, such as biocompatibility and biodegradability (Ke et al., 2021). Additionally, they can encapsulate and release drugs in a controlled manner, improving the efficacy of pharmacological treatments and reducing side effects; for biofilm control and eradication, chitosan has been combined with bacteriophages (Sharifi-Rad et al., 2021). Encapsulating bacteriophages in chitosan nanoparticles can protect them from harsh gastrointestinal conditions and improve delivery to the target site for effective results. Adamu and coworkers synthesized chitosan nanoparticles to encapsulate phages targeting *Escherichia coli*, offering considerable protection of the ΦKAZ14 bacteriophage against enzymatic degradation and acidic environments. This innovation makes the phage suitable for oral applications, improving its delivery (Adamu Ahmad et al., 2016). In a similar approach using chitosan, Li and coworkers introduced an innovative method of using polyvalent phages attached to magnetic colloidal nanoparticle clusters (CNCs) under a small magnetic field. The phage PEL1 immobilized onto chitosan-coated Fe_3O_4-based CNCs showed enhanced phage loading and improved biofilm penetration. The author concluded this conjugation method could broaden the use of phages for microbial control by improving their delivery to relatively hard-to-reach areas within biofilms (Li et al., 2017).

Gold nanoparticles (AuNPs) have been used to target phages in *P. aeruginosa* biofilms, demonstrating a significant reduction in biofilm production, which suggests that phage-inspired AuNPs could serve as potent therapeutic agents against human pathogens (Ahiwale et al., 2017). Similar research used AuNPs but combined with the C3 phage to treat *P. aeruginosa* in planktonic and biofilm states. This combination exhibited high stability under various temperatures, pH levels, and salt concentrations, indicating a more efficient delivery (Abdelsattar et al., 2021).

In a recent approach, a phage-Chlorin e6 (Ce6)-manganese dioxide nanocomposite (PCM) was created, combining the benefits of phage therapy with other therapeutic modalities. The phage component of the nanocomposite plays a crucial role in targeting host bacteria and aiding in the efficient delivery of Ce6 to penetrate biofilms. By incorporating phages into the nanocomposite, the

study improves the targeting of host bacteria, facilitating the effective delivery of Ce6 within the biofilm structure (Wang et al., 2023).

Similarly, Manoharadas and coworkers showed an enhanced phage delivery method by combining green-synthesized silver nanoparticles and bacteriophages to effectively disperse pre-formed *S. aureus* biofilms from inert surfaces. This approach not only removes the biofilms but also prevents the establishment of new infections and subsequent colonization by causing the loss of viability of the biofilm-entrapped bacterial cells (Manoharadas et al., 2021).

Recent advancements in nanoparticle-based delivery systems have emphasized the importance of surface modifications and functionalization to enhance their further interaction with biofilms and bacteriophages. The attachment of polyethylene glycol (PEG) chains to nanoparticles, known as PEGylation, has improved nanoparticles' stability and circulation time, thereby enhancing the delivery of bacteriophages to biofilm sites (Mura et al., 2013). Additionally, dual-functional nanoparticles that combine targeting ligands with antimicrobial agents offer a promising strategy for enhancing the specificity and efficacy of bacteriophage therapy. For example, mannose-functionalized nanoparticles have been developed to target lectin receptors on the surface of biofilm-forming bacteria, improving phage adherence and biofilm disruption (Pawde et al., 2020). Furthermore, stimuli-responsive nanoparticles that release their payload in response to environmental triggers such as pH or enzymatic activity have shown potential in improving the targeted delivery of bacteriophages within biofilms (Karimi et al., 2016).

4.3 Liposome and hydrogel encapsulation-based delivery

Liposomes and vesicles constitute a versatile delivery system for hydrophilic and hydrophobic substances and represent the most promising vehicles for a variety of therapeutic agents, including bacteriophages. Liposome and vesicle encapsulation have recently emerged as an efficient approach for enhancing the efficient delivery and improved the efficacy of phages used to treat biofilms (Kaszuba et al., 1997; Sihorkar and Vyas, 2001). These exploit lipid-based carriers' biocompatibility and tailor-made nature to improve biofilm phage interactions such as stability, targeting, or penetration into the biofilm structures (Singla et al., 2016).

The mechanisms to enhance bacteriophage therapy by using liposomes are: (I) Protection from environmental stress, where the encapsulation of bacteriophages in liposomes protects them from different environmental stressors, such as pH changes and enzymatic degradation, and thereby maintain their infectivity (Loh et al., 2021), (II) improved penetration into the biofilm thanks to the presence of the lipid bilayer structure that facilitates the delivery of phages into biofilms due to easy fusion with the bacterial membrane (Malik et al., 2017), and (III) targeted delivery through the functionalization with the targeting moieties to ensure that the phages are specifically targeted on the bacterial biofilms, which decreases off-target effects and enhances the therapeutic impact.

Recent advancements in liposomes and hydrogels for bacteriophage delivery have demonstrated significant potential in enhancing biofilm removal. In the context of orthopedic device infections, engineered injectable hydrogels encapsulating *P.aeruginosa* bacteriophages have shown promising results. These hydrogels, capable of controlled phage release, retain bacteriolytic activity and effectively target planktonic and biofilm bacteria without affecting human mesenchymal stromal cells. The authors concluded that the hydrogels efficiently deliver bacteriophages to treat localized bone infections (Wroe et al., 2020).

Furthermore, incorporating bacteriophages into liposomes and other amphiphilic nanoparticles offers the advantage of targeted delivery through ligand interaction with target cells. Although this approach presents challenges, such as ensuring amphiphilic properties or conjugation with anchoring molecules, it provides a sophisticated means of enhancing the directed delivery of bacteriophages (Loh et al., 2021).

Finally, an innovative delivery system has been developed for local tissue regeneration and infection control using bacteriophage-loaded alginate-nanohydroxyapatite hydrogel. This system efficiently encapsulates bacteriophages, with release influenced by environmental pH, without compromising their viability or functionality, thus improving their delivery. The hydrogels showed good tissue response and exhibited excellent antimicrobial effectiveness, inhibiting the attachment and colonization of multidrug-resistant *E. faecalis* (Barros et al., 2020).

Together, these studies illustrate the diverse strategies and significant progress made in using nanoparticle-encapsulated bacteriophages to address biofilm-related infections, paving the way for innovative treatments that enhance targeted delivery and efficacy.

4.4 Genetically engineered bacteriophages

Phage engineering has shown promise in enhancing the effectiveness of tailored phage therapies in combating biofilm-related challenges. Most genetic engineering approaches for biofilm control focus on improving the specificity, affinity, and efficacy of bacteriophages rather than enhancing their delivery to eradicate biofilms (Lu and Collins, 2007; Gutiérrez et al., 2016; Chegini et al., 2020; Yue et al., 2022). Another application of genetic engineering of phages is the potential to extend their natural host range and modify phage display (Khambhati et al., 2023). However, improved delivery is often a beneficial consequence rather than the primary goal of these modifications. Recently, to overcome the challenge of eradicating biofilms in water distribution systems, the filamentous coliphage M13 was engineered to enhance biofilm affinity and deliver lytic polyvalent phages. Modified M13 showed a significantly higher affinity for *P.aeruginosa* biofilms and improved delivery capabilities (Sun et al., 2022). This tunable approach could enable enhanced phage delivery and higher biofilm eradication efficacy to expand the scope

of phage applications. A summary of the innovations regarding phage delivery is shown in Figure 1.

Exploring innovative approaches to intentionally enhance phage delivery, such as engineering phages to improve phage entrance or withstand harsh conditions within biofilms, could offer significant advancements in biofilm control strategies. This gap suggests an opportunity for innovative approaches to enhance phage delivery to biofilms. For example, engineering phages to produce surface modifications that increase their ability to penetrate biofilms or survive harsh biofilm environments could significantly improve their therapeutic efficacy. Such targeted delivery strategies would be a novel direction for research and development in bacteriophage therapy.

5 Using bacteriophages to dismantle biofilms

The rise of antibiotic-resistant microorganisms has become a significant global public health concern, especially in chronic infections associated with bacterial biofilms growing over medical instruments. These biofilms demonstrate heightened antibiotic tolerance and host immunity (Singh et al., 2022a; Cangui-Panchi et al., 2023). Phage therapy, recognized for its efficacy against antibiotic-resistant bacteria, is being explored by several research groups worldwide (Pires et al., 2020). Technological advancements have facilitated phage-based therapy research, revealing promising results in addressing antibiotic-resistant bacterial infections. Notably, phages have reduced contamination in medical catheters (Joo et al., 2023; Erol et al., 2024). However, phage application shows potential for the sanitation of medical instruments and holds great promise for a prospective application in clinical practice and patient treatment (Suh et al., 2022).

5.1 Environmental sanitation

5.1.1 Phage application: prevention of biofilm in water environment

Contamination of water sources by enteric pathogens poses a significant threat to public health. These microorganisms can originate from various human activities, such as runoff from livestock facilities, intensive farming practices, and wastewater treatment plants (WWTPs) effluents. Infrastructure failures in sewage systems can exacerbate this issue, resulting in fecal pollution of surface waters (Shivaram et al., 2023). Traditional methods of microbial removal include chemical disinfection and antibiotic treatments, contributing to the emergence of antibiotic resistance among waterborne pathogens (Mancuso et al., 2021).

Bacteriophage therapy has emerged as a promising approach to combat antibiotic-resistant bacteria (Karthikeyan and Meyer, 2006; Shivaram et al., 2023). In WWTPs, filamentous bacteria commonly cause bulking and foaming, reducing treatment efficiency (Ballesté et al., 2022). Laboratory studies have shown that isolated phages targeting these foam-causing bacteria can prevent foam stabilization, offering potential solutions to this issue (Petrovski et al., 2011; Liu et al., 2015). Moreover, bacterial biofilms on membrane-based WWTPs can impair treatment processes (Wu et al., 2017). Lytic phages have demonstrated effectiveness in

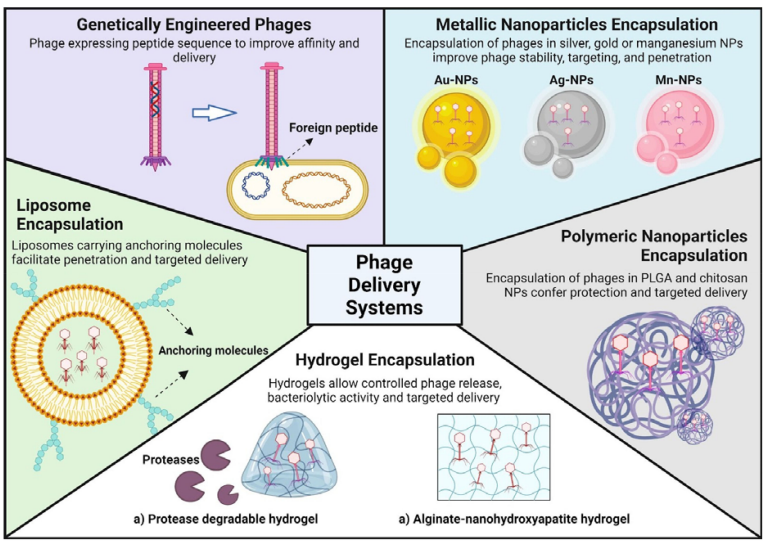

FIGURE 1
Advanced encapsulation strategies for phage delivery systems. The figure illustrates various methodologies for enhancing the stability and targeting of phages for therapeutic applications. Genetically engineered phages are modified to express specific peptides that improve their delivery efficiency. Liposomes, metallic nanoparticles (silver, gold, magnesium, etc.) and polymeric nanoparticles (PLGA and chitosan) are utilized to encapsulate phages, thereby bolstering their stability, penetration capabilities and ensuring targeted delivery. Moreover, the use of hydrogels (protease-degradable and alginate-nanohydroxyapatite) allows for controlled release and targeted delivery while maintain the phages innate bacteriolytic activity.

inhibiting bacterial fouling of membranes (Goldman et al., 2009; Bhattacharjee et al., 2015; Ayyaru et al., 2018); for instance, phage DTP1 showed promise as a biocontrol agent against *Delftia tsuruhatensis* ARB1, an antibiotic-resistant bacterium commonly found in WWTPs (Bhattacharjee et al., 2015).

P. aeruginosa biofilms frequently clog filters in water treatment plants and increase cleaning costs (Tian et al., 2021). Studies have explored the use of phages in combination with other disinfectants to achieve significant reductions (up to 96% removal rate) in *P. aeruginosa* biofilms, highlighting the potential of phage-based interventions in water treatment (Zhang and Hu, 2013). Antibiotic-resistant *Vibrio* species have been isolated from aquatic environments like dams, boreholes, and tap water (Maje et al., 2020); in aquaculture, preventive antibiotic treatment is commonly applied to reduce pathogenic *Vibrio* spp. and its biofilm (Tian et al., 2021; Lomelí-Ortega et al., 2023; Srisangthong et al., 2023). Also, lysins derived from a *Vibrio parahaemolyticus* phage have been proposed as a promising alternative to reducing antibiotic overuse in aquaculture (Matamp and Bhat, 2019). Overall, there is great potential in using phage-based interventions to eliminate waterborne pathogen contamination and reduce the reliance on antibiotics in water treatment and aquaculture practices.

5.1.2 Phage application: prevention of biofilm in the food industry

In agriculture and livestock food production, infectious diseases pose significant challenges to food sustainability, causing crop losses, animal welfare issues, and environmental pollution with antimicrobial agents (Abebe et al., 2020). These diseases can also lead to emerging infectious diseases in humans and animals, facilitated by zoonotic transmission from microbial contamination (Rohr et al., 2019). Biofilms formed by foodborne pathogens have substantial public health implications, particularly in mixed-species biofilms common in the food industry (Galié et al., 2018). Bacteriophages have also been proposed as a green biocontrol tool for eliminating these microorganisms in food production (Moye et al., 2018).

Research has employed bacteriophages (Phage K and T4-like phages) for the treatment of *S. aureus* and *E. coli* that induced mastitis, a prevalent infectious disease in livestock (da Silva Duarte et al., 2018; Loponte et al., 2021). In 2006, the U.S. Food and Drug Administration (FDA) approved a phage cocktail sanitation product (ListShieldTM) to eliminate *Listeria monocytogenes* and marked a milestone for subsequent phage-based food preservation products (Zhang, 2018; Vikram et al., 2021). Biofilm formation on food production surfaces, often resistant to biocides, is a significant challenge (Meade et al., 2020). A recent study assessed the effectiveness of phage cocktails in the elimination of Shiga-toxigenic *E. coli* (STEC) growth over several types of surfaces (polystyrene well plates, stainless, steel, and high-density polyethylene) and found that STEC populations were reduced to undetectable levels after 16 hours of treatment (Jaroni et al., 2023). Similarly, another study used phage phT4A to reduce *E. coli* biofilm growth over plastic and reported its maximum inhibition percentage after only 6 hours of phage application (Brás et al., 2024).

Some studies have assessed the potential use of phage cocktails to combat dual-species biofilms, which are also relatively common biofilm arrangements over food production surfaces (Kim et al., 2023b). The effectiveness of these approaches depends on the combination of bacteria inside the mixed-species biofilm. For instance, one study showed that phages are more effective in eliminating single species than mixed biofilms in an *E. coli* and *Salmonella enteritidis* biofilm (Milho et al., 2019). In contrast, it has been suggested that phages tackling *Staphylococcus lentus* and *Pseudomonas fluorescens* mixed biofilms are able to eliminate their respective host within the biofilm (Sillankorva et al., 2010; Milho et al., 2019). Although studies have demonstrated the efficacy of phages in controlling single-species biofilms, further research is needed to explore their application in mixed-species biofilms in food environments.

5.2 Clinical treatment

The global impact of antibiotic-resistant bacteria, contributing to over 1.27 million annual deaths, underscores the urgent need for novel treatments (Antimicrobial Resistance Collaborators, 2022; Fongang et al., 2023). Bacterial biofilms are particularly problematic due to their ability to cause chronic and resilient infections. These biofilms offer protection and tolerance to antibiotics, antiseptics, antimicrobials, and host immune responses, leading to persistent infections (Yang et al., 2012). Eradicating biofilms within a host proves difficult due to physiological and physical barriers. Moreover, the minimum inhibitory concentration of antibiotics required against biofilms can be substantially higher than planktonic bacteria (Høiby et al., 2011). Biofilms on medical surfaces, such as catheters and implants, exacerbate the problem (Srivastava et al., 2019; Joo et al., 2023; Erol et al., 2024). Phage therapy has demonstrated significant potential in combating these infections through various therapeutic approaches (Figure 2). A summary of bacteriophage-based clinical studies is shown in Table 1.

5.2.1 Bacteriophage and antibiotic combination therapy

The use of bacteriophages and antibiotics during a combination therapy has shown a synergizing effect that increases the effectiveness of biofilm eradication. This approach reduces antibiotic concentrations while maintaining efficacy (Morrisette et al., 2020). In 2018, a study assessed the synergistic effect of pre-treatment application of Sb-1 *S. aureus* phage followed by antibiotic administration and demonstrated the effective elimination of MRSA biofilms (Tkhilaishvili et al., 2018). Previously, combination therapy of T4 phage and antibiotics showed potential to reduce biofilms formed by antibiotic-resistant and phage-resistant *E. coli* biofilms (Coulter et al., 2014). Notably, studies in *P. aeruginosa* biofilms using phage-antibiotic

combination therapy also demonstrated high efficacy. In 2017, one study assessed the effects of the concurrent administration of a 12-phage cocktail PP1131 with various antibiotics. It concluded that this combination exhibited efficacy in treating bacterial infections in laboratory rats, compared to administering only one of the components individually (Oechslin et al., 2017).

More recently, some clinical studies have already applied the combination of phage and antibiotic treatments in patients with recurrent or unresolved infections (Table 1). For instance, during a case study, a 62-year-old woman was treated with a combination of phage Pa53 and meropenem to treat a chronic right hip prosthesis infection caused by *P. aeruginosa* since 2016. The patient could self-administer the phage suspension with no observable side effects during the treatment. A 2-year follow-up evaluation concluded the success of the treatment as no signs of infection relapse were found (Cesta et al., 2023). The question regarding the effectiveness of phage application with other types of drugs has also started to be investigated. One study observed that certain anticancer drugs can inhibit the activity of potential therapeutic phages in an *S. aureus* infection model (Li et al., 2023). Immunocompromised cancer patients are highly vulnerable to opportunistic infection; for example, lung cancer patients can present high rates of *S. aureus*-derived pneumonia during chemotherapy (Rolston, 2017). Chemotherapeutic drugs can be seen as a limitation for using antibiotic approaches such as antibiotics or phage therapy due to interference or incompatibility. Li and coworkers studied the synergetic potential of phages with common anti-cancer drugs. Combining phage K with Doxorubicin effectively eliminated *S. aureus* intracellular infections and migration (Li et al., 2023).

5.2.2 Bacteriophage cocktail therapy

Recent findings suggest the efficacy of phage cocktails against bacterial biofilms, particularly in multispecies environments, offering advantages like a broader host range and reduced risk of phage resistance (Morrisette et al., 2020). Using multiple phages enables the recognition of different bacterial receptors, which increases their effectiveness (Singh et al., 2022b; Naknaen et al., 2023). For example, a study utilized six lytic phages against a wide range of *P. aeruginosa* clinical isolates and assessed biofilm-inhibiting in static and dynamic biofilm models. The phage cocktail effectively eliminated most biofilm biomass within 4 hours for the static model and within 48 hours in the dynamic biofilm model (Alves et al., 2016). Another promising phage cocktail (EFDG1 and EFLK1) was able to target and eliminate planktonic and biofilm cultures of vancomycin-resistant *E. faecalis* V583 strains (Khalifa et al., 2018).

A major pathogen in orthopedic and joint implant infections is *Staphylococcus*, specifically coagulase-negative *Staphylococcus* or MRSA (Bozhkova et al., 2013; Lu et al., 2022). Using phage cocktails combined with linezolid reduced adherence to MRSA after being surgically implanted in the intramedullary canal of the mouse femur bone (Kaur et al., 2016). Finally, in a phase I clinical trial, nine patients with *S. aureus*-derived chronic rhinosinusitis were treated with intranasal irrigants of phage cocktail AB-SA01 and presented no serious adverse effects (Ooi et al., 2019).

More recently, the application of phage cocktails and antibiotic courses has already been investigated in several clinical trials. For example, during a case study, a 54-year-old male patient was treated with a combination of two phages (PNM and PT07) and antibiotics

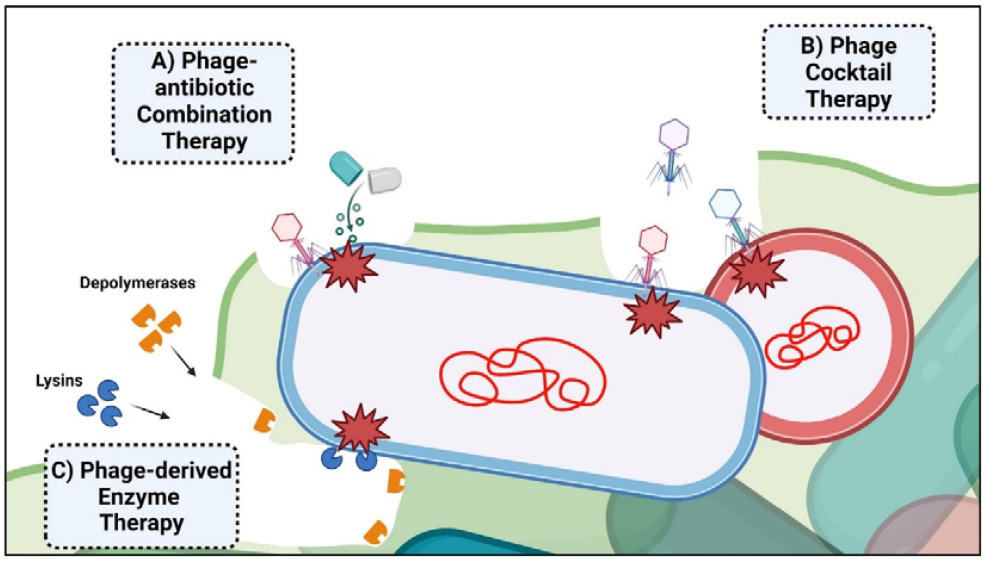

FIGURE 2
Bacteriophage-based therapeutic approaches employed for biofilm-derived infection. The figure illustrates the three main phage-associated mechanisms employed for clinical treatment. **(A)** Phage-antibiotic combination therapy can disrupt biofilm formation, making bacteria more vulnerable to phage attack and the effects of antibiotics. **(B)** Phage cocktail therapy involves using a mixture of bacteriophages to target and eliminate multiple strains or species of bacteria in poly-bacterial infections. **(C)** Phage-derived enzyme therapy utilizes enzymes, such as lysins and depolymerases, to degrade bacterial cell walls and biofilm matrices, degrading biofilms and eliminating bacteria.

TABLE 1 Clinical studies regarding bacteriophage therapy used to treat biofilm-related infections.

Target bacteria	Biofilm model	Treatment	Outcomes	Ref.
Multiple species	Chronic wound infection	Phage cocktail-antibiotic combination (ceftazidime-avibactam)	Infection was resolved in 90 days	(Karn et al., 2024)
Pseudomonas aeruginosa	Left Ventricular Assist Device Driveline Infection	Phage cocktail-antibiotic combination (ceftazidime/avibactam-amikacin)	Infection was resolved. No adverse effects were observed	(Racenis et al., 2023)
Enterococcus faecalis	Prosthetic joint infections	Phage-antibiotic combination (daptomycin and amoxicillin)	*E. faecalis* infection was resolved but the patient presented a posterior MRSA infection.	(Doub et al., 2023)
Pseudomonas aeruginosa	Prosthetic vascular graft infection	Phage cocktail-antibiotic combination (ceftazidime-avibactam)	Therapy did not resolve the infection	(Blasco et al., 2023)
Pseudomonas aeruginosa	Hip prosthetic infection	Phage-antibiotic combination (meropenem)	Infection was resolved. No adverse effects were observed	(Cesta et al., 2023)
***Staphylococcal* spp.**	Peri-Prosthetic joint infections	Phage cocktail-antibiotic combination	Lower rate of periprosthetic joint infection relapse	(Fedorov et al., 2023)
MRSA	Knee and hip prosthetic joint infection	Phage-antibiotic combination (daptomycin and vancomycin)	Infection was resolved. No adverse effects were observed	(Schoeffel et al., 2022)
MRSA	Prosthetic joint infection	Phage-antibiotic combination (daptomycin)	Infection was resolved. No adverse effects were observed	(Doub et al., 2022a)
Klebsiella pneumoniae	Prosthetic shoulder infection	Phage cocktail combination (ertapenem)	Infection was resolved. No adverse effects were observed	(Doub et al., 2022b)
Pseudomonas aeruginosa	Left Ventricular Assist Device Driveline Infection	Phage-antibiotic combination (Ceftolozane/tazobactam)	Infection was resolved. No adverse effects were observed	(Tkhilaishvili et al., 2021)
Staphylococcus aureus*	Pelvic bone allograft infection	Phage-antibiotic combination (intravenous clindamycin, rifampin and ciprofloxacin)	Therapy did not resolve the infection	(Van Nieuwenhuyse et al., 2021)
Staphylococcus epidermidis	Prosthetic knee infection	Phage-antibiotic combination (daptomycin and doxycycline)	Phage therapy discontinued by patient request due to mild transaminitis	(Doub et al., 2021)

MRSA, methicillin-resistant S. aureus.
(*Multispecies infection was diagnosed but only S. aureus phages were available for the phage therapy).

(ceftazidime/avibactam and amikacin) to treat a left ventricular assist device driveline infection caused by multidrug-resistant *P. aeruginosa*. Follow-up evaluations were recorded at six weeks, 34 weeks, and 48 months after intervention, where the patient showed no signs of relapse (Racenis et al., 2023). The same year, a necessary clinical trial assessed the effect of an antibiotic phage cocktail in combination with several etiotropic antibiotics (Fedorov et al., 2023). During this trial, twenty-three adult patients with deep periprosthetic joint infection received phage-antibiotic therapeutic intervention during and after surgery, with two patients presenting mild adverse effects (fever) after phage administration, which were eventually resolved. In the end, the periprosthetic joint infection relapse rate was around 12 times lower than that in the control group (Fedorov et al., 2023).

5.2.3 Bacteriophage-derived enzymes application

Several limitations can interfere with phage penetration, propagation, and diffusion through the EPS matrix, hindering the use of lytic phages to eliminate biofilms. Phage-derived enzymes, namely endolysins and depolymerizes, have emerged as potential mechanisms of EPS matrix degradation, as explained in Section 4.1. The efficacy of endolysins as tools for biofilm treatment has been extensively covered in the literature (de Miguel et al., 2020; Ghose and Euler, 2020; Abdelrahman et al., 2021).

In the field of clinical trials, some advancements have been made in the elimination of biofilm-forming bacteria of medical relevance. For instance, research has demonstrated that the phage depolymerase KPO1K1 can eliminate *Klebsiella pneumoniae* B5055 even on an old biofilm matrix (Fernandes and São-José, 2018). Recently, the multidrug-resistant clinical strain Kl 315 of *K. pneumoniae* and its biofilm were also shown to be effectively eliminated by phage displaying depolymerase activity (Zurabov et al., 2023).

In this regard, both endolysins and depolymerizes exhibit a narrow antibacterial spectrum, offering advantages over broad-spectrum antibiotics. They are suitable for selective elimination of drug-resistant pathogenic bacteria with lesser adverse effects on the host microbiome (Singh et al., 2022b).

5.2.4 Novel bacteriophage-based clinical approaches

In recent years, novel bacteriophage approaches have gained significant attention as promising strategies for treating biofilm-associated infections, effectively addressing the limitations of

traditional antibiotics and earlier phage therapies. These approaches have been assessed *in vivo* models and tackle critical challenges such as efficient phage delivery, resilience against harsh environmental conditions within the host, neutralization by host antibodies, and the internalization of phages to combat intracellular infections. As mentioned in Section 4, bacteriophage encapsulation represents an innovative method for biofilm infection treatment, leveraging bacteriophages' inherent potential while overcoming issues related to their stability and targeted delivery (Yan et al., 2021).

Clinical applications of hydrogel-based bacteriophage encapsulation have shown significant potential *in vivo* for treating multidrug-resistant (MDR) infections. In 2015, a study evaluated the temperate phage ΦPan70 for its efficacy against MDR *P. aeruginosa* in planktonic, biofilm, and mouse burn models. The phage significantly reduced bacterial populations and improved the survival rate of burned mice from 80% to 100%. Researchers suggested that phages could prevent bacterial spread into the bloodstream and enhance immune responses at the injection site (Holguín et al., 2015).

Further advancements in wound therapy have led to the development of wound dressings composed of chitosan, sodium alginate, and carboxymethyl cellulose, targeting MDR bacteria and biofilm-mediated infections in mice wound models (Mabrouk et al., 2022; Dehari et al., 2023; Mukhopadhyay et al., 2023). For instance, a study highlighted the synergistic effect of a phage-ciprofloxacin hydrogel in a mouse wound healing model, showing enhanced wound healing and improving mice recovery (Shafigh Kheljan et al., 2023). Figure 3 showcases the concept of wound dressing with hydrogel-coated bacteriophages. Some studies suggest that hydrogel-coated bacteriophages can be delivered via injectable application into specific tissues. For instance, a recent study utilized a fracture-related infection (FRI) mouse model to assess the effectiveness of a hydrogel containing both a phage cocktail and antibiotic meropenem to treat a *P. aeruginosa* FRI. Compared with the application of free bacteriophages, the phage-meropenem hydrogel exhibited a lower incidence of phage resistance and reduced serum neutralization (Chen et al., 2023).

On the other hand, encapsulating bacteriophages in liposomes also shows promise in enhancing their stability and protection from the host immune system, ensuring controlled release at the infection site (Figure 3). Studies have employed various methods for effective phage encapsulation, such as a microfluidic-based technique to create liposomes with adjustable sizes (Cinquerrui et al., 2018). In a 2016 study, liposomes were evaluated for their ability to deliver phages intracellularly and their susceptibility to anti-phage antibodies. Liposome-encapsulated phages were fully protected from neutralizing antibodies, whereas free phages were neutralized within three hours. Additionally, liposome-encapsulated phages were able to enter mouse peritoneal macrophages and achieve a 94.6% killing rate of intracellular *K. pneumoniae* (Singla et al., 2016).

Another *in vivo* study in mice examined the biodistribution of orally administered, liposome-encapsulated fluorescent bacteriophages and their transport through intestinal cell layers. This study showed that liposome-encapsulated phages persisted longer in the stomach and adhered to the intestinal membrane, suggesting greater long-term efficacy of phage therapy (Otero et al., 2019). Murine models are not the only *in vivo* models used for these

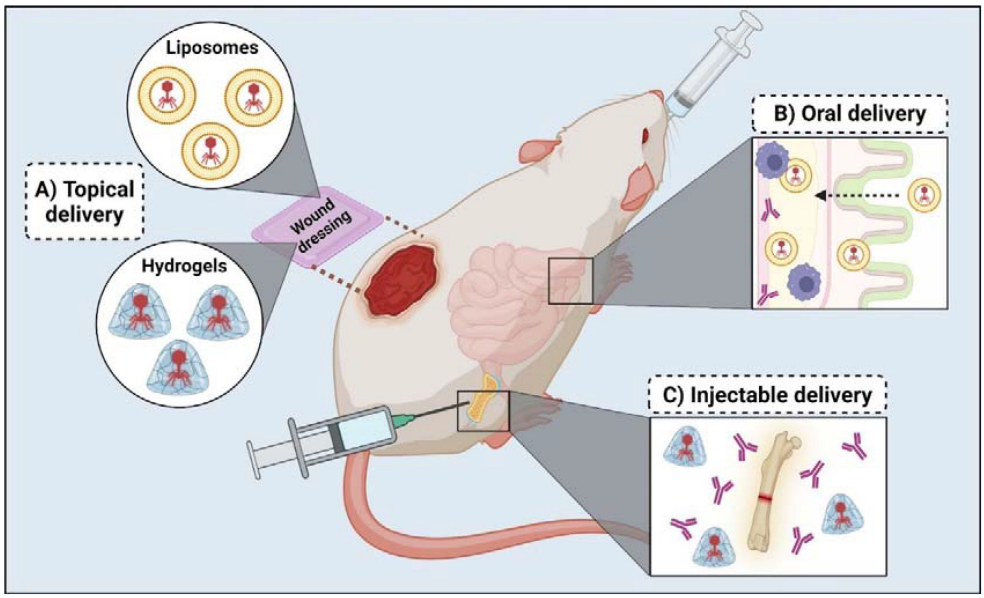

FIGURE 3
In vivo studies regarding bacteriophage delivery for clinical application. **(A)** Topical delivery has been used in mice wound models and involves wound dressing coated with liposomes or hydrogels containing bacteriophages. **(B)** Oral delivery mainly uses liposome encapsulation to protect bacteriophages on their transit to the intestinal tract, facilitate transportation through the intestinal layer and avoid antibody interference. **(C)** Injectable delivery allows the intradermal and intramuscular application of bacteriophage therapy in case of bone and prosthetic joint infection; it usually involves using hydrogels to protect bacteriophages from antibodies and other immune responses.

studies. For instance, in 2022, a study demonstrated that asymmetric phosphatidylserine/phosphatidic acid (PS/PA) liposomes, used in both prophylactic and treatments, reduced bacterial burden in zebrafish embryos infected with *P. aeruginosa* by enhancing macrophage phagocytic activity. In this regard, combining liposomes and phage cocktails improves antimicrobial effects and is effective against phage-resistant bacteria (Cafora et al., 2022).

Phage engineering has also shown great potential to develop novel approaches for targeting infections in clinical settings. Genetic modifications can enhance the expression of lytic enzymes, such as phage hydrolases, and facilitate the degradation of the biofilm matrix. For instance, genetically modified (GM) T7 *E. coli* phages have enhanced biofilm matrix degradation efficacy (Waturangi et al., 2021).

Studies have shown that phages can be engineered to augment their antimicrobial properties. In 2023, modification of the capsid of K1F phages increased their affinity for human tissue, potentially enhancing their ability to target intracellular infections caused by their host bacteria, *E. coli* K1 (Williams et al., 2023). Furthermore, eliminating lysogeny-related genes in Ef11 *E. faecalis* phages has shown promising results in eradicating *E. faecalis* biofilm populations, including vancomycin-resistant strains (Tinoco et al., 2016). Overall, genetic modification of phages also represents a valuable tool to enhance the effectiveness of phage-based biofilm treatment in clinical settings.

6 Future perspectives and challenges

Bacteriophage therapy, an innovative approach for targeting biofilm-associated infections and antibiotic-resistant bacteria, holds significant potential. However, its application is accompanied by significant challenges and limitations that necessitate critical examination. These challenges encompass a range of technical, biological, and regulatory issues that must be addressed to harness the full potential of phages in clinical and environmental applications.

6.1 Enhancing phage efficacy and delivery

A primary limitation of bacteriophage therapy is its narrow host range, which restricts its application to specific bacterial strains (Magaziner and Salmond, 2022; Ratnakar, 2022). This specificity, though beneficial in minimizing off-target effects, significantly limits the broader clinical applicability of phage therapy, especially in polymicrobial infections. Phage cocktails, comprising multiple phages with varying host ranges, have been suggested as a solution to this limitation (Schooley et al., 2017; Zaczek-Moczydłowska et al., 2020). However, the formulation of such cocktails must carefully consider the potential antagonistic interactions between phages, which could compromise their efficacy. Additionally, identifying and formulating effective phage cocktails is resource-intensive and requires extensive screening and validation.

6.2 Addressing phage resistance

Similar to antibiotics, bacteriophages face the challenge of bacterial resistance. Bacteria can evolve mechanisms to evade phage predation (Teklemariam et al., 2023), such as altering surface receptors required for phage attachment and infection (Rendueles et al., 2023). This phenomenon requires ongoing monitoring and the development of new phages, a process that demands significant resources and time. To mitigate resistance, strategies such as combining phages with antibiotics have shown promise in enhancing biofilm eradication and preventing resistance (Lu et al., 2023; Meneses et al., 2023).

6.3 Structural complexity of biofilms

The dense extracellular matrix of biofilms presents a significant barrier to effective phage therapy. This matrix can impede phage penetration and reduce bactericidal efficiency. Advanced delivery systems, including nanoparticles, liposomes, and hydrogels, are being explored to enhance phage stability and facilitate deeper penetration into biofilm structures (Kluzek et al., 2022; Costa et al., 2023). Despite promising results, these delivery mechanisms' development and clinical application remain in their early stages and require further validation.

6.4 Stability in various environments

The stability of phages in different environments, including the human body, is a concern. Factors such as pH, temperature, and the presence of immune components can influence phage viability and activity. Strategies like encapsulating phages in protective carriers or engineering phages to evade immune detection are under investigation (Arias et al., 2022; Hufziger et al., 2022; Gao and Feng, 2023). However, these approaches add complexity to treatment protocols.

6.5 Environmental and industrial applications

Beyond clinical settings, phage therapy holds potential for environmental sanitation and industrial applications. Phages can be utilized to control biofilms in water treatment plants (Shivaram et al., 2023), food processing environments (Vikram et al., 2021; Brás et al., 2024), and agricultural settings (Ascaño et al., 2022), providing sustainable and effective alternatives to chemical treatments. Future research should focus on optimizing phage application methods to ensure environmental compatibility and effectiveness across diverse conditions.

6.6 Phage-host interactions and evolutionary dynamics

Understanding the complex interactions between phages and their bacterial hosts is crucial for successfully applying phage therapy. Phage-host dynamics are influenced by various factors, including the genetic diversity of phages and bacteria, environmental conditions (Fister et al., 2016; Goehlich et al., 2024), and the presence of other microorganisms (Alkhalil, 2023). Studying these interactions can provide insights into the mechanisms of bacterial resistance and inform the development of more effective phage therapies.

6.7 Integration with other therapies

Combining phage therapy with other treatment modalities, such as antibiotics, antimicrobial peptides, and immune modulators, has shown promise in enhancing therapeutic outcomes (Coulter et al., 2014; Morrisette et al., 2020; Joo et al., 2023; Lu et al., 2023). This approach requires careful consideration of potential interactions, dosing regimens, and treatment protocols. Clinical trials and studies are needed to evaluate the safety and efficacy of combination therapies and establish guidelines for their use in clinical practice.

6.8 Release of endotoxins by lysis of Gram-negative bacteria

A critical impediment to the deployment of phage therapy for infections caused by Gram-negative bacteria is the simultaneous release of endotoxins, particularly LPS, during the lysis of bacterial cells. Gram-negative bacteria are characterized by an outer membrane enriched with LPS, a potent elicitor of human immune responses. Bacteriophage-induced lysis releases these cell wall components, including endotoxins, into the extracellular milieu, precipitating a severe inflammatory reaction. This response, known as endotoxin shock or septic shock, is marked by symptoms such as fever and hypotension, which can lead to fatal outcomes if not adequately controlled. The efficacy of phage therapy in reducing bacterial populations is paradoxically undermined by the exacerbation of clinical symptoms due to the rapid liberation of endotoxins (Hibstu et al., 2022). Strategies to mitigate this issue include the development of genetically engineered phages designed to either preclude the release of endotoxins or facilitate their degradation post-release (Matsuda et al., 2005; Łobocka et al., 2021).

In conclusion, while bacteriophage therapy offers a promising alternative to traditional antibiotics, continued research, innovation, and a multidisciplinary approach that addresses its myriad challenges and complexities is needed. The path forward involves enhancing phage delivery systems, developing strategies to mitigate resistance, expanding host range specificity, navigating the regulatory landscape, and fostering public engagement to ensure phage therapy's sustainable and effective application across multiple domains.

Author contributions

LG: Conceptualization, Data curation, Formal Analysis, Methodology, Supervision, Writing – review & editing. AM-R: Investigation, Methodology, Validation, Visualization, Writing – original draft. SC-P: Formal Analysis, Investigation, Resources, Writing – review & editing. CB-O: Data curation, Formal Analysis, Validation, Writing – original draft.

Funding

The author(s) declare that no financial support was received for the research, authorship, and/or publication of this article.

Acknowledgments

Figures were created with BioRender.com.

Conflict of interest

The authors declare that the research was conducted in the absence of any commercial or financial relationships that could be construed as a potential conflict of interest.

Publisher's note

References

Abdelrahman, F., Easwaran, M., Daramola, O. I., Ragab, S., Lynch, S., Oduselu, T. J., et al. (2021). Phage-encoded endolysins. *Antibiot. (Basel)* 10, 124. doi: 10.3390/antibiotics10020124

Abdelsattar, A. S., Nofal, R., Makky, S., Safwat, A., Taha, A., and El-Shibiny, A. (2021). The synergistic effect of biosynthesized silver nanoparticles and phage ZCSE2 as a novel approach to combat multidrug-resistant *Salmonella enterica*. *Antibiot. (Basel)* 10, 678. doi: 10.3390/antibiotics10060678

Abebe, E., Gugsa, G., and Ahmed, M. (2020). Review on major food-borne zoonotic bacterial pathogens. *J. Trop. Med.* 2020, 4674235. doi: 10.1155/2020/4674235

Abedon, S. T. (2015). Ecology of anti-biofilm agents II: Bacteriophage exploitation and biocontrol of biofilm bacteria. *Pharm. (Basel)* 8, 559–589. doi: 10.3390/ph8030559

Adamu Ahmad, K., Sabo Mohammed, A., and Abas, F. (2016). Chitosan nanoparticles as carriers for the delivery of ΦKAZ14 bacteriophage for oral biological control of colibacillosis in chickens. *Molecules* 21, 256. doi: 10.3390/molecules21030256

Ahiwale, S. S., Bankar, A. V., Tagunde, S., and Kapadnis, B. P. (2017). A bacteriophage mediated gold nanoparticles synthesis and their anti-biofilm activity. *Indian J. Microbiol.* 57, 188–194. doi: 10.1007/s12088-017-0640-x

Ali, A., Zahra, A., Kamthan, M., Husain, F. M., Albalawi, T., Zubair, M., et al. (2023). Microbial biofilms: Applications, clinical consequences, and alternative therapies. *Microorganisms* 11, 1934. doi: 10.3390/microorganisms11081934

Alkhalil, S. S. (2023). The role of bacteriophages in shaping bacterial composition and diversity in the human gut. *Front. Microbiol.* 14. doi: 10.3389/fmicb.2023.1232413

Alves, D. R., Perez-Esteban, P., Kot, W., Bean, J. E., Arnot, T., Hansen, L. H., et al. (2016). A novel bacteriophage cocktail reduces and disperses *Pseudomonas aeruginosa* biofilms under static and flow conditions. *Microbial. Biotechnol.* 9, 61–74. doi: 10.1111/1751-7915.12316

Amankwah, S., Abdella, K., and Kassa, T. (2021). Bacterial biofilm destruction: A focused review on the recent use of phage-based strategies with other antibiofilm agents. *Nanotechnol. Sci. Appl.* 14, 161–177. doi: 10.2147/NSA.S325594

Antimicrobial Resistance Collaborators (2022). Global burden of bacterial antimicrobial resistance in 2019: A systematic analysis. *Lancet* 399, 629–655. doi: 10.1016/S0140-6736(21)02724-0

Arias, C. F., Acosta, F. J., Bertocchini, F., Herrero, M. A., and Fernández-Arias, C. (2022). The coordination of anti-phage immunity mechanisms in bacterial cells. *Nat. Commun.* 13, 7412. doi: 10.1038/s41467-022-35203-7

Armbruster, C. R., and Parsek, M. R. (2018). New insight into the early stages of biofilm formation. *Proc. Natl. Acad. Sci. U.S.A.* 115, 4317–4319. doi: 10.1073/pnas.1804084115

Ascaño, M. A., Caiñza, M. A., and Dy, R. L. (2022). "Sustainable Phage-Based Strategies to Control Bacterial Diseases in Agriculture," in *Agricultural biocatalysis: Biological and chemical applications* (Jenny Stanford Publishing, New York), 41–79. doi: 10.1201/9781003313144-3

Ayyaru, S., Choi, J., and Ahn, Y.-H. (2018). Biofouling reduction in a MBR by the application of a lytic phage on a modified nanocomposite membrane. *Environ. Sci.: Water Res. Technol.* 4, 1624–1638. doi: 10.1039/C8EW00316E

Azulay, D. N., Spaeker, O., Ghrayeb, M., Wilsch-Bräuninger, M., Scoppola, E., Burghammer, M., et al. (2022). Multiscale X-ray study of *Bacillus subtilis* biofilms reveals interlinked structural hierarchy and elemental heterogeneity. *Proc. Natl. Acad. Sci. U.S.A.* 119, e2118107119. doi: 10.1073/pnas.2118107119

Ballesté, E., Blanch, A. R., Muniesa, M., García-Aljaro, C., Rodríguez-Rubio, L., Martín-Díaz, J., et al. (2022). Bacteriophages in sewage: Abundance, roles, and applications. *FEMS Microbes* 3, xtac009. doi: 10.1093/femsmc/xtac009

Barros, J. A. R., de Melo, L. D. R., da Silva, R. A. R., Ferraz, M. P., de Rodriguez Azeredo, J. C. V., de Carvalho Pinheiro, V. M., et al. (2020). Encapsulated bacteriophages in alginate-nanohydroxyapatite hydrogel as a novel delivery system to prevent orthopedic implant-associated infections. *Nanomedicine* 24, 102145. doi: 10.1016/j.nano.2019.102145

Bhattacharjee, A. S., Choi, J., Motlagh, A. M., Mukherji, S. T., and Goel, R. (2015). Bacteriophage therapy for membrane biofouling in membrane bioreactors and antibiotic-resistant bacterial biofilms. *Biotechnol. Bioeng.* 112, 1644–1654. doi: 10.1002/bit.25574

Blasco, L., López-Hernández, I., Rodríguez-Fernández, M., Pérez-Florido, J., Casimiro-Soriguer, C. S., Djebara, S., et al. (2023). Case report: Analysis of phage therapy failure in a patient with a *P. aeruginosa* prosthetic vascular graft infection. *Front. Med. (Lausanne)* 10. doi: 10.3389/fmed.2023.1199657

Bozhkova, S. A., Tikhilov, R. M., Krasnova, M. V., and Rukina, A. N. (2013). Orthopedic implant-associated infection: The main etiological agents, local resistance and antimicrobial therapy recommendations. *Travmatol. ortop. Ross.* 19, 5–15. doi: 10.21823/2311-2905-2013–4-5-15

Brás, A., Braz, M., Martinho, I., Duarte, J., Pereira, C., and Almeida, A. (2024). Effect of bacteriophages against biofilms of *Escherichia coli* on food processing surfaces. *Microorganisms* 12, 366. doi: 10.3390/microorganisms12020366

Briers, Y., Schmelcher, M., Loessner, M. J., Hendrix, J., Engelborghs, Y., Volckaert, G., et al. (2009). The high-affinity peptidoglycan binding domain of *Pseudomonas* phage endolysin KZ144. *Biochem. Biophys. Res. Commun.* 383, 187–191. doi: 10.1016/j.bbrc.2009.03.161

Bull, J. J., Christensen, K. A., Scott, C., Jack, B. R., Crandall, C. J., and Krone, S. M. (2018). Phage-bacterial dynamics with spatial structure: Self-on organization around phage sinks can promote increased cell densities. *Antibiot. (Basel)* 7, 1–25. doi: 10.3390/antibiotics7010008

Cady, K. C., and O'Toole, G. A. (2011). Non-identity-mediated CRISPR-bacteriophage interaction mediated via the Csy and Cas3 proteins. *J. Bacteriol.* 193, 3433–3445. doi: 10.1128/JB.01411-10

Cafora, M., Poerio, N., Forti, F., Loberto, N., Pin, D., Bassi, R., et al. (2022). Evaluation of phages and liposomes as combination therapy to counteract *P. aeruginosa* infection in wild-type and CFTR-null models. *Front. Microbiol.* 13. doi: 10.3389/fmicb.2022.979610

Cahill, J., and Young, R. (2019). Phage lysis: Multiple genes for multiple barriers. *Adv. Virus Res.* 103, 33–70. doi: 10.1016/bs.aivir.2018.09.003

Cangui-Panchi, S. P., Ñacato-Toapanta, A. L., Enríquez-Martínez, L. J., Salinas-Delgado, G. A., Reyes, J., Garzon-Chavez, D., et al. (2023). Battle royale: Immune response on biofilms - host-pathogen interactions. *Curr. Res.Immunol.* 4, 100057. doi: 10.1016/j.crimmu.2023.100057

Carrasco, B., Escobedo, S., Alonso, J. C., and Suárez, J. E. (2016). Modulation of *Lactobacillus casei* bacteriophage A2 lytic/lysogenic cycles by binding of Gp25 to the early lytic mRNA. *Mol. Microbiol.* 99, 328–337. doi: 10.1111/mmi.13234

Cesta, N., Pini, M., Mulas, T., Materazzi, A., Ippolito, E., Wagemans, J., et al. (2023). Application of phage therapy in a case of a chronic hip-prosthetic joint infection due to *P. aeruginosa*: An Italian real-life experience and in *vitro* analysis. *Open Forum Infect. Dis.* 10, ofad051. doi: 10.1093/ofid/ofad051

Chávez-Jacobo, V. M., Becerra-Rivera, V. A., Guerrero, G., and Dunn, M. F. (2023). The *Sinorhizobium meliloti* NspS-MbaA system affects biofilm formation, exopolysaccharide production and motility in response to specific polyamines. *Microbiol. (Reading Engl)* 169, 1–15. doi: 10.1099/mic.0.001293

Chegini, Z., Khoshbayan, A., Taati Moghadam, M., Farahani, I., Jazireian, P., and Shariati, A. (2020). Bacteriophage therapy against *P. aeruginosa* biofilms: A review. *Ann. Clin. Microbiol. Antimicrob.* 19, 45. doi: 10.1186/s12941-020-00389-5

Chen, B., Benavente, L. P., Chittò, M., Wychowaniec, J. K., Post, V., D'Este, M., et al. (2023). Alginate microbeads and hydrogels delivering meropenem and bacteriophages to treat *P. aeruginosa* fracture-related infections. *J. Control. Release* 364, 159–173. doi: 10.1016/j.jconrel.2023.10.029

Cinquerrui, S., Mancuso, F., Vladisavljević, G. T., Bakker, S. E., and Malik, D. J. (2018). Nanoencapsulation of bacteriophages in liposomes prepared using microfluidic hydrodynamic flow focusing. *Front. Microbiol.* 9. doi: 10.3389/fmicb.2018.02172

Costa, M. J., Pastrana, L. M., Teixeira, J. A., Sillankorva, S. M., and Cerqueira, M. A. (2023). Bacteriophage delivery systems for food applications: Opportunities and perspectives. *Viruses* 15, 1271. doi: 10.3390/v15061271

Coulter, L. B., McLean, R. J. C., Rohde, R. E., and Aron, G. M. (2014). Effect of bacteriophage infection in combination with tobramycin on the emergence of resistance in *E. coli* and *P. aeruginosa* biofilms. *Viruses* 6, 3778–3786. doi: 10.3390/v6103778

da Silva Duarte, V., Dias, R. S., Kropinski, A. M., Campanaro, S., Treu, L., Siqueira, C., et al. (2018). Genomic analysis and immune response in a murine mastitis model of vB_EcoM-UFV13, a potential biocontrol agent for use in dairy cows. *Sci. Rep.* 8, 6845. doi: 10.1038/s41598-018-24896-w

Dehari, D., Kumar, D. N., Chaudhuri, A., Kumar, A., Kumar, R., Kumar, D., et al. (2023). Bacteriophage entrapped chitosan microgel for the treatment of biofilm-mediated polybacterial infection in burn wounds. *Int. J. Biol. Macromol.* 253, 127247. doi: 10.1016/j.ijbiomac.2023.127247

de Miguel, T., Rama, J. L. R., Sieiro, C., Sánchez, S., and Villa, T. G. (2020). Bacteriophages and lysins as possible alternatives to treat antibiotic-resistant urinary tract infections. *Antibiot. (Basel)* 9, 466. doi: 10.3390/antibiotics9080466

Doub, J. B., Chan, B., and Johnson, A. J. (2023). Salphage: Salvage bacteriophage therapy for a chronic *Enterococcus faecalis* prosthetic joint infection. *IDCases* 33, e01854. doi: 10.1016/j.idcr.2023.e01854

Doub, J. B., Ng, V. Y., Lee, M., Chi, A., Lee, A., Würstle, S., et al. (2022a). Salphage: Salvage bacteriophage therapy for recalcitrant MRSA prosthetic joint infection. *Antibiot. (Basel)* 11, 616. doi: 10.3390/antibiotics11050616

Doub, J. B., Ng, V. Y., Wilson, E., Corsini, L., and Chan, B. K. (2021). Successful treatment of a recalcitrant *Staphylococcus epidermidis* prosthetic knee infection with intraoperative bacteriophage therapy. *Pharm. (Basel)* 14, 231. doi: 10.3390/ph14030231

Doub, J. B., Shishido, A., Srikumaran, U., Haskoor, J., Tran-Nguyen, P., Lee, M., et al. (2022b). Salphage: Salvage bacteriophage therapy for a recalcitrant Klebsiella pneumoniae prosthetic shoulder infection - a case report. *Acta Orthop.* 93, 756–759. doi: 10.2340/17453674.2022.4579

Erol, H. B., Kaskatepe, B., Yildiz, S., Altanlar, N., and Bayrakdar, F. (2024). Characterization of two bacteriophages specific to *Acinetobacter baumannii* and their effects on catheters biofilm. *Cell Biochem. Funct.* 42, e3966. doi: 10.1002/cbf.3966

Fedorov, E., Samokhin, A., Kozlova, Y., Kretien, S., Sheraliev, T., Morozova, V., et al. (2023). Short-term outcomes of phage-antibiotic combination treatment in adult patients with periprosthetic hip joint infection. *Viruses* 15, 396. doi: 10.3390/v15020499

Fernandes, S., and São-José, C. (2018). Enzymes and mechanisms employed by tailed bacteriophages to breach the bacterial cell barriers. *Viruses* 10. doi: 10.3390/v10080396

Fernández, L., Rodríguez, A., and García, P. (2018). Phage or foe: An insight into the impact of viral predation on microbial communities. *ISME J.* 12, 1171–1179. doi: 10.1038/s41396-018-0049-5

Ferriol-González, C., and Domingo-Calap, P. (2020). Phages for biofilm removal. *Antibiot. (Basel)* 9, 268. doi: 10.3390/antibiotics9050268

Fister, S., Robben, C., Witte, A. K., Schoder, D., Wagner, M., and Rossmanith, P. (2016). Influence of environmental factors on phage-bacteria interaction and on the efficacy and infectivity of phage P100. *Front. Microbiol.* 7. doi: 10.3389/fmicb.2016.01152

Fongang, H., Mbaveng, A. T., and Kuete, V. (2023). "Global burden of bacterial infections and drug resistance," in *African Flora to Fight Bacterial Resistance, Part I: Standards for the Activity of Plant-Derived Products* (London: Elsevier), 1–20. doi: 10.1016/bs.abr.2022.08.001

Galié, S., García-Gutiérrez, C., Miguélez, E. M., Villar, C. J., and Lombó, F. (2018). Biofilms in the food industry: Health aspects and control methods. *Front. Microbiol.* 9. doi: 10.3389/fmicb.2018.00898

Gao, Z., and Feng, Y. (2023). Bacteriophage strategies for overcoming host antiviral immunity. *Front. Microbiol.* 14. doi: 10.3389/fmicb.2023.1211793

Ghose, C., and Euler, C. W. (2020). Gram-negative bacterial lysins. *Antibiot. (Basel)* 9, 74. doi: 10.3390/antibiotics9020074

Goehlich, H., Roth, O., Sieber, M., Chibani, C. M., Poehlein, A., Rajkov, J., et al. (2024). Suboptimal environmental conditions prolong phage epidemics in bacterial populations. *Mol. Ecol.* 33, e17050. doi: 10.1111/mec.17050

Goldman, G., Starosvetsky, J., and Armon, R. (2009). Inhibition of biofilm formation on UF membrane by use of specific bacteriophages. *J. Memb. Sci.* 342, 145–152. doi: 10.1016/j.memsci.2009.06.036

González, S., Fernández, L., Gutiérrez, D., Campelo, A. B., Rodríguez, A., and García, P. (2018). Analysis of different parameters affecting diffusion, propagation and survival of staphylophages in bacterial biofilms. *Front. Microbiol.* 9. doi: 10.3389/fmicb.2018.02348

Gulec, F., and Eckford, A. W. (2023). A stochastic biofilm disruption model based on quorum sensing mimickers. *IEEE Trans. Mol. Biol. Multi-Scale Commun.* 9, 346–350. doi: 10.1109/TMBMC.2023.3292321

Gutiérrez, D., Rodríguez-Rubio, L., Martínez, B., Rodríguez, A., and García, P. (2016). Bacteriophages as weapons against bacterial biofilms in the food industry. *Front. Microbiol.* 7. doi: 10.3389/fmicb.2016.00825

Guttenplan, S. B., Blair, K. M., and Kearns, D. B. (2010). The EpsE flagellar clutch is bifunctional and synergizes with EPS biosynthesis to promote *B. subtilis* biofilm formation. *PloS Genet.* 6, e1001243. doi: 10.1371/journal.pgen.1001243

Hanlon, G. W. (2007). Bacteriophages: An appraisal of their role in the treatment of bacterial infections. *Int. J. Antimicrob. Agents* 30, 118–128. doi: 10.1016/j.ijantimicag.2007.04.006

Hassan, A. Y., Lin, J. T., Ricker, N., and Anany, H. (2021). The age of phage: Friend or foe in the new dawn of therapeutic and biocontrol applications? *Pharm. (Basel)* 14, 199. doi: 10.3390/ph14030199

Hibstu, Z., Belew, H., Akelew, Y., and Mengist, H. M. (2022). Phage therapy: A different approach to fight bacterial infections. *Biologics* 16, 173–186. doi: 10.2147/BTT.S381237

Høiby, N., Ciofu, O., Johansen, H. K., Song, Z., Moser, C., Jensen, P.Ø., et al. (2011). The clinical impact of bacterial biofilms. *Int. J. Oral. Sci.* 3, 55–65. doi: 10.4248/IJOS11026

Holguín, A. V., Rangel, G., Clavijo, V., Prada, C., Mantilla, M., Gomez, M. C., et al. (2015). Phage ΦPan70, a putative temperate phage, controls *P. aeruginosa* in planktonic, biofilm and burn mouse model assays. *Viruses* 7, 4602–4623. doi: 10.3390/v7082835

Hufziger, K. A., Farquharson, E. L., Werner, B. G., Chen, Q., Goddard, J. M., and Nugen, S. R. (2022). *In vivo* capsid engineering of bacteriophages for oriented surface conjugation. *ACS Appl. Bio Mater.* 5, 5104–5112. doi: 10.1021/acsabm.2c00428

Jaroni, D., Litt, P. K., Bule, P., and Rumbaugh, K. (2023). Effectiveness of bacteriophages against biofilm-forming shiga-toxigenic *E. coli in vitro* and on food-contact surfaces. *Foods* 12, 2787. doi: 10.3390/foods12142787

Joo, H., Wu, S. M., Soni, I., Wang-Crocker, C., Matern, T., Beck, J. P., et al. (2023). Phage and antibiotic combinations reduce *Staphylococcus aureus* in static and dynamic biofilms grown on an implant material. *Viruses* 15, 460. doi: 10.3390/v15020460

Karimi, M., Eslami, M., Sahandi-Zangabad, P., Mirab, F., Farajisafiloo, N., Shafaei, Z., et al. (2016). pH-Sensitive stimulus-responsive nanocarriers for targeted delivery of therapeutic agents. *Wiley Interdiscip. Rev. Nanomed. Nanobiotechnol.* 8, 696–716. doi: 10.1002/wnan.1389

Karn, S. L., Bhartiya, S. K., Pratap, A., Saroj, S. K., Kumar, R., Sahu, M., et al. (2024). A randomized, placebo-controlled, double-blind clinical trial of bacteriophage cocktails in chronic wound infections. *Int. J. Low. Extrem. Wounds*, 15347346231226342. doi: 10.1177/15347346231226342

Karthikeyan, K. G., and Meyer, M. T. (2006). Occurrence of antibiotics in wastewater treatment facilities in Wisconsin, USA. *Sci. Total Environ.* 361, 196–207. doi: 10.1016/j.scitotenv.2005.06.030

Kaszuba, M., Robinson, A. M., Song, Y. H., Creeth, J. E., and Jones, M. N. (1997). The visualisation of the targeting of phospholipid liposomes to bacteria. *Colloids Surfaces B: Biointerfaces* 8, 321–332. doi: 10.1016/S0927-7765(97)00007-6

Kaur, S., Harjai, K., and Chhibber, S. (2016). *In vivo* assessment of phage and linezolid based implant coatings for treatment of methicillin resistant *S. aureus* (MRSA) mediated orthopaedic device related infections. *PloS One* 11, e0157626. doi: 10.1371/journal.pone.0157626

Ke, C.-L., Deng, F.-S., Chuang, C.-Y., and Lin, C.-H. (2021). Antimicrobial actions and applications of chitosan. *Polym. (Basel)* 13, 904. doi: 10.3390/polym13060904

Khalifa, L., Gelman, D., Shlezinger, M., Dessal, A. L., Coppenhagen-Glazer, S., Beyth, N., et al. (2018). Defeating antibiotic- and phage-resistant *E. faecalis* using a phage cocktail in *vitro* and in a clot model. *Front. Microbiol.* 9. doi: 10.3389/fmicb.2018.00326

Khambhati, K., Bhattacharjee, G., Gohil, N., Dhanoa, G. K., Sagona, A. P., Mani, I., et al. (2023). Phage engineering and phage-assisted CRISPR-Cas delivery to combat multidrug-resistant pathogens. *Bioeng. Transl. Med.* 8, e10381. doi: 10.1002/btm2.10381

Kim, U., Lee, S.-Y., and Oh, S.-W. (2023b). A review of mechanism analysis methods in multi-species biofilm of foodborne pathogens. *Food Sci. Biotechnol.* 32, 1665–1677. doi: 10.1007/s10068-023-01317-x

Kim, B., Madukoma, C. S., Shrout, J. D., and Nerenberg, R. (2023a). Effect of EPS production on the performance of membrane-based biofilm reactors. *Water Res.* 240, 120101. doi: 10.1016/j.watres.2023.120101

Kluzek, M., Oppenheimer-Shaanan, Y., Dadosh, T., Morandi, M. I., Avinoam, O., Raanan, C., et al. (2022). Designer liposomic nanocarriers are effective biofilm eradicators. *ACS Nano* 16, 15792–15804. doi: 10.1021/acsnano.2c04232

Knecht, L. E., Veljkovic, M., and Fieseler, L. (2019). Diversity and function of phage encoded depolymerases. *Front. Microbiol.* 10. doi: 10.3389/fmicb.2019.02949

Krishnan, S., Patil, S. A., and Nancharaiah, Y. V. (2023). "Environmental microbial biofilms," in *Material-Microbes Interactions* (Cambridge, MA, USA: Elsevier), 3–45. doi: 10.1016/B978-0-323-95124-1.00013-9

Kushwaha, S. O., Sahu, S. K., Yadav, V. K., Rathod, M. C., Patel, D., Sahoo, D. K., et al. (2024). Bacteriophages as a potential substitute for antibiotics: A comprehensive review. *Cell Biochem. Funct.* 42, e4022. doi: 10.1002/cbf.4022

Kwiatek, M., Parasion, S., Rutyna, P., Mizak, L., Gryko, R., Niemcewicz, M., et al. (2017). Isolation of bacteriophages and their application to control *P. aeruginosa* in planktonic and biofilm models. *Res. Microbiol.* 168, 194–207. doi: 10.1016/j.resmic.2016.10.009

Laganenka, L., Sander, T., Lagonenko, A., Chen, Y., Link, H., and Sourjik, V. (2019). Quorum sensing and metabolic state of the host control lysogeny-lysis switch of bacteriophage T1. *MBio* 10, e01884-19. doi: 10.1128/mBio.01884-19

Lee, H. J., Kim, H. J., and Lee, S. J. (2022). Control of λ lysogenic *E. coli* cells by synthetic λ phage carrying cIantisense. *ACS Synth. Biol.* 11, 3829–3835. doi: 10.1021/acssynbio.2c00409

Lee, K. W. K., Periasamy, S., Mukherjee, M., Xie, C., Kjelleberg, S., and Rice, S. A. (2014). Biofilm development and enhanced stress resistance of a model, mixed-species community biofilm. *ISME J.* 8, 894–907. doi: 10.1038/ismej.2013.194

Li, J., Zheng, H., and Leung, S. S. Y. (2023). Potential of bacteriophage therapy in managing *S. aureus* infections during chemotherapy for lung cancer patients. *Sci. Rep.* 13, 9534. doi: 10.1038/s41598-023-36749-2

Li, L.-L., Yu, P., Wang, X., Yu, S.-S., Mathieu, J., Yu, H.-Q., et al. (2017). Enhanced biofilm penetration for microbial control by polyvalent phages conjugated with magnetic colloidal nanoparticle clusters (CNCs). *Environ. Sci.: Nano* 4, 1817–1826. doi: 10.1039/C7EN00414A

Li, Y., Xiao, P., Wang, Y., and Hao, Y. (2020). Mechanisms and control measures of mature biofilm resistance to antimicrobial agents in the clinical context. *ACS Omega* 5, 22684–22690. doi: 10.1021/acsomega.0c02294

Li, Z., Wang, X., Wang, J., Yuan, X., Jiang, X., Wang, Y., et al. (2022). Bacterial biofilms as platforms engineered for diverse applications. *Biotechnol. Adv.* 57, 107932. doi: 10.1016/j.biotechadv.2022.107932

Limoli, D. H., Jones, C. J., and Wozniak, D. J. (2015). Bacterial extracellular polysaccharides in biofilm formation and function. *Microbiol. Spectr.* 3. doi: 10.1128/microbiolspec.MB-0011-2014

Liu, M., Gill, J. J., Young, R., and Summer, E. J. (2015). Bacteriophages of wastewater foaming-associated filamentous *Gordonia* reduce host levels in raw activated sludge. *Sci. Rep.* 5, 13754. doi: 10.1038/srep13754

Łobocka, M., Dąbrowska, K., and Górski, A. (2021). Engineered bacteriophage therapeutics: Rationale, challenges and future. *BioDrugs* 35, 255–280. doi: 10.1007/s40259-021-00480-z

Loh, B., Gondil, V. S., Manohar, P., Khan, F. M., Yang, H., and Leptihn, S. (2021). Encapsulation and delivery of therapeutic phages. *Appl. Environ. Microbiol.* 87, e01979-20. doi: 10.1128/AEM.01979-20

Lomelí-Ortega, C. O., Barajas-Sandoval, D. R., Martínez-Villalobos, J. M., Jaramillo, C. R., Chávez, E. M., Gómez-Gil, B., et al. (2023). A broad-host-range phage cocktail selectively and effectively eliminates *Vibrio* species from shrimp aquaculture environment. *Microb. Ecol.* 86, 1443–1446. doi: 10.1007/s00248-022-02118-1

Loponte, R., Pagnini, U., Iovane, G., and Pisanelli, G. (2021). Phage therapy in veterinary medicine. *Antibiot. (Basel)* 10, 421. doi: 10.3390/antibiotics10040421

Lu, H., Li, Z., Elbaz, A., and Ni, S.-Q. (2023). Synergistic action of phages and lytic proteins with antibiotics: A combination strategy to target bacteria and biofilms. *BMC Microbiol.* 23, 149. doi: 10.1186/s12866-023-02881-2

Lu, T. K., and Collins, J. J. (2007). Dispersing biofilms with engineered enzymatic bacteriophage. *Proc. Natl. Acad. Sci. U.S.A.* 104, 11197–11202. doi: 10.1073/pnas.0704624104

Lu, Y., Cai, W.-J., Ren, Z., and Han, P. (2022). The role of staphylococcal biofilm on the surface of implants in orthopedic infection. *Microorganisms* 10, 1909. doi: 10.3390/microorganisms10101909

Mabrouk, S., Abdellatif, G. R., Abu Zaid, A. S., Aziz, R. K., and Aboshanab, K. M. (2022). *In Vitro* and pre-clinical evaluation of locally isolated phages, vB_Pae_SMP1 and vB_Pae_SMP5, formulated as hydrogels against carbapenem-resistant *P. aeruginosa*. *Viruses* 14, 2760. doi: 10.3390/v14122760

Magaziner, S. J., and Salmond, G. P. C. (2022). A novel T4- and λ-based receptor binding protein family for bacteriophage therapy host range engineering. *Front. Microbiol.* 13. doi: 10.3389/fmicb.2022.1010330

Mah, T. F., and O'Toole, G. A. (2001). Mechanisms of biofilm resistance to antimicrobial agents. *Trends Microbiol.* 9, 34–39. doi: 10.1016/S0966-842X(00)01913-2

Maje, M. D., Kaptchouang Tchatchouang, C. D., Manganyi, M. C., Fri, J., and Ateba, C. N. (2020). Characterisation of *Vibrio* species from surface and drinking water sources and assessment of biocontrol potentials of their bacteriophages. *Int. J. Microbiol.* 2020, 1–15. doi: 10.1155/2020/8863370

Malik, D. J., Sokolov, I. J., Vinner, G. K., Mancuso, F., Cinquerrui, S., Vladisavljevic, G. T., et al. (2017). Formulation, stabilisation and encapsulation of bacteriophage for phage therapy. *Adv. Colloid Interface Sci.* 249, 100–133. doi: 10.1016/j.cis.2017.05.014

Mancuso, G., Midiri, A., Gerace, E., and Biondo, C. (2021). Bacterial antibiotic resistance: The most critical pathogens. *Pathogens* 10, 1310. doi: 10.3390/pathogens10101310

Manoharadas, S., Altaf, M., Alrefaei, A. F., Devasia, R. M., Badjah Hadj, A. Y. M., and Abuhasil, M. S. A. (2021). Concerted dispersion of *S. aureus* biofilm by bacteriophage and "green synthesized" silver nanoparticles. *RSC Adv.* 11, 1420–1429. doi: 10.1039/D0RA09725J

Matamp, N., and Bhat, S. G. (2019). Phage endolysins as potential antimicrobials against multidrug resistant *Vibrio alginolyticus* and *Vibrio parahaemolyticus*: Current status of research and challenges ahead. *Microorganisms* 7, 84. doi: 10.3390/microorganisms7030084

Matsuda, T., Freeman, T. A., Hilbert, D. W., Duff, M., Fuortes, M., Stapleton, P. P., et al. (2005). Lysis-deficient bacteriophage therapy decreases endotoxin and inflammatory mediator release and improves survival in a murine peritonitis model. *Surgery* 137, 639–646. doi: 10.1016/j.surg.2005.02.012

Meade, E., Savage, M., and Garvey, M. (2020). Investigation of alternative biocidal options against foodborne multidrug resistant pathogens. *Eur. J. Exp. Biol.* 10, 2248–9215. doi: 10.36648/2248-9215.10.3.105

Meneses, L., Brandão, A. C., Coenye, T., Braga, A. C., Pires, D. P., and Azeredo, J. (2023). A systematic review of the use of bacteriophages for in *vitro* biofilm control. *Eur. J. Clin. Microbiol. Infect. Dis.* 42, 919–928. doi: 10.1007/s10096-023-04638-1

Milho, C., Silva, M. D., Alves, D., Oliveira, H., Sousa, C., Pastrana, L. M., et al. (2019). *E. coli* and *Salmonella enteritidis* dual-species biofilms: Interspecies interactions and antibiofilm efficacy of phages. *Sci. Rep.* 9, 18183. doi: 10.1038/s41598-019-54847-y

Mohanta, Y. K., Chakrabartty, I., Mishra, A. K., Chopra, H., Mahanta, S., Avula, S. K., et al. (2023). Nanotechnology in combating biofilm: A smart and promising therapeutic strategy. *Front. Microbiol.* 13. doi: 10.3389/fmicb.2022.1028086

Morrisette, T., Kebriaei, R., Lev, K. L., Morales, S., and Rybak, M. J. (2020). Bacteriophage therapeutics: A primer for clinicians on phage-antibiotic combinations. *Pharmacotherapy* 40, 153–168. doi: 10.1002/phar.2358

Moye, Z. D., Woolston, J., and Sulakvelidze, A. (2018). Bacteriophage applications for food production and processing. *Viruses* 10, 205. doi: 10.3390/v10040205

Mukhopadhyay, S., To, K. K. W., Liu, Y., Bai, C., and Leung, S. S. Y. (2023). A thermosensitive hydrogel formulation of phage and colistin combination for the management of multidrug-resistant *A. baumannii* wound infections. *Biomater. Sci.* 12, 151–163. doi: 10.1039/D3BM01383A

Mura, S., Nicolas, J., and Couvreur, P. (2013). Stimuli-responsive nanocarriers for drug delivery. *Nat. Mater.* 12, 991–1003. doi: 10.1038/nmat3776

Naknaen, A., Samernate, T., Wannasrichan, W., Surachat, K., Nonejuie, P., and Chaikeeratisak, V. (2023). Combination of genetically diverse *Pseudomonas* phages enhances the cocktail efficiency against bacteria. *Sci. Rep.* 13, 8921. doi: 10.1038/s41598-023-36034-2

Ngiam, L., Weynberg, K. D., and Guo, J. (2022). The presence of plasmids in bacterial hosts alters phage isolation and infectivity. *ISME Commun.* 2, 75. doi: 10.1038/s43705-022-00158-9

Nie, P., Alarcon, F., López-Montero, I., Orgaz, B., Valeriani, C., and Pica Ciamarra, M. (2021). *In-silico* modeling of early-stage biofilm formation. *Soft Mater.* 19, 346–358. doi: 10.1080/1539445X.2021.1887220

Oechslin, F., Piccardi, P., Mancini, S., Gabard, J., Moreillon, P., Entenza, J. M., et al. (2017). Synergistic interaction between phage therapy and antibiotics clears *P. aeruginosa* infection in endocarditis and reduces virulence. *J. Infect. Dis.* 215, 703–712. doi: 10.1093/infdis/jiw632

Ooi, M. L., Drilling, A. J., Morales, S., Fong, S., Moraitis, S., Macias-Valle, L., et al. (2019). Safety and tolerability of bacteriophage therapy for chronic rhinosinusitis due to *S. aureus*. *JAMA Otolaryngol. Head Neck Surg.* 145, 723–729. doi: 10.1001/jamaoto.2019.1191

Otero, J., García-Rodríguez, A., Cano-Sarabia, M., Maspoch, D., Marcos, R., Cortés, P., et al. (2019). Biodistribution of liposome-encapsulated bacteriophages and their transcytosis during oral phage therapy. *Front. Microbiol.* 10. doi: 10.3389/fmicb.2019.00689

Oyewole, O. A., Raji, R. O., and Yakubu, J. G. (2022). "The role of quorum sensing in microbial biofilm formation," in *Microbial biofilms: Applications and control* (CRC Press, Boca Raton), 47–63. doi: 10.1201/9781003184942-4

Papaianni, M., Cuomo, P., Fulgione, A., Albanese, D., Gallo, M., Paris, D., et al. (2020). Bacteriophages promote metabolic changes in bacteria biofilm. *Microorganisms* 8, 480. doi: 10.3390/microorganisms8040480

Pawde, D. M., Viswanadh, M. K., Mehata, A. K., Sonkar, R., Narendra,, Poddar, S., et al. (2020). Mannose receptor targeted bioadhesive chitosan nanoparticles of clofazimine for effective therapy of tuberculosis. *Saudi Pharm. J.* 28, 1616–1625. doi: 10.1016/j.jsps.2020.10.008

Penesyan, A., Paulsen, I. T., Kjelleberg, S., and Gillings, M. R. (2021). Three faces of biofilms: a microbial lifestyle, a nascent multicellular organism, and an incubator for diversity. *NPJ Biofilms Microbiomes* 7, 80. doi: 10.1038/s41522-021-00251-2

Petrovski, S., Seviour, R. J., and Tillett, D. (2011). Prevention of *Gordonia* and *Nocardia* stabilized foam formation by using bacteriophage GTE7. *Appl. Environ. Microbiol.* 77, 7864–7867. doi: 10.1128/AEM.05692-11

Pires, D. P., Costa, A. R., Pinto, G., Meneses, L., and Azeredo, J. (2020). Current challenges and future opportunities of phage therapy. *FEMS Microbiol. Rev.* 44, 684–700. doi: 10.1093/femsre/fuaa017

Pires, D. P., Oliveira, H., Melo, L. D. R., Sillankorva, S., and Azeredo, J. (2016). Bacteriophage-encoded depolymerases: their diversity and biotechnological applications. *Appl. Microbiol. Biotechnol.* 100, 2141–2151. doi: 10.1007/s00253-015-7247-0

Quan, K., Zhang, Z., Chen, H., Ren, X., Ren, Y., Peterson, B. W., et al. (2019). Artificial channels in an infectious biofilm created by magnetic nanoparticles enhanced bacterial killing by antibiotics. *Small* 15, e1902313. doi: 10.1002/smll.201902313

Racenis, K., Lacis, J., Rezevska, D., Mukane, L., Vilde, A., Putnins, I., et al. (2023). Successful bacteriophage-antibiotic combination therapy against multidrug-resistant *P. aeruginosa* left ventricular assist device driveline infection. *Viruses* 15, 1210. doi: 10.3390/v15051210

Ramzan, A., Rehman, T., But, M. S., Imran, M., and Qaisar, U. (2022). Biofilm formation and its regulation by extracellular appendages in *P. aeruginosa*. *World J. Biol. Biotechnol.* 7, 1. doi: 10.33865/wjb.007.03.0516

Ratnakar, I. S. (2022). Phage therapy: Challenges and opportunities. *Fine Focus* 8, 12–35. doi: 10.33043/FF.8.1.12-35

Rendueles, O., de Sousa, J. A. M., and Rocha, E. P. C. (2023). Competition between lysogenic and sensitive bacteria is determined by the fitness costs of the different emerging phage-resistance strategies. *eLife* 12, e83479. doi: 10.7554/eLife.83479

Richter, L. V., Franks, A. E., Weis, R. M., and Sandler, S. J. (2017). Significance of a posttranslational modification of the PilA protein of *geobacter sulfurreducens* for surface attachment, biofilm formation, and growth on insoluble extracellular electron acceptors. *J. Bacteriol.* 199, e00716-16. doi: 10.1128/JB.00716-16

Rohr, J. R., Barrett, C. B., Civitello, D. J., Craft, M. E., Delius, B., DeLeo, G. A., et al. (2019). Emerging human infectious diseases and the links to global food production. *Nat. Sustain.* 2, 445–456. doi: 10.1038/s41893-019-0293-3

Rolston, K. V. I. (2017). Infections in cancer patients with solid tumors: A Review. *Infect. Dis. Ther.* 6, 69–83. doi: 10.1007/s40121-017-0146-1

Römling, U., and Balsalobre, C. (2012). Biofilm infections, their resilience to therapy and innovative treatment strategies. *J. Intern. Med.* 272, 541–561. doi: 10.1111/joim.12004

Rumbaugh, K. P., and Sauer, K. (2020). Biofilm dispersion. *Nat. Rev. Microbiol.* 18, 571–586. doi: 10.1038/s41579-020-0385-0

Schoeffel, J., Wang, E. W., Gill, D., Frackler, J., Horne, B., Manson, T., et al. (2022). Successful use of salvage bacteriophage therapy for a recalcitrant MRSA knee and hip prosthetic joint infection. *Pharm. (Basel)* 15, 177. doi: 10.3390/ph15020177

Schooley, R. T., Biswas, B., Gill, J. J., Hernandez-Morales, A., Lancaster, J., Lessor, L., et al. (2017). Development and use of personalized bacteriophage-based therapeutic cocktails to treat a patient with a disseminated resistant *A. baumannii* infection. *Antimicrob. Agents Chemother.* 61. doi: 10.1128/AAC.00954-17

Schulze, A., Mitterer, F., Pombo, J. P., and Schild, S. (2021). Biofilms by bacterial human pathogens: Clinical relevance - development, composition and regulation - therapeutical strategies. *Microb. Cell* 8, 28–56. doi: 10.15698/mic2021.02.741

Secor, P. R., Burgener, E. B., Kinnersley, M., Jennings, L. K., Roman-Cruz, V., Popescu, M., et al. (2020). Pf bacteriophage and their impact on *Pseudomonas* virulence, mammalian immunity, and chronic infections. *Front. Immunol.* 11. doi: 10.3389/fimmu.2020.00244

Shafigh Kheljan, F., Sheikhzadeh Hesari, F., Aminifazl, M. S., Skurnik, M., Gholadze, S., and Zarrini, G. (2023). Design of phage-cocktail-containing hydrogel for the treatment of *P. aeruginosa*-infected wounds. *Viruses* 15, 803. doi: 10.3390/v15030803

Sharifi-Rad, J., Quispe, C., Butnariu, M., Rotariu, L. S., Sytar, O., Sestito, S., et al. (2021). Chitosan nanoparticles as a promising tool in nanomedicine with particular emphasis on oncological treatment. *Cancer Cell Int.* 21, 318. doi: 10.1186/s12935-021-02025-4

Sharma, D., Misba, L., and Khan, A. U. (2019). Antibiotics versus biofilm: An emerging battleground in microbial communities. *Antimicrob. Resist. Infect. Control* 8, 76. doi: 10.1186/s13756-019-0533-3

Shivaram, K. B., Bhatt, P., Applegate, B., and Simsek, H. (2023). Bacteriophage-based biocontrol technology to enhance the efficiency of wastewater treatment and reduce targeted bacterial biofilms. *Sci. Total Environ.* 862, 160723. doi: 10.1016/j.scitotenv.2022.160723

Sihorkar, V., and Vyas, S. P. (2001). Biofilm consortia on biomedical and biological surfaces: delivery and targeting strategies. *Pharm. Res.* 18, 1247–1254. doi: 10.1023/A:1013073508318

Sillankorva, S., Neubauer, P., and Azeredo, J. (2010). Phage control of dual species biofilms of *Pseudomonas fluorescens* and *Staphylococcus lentus*. *Biofouling* 26, 567–575. doi: 10.1080/08927014.2010.494251

Singh, A., Amod, A., Pandey, P., Bose, P., Pingali, M. S., Shivalkar, S., et al. (2022a). Bacterial biofilm infections, their resistance to antibiotics therapy and current treatment strategies. *Biomed. Mater.* 17, 022003. doi: 10.1088/1748-605X/ac50f6

Singh, A., Padmesh, S., Dwivedi, M., and Kostova, I. (2022b). How good are bacteriophages as an alternative therapy to mitigate biofilms of nosocomial infections. *Infect. Drug Resist.* 15, 503–532. doi: 10.2147/IDR.S348700

Singla, S., Harjai, K., Katare, O. P., and Chhibber, S. (2016). Encapsulation of bacteriophage in liposome accentuates its entry in to macrophage and shields it from neutralizing antibodies. *PloS One* 11, e0153777. doi: 10.1371/journal.pone.0153777

Srisangthong, I., Sangseedum, C., Chaichanit, N., Surachat, K., Suanyuk, N., and Mittraparp-Arthorn, P. (2023). Characterization and genome analysis of *Vibrio campbellii* lytic bacteriophage OPA17. *Microbiol. Spectr.* 11, e0162322. doi: 10.1128/spectrum.01623-22

Srivastava, A., Chandra, N., and Kumar, S. (2019). "The role of biofilms in medical devices and implants," in *Biofilms in human diseases: Treatment and control*. Eds. S. Kumar, N. Chandra, L. Singh, M. Z. Hashmi and A. Varma (Springer International Publishing, Cham), 151–165. doi: 10.1007/978-3-030-30757-8_11

Suh, G. A., Lodise, T. P., Tamma, P. D., Knisely, J. M., Alexander, J., Aslam, S., et al. (2022). Considerations for the use of phage therapy in clinical practice. *Antimicrob. Agents Chemother.* 66, e0207121. doi: 10.1128/aac.02071-21

Sun, R., Yu, P., Zuo, P., Villagrán, D., Mathieu, J., and Alvarez, P. J. J. (2022). Biofilm control in flow-through systems using polyvalent phages delivered by peptide-modified M13 coliphages with enhanced polysaccharide affinity. *Environ. Sci. Technol.* 56, 17177–17187. doi: 10.1021/acs.est.2c06561

Sutherland, I. W., Hughes, K. A., Skillman, L. C., and Tait, K. (2004). The interaction of phage and biofilms. *FEMS Microbiol. Lett.* 232, 1–6. doi: 10.1016/S0378-1097(04)00041-2

Talapko, J., and Škrlec, I. (2020). The principles, mechanisms, and benefits of unconventional agents in the treatment of biofilm infection. *Pharm. (Basel)* 13, 299. doi: 10.3390/ph13100299

Teklemariam, A. D., Al-Hindi, R. R., Qadri, I., Alharbi, M. G., Ramadan, W. S., Ayubu, J., et al. (2023). The battle between bacteria and bacteriophages: A conundrum to their immune system. *Antibiot. (Basel)* 12, 381. doi: 10.3390/antibiotics12020381

Tian, F., Li, J., Nazir, A., and Tong, Y. (2021). Bacteriophage - a promising alternative measure for bacterial biofilm control. *Infect. Drug Resist.* 14, 205–217. doi: 10.2147/IDR.S290093

Tinoco, J. M., Buttaro, B., Zhang, H., Liss, N., Sassone, L., and Stevens, R. (2016). Effect of a genetically engineered bacteriophage on *E. faecalis* biofilms. *Arch. Oral. Biol.* 71, 80–86. doi: 10.1016/j.archoralbio.2016.07.001

Tkhilaishvili, T., Lombardi, L., Klatt, A.-B., Trampuz, A., and Di Luca, M. (2018). Bacteriophage Sb-1 enhances antibiotic activity against biofilm, degrades exopolysaccharide matrix and targets persisters of *S. aureus*. *Int. J. Antimicrob. Agents* 52, 842–853. doi: 10.1016/j.ijantimicag.2018.09.006

Tkhilaishvili, T., Merabishvili, M., Pirnay, J.-P., Starck, C., Potapov, E., Falk, V., et al. (2021). Successful case of adjunctive intravenous bacteriophage therapy to treat left ventricular assist device infection. *J. Infect.* 83, e1–e3. doi: 10.1016/j.jinf.2021.05.027

Topka-Bielecka, G., Dydecka, A., Necel, A., Bloch, S., Nejman-Faleńczyk, B., Węgrzyn, G., et al. (2021). Bacteriophage-derived depolymerases against bacterial biofilm. *Antibiot. (Basel)* 10, 175. doi: 10.3390/antibiotics10020175

Uchiyama, J., Takemura-Uchiyama, I., Kato, S.-I., Sato, M., Ujihara, T., Matsui, H., et al. (2014). *In silico* analysis of AHJD-like viruses, *S. aureus* phages S24-1 and S13', and study of phage S24-1 adsorption. *Microbiologyopen* 3, 257–270. doi: 10.1002/mbo3.166

Usui, M., Yoshii, Y., Thiriet-Rupert, S., Ghigo, J.-M., and Beloin, C. (2023). Intermittent antibiotic treatment of bacterial biofilms favors the rapid evolution of resistance. *Commun. Biol.* 6, 275. doi: 10.1038/s42003-023-04601-y

Van Nieuwenhuyse, B., Galant, C., Brichard, B., Docquier, P.-L., Djebara, S., Pirnay, J.-P., et al. (2021). A case of in *situ* phage therapy against *S. aureus* in a bone allograft polymicrobial biofilm infection: Outcomes and phage-antibiotic interactions. *Viruses* 13, 1898. doi: 10.3390/v13101898

Vera-González, N., and Shukla, A. (2020). Advances in biomaterials for the prevention and disruption of candida biofilms. *Front. Microbiol.* 11. doi: 10.3389/fmicb.2020.538602

Vikram, A., Woolston, J., and Sulakvelidze, A. (2021). Phage biocontrol applications in food production and processing. *Curr. Issues Mol. Biol.* 40, 267–302. doi: 10.21775/cimb.040.267

Wang, I. N., Smith, D. L., and Young, R. (2000). Holins: The protein clocks of bacteriophage infections. *Annu. Rev. Microbiol.* 54, 799–825. doi: 10.1146/annurev.micro.54.1.799

Wang, J., Zhao, S., Chen, J., Liu, X., Chen, H., Lu, T., et al. (2023). Phage-Ce6-manganese dioxide nanocomposite-mediated photodynamic, photothermal, and chemodynamic therapies to eliminate biofilms and improve wound healing. *ACS Appl. Mater. Interfaces* 15, 21904–21916. doi: 10.1021/acsami.3c01762

Waturangi, D. E., Kasriady, C. P., Guntama, G., Sahulata, A. M., Lestari, D., and Magdalena, S. (2021). Application of bacteriophage as food preservative to control enteropathogenic *E. coli* (EPEC). *BMC Res. Notes* 14, 336. doi: 10.1186/s13104-021-05756-9

Weinbauer, M. G., Brettar, I., and Höfle, M. G. (2003). Lysogeny and virus-induced mortality of bacterioplankton in surface, deep, and anoxic marine waters. *Limnol. Oceanogr.* 48, 1457–1465. doi: 10.4319/lo.2003.48.4.1457

Werneburg, G. T., Nguyen, A., Henderson, N., Sueur, A. L., Corcoran, A., Katz, A., et al. (2019). Progression and formation of bacterial biofilms on indwelling urinary catheters over time. *J. Urol.* 201, e1136. doi: 10.1097/01.JU.0000557322.77175.6f

Williams, J., Kerven, J., Chen, Y., and Sagona, A. P. (2023). Genetic engineering of bacteriophage K1F with human epidermal growth factor to enhance killing of intracellular *E. coli* K1. *ACS Synth. Biol.* 12, 2094–2106. doi: 10.1021/acssynbio.3c00135

Wroe, J. A., Johnson, C. T., and García, A. J. (2020). Bacteriophage delivering hydrogels reduce biofilm formation in *vitro* and infection in *vivo*. *J. Biomed. Mater. Res. A* 108, 39–49. doi: 10.1002/jbm.a.36790

Wu, B., Wang, R., and Fane, A. G. (2017). The roles of bacteriophages in membrane-based water and wastewater treatment processes: A review. *Water Res.* 110, 120–132. doi: 10.1016/j.watres.2016.12.004

Xiu, W., Wan, L., Yang, K., Li, X., Yuwen, L., Dong, H., et al. (2022). Potentiating hypoxic microenvironment for antibiotic activation by photodynamic therapy to combat bacterial biofilm infections. *Nat. Commun.* 13, 3875. doi: 10.1038/s41467-022-31479-x

Yan, J., Mao, J., and Xie, J. (2014). Bacteriophage polysaccharide depolymerases and biomedical applications. *BioDrugs* 28, 265–274. doi: 10.1007/s40259-013-0081-y

Yan, W., Banerjee, P., Xu, M., Mukhopadhyay, S., Ip, M., Carrigy, N. B., et al. (2021). Formulation strategies for bacteriophages to target intracellular bacterial pathogens. *Adv. Drug Deliv. Rev.* 176, 113864. doi: 10.1016/j.addr.2021.113864

Yang, L., Liu, Y., Wu, H., Song, Z., Høiby, N., Molin, S., et al. (2012). Combating biofilms. *FEMS Immunol. Med. Microbiol.* 65, 146–157. doi: 10.1111/j.1574-695X.2011.00858.x

Yasir, M., Willcox, M. D. P., and Dutta, D. (2018). Action of antimicrobial peptides against bacterial biofilms. *Mater. (Basel)* 11, 2468. doi: 10.3390/ma11122468

Yin, W., Wang, Y., Liu, L., and He, J. (2019). Biofilms: The microbial "protective clothing" in extreme environments. *Int. J. Mol. Sci.* 20, 3423. doi: 10.3390/ijms20143423

Yue, H., Li, Y., Yang, M., and Mao, C. (2022). T7 phage as an emerging nanobiomaterial with genetically tunable target specificity. *Adv. Sci. (Weinh)* 9, e2103645. doi: 10.1002/advs.202103645

Zaczek-Moczydłowska, M. A., Young, G. K., Trudgett, J., Plahe, C., Fleming, C. C., Campbell, K., et al. (2020). Phage cocktail containing podoviridae and myoviridae bacteriophages inhibits the growth of *Pectobacterium* spp. under in *vitro* and in *vivo* conditions. *PloS One* 15, e0230842. doi: 10.1371/journal.pone.0230842

Zhang, L. (2018). "The use of biological agents in processing: Antimicrobials, fermentation, and antagonistic control," in *Packaging for nonthermal processing of food*. Eds. M. A. Pascall and J. H. Han (John Wiley & Sons, Ltd, Chichester, UK), 83–94. doi: 10.1002/9781119126881.ch5

Zhang, Y., Gao, J., Wang, L., Liu, S., Bai, Z., Zhuang, X., et al. (2018). Environmental adaptability and quorum sensing: Iron uptake regulation during biofilm formation by *Paracoccus denitrificans*. *Appl. Environ. Microbiol.* 84, e00865-18. doi: 10.1128/AEM.00865-18

Zhang, Y., and Hu, Z. (2013). Combined treatment of *P. aeruginosa* biofilms with bacteriophages and chlorine. *Biotechnol. Bioeng.* 110, 286–295. doi: 10.1002/bit.24630

Zhao, M., Tan, X., Liu, Z.-Q., Dou, L., Liu, D., Pan, Y.-J., et al. (2023). Engineered phage with cell-penetrating peptides for intracellular bacterial infections. *mSystems* 8, e0064623. doi: 10.1128/msystems.00646-23

Zurabov, F., Glazunov, E., Kochetova, T., Uskevich, V., and Popova, V. (2023). Bacteriophages with depolymerase activity in the control of antibiotic resistant *K. pneumoniae* biofilms. *Sci. Rep.* 13, 15188. doi: 10.1038/s41598-023-42505-3

frontiers | Frontiers in Cellular and Infection Microbiology

TYPE Original Research
PUBLISHED 14 October 2024
DOI 10.3389/fcimb.2024.1456700

OPEN ACCESS

EDITED BY
Maria Gabriela Paraje,
National University of Cordoba, Argentina

REVIEWED BY
Luisa Jordao,
National Health Institute Doutor Ricardo Jorge (INSA), Portugal
Mauro Nicolas Gallucci,
National Scientific and Technical Research Council (CONICET), Argentina
Graciela Pucci,
National University of Patagonia San Juan Bosco, Argentina

*CORRESPONDENCE
Khristina G. Judan Cruz
kjcruz@clsu.edu.ph
Kozo Watanabe
watanabe.kozo.mj@ehime-u.ac.jp

RECEIVED 29 June 2024
ACCEPTED 18 September 2024
PUBLISHED 14 October 2024

CITATION
Judan Cruz KG, Takumi O, Bongulto KA, Gandalera EE, Kagia N and Watanabe K (2024) Natural compound-induced downregulation of antimicrobial resistance and biofilm-linked genes in wastewater *Aeromonas* species. *Front. Cell. Infect. Microbiol.* 14:1456700. doi: 10.3389/fcimb.2024.1456700

Natural compound-induced downregulation of antimicrobial resistance and biofilm-linked genes in wastewater *Aeromonas* species

Khristina G. Judan Cruz[1,2]*, Okamoto Takumi[1], Kenneth A. Bongulto[1], Emmanuel E. Gandalera[1,2], Ngure Kagia[1] and Kozo Watanabe[1]*

[1]Center for Marine Environmental Studies (CMES), Ehime University, Matsuyama, Ehime, Japan, [2]Department of Biological Sciences, College of Science, Central Luzon State University, Science City of Muñoz, Nueva Ecija, Philippines

Addressing the global antimicrobial resistance (AMR) crisis requires a multifaceted innovative approach to mitigate impacts on public health, healthcare and economic systems. In the complex evolution of AMR, biofilms and the acquisition of antimicrobial resistance genes (ARGs) play a pivotal role. *Aeromonas* is a major AMR player that often forms biofilm, harbors ARGs and is frequently detected in wastewater. Existing wastewater treatment plants (WWTPs) do not have the capacity to totally eliminate antimicrobial-resistant bacteria favoring the evolution of ARGs in wastewater. Besides facilitating the emergence of AMR, biofilms contribute significantly to biofouling process within the activated sludge of WWTP bioreactors. This paper presents the inhibition of biofilm formation, the expression of biofilm-linked genes and ARGs by phytochemicals andrographolide, docosanol, lanosterol, quercetin, rutin and thymohydroquinone. *Aeromonas* species were isolated and purified from activated sludge samples. The ARGs were detected in the isolated *Aeromonas* species through PCR. *Aeromonas* biofilms were quantified following the application of biocompounds through the microtiter plate assay. qPCR analyses of related genes were done for confirmation. Findings showed that the natural compounds inhibited the formation of biofilms and reduced the expression of genes linked to biofilm production as well as ARGs in wastewater *Aeromonas*. This indicates the efficacy of these compounds in targeting and controlling both ARGs and biofilm formation, highlighting their potential as innovative solutions for combating antimicrobial resistance and biofouling.

KEYWORDS

ARGS, antimicrobial resistance, biofilm, natural compounds, *Aeromonas*, wastewater

1 Introduction

Wastewater treatment plants (WWTPs) and wastewater are critical transition points for the emergence of antimicrobial-resistant bacteria (ARB) and antimicrobial resistance genes (ARG) (Skwor et al., 2020) following the release of residual antibiotics not fully metabolized after therapeutic use. Since existing WWTPs do not have the capacity to totally eliminate pollutants specifically ARB (Shrout and Nerenberg, 2012; Uluseker et al., 2021; Perveen et al., 2023), this creates a favorable environment for the expansion of antimicrobial resistance. Among the diverse bacterial species found in wastewater, *Aeromonas* species are known to harbor a wide range of ARGs and virulence factors, making them ideal model organisms for monitoring AMR and studying the mechanisms of resistance development (Usui et al., 2016; Skwor et al., 2020). *Aeromonas* genomes harboring ARGs have increased considerably (Roh and Kannimuthu, 2023) and highlights their potential as a global public health risk (Piotrowska et al., 2017; Skwor et al., 2020).

Aside from facilitating the acquisition and exchange of ARGs, *Aeromonas* is also known for forming biofilms in water systems (Talagrand-Reboul et al., 2017). Biofilm architecture ensures stability and barrier (Hall-Stoodley et al., 2004; Rather et al., 2021) and makes biofilms particularly resistant to antibiotics. Studies have shown a substantial increase in antibiotic resistance in biofilm-associated bacteria compared to their planktonic forms, as well as a high frequency of ARGs (Chen et al., 2020; Michaelis and Grohmann, 2023). *Aeromonas*, akin to other bacteria, can induce biofouling in WWTP activated sludge bioreactors by forming biofilms on surfaces, filters, pumps, and membranes (Taiswa et al., 2024). This compromises the flow of water through the system, leading to decreased pressure and increased energy consumption, resulting in reduced efficiency of filters, membranes and flux rate and surge in maintenance costs.

ARGs and biofilm play a key part in the emergence of antimicrobial resistance and has been linked to most persistent infections. Strategies and emerging therapeutic options for antipathogenesis in MDR bacteria are limited, leading to higher risks of AMR development, increased morbidity and mortality rates and consequently, significant economic burdens. As antibiotics become less effective while more multi-drug resistant (MDR) pathogens emerge and spread globally, research efforts and new antimicrobials are urgently needed to produce novel, effective strategies not only for the public health but also to mitigate effects on significant economic losses (WHO, 2023). Targeting two mechanisms at the same time, such as ARGs and biofilm is a practical alternative to antibiotics use and display high potential in efficiently managing bacterial pathogenicity and antimicrobial resistance.

Natural products are now being extensively explored for their ability to interfere with ARGs and biofilm formation in bacteria. Plants have evolved intricate defense mechanisms, including the production of a wide array of secondary metabolites, many of which exhibit antimicrobial properties and play an integral part in the plant's immune system (Algburi et al., 2017). The exploration of natural products for their potential to interfere with ARGs and biofilms is an emerging area of antimicrobial research. Several natural products have been shown to modulate or inhibit biofilm formation and downregulate ARG and biofilm-linked genes. The enormous diversity of natural products provides a vast reservoir of antimicrobial compounds that may contribute to the development of novel antimicrobial drugs to combat resistance mechanisms in bacteria.

The role in pathogenesis and increasing incidences of persistent infections influenced by ARGs and biofilm formation makes these important targets in the development of antimicrobials for *Aeromonas* sp. while avoiding the development of AMR driven by antibiotic over-use and mis-use. The capacity of natural compounds to influence biofilm formation and the expression of biofilm-linked genes and ARGs offers a plausible approach to addressing AMR in *Aeromonas*. Hence, this paper explores the action of six plant-derived compounds to inhibit the formation of biofilm and downregulate the expression of biofilm-linked genes and ARGs in 6 wastewater *Aeromonas* species.

2 Materials and methods

2.1 Isolation and purification of bacteria

Aeromonas species were isolated from wastewater activated sludge collected from bioreactors in 2 wastewater treatment facilities in Japan. A total of 3 liters of water were collected. The water samples were immediately filtered using a 50 µm mesh, stored in ice and processed within 3 hours. Appropriately diluted samples were plated onto Mueller-Hinton Agar plates and incubated at 37°C for 24 h. Colonies were picked on the plates and inoculated to 20 ml Luria-Bertani (LB) Broth and incubated for 24 h at 37 ^{0}C. Pure bacterial cultures were obtained after successive subculture of colonies in LB plates.

2.2 Identification of bacteria

Sixty isolates were subjected to DNA extraction and 16srRNA PCR amplification to identify the bacterial species present in the collected wastewater activated sludge. Genomic DNA was extracted using the DNeasy kit (Qiagen) following the manufacturer's protocol. In 2ml tubes, 1.75 ml of bacterial culture was centrifuged at 20,000 x g for 5 minutes. The resulting supernatant was decanted. 180 µl of lysis buffer was added to the tube, vortexed and incubated at 37°C for 30 minutes. 25 µl of proteinase K and 200 ul of Buffer AL were added to the tube, vortexed and incubated at 56°C for 30 minutes. 200 µl 95% ethanol was added to the sample and vortexed. This was transferred to the DNeasy spin column placed in a 2 ml collection tube centrifuged at ≥6000 x g (8000 rpm) for 1 minute. The flow-through and collection tube was discarded. The spin column was placed in a new 2 ml collection tube. 500 µl Buffer AW1 was added and centrifuged for 1 min at ≥6000 x g. The flow-through and collection tube was discarded. The spin column was placed in a new 2 ml collection tube. 500 µl Buffer AW2 was added and centrifuged for 3 min at 20,000 x g (14,000 rpm). The flow-through and collection tube was discarded. The spin column was transferred to a new 1.5 ml or 2 ml microcentrifuge tube. To elute the DNA, 100 µl Buffer AE was

added to the center of the spin column membrane, incubated for 1 min at room temperature (15–25°C) and centrifuge for 1 min at ≥6000 x g. The DNA was stored at -20°C until use. 16S PCR amplification was performed to accurately identify the bacteria. PCR amplification was done in a mix containing molecular-grade water, 10X Taq buffer, DMSO, $MgCl_2$, dNTPs, primers, Taq polymerase and DNA samples. Primers used are the following: 16S 341F 5'-CCTACGGGAGGCAGCAG-3' and 16S 907R 5'-CCGTCAATTCMTTTRAGTTT-3' (Lane, 1991). PCR conditions include initial denaturation at 94 °C for 3 minutes followed by 30 cycles of 94 °C, 52 °C and 72 °C; and a final extension of 72°C for 5 minutes. The PCR products were visualized using 1.5% agarose gel and sequenced. Sequences were run in NCBI BLAST for the identification of *Aeromonas* species.

2.3 Detection of ARGs

For the detection of ARGs, PCR amplification was done using specific primers (Table 1). Primers generated in this study were designed using the Primer3 program (Untergasser et al., 2012). The reaction mix included molecular-grade water, 10X Taq buffer, DMSO, $MgCl_2$, dNTPs, primers, Taq polymerase and DNA. PCR conditions include initial denaturation at 94 °C for 5 minutes followed by 30 cycles of denaturation 94°C, annealing temperature range of 50 °C – 60 °C and extension of 72 °C; and a final extension of 72 °C for 5 minutes. The PCR products were visualized using 1.5% agarose gel and sequenced. Known DNA samples positive for the ARGs were ran alongside the samples of this study on agarose gel electrophoresis. The ARG sequences were checked on ResFinder 4.5.0 - Center for Genomic Epidemiology (CGE) (Clausen et al., 2018; Bortolaia et al., 2020). The selection of the primer pairs facilitated the identification of prevalent and clinically significant ARGs, allowing an initial assessment of compound effects.

TABLE 1 Gene primer sequences and references used for the detection of ARGs.

ARGs	Primer sequences	References
TetS F	GAAAGCTTACTATACAGTAGC	Aminov et al., 2001
TetS R	AGGAGTATCTACAATATTTAC	
FloR817 F	AGGTGATTTTTGGTCCGCTCT	This study
FloR817 R	ATGTCGTCGAACTCTGCCAAA	
aadA2:510 F	TTGTTGGTTACTGTGGCCGT	This study
aadA2:510 R	CTGGGCAGGTAGGCGTTTTA	
TetM F	GTTAAATAGTGTTCTTGGAG	Aarestrup et al., 2000
TetM R	CTAAGATATGGCTCTAACAA	
TetE F	TCGGGATTGTTAGTTGTCTTTTTC	Fan et al., 2007
TetE R	GTGGATTACCCTACCTGGATGGA	
TetA F	GCTACATCCTGCTTGCCTTC	Dahshan et al., 2010
TetA R	CATAGATCGCCGTGAAGAGG	
Sul1F	CTGAACGATATCCAAGGATTYCC	Heuer and Smalla, 2007
Sul1R	AAAAATCCCATCCCCGGRTC	
Sul2 F	CTCAATGATATTCGCGGTTTYCC	
Sul2 R	AAAAACCCCATGCCGGGRTC	
StrB F	ATCGTCAAGGGATTGAAACC	Rosengren et al., 2009
StrB R	GGATCGTAGAACATATTGGC	
StrA F	CTTGGTGATAACGGCAATTC	
StrA R	CCAATCGCAGATAGAAGGC	

2.4 Biocompounds for bioassays

Biocompounds andrographolide (ANDR), rutin (RUT), quercetin (QUE), docosanol (DOC), lanosterol (LAN), and thymohydroquinone (THQ) were obtained from Sigma-Aldrich (St. Louis, MO, United States) and were prepared as corresponding stock solutions following product information: ANDR - 3mg/ml in DMSO; RUT 2.5 mg/ml using DMSO; QUE-0.5 mg/ml in DMSO; DOC - 1mg/ml in ethanol; LAN - 1mg/ml in DMSO; THQ - 1mg/ml in DMSO. All stock solutions were stored at -20°C upon preparation and used immediately to ensure freshness and stability.

2.5 Antibacterial assay and determination of minimum inhibitory concentration

Disc diffusion method for antimicrobial susceptibility testing was carried out to assess the presence of antibacterial activities of biocompounds (Rezaei et al., 2011). The 24-hour culture of *Aeromonas* spp. in nutrient broth was adjusted to 0.5 McFarland standard. Sterile swabs were immersed into the bacterial culture and were aseptically swabbed onto the surface of bacterial medium plates evenly. Twenty µl of each treatment, positive control Enrofloxacin and distilled water for negative control, were pipetted on sterile petri plates containing sterile paper discs which were dipped for 30 minutes. The discs were placed equidistantly on the surface of the agar medium specific for each pathogen using sterile forceps. Treatments were done in triplicates and incubated at 37°C for 24 hours. The zone of inhibition was observed after 12 and 24 hours of incubation. Positive result in the antibacterial assay established the command to proceed on the determination of Minimum Inhibitory Concentration (MIC) determination. The determination of Minimal Inhibitory Concentrations (MICs in mg/ml) of the treatments were determined by performing an adaptation of the method according to Clinical and Laboratory Standards Institute (2015) and with an inoculum of 1×10^5 Colony-Forming Unit/ml. Two-fold dilution method using Nutrient Broth was used to prepare a series of concentrations for the assay. The assay was carried out in a 96-well polystyrene microtiter plate, with 10 wells for each concentration. MIC is defined as the minimum concentration of the biocompounds which inhibit the visible growth of the *Aeromonas* sp. The lowest concentration that

reduced the rezasurin dye was considered the MIC. In the case of THQ with observed antibacterial activity, the sub-MIC was through rezasurin-based assay in microtiter plates with two-fold dilution consisting of 8 concentrations – 1 mg/ml, 0.5 mg/ml, 0.25 mg/ml, 0.125 mg/ml, 0.0625 mg/ml, 0.03125 mg/ml, 0.0156 mg/ml and 0.0078 mg/ml (Gajic et al., 2022).

2.6 Microtiter plate biofilm formation assay

180 µl of overnight cultures of *Aeromonas* sp. were added to 20 µl biocompounds in each well and incubated at 30°C for 40 h. Untreated bacterial cultures served as negative control. A biological blank (PBS) was also prepared. The setup was run twice, with each run consisting of 6 replicates. After incubation, microtiter plates were rinsed with sterile distilled water five (5) times to remove planktonic cells, air-dried for 45 min, and stained with 150 µl of 1% crystal violet solution. Plates were rinsed five (5) times to remove excess stain. Quantification of biofilm production was done by adding 200 µl of 95% ethanol to destain the wells. Then, 100 µl from each well was transferred to a new microtiter plate and the optical density (OD) values were measured at 595 nm (MultiSkan FC, Thermo Scientific) (Fernando and Judan Cruz, 2020).

2.7 Expression analysis of ARGs and biofilm-linked genes

The total RNA of the bacteria were extracted using the RNeasy Minikit protocol (Qiagen, GmbH, Germany). For each sample, 25-50 mg acid-washed glass beads (150-600 µm diameter) were weighed in 2 ml safe-lock tubes. Bacteria were collected by centrifugation at 5000 x g for five minutes at 4°C. The supernatant was decanted and aspirated to ensure the removal of the remaining media. Buffer RLT was added (350 µl for $<5 \times 10^8$ and 700 µl for $5 \times 10^8 - 1 \times 10^9$ number of bacteria). The suspension was transferred into the 2ml safe-lock tube containing the acid-washed beads. Cells were disrupted in the Tissue Lyser for five minutes at maximum speed. The suspension was centrifuged for 10 seconds at maximum speed. The supernatant was transferred into a new tube and the volume of the sample was determined. An equal volume of 70% ethanol was added and mixed by pipetting. Up to 700 µl lysate was transferred to a spin column placed in a 2 ml collection tube and centrifuged for 15 seconds at ≥8000 x g. The flow-through tube was discarded. 700 µl Buffer RW1 was added to the spin column. With the lid closed gently, the spin column was centrifuged for 15 seconds at ≥8000 x g to wash the spin column membrane. The spin-column was placed in a new 2 ml collection tube with the flow-through. Lids were closed gently and centrifuged at full speed for one minute. The spin-column was placed in a new 1.5 ml collection tube. 30-50 µl RNase-free water was added directly to the spin column membrane and was centrifuged for one minute at ≥8000 x g to elute the RNA (Qiagen, 2023).

The expression analysis of ARGs and biofilm-linked genes was done using qRT-PCR with specific primers (Tables 1, 2) using Promega GoTaq ® 1-step RT-qPCR kit following the recommended proportions. A 10 µl reaction mix was prepared for each of the samples. qRT-PCR conditions included the following: 1 cycle at 42°C for 5 min and 95°C for 2 min for initial denaturation, followed by 45 cycles at 95°C for 20 s for denaturation, 55°C for 20 s for annealing, and 72°C for 20 s for the extension. For the ARGs expression, annealing temperature ranged from 55°C to 60°C. The relative expression of genes was analyzed using the LIVAK method of $2^{-\Delta\Delta Ct}$ (Livak and Schmittgen, 2001).

2.8 Statistical analysis

To determine statistical differences in biofilm formation, quantification through OD values were analyzed through an independent sample non-parametric Mann-Whitney U test with 0.05 level of significance using SPSS 13.0 program. The statistical analyses for the gene regulation were done using the Kruskal-Wallis test (non-parametric ANOVA) where means between the control and experimental setup were compared and the significance were determined if the F-values were greater than the F-crit at 0.05 level of significance. For the analysis of the relative mRNA expression in qPCR, the LIVAK method (2−ΔΔCt) was used. The correlation analyses between biofilm formation and biofilm-linked genes, biofilm formation and ARGs as well as biofilm-linked genes and ARGS were done through Spearman correlation coefficient using the function pairs.*panel* in *psychs* package in R v. 4.3.1 following the standard procedure for non-parametric correlation analysis.

3 Results

3.1 16S rRNA Identification of *Aeromonas* wastewater bacteria

Comparison of 16S rRNA sequences of 60 wastewater bacterial isolates with the NCBI database (BLAST) confirmed the presence of known bacterial pathogens, from which five (5) species of *Aeromonas* were selected for further experiments on the detection and inhibition of ARGs and biofilm formation. These are *Aeromonas veronii, Aeromonas jandaei, Aeromonas hydrophila, Aeromonas dhakensis* and *Aeromonas caviae*.

3.2 Detection of ARGs

Major ARGs coding resistance to streptomycin, tetracyclines, sulfonamide and aminoglycosides were evaluated for their occurrence in the identified wastewater *Aeromonas* species. To identify and analyze the presence of ARGs within the *Aeromonas* spp., sequences were checked on ResFinder 4.5.0 - Center for Genomic Epidemiology (CGE) (Clausen et al., 2018; Bortolaia et al., 2020). Eleven ARGs were evaluated for their presence: *StrA, StrB, TetS, TetM, TetE, TetA, FloR, Sul1, Sul2, aadA1* and *aadA2*. The results obtained from ResFinder revealed the presence of three ARGs in two *Aeromonas* spp: *A. caviae* carries three ARGs namely *aadA1*, *aadA2* and *sul1; sul1* was also detected in *A. jandaei.*

TABLE 2 Primers used in qRT-PCR analysis of biofilm-linked genes.

Primer	Primer sequence (5′-3′)	References
ahyR -F	TTTACGGGTGACCTGATTGAG	Patel et al., 2017
ahyR -R	CCTGGATGTCCAACTACATCTT	
ahyI -F	GTCAGCTCCCACACGTCGTT	Dong et al., 2020
ahyI -R	GGGATGTGGAATCCCACCGT	
litR -F	CATCGAGGTGTTCTCCCGTC	Sun et al., 2021
litR -R	TCATCCACCAGCTCTTCACG	
casgAB -F	TTGTTTCTGGTGGATCTGGATTA	
casgAB -R	GGCATTGAGCAGCACGGTA	
fleQ -F	ACTTCCCACAGCAACTTCA	
fleQ -R	CCTTGTCGTGGGTCTGTTGA	
16S F	GCACAAGCGGTGGAGCATGTGG	
16S R	CGTGTGTAGCCCTGGTCGTA	

3.3 Biocompounds inhibit the expression of *Aeromonas* ARGs

The changes in gene expression levels were visualized using a heatmap to present effect of the biocompounds on the expression of ARGs (Figure 1; Supplementary Table 1). The numbers on the right side of the heat map indicate the standardized relative quantification values. The cluster delineating between the effect of the biocompounds versus the untreated sample is clear and distinct. The decrease in *aadA1*, *aadA2* and *sul1*expression was statistically significant ($p < 0.05$) indicating a downregulating effect of the biocompounds. While RUT's effects on ARG expression varied slightly from the other biocompounds, still, showed substantial downregulation as compared to the untreated (UN) ($p < 0.05$).

3.4 Antibacterial activity of biocompounds against the *Aeromonas* spp.

Before conducting evaluations on biofilm activity, an antibacterial screening was performed to ensure that any observed reduction in the production of biofilm was not due to antibacterial properties. For biocompounds with confirmed antibacterial activity as noted by a zone of inhibition, the sub MIC was determined through a rezasurin-based assay. The biocompounds ANDR, RUT, QUE, DOC and LAN did not show any antibacterial activity in the disk diffusion assay across all tested *Aeromonas* spp, hence, their original concentrations were retained for further assessments. THQ demonstrated antibacterial activity against all Aeromonas spp. except *A. veronii*, hence, the rezasurin-based assay was performed to determine the sub-MIC that resulted to 0.5 mg/ml. This sub-MIC was then used for both assays on ARGs and biofilm since the objective was to see the effects on both mechanisms using the same concentration.

3.5 Biofilm formation inhibitory effect of the biocompounds against *Aeromonas* spp.

The biofilm formation activity in *Aeromonas* spp as affected by the biocompounds was lower than the control (UN) (Figure 2). The values presented are OD values for each treatment. In *A. caviae* strong inhibition by ANDR (0.127), RUT (0.129), DOC (0.174), LAN (0.156) and THQ (0.118) were noted compared to (UN) (0.327) ($p < 0.01$). *A. caviae* treated with QUE was not significantly different but showed lower OD values at 0.207 compared to UN ($p > 0.05$). The OD values in *A. dhakensis* also significantly decreased ($p < 0.01$) when treated with AND (0.059), RUT (0.056), QUE (0.65) and LAN (0.178). DOC (0.246) and THQ (0.133) showed lower OD values but was not significantly different from the UN (control) (0.306) ($p > 0.05$). The same significant observations were seen in *A. hydrophila* when exposed to ANDR (0.055), RUT (0.057), QUE (0.092) and DOC (0.086) ($p < 0.01$). Although LAN (0.240) and THQ (0.193) showed decrease in biofilm formation, it showed no significant difference with UN (0.33) ($p > 0.05$); in *A. jandaei*, all compounds except QUE (0.175) have strong anti-biofilm activity versus UN (0.298) ($p < 0.01$) as ANDR (0.069), RUT (0.068), docosanol (0.093), lanosterol (0.123) and THQ (0.092; and in *A. veronii*, ANDR (0.046), rutin (0.052), quercetin (0.088), docosanol (0.165) substantially suppressed biofilm formation ($p < 0.01$); OD values of LAN (0.222) and THQ (0.181) was observed lower but not significant compared to UN (0.323) ($p > 0.05$). The mean OD values in *Aeromonas* spp. treated with the biocompounds showed significant decrease in biofilm formation indicates efficiency in controlling the growth of biofilm. Overall, all biocompounds showed inhibition in biofilm formation against the wastewater *Aeromonas* spp.

3.6 Biocompounds inhibit the expression of *Aeromonas* biofilm-linked genes

The changes in gene expression levels were visualized in a heatmap, indicating the relative expression levels of key biofilm-linked genes across different samples. The heatmap of relative gene expression of biofilm-linked genes as affected by the compounds clearly shows defined clustering (Figure 3; Supplementary Table 2). The biocompounds ANDR, QUE, RUT, DOC, LAN and THQ clustered in one group showing similar downregulation of all genes compared to the untreated culture (UN) which suggests significant effects ($p < 0.05$) of these compounds against the expression of the genes. This can be noted in *A. dhakensis* and *A. jandaei* ($p < 0.05$). Different effects were observed in *A. caviae*, *A. hydrophila*, and *A. veronii*. For instance, fleQ as affected by RUT (*A. caviae*), *AhyI, AhyR, fleQ*, and *casgAB* in ANDR (*A. hydrophila* and *A. veronii*), DOC (*A. hydrophila*), RUT (*A. veronii*) showed higher expression of genes than other compounds, nevertheless, still showed significant downregulation when compared to treatments without the compounds ($p < 0.05$).

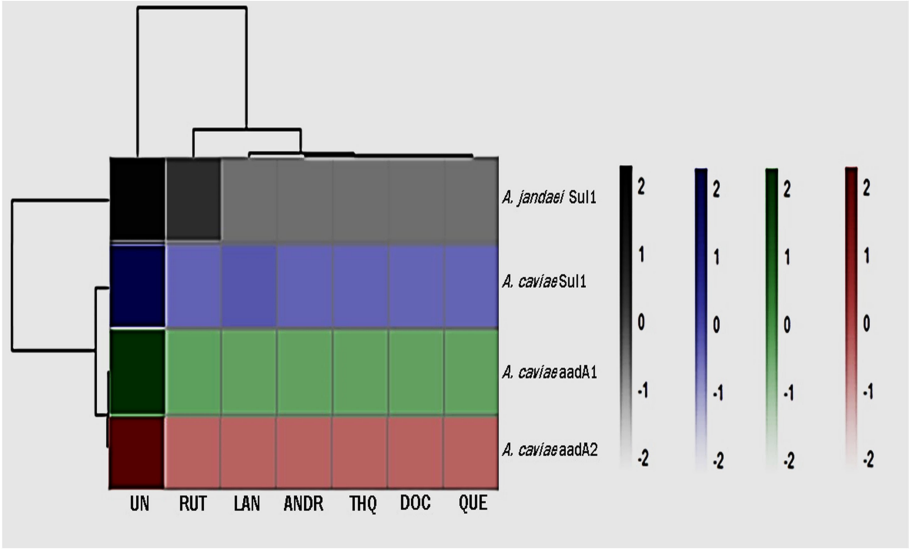

FIGURE 1
Heatmap of gene expression of ARGs as affected by the treatments. UN (untreated); RUT (rutin); LAN (lanosterol); QUE (quercetin); ANDR (andrographolide); DOC (docosanol); THQ.

3.7 Correlation analysis

The Spearman's rank correlation coefficient (R) and its significance level (p-value) were calculated to analyze the relationship between the expression levels of genes and biofilm formation (Figure 4). In *A. caviae*, a strong significant positive correlation between biofilm-linked gene expression and biofilm formation was noted: *AhyR* (R = 0.89; $p < 0.01$), *AhyI* (R = 0.76; $p < 0.05$) and *casgAB* (R = 0.89; $p < 0.01$). This was also observed between biofilm formation and expression of ARGs *aadA1* (R = 0.87; $p < 0.05$) and *aadA2* (R = 0.87; $p < 0.05$). A strong positive correlation was also noted between the *aadA1* and biofilm-linked genes *AhyR* (R = 0.91; $p < 0.01$), *casgAB* (R = 0.97; $p < 0.001$) and *fleQ* (R = 0.78; $p < 0.05$), as well as in *aadA2*: *AhyR* (R = 0.88; $p < 0.01$), *casgAB* (R = 0.98; $p < 0.001$) and *fleQ* (R = 0.84; $p < 0.05$. A strong significant positive correlation between biofilm-linked gene expression and biofilm formation was also seen in *A. jandaei*: *AhyI* (R = 0.77; $p < 0.05$), *casgAB* (R = 0.84; $p < 0.05$), *fleQ* (R = 0.79; $p < 0.05$). sul1 expression registered high significant correlation values between all biofilm-linked genes *AhyR* (R = 0.79; $p < 0.01$), *AhyI* (R = 0.95; $p < 0.01$), *casgAB* (R = 0.91; $p < 0.01$) and *fleQ* (R = 0.94; $p < 0.01$). The R value between biofilm formation and sul1 expression (0.73) was not significant, nevertheless, still showed a strong correlation. No ARGs were detected in *A. dhakensis*, *A. hydrophila* and *A. veronii*, hence, the correlation only presented biofilm and biofilm-linked genes. R values displayed positive

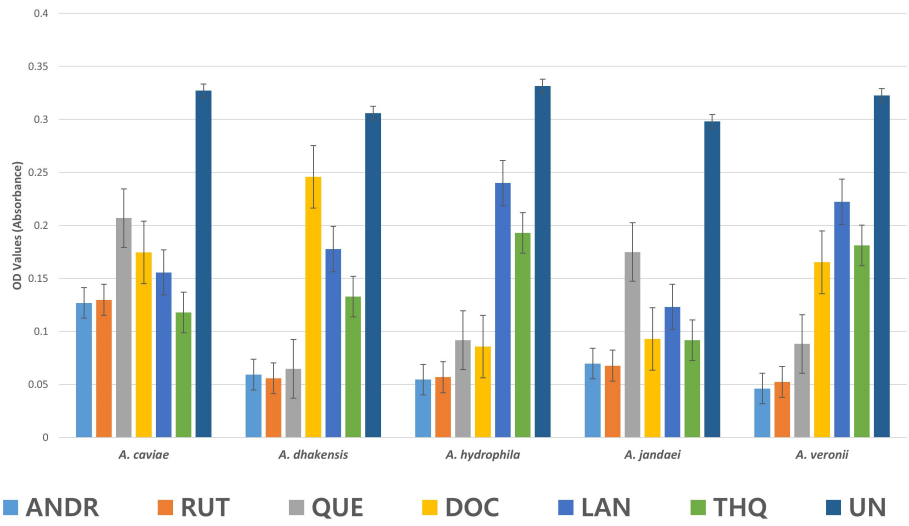

FIGURE 2
Mean OD values in *Aeromonas* sp. as affected by the biocompounds.

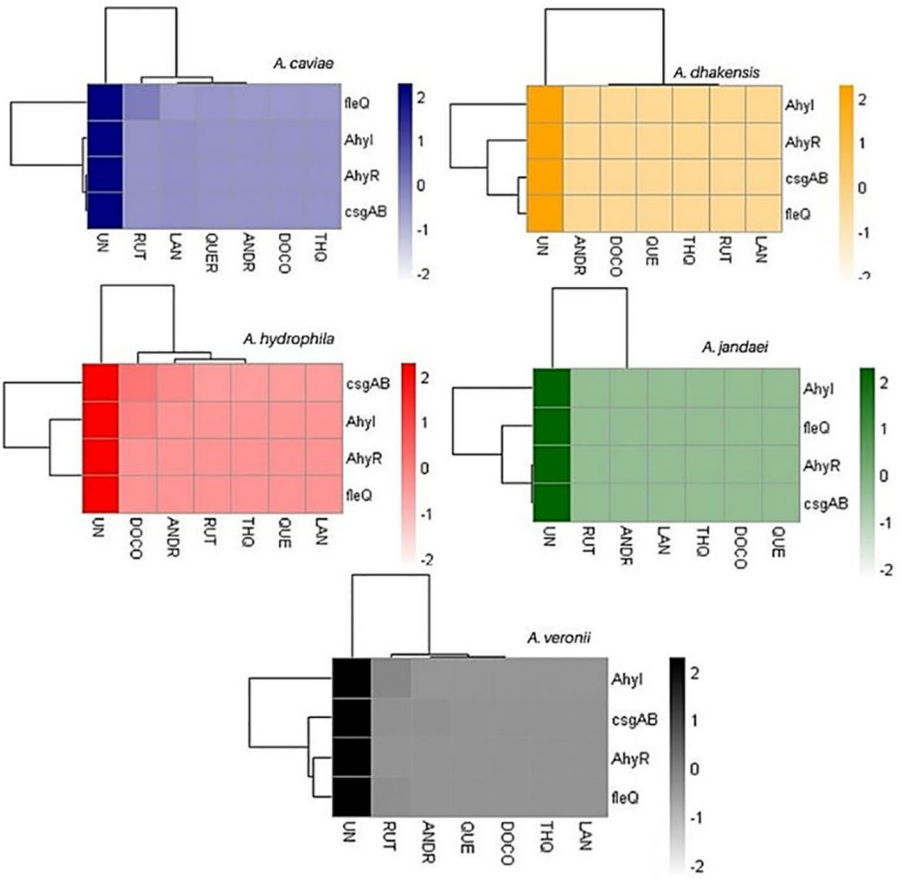

FIGURE 3
Heatmap of gene expression of biofilm-linked genes as affected by the treatments. UN (untreated); RUT (rutin); LAN (lanosterol); QUE (quercetin); ANDR (andrographolide); DOC (docosanol); THQ (thymohydroquinone).

correlation between biofilm formation and biofilm-linked genes in *A. dhakensis*, *A. hydrophila* and *A. veronii* through the R values but were not significant. However, strong interactions ($p < 0.001$) were observed between biofilm-linked genes.

4 Discussion

In this study, three ARGs—aminoglycoside resistance genes *aadA1* and *aadA2*, and sulfonamide resistance gene *sul1*—were identified in wastewater *Aeromonas* spp. This work shows effective downregulation of these ARGs when exposed to the biocompounds, suggesting their potential in targeting AMR. These ARGs are involved in enzymatic degradation or modification of respective antibiotics i.e., *sul1* encoding the DHPS enzymes with pronounced insensitivity to sulfonamides (Venkatesan et al., 2023); *aadA1* and *aadA2* modify aminoglycosides by adding an adenyl group rendering them inactive. As such, their efficiency adds up to strategies targeting antimicrobial-resistant enzymes and opens up the possibility of potentially developing these compounds for use in combination therapies as antibiotic adjuvants. Bacteria employ various mechanisms to resist antibiotics, including efflux pumps, antibiotic structural modifications, and in enzyme-catalyzed deactivation (El-Khoury et al., 2022; Murugaiyan et al., 2022). Targeting these mechanisms is crucial for enhancing antibiotic efficacy. Antibiotic adjuvants are used in cases of combination therapies (Kumar and Tudu, 2023) to augment the action of antibiotics by suppressing a mechanism of resistance thereby increasing bacterial susceptibility (Álvarez-Martínez et al., 2020). Natural products, for example, extracts from *Rhus coriaria* (Adwan et al., 2010) and plant-based compounds like tea catechins (Hu et al., 2002), quercetin and kaempferol (Lin et al., 2008), have shown synergy with antibiotics against resistant pathogens, such as *Pseudomonas aeruginosa* and MRSA (methicillin-resistant *Staphylococcus aureus*). While adjuvants are less effective in monotherapy, their combination with traditional antibiotics enhances therapeutic outcomes (Álvarez-Martínez et al., 2020). Efflux pump inhibitors (EPIs), a class of antibiotic adjuvants, have shown promise in preclinical and clinical settings (Van Bambeke et al., 2006; Zhang et al., 2023; Compagne et al., 2023) though challenges remain in their development, including pharmacokinetic profiling and addressing bacterial specificity, particularly their potential side effects on beneficial bacteria. Combination therapy of antibiotics + natural product adjuvants offer new promising strategies in synergistic approaches to manage recurring infections and control the spread of AMR.

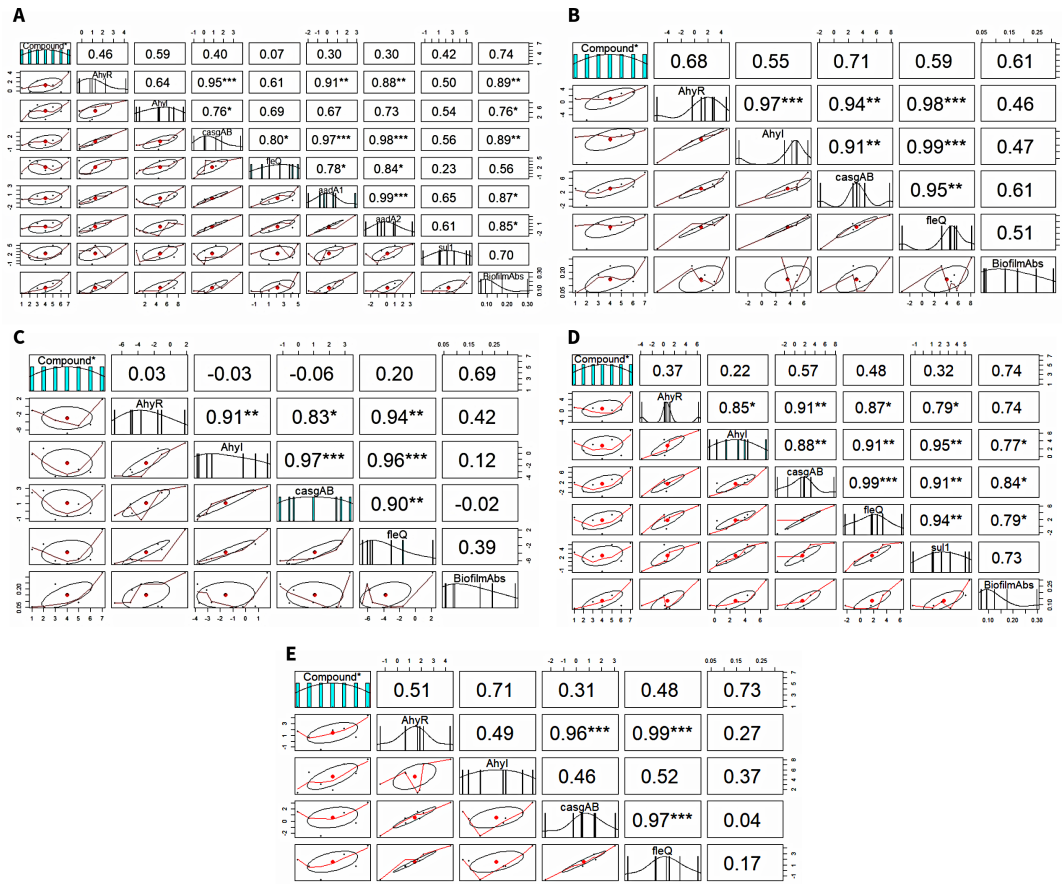

FIGURE 4
Correlation analysis between biofilm formation, biofilm-linked genes and ARGs. **(A)** *A. caviae*, **(B)** *A. dhakensis*, **(C)** *A. hydrophila*, **(D)** *A. jandaei*, **(E)** *A. veronii*.

The *Aeromonas* spp. identified in activated sludge in this study aligns with the previous reports of their consistent presence and ubiquity in wastewater samples (Skwor et al., 2020). *Aeromonas* spp are key indicator bacteria for assessing water quality risks, chiefly in antimicrobial resistance and health issues related to aquatic environments (Usui et al., 2016). The presence of the detected ARGs likely reflects past exposure and selective pressure from antibiotics, notably aminoglycosides and sulfonamides, which are frequently detected in wastewater before and after treatment (Antunes et al., 2005). Sulfonamides are widely disseminated in wastewater, often exceeding sulfonamide levels in aquatic environments linked to wastewater discharge (Proia et al., 2016; Hanna et al., 2018; Kovalakova et al., 2020). In contrast, aminoglycosides, like streptomycin, are typically found at lower concentrations, possibly due to reduced clinical use attributed to toxicity effects and has been in applied only in veterinary practices (Mutuku et al., 2022). *Aeromonas* spp. exhibits broad antibiotic resistance, notably to β-lactams, quinolones, aminoglycosides, sulfonamides, and tetracyclines, mediated by ARGs on mobile genetic elements (MGEs) such as plasmids, insertion sequences, transposons, and mobile integron gene cassettes (Piotrowska and Popowska, 2015). In *Aeromonas*, *aadA1* and *aadA2* are the most predominant ARGs in resistance integrons (Partridge et al., 2009; Piotrowska and Popowska, 2014; Khorshidi et al., 2022) while *sul*1 is considered a good marker of Class 1 integrons (Arabi et al., 2015; De los Santos et al., 2021). As also seen in this work, *sul1* and *aadA* are found to be colocalized in *Aeromonas* species (Lee et al., 2023) which provides higher risk of transmission and renders the *Aeromonas* spp co-resistance to wider spectrum of antibiotics. Although this study only detected three out of 11 target ARGs, their detection in two isolated *Aeromonas* species in WWTPs already provides evidence not only of their presence but also shows their diversity of AMR mechanisms (Piotrowska and Popowska, 2014).

Biofilm formation in *Aeromonas* spp was also effectively inhibited by all biocompounds evaluated in this study (Figure 2). When comparing the OD values, the treatment without biocompounds showed considerably higher values, indicating higher biofilm formation. Biofilm is a critical factor in bacterial virulence and the evolution of AMR, directly contributing to approximately 80% of human microbial infections (Shunmugaperumal, 2010; Davies, 2003). Our findings demonstrate that the evaluated biocompounds disrupt biofilm formation, potentially through interference with quorum sensing (QS). QS is a communication mechanism that bacteria use to coordinate biofilm formation by influencing adhesion and

exopolysaccharide (EPS) production (Miller and Bassler, 2001; Shrout and Nerenberg, 2012). By targeting QS, the biocompounds in this work may reduce pathogenicity without affecting bacterial growth, thereby lowering selective pressure and the development of antimicrobial resistance. This alternative therapeutic approach of inhibiting QS and biofilm formation offers a promising strategy for managing bacterial infections and combating AMR.

By interfering with QS cell-cell signaling, biofilm synthesis genetic pathways, adhesins, efflux pumps, and motility by repressing flagellar genes, phytochemicals function as natural antibiofilm agents that can target all stages of development (Mishra et al., 2020). Corollary to the inhibition of biofilm formation, biofilm-linked genes *ahyR*, *ahyI*, *fleQ* and *casgAB* were subsequently downregulated confirming the effects of the biocompounds and likewise points out that the compounds were able to target these genetic pathways. AhyR and AhyI are homologues of the Lux QS proteins (Kirke et al., 2004). Biofilm development in *Aeromonas* is dependent on the production of many QS signaling molecules, *N*-acylhomoserine lactone (AHL), via the AhyRI pathways (Lynch et al., 2002; Jin et al., 2020) wherein *ahyR* encodes AhyR which acts as a transcription regulator of *ahyI* for the synthesis of AHLs. *fleQ* is involved in the regulation of flagellar biogenesis and motility which is closely intertwined with the processes leading to biofilm formation (Du et al., 2020; Laganenka et al., 2020; Benyoussef et al., 2022). *csgAB* operon is responsible for the production of curli fimbriae which facilitates cell adhesion and biofilm formation (Barnhart and Chapman, 2006; Kozlova et al., 2011; Boya et al., 2022).

Our study evaluated the efficacy of six biocompounds in inhibiting biofilm formation and ARG expression in *Aeromonas* spp. The results demonstrated significant antibiofilm activity for all tested compounds, with andrographolide consistently showing substantial inhibition. Quercetin also showed significant inhibition in the majority of cases but was not as effective in all *Aeromonas* spp. tested. Andrographolide, a diterpenoid from *A. paniculata*, effectively reduced biofilm formation in *Aeromonas*, corroborating its known antimicrobial properties against high-risk pathogens such as *S. aureus*, *Escherichia coli*, and *P. aeruginosa* (Guo et al., 2014; Banerjee et al., 2017; Zhang et al., 2020). Andrographolide has also been reported to inhibit QS in *Listeria monocytogenes* by targeting the *Agr* system (Yu et al., 2022). Quercetin, a flavonoid, suppressed QS molecules and biofilm-related genes in *Aeromonas*, aligning with its previously reported effects on *P. aeruginosa* and *Klebsiella pneumoniae*, where it inhibited QS molecules *lasI, lasR, rhlI*, and *rhlR*, reducing pyocyanin production and swarming (Gopu et al., 2015; Ouyang et al., 2016; Paczkowski et al., 2017; Wang et al., 2021). It also affected gene expression linked to flagellar motility, biofilm formation, and virulence in *Vibrio parahaemolyticus* (Roy et al., 2022). Docosanol, primarily recognized for its antiviral properties (Katz et al., 1991; Pope et al., 1998; Sadowski et al., 2021), also exhibited antibiofilm activity in our study. This finding is consistent with limited reports on its bacterial effects, such as the suppression of biofilm and virulence factors in MRSA and the downregulation of stress response proteins (Lakshmi et al., 2020, 2022), and in *K. pneumoniae* (Umaru et al., 2019). Similarly, rutin has shown effectiveness against QS, biofilm formation, and expression of virulence genes in *E. coli* and *S. aureus* (Peng et al., 2018; Matilla-Cuenca et al., 2020). lanosterol and thymohydroquinone (THQ), despite their limited prior research on antimicrobial properties, showed promising results in our assays. Lanosterol has documented anticancer (Ivankovic et al., 2006) and antioxidant attributes (Tesarova et al., 2011), while THQ has shown potential but remains largely unexplored in terms of antimicrobial properties. Natural products display a rich repertoire of chemically and structurally diverse molecules with novel antimicrobial activities. This diversity can target different aspects of bacterial mechanisms and ensures that bacteria cannot easily predict or develop resistance to phytochemicals simultaneously. The dynamic nature of these compounds allows them to interfere with various bacterial processes, making them promising candidates for combating biofilm-related infections and reducing the evolution of antimicrobial resistance. Our findings provide new insights into the antibiofilm and QS-inhibiting properties of these natural biocompounds in *Aeromonas* spp., suggesting their potential as alternative therapeutic agents to combat biofilm-related infections and reduce the evolution of antimicrobial resistance. This study contributes to the limited research on the effects of these compounds on biofilm formation and ARG expression, highlighting their promise as antibiotic adjuvants.

The association between the ARGs, biofilm-linked genes and biofilm formation within the *Aeromonas* species as affected by the compounds was explored. The strong positive correlations identified in our study suggest a clear interaction between biofilm formation and the expression of biofilm-linked genes along with ARGs. Our findings align with previous studies suggesting a link between antibiotic resistance and biofilm formation, reinforcing that biofilms play a crucial role in the persistence and spread of antibiotic-resistant strains. The correlation between ARGs and biofilm-linked genes somehow suggests the coordinated regulation of these genes in the development of biofilm-associated antibiotic resistance. To strengthen these findings, future studies could consider increasing the sample size or conducting relevant experiments to further elucidate these correlations. This association has significant implications for simultaneously managing two resistance mechanisms, as well as understanding bacterial resistance mechanisms in biofilms. ARGs, such as in efflux pumps and antibiotic-modifying enzymes, have been linked to AMR in bacteria in biofilms (Kvist et al., 2008; Soto, 2013) wherein their absence can lead to diminished biofilm formation due to compromised adherence of microorganisms and the establishment of mature biofilm structures (Ren et al., 2024), thus, ARGs are now an emerging target for anti-biofilm applications and in enhancing the efficacy of AMR strategies. The limitations of this study confined the number of ARGs that could be detected to only 11, and given that only three ARGs were found and none were efflux pumps, it is plausible that other efflux pumps associated with biofilm formation in *Aeromonas* spp. were also affected. Hence, given this limitation, it is evident that further detection of other ARGs should be done, particularly those associated with efflux pumps. This will enhance the evaluations on the full spectrum of AMR mechanisms influenced by the biocompounds.

Suppression of both ARGs and biofilm formation by the biocompounds point to their significant role in the future of wastewater treatment. Since WWTPs are recognized as hotspots for horizontal gene transfer (HGT) of ARGs between bacterial populations, targeting these mechanisms in wastewater can prevent the transmission of antibiotic resistance, a critical issue concerning wastewater treatment. By reducing the transmission of ARGs in wastewater, there is a decreased risk of antibiotic resistance spreading into the environment, which could affect human health and ecosystems (Che et al., 2019). This also addresses reduction of biofouling in bioreactors. Reduction in biofouling, is a constant concern in wastewater treatment, and this justifies the application of biocompounds substances as a cost-effective and environmentally friendly solution paving the way for sustainable solutions to wastewater treatments and its implication to global health.

5 Conclusion

To combat the increasing multidrug resistance in *Aeromonas*, a comprehensive, multifaceted approach is essential, targeting both ARGs and biofilm formation. This work demonstrates that naturally-derived compounds effectively address these issues. Specifically, our results revealed that these compounds significantly reduced ARG expression levels and markedly decreased biofilm formation in *Aeromonas*.

The study highlights the effectiveness of these natural products in mitigating the development and transmission of AMR in wastewater bacteria. By disrupting biofilm formation and inhibiting ARG expression, these compounds present a promising strategy for enhancing sustainable wastewater treatment and preventing biofouling in treatment facilities. Furthermore, the ability of these biocompounds to act as adjuvants to antibiotics — by inhibiting ARGs and biofilms — offers a significant advancement in improving the efficacy of antibiotic therapies for biofilm-forming pathogens.

Overall, the findings underscore the potential of these natural products to provide a dual-action approach against AMR, both in molecular and structural aspects of bacterial resistance. This work not only addresses the challenge of AMR in wastewater bacteria but also contributes to reducing the broader burden of AMR. The study emphasizes the need for continued exploration of these bioactive compounds to fully understand their mechanisms and maximize their potential in addressing the global AMR crisis.

Data availability statement

All relevant data is contained within the article: The original contributions presented in the study are included in the article/Supplementary Material, further inquiries can be directed to the corresponding author/s.

Author contributions

KJ: Conceptualization, Data curation, Formal analysis, Investigation, Methodology, Resources, Software, Supervision, Validation, Visualization, Writing – original draft. OT: Data curation, Formal analysis, Investigation, Methodology, Software, Visualization, Writing – original draft. KB: Formal analysis, Methodology, Software, Validation, Visualization, Writing – review & editing. EG: Investigation, Methodology, Writing – review & editing. NK: Methodology, Validation, Writing – review & editing. KW: Funding acquisition, Project administration, Resources, Supervision, Validation, Writing – review & editing.

Funding

The author(s) declare financial support was received for the research, authorship, and/or publication of this article. This work was supported by the Japan Society for the Promotion of Science (JSPS) and the Ministry of Education, Culture, Sports, Science and Technology (MEXT), Japan.

Conflict of interest

The authors declare that the research was conducted in the absence of any commercial or financial relationships that could be construed as a potential conflict of interest.

Publisher's note

Supplementary material

The Supplementary Material for this article can be found online at: https://www.frontiersin.org/articles/10.3389/fcimb.2024.1456700/full#supplementary-material

References

Aarestrup, F. M., Agerso, Y., Gerner-Smidt, P., Madsen, M., and Jensen, L. B. (2000). Comparison of antimicrobial resistance phenotypes and resistance genes in *Enterococcus faecalis* and *Enterococcus faecium* from humans in the community, broilers, and pigs in Denmark. *Diagn. Microbiol. Infect. Dis.* 37, 127–137. doi: 10.1016/s0732-8893(00)00130-9

Adwan, G., Abu-Shanab, B., and Adwan, K. (2010). Antibacterial activities of some plant extracts alone and in combination with different antimicrobials against multidrug–resistant *Pseudomonas aeruginosa* strains. *Asia Pac J. Trop. Med.* 3 (4), 266–269. doi: 10.1016/S1995-7645(10)60064-8

Algburi, A., Comito, N., Kashtanov, D., Dicks, L. M. T., and Chikindas, M. L. (2017). Control of biofilm formation: antibiotics and beyond. *Appl. Environ. Microbiol.* 83, e02508–e02516. doi: 10.1128/AEM.02508-16

Álvarez-Martínez, F. J., Barrajón-Catalán, E., and Micol, V. (2020). Tackling antibiotic resistance with compounds of natural origin: A comprehensive review. *Biomedicines* 8, 405. doi: 10.3390/biomedicines8100405

Aminov, R. I., Garrigues-Jeanjean, N., and Mackie, R. I. (2001). Molecular ecology of tetracycline resistance: development and validation of primers for detection of tetracycline resistance genes encoding ribosomal protection proteins. *Appl. Environ. Microbiol.* 67, 2–32. doi: 10.1128/AEM.67.1.22-32.2001

Antunes, P., Machado, J., Sousa, J. C., and Peixe, L. (2005). Dissemination of sulfonamide resistance genes (sul1, sul2, and sul3) in portuguese *Salmonella enterica* strains and relation with integrons. *Antimicrob. Agents Chemother.* 49 (2), 836–839. doi: 10.1128/AAC.49.2.836-839.2005

Arabi, H., Pakzad, I., Nasrollahi, A., Hosainzadegan, H., Azizi Jalilian, F., Taherikalani, M., et al. (2015). Sulfonamide resistance genes (sul) M in Extended Spectrum Beta Lactamase (ESBL) and Non-ESBL producing *Escherichia coli* isolated from Iranian hospitals. *Jundishapur J. Microbiol.* 8, e19961. doi: 10.5812/jjm.19961v2

Banerjee, M., Parai, D., Chattopadhyay, S., and Mukherjee, S. K. (2017). Andrographolide: antibacterial activity against common bacteria of human health concern and possible mechanism of action. *Folia Microbiol. (Praha).* 62 (3), 237–244. doi: 10.1007/s12223-017-0496-9

Barnhart, M. M., and Chapman, M. R. (2006). Curli biogenesis and function. *Annu. Rev. Microbiol.* 60, 131–147. doi: 10.1146/annurev.micro.60.080805.142106

Benyoussef, W., Deforet, M., Monmeyran, A., and Henry, N. (2022). Flagellar motility during *E. coli* biofilm formation provides a competitive disadvantage which recedes in the presence of co-colonizers. *Front. Cell. Infect. Microbiol.* 12. doi: 10.3389/fcimb.2022.896898

Bortolaia, V., Kaas, R. S., Ruppe, E., Roberts, M. C., Schwarz, S., Cattoir, V., et al. (2020). ResFinder 4.0 for predictions of phenotypes from genotypes. *J. Antimicrob. Chemother.* 75, 3491–3500. doi: 10.1093/jac/dkaa345

Boya, B. R., Lee, J. H., and Lee, J. (2022). Antibiofilm and antimicrobial activities of chloroindoles against uropathogenic. *Escherichia coli. Front. Microbiol.* 13. doi: 10.3389/fmicb.2022.872943

Che, Y., Xia, Y., Liu, L., Li, A.-D., Yang, Y., and Zhang, T. (2019). Mobile antibiotic resistome in wastewater treatment plants revealed by nanopore metagenomic sequencing. *Microbiome* 7, 44. doi: 10.1186/s40168-019-0663-0

Chen, J., Li, W., Zhang, J., Qi, W., Li, Y., Chen, S., et al. (2020). Prevalence of antibiotic resistance genes in drinking water and biofilms: The correlation with the microbial community and opportunistic pathogens. *Chemosphere* 259, 127483. doi: 10.1016/j.chemosphere.2020.127483

Clausen, P. T. L. C., Aarestrup, F. M., and Lund, O. (2018). Rapid and precise alignment of raw reads against redundant databases with KMA. *BMC Bioinf.* 19, 307. doi: 10.1186/s12859-018-2336-6

Clinical and Laboratory Standards Institute (2015). *Performance Standards for Antimicrobial Susceptibility Testing; 25th Informational Supplement* (Wayne, PA: Clinical and Laboratory Standards Institute). CLSI Document M100-S25.

Compagne, N., Vieira Da Cruz, A., Müller, R. T., Hartkoorn, R. C., Flipo, M., and Pos, K. M. (2023). Update on the discovery of efflux pump inhibitors against critical priority gram-negative bacteria. *Antibiotics* 12, 180. doi: 10.3390/antibiotics12010180

Dahshan, H., Chuma, T., Shahada, F., Akiba, M., Fujimoto, H., Akasaka, K., et al. (2010). Characterization of antibiotic resistance and the emergence of AmpC-producing *Salmonella* Infantis from pigs. *J. Vet. Med. Sci.* 72, 1437–1442. doi: 10.1292/jvms.10-0186

Davies, D. (2003). Understanding biofilm resistance to antibacterial agents. *Nat. Rev. Drug Discovery.* 2, 114–122.

De los Santos, E., Laviña, M., Poey, M. E., and Part, A. (2021). Strict relationship between class 1 integrons and resistance to sulfamethoxazole in *Escherichia coli. Microb. Pathog.* 161, 105206. doi: 10.1016/j.micpath.2021.105206

Dong, J., Zhang, L., Liu, Y., Xu, N., Zhou, S., Yang, Q., et al. (2020). Thymol protects channel catfish from *Aeromonas hydrophila* infection by inhibiting aerolysin expression and biofilm formation. *Microorganisms* 8, 636. doi: 10.3390/microorganisms8050636

Du, B., Gu, Y., Chen, G., Wang, G., and Liu, L. (2020). Flagellar motility mediates early-stage biofilm formation in oligotrophic aquatic environment. *Ecotoxicol Environ. Saf.* 194, 110340. doi: 10.1016/j.ecoenv.2020.110340

El-Khoury, C., Mansour, E., Yuliandra, Y., Lai, F., Hawkins, B. A., Du, J. J., et al. (2022). The role of adjuvants in overcoming antibacterial resistance due to enzymatic drug modification. *RSC Med. Chem.* 13, 1276–1299. doi: 10.1039/d2md00263a

Fan, W., Hamilton Webster-Sesay, T. S., Nikolich, M. P., and Lindler, L. E. (2007). Multiplex real-time SYBR Green I PCR assay for detection of tetracycline efflux genes of gram-negative bacteria. *Mol. Cell Probes.* 21, 245–256. doi: 10.1016/j.mcp.2006.12.005

Fernando, S. I. D., and Judan Cruz, K. G. (2020). Ethnobotanical biosynthesis of gold nanoparticles and its downregulation of quorum sensing-linked *AhyR* gene in *Aeromonas hydrophila. SN Appl. Sci.* 2, 570. doi: 10.1007/s42452-020-2368-1

Gajic, I., Kabic, J., Kekic, D., Jovicevic, M., Milenkovic, M., Mitic Culafic, D., et al. (2022). Antimicrobial susceptibility testing: A comprehensive review of currently used methods. *Antibiot. (Basel)* 11, 427. doi: 10.3390/antibiotics11040427

Gopu, V., Kothandapani, S., and Shetty, P. H. (2015). Quorum quenching activity of *Syzygium cumini* (L.) skeels and its anthocyanin malvidin against *Klebsiella pneumoniae. Microb. Pathog.* 79, 61–69. doi: 10.1016/j.micpath.2015.01.010

Guo, X., Zhang, L. Y., Wu, S. C., Xia, F., Fu, Y. X., Wu, Y. L., et al. (2014). Andrographolide interferes quorum sensing to reduce cell damage caused by avian pathogenic *Escherichia coli. Vet. Microbiol.* 174, 496–503. doi: 10.1016/j.vetmic.2014.09.021

Hall-Stoodley, L., Costerton, J. W., and Stoodley, P. (2004). Bacterial biofilms: from the natural environment to infectious diseases. *Nat. Rev. Microbiol.* 2, 95–108. doi: 10.1038/nrmicro821

Hanna, N., Sun, P., Sun, Q., Li, X., Yang, X., Ji, X., et al. (2018). Presence of antibiotic residues in various environmental compartments of Shandong province in eastern China: its potential for resistance development and ecological and human risk. *Environ. Int.* 114, 131–142. doi: 10.1016/j.envint.2018.02.003

Heuer, H., and Smalla, K. (2007). Manure and sulfadiazine synergistically increased bacterial antibiotic resistance in soil over at least two months. *Environ. Microbiol.* 9, 657–666. doi: 10.1111/j.1462-2920.2006.01185.x

Hu, Z. Q., Zhao, W. H., Yoda, Y., Asano, N., Hara, Y., and Shimamura, T. (2002). Additive, indifferent and antagonistic effects in combinations of epigallocatechin gallate with 12 non-beta-lactam antibiotics against methicillin-resistant *Staphylococcus aureus. J. Antimicrob. Chemother.* 50, 1051–1054. doi: 10.1093/jac/dkf250

Ivankovic, S., Stojkovic, R., Jukic, M., Milos, M., Milos, M., and Jurin, M. (2006). The antitumor activity of thymoquinone and thymohydroquinone in *vitro* and in *vivo*. *Exp. Oncol.* 28, 220–224.

Jin, L., Zhang, X., Shi, H., Wang, W., Qiao, Z., Yang, W., et al. (2020). Identification of a novel *N*-acyl homoserine lactone synthase, *AhyI*, in *Aeromonas hydrophila* and structural basis for its substrate specificity. *J. Agri Food Chem.* 68 (8), 2516–2527. doi: 10.1021/acs.jafc.9b07833

Katz, D. H., Marcelletti, J. F., Khalil, M. H., Pope, L. E., and Katz, L. R. (1991). Antiviral activity of 1-docosanol, an inhibitor of lipid-enveloped viruses including herpes simplex. *Proc. Natl. Acad. Sci. U.S.A.* 88, 10825–10829. doi: 10.1073/pnas.88.23.10825

Khorshidi, A., Zadeh, N. M., Khaledi, A., Moosavi, G. A., Shakerimoghaddam, A., and Matinpur, A. (2022). Investigation of class 1 integrons and biofilm formation in multi-drug resistance uropathogenic *Escherichia coli* isolated from patients with urinary tract infection in Shohadaye Qom Hospital, Iran. *IntArch Heal Sci.* 9, 47–52. doi: 10.4103/iahs.iahs_163_21

Kirke, D. F., Swift, S., Lynch, M. J., and Williams, P. (2004). The *Aeromonas hydrophila* LuxR homologue AhyR regulates the *N*-acyl homoserine lactone synthase, AhyI positively and negatively in a growth phase-dependent manner. *FEMS Microbiol. Lett.* 241, 109–117. doi: 10.1016/j.femsle.2004.10.011

Kovalakova, P., Cizmas, L., McDonald, T. J., Marsalek, B., Feng, M., and Sharma, V. K. (2020). Occurrence and toxicity of antibiotics in the aquatic environment: A review. *Chemosphere.* 251, 126351. doi: 10.1016/j.chemosphere.2020.126351

Kozlova, E. V., Khajanchi, B. K., Sha, J., and Chopra, A. K. (2011). Quorum sensing and c-di-GMP-dependent alterations in gene transcripts and virulence-associated phenotypes in a clinical isolate of *Aeromonas hydrophila. Microb. Pathog.* 50, 213–223. doi: 10.1016/j.micpath.2011.01.007

Kumar, G., and Tudu, A. K. (2023). Tackling multidrug-resistant *Staphylococcus aureus* by natural products and their analogues acting as NorA efflux pump inhibitors. *Bioorg. Med. Chem.* 80, 117187. doi: 10.1016/j.bmc.2023.117187

Kvist, M., Hancock, V., and Klemm, P. (2008). Inactivation of efflux pumps abolishes bacterial biofilm formation. *Appl. Environ. Microbiol.* 74, 7376–7382. doi: 10.1128/AEM.01310-08

Laganenka, L., López, M. E., Colin, R., and Sourjik, V. (2020). Flagellum-mediated mechanosensing and RflP control motility state of pathogenic *Escherichia coli. mBio.* 11 (2), 3e02269–19. doi: 10.1128/mbio.02269-19

Lakshmi, S. A., Bhaskar, J. P., Krishnan, V., Sethupathy, S., Pandipriya, S., Aruni, W., et al. (2020). Inhibition of biofilm and biofilm-associated virulence factor production in methicillin-resistant *Staphylococcus aureus* by docosanol. *J. Biotechnol.* 317, 59–69. doi: 10.1016/j.jbiotec.2020.04.014

Lakshmi, S. A., Prasath, K. G., Tamilmuhilan, K., Srivathsan, A., Shafreen, R. M. B., Kasthuri, T., et al. (2022). Suppression of thiol-dependent antioxidant system and stress response in methicillin-resistant *Staphylococcus aureus* by docosanol: explication through proteome investigation. *Mol. Biotechnol.* 64, 575–589. doi: 10.1007/s12033-021-00434-4

Lane, D. J. (1991). "16S/23S rRNA sequencing," in *Nucleic Acid Techniques in Bacterial Systematics*. Eds. E. Stackebraundt and M. Goodfellow (John Wiley & Sons Ltd, New York), 115–175.

Lee, H. J., Storesund, J. E., Lunestad, B. T., Hoel, S., Lerfall, J., and Jakobsen, A. N. (2023). Whole genome sequence analysis of Aeromonas spp. isolated from ready-to-eat seafood: antimicrobial resistance and virulence factors. *Front. Microbiol.* 14. doi: 10.3389/fmicb.2023.1175304

Livak, K. J., and Schmittgen, T. D. (2001). Analysis of relative gene expression data using real-time quantitative PCR and the 2(-Delta Delta C(T)) Method. *Methods* 25, 402–408. doi: 10.1006/meth.2001.1262

Lynch, M. J., Swift, S., Kirke, D. F., Keevil, C. W., Dodd, C. E., and Williams, P. (2002). The regulation of biofilm development by quorum sensing in *Aeromonas hydrophila*. *Environ. Microbiol.* 4, 18–28.

Matilla-Cuenca, L., Gil, C., Cuesta, S., Rapún-Araiz, B., Žiemytė, M., Mira, A., et al. (2020). Antibiofilm activity of flavonoids on staphylococcal biofilms through targeting BAP amyloids. *Sci. Rep.* 10 (1), 18968. doi: 10.1038/s41598-020-75929-2

Michaelis, C., and Grohmann, E. (2023). Horizontal gene transfer of antibiotic resistance genes in biofilms. *Antibiot. (Basel).* 12, 328. doi: 10.3390/antibiotics12020328

Miller, M. B., and Bassler, B. L. (2001). Quorum sensing in bacteria. *Ann. Rev. Microbiol.* 55, 165–199. doi: 10.1146/annurev.micro.55.1.165

Mishra, R., Panda, A. K., De Mandal, S., Shakeel, M., Bisht, S. S., and Khan, J. (2020). Natural anti-biofilm agents: strategies to control biofilm-forming pathogens. *Front. Microbiol.* 11. doi: 10.3389/fmicb.2020.566325

Murugaiyan, J., Kumar, P. A., Rao, G. S., Iskandar, K., Hawser, S., Hays, J. P., et al. (2022). Progress in alternative strategies to combat antimicrobial resistance: Focus on antibiotics. *Antibiotics.* 11 (2), 200. doi: 10.3390/antibiotics11020200

Mutuku, C., Gazdag, Z., and Melegh, S. (2022). Occurrence of antibiotics and bacterial resistance genes in wastewater: resistance mechanisms and antimicrobial resistance control approaches. *World J. Microbiol. Biotechnol.* 38, 152. doi: 10.1007/s11274-022-03334-0

Ouyang, J., Sun, F., Feng, W., Sun, Y., Qiu, X., Xiong, L., et al. (2016). Quercetin is an effective inhibitor of quorum sensing, biofilm formation and virulence factors in *Pseudomonas aeruginosa*. *J. Appl. Microbiol.* 120, 966–974. doi: 10.1111/jam.13073

Paczkowski, J. E., Mukherjee, S., McCready, A. R., Cong, J. P., Aquino, C. J., Kim, H., et al. (2017). Flavonoids suppress *Pseudomonas aeruginosa* virulence through allosteric inhibition of quorum-sensing receptors. *J. Biol. Chem.* 292, 4064–4076. doi: 10.1074/jbc.M116.770552

Partridge, S. R., Tsafnat, G., Coiera, E., and Iredell, J. R. (2009). Gene cassettes and cassette arrays in mobile resistance integrons. *FEMS Microbiol. Rev.* 33, 757–784. doi: 10.1111/j.1574-6976.2009.00175.x

Patel, B., Kumari, S., Banerjee, R., Samanta, M., and Das, S. (2017). Disruption of the quorum sensing regulated pathogenic traits of the biofilm-forming fish pathogen *Aeromonas hydrophila* by tannic acid, a potent quorum quencher. *Biofouling* 33, 580–590. doi: 10.1080/08927014.2017.1336619

Peng, L. Y., Yuan, M., Cui, Z. Q., Wu, Z. M., Yu, Z. J., Song, K., et al. (2018). Rutin inhibits quorum sensing, biofilm formation and virulence genes in avian pathogenic *Escherichia coli*. *Microb. Pathog.* 119, 54–59. doi: 10.1016/j.micpath.2018.04.007

Perveen, S., Pablos, C., Reynolds, K., Stanley, S., and Marugán, J. (2023). Growth and prevalence of antibiotic-resistant bacteria in microplastic biofilm from wastewater treatment plant effluents. *Sci. Total Environ.* 856, 159024. doi: 10.1016/j.scitotenv.2022.159024

Piotrowska, M., and Popowska, M. (2014). The prevalence of antibiotic resistance genes among *Aeromonas* species in aquatic environments. *Ann. Microbiol.* 64, 921–934. doi: 10.1007/s13213-014-0911-2

Piotrowska, M., and Popowska, M. (2015). Insight into the mobilome of *Aeromonas* strains. *Front. Microbiol.* 6. doi: 10.3389/fmicb.2015.00494

Piotrowska, M., Przygodzińska, D., Matyjewicz, K., and Popowska, M. (2017). Occurrence and variety of β-lactamase genes among Aeromonas spp. isolated from urban wastewater treatment plant. *Front. Microbiol.* 8. doi: 10.3389/fmicb.2017.00863

Pope, L. E., Marcelletti, J. F., Katz, L. R., Lin, J. Y., Katz, D. H., Parish, M. L., et al. (1998). The anti-herpes simplex virus activity of n-docosanol includes inhibition of the viral entry process. *Antiviral Res.* 40, 85–94. doi: 10.1016/s0166-3542(98)00048-5

Proia, L., von Schiller, D., Sànchez-Melsió, A., Sabater, S., Borrego, C. M., Rodríguez-Mozaz, S., et al. (2016). Occurrence and persistence of antibiotic resistance genes in river biofilms after wastewater inputs in small rivers. *Environ. pollut.* 210, 121–128. doi: 10.1016/j.envpol.2015.11.035

Qiagen (2023). *RNeasy Mini Kit Handbook*. Available online at: https://www.qiagen.com/us/resources (Accessed November 15, 2023).

Rather, M., Gupta, K., and Mandal, M. (2021). Microbial biofilm: formation, architecture, antibiotic resistance, and control strategies. *Braz. J. Microbiol.* 52, 1701–1718. doi: 10.1007/s42770-021-00624-x

Ren, J., Wang, M., Zhou, W., and Liu, Z. (2024). Efflux pumps as potential targets for biofilm inhibition. *Front. Microbiol.* 15. doi: 10.3389/fmicb.2024.1315238

Rezaei, A., Oyong, G. G., Borja, V. B., Inoue, M., Abe, T., Tamamura, R., et al. (2011). Molecular screening of anti-quorum sensing capability of *Salvadora persica* on *Enterococcus faecalis*. *J. Hard Tis Bio.* 20 (2), 115–124. doi: 10.2485/jhtb.20.115

Roh, H., and Kannimuthu, D. (2023). Comparative resistome analysis of *Aeromonas* species in aquaculture reveals antibiotic resistance patterns and phylogeographic distribution. *Env. Res.* 239, 117273. doi: 10.1016/j.envres.2023.117273

Rosengren, L. B., Waldner, C. L., and Reid-Smith, R. J. (2009). Associations between antimicrobial resistance phenotypes, antimicrobial resistance genes, and virulence genes of fecal *Escherichia coli* isolates from healthy grow-finish pigs. *Appl. Environ. Microbiol.* 75 (5), 1373–1380. doi: 10.1128/AEM.01253-08

Roy, P. K., Song, M. G., Jeon, E. B., Kim, S. H., and Park, S. Y. (2022). Antibiofilm efficacy of quercetin against *Vibrio parahaemolyticus* biofilm on food-contact surfaces in the food industry. *Microorganisms* 10, 1902. doi: 10.3390/microorganisms10101902

Sadowski, L. A., Upadhyay, R., Greeley, Z. W., and Margulies, B. J. (2021). Current drugs to treat infections with herpes simplex viruses-1 and -2. *Viruses* 13, 1228. doi: 10.3390/v13071228

Shrout, J. D., and Nerenberg, R. (2012). Monitoring bacterial twitter: does quorum sensing determine the behavior of water and wastewater treatment biofilms? *Environ. Sci. Technol.* 46, 1995–2005. doi: 10.1021/es203933h

Shunmugaperumal, T. (2010). *Biofilm eradication and prevention: a pharmaceutical approach to medical device infections* (Hoboken NJ: John Wiley & Sons).

Skwor, T., Stringer, S., Haggerty, J., Johnson, J., Duhr, S., Johnson, M., et al. (2020). Prevalence of potentially pathogenic antibiotic-resistant Aeromonas spp. in treated urban wastewater effluents versus recipient riverine populations: a 3-year comparative study. *Appl. Environ. Microbiol.* 86, e02053–e02019. doi: 10.1128/AEM.02053-19

Soto, S. M. (2013). Role of efflux pumps in the antibiotic resistance of bacteria embedded in a biofilm. *Virulence* 4, 223–229. doi: 10.4161/viru.23724

Sun, B., Luo, H., Jiang, H., Wang, Z., and Jia, A. (2021). Inhibition of quorum sensing and biofilm formation of esculetin on *Aeromonas Hydrophila*. *Front. Microbiol.* 12. doi: 10.3389/fmicb.2021.737626

Taiswa, A., Andriolo, J. M., Hailer, M. K., and Skinner, J. K. (2024). Electrospun controlled release anti-quorum sensing filter for biofouling prevention in MCE membranes. *Sep Pur Tech.* 332, 125874. doi: 10.1016/j.seppur.2023.125874

Talagrand-Reboul, E., Jumas-Bilak, E., and Lamy, B. (2017). The social life of *Aeromonas* through biofilm and quorum sensing systems. *Front. Microbiol.* 8. doi: 10.3389/fmicb.2017.00037

Tesarova, H., Svobodova, B., Kokoska, L., Marsik, P., Pribylova, M., Landa, P., et al. (2011). Determination of oxygen radical absorbance capacity of black cumin (*Nigella sativa*) seed quinone compounds. *Nat. ProdComm* 6 (2), 213–216. doi: 10.1177/1934578X1100600214

Uluseker, C., Kaster, K. M., Thorsen, K., Basiry, D., Shobana, S., Jain, M., et al. (2021). A review on occurrence and spread of antibiotic resistance in wastewaters and in wastewater treatment plants: mechanisms and perspectives. *Front. Microbiol.* 12, 717809. doi: 10.3389/fmicb.2021.717809

Umaru, I. J., Ahmad, F. B., and Aduwamai, U. H. (2019). Extraction, elucidation, characterization and evaluation of antibacterial activity of four pure compounds from *Barringtonia racemosa* leaf extract. *World Jour Pharm. Pharma Sci.* 8, 184–223. doi: 10.20959/wjpps20198-14476

Untergasser, A., Cutcutache, I., Koressaar, T., Ye, J., Faircloth, B. C., Remm, M., et al. (2012). Primer3–new capabilities and interfaces. *Nucleic Acids Res.* 40, e115. doi: 10.1093/nar/gks596

Usui, M., Tagaki, C., Fukuda, A., Okubo, T., Boonla, C., Suzuki, S., et al. (2016). Use of Aeromonas spp. as general indicators of antimicrobial susceptibility among bacteria in aquatic environments in Thailand. *Front. Microbiol.* 7. doi: 10.3389/fmicb.2016.00710

Van Bambeke, F., Pagès, J. M., and Lee, V. J. (2006). Inhibitors of bacterial efflux pumps as adjuvants in antibiotic treatments and diagnostic tools for detection of resistance by efflux. *Recent Pat. Antiinfect. Drug Discovery* 1, 157–175. doi: 10.2174/157489106777452692

Venkatesan, M., Fruci, M., Verellen, L. A., Skarina, T., Mesa, N., Flick, R., et al. (2023). Molecular mechanism of plasmid-borne resistance to sulfonamide antibiotics. *Nat. Commun.* 4, 4031. doi: 10.1038/s41467-023-39778-7

Wang, Z., Ding, Z., Li, Z., Ding, Y., Jiang, F., and Liu, J. (2021). Antioxidant and antibacterial study of 10 flavonoids revealed rutin as a potential antibiofilm agent in *Klebsiella pneumoniae* strains isolated from hospitalized patients. *Microb. Pathog.* 159, 105121. doi: 10.1016/j.micpath.2021.105121

World Health Organization (2023). *Antimicrobial resistance*. Available online at: https://www.who.int/news-room/fact-sheets/detail/antimicrobial-resistance (Accessed February 15, 2024).

Zhang, L., Bao, M., Liu, B., Zhao, H., Zhang, Y., Ji, X., et al. (2020). Effect of andrographolide and its analogs on bacterial infection: a review. *Pharmacology* 105, 123–134. doi: 10.1159/000503410

Yu, T., Jiang, X., Xu, X., Jiang, C., Kang, R., and Jiang, X. (2022). Andrographolide inhibits biofilm and virulence in *Listeria monocytogenes* as a quorum-sensing inhibitor. *Molecules.* 27 (10), 3234. doi: 10.3390/molecules27103234

Zhang, S., Wang, J., and Ahn, J. (2023). Advances in the discovery of efflux pump inhibitors as novel potentiators to control antimicrobial-resistant pathogens. *Antibiot. (Basel).* 12, 1417. doi: 10.3390/antibiotics12091417

frontiers | Frontiers in Cellular and Infection Microbiology

TYPE Brief Research Report
PUBLISHED 17 October 2024
DOI 10.3389/fcimb.2024.1458652

OPEN ACCESS

EDITED BY
Maria Gabriela Paraje,
National University of Cordoba, Argentina

REVIEWED BY
Wang Ke,
Guangxi Medical University, China
Laura Gabriela Hedemann,
National University of Cordoba, Argentina

*CORRESPONDENCE
Shamus R. Carr
Shamus.Carr@nih.gov

RECEIVED 02 July 2024
ACCEPTED 04 October 2024
PUBLISHED 17 October 2024

CITATION
Gustafson AM, Larrain CM, Friedman LR, Repkorwich R, Anidi IU, Forrest KM, Fennelly KP and Carr SR (2024) Novel management of pseudomonas biofilm-like structure in a post-pneumonectomy empyema.
Front. Cell. Infect. Microbiol. 14:1458652.
doi: 10.3389/fcimb.2024.1458652

Novel management of pseudomonas biofilm-like structure in a post-pneumonectomy empyema

Alexandra M. Gustafson[1], Carolina M. Larrain[1], Lindsay R. Friedman[1], Rachel Repkorwich[2], Ifeanyichukwu U. Anidi[3], Karen M. Forrest[4], Kevin P. Fennelly[3] and Shamus R. Carr[2]*

[1]National Institutes of Health, National Cancer Institute, Surgery Branch, Bethesda, MD, United States, [2]National Institutes of Health, National Cancer Institute, Thoracic Surgery Branch, Bethesda, MD, United States, [3]National Institutes of Health, National Heart, Lung and Blood Institute, Critical Care Medicine and Pulmonary Branch, Bethesda, MD, United States, [4]Medical Research Council Unit the Gambia, London School of Hygiene and Tropical Medicine, Fajara, Gambia

We present a patient with a post-pneumonectomy empyema refractory to surgical debridement and systemic antibiotics. The patient initially presented with a bronchopleural fistula and pneumothorax secondary to tuberculosis (TB) destroyed lung, which required a pneumonectomy with Eloesser flap. Ongoing pleural infection delayed the closure of the Eloesser flap, and thoracoscopic inspection of his chest cavity revealed a green, mucous biofilm-like structure lining the postpneumonectomy pleural cavity. Cultures identified pan-susceptible *Pseudomonas aeruginosa*. Despite debriding this biofilm-like structure and administering systemic antibiotics, the patient continued to show persistent signs of infection and regrowth of the film. We employed a novel approach to dissolve the biofilm-like structure using intrapleural dornase alfa followed by intrapleural antibiotic washes. After 3 weeks of daily washes, repeat inspection demonstrated the biofilm-like structure had completely resolved. Resolving the pseudomonas biofilm-like structure allowed permanent closure of his chest without further need for systemic antibiotics. At follow up 3 months later, he showed no sequalae. This treatment option can be an important adjunct to improve likelihood of chest closure in patients with post-pneumonectomy empyema that resists standard treatment options due to biofilm formation.

KEYWORDS

biofilm-like structure, pseudomonas, tuberculosis, empyema, dornase, alfa, pneumonectomy

1 Introduction

Empyema in patients who have undergone pneumonectomies, while uncommon, carries a high mortality. Diagnosing empyema can be challenging due to an insidious onset, but typically presents with fevers, leukocytosis and elevated C-reactive protein (CRP). Cultures of the pleural space most often yield growth of *Pseudomonas aeruginosa* or *Staphylococcus aureus* (Deschamps et al., 2001). Postpneumonectomy empyema outcomes are typically worse in patients with a bronchopleural fistula (BPF). Treatment focuses on debriding the pleural cavity, ensuring adequate drainage, and systemic antibiotics, which have variable penetration to pleural tissue (Teixeira et al., 2000; Bedawi et al., 2023). Despite limited advancements in the management of post-pneumonectomy empyema, standard care still carries elevated morbidity and mortality, with some studies showing a 7.1% operative mortality and 5-year survival of 44.5% (Zaheer et al., 2006).

Treatment options for empyema often require operative intervention, especially when a BPF is present. Historically, treatment involved an open thoracotomy and rib resection, as described by Clagett and Geraci (1963). The current approach, however, involves using video-assisted thoracoscopic surgery (VATS) to debride the pleural cavity and either fill the pleural space with an antibiotic solution or obliterate it by filling the space with various tissue flaps (Azevedo et al., 2020). Despite these new operative techniques, empyema may still be recalcitrant to standard therapy due to growth of a bacterial associated biofilm that may provide a sheltered environment allowing the bacteria to persist despite direct appropriate antibiotic treatment (Yin et al., 2019). Intrapleural administration of dornase alfa (Pulmozyme®, Genentech, USA), a DNase, has been used to treat loculated pleural infections (Rahman et al., 2011). In our patient, we used 5 mg of dornase alfa along with intrapleural amikacin to resolve the pleural infection. This novel technique successfully cleared the pleural biofilm-like structure and allowed for closure of the open chest. We present this case, demonstrating the use of intrapleural dornase alfa to treat a bacterial biofilm-like structure contributing to a post-pneumonectomy empyema that was recalcitrant to intrapleural antibiotics. The persistent empyema initially prevented closure of the open thoracotomy window used in the management of this patient.

2 Case presentation

A 20-year-old male from The Gambia, West Africa was admitted locally with a right sided hydro-pneumothorax, initially managed with a chest thoracostomy tube. Chest radiographs demonstrated left upper lobe patchy opacities. At that time sputum microscopy was positive for acid-fast bacilli (AFB), and the Xpert MTB/RIF molecular assay of the sputum detected *Mycobacterium tuberculosis* that was negative for resistance to rifampin. However, due to local economic issues and standard of care, sputum cultures were not performed. His serology for HIV was negative.

The patient began standard daily treatment with rifampin 600 mg, isoniazid 300 mg, pyridoxine 1600 mg, and ethambutol 1100 mg. Despite the chest thoracostomy tube, his lung remained entrapped (Figure 1A), and he continued to experience fever and illness. After one month of treatment, the Xpert MTB/RIF panel was negative, but the patient remained febrile after exhausting all local treatment options. Consequently, his treating team referred

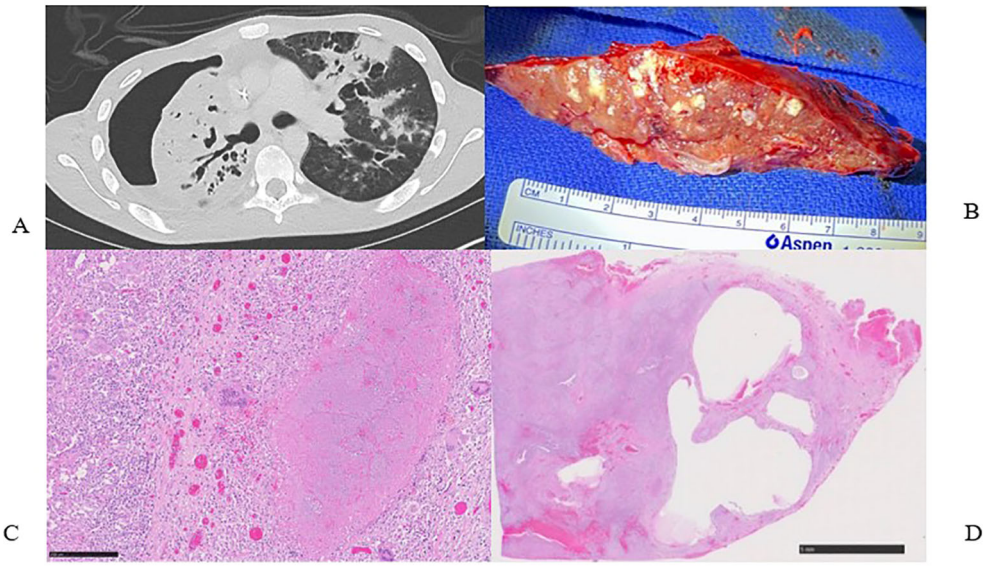

FIGURE 1
(A) Pre-operative computed tomography scan showing right hydropneumothorax, right lung consolidations and collapse. **(B)** Surgical specimen, right pneumonectomy with innumerable micro abscesses and caseating granulomas. **(C)** H&E stain of surgical specimen showing large necrotizing granuloma surrounded by multinucleated giant cells and epithelioid histiocytes (250μm). **(D)** Low power view of lung parenchyma showing diffuse involvement by granulomatous inflammation and cystic lesions (5mm).

him for consultation and additional treatment. Upon admission to our institution in the United States, 8 months after his initial presentation, the patient reported persistent low-grade fevers, a dry cough, and an unintentional 9 kg weight loss since his initial admission. He presented as cachectic, weighing 42 kg, but in no acute distress. He had a right chest tube with Heimlich valve in place, decreased breath sounds over his right chest with a pleural rub, and a resting tachycardia of 140 beats per minute. The neurological examination was remarkable for a lower extremity motor and sensory peripheral neuropathy with a right foot drop.

Pleural fluid from his chest tube grew heavy amounts of *Achromobacter* species, *Stenotrophomonas maltophilia*, and *P. aeruginosa*. The initial Mycobacteria Growth Indicator Tube (MGIT) liquid culture of the pleural fluid reported growth of *M. tuberculosis*. This was later amended as a false positive due to the overgrowth of the gram-negative species in the MGIT. However, the Cepheid Xpert MTB/RIF molecular assay detected *M. tuberculosis* that was not resistant to rifampin in the pleural fluid. The isoniazid and ethambutol were discontinued, and the treatment regimen was modified to oral rifampin, moxifloxacin, pyrazinamide, and trimethoprim-sulfamethoxazole, in addition to intravenous amikacin and meropenem to cover all detected microorganisms.

The primary team consulted thoracic surgery, and the initial plan aimed to salvage the lung with total pulmonary pleural decortication to permit lung re-expansion to fill the pleural space. However, due to the patient's malnutrition and poor health status, surgery was delayed until the patient was medically optimized. Over the ensuing 4 weeks, the patient worked with physical therapy and nutrition, eventually regaining 6 kg. The patient underwent a right thoracotomy and pleurectomy with decortication in attempts to preserve the lung. However, inspection of the lung revealed extensive inflammation along with micro abscesses and granulomas involving all three lobes of the right lung (Figure 1B). After intraoperative multidisciplinary discussion with pulmonary medicine, the decision was to proceed with a right pneumonectomy. A pedicled rotational pericardial patch was used to buttress the right bronchial stump, and an Eloesser flap was created for open drainage of the infected space (Figure 2A).

Final pathology demonstrated necrotizing and non-necrotizing granulomas involving almost the entire right lung parenchyma (Figures 1C, D); AFB were present in the necrotizing granulomas. The visceral and parietal pleura was fibrous and contained multiple necrotizing and non-necrotizing granulomas with acid-fast bacilli. All cultures of the resected lung tissue were negative for microbial growth.

The patient experienced an expected Intensive Care Unit stay and transferred to the surgical floor after 11 days. During the immediate postoperative period, he underwent two planned VATS to aid in pleural debridement. There were no signs of gross infection. He continued aggressive management and rehabilitation, and 4 months after his pneumonectomy, plans were formulated to close his Eloesser flap. However, the patient developed a fever with a rising CRP, and leukocytosis. Bronchoscopy with bronchoalveolar washings grew *P. aeruginosa*, and a right sided VATS showed a green film lining the entire right parietal pleura (Figure 3A). His chest was debrided and washed out; he received intravenous antibiotics, resulting in eventual improvement. Plans to close the chest were again delayed when a low-grade fever, rising CRP, and leukocytosis recurred. Repeat VATS demonstrated a recurrent green film, suggesting a biofilm-like structure had reformed, with redemonstration of only a pan-sensitive strain of *P. aeruginosa* in pleural microbiology cultures.

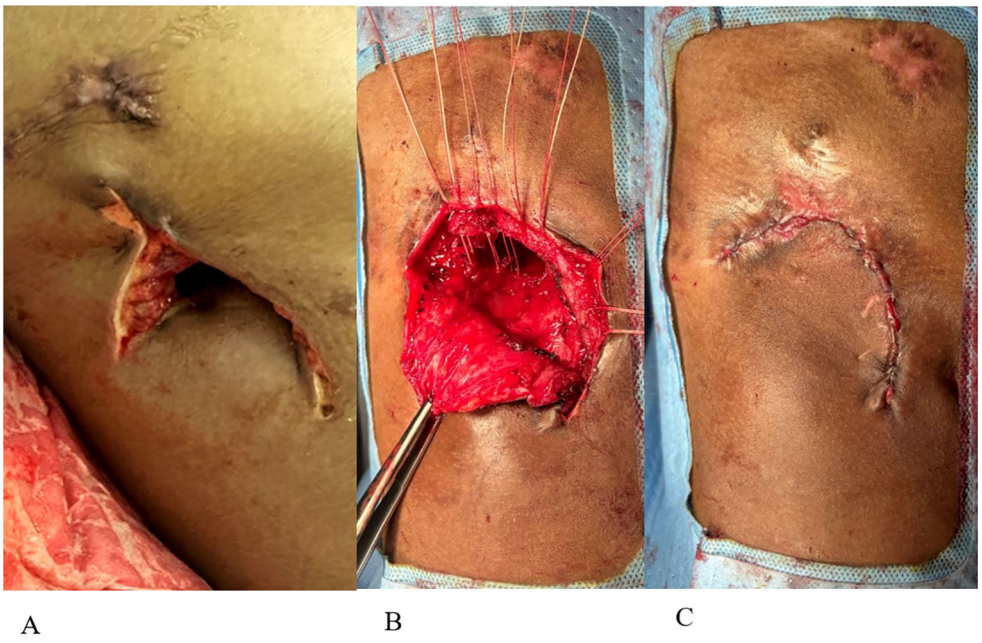

FIGURE 2
(A) Eloesser flap creation. **(B)** Closure of Eloesser flap. **(C)** Final flap closure with skin reapproximated.

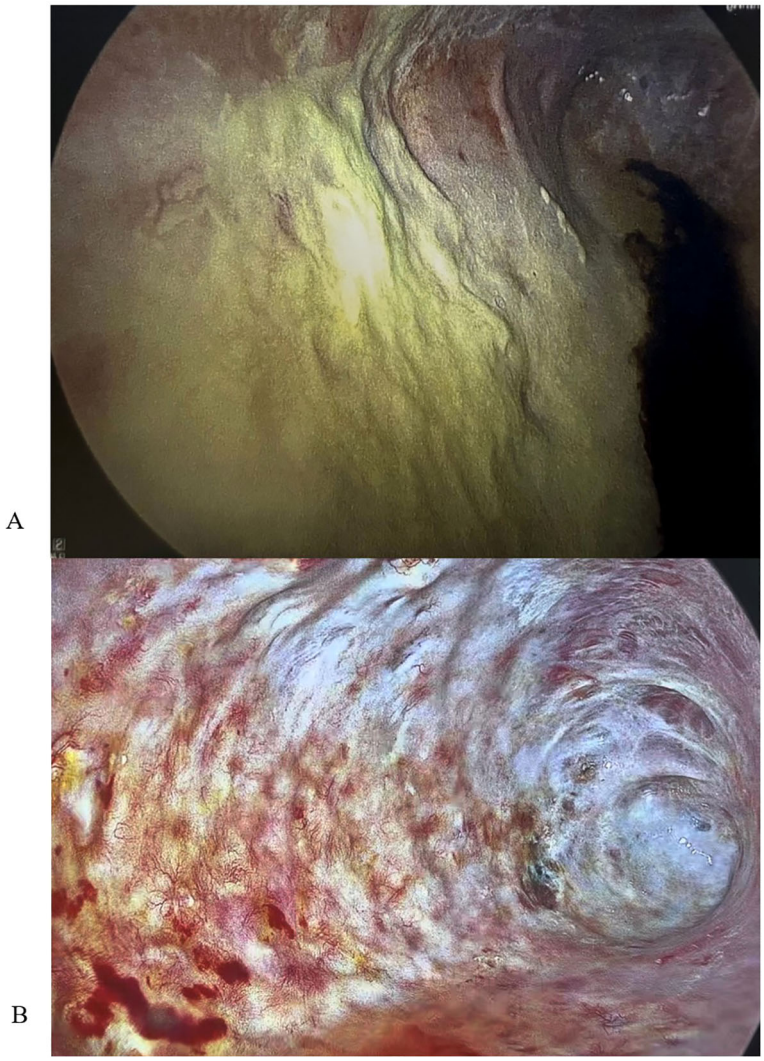

FIGURE 3
(A) VATS image showing biofilm-like structure prior to dornase alfa application. **(B)** VATS image showing resolution of biofilm-like structure after 21 days of dornase alfa application.

After consulting with pulmonology and infectious disease teams, we began intrapleural instillation of 5 mg of dornase alfa in 50 ml of normal saline. The dose of 5 mg was chosen since this has been proven to safely and effectively improve drainage of pleural infections (Rahman et al., 2011). We performed daily dornase alfa instillation followed by intrapleural instillation of antibiotic solution with 500mg amikacin, to which the *P. aeruginosa* was susceptible. The patient then followed a turning protocol to allow the antibiotic solution to contact all areas of the right pleural space. We chose the intrapleural route due to the known poor pleural penetration of systemically administered amnioglycosides (Thys et al., 1988). We monitored serum amikacin levels for up to eight hours after installation due to the unknown systemic absorption of amikacin through an infected pleural space (Thys et al., 1984; Thys et al., 1988).

On the first day of dornase alfa and amikacin instillation, the patient's serum amikacin level prior to antibiotic administration was <0.8 mcg/mL. We then measured serum amikacin levels 1, 2, 4, and 8 hours post intrapleural administration. The levels were 1.4, 3.7, 3.6, and 1.7 mcg/mL respectively. We repeated this daily; on the subsequent day the patient's serum amikacin levels were 7.2, 10.4, 9.3, and 3.1 mcg/mL 1, 2, 4, and 8 hours post intrapleural administration. The highest serum amikacin level ever measured was 10.9 mcg/mL. Since maximum safe serum amikacin levels are 20.0.-30.0 mcg/mL (Kovačević et al., 2016), we elected to stop measuring serum amikacin levels while continuing the dornase alfa and amikacin intrapleural washes.

The patient never exhibited symptoms or signs of amikacin toxicity, and serum levels remained low. Audiometry exams and renal function remained normal. DNase and amikacin washes were repeated daily for 21 days. On subsequent VATS, there was no green film seen, implying resolution of the *P. aeruginosa* biofilm-like structure (Figure 3B). Due to no further evidence of infection, we stopped intrapleural dornase alfa administration. Clinically, the patient remained afebrile with no leukocytosis and resolution of the elevated CRP during this time (Figures 4A, B). We continued daily

amikacin washes only from that time forward, and two weeks later, his Eloesser flap was closed (Figures 2B, C).

Immediately prior to closure of the patient's chest, we instilled 500 mg of amikacin in one liter of normal saline. This solution remained in his chest to fill the pleural cavity as previously described (Zaheer et al., 2006). The patient was discharged home, and on follow up visits he has no complaints and continues to do well (Figure 4C).

3 Discussion

Post-pneumonectomy empyemas pose a complex clinical challenge. Although occurring in only 5-10% of cases, mortality rates can reach as high as 20% (Schneiter et al., 2001; Zaheer et al., 2006). The hallmark of treatment for post-pneumonectomy empyema involves debridement of infected tissue, pleural drainage, and administration of parenteral antibiotics (Deschamps et al., 2001). Surgeons have developed several techniques to facilitate pleural drainage, the predominant two being Eloesser flap and Clagett window; the main difference is the Eloesser flap is smaller with the possibility of remaining permanent as a drainage site (Denlinger, 2010). While both techniques successfully manage empyemas and result in chest closure in most patients, a small subset are unable to undergo closure. Persistent infection of the pleural space, sometimes associated with a recurrent bronchopleural fistula, often accounts for this. When eradicating bacterial infection from the pleural cavity proves impossible, patients may be left with a permanent drainage window.

Maintaining a chest wall opening, though viable, can impact quality of life. Patients must diligently irrigate the chest cavity and frequently change dressings. The patient we present here experienced recurrent empyema, which repeatedly prevented closure of his chest. For a young, otherwise healthy patient, discharge home with an open chest is less than ideal, particularly if returning to a community with limited health resources. Thus, to treat this recalcitrant empyema, we employed a novel technique. While clinicians frequently instill dornase alfa through a tube thoracostomy to break apart loculated pleural effusions (Thomas et al., 2015), its instillation to destabilize a post-pneumonectomy biofilm, followed by subsequent antibiotic solution, has not been previously described in humans. Although the purpose of dornase alfa in treating infected pleural collections is to reduce the viscosity of recruited leukocytes via hydrolysis of extracellular DNA from exuberant neutrophil extracellular trap formation, we specifically administered dornase alfa to target the bacterial biofilm lining the pleural cavity of the pneumonectomy

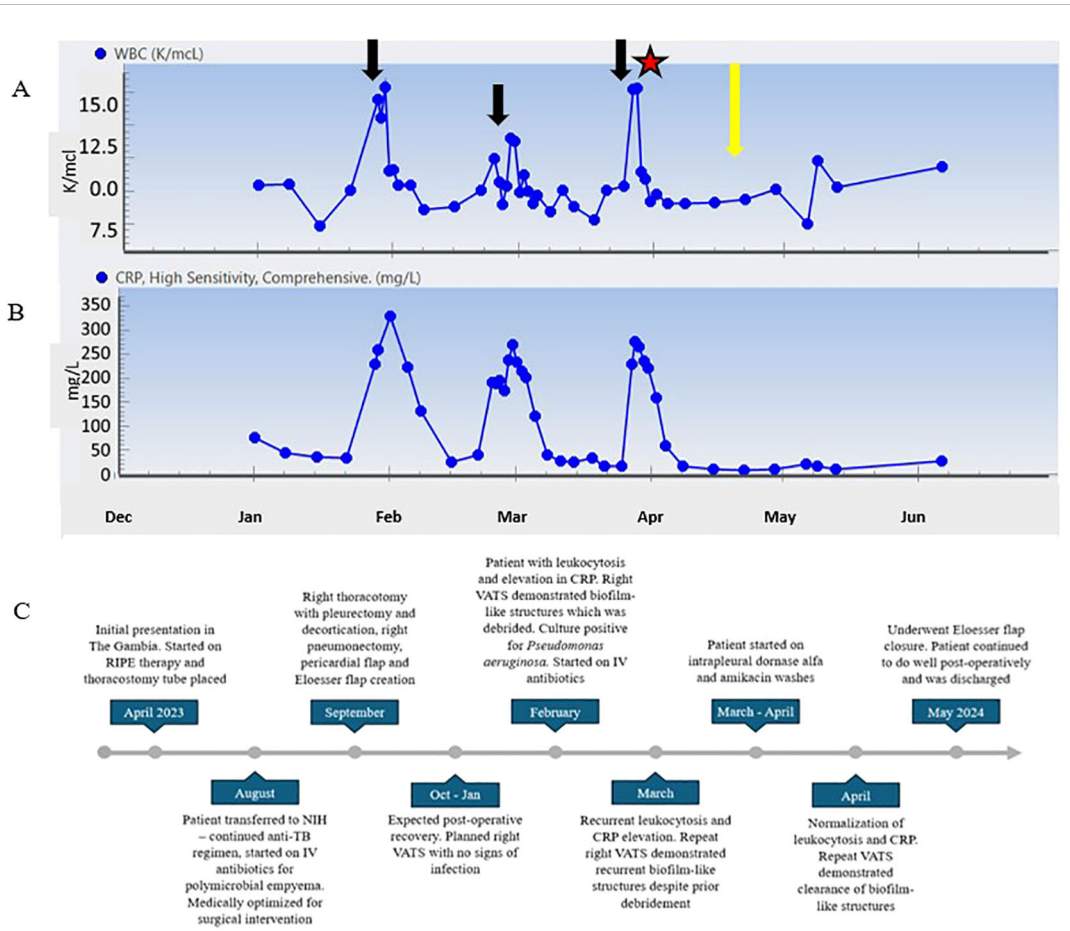

FIGURE 4
(A) WBC count trend throughout clinical course. **(B)** CRP trend from 2 months post operatively until follow up 8 months post operatively. **(C)** Timeline of patient clinical course. Black arrows represent time points at which patient developed symptoms and procedures revealed *P. aeruginosa* growth. Star represents initiation of dornase alfa and amikacin washes. Yellow arrow represents VATS showing resolution of biofilm-like structures.

space. Dornase alfa acts to destabilize the biofilm and permit antibiotics to penetrate the chronically infected pleural space, thereby aiding in eradicating *P. aeruginosa*. Here, we present the successful use of dornase alfa to disintegrate a bacterial biofilm-like structure. We hypothesize the biofilm-like structure contributed to the difficulty in eradication of a polymicrobial post-pneumonectomy empyema preventing closure of an Eloesser flap.

Various microorganisms produce biofilms that share common traits. They often harbor dormant populations of pathogens that cause recalcitrant infections, as seen in our patient with persistent *P. aeruginosa* growth. The extracellular matrix constitutes a major component of biofilms. These unique extracellular matrix compositions contribute to the virulence of biofilms. Moreover, even if antibiotics are bactericidal, the biofilm often remains, sheltering bacteria from the antibiotic and increasing the likelihood of recurrent infections (Koo et al., 2017; Yin et al., 2022). Current strategies to eradicate biofilms must target multiple aspects that lead to biofilm formation. Hence, we employed a multimodal approach with surgical debridement, dornase alfa for mechanical disruption of the extracellular matrix of the biofilm, and pleural instillation of amikacin solution to reach a high concentration of antibiotic directly in the infected tissue. When delivering antibiotics in this manner, there must still be consideration for systemic absorption. Measurements of systemic amikacin levels after pleural wash demonstrated low systemic absorption. This finding differs from other studies using intrapleural amikacin, however these studies were done in a noninfected pleural space (Clagett and Geraci, 1963; Zaheer et al., 2006).

P. aeruginosa creates biofilms, a bacterial attribute that leads to chronic infections due to the inability of the antibiotic to penetrate the biofilm. The biofilm matrix primarily comprises proteins, carbohydrates, and DNA; pseudomonal biofilms contain a large amount of extracellular DNA (Allesen-Holm et al., 2006). DNases target and break down these foreign DNA particles by an enzymatic process. Degrading extracellular DNA has many medical applications, one of which is to prevent pulmonary infections (Lauková et al., 2020). In one study, mice deficient in DNase exhibited increased susceptibility to bloodstream infections (Lacey et al., 2023). Additionally, these mice had bacterial lesions that resembled a biofilm and contained bacterial DNA while excluding neutrophils (Lacey et al., 2023). *P. aeruginosa* can cause severe, life-threatening pulmonary infections in patients with cystic fibrosis (CF), and one preventive method involves CF patients inhaling dornase alfa. This acts by breaking up the thick, viscous secretions while also cleaving the extracellular DNA that allows *P. aeruginosa* to form biofilms (Gnanadhas et al., 2015). A study evaluating the use of L-methionine to increase DNase activity showed that chronic infections with *P. aeruginosa* biofilm can be treated with DNase and antibiotics (Gnanadhas et al., 2015). Thus, we extrapolate that the same treatment could be used in patients with recurrent chronic empyemas due to *P. aeruginosa* biofilm, as in our presented patient.

While limitations exist, this report is, to our knowledge, the first to utilize intrapleural dornase alfa and amikacin to dissolve and treat a biofilm-like structure of the pleural cavity. Previously, Deng and colleagues have shown that DNase effectively inhibits early biofilm formation (Deng et al., 2022). However, no *in-vitro* studies have assessed the ability of DNase to treat mature biofilms. Moving forward, this method could be improved by measuring clearance of the biofilm using laboratory testing rather than imaging alone.

Data availability statement

The original contributions presented in the study are included in the article/Supplementary Material, further inquiries can be directed to the corresponding author.

Ethics statement

The studies involving humans were approved by Institutional Review Board-approved investigational protocols NIH IRB: 06C0014 and 93I0119. The studies were conducted in accordance with the local legislation and institutional requirements. The participants provided their written informed consent to participate in this study. Written informed consent was obtained from the individual(s) for the publication of any potentially identifiable images or data included in this article.

Author contributions

AG: Writing – original draft, Writing – review & editing, Investigation, Visualization. CL: Writing – review & editing, Investigation, Data curation, Methodology, Project administration. LF: Writing – review & editing, Data curation, Investigation, Methodology, Project administration. RR: Writing – review & editing, Investigation. IA: Conceptualization, Writing – review & editing. KF: Conceptualization, Writing – review & editing, Investigation. KF: Conceptualization, Resources, Supervision, Writing – review & editing. SC: Conceptualization, Methodology, Project administration, Supervision, Writing – review & editing.

Funding

The author(s) declare that financial support was received for the research, authorship, and/or publication of this article. This research was supported fully or in part by the Intramural Research Program of the National Institutes of Health, NHLBI, and NCI (AG, RR, IA, KPF, and SC). Funding is also from MRC (UK) Grant: MC_UU_00031/7 (KMF).

Acknowledgments

The authors would like to thank Dr. Steven M. Holland, Scientific Director of NIAID, for his unwavering support and assistance in the care of this patient.

Conflict of interest

The authors declare that the research was conducted in the absence of any commercial or financial relationships that could be construed as a potential conflict of interest.

Publisher's note

All claims expressed in this article are solely those of the authors and do not necessarily represent those of their affiliated organizations, or those of the publisher, the editors and the reviewers. Any product that may be evaluated in this article, or claim that may be made by its manufacturer, is not guaranteed or endorsed by the publisher.

Supplementary material

The Supplementary Material for this article can be found online at: https://www.frontiersin.org/articles/10.3389/fcimb.2024.1458652/full#supplementary-material

References

Allesen-Holm, M., Barken, K. B., Yang, L., Klausen, M., Webb, J. S., Kjelleberg, S., et al. (2006). A characterization of DNA release in *Pseudomonas aeruginosa* cultures and biofilms. *Mol. Microbiol.* 59, 1114–1128. doi: 10.1111/j.1365-2958.2005.05008.x

Azevedo, I., Oliveira, R. L., and Ugalde, P. A. (2020). Management of postpneumonectomy empyema and bronchopleural fistula. *Shanghai Chest.* 5. doi: 10.21037/shc.2020.03.11

Bedawi, E. O., Ricciardi, S., Hassan, M., Gooseman, M. R., Asciak, R., Castro-Añón, O., et al. (2023). ERS/ESTS statement on the management of pleural infection in adults. *Eur. Respir. J.* 61. doi: 10.1183/13993003.01062-2022

Clagett, O. T., and Geraci, J. E. (1963). A procedure for the management of postpneumonectomy empyema. *J. Thorac. Cardiovasc. Surg.* 45, 141–145. doi: 10.1016/S0022-5223(19)32877-6

Deng, W., Lei, Y., Tang, X., Li, D., Liang, J., Luo, J., et al. (2022). DNase inhibits early biofilm formation in *Pseudomonas aeruginosa*- or *Staphylococcus aureus*-induced empyema models. *Front. Cell Infect. Microbiol.* 12, 917038. doi: 10.3389/fcimb.2022.917038

Denlinger, C. E. (2010). Eloesser flap tthoracostomy window. *Operative Techniques Thorac. Cardiovasc. Surgery.* 15, 61–69. doi: 10.1053/j.optechstcvs.2010.03.003

Deschamps, C., Allen, M. S., Miller, D. L., Nichols, F. C. 3rd, and Pairolero, P. C. (2001). Management of postpneumonectomy empyema and bronchopleural fistula. *Semin. Thorac. Cardiovasc. Surg.* 13, 13–19. doi: 10.1053/stcs.2001.22495

Gnanadhas, D. P., Elango, M., Datey, A., and Chakravortty, D. (2015). Chronic lung infection by *Pseudomonas aeruginosa* biofilm is cured by L-Methionine in combination with antibiotic therapy. *Sci. Rep.* 5, 16043. doi: 10.1038/srep16043

Koo, H., Allan, R. N., Howlin, R. P., Stoodley, P., and Hall-Stoodley, L. (2017). Targeting microbial biofilms: current and prospective therapeutic strategies. *Nat. Rev. Microbiol.* 15, 740–755. doi: 10.1038/nrmicro.2017.99

Kovačević, T., Avram, S., Milaković, D., Špirić, N., and Kovačević, P. (2016). Therapeutic monitoring of amikacin and gentamicin in critically and noncritically ill patients. *J. Basic Clin. Pharm.* 7, 65. doi: 10.4103/0976-0105.183260

Lacey, K. A., Serpas, L., Makita, S., Wang, Y., Rashidfarrokhi, A., Soni, C., et al. (2023). Secreted mammalian DNases protect against systemic bacterial infection by digesting biofilms. *J. Exp. Med.* 220. doi: 10.1084/jem.20221086

Lauková, L., Konečná, B., Janovičová, Ľ, Vlková, B., and Celec, P. (2020). Deoxyribonucleases and their applications in biomedicine. *Biomolecules.* 10. doi: 10.3390/biom10071036

Rahman, N. M., Maskell, N. A., West, A., Teoh, R., Arnold, A., Mackinlay, C., et al. (2011). Intrapleural use of tissue plasminogen activator and DNase in pleural infection. *N Engl. J. Med.* 365, 518–526. doi: 10.1056/NEJMoa1012740

Schneiter, D., Cassina, P., Korom, S., Inci, I., Al-Abdullatief, M., Dutly, A., et al. (2001). Accelerated treatment for early and late postpneumonectomy empyema. *Ann. Thorac. Surg.* 72, 1668–1672. doi: 10.1016/S0003-4975(01)03083-1

Teixeira, L. R., Sasse, S. A., Villarino, M. A., Nguyen, T., Mulligan, M. E., and Light, R. W. (2000). Antibiotic levels in empyemic pleural fluid. *Chest.* 117, 1734–1739. doi: 10.1378/chest.117.6.1734

Thomas, R., Piccolo, F., Miller, D., MacEachern, P. R., Chee, A. C., Huseini, T., et al. (2015). Intrapleural fibrinolysis for the treatment of indwelling pleural catheter-related symptomatic loculations: A multicenter observational study. *Chest.* 148, 746–751. doi: 10.1378/chest.14-2401

Thys, J. P., Serruys-Schoutens, E., Rocmans, P., Herchuelz, A., Vanderlinden, M. P., and Yourassowsky, E. (1984). Amikacin concentrations in uninfected postthoracotomy pleural fluid and in serum after intravenous and intrapleural injection. *Chest.* 85, 502–505. doi: 10.1378/chest.85.4.502

Thys, J. P., Vanderhoeft, P., Herchuelz, A., Bergmann, P., and Yourassowsky, E. (1988). Penetration of aminoglycosides in uninfected pleural exudates and in pleural empyemas. *Chest.* 93, 530–532. doi: 10.1378/chest.93.3.530

Yin, R., Cheng, J., Wang, J., Li, P., and Lin, J. (2022). Treatment of Pseudomonas aeruginosa infectious biofilms: Challenges and strategies. *Front. Microbiol.* 13. doi: 10.3389/fmicb.2022.955286

Yin, W., Wang, Y., Liu, L., and He, J. (2019). Biofilms: The microbial "Protective Clothing" in extreme environments. *Int. J. Mol. Sci.* 20. doi: 10.3390/ijms20143423

Zaheer, S., Allen, M. S., Cassivi, S. D., Nichols, F. C. 3rd, Johnson, C. H., Deschamps, C., et al. (2006). Postpneumonectomy empyema: results after the Clagett procedure. *Ann. Thorac. Surg.* 82, 279–86;discussion 86-7. doi: 10.1016/j.athoracsur.2006.01.052

frontiers | Frontiers in Cellular and Infection Microbiology

TYPE Original Research
PUBLISHED 21 January 2025
DOI 10.3389/fcimb.2024.1508016

OPEN ACCESS

EDITED BY
Maria Gabriela Paraje,
National University of Cordoba, Argentina

REVIEWED BY
Li Li,
South China University of Technology, China
Zhenbo Xu,
South China University of Technology, China
Olivier Braissant,
University of Basel, Switzerland

*CORRESPONDENCE
Tinatini Tchatchiashvili
Tinatini.tchatchiashvili@med.uni-jena.de

RECEIVED 08 October 2024
ACCEPTED 23 December 2024
PUBLISHED 21 January 2025

CITATION
Tchatchiashvili T, Jundzill M, Marquet M, Mirza KA, Pletz MW, Makarewicz O and Thieme L (2025) CAM/TMA-DPH as a promising alternative to SYTO9/PI for cell viability assessment in bacterial biofilms. *Front. Cell. Infect. Microbiol.* 14:1508016. doi: 10.3389/fcimb.2024.1508016

CAM/TMA-DPH as a promising alternative to SYTO9/PI for cell viability assessment in bacterial biofilms

Tinatini Tchatchiashvili[1,2]*, Mateusz Jundzill[1,2], Mike Marquet[1], Kamran A. Mirza[1,2], Mathias W. Pletz[1,2], Oliwia Makarewicz[1,2] and Lara Thieme[1,2]

[1]Institute of Infectious Disease and Infection Control, Jena University Hospital, Friedrich-Schiller-University Jena, Jena, Germany, [2]Institute of Infectious Disease and Infection Control, Member of the Leibniz Center for Photonics in Infection Research (LPI), Jena, Germany

Introduction: Accurately assessing biofilm viability is essential for evaluating both biofilm formation and the efficacy of antibacterial treatments. Traditional SYTO9 and propidium iodide (PI) live/dead staining in biofilm viability assays often ace challenges due to non-specific staining, limiting precise differentiation between live and dead cells. To address this limitation, we investigated an alternative staining method employing calcein acetoxymethyl (CAM) to detect viable cells based on esterase activity, and 1-(4-trimethylammoniumphenyl)-6-phenyl-1,3,5-hexatriene p-toluenesulfonate (TMA-DPH) to assess the remaining biofilm population.

Methods: Biofilms of *Pseudomonas aeruginosa, Klebsiella pneumoniae*, *Staphylococcus aureus*, and *Enterococcus faecium* were matured and exposed to varying concentrations of antibiotics or sterile medium. Biofilm viability was assessed using CAM/TMA-DPH or SYTO9/PIstaining, followed by analysis with confocal laser scanning microscopy (CLSM) and ImageJ-based biofilm surface coverage quantification. Viability findings were compared with colony-forming units (CFU/mL), a standard microbial viability measure.

Results: CAM/TMA-DPH staining demonstrated strong positive correlations with CFU counts across all bacterial species (r = 0.59 - 0.91), accurately reflecting biofilm vitality. In contrast, SYTO9/PI staining consistently underestimated the viability of untreated biofilms, particularly in *Klebsiella pneumoniae*, where a negative correlation with CFU/mL was observed (r = −0.04). Positive correlations for SYTO9/PI staining were noted in other species (r = 0.65 - 0.79). These findings underscore the limitations of membrane integrity-based staining methods and highlight the advantages of metabolic-based probes like CAM/TMA-DPH.

Discussion: Our findings suggest that CAM/TMA-DPH staining provides a promising alternative to SYTO9/PI for cell viability assessment in bacterial biofilms, highlighting the advantages of metabolic-based probes over traditional membrane integrity

assays. The consistency of CAM/TMA-DPH staining across different bacterial species underscores its potential to advance studies on biofilm and contribute to the development of more effective anti-biofilm treatments, which is essential for clinical management of biofilm-associated infections.

KEYWORDS

biofilm, viability, staining, metabolism, calcein acetoxymethyl, live/dead assay

1 Introduction

Biofilms represent complex microbial aggregates enclosed within a self-produced extracellular polymeric substance (EPS) (Donlan, 2002), providing structural stability and protection to the bacterial communities in various environments (Kim and Lee, 2016). Biofilms are associated with numerous tissue and device-related infections, such as native and prosthetic valve endocarditis or cystic fibrosis (CF) (Costerton et al., 1999). Bacteria in biofilms demonstrate increased tolerance to antibiotics and the immune system, compared to their planktonic (free-living) counterparts (Fux et al., 2005). This heightened phenotypic resistance is partly due to the EPS, which acts as a barrier that impedes antibiotic penetration and restricts immune cell access. Moreover, altered gene expression and metabolic changes within the biofilm contribute to heterogeneous cell populations with diverse physiological states (Rani et al., 2007), a key factor in their resilience and treatment resistance (Sadiq et al., 2017). Addressing biofilm-associated infections therefore remains a significant challenge, leading to ongoing research to develop compounds that can effectively disrupt and eliminate biofilms (Taylor et al., 2014; Li and Lee, 2017). Accurate *in vitro* assessment of bacterial cell viability within biofilms is essential for determining the efficacy of these anti-biofilm agents during drug development (Costerton et al., 1999).

Biofilm research employs a variety of microbiological, chemical, physical, and molecular techniques, each with distinct advantages and limitations (Azeredo et al., 2017). Among the most utilized quantitative biochemical methods are crystal violet (CV) staining, or colorimetric metabolic assays based on tetrazolium salts. CV targets the biomass of biofilms, specifically binding to negatively charged molecules, such as acidic polysaccharides and other components in the biofilm matrix without distinguishing between viable and non-viable cells. CV staining is straightforward and widely used for quantifying biofilm biomass, but it can be error-prone due to inconsistencies in staining intensity, incomplete removal of excess dye, and variability in washing and drying steps, all of which can lead to inaccuracies in biofilm quantification (Wilson et al., 2017). Tetrazolium-based assays, such as reduction of XTT (2,3-bis(2-methoxy-4-nitro-5-sulfophenyl)-5-[(phenylamino)carbonyl]-2H-tetrazolium hydroxide) and TTC (2,3,5-triphenyl-2H-tetrazolium chloride) are widely used to assess the respiratory activity of cells within biofilms. These techniques provide efficient, indirect biofilm quantification but are limited in their ability to visualize the detailed structure and organization of biofilms. They generally have low sensitivity thresholds, which can reduce accuracy, especially for biofilms with sparse biomass or those containing anaerobic organisms (Stewart and Franklin, 2008; Azeredo et al., 2017). These limitations make these methods less effective for comprehensive biofilm analysis, particularly in studies requiring precise structural or viability information.

In contrast, confocal laser scanning microscopy (CLSM) provides a robust approach for biofilm analysis by enabling direct spatial visualization of biofilm architecture and its bacterial constituents. Through the use of targeted fluorescent probes, CLSM allows for specific labelling of distinct bacterial components, facilitating detailed examination of biofilm structure, organization, and cell viability (Bridier and Briandet, 2014). Commonly used fluorescent probes for evaluating biofilm vitality include SYTO9 and propidium iodide (PI), which are both nucleic acid-binding dyes. SYTO9 (green-fluorescent stain) is a membrane-permeable dye, while PI (red-fluorescent stain) penetrates only bacteria with compromised cell membranes, such as dead or dying cells, and is excluded from intact cells (Bunthof et al., 2001). In the analysis of SYTO9/PI-stained bacteria, cells emitting green fluorescence are classified as the total cell population (alive and dead), whereas those exhibiting additional red fluorescence are identified as dead. To distinguish fluorescent signals of vital cells the green and red channels should be subtracted (Boulos et al., 1999) (Figure 1A). However, researchers have reported several limitations of SYTO9/PI dual staining, despite its use in biofilm research for over 20 years. Both false positive and negative live/dead staining patterns have been observed in various bacterial species due to off-label target binding (Stiefel et al., 2015; Rosenberg et al., 2019), changes in membrane potential (Kirchhoff and Cypionka, 2017) or dye excretion (Minero et al., 2024). Additionally, the SYTO9/PI staining combination evaluates cell viability status by merely assessing the membrane integrity, overlooking metabolic activity. These limitations necessitate the exploration of alternative staining methods that can more accurately evaluate cell viability in biofilms.

As an alternative approach, we employed a combination of calcein acetoxymethyl (CAM) and 1-(4-trimethylammoniumphenyl)-6-phenyl-1,3,5-hexatriene p-toluenesulfonate (TMA-DPH). To the best

10.3389/fcimb.2024.1508016

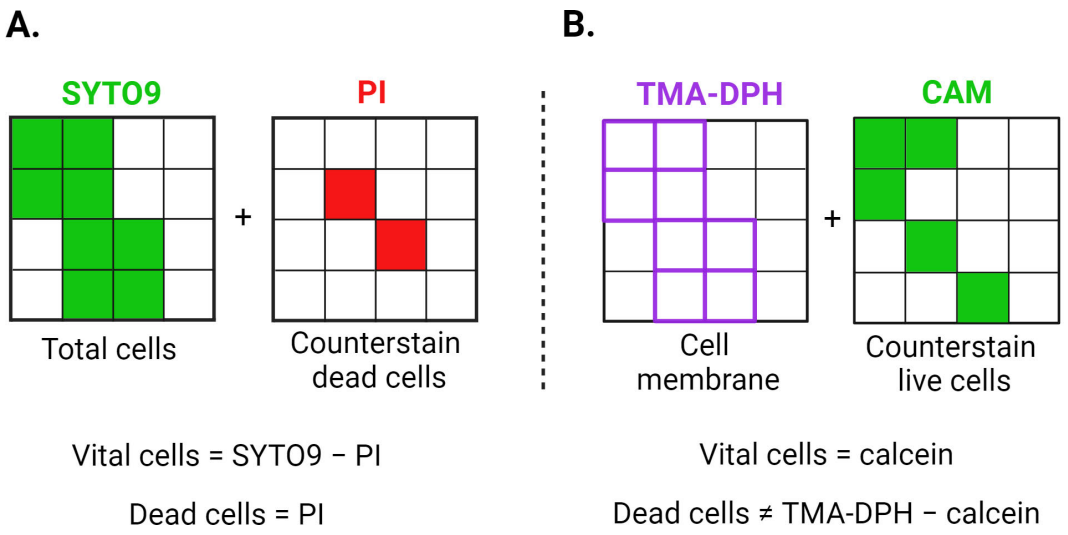

FIGURE 1
Graphical representation of the theoretical staining principles of SYTO9/PI **(A)** and CAM/TMA-DPH **(B)** dyes. One small square corresponds to one bacterium, while the entire large square represents the total image area recorded via CLSM. PI can only penetrate cells with compromised membranes, whereas SYTO9 can enter both intact and damaged cells. Both SYTO9 and PI intercalate with DNA, staining the entire cell. TMA-DPH intercalates with the lipid bilayer of bacterial membranes, staining the cell boundary without distinguishing between live and dead cells. Cellular esterases in viable cells convert CAM into fluorescent calcein, causing the entire cell to fluoresce. CAM, calcein acetoxymethyl; PI, propidium iodide; TMA-DPH, 1-(4-trimethylammoniumphenyl)-6-phenyl-1,3,5-hexatriene p-toluenesulfonate. Created in BioRender. Röll, D. (2024) BioRender.com/f07q170.

of our knowledge, while both dyes are well-established, this is the first time these dyes have been used together for biofilm analysis. CAM, a non-fluorescent ester, permeates cell membranes and is converted by cellular esterases into fluorescent calcein, which is retained within vital cells due to its inability to cross intact membranes (Wiederschain, 2011; Tawakoli et al., 2013). This transformation enables CAM to differentiate between functionally active and inactive cells, as dead cells cannot hydrolyse or retain calcein.

To complement the visualization of remaining biofilm population, we repurposed the lipophilic fluorescent dye TMA-DPH which is commonly used in biophysics for studying cell membrane fluidity, dynamics, and lipid organization. The cationic trimethylammonium group of TMA-DPH interacts with the polar head groups of phospholipids, anchoring the dye in a specific orientation within the membrane (Yoon et al., 2011). This interaction helps TMA-DPH to stay in the membrane, making it suitable for studying membrane dynamics over time, but also for visualizing the cell membrane of both viable and non-viable bacteria (Figure 1B).

The study evaluated the reliability of the CAM/TMA-DPH assay in assessing biofilm viability compared to conventional SYTO9/PI staining. Mature biofilms of *Pseudomonas aeruginosa* (*P. aeruginosa*), *Klebsiella pneumoniae* (*K. pneumoniae*), *Staphylococcus aureus* (*S. aureus*), and *Enterococcus faecium* (*E. faecium*) were treated with increasing concentrations of antibiotics and stained with either CAM/TMA-DPH or SYTO9/PI. CLSM images of the biofilms were quantitatively analyzed via Biofilm Viability Checker (Mountcastle et al., 2021), and results were compared to colony-forming units (CFU/mL), the microbiological standard for assessing viability.

2 Materials and methods

2.1 Bacterial strains and antibiotics

This study used different Gram-positive and Gram-negative bacterial species available as laboratory stocks. The strains included *S. aureus* ATCC 43300, with a vancomycin minimum inhibitory concentration (MIC) of 1 mg/L; an *E. faecium* endocarditis isolate, MIBI701, exhibiting a gentamicin MIC of 32 mg/L; a mucoid *P. aeruginosa* strain, MIBI685, isolated from a cystic fibrosis patient with a ciprofloxacin MIC of 0.125 mg/L; and a bloodstream isolate of *K. pneumoniae*, IIMK 217, with a ciprofloxacin MIC of 0.0625 mg/L. The clinical isolates with various clinical backgrounds were previously collected in studies approved by the ethical committee of Jena University Hospital (3852/07-13 and 3694-02/13). MICs of vancomycin (Sigma Aldrich, St. Louis, United States), gentamicin (TCI Europe, Zwijndrecht, Belgium), and ciprofloxacin (AppliChem GmbH, Darmstadt, Germany) were determined by the broth microdilution method according to EUCAST guideline (ISO 20776-2:2021).

2.2 Testing of the anti-biofilm activity of selected antibiotics by CFU counting

Bacterial overnight cultures were prepared in either Todd Hewitt (TH) (*E. faecium*) or Mueller-Hinton (MH) broth (all other strains). Subsequently, the optical density (OD) was measured at 600 nm using the Thermo Scientific™ Multiskan™ GO (Thermo Fischer Scientific, Waltham, MA, USA) and adjusted to an OD of 0.08,

corresponding to approximately 10^7–10^8 CFU/mL (Zhang et al., 2015). Biofilms were grown in triplicate by adding 200 µL of the adjusted cultures per well in 96-well flat-bottom glass microtiter plates (Greiner Bio-one, Kremsmünster, Austria). The plates were placed in a humidified chamber and incubated at 37°C with 5% CO_2 without shaking for 48 hours. Before antibiotic treatment, the supernatants containing planktonic bacteria were carefully removed. The antibiotics were prepared as 10 mg/mL stock solutions in distilled water and freshly diluted to the needed concentrations in the respective broth (see above). As biofilms are more tolerant to antibiotics, the concentrations for biofilm treatments were chosen higher than the determined MICs. Antibiotic or mock solutions (medium only) of 200 µL per well were added for 24 h to the mature biofilms. For CFU determination, the drop plate method was employed as described by Thieme et al (Thieme et al., 2020). In brief, biofilms were washed twice with 200 µL of sterile saline to remove non-adherent cells, carefully scraped off using a loop, and serially diluted. For *S. aureus*, *E. faecium*, and *K. pneumoniae*, 10 µL aliquots of the serial dilutions were deposited in triplicate on TH or MH agar plates. In contrast, *P. aeruginosa* suspensions were conventionally plated (100 µL per plate) due to the mucoid phenotype, which results in the formation of large colonies. After overnight incubation at 37°C, bacterial colonies were counted, and CFU/mL values were calculated. Three independent biological experiments were conducted, each comprising three replicates.

2.3 Fluorescent staining and imaging

For fluorescent image analysis, biofilms were grown and treated as described above in parallel to the CFU assays. For fluorescent staining, an aqueous working solution of CAM and TMA-DPH (both purchased from Thermo Fisher Scientific Inc., Waltham, MA, USA) was prepared by adding 2 µL of TMA-DPH and 100 µL of CAM to 900 µL of distilled water, resulting in concentrations of 20 µM and 100 µM for TMA-DPH and CAM, respectively (Calcein AM, cell-permeant green and blue dyes, n.d). The SYTO9/PI staining working solution (FilmTracer™ LIVE/DEAD® Biofilm Viability Kit, Thermo Fisher Scientific Inc.) was prepared according to the manufacturer's protocol, with 3 µL of SYTO9 stain and 3 µL of PI stain in 1 mL of distilled water (Filmtracer™ LIVE/DEAD™ Biofilm Viability Kit, n.d). Intact, washed biofilms were subsequently stained by adding 50 µL of the respective staining solution per well. Samples were incubated for 20 min (stained with SYTO9/PI) or 60 min (stained with CAM/TMA-DPH) at room temperature, protected from light. Subsequently, the staining solutions were carefully removed, and the respective fresh broth was added to prevent the biofilms from drying up during microscopy. Toxic effects of the single dyes on the biofilms independent from the antibiotic treatment were excluded by prior CFU analysis of stained versus unstained biofilms.

Biofilms were visualized using CLSM on an LSM 980 microscope system (Carl Zeiss AG, Oberkochen, Germany), equipped with air objectives of 63×/0.65, 40×/0.65, and 20×/0.65 magnifications. Three independent microscopy experiments were conducted, each comprising three replicates. The SYTO9, CAM, and PI fluorophores were excited using an argon laser with a wavelength of 488 nm. SYTO9 and CAM emitted in the green channel at 522 nm, while PI emitted in the red channel at 635 nm. TMA-DPH was excited at a wavelength of 405 nm, with emission detected in the blue channel at 430 nm. For each sample, three observation fields were randomly selected across three replicates to ensure representativeness. An area of approximately 200 µm (X) × 200 µm (Y) was scanned at 1 µm intervals along the Z-axis (Z-stack). Z-stacks were acquired starting from the first plane where bacteria were detected. Typically, a single Z-stack was recorded per well. However, in wells where biofilms appeared non-homogeneous or exhibited variations across the well, multiple Z-stacks were captured to ensure accurate representation. The pinhole was adjusted to 0.95 Airy Units (corresponding to 1 µm). Images were processed using the ZEN 9.0 Black software package (Carl Zeiss AG).

2.4 Computed image analysis

The open-source tool Biofilm Viability Checker (Mountcastle et al., 2021) was used for quantitative analysis of biofilm micrographs. We adapted the original code (Mountcastle et al., 2021) to process images stained with the CAM/TMA-DPH assay (see the section 2.6). First, we adjusted the analysis to utilize the appropriate channels for CAM (green) and TMA-DPH (blue). Second, channel subtraction was excluded, as the two dyes target distinct cellular components, rendering subtraction unnecessary. Additionally, we omitted the background subtraction step, as neither dye stains extracellular DNA (eDNA). Furthermore, the tool was reprogrammed to report the absolute count of stained pixels rather than percentage values for improved accuracy. Biofilm surface area coverage was then calculated as a percentage using the formula: Surface area coverage (%) = (Biofilm covered area/Total area) × 100 (Halsted et al., 2022). The total pixel area was set at 2024 × 2024, based on the micrograph dimensions. This method was consistently applied to each image within a confocal Z-stack.

2.5 Statistical analysis

To assess data normality, a Shapiro-Wilk test was conducted using GraphPad Software (version 9.4.0, Boston, MA, USA), indicating a deviation from normality. All statistical analyses were then performed using the R Statistical Software (v. 4.4.1, R Core Team 2021, Vienna, Austria) using dplyr package (v. 1.1.4) (Wickham, 2014). Spearman's rank correlation was calculated with the cor.test function (method = "spearman") to evaluate the association between image analysis measurements and corresponding CFU values. Data visualization was carried out in GraphPad Software, and a p-value < 0.05 was considered statistically significant for all analyses.

2.6 Code availability

The macro script was adapted from (Mountcastle et al., 2021), and the modified version is available at: https://github.com/Tiktcha/Biofilm-Viability-Checker.

10.3389/fcimb.2024.1508016

3 Results

3.1 Qualitative analysis of CLSM micrographs

To determine the staining quality at the individual level, CLSM images were captured at the highest resolution for single and combined staining of *P. aeruginosa, S. aureus*, *K. pneumoniae* and *E. faecium* biofilms (Figure 2).

In all species SYTO9 and PI exhibited strong intracellular staining, clearly delineating septum formation within the cells, which indicates ongoing cell division and membrane retraction between the developing daughter cells. Notably, in *P. aeruginosa* rods, green structures are visible under SYTO9 staining, potentially indicating the release of eDNA into the biofilm matrix. Interestingly, this phenomenon is much less pronounced with PI. In the combined staining, bacterial cells penetrated by both dyes appear yellow due to the overlap of the two fluorescence channels. However, distinct populations of cells are observed: those stained predominantly red (presumably dead) and those stained green (presumably alive). Notably, red fluorescence appears to be leaking from some cells visible as a red blur, which is indicative of compromised membrane integrity, a hallmark of cell death.

Using the membrane-specific dye TMA-DPH, the outer cell layer of all species could be specifically visualized as violet-colored cell borders. In contrast, the CAM dye produced an almost homogeneous intracellular staining. However, in some cells, the staining appeared uneven, suggesting possible septum formation. Interestingly, in Gram-negative species, combined staining with CAM and TMA-DPH revealed that the violet membrane dye signal was barely visible when cells exhibited strong green fluorescence from CAM, clearly highlighting them (Figure 2). In contrast, for Gram-positive species, the hypothesized outcome was observed during combined staining: CAM stained the cytoplasm, while TMA-DPH marked the membrane.

3.2 Qualitative analysis of biofilm micrographs after antibiotic treatment

The staining efficacy of SYTO9/PI and CAM/TMA-DPH was evaluated at the population level in both untreated and antibiotic-treated biofilms. Untreated *P. aeruginosa* biofilms stained with SYTO9/PI exhibited a weak SYTO9 and strong PI signal, contrasting with strong CAM fluorescence observed in biofilms stained with CAM/TMA-DPH (Figure 3). As expected, increasing

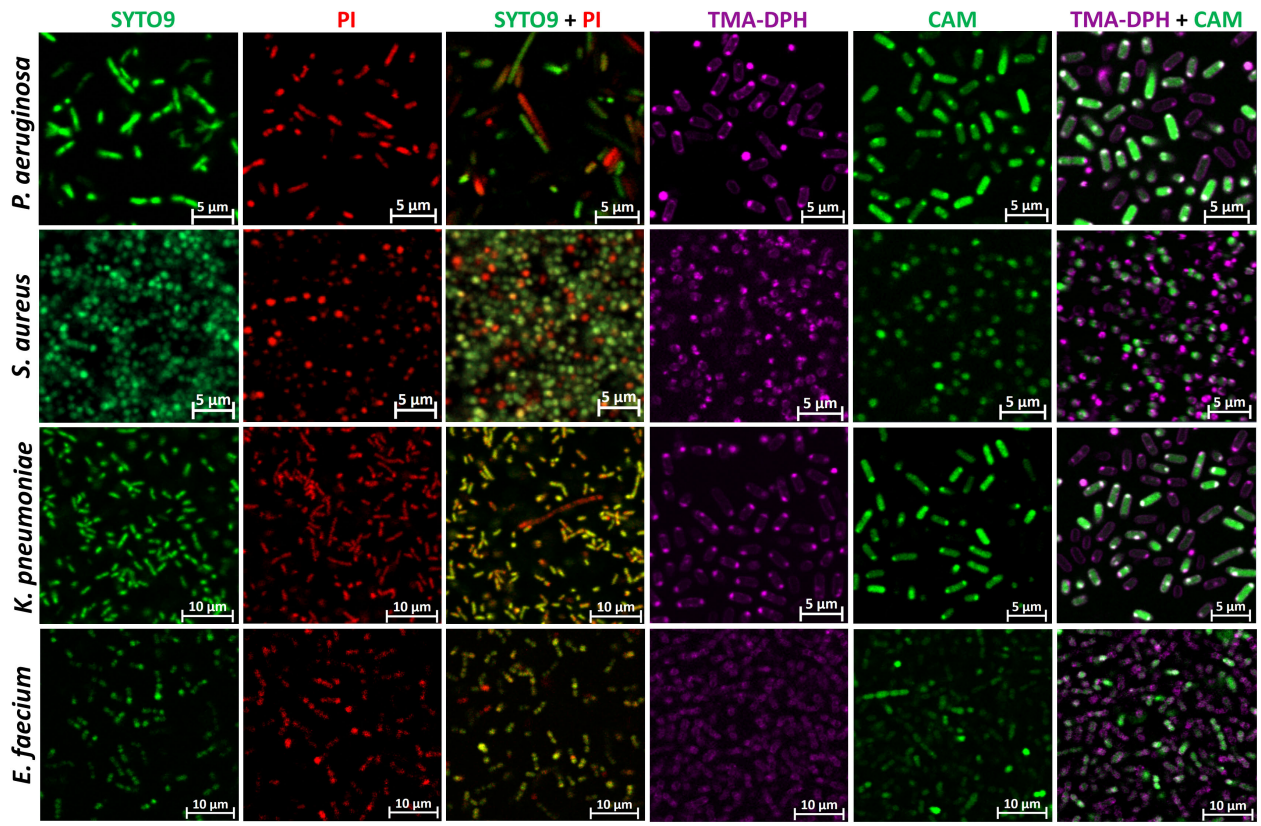

FIGURE 2
Representative CLSM images of single and combination staining of different dyes in *P. aeruginosa*, *S. aureus*, *K. pneumoniae*, and *E. faecium* biofilms. CAM, calcein acetoxymethyl; PI, propidium iodide; TMA-DPH, 1-(4-trimethylammoniumphenyl)-6-phenyl-1,3,5-hexatriene p-toluenesulfonate. Images were captured from three randomly selected fields per sample, with similar observations across all replicates. Imaging was conducted at 63× magnification.

10.3389/fcimb.2024.1508016

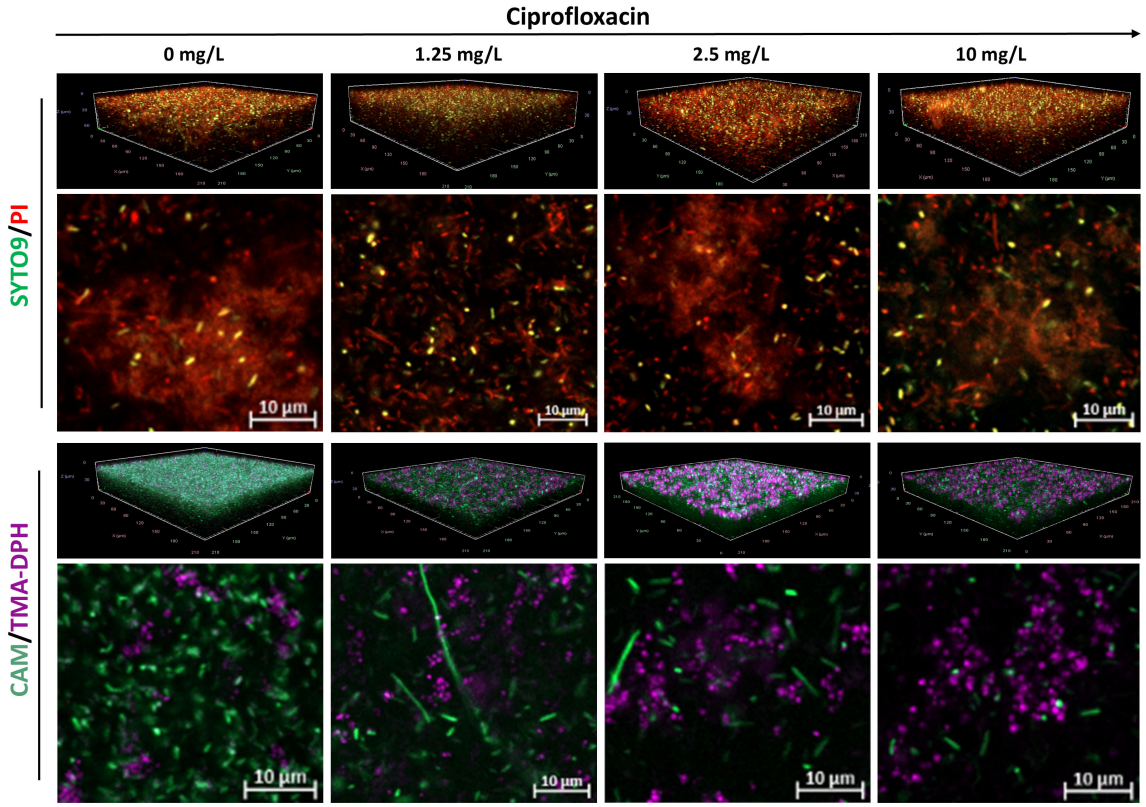

FIGURE 3
Representative CLSM images of *P. aeruginosa* MIBI685 biofilms treated with increasing concentrations of ciprofloxacin. Shown are 3D visualizations of the biofilms and representative X-Y intersections, stained with SYTO/PI (upper panel) or CAM/TMA-DPH (lower panel). CAM, calcein acetoxymethyl; PI, propidium iodide; TMA-DPH, 1-(4-trimethylammoniumphenyl)-6-phenyl-1,3,5-hexatriene p-toluenesulfonate. Images were captured from three randomly selected fields per sample, with similar observations across all replicates. Imaging was conducted at 40× magnification.

concentrations of ciprofloxacin led to a progressive decrease in CAM-stained cells, while concurrently increasing the fluorescence intensity of TMA-DPH. Conversely, *P. aeruginosa* biofilms stained with SYTO9/PI, showed thick aggregates of PI-stained matrix components and cells regardless the antibiotic treatment (Figure 3).

In the CAM and PI channels, morphological changes toward elongated rod shapes were observed in response to ciprofloxacin treatment. Both the length and the number of these cells progressively decreased with increasing concentrations of ciprofloxacin.

In untreated *K. pneumoniae* samples, SYTO9/PI-stained micrographs displayed a dense biofilm architecture characterized by red/yellowish fluorescence, whereas antibiotic-treated biofilms exhibited significant disruption of the biofilm structure, with no observable staining of matrix components (Figure 4). Conversely, *K. pneumoniae* biofilms stained with CAM/TMA-DPH showed a decrease in calcein fluorescence and an increase in TMA-DPH fluorescence with increasing concentrations of ciprofloxacin, similar to the observations in *P. aeruginosa* biofilms. Also here, morphological changes to elongated rods were observed due to ciprofloxacin treatment, but those were visible in the CAM and SYTO9 Channels (Figure 4).

Unlike Gram-negative species, untreated *S. aureus* biofilms stained with SYTO9/PI showed strong green and weak red fluorescence (Figure 5). As antibiotic concentrations increased, the PI signal became more intense. Remarkably, *S. aureus* biofilms treated with 2048 mg/L of vancomycin exhibited unusually intense SYTO9 fluorescence. Furthermore, untreated biofilms stained with CAM/TMA-DPH displayed strong green fluorescence, which predictably diminished as antibiotic concentrations increased (Figure 5).

Compared to other species, *E. faecium* exhibited relatively weaker biofilm formation (Figure 6). Interestingly, similar staining patterns were observed between the SYTO9/PI and CAM/TMA-DPH staining techniques. Untreated biofilms stained with either SYTO9/PI or CAM/TMA-DPH predominantly exhibited green fluorescence but lacked a dense structure or eDNA, as indicated by PI staining. The green fluorescence progressively diminished with increasing gentamicin concentrations, correlating with the disruption of biofilm structure in treated samples (Figure 6).

3.3 Computational image analysis and comparison with CFU counts

To assess biofilm viability in CLSM micrographs of untreated and antibiotic-treated biofilms that were stained with SYTO9/PI or CAM/TMA-DPH, we quantified the respective surface coverage: either as the sum of the recorded calcein fluorescence signals, or as

10.3389/fcimb.2024.1508016

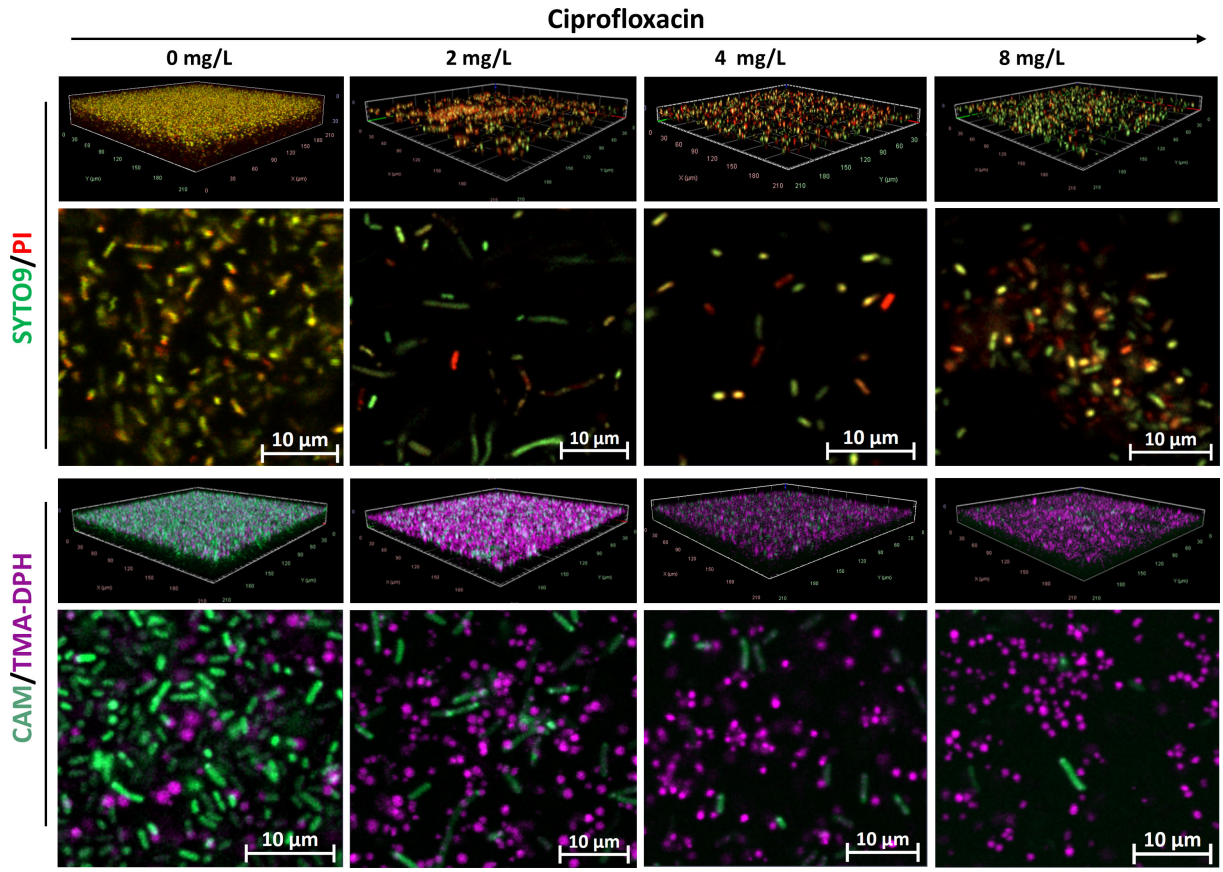

FIGURE 4
Representative CLSM images of *K. pneumoniae* IIMK217 biofilms treated with increasing concentrations of ciprofloxacin. Shown are 3D visualizations of the biofilms and representative X-Y intersections, stained with SYTO/PI (upper panel) or CAM/TMA-DPH (lower panel). CAM, calcein acetoxymethyl; PI, propidium iodide; TMA-DPH, 1-(4-trimethylammoniumphenyl)-6-phenyl-1,3,5-hexatriene p-toluenesulfonate. Images were captured from three randomly selected fields per sample, with similar observations across all replicates. Imaging was conducted at 40× magnification.

the difference of the SYTO9 – PI signals, subtracting the PI fluorescence from the SYTO9 fluorescence.

In untreated *P. aeruginosa* biofilms, the calcein-stained area was substantially larger than that stained by SYTO9 – PI, with respective coverage values of 56.80% ± 8.33% and 0.56% ± 0.14% (Figure 7A) (Supplementary Table 1). Similarly, at all tested ciprofloxacin concentrations, calcein-stained biofilms consistently showed higher area coverage compared to SYTO9 – PI-stained samples. A strong significant positive correlation (r = 0.91, p < 0.0001) was observed between calcein-stained area coverage and CFU counts in both untreated and treated *P. aeruginosa* biofilms. Conversely, SYTO9 – PI-stained biofilm area coverage exhibited significant but moderate correlation (r = 0.65, p = 0.02) with CFU counts (Figure 7A) (Supplementary Table 1).

Similar to *P. aeruginosa*, untreated *K. pneumoniae* biofilms showed higher calcein-stained area coverage compared to those stained with SYTO9 – PI, with mean values of 25.23% ± 12.35% and 1.0% ± 0.20%, respectively (Figure 7B). As the ciprofloxacin concentration increased, the calcein-stained area coverage decreased, showing a positive correlation (r = 0.59, p = 0.03) with viable cell counts obtained from CFU experiments. Contrarily, no correlation (r = – 0.04, p = 0.87) was observed between SYTO9-stained biofilm area coverage and CFU counts in *K. pneumoniae* biofilms (Figure 7B) (Supplementary Table 1). Notably, SYTO9/PI-stained biofilms treated with the highest concentration of ciprofloxacin showed greater SYTO9 – PI surface coverage compared to the untreated samples, with the mean values of 7.71% and 1.0%, respectively (Figure 7B) (Supplementary Table 1).

Similar to Gram-negative species, untreated *S. aureus* biofilms exhibited higher calcein-stained surface area coverage compared to those stained with SYTO9 – PI, albeit with a smaller difference (respective mean values of 85.85% ± 2.42% and 70.27% ± 6.99%). (Figure 7C). As antibiotic concentrations increased, calcein-stained surface area progressively decreased and showed a strong positive correlation (r = 0.88, p = 0.00015) with CFU counts. Interestingly, biofilms treated with 2048 mg/L vancomycin exhibited increased SYTO9 – PI area coverage, with mean value of 36.60% ± 5.94%, while biofilms stained with calcein showed lower area coverage with mean value of 26.76% ± 7.63 (Figure 7C) (Supplementary Table 1). However, there was a positive correlation between SYTO9-stained biofilm area coverage and the corresponding CFU counts (r = 0.74, p = 0.005).

In untreated *E. faecium* biofilms, areas stained with calcein or SYTO9 – PI covered approximately 4.13% ± 1.26% and 5.37% ±

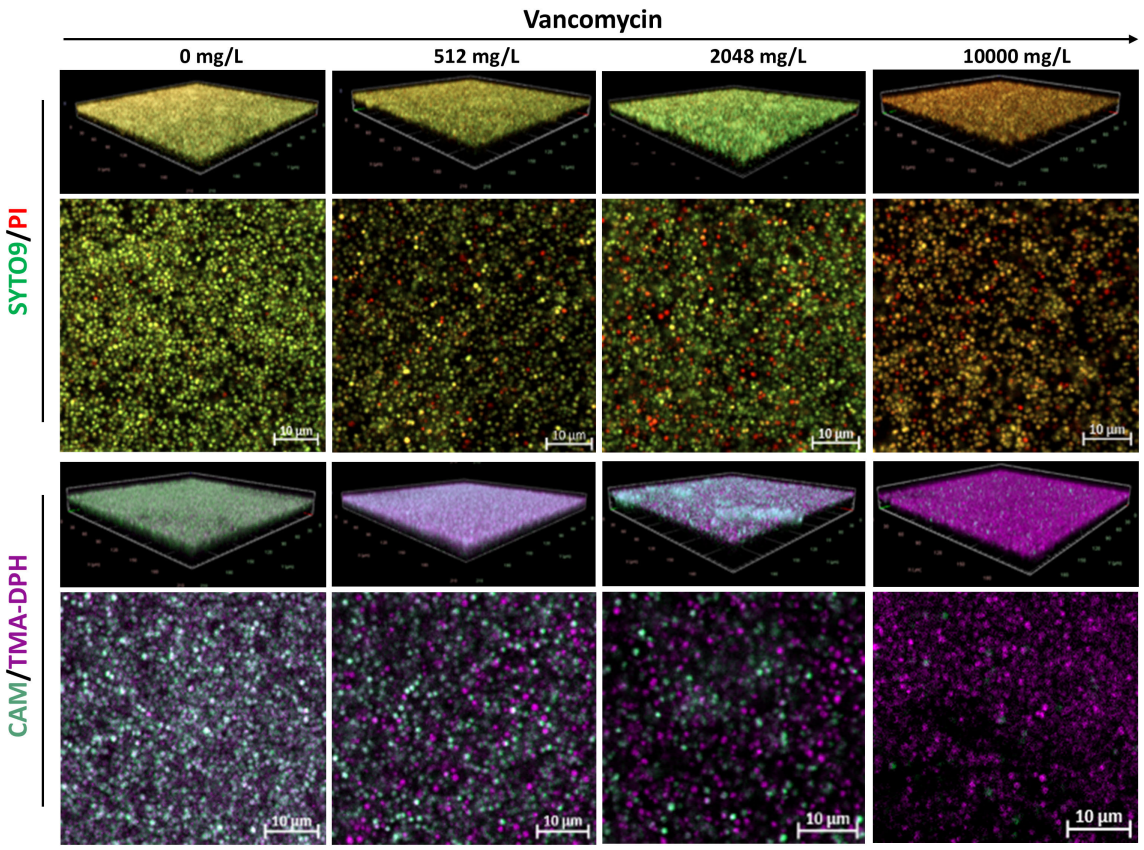

FIGURE 5
Representative CLSM images of S. aureus ATCC 43300 biofilms treated with increasing concentrations of vancomycin. Shown are 3D visualizations of the biofilms and representative X-Y intersections, stained with SYTO/PI (upper panel) or CAM/TMA-DPH (lower panel). CAM, calcein AM; PI, propidium iodide; TMA-DPH, 1-(4-trimethylammoniumphenyl)-6-phenyl-1,3,5-hexatriene p-toluenesulfonate. Images were captured from three randomly selected fields per sample, with similar observations across all replicates. Imaging was conducted at 40× magnification.

1.59% of the surface area, respectively (Figure 7D). A strong positive correlation was found between calcein-stained area coverage and viable cell counts (r = 0.83, p = 0.00083). Similarly, a significant positive correlation was observed between SYTO9/PI-stained area and CFU counts (r = 0.79, p = 0.001) (Figure 7D) (Supplementary Table 1).

4 Discussion

This study aimed to assess biofilm viability across diverse bacterial species using CAM/TMA-DPH staining as an alternative to the conventional SYTO9/PI method, leveraging CAM's ability to selectively stain live cells. The findings indicate that CAM/TMA-DPH staining demonstrates a strong correlation with viable cell counts across all tested species. This underscores the importance of incorporating assessments of cellular activity into biofilm viability evaluations, thereby addressing the limitations of membrane integrity-based methods, such as the SYTO9/PI approach.

CAM presents several advantages over SYTO9/PI staining for assessing bacterial biofilm viability. Its cleavage product, calcein, fluoresces solely within live cells due to its reliance on intracellular esterase activity (Wilson et al., 2017). This mechanism enables highly specific staining of viable cells with active metabolism. Unlike SYTO9/PI CAM's targeted fluorescence prevents calcein from accumulating in extracellular fluid, eliminating the need for extra wash steps and improving both the accuracy and efficiency of viability measurements (Wilson et al., 2017). Notably, CAM does not bind to eDNA, thereby enhancing staining precision by exclusively targeting live cells. This contrasts with SYTO9/PI, which is prone to intercalate with eDNA in biofilms (Rosenberg et al., 2019). Furthermore, calcein provides stable fluorescence, shows strong resistant to photobleaching, and remains unaffected by pH fluctuations (Hiraoka and Kimbara, 2002). In contrast, SYTO9/PI staining is more prone to photobleaching, resulting in reduced signal intensity over time (Stiefel et al., 2015). Despite these benefits, CAM's application in biofilm studies remains relatively uncommon.

Biofilms are highly heterogeneous communities consisting of various subpopulations with differing levels of viability (Stewart and Franklin, 2008). These subpopulations include viable but non-culturable (VBNC) cells (Pasquaroli et al., 2013; Dong et al., 2020), persisters (Lewis, 2007; Stewart and Franklin, 2008), dormant cells (Lewis, 2007), hollow membrane-enclosed vessels (Liu et al., 2023), and phenotypic variants such as small colony variants (SCVs) (Häußler, 2004). Calcein, which simultaneously

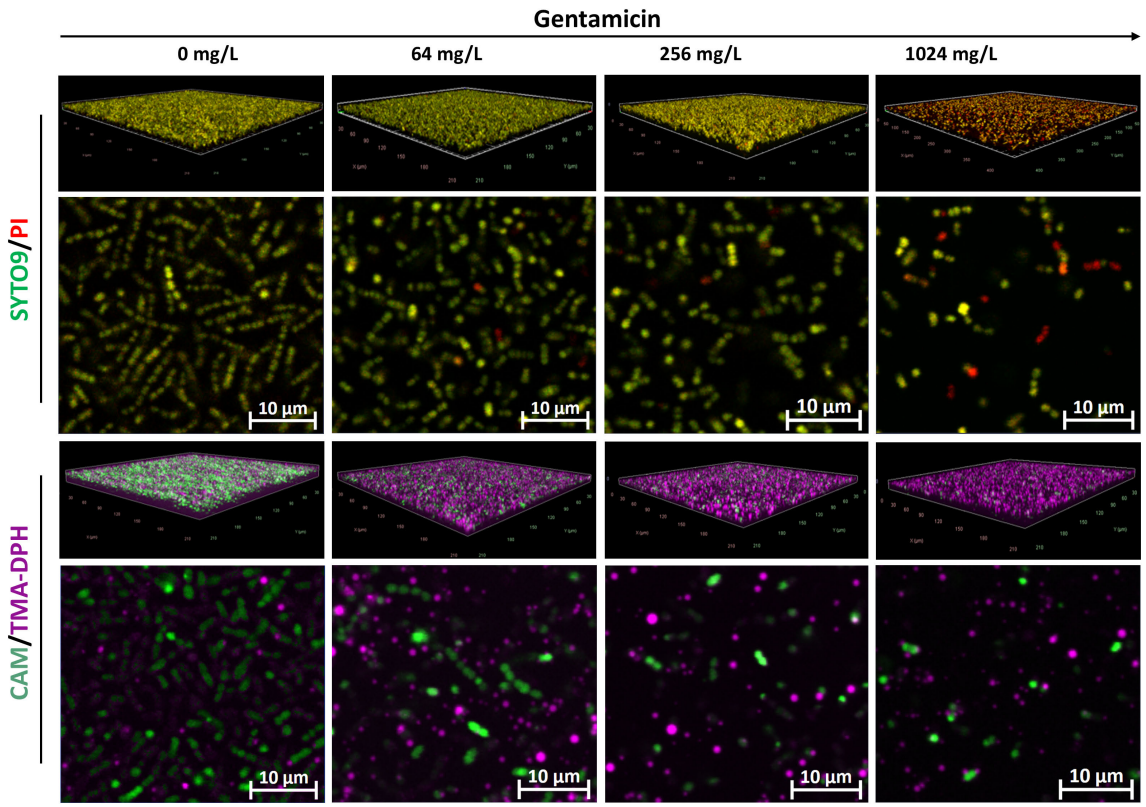

FIGURE 6
Representative CLSM images of *E. faecium* MIBI701 biofilms treated with increasing concentrations of gentamicin. Shown are 3D visualizations of the biofilms and representative X-Y intersections, stained with SYTO/PI (upper panel) or CAM/TMA-DPH (lower panel). CAM, calcein acetoxymethyl; PI, propidium iodide; TMA-DPH, 1-(4-trimethylammoniumphenyl)-6-phenyl-1,3,5-hexatriene p-toluenesulfonate. Images were captured from three randomly selected fields per sample, with similar observations across all replicates. Imaging was conducted at 40× magnification.

targets metabolic activity and cell membrane integrity (Lichtenfels et al., 1994), can be used to detect survival subpopulations within biofilms, such as VBNC and persister cells that maintain both metabolic functions and intact membranes (Liu et al., 2023). However, a commonly employed method to study VBNC cells in biofilms is membrane integrity-based SYTO9/PI staining (Gao et al., 2021), which overlooks the fact that this method can be significantly constrained. Specifically, hollow membrane-enclosed vessels may be mistakenly identified as viable cells, reducing the accuracy of membrane-integrity-based approaches (Song and Wood, 2021) for identifying VBNC populations in biofilms.

In this study, our primary objective was to quantify the antimicrobial effects on mature biofilms, recognized as one of the most structurally complex and resilient biofilm forms, presenting substantial challenges in clinical antimicrobial testing (Römling and Balsalobre, 2012). To our knowledge, this is the first study to combine CAM and TMA-DPH staining to evaluate biofilm viability while simultaneously quantifying antimicrobial effects. We were able to visualize both the viable cells stained with CAM and the residual biofilm population co-stained with TMA-DPH to detect structural changes in cell membranes triggered by antibiotic exposure.

To address the diversity of biofilm structures, we applied a range of antibiotic concentrations, targeting biofilms at varying structural and developmental stages. The efficacy of the CAM/TMA-DPH and SYTO9/PI staining methods was assessed relative to CFU counts, which provide a more sensitive and specific measure of viability, in contrast to commonly used CV or tetrazolium salt assays. CV staining was not employed because it indiscriminately labels total biofilm biomass without differentiating between live and dead cells (Wilson et al., 2017), reducing its utility in viability-focused studies. Likewise, XTT and TTC assays were not utilized, as these reagents have demonstrated inhibitory effects on bacterial cells (Ullrich et al., 1996). Additionally, the outcomes can vary significantly due to metabolic differences among isolates and species, limiting their reliability for accurately quantifying biofilm development (Ramage, 2016).

Our results, particularly the strong correlation between CAM/TMA-DPH staining and CFU counts, is not surprising as both techniques detect active, living cells. This was particularly evident in *P. aeruginosa* and *S. aureus* biofilms, where the calcein signal exhibited a near-perfect correlation with CFU values. The decrease in calcein fluorescence with increasing antibiotic concentrations, indicating a reduction in viable cells, suggests that the CAM/TMA-DPH staining method accurately reflects the effects of antibiotics. In contrast, the SYTO9/PI staining method often failed to quantitatively capture the full extent of viability, particularly in biofilms of Gram-negative species. In *P. aeruginosa* this was likely due to high eDNA

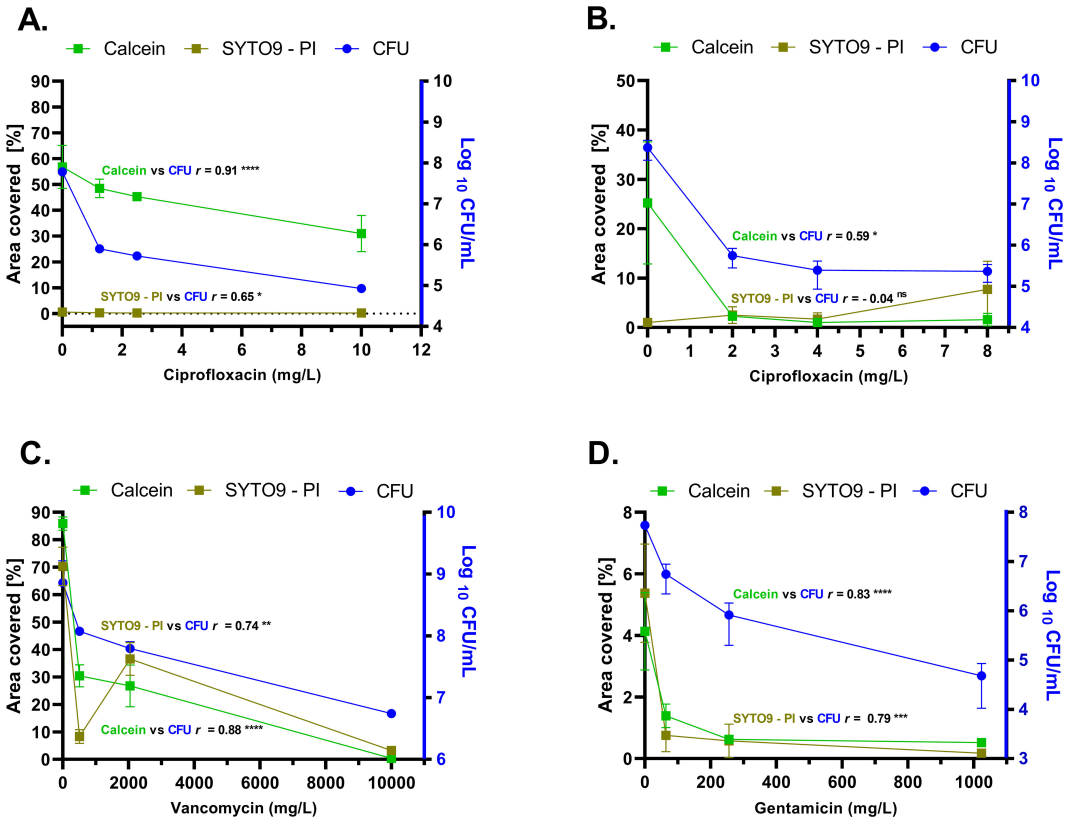

FIGURE 7
Comparative analysis of biofilm surface area coverage (left Y-axis) and number of viable cells (CFU/mL) (right Y-axis) across biofilms of *P. aeruginosa* **(A)**, *K. pneumoniae* **(B)**, *S. aureus* **(C)**, and *E. faecium* **(D)**. "SYTO9 – PI" indicates the net fluorescence differential between SYTO9 and PI signals post-subtraction. "Calcein" indicates the signal of the fluorophore calcein after digestion of CAM by intracellular esterases. The biofilm surface area coverage was calculated with the formula: Surface area coverage (%) = (Biofilm covered area/Total area) × 100. The total pixel area for analysis was equal to 2024 × 2024, derived from CLSM micrographs. Three independent experiments, each with three replicates were performed. In some cases, the error bars are too small to be visible, as they are obscured by the data symbols. CAM, calcein acetoxymethyl; CFU, colony forming unit; PI, propidium iodide; vs: versus. *r* = Spearman correlation rank. Significance was assumed at the *p* value < 0.05 and was indicated by asterisks: * < 0.05, ** < 0.01, *** < 0.001, **** < 0.0001, ns, not significant.

content masking viable cells (Rosenberg et al., 2019) leading to an underestimation of biofilm viability. However, the positive correlation observed in *P. aeruginosa* biofilms between SYTO9/PI staining and viable cell counts is likely attributed to the computational approach used, which helps minimize interference from EPS and non-specific staining (Mountcastle et al., 2021).

In *K. pneumoniae* biofilms, the persistence of SYTO9 fluorescence following treatment with the highest antibiotic concentration can be attributed to generally stronger binding affinity of SYTO9 to dead cells (Stiefel et al., 2015), even when counterstained with PI. The preferentially more effectively SYTO9-stained dead Gram-negative bacteria over intact ones may also result from lower membrane permeability and active efflux mechanisms of viable cells that limit dye uptake (Minero et al., 2024). This hypothesis is further supported by the lack of a significant correlation between SYTO9 – PI-stained biofilm area coverage and CFU counts. In contrast, the strong positive correlation between calcein fluorescence and culturable cell counts suggests that the CAM staining method accurately reflects the presence of viable cells in the *K. pneumoniae* biofilm.

Cell shape changes observed in Gram-negative species at lower ciprofloxacin doses suggest that the drug inhibits cell division. This effect was most pronounced at these lower concentrations, indicating that cell division inhibition occurs at doses below those required for biofilm eradication. Fluoroquinolones passively penetrate bacterial membranes (Cramariuc et al., 2012) primarily targeting DNA gyrase and topoisomerase IV, thereby inhibiting DNA replication and, consequently, cell division. At higher concentrations, however, this inhibition escalates, ultimately leading to cell death (Pommier et al., 2010) before significant morphological alterations can be established. Interestingly these phenotypes were CAM-stained in both *K. pneumoniae* and *P. aeruginosa*, but were differentially stained by SYTO9 (in *K. pneumoniae*) and PI (in *P. aeruginosa*). We cannot clearly explain this observation but due to the calcein fluorescence in those phenotypes, we must assume activity and viability.

In antibiotic-treated *S. aureus* biofilms, the intriguing shift with increased SYTO9 – PI-stained area coverage at 2048 mg/L vancomycin could be attributed to *S. aureus*' ability to enter a dormant state after antibiotic exposure (Pasquaroli et al., 2013),

during which cells maintain intact membranes but exhibit reduced metabolic activity (Li et al., 2014). Since SYTO9 uptake is independent of the membrane potential, it can stain dormant cells, keeping the SYTO9 signal relatively high despite the reduced activity. This can explain the decreased fluorescence of calcein while the SYTO9 signal remained relatively high.

In this study, the weak biofilm formation and limited EPS production observed in *E. faecium* likely explain the comparable performance of both vital staining techniques. As a result, both the SYTO9/PI and CAM/TMA-DPH methods were found to be effective for assessing biofilm viability in *E. faecium*.

The enhanced detection of simultaneous fluorescence from CAM and TMA-DPH co-staining in Gram-positive bacteria, compared to Gram-negative species, can be attributed to structural and functional differences between Gram-positive and Gram-negative bacteria, particularly in their cell wall composition and efflux mechanisms. It was demonstrated that multiple xenobiotic efflux pumps, in combination with the outer membrane permeability barrier, play a critical role in *P. aeruginosa* by expelling fluorescent probes (Germ et al., 1999). Similarly, Ocaktan et al. emphasized the synergy between the efflux pump and outer membrane permeability in reducing the intracellular concentrations of TMA-DPH in *P. aeruginosa* (Ocaktan et al., 1997). These findings support our hypothesis that the presence of active metabolic processes in *P. aeruginosa* may trigger an efflux mechanism that prevents effective TMA-DPH accumulation in calcein-stained cells. This interaction may be absent or minimal in Gram-positive *S. aureus*, which lacks an outer membrane and has a thicker peptidoglycan layer that is more permeable to cationic molecules (Lambert, 2002). As a result, both TMA-DPH and CAM can penetrate and accumulate within *S. aureus* cells, leading to detectable fluorescence signals. The differences in the staining effectiveness of TMA-DPH and CAM in Gram-positive and Gran-negative species could potentially lead to misinterpretations. However, the comparison with CFU counts indicates that this bias is negligible, at least under the conditions of our experimental setup.

Previous studies comparing fluorescence-based assays with CFU measurements for quantifying adherent bacteria (Hannig et al., 2007; Tawakoli et al., 2013) were unable to establish a correlation between the two methods, likely due to computational approaches used for viability assessment. In contrast, our study utilized an ImageJ-based automated image analysis method, the Biofilm Viability Checker (Mountcastle et al., 2021), which quantifies biofilm cell vitality by analyzing stained pixels in CLSM micrographs. The software enables image preprocessing and automated thresholding, specifically accounting for the presence of eDNA by removing uniform, consistent backgrounds from images, distinguishing it from other biofilm analysis tools (Mountcastle et al., 2021). Although the original code was developed for SYTO9/PI-stained confocal micrographs, we adapted it to support CAM/TMA-DPH staining. (Detailed modifications are provided in Section 2.4, and the link of updated macro code is available in Section 2.6).

Accurately assessing biofilm viability is crucial for evaluating the efficacy of antibacterial treatments, particularly in clinical settings where biofilm-associated infections pose significant treatment challenges. Our study highlights the potential of CAM/TMA-DPH staining as a valuable tool in drug development and biofilm research, providing reliable insights by directly targeting cell viability. This approach is especially timely given the rise of antibiotic-resistant biofilms in chronic infections, such as those linked to cystic fibrosis and endocarditis. Supporting this, recent research (Kolpen et al., 2022), emphasizes the importance of evaluating cellular activity in biofilms, revealing that biofilms in chronic lung infections exhibit lower metabolic rates than those in acute infections, contributing to heightened treatment resistance.

Furthermore, the CAM/TMA-DPH staining method may be particularly suitable for studies exploring alternative antibiofilm compounds. Its stable fluorescence, combined with the elimination of multiple wash steps, allows for real-time monitoring of biofilm dynamics during treatment. This approach can provide valuable insights into the progression of biofilm disruption and bacterial eradication over time.

Despite the advantages of the CAM/TMA-DPH staining approach, some limitations should be acknowledged. Firstly, the potential overestimation of viability in specific bacterial species due to residual esterase activity (Hiraoka and Kimbara, 2002), or the presence of proteases capable of hydrolyzing ester bonds remains a concern (Lee and deMan, 2018). Proteases, which can retain activity after cellular metabolism has ceased, may lead to misleading results. This limitation can be mitigated by conducting parallel CFU/mL analysis to validate viability assessments.

Secondly, the reliance on metabolic activity as a viability marker renders CAM/TMA-DPH staining ineffective for identifying non-metabolic biofilm populations, such as dormant cells. Although TMA-DPH theoretically targets membrane integrity, it cannot differentiate dormant populations from dead cells, emphasizing the need for advanced assays that better discriminate among biofilm subpopulations.

Finally, the structural and phenotypic diversity of biofilms poses a challenge to the universal applicability of this method. While this study demonstrated efficacy across biofilms formed by four clinically relevant species, further research is needed to validate its performance on a broader range of isolates, especially those with atypical biofilm characteristics (e.g., robust but thin or loose but thick structures).

In conclusion, the CAM/TMA-DPH staining method offers a compelling alternative to traditional membrane integrity-based viability assays, particularly when the assessment of biofilm viability requires a focus on metabolic activity. By emphasizing cellular activity, this method delivers valuable insights into the physiological state of biofilm-embedded bacteria, which is essential for both fundamental biofilm research and the clinical management of biofilm-associated infections.

Data availability statement

The raw data supporting the conclusions of this article will be made available by the authors, without undue reservation. For further inquiries, please contact the corresponding author.

Author contributions

TT: Investigation, Methodology, Software, Validation, Visualization, Writing – original draft, Writing – review & editing, Conceptualization. MJ: Formal analysis, Writing – review & editing. MM: Software, Writing – review & editing. KM: Writing – review & editing. MP: Funding acquisition, Writing – review & editing. OM: Conceptualization, Funding acquisition, Project administration, Resources, Supervision, Validation, Writing – review & editing. LT: Conceptualization, Supervision, Validation, Visualization, Writing – review & editing.

Funding

The author(s) declare that financial support was received for the research, authorship, and/or publication of this article. This project has received funding from the Federal Ministry of Education and Research (BMBF, Germany) grant numbers 13N15467 and 13N15720. This work was further supported by the Thüringer Innovationszentrum für Medizintechnik-Lösungen (ThIMEDOP) (FKZ IZN 2018 0002).

Acknowledgments

We sincerely thank Dr. Astrid Tannert for her expert assistance with the CLSM settings and Dr. Ekaterine Gabashvili for her valuable feedback on the manuscript. We acknowledge the support by the German Research Foundation and the Open Access Publication Fund of the Thueringer Universitaets - und Landesbibliothek Jena (Projekt-Nr. 512648189). We acknowledge the use of BioRender® (BioRender.com) for the preparation of Figure 1.

Conflict of interest

The authors declare that the research was conducted in the absence of any commercial or financial relationships that could be construed as a potential conflict of interest.

Generative AI statement

The authors declare that Gen AI was used in the creation of this manuscript. Gen AI was used to enhance spelling and grammar. Following its use, the authors thoroughly reviewed and edited the content, taking full responsibility for the final version of the publication.

Publisher's note

Supplementary material

The Supplementary Material for this article can be found online at: https://www.frontiersin.org/articles/10.3389/fcimb.2024.1508016/full#supplementary-material

References

Calcein AM, cell-permeant green and blue dyes. Available online at: https://www.thermofisher.com/order/catalog/product/de/en/C3099 (Accessed December 20, 2024).

Filmtracer™ LIVE/DEAD™ Biofilm viability kit. Available online at: https://www.thermofisher.com/order/catalog/product/de/en/L10316 (Accessed December 20, 2024).

Azeredo, J., Azevedo, N. F., Briandet, R., Cerca, N., Coenye, T., Costa, A. R., et al. (2017). Critical review on biofilm methods. *Crit. Rev. Microbiol.* 43, 313–351. doi: 10.1080/1040841X.2016.1208146

Boulos, L., Prévost, M., Barbeau, B., Coallier, J., and Desjardins, R. (1999). LIVE/DEAD® *Bac*Light™: application of a new rapid staining method for direct enumeration of viable and total bacteria in drinking water. *J. Microbiol. Methods* 37, 77–86. doi: 10.1016/S0167-7012(99)00048-2

Bridier, A., and Briandet, R. (2014). Contribution of confocal laser scanning microscopy in deciphering biofilm tridimensional structure and reactivity. *Methods Mol. Biol.* 1147, 255–266. doi: 10.1007/978-1-4939-0467-9_18

Bunthof, C. J., van Schalkwijk, S., Meijer, W., Abee, T., and Hugenholtz, J. (2001). Fluorescent method for monitoring cheese starter permeabilization and lysis. *Appl. Environ. Microbiol.* 67, 4264–4271. doi: 10.1128/AEM.67.9.4264-4271.2001

Costerton, J. W., Stewart, P. S., and Greenberg, E. P. (1999). Bacterial Biofilms: A common cause of persistent infections. *Science* 284, 1318–1322. doi: 10.1126/science.284.5418.1318

Cramariuc, O., Rog, T., Javanainen, M., Monticelli, L., Polishchuk, A. V., and Vattulainen, I. (2012). Mechanism for translocation of fluoroquinolones across lipid membranes. *Biochim. Biophys. Acta BBA - Biomembr.* 1818, 2563–2571. doi: 10.1016/j.bbamem.2012.05.027

Dong, K., Pan, H., Yang, D., Rao, L., Zhao, L., Wang, Y., et al. (2020). Induction, detection, formation, and resuscitation of viable but non-culturable state microorganisms. *Compr. Rev. Food Sci. Food Saf.* 19, 149–183. doi: 10.1111/1541-4337.12513

Donlan, R. M. (2002). Biofilms: microbial life on surfaces. *Emerg. Infect. Dis.* 8, 881–890. doi: 10.3201/eid0809.020063

Fux, C. A., Costerton, J. W., Stewart, P. S., and Stoodley, P. (2005). Survival strategies of infectious biofilms. *Trends Microbiol.* 13, 34–40. doi: 10.1016/j.tim.2004.11.010

Gao, R., Liao, X., Zhao, X., Liu, D., and Ding, T. (2021). The diagnostic tools for viable but nonculturable pathogens in the food industry: Current status and future prospects. *Compr. Rev. Food Sci. Food Saf.* 20, 2146–2175. doi: 10.1111/1541-4337.12695

Germ, M., Yoshihara, E., Yoneyama, H., and Nakae, T. (1999). Interplay between the efflux pump and the outer membrane permeability barrier in fluorescent dye accumulation in *Pseudomonas aeruginosa*. *Biochem. Biophys. Res. Commun.* 261, 452–455. doi: 10.1006/bbrc.1999.1045

Halsted, M. C., Bible, A. N., Morrell-Falvey, J. L., and Retterer, S. T. (2022). Quantifying biofilm propagation on chemically modified surfaces. *Biofilm* 4, 100088. doi: 10.1016/j.bioflm.2022.100088

Hannig, C., Hannig, M., Rehmer, O., Braun, G., Hellwig, E., and Al-Ahmad, A. (2007). Fluorescence microscopic visualization and quantification of initial bacterial colonization on enamel in *situ*. *Arch. Oral. Biol.* 52, 1048–1056. doi: 10.1016/j.archoralbio.2007.05.006

Häußler, S. (2004). Biofilm formation by the small colony variant phenotype of *Pseudomonas aeruginosa*. *Environ. Microbiol.* 6, 546–551. doi: 10.1111/j.1462-2920.2004.00618.x

Hiraoka, Y., and Kimbara, K. (2002). Rapid assessment of the physiological status of the polychlorinated biphenyl degrader *Comamonas testosteroni* TK102 by flow cytometry. *Appl. Environ. Microbiol.* 68, 2031–2035. doi: 10.1128/AEM.68.4.2031-2035.2002

Kim, S.-K., and Lee, J.-H. (2016). Biofilm dispersion in *Pseudomonas aeruginosa*. *J. Microbiol.* 54, 71–85. doi: 10.1007/s12275-016-5528-7

Kirchhoff, C., and Cypionka, H. (2017). Propidium ion enters viable cells with high membrane potential during live-dead staining. *J. Microbiol. Methods* 142, 79–82. doi: 10.1016/j.mimet.2017.09.011

Kolpen, M., Kragh, K. N., Enciso, J. B., Faurholt-Jepsen, D., Lindegaard, B., Egelund, G. B., et al. (2022). Bacterial biofilms predominate in both acute and chronic human lung infections. *Thorax* 77, 1015–1022. doi: 10.1136/thoraxjnl-2021-217576

Lambert, P. A. (2002). Cellular impermeability and uptake of biocides and antibiotics in Gram-positive bacteria and mycobacteria. *J. Appl. Microbiol.* 92 Suppl, 46S–54S. doi: 10.1046/j.1365-2672.92.5s1.7.x

Lee, C. Y., and deMan, J. M. (2018). "Enzymes," in *Principles of Food Chemistry*. Eds. J. M. deMan, J. W. Finley, W. J. Hurst and C. Y. Lee (Springer International Publishing, Cham), 397–433. doi: 10.1007/978-3-319-63607-8_10

Lewis, K. (2007). Persister cells, dormancy and infectious disease. *Nat. Rev. Microbiol.* 5, 48–56. doi: 10.1038/nrmicro1557

Li, X.-H., and Lee, J.-H. (2017). Antibiofilm agents: A new perspective for antimicrobial strategy. *J. Microbiol. Seoul Korea* 55, 753–766. doi: 10.1007/s12275-017-7274-x

Li, L., Mendis, N., Trigui, H., Oliver, J. D., and Faucher, S. P. (2014). The importance of the viable but non-culturable state in human bacterial pathogens. *Front. Microbiol.* 5. doi: 10.3389/fmicb.2014.00258

Lichtenfels, R., Biddison, W. E., Schulz, H., Vogt, A. B., and Martin, R. (1994). CARE-LASS (calcein-release-assay), an improved fluorescence-based test system to measure cytotoxic T lymphocyte activity. *J. Immunol. Methods* 172, 227–239. doi: 10.1016/0022-1759(94)90110-4

Liu, J., Yang, L., Kjellerup, B. V., and Xu, Z. (2023). Viable but nonculturable (VBNC) state, an underestimated and controversial microbial survival strategy. *Trends Microbiol.* 31, 1013–1023. doi: 10.1016/j.tim.2023.04.009

Minero, G. A. S., Larsen, P. B., Hoppe, M. E., and Meyer, R. L. (2024). Bacterial efflux pumps excrete SYTO™ dyes and lead to false-negative staining results. *Analyst* 149, 2232–2235. doi: 10.1039/D3AN02112B

Mountcastle, S. E., Vyas, N., Villapun, V. M., Cox, S. C., Jabbari, S., Sammons, R. L., et al. (2021). Biofilm viability checker: An open-source tool for automated biofilm viability analysis from confocal microscopy images. *NPJ Biofilms Microbiomes* 7, 1–12. doi: 10.1038/s41522-021-00214-7

Ocaktan, A., Yoneyama, H., and Nakae, T. (1997). Use of fluorescence probes to monitor function of the subunit proteins of the MexA-MexB-OprM drug extrusion machinery in *Pseudomonas aeruginosa*. *J. Biol. Chem.* 272, 21964–21969. doi: 10.1074/jbc.272.35.21964

Pasquaroli, S., Zandri, G., Vignaroli, C., Vuotto, C., Donelli, G., and Biavasco, F. (2013). Antibiotic pressure can induce the viable but non-culturable state in *Staphylococcus aureus* growing in biofilms. *J. Antimicrob. Chemother.* 68, 1812–1817. doi: 10.1093/jac/dkt086

Pommier, Y., Leo, E., Zhang, H., and Marchand, C. (2010). DNA Topoisomerases and their poisoning by anticancer and antibacterial drugs. *Chem. Biol.* 17, 421–433. doi: 10.1016/j.chembiol.2010.04.012

Ramage, G. (2016). Comparing apples and oranges: considerations for quantifying candidal biofilms with XTT [2,3-bis(2-methoxy-4-nitro-5-sulfo-phenyl)-2H-tetrazolium-5-carboxanilide] and the need for standardized testing. *J. Med. Microbiol.* 65, 259–260. doi: 10.1099/jmm.0.000237

Rani, S. A., Pitts, B., Beyenal, H., Veluchamy, R. A., Lewandowski, Z., Davison, W. M., et al. (2007). Spatial patterns of DNA replication, protein synthesis, and oxygen concentration within bacterial biofilms reveal diverse physiological states. *J. Bacteriol.* 189, 4223–4233. doi: 10.1128/JB.00107-07

Römling, U., and Balsalobre, C. (2012). Biofilm infections, their resilience to therapy and innovative treatment strategies. *J. Intern. Med.* 272, 541–561. doi: 10.1111/joim.12004

Rosenberg, M., Azevedo, N. F., and Ivask, A. (2019). Propidium iodide staining underestimates viability of adherent bacterial cells. *Sci. Rep.* 9, 6483. doi: 10.1038/s41598-019-42906-3

Sadiq, F. A., Flint, S., Li, Y., Ou, K., Yuan, L., and He, G. Q. (2017). Phenotypic and genetic heterogeneity within biofilms with particular emphasis on persistence and antimicrobial tolerance. *Future Microbiol.* 12, 1087–1107. doi: 10.2217/fmb-2017-0042

Song, S., and Wood, T. K. (2021). [amp]]lsquo;Viable but non-culturable cells' are dead. *Environ. Microbiol.* 23, 2335–2338. doi: 10.1111/1462-2920.15463

Stewart, P. S., and Franklin, M. J. (2008). Physiological heterogeneity in biofilms. *Nat. Rev. Microbiol.* 6, 199–210. doi: 10.1038/nrmicro1838

Stiefel, P., Schmidt-Emrich, S., Maniura-Weber, K., and Ren, Q. (2015). Critical aspects of using bacterial cell viability assays with the fluorophores SYTO9 and propidium iodide. *BMC Microbiol.* 15, 36. doi: 10.1186/s12866-015-0376-x

Tawakoli, P. N., Al-Ahmad, A., Hoth-Hannig, W., Hannig, M., and Hannig, C. (2013). Comparison of different live/dead stainings for detection and quantification of adherent microorganisms in the initial oral biofilm. *Clin. Oral. Investig.* 17, 841–850. doi: 10.1007/s00784-012-0792-3

Taylor, P. K., Yeung, A. T. Y., and Hancock, R. E. W. (2014). Antibiotic resistance in *Pseudomonas aeruginosa* biofilms: Towards the development of novel anti-biofilm therapies. *J. Biotechnol.* 191, 121–130. doi: 10.1016/j.jbiotec.2014.09.003

Thieme, L., Hartung, A., Makarewicz, O., and Pletz, M. W. (2020). *In vivo* synergism of ampicillin, gentamicin, ceftaroline and ceftriaxone against *Enterococcus faecalis* assessed in the *Galleria mellonella* infection model. *J. Antimicrob. Chemother.* 75, 2173–2181. doi: 10.1093/jac/dkaa129

Ullrich, S., Karrasch, B., Hoppe, H., Jeskulke, K., and Mehrens, M. (1996). Toxic effects on bacterial metabolism of the redox dye 5-cyano-2,3-ditolyl tetrazolium chloride. *Appl. Environ. Microbiol.* 62, 4587–4593. doi: 10.1128/aem.62.12.4587-4593.1996

Wickham, H. (2014). Tidy data. *J. Stat. Software* 59, 1–23. doi: 10.18637/jss.v059.i10

Wiederschain, G. (2011). The Molecular Probes handbook. A guide to fluorescent probes and labeling technologies. *Biochem. Mosc.* 76, 1276–1276. doi: 10.1134/S0006297911110101

Wilson, C., Lukowicz, R., Merchant, S., Valquier-Flynn, H., Caballero, J., Sandoval, J., et al. (2017). Quantitative and qualitative assessment methods for biofilm growth: A mini-review. *Res. Rev. J. Eng. Technol.* 6, 4. Available at: http://www.rroij.com/open-access/quantitative-and-qualitative-assessment-methods-for-biofilm-growth-a-minireview-.pdf.

Yoon, M. Y., Lee, K.-M., Park, Y., and Yoon, S. S. (2011). Contribution of cell elongation to the biofilm formation of *Pseudomonas aeruginosa* during anaerobic respiration. *PLoS One* 6, e16105. doi: 10.1371/journal.pone.0016105

Zhang, X., Wang, Y., Guo, J., YU, Y., Li, Y., and Liu, C. (2015). Comparing two functions for optical density and cell numbers in bacterial exponential growth phase. *J. Pure Appl. Microbiol.* 9, 299–305.

frontiers | Frontiers in Cellular and Infection Microbiology

TYPE Original Research
PUBLISHED 31 January 2025
DOI 10.3389/fcimb.2025.1507486

OPEN ACCESS

EDITED BY
Maria Gabriela Paraje,
National University of Cordoba, Argentina

REVIEWED BY
Maciej Jaśkiewicz,
Medical University of Gdansk, Poland
Farida Bendali,
University of Béjaïa, Algeria

*CORRESPONDENCE
Yong Li
yong.li@wmed.edu

RECEIVED 07 October 2024
ACCEPTED 09 January 2025
PUBLISHED 31 January 2025

CITATION
Grooters KE, Hayes SL, Richter DM, Ku JC, Sawyer R and Li Y (2025) A novel strategy for eradication of staphylococcal biofilms using blood clots. *Front. Cell. Infect. Microbiol.* 15:1507486. doi: 10.3389/fcimb.2025.1507486

A novel strategy for eradication of staphylococcal biofilms using blood clots

Kayla E. Grooters[1], Sheridan L. Hayes[2], David M. Richter[1], Jennifer C. Ku[1], Robert Sawyer[2] and Yong Li[2]*

[1]Department of Medicine, Western Michigan University Homer Stryker M.D. School of Medicine, Kalamazoo, MI, United States, [2]Division of Medical Engineering, Department of Surgical Science, Western Michigan University Homer Stryker MD School of Medicine, Kalamazoo, MI, United States

Introduction: Infections with coagulase negative staphylococcal species (CoNS) are a major cause of mortality and morbidity in joint and heart valve replacement procedures, largely due to biofilm formation. Cells within biofilms have higher rates of antibiotic resistance than their planktonic counterparts; consequently, novel mechanisms are needed to combat these infections.

Methods: To enhance antibiotic delivery and penetration, this innovative study involved treating CoNS biofilms with murine blood clots impregnated with antibiotics. We then investigated the impact of this treatment on biofilm density, metabolism, and architecture.

Results: Our pilot study demonstrates that this method of antibiotic delivery results in improved biofilm clearance, relative to conventional exposure methods.

Discussion: Our results demonstrate that blood clot exposure has an intrinsic impact on biofilm density and potentially reduces colonization, warrenting further investigation into the mechanism.

KEYWORDS

biofilm, antibiotic resistance, staphylococci, prosthetic joint infections, biomaterials

1 Introduction

A biofilm is a three-dimensional structure consisting of microscopic organisms and a robust extracellular matrix (ECM) produced by such organisms. This ECM functions to enhance adhesion to the local environment, reduce desiccation, mitigate environmental hazards, and provide protection from antimicrobial compounds. Accordingly, these biofilms become highly resistant to antibiotics (Sharma et al., 2019). Biofilm infections are a major cause of morbidity and mortality—particularly impacting prosthetic joints and valves. Prosthetic medical implants are susceptible to colonization by microorganisms during the perioperative and postoperative period (Khatoon et al., 2018; Skovdal et al., 2022). Infections during the perioperative period are

most commonly due to inoculation of microorganisms during the surgery due to a lapse in sterile technique. Rarely, inoculation can occur during the manufacturing process (Ribeiro et al., 2012). Postoperative infections occur when the implant is seeded by microorganisms after the initial implantation. These microorganisms can be introduced through hematogenous or contiguous routes. Infections can further be classified as early, which occur within 3 months of the operation, delayed, which occur within 3-24 months, and late, occurring more than 24 months postoperatively (Ribeiro et al., 2012).

Staphylococci, including the coagulase negative *Staphylococcus epidermidis*, are the most prevalent biofilm-producing species (Oliveira et al., 2018; Otto, 2008, 2018). Staphylococcal species are responsible for over two thirds of implantable device associated infections (Darouiche, 2004; Oliveira et al., 2018; Severn and Horswill, 2023). These gram-positive bacteria are part of the naturally occurring skin and soft tissue microbiota in humans, and therefore can easily contaminate the surgical field. (Khatoon et al., 2018; Severn and Horswill, 2023). Biofilm formation can start within 24 h of inoculation. These infections are often refractory to antibiotic treatment and require surgical revision (Skovdal et al., 2022). The annual cost of revision surgery due to biofilm-mediated infections is $7.849 million globally (Cámara et al., 2022).

One of the key issues with using antibiotics to treat biofilms is achieving the required minimum bactericidal concentration (MBC) of a drug at the infection site. The MBC for a biofilm can be thousands of times greater than the MBC for planktonic cells (Oliveira et al., 2018). This is because the ECM provides a physical barrier which protects cells from antibiotic exposure. In addition, there exists a stratification of metabolic activity through the layers of the biofilm (Shree et al., 2023; Wood et al., 2013). The metabolically inactive basement cells form the foundation for the biofilm and can persist to reform the biofilm despite eradication of the upper layers (Wood et al., 2013). For these reasons, there is a growing need to develop new technology capable of penetrating and eradicating biofilm infections. One idea is to use a biologic delivery system that can adhere to the biofilm itself, allowing direct exposure and penetration of the drug. Previous studies have implemented fibrin clots as substrates to model biofilms, indicating that they are capable of biofilm integration (Domínguez-Herrera et al., 2012). Our team elected to suspend antibiotics within a blood clot and then adhere it to the biofilm. Our recent studies have shown that these blood clots can release a steady concentration of antibiotics into the target environment for at least 7 days (Ku et al., 2024). We hypothesized that this Trojan horse model would facilitate penetration of the antibiotic throughout the biofilm, leading to an increased rate of clearance compared to conventional treatments.

2 Materials and methods

2.1 Chemicals, media, and strains

Staphylococcus epidermidis FDA strain PCI 1200 (ATCC Cat#12228) was routinely maintained as a frozen –80°C stock and grown on Luria–Bertani (LB) agar (Fisher Scientific). Gentamicin (Gibco; 10 µg/mL in LB broth) and vancomycin (Thermofisher; 20 µg/mL in LB broth) were suspended in LB broth for inhibition experiments.

2.2 Biofilm formation

Biofilm formation was assessed using a 12-well micro-titer plate model, adapted from the design in Kumar et al., 2019 as well as Bailey and Scott's Diagnostic Microbiology, 14th edition (Tille, 2017). Cells from an overnight culture were washed, counted, and resuspended to a final concentration of 1x10^{6} CFU/mL in LB. Aliquots of 1000 µL were used to seed the 12-well micro-titer plate (Corning Incorporated Costar). Plates were incubated for 24 h at 37°C and thrice washed with PBS to remove non-adherent cells (Figure 1).

2.3 Minimum bactericidal concentration and minimum biofilm eradication concentration

The Minimum Bactericidal Concentration (MBC) and Minimum Biofilm Eradication Concentration (MBEC) assays were adapted from Bailey and Scott's Diagnostic Microbiology, 14th edition (Tille, 2017) and the *In Vitro* MBEC Assay in Okae et al., 2022 to fit the parameters of this study. According to the European Committee for Antimicrobial Susceptibility Testing (EUCAST), the minimum bactericidal concentration is "the lowest concentration of an antibiotic that under defined *in vitro* conditions reduces by 99.9% the number of organisms in a medium containing a defined inoculum of bacteria within a defined period of time." (European Committe for Antimicrobial Susceptibility Testing, 2000) The Minimum Biofilm Eradication Concentration can be defined as "the lowest concentration of antibiotic required to eradicate the biofilm (Ceri et al., 1999) or, in other words, the lowest concentration of antimicrobial agent that prevents visible growth in the recovery medium used to collect biofilm cells." (Macia et al., 2014). Historically, these measures have been paired together because they are complementary, describing the concentration needed for complete cell death in planktonic and biofilm culture (Evans and Holmes, 1987). For the MBC, increasing concentrations of select antibiotics (gentamicin or vancomycin) were incubated with planktonic bacteria in a 12-well micro-titer plate for 24 h in a stagnant 37°C incubator. For gentamicin, the intervals ranged from 0 to 40 µg/mL (see supplemental 1). For vancomycin, the intervals ranged from 0 to 5 µg/mL. Wells were then thrice washed with PBS and the remaining bacteria was scrapped and resuspended in 3 mL of LB media, which was placed in a shaking 37°C incubator overnight. Following the bacterial recovery period, a colony forming unit (CFU) assay in the form of the drop plate method was performed, and 24 h later, colony formation was counted at the 10^{-4} dilution (Herigstad et al., 2001). For the MBEC, biofilms were formed as previously described over 24 h, were then thrice washed with PBS and treated with select antibiotics (gentamicin or vancomycin). For gentamicin, the intervals ranged from 0 to 10,000 µg/mL. For vancomycin, the intervals ranged from 0 to 1,000 µg/mL (see supplemental 1). After 24 h treatment, the MBEC was conducted in the same manner as the MBC. Each concentration for each condition was tested in triplicate.

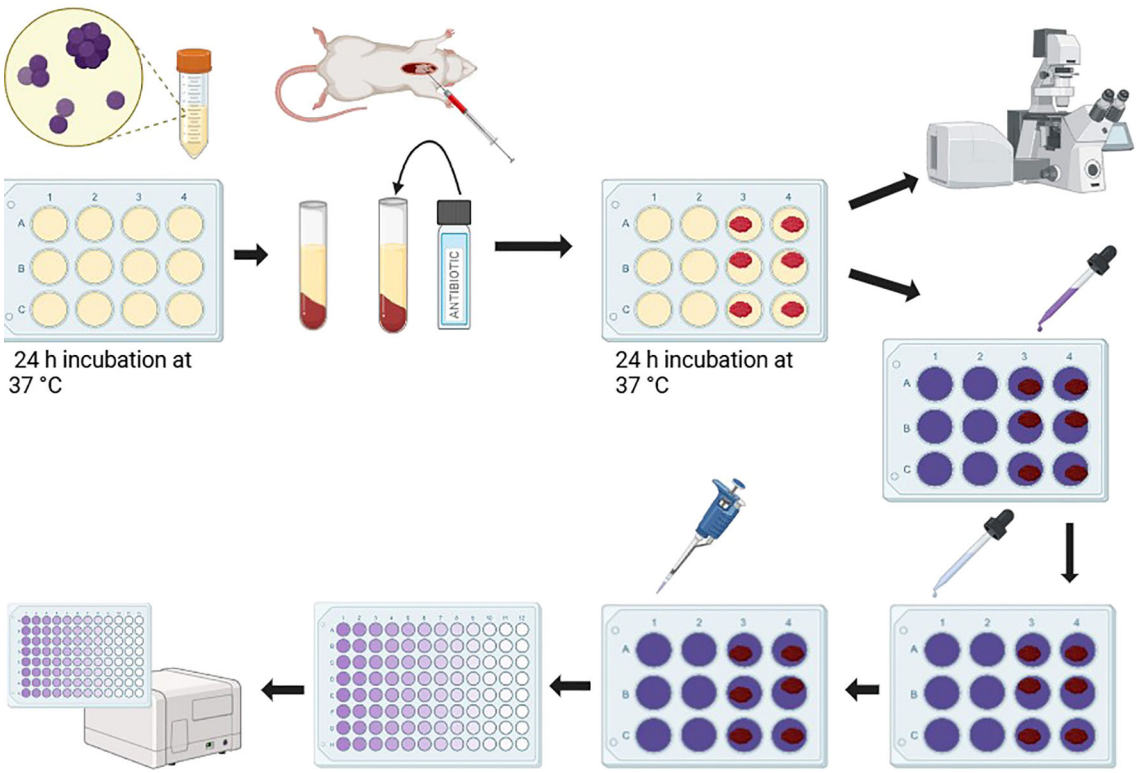

FIGURE 1
Schematic representation of experimental design.Figure generated with BioRender ®.

2.4 Blood clot harvesting and preparation

All animal procedures were approved by the host institution's Institutional Animal Care and Use Committee (IACUC protocol number 2020-0023). This protocol was adapted from Ku et al., 2024. C57 BL/6J mice (6–8 weeks of age; male) were anesthetized with 1–1.5% isoflurane. After reaching the surgical plane of anesthesia, approximately 300–500 µL of blood was removed via cardiac puncture. Animals were subsequently euthanized in accordance with institutional protocols. The blood was subsequently transferred to microcentrifuge tubes, where it was allowed to clot in the presence of LB media, LB media supplemented with vancomycin (20 µg/mL), or LB media supplemented with gentamycin (10 µg/mL). These blood clot preparations were subsequently applied to the biofilms, as outlined below.

2.5 Crystal violet assay

This assay was modeled after the protocol in O'Toole, 2011; Kumar et al., 2019, and Bailey and Scott's Diagnostic Microbiology, 14th edition (Tille, 2017). Select wells were exposed to the experimental condition. The following conditions were tested: no treatment, 20 µg/mL gentamicin suspension, 10 µg/mL vancomycin suspension, gentamicin impregnated blood clot, vancomycin impregnated blood clot, and blood clot alone. Fresh LB media was replaced in each well such that the total volume remained 1000 µL. Plates were incubated for 24 h at 37°C, thrice washed with PBS to remove non-adherent cells, and stained with 0.1% crystal violet for 10 minutes. Biofilms were washed with sterile water to remove excess stain, then destained with 33% acetic acid (Fisher Scientific). The supernatant was transferred to empty wells and the absorbance was measured at 550 nm using a plate reader (BioTek EPOCH 2). The results were analyzed by Student's t-test, comparing each transformant strain with its parent strain (Figure 1).

2.6 Metabolic assay

The following procedure was adapted from Haney et al., 2018 to fit the parameters of this study. Following a 24 h incubation of 24-well plates (Corning Incorporated Costar) in static conditions, media and planktonic cells were removed from their respective wells and replaced with the following treatments: control, gentamicin, vancomycin, blood clot, blood clot with gentamicin, and blood clot with vancomycin. In addition to the treatment, fresh LB Media containing 0.05% 2,3,5-Triphenyl Tetrazolium Chloride (TTC) (Carolina Biological Supply Company) was added to each well for a total volume of 1000 µL. Plates were then incubated at 37°C for 24 h. To remove used media and residual treatments, the biofilms were carefully washed three times with deionized water. To isolate the metabolized TTC, 500 µL of methanol was mixed gently in each well. To quantify the metabolized TTC, 200 µL from each well was aliquoted to a 96-well micro-titer plate (Wuxi NEST Biotechnology Co) and read on a plate reader (BioTek EPOCH 2) at an absorbance of 500 nm.

2.7 Architectural analysis

The following procedure was adapted from Haney et al., 2018 to fit the parameters of this study. Cells from an overnight culture were diluted to a final density of 0.005 at an absorbance reading of 600 nm, and 2 mL was seeded in MatTek 35 mm Glass Bottom Culture Dishes. After being incubated at 37°C for 24 h, media and unadhered cells were removed. Fresh media (2 mL) and treatments were added, as described above, centralized on the glass microwells of the dishes. After another 24 h incubation, dishes were washed twice with DI water. Care was taken to ensure the biofilms were not disrupted. The biofilms were centrally stained with 10.2µM SYTO®9 and 60µM propidium iodide diluted in DI water (FilmTracer™ LIVE/DEAD® Biofilm Viability Kit; Invitrogen Molecular Probes), protected from light, and allowed to sit for 20 minutes. The excess stain was removed and washed with DI water.

Samples were imaged using a Nikon A1R+ Confocal Microscope System equipped with a 60X objective, with analysis and 3D rendering performed using NIS-Elements C software. Bacterial quantification was performed with the open-source software ImageJ (version 1.54f, National Institutes of Health, USA) by Fiji (Schindelin et al., 2012). Specifically, the live and dead percentages were determined using the MorphoLibJ plugin and Biofilm Viability Checker macro (Mountcastle et al., 2021). Imaging was performed in biological triplicates. Imaging data were generated in the Flow Cytometry and Imaging Core at Western Michigan University Homer Stryker M.D. School of Medicine (Figure 1).

2.8 Statistical analysis

Data are expressed as mean ± SD and n represents the number of discrete samples. Paired t-tests were used to compare the effect of a given treatment condition on A_{500}. GraphPad Prism 10.2.2 was used for data analysis and figure generation.

3 Results

3.1 Crystal violet assay

To examine the impact of our blood clot/antibiotic system on biofilm density, we formed *S. epidermidis* biofilms and then exposed them to antibiotics suspended in media vs blood clots impregnated with an equal concentration of antibiotics. A blood clot alone condition and an untreated condition served as controls. We selected two antibiotics with differing mechanisms of action to test, vancomycin and gentamicin. In clinical settings, vancomycin, a glycopeptide, is often selected as the first line option against *S. epidermidis* infections due to the frequency of methicillin resistance (Lee and Anjum, 2024). Gentamicin, an aminoglycoside, has been proposed as an alternative option (Chambers and Pallagrosi, 1973) (Karmakar et al., 2016). Our experiments showed that after 24 h, there was a significant reduction in biofilm density after blood clot/antibiotic exposure compared to antibiotic alone (Figure 2). There was approximately a 50% reduction in density between the biofilm control group and the

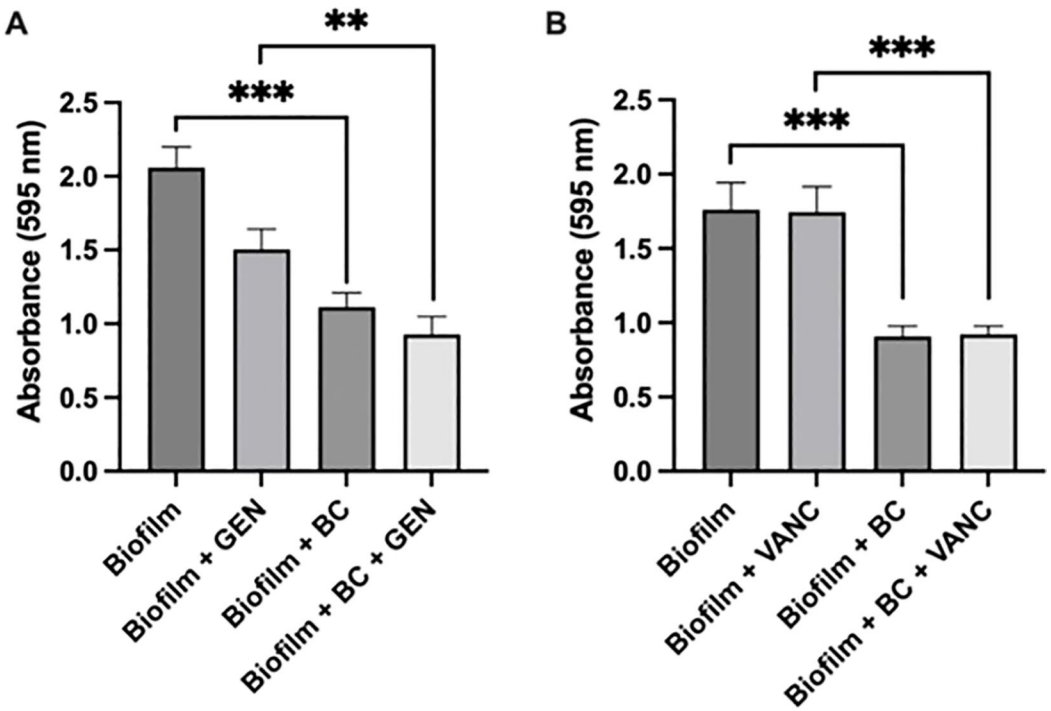

FIGURE 2
Biofilm formation and Crystal Violet Assay. Crystal Violet assay measuring *Staphylococcus epidermidis* biofilm formation following exposure to blood clot, gentamicin **(A)**, vancomycin **(B)**, or their combination. Significance indicated by ** ($p<0.0032$) and **** ($p<0.0008$). Each experiment was performed in triplicate. Gentamicin trials were conducted across 6 independent experiments, while vancomycin trials were conducted across 3 independent experiments.

biofilm with blood clot, with a p value less than 0.0008. Between the biofilm with gentamicin condition and the biofilm with gentamicin and blood clot condition, the reduction was approximately 33%, with a p value less than 0.0032. For the biofilm with vancomycin condition compared to the biofilm with vancomycin and blood clot, the reduction was approximately 40%, with a p value less than 0.0008. This trend, being evident across both antibiotics tested, suggests that the blood clot facilitates antibiotic susceptibility, potentially due to increased penetration. Additionally, exposure to liquid antibiotics alone caused a significant increase in biofilm density compared to the untreated control. This aligns with the current literature, which suggests that exposing biofilms to subtherapeutic concentrations of antibiotics elicits a stress response, subsequently increasing ECM production (Lories et al., 2020). Surprisingly, we observed that exposure to the blood clot alone caused a reduction in biofilm density. This reduction was not statistically different than the effect of the blood clot/antibiotic combination, suggesting that the mechanism of effect is dependent on the blood clot, and not the antibiotic. Elucidating the mechanism behind this requires further investigation. We hypothesize that select enzymes within the blood clot may play a role in breaking down the ECM. One potential enzyme is matrix metalloprotease 1 (MMP-1) which has already been shown to disrupt *Enterococcus* biofilms (Kumar et al., 2019).

3.2 Metabolic changes

To determine the impact of the blood clot/antibiotic system on the metabolic activity of the biofilm, we repeated the experiment using a TTC assay. The conditions and antibiotics tested during the Crystal Violet assay were maintained. Our results mirrored the results of the crystal violet assay (Figure 3). There was approximately a 55% reduction in density between the biofilm control group and the biofilm with blood clot, with a p value less than 0.0001. Between the biofilm with gentamicin condition and the biofilm with gentamicin and blood clot condition, the reduction was approximately 40%, with a p value less than 0.0032. For the biofilm with vancomycin condition compared to the biofilm with vancomycin and blood clot, the reduction was approximately 55%, with a p value less than 0.0001. After 24 h, there was a significant reduction in the metabolic activity of the biofilm after exposure to the blood clot/antibiotic and blood clot alone compared to the untreated control and antibiotic alone. Once more, the biofilms treated with antibiotics displayed an increase in metabolic activity.

3.3 Alterations in biofilm architecture

Recognizing the density and metabolic differences between treatments, we sought to visually confirm these relations through architectural imaging. Such imaging was performed via confocal microscopy, a critical technology used to determine specific relations not otherwise discovered within a biofilm. Confocal microscopy non-invasively visualizes the overall components and individual bacteria within a fully hydrated biofilm (Pitts and Stewart, 2008; Palmer et al., 2006). Additionally, the 3D capabilities through z-plane imaging allows for visualization of

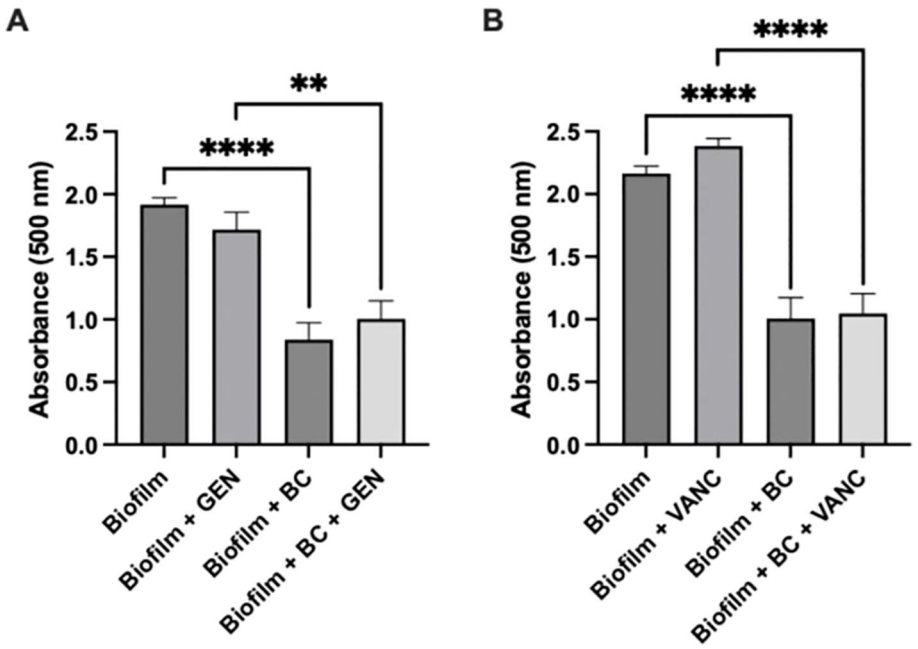

FIGURE 3
Metabolic Assay. Tetrazolium chloride assay of *Staphylococcus epidermidis* biofilm viability following exposure to blood clot, gentamicin **(A)**, vancomycin **(B)**, or their combination. Statistical significance indicated by ** ($p<0.0032$) and **** ($p<0.0001$). Each experiment was performed in triplicate, with a total of 2 independent experiments conducted.

spatial positioning and treatment penetration into the biofilm (Reichhardt and Parsek, 2019).

Utilizing the same 24 h treatments as above, the biofilms were stained with a Live/Dead stain, SYTO®9 and propidium iodide, then imaged in multiple slices along the z-plane and visualized in both a maximum intensity projection and a 3D rendering (Figure 4). A portrayal of a *S. epidermidis* biofilm is seen within the control condition, as it creates a cohesive sheet of bacteria (Figure 4A). The vancomycin treatment exhibits an increased abundance of bacteria compared to the control condition (Figure 4B). In contrast to the vancomycin, the gentamicin treatment appears to create a slightly dispersed biofilm, consisting of a more scattered array of clumps and planktonic bacteria (Figure 4C). This relation between antibiotic treatments is supported previously in the densities of each condition.

Meanwhile, the biofilms treated with blood clots (Figures 4D-F), exhibit a noticeable visual decrease of bacteria compared to the bacterial sheets seen in conditions without blood clots. Rather than the cohesive bacterial unit, these conditions have greater separation between colonies, with multiple areas absent of bacteria. Moreover, within the blood clot treatments, there appears to be less bacteria in the conditions where blood clot was impregnated with antibiotic (Figures 4E, F), suggesting an amplified effect when these treatments are used together.

This visual relation of treatment type to bacteria coverage is further supported through the quantification of these images, with the open-source domain ImageJ by Fiji and the Biofilm Viability Checker (Mountcastle et al., 2021; Schindelin et al., 2012). The percentage of the visual plane covered with bacteria, live or dead, appears greatly dependent on the presence of blood clot (Figure 5A). The percentages for total bacterial coverage for no treatment range from 55.5% to 84.1%, for gentamicin values range from 58.5% to 69.4%, for vancomycin values range from 49.5% to 86.9%, for blood clot values range from 31.4% to 57.8%, for blood clot with gentamicin values range from 27.1% to 59.8%, and for blood clot with vancomycin values range from 28.9% to 48.7%. The

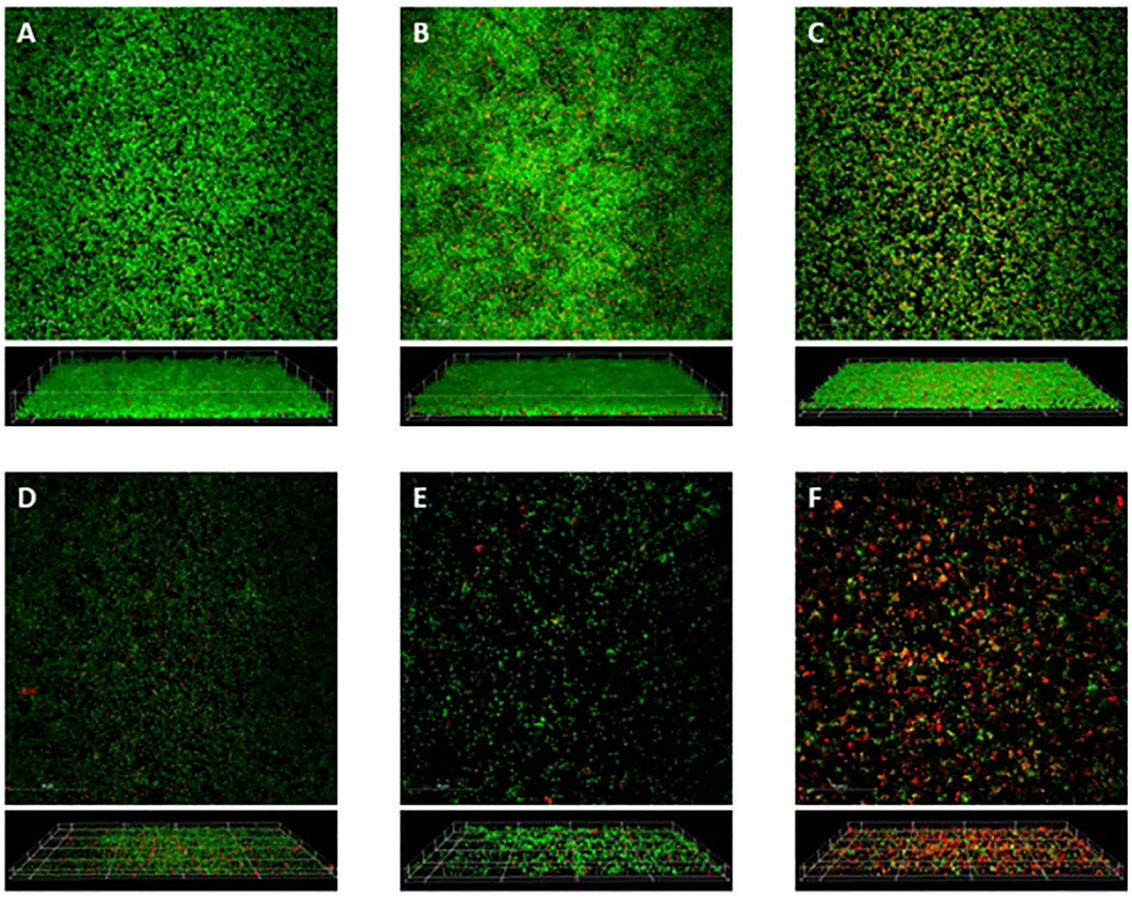

FIGURE 4
Confocal Microscopy. Confocal microscopy of 24 h old *S. epidermidis* biofilms formed on glass bottom culture dishes when either left untreated **(A)**, or treated with vancomycin (20 μg/mL) **(B)**, gentamicin (10 μg/mL) **(C)**, blood clot **(D)**, blood clot impregnated with vancomycin (20 μg/mL) **(E)**, or blood clot impregnated with gentamicin (10 μg/mL) **(F)**. Following 24 h treatments, biofilms were stained with SYTO-9 (green=live) and propidium iodide (red=dead). Image stacks were acquired along the z-plane using a Nikon A1R+ Confocal Microscope System. Top-down maximum projections (top panels) and 3D reconstructions (bottom panels) were made using NIS-Elements C software. The scale bars in the top panels represent 50 μm.

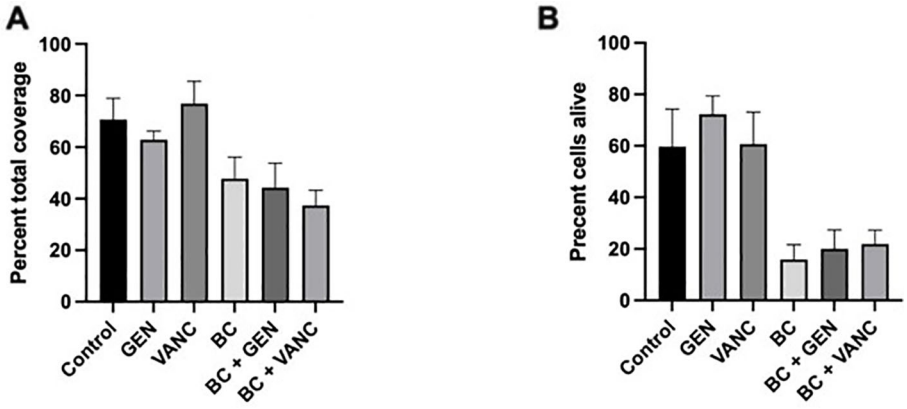

FIGURE 5
Confocal Analysis of Biofilm Coverage. Live-dead staining of *Staphylococcus epidermidis* biofilms without treatment (control) and following administration of gentamicin (GEN) and vancomycin (VANC), alone and conjugated with a blood clot (bc). **(A)** Depicts percentage of total bacterial coverage, and **(B)** depicts percentage of living cells. Analysis performed using Prism. Each experiment was preformed in triplicate, with a total of 3 independent experiments conducted.

addition of a blood clot appears to decrease the bacterial coverage by an average of a third to that of the non-blood clot condition. Additionally, the biofilms treated with blood clot appear to be comprised of more dead cells throughout (Figure 4). This is supported in the quantification of the biofilm viability, in which more propidium iodide staining is present in the biofilms treated with blood clots (Figure 5B). Thus, the combination of a dispersed biofilm, increased death, and planktonic form visualization throughout the biofilms treated with blood clot, and to a greater degree when impregnated with antibiotic, suggests its effectiveness as a viable treatment. The percentages for alive cells for no treatment range from 32.3% to 78.7%, for gentamicin the values range from 58.8% to 83.1%, for vancomycin the values range from 41.3% to 83.9%, for blood clot the values range from 5.8% to 35.7%, for blood clot with gentamicin the values range from 5.6% to 29.2%, for blood clot with vancomycin the values range from 11.1% to 36.0%.

Qualitatively, the presence of a 24 h blood clot treatment alone or impregnated with antibiotics appears to decrease bacteria abundance. This trend warrants further testing and investigation as despite the appearance, there is no significant difference in total bacterial coverage between samples. The p-values for total bacterial coverage are as follows: control to gentamicin p=0.98, control to vancomycin p=0.99, blood clot to control p=0.43, blood clot with gentamicin to control p=0.29, blood clot with vancomycin to control p=0.12, blood clot to gentamicin p=0.78, blood clot to vancomycin p=0.32, blood clot to blood clot with gentamicin p=0.99, blood clot to blood clot with vancomycin p=0.94, blood clot with gentamicin to gentamicin p=0.62, and blood clot with vancomycin to vancomycin p=0.08. When looking at the percentage of alive cells, there are two significant p-values (blood clot to gentamicin and blood clot with gentamicin to gentamicin), however the rest have no significant differences. The p-values for percent of alive cells are as follows: blood clot to gentamicin p=0.02, blood clot with gentamicin to gentamicin p=0.03, control to gentamicin p=0.73, control to vancomycin p=0.99, blood clot to control p=0.22, blood clot with gentamicin to control p=0.24, blood clot with vancomycin to control p=0.39, blood clot to vancomycin p=0.09, blood clot to blood clot with gentamicin p=1.0, blood clot to blood clot with vancomycin p=0.99, and blood clot with vancomycin to vancomycin p=0.18.

The variations between visual appearance and quantification may be due to the multiple limitations with quantifying Live/Dead staining of biofilms through confocal microscopy. These include thickness and density of biofilm, flatness of biofilm, and background staining (Mountcastle et al., 2021). Additional limitations occur with the binding of propidium iodide to biofilm extracellular matrices and extracellular DNA which in turn can overestimate dead cell counts (Rosenberg et al., 2019). In response to these limitations, the primary use of confocal microscopy in biofilm analysis is to demonstrate qualitative results through biofilm visualization (Mountcastle et al., 2021). Thus, despite the limitations and the variation in quantifying the confocal microscopy images, the qualitative trends express a promising decrease in bacterial abundance and viability in the presence of blood clot treatment.

To further determine the quantifiable and mechanistic properties of the blood clot treatment, we recommend further comprehensive procedures. This includes the utilization of fluorescently tagged *S. epidermidis* combined with time-lapse imaging to allow for the visualization of treatment penetration and biofilm degradation in real time (Palmer et al., 2006) (Schlafer and Meyer, 2017). Additionally, to determine individual bacteria viability throughout the biofilm and in relation to the placement of the blood clot, we propose the use of flow cytometry (Servain-Viel et al., 2024).

4 Discussion and conclusion

Our study shows that fresh fibrin blood clots offer a promising option for the treatment of *S. epidermidis* biofilms and have the potential to prevent infections. Specifically, we saw that the use of blood clot treatments reduces cell load and disrupts architecture. As the

U.S population ages, the number of patients with prosthetic implants susceptible to these infections will continue to rise (Fischbacher and Borens, 2019). Autologous blood clots potentially serve as a cost effective, immunologically inert option for treating these highly resistant infections. It is therefore necessary to continue exploring this treatment through multiple avenues. Primarily, further exploration of the intrinsic mechanism of the blood clot is warranted. To start, continued confocal imaging analysis especially through bacterial staining percentages will foster a mechanistic hypothesis. From there, to identify a more comprehensive understanding of the treatment impact on biofilm structure and environment we will employ scanning electron microscopy (Alhede et al., 2012). Further, a novel approach would be to utilize single-cell RNA sequencing to identify the transcriptional stress response of the bacteria to the blood clot treatment (Korshoj and Kielian, 2024). Once a mechanistic pathway is determined, we suggest further identification of blood clot characteristics, including the blood clot proximity to the biofilm using transwell inserts, and the effects of individual blood clot components, specifically MMP (Kumar et al., 2019). We also suggest further investigation into the relationship between antibiotics and blood clots in suspension, including potential binding mechanisms. Other investigations have suggested certain antibiotics are capable of binding individual components of blood clots, such as fibrin. Recently, fibrin-based nanoparticles have been used to bind and deliver the antibiotic vancomycin into *Staphylococcus aureus* biofilms (Scull et al., 2024). Platelet rich fibrin has also been used as a delivery mechanism for the antibiotic's vancomycin, linezolid, and gentamicin in an oral surgery context, although specific binding mechanism was not ascertained. They found that vancomycin interfered with PRF formation. Gentamicin and linezolid did not change the physical properties of PRF and were released from membranes in the time intervals examined (Bennardo et al., 2023). It is likely that unique properties of the different antibiotics contribute to the viability of molecular binding, if it is occurring, and therefore we encourage further exploration of these models.

Additionally, it is known that biofilm susceptibility to treatments is impacted by its developmental stage, thus we suggest investigating the addition of blood clot treatments at various biofilm stages (Wang et al., 2023). Through these continued studies, the specificities and mechanism of the blood clot treatment will be established, and additional, translational studies can be focused on. Imperatively, this treatment needs to be investigated using animal models, with and without antibiotics. It would also be beneficial to understand if treatment improves the effectiveness of consequent IV antibiotic treatment, reducing the need for surgical debridement. Finally, we recommend exploring the impact that this treatment can have on polyclonal biofilms, particularly in other clinical models including chronic wounds and burns. Ultimately, the encouraging results found within this study promote a wide range of prospective investigations utilizing blood clots to eradicate biofilms.

Data availability statement

The raw data supporting the conclusions of this article will be made available by the authors, without undue reservation.

Author contributions

KG: Conceptualization, Investigation, Methodology, Writing – original draft, Writing – review & editing. SH: Investigation, Methodology, Writing – original draft, Writing – review & editing. DR: Investigation, Writing – original draft, Writing – review & editing. JK: Investigation, Methodology, Writing – original draft, Writing – review & editing. RS: Resources, Writing – review & editing. YL: Resources, Supervision, Writing – review & editing.

Funding

The author(s) declare financial support was received for the research, authorship, and/or publication of this article. Funding for this project was provided by YL's start up package and partially supported by a WMed pilot grant.

Acknowledgments

We would like to thank the Larson Lab at Western Michigan University Homer Stryker M.D. School of Medicine for generously offering their laboratory space for a selection of this research. We would also like to acknowledge the help of the Flow Cytometry and Imaging Core at Western Michigan University Homer Stryker M.D. School of Medicine.

Conflict of interest

The authors declare that the research was conducted in the absence of any commercial or financial relationships that could be construed as a potential conflict of interest.

Generative AI statement

The author(s) declare that no Generative AI was used in the creation of this manuscript.

Publisher's note

Supplementary material

The Supplementary Material for this article can be found online at: https://www.frontiersin.org/articles/10.3389/fcimb.2025.1507486/full#supplementary-material

References

Alhede, M., Qvortrup, K., Liebrechts, R., Høiby, N., Givskov, M., and Bjarnsholt, T. (2012). Combination of microscopic techniques reveals a comprehensive visual impression of biofilm structure and composition. *FEMS Immunol. Med. Microbiol.* 65, 335–342. doi: 10.1111/j.1574-695X.2012.00956.x

Bennardo, F., Gallelli, L., Palleria, C., Colosimo, M., Fortunato, L., De Sarro, G., et al. (2023). Can platelet-rich fibrin act as a natural carrier for antibiotics delivery? A proof-of-concept study for oral surgical procedures. *BMC Oral. Health* 23, 134. doi: 10.1186/s12903-023-02814-5

Cámara, M., Green, W., MacPhee, C. E., Rakowska, P. D., Raval, R., Richardson, M. C., et al. (2022). Economic significance of biofilms: a multidisciplinary and cross-sectoral challenge. *NPJ Biofilms. Microbiom.* 8, 42. doi: 10.1038/s41522-022-00306-y

Ceri, H., Olson, M. E., Stremick, C., Read, R. R., Morck, D., and Buret, A. (1999). The calgary biofilm device: new technology for rapid determination of antibiotic susceptibilities of bacterial biofilms. *J. Clin. Microbiol.* 37, 1771–1776. doi: 10.1128/JCM.37.6.1771-1776.1999

Chambers, W. B., and Pallagrosi, A. U. (1973). Gentamicin in the treatment of staphylococcal infections. *J. Int. Med. Res.* 1, 442–449. doi: 10.1177/030006057300100211

Darouiche, R. O. (2004). Treatment of infections associated with surgical implants. *N. Engl. J. Med.* 350, 1422–1429. doi: 10.1056/NEJMra035415

Domínguez-Herrera, J., Docobo-Perez, F., López-Rojas, R., Pichardo, C., Ruiz-Valderas, R., Lepe, J. A., et al. (2012). Efficacy of Daptomycin versus Vancomycin in an Experimental Model of Foreign-Body and Systemic Infection Caused by Biofilm Producers and Methicillin-Resistant Staphylococcus epidermidis. *Antimicrobial. Agents Chemother.* 56 (2), 613–617. doi: 10.1128/AAC.05606-11

European Committe for Antimicrobial Susceptibility Testing (2000). Terminology relating to methods for the determination of susceptibility of bacteria to antimicrobial agents. *EUCAST. Definitive. Document. E.Def. 1.2* 6 (9), 503–508. doi: 10.1046/j.1469-0691.2000.00149.x

Evans, R. C., and Holmes, C. J. (1987). Effect of vancomycin hydrochloride on Staphylococcus epidermidis biofilm associated with silicone elastomer. *Antimicrob. Agents Chemother.* 31, 889–894. doi: 10.1128/AAC.31.6.889

Fischbacher, A., and Borens, O. (2019). Prosthetic-joint infections: mortality over the last 10 years. *J. Bone Joint Infect.* 4, 198–202. doi: 10.7150/jbji.35428

Haney, E., Trimble, M., Cheng, J., Vallé, Q., and Hancock, R. (2018). Critical assessment of methods to quantify biofilm growth and evaluate antibiofilm activity of host defence peptides. *Biomolecules* 8, 29. doi: 10.3390/biom8020029

Herigstad, B., Hamilton, M., and Heersink, J. (2001). How to optimize the drop plate method for enumerating bacteria. *J. Microbiol. Methods* 44, 121–129. doi: 10.1016/S0167-7012(00)00241-4

Karmakar, A., Dua, P., and Ghosh, C. (2016). Biochemical and molecular analysis of staphylococcus aureus clinical isolates from hospitalized patients. *Can. J. Infect. Dis. Med. Microbiol.* 2016 (1), 9041636. doi: 10.1155/2016/9041636

Khatoon, Z., McTiernan, C. D., Suuronen, E. J., Mah, T.-F., and Alarcon, E. I. (2018). Bacterial biofilm formation on implantable devices and approaches to its treatment and prevention. *Heliyon* 4, e01067. doi: 10.1016/j.heliyon.2018.e01067

Korshoj, L. E., and Kielian, T. (2024). Bacterial single-cell RNA sequencing captures biofilm transcriptional heterogeneity and differential responses to immune pressure. *Nat. Commun.* 15, 10184. doi: 10.1038/s41467-024-54581-8

Ku, J. C., Pan, H., Abd, G. M., Richter, D. M., Minor, A., Sawyer, R. G., et al. (2024). Blood clots used as natural biomaterials for antibiotic delivery in *vitro*. *J. Surg. Res.* 303, 224–232. doi: 10.1016/j.jss.2024.09.018

Kumar, L., Cox, C. R., and Sarkar, S. K. (2019). Matrix metalloprotease-1 inhibits and disrupts E*nterococcus faecalis* biofilms. *PloS One* 14, e0210218. doi: 10.1371/journal.pone.0210218

Lee, E., and Anjum, F. (2024).Staphylococcus epidermidis Infection. In: *StatPearls* (Treasure Island (FL: StatPearls Publishing). Available online at: http://www.ncbi.nlm.nih.gov/books/NBK563240/ (Accessed December 20, 2024).

Lories, B., Roberfroid, S., Dieltjens, L., De Coster, D., Foster, K. R., and Steenackers, H. P. (2020). Biofilm bacteria use stress responses to detect and respond to competitors. *Curr. Biol.* 30, 1231–1244.e4. doi: 10.1016/j.cub.2020.01.065

Macia, M. D., Rojo-Molinero, E., and Oliver, A. (2014). Antimicrobial susceptibility testing in biofilm-growing bacteria. *Clin. Microbiol. Infect.* 20, 981–990. doi: 10.1111/1469-0691.12651

Mountcastle, S. E., Vyas, N., Villapun, V. M., Cox, S. C., Jabbari, S., Sammons, R. L., et al. (2021). Biofilm viability checker: An open-source tool for automated biofilm viability analysis from confocal microscopy images. *NPJ Biofilms. Microbiom.* 7, 44. doi: 10.1038/s41522-021-00214-7

O'Toole, G. A. (2011). Microtiter dish biofilm formation assay. *JoVE* 2437. doi: 10.3791/2437-v

Okae, Y., Nishitani, K., Sakamoto, A., Kawai, T., Tomizawa, T., Saito, M., et al. (2022). Estimation of minimum biofilm eradication concentration (MBEC) on *in vivo* biofilm on orthopedic implants in a rodent femoral infection model. *Front. Cell. Infect. Microbiol.* 12. doi: 10.3389/fcimb.2022.896978

Oliveira, W. F., Silva, P. M. S., Silva, R. C. S., Silva, G. M. M., MaChado, G., Coelho, L. C. B. B., et al. (2018). Staphylococcus aureus and Staphylococcus epidermidis infections on implants. *J. Hosp. Infect.* 98, 111–117. doi: 10.1016/j.jhin.2017.11.008

Otto, M. (2008). Staphylococcal biofilms. *Curr. Top. Microbiol. Immunol.* 322, 207–228. Available at: https://www.ncbi.nlm.nih.gov/pmc/articles/PMC2777538/.

Otto, M. (2018). Staphylococcal biofilms. *Microbiol. Spectr.* 6, 6.4.27. doi: 10.1128/microbiolspec.GPP3-0023-2018

Palmer, R. J., Haagensen, J. A. J., Neu, T. R., and Sternberg, C. (2006). "Confocal microscopy of biofilms — Spatiotemporal approaches," in *Handbook Of Biological Confocal Microscopy*. Ed. J. B. Pawley (Springer US, Boston, MA), 870–888. doi: 10.1007/978-0-387-45524-2_51

Pitts, B., and Stewart, P. (2008). Confocal laser microscopy on biofilms: successes and limitations. *Microscopy. Today* 16, 18–23. doi: 10.1017/S1551929500059733

Reichhardt, C., and Parsek, M. R. (2019). Confocal laser scanning microscopy for analysis of pseudomonas aeruginosa biofilm architecture and matrix localization. *Front. Microbiol.* 10. doi: 10.3389/fmicb.2019.00677

Ribeiro, M., Monteiro, F. J., and Ferraz, M. P. (2012). Infection of orthopedic implants with emphasis on bacterial adhesion process and techniques used in studying bacterial-material interactions. *Biomatter* 2, 176–194. doi: 10.4161/biom.22905

Rosenberg, M., Azevedo, N. F., and Ivask, A. (2019). Propidium iodide staining underestimates viability of adherent bacterial cells. *Sci. Rep.* 9. doi: 10.1038/s41598-019-42906-3

Schindelin, J., Arganda-Carreras, I., Frise, E., Kaynig, V., Longair, M., Pietzsch, T., et al. (2012). Fiji: an open-source platform for biological-image analysis. *Nat. Methods* 9, 676–682. doi: 10.1038/nmeth.2019

Schlafer, S., and Meyer, R. L. (2017). Confocal microscopy imaging of the biofilm matrix. *J. Microbiol. Methods* 138, 50–59. doi: 10.1016/j.mimet.2016.03.002

Scull, G., Aligwekwe, A., Rey, Y., Koch, D., Nellenbach, K., Sheridan, A., et al. (2024). Fighting fibrin with fibrin: Vancomycin delivery into coagulase-mediated *Staphylococcus aureus* biofilms via fibrin-based nanoparticle binding. *J. Biomed. Mater. Res.* 112, 2071–2085. doi: 10.1002/jbm.a.37760

Servain-Viel, S., Aknin, M.-L., Domenichini, S., Perlemuter, G., Cassard, A.-M., Schlecht-Louf, G., et al. (2024). A flow cytometry method for safe detection of bacterial viability. *Cytomet. Pt. A.* 105, 146–156. doi: 10.1002/cyto.a.24794

Severn, M. M., and Horswill, A. R. (2023). Staphylococcus epidermidis and its dual lifestyle in skin health and infection. *Nat. Rev. Microbiol.* 21, 97–111. doi: 10.1038/s41579-022-00780-3

Sharma, D., Misba, L., and Khan, A. U. (2019). Antibiotics versus biofilm: an emerging battleground in microbial communities. *Antimicrob. Resist. Infect. Control.* 8, 76. doi: 10.1186/s13756-019-0533-3

Shree, P., Singh, C. K., Sodhi, K. K., Surya, J. N., and Singh, D. K. (2023). Biofilms: Understanding the structure and contribution towards bacterial resistance in antibiotics. *Med. Microecol.* 16, 100084. doi: 10.1016/j.medmic.2023.100084

Skovdal, S. M., Jørgensen, N. P., and Meyer, R. L. (2022). JMM profile: staphylococcus epidermidis. *J. Med. Microbiol.* 71, 1597. doi: 10.1099/jmm.0.001597

Tille, P. M. (2017). *Bailey & Scott's diagnostic microbiology. Fourteenth edition* (St. Louis, Missouri: Elsevier).

Wang, X., Liu, M., Yu, C., Li, J., and Zhou, X. (2023). Biofilm formation: mechanistic insights and therapeutic targets. *Mol. BioMed.* 4, 49. doi: 10.1186/s43556-023-00164-w

Wood, T. K., Knabel, S. J., and Kwan, B. W. (2013). Bacterial persister cell formation and dormancy. *Appl. Environ. Microbiol.* 79, 7116–7121. doi: 10.1128/AEM.02636-13

frontiers | Frontiers in Cellular and Infection Microbiology

TYPE Original Research
PUBLISHED 14 July 2025
DOI 10.3389/fcimb.2025.1545119

OPEN ACCESS

EDITED BY
Olivier Habimana,
Guangdong Technion-Israel Institute of Technology (GTIIT), China

REVIEWED BY
Ifeanyi Elibe Mba,
University of Ibadan, Nigeria
Rajwinder Kaur,
Chitkara University, India

*CORRESPONDENCE
María Gabriela Paraje
gparaje@unc.edu.ar;
gabrielaparaje@gmail.com

RECEIVED 14 December 2024
ACCEPTED 19 June 2025
PUBLISHED 14 July 2025

CITATION
Lopez Venditti ED, Crespo Andrada KF, Bustos PS, Maldonado Torales M, Manrrique Hughes I, Paraje MG and Guiñazú N (2025) Antibacterial, antifungal, and antibiofilm activities of biogenic zinc nanoparticles against pathogenic microorganisms. *Front. Cell. Infect. Microbiol.* 15:1545119. doi: 10.3389/fcimb.2025.1545119

Antibacterial, antifungal, and antibiofilm activities of biogenic zinc nanoparticles against pathogenic microorganisms

Eliana Daniela Lopez Venditti[1,2], Karina Fernanda Crespo Andrada[3,4], Pamela Soledad Bustos[5], Manuela Maldonado Torales[3,4], Iván Manrrique Hughes[3,4], María Gabriela Paraje[3,4]* and Natalia Guiñazú[1,2]

[1]Centro de Investigaciones en Toxicología Ambiental y Agrobiotecnología del Comahue (CITAAC), Consejo Nacional de Investigaciones Científicas y Técnicas (CONICET), Neuquén, Argentina, [2]Departamento de Ciencias del Ambiente y la Salud, Facultad de Ciencias del Ambiente y la Salud, Universidad Nacional del Comahue, Neuquén, Argentina, [3]Cátedra de Microbiología, Facultad de Ciencias Exactas, Físicas y Naturales, Universidad Nacional de Córdoba, Córdoba, Argentina, [4]Instituto Multidisciplinario de Biología Vegetal (IMBIV), Consejo Nacional de Investigaciones Científicas y Técnicas (CONICET), Córdoba, Argentina, [5]Departamento de Ciencias Farmacéuticas, Facultad de Ciencias Químicas, Universidad Nacional de Córdoba, Haya de la Torre y Medina Allende, Córdoba, Argentina

Introduction: The increasing resistance to antimicrobial drugs has prompted global efforts to combat pathogenic bacteria and fungi. The World Health Organization's recent report underscores the urgent need for innovative antimicrobial strategies to address infections caused by *Staphylococcus aureus*, *Escherichia coli*, *Candida albicans*, and *Candida tropicalis*. This study presents a comparative evaluation of the effects of biogenically synthesized zinc nanoparticles (ZnNPs) from *Pseudomonas aeruginosa*, highlighting their effectiveness against both planktonic and sessile forms of these tested pathogens.

Methods: The antimicrobial effects were assessed using the Kirby-Bauer disk diffusion method, broth microdilution, and time-kill assays. Biofilm formation and eradication were evaluated through crystal violet staining, resazurin assays, and colony-forming unit quantification. Additionally, the oxidative and nitrosative stress toxicity mechanisms triggered by ZnNPs, particularly those related to cellular stress, were investigated.

Results: The results demonstrated that ZnNPs exhibit concentration-dependent inhibitory effects on both prokaryotic and eukaryotic microorganisms. ZnNPs inhibit biofilm formation by up to 50% in *E. coli* and yeast species, and up to 80% in *S. aureus*.

Discussion: These antibiofilm activities were attributed to disruptions in cellular stress metabolism, primarily driven by nitrosative stress through enhanced production of reactive nitrogen intermediates. ZnNPs synthesized through green methods offer significant advantages due to their biocompatibility and potential biomedical applications. These findings advance our understanding of ZnNPs in combating biofilm-associated infections, offering promising strategies to address pathogenic bacteria and fungi, which pose a critical threat to global health.

KEYWORDS

biogenic zinc nanoparticles, antibacterial activity, antifungal activity, biofilm associated infections, oxidative stress, nitrosative stress, total antioxidant capacity

1 Introduction

The increasing resistance to antimicrobial drugs has complicated the effective treatment of infections, leading to the establishment of global priorities and guidelines to improve the management of pathogenic bacteria and fungi, which pose a critical threat to global health. The World Health Organization (WHO) recently published a report prioritizing pathogenic bacteria and fungi to guide research and public health efforts in combating resistant infections. This report highlights key bacteria and fungi associated with antimicrobial resistance and underscores the urgent need for innovative strategies, including the development of new antimicrobial agents (Vitiello et al., 2023; WHO, 2024). For instance, *Staphylococcus aureus*, particularly methicillin-resistant *S. aureus*, is classified as a high priority due to its widespread resistance and significant burden on healthcare systems. Similarly, *Escherichia coli*, especially extended-spectrum beta-lactamase (ESBL)-producing and carbapenem-resistant strains, is listed as a critical priority because of its association with life-threatening infections and limited therapeutic options. Among fungal pathogens, *Candida albicans* is recognized as a critical priority, while *Candida tropicalis* is classified as a high priority (Jesudason, 2024).

Biogenic metal nanoparticles (NPs) have significant potential in biomedical applications, providing innovative solutions to various health challenges. In particular, microbial resistance to conventional antimicrobial treatments and the persistent infections caused by bacteria and fungi represent critical health concerns that can potentially be addressed using metal NPs (Paraje, 2023; Arora et al., 2024). Both bacteria and yeast have evolved various virulence strategies to ensure infection persistence, one of the most significant being biofilm formation. Biofilms are structured, three-dimensional communities of microorganisms that play a crucial role in infection development and persistence, significantly increasing antimicrobial resistance compared to their planktonic (free-floating) counterparts (Paraje, 2023; Coenye et al., 2024).

Zinc (Zn), a trace metal essential for human health, is critical for optimal enzyme activity across various organs and systems. It plays a fundamental role in numerous physiological and metabolic processes (Costa et al., 2023). Zn is a promising candidate for NPs production due to its high reduction potential. As an active element and a powerful reducing agent, Zn can be easily oxidized to form zinc oxide (ZnO) (Kalaba et al., 2024). Zinc nanoparticles (ZnNPs) and zinc oxide nanoparticles (ZnO NPs) have emerged as promising materials for various medical applications due to their biocompatibility, antimicrobial activity, and multifunctional properties (Krol et al., 2017). This property makes Zn advantageous for the synthesis of ZnO NPs, which have potential applications for nano-optical and nano-electronic devices, as well as in food packaging and medicine, where they exhibit antimicrobial and antitumor properties (Costa et al., 2023; Masoudi et al., 2024).

Biological methods have been developed for NP synthesis and various studies have demonstrated that bacteria can produce metal NPs both intra- and extracellularly (Kulkarni et al., 2023; Rasheed et al., 2024). Intracellular biosynthesis occurs within the bacterial biomass, whereas extracellular biosynthesis is achieved using cell-free extracts or bacterial culture supernatants (Borehalli Mayegowda et al., 2023). Particularly, *E. coli* and *Pseudomonas aeruginosa* have been shown to produce metallic NPs from iron, silver, and gold salts. Among these, *P. aeruginosa* can transform metal salts into stable metallic NPs through biochemical processes involving enzymes, proteins, and polysaccharides that act as reducing and stabilizing agents. This environmentally friendly and cost-effective green synthesis approach, combined with *P. aeruginosa*'s adaptability to diverse environmental conditions and rapid growth rate, makes it a promising candidate for the sustainable biosynthesis of ZnNPs (Crespo et al., 2016; Ihsan et al., 2023; Okaiyeto et al., 2024).

This research hypothesizes that biogenic ZnNPs display antimicrobial and antibiofilm capabilities, in both bacteria and yeast strains. Thus, the present study explored the antimicrobial and antibiofilm activities of ZnNPs synthesized with green methods, obtained by microbial synthesis using *P. aeruginosa*. For this purpose, a comparative evaluation was conducted to assess the antimicrobial activity against both planktonic and sessile cells of two bacterial strains, *S. aureus* and *E. coli*, as well as two yeast strains, *C. albicans* and *C. tropicalis*. Research also focused on ZnNP toxicity mechanisms by the determination of reactive oxygen species (ROS), reactive nitrogen intermediates (RNI) and total oxidative stress response (OSR), in the bacteria and yeast treated with the ZnNPs.

To the best of our knowledge, this is the first study to comprehensively investigate the multifunctional antimicrobial of biogenic ZnNPs synthesized by *P. aeruginosa*, demonstrating their effectiveness against both bacterial and yeast biofilms. Our findings provide valuable insights into how these eco-friendly nanoparticles combat biofilm-associated infections caused by *S. aureus, E. coli, C. albicans*, and *C. tropicalis*. Furthermore, the development of novel strategies to eradicate biofilms holds significant clinical promise, particularly for treating the growing population of at-risk patients.

2 Materials and methods

2.1 Reagents

Trypticase Soy Broth (TSB), Trypticase Soy Agar (TSA), Sabouraud Dextrose Broth (SDB), and Sabouraud Dextrose Agar (SDA) were purchased from Difco (MI, USA) and prepared according to the manufacturer's instructions. Muller-Hinton Broth (MHB) and Mueller-Hinton agar (MHA) were obtained from Britania (Buenos Aires, Argentina) and prepared as per the manufacturer's guidelines. Zinc sulfate heptahydrate ($ZnSO_4{\cdot}7H_2O$), $NaNO_2$, $FeSO_4$, $FeCl_3{\cdot}6H_2O$ and Crystal Violet (CV) were acquired from Cicarelli (Santa Fe, Argentina). Resazurin-resorufin (Alamar Blue, AB), Amphotericin B (AmB), Nitro Blue Tetrazolium (NBT), fetal bovine serum sulfanilamide, N-1-naphthyl ethylene diamine dihydrochloride, Roswell Park Memorial Institute (RPMI) 1640 medium, D-glucose, glutamine,

morpholinepropanesulfonic acid, and 2,4,6-tripyridyl-s-triazine, were sourced from Sigma-Aldrich Co. (St. Louis, MO, USA). Ciprofloxacin (CIP) was supplied by Roemmers (Buenos Aires, Argentina). HCl, dimethyl sulfoxide (DMSO), ethanol, acetic acid, and glycerol were obtained from Anedra (Buenos Aires, Argentina). Phosphate-buffered saline (PBS) 10x stock (8% NaCl, 0.2% KCl, 1.44% Na_2HPO_4, 0.24% KH_2PO_4) was prepared and filter-sterilized. Petri dishes and flat-bottom 96-well plates were provided by Greiner Bio-One (Frickenhausen, Germany).

2.2 Bacterial and fungal strains and biogenic ZnNPs

The bacterial strains *S. aureus* ATCC 29213 and *E. coli* ATCC 25922 were used for antimicrobial studies (Arce Miranda et al., 2011; Angel Villegas et al., 2015). Additionally, the yeast strains *C, albicans* SC 5314 and *C. tropicalis* NCPF 311 were employed (Miranda et al., 2019; Da Silva et al., 2021). All strains were stored in cryovials containing 20% glycerol at −80°C until use in the *in vitro* studies. For antimicrobial activity assays, the bacterial genus was subcultured on TSA, while the yeast genus was subcultured on SDA. The cultures were incubated at 37°C for 24 hours prior to use. The biogenic ZnNPs described in previous studies were utilized in this work (Crespo et al., 2016; Okaiyeto et al., 2024). Experimental flowchart including biosynthesis and following experiments is shown as Supplementary material 1 (Supplementary Figure S1).

The ZnNPs physicochemical properties are detailed in Supplementary Material 2, which includes UV-Vis spectroscopy (Supplementary Figure S2A), zeta potential analysis (Supplementary Figure S2B), transmission electron microscopy (TEM; Supplementary Figure S2C), and scanning electron microscopy (SEM; Supplementary Figure S2D). Additionally, Supplementary Material 3 presents Fourier-transform infrared (FT-IR) spectroscopy (Supplementary Figure S3A), SDS-PAGE with silver staining (Supplementary Figure S3B), and fluorescence (FL) spectroscopy (Supplementary Figure S3C). Together, these analyses provide comprehensive information on the size, surface charge, morphology, and surface chemistry of the ZnNPs.

2.3 Determination of microbial susceptibility to ZnNPs by the Kirby-Bauer method

MHB was used to prepare the agar medium for bacterial cultures. Fresh overnight cultures of *S. aureus* and *E. coli* were grown in TSB until reaching the logarithmic growth phase. The bacterial suspensions were standardized by adjusting the turbidity to 0.5 McFarland standards with McFarland Densitometer DEN-1B (Britania, Argentina). For the candidal species, fresh overnight cultures of *C. albicans* and *C. tropicalis* were prepared in SDB and standardized to 0.5 McFarland (Kourmouli et al., 2018).

The inoculum was uniformly swabbed onto individual Petri dishes containing MHA, following the Clinical and Laboratory Standards Institute (CLSI) guidelines (Clinical and Laboratory Standards Institute, 2018). A sterile cotton swab, moistened with each inoculum suspension, was used to inoculate 30 mL of MHA in 90-mm diameter plates. The agar plates were left to dry for 3–15 minutes, after which wells were created using a cork borer (5 mm diameter). Reference antibiotics agents (CIP and AmB, in DMSO 1% v/v), biogenic ZnNPs, biosynthesis supernatant (SN) and $ZnSO_4$, were dispensed into the wells on the inoculated plates, which were subsequently incubated at 37°C for 24 hours. After incubation, diameter of the zones of inhibition was measured using a standard caliper (mm), based on three independent determinations performed in duplicate. The zone of clearing around each well was measured to evaluate the susceptibility of the tested microorganisms, taking into account the diameter of the wells themselves (5 mm ± 1 mm).

The percentage inhibition of diameter growth (PIDG) was calculated to evaluate the antimicrobial activity of the ZnNPs relative to the positive control. PIDG values were estimated according to the following equation (Himratul-Aznita et al., 2011):

$$PIDG(\%) = \frac{Diameter\ \ of\ \ trated\ \ sample - Diameter\ \ of\ \ positive\ \ control}{Diameter\ \ of\ \ positive\ \ control} X\ \ 100$$

2.4 Antibacterial and antifungal activity in planktonic cells

An important limitation of the Kirby-Bauer method is that it does not provide a minimum inhibitory concentration (MIC) value. The MIC was defined as the lowest concentration of the antimicrobial agent that resulted in a 99.9% reduction of the initial inoculum after subculturing onto fresh media. Therefore, the MIC, the minimum bactericidal concentration (MBC) and the minimum fungicidal concentration (MFC) were determined using the standard tube dilution method, following the guidelines established by the CLSI (Clinical and Laboratory Standards Institute, 2017, 2020). The antibacterial and antifungal effects of ZnNPs were assessed using overnight cultures of each microorganism, diluted to achieve a cell density equivalent to 0.5 on the McFarland scale. Serial dilutions of ZnNPs (ranging from 0 to 6600 μg/mL) were prepared in a 96-well microtiter plate and incubated at 37°C for 24 hours in triplicate (Pierce et al., 2008; Da Silva et al., 2022, 2024; Herman et al., 2024).

To assess metabolic activity and confirm the MIC value, the resazurin-resorufin (AB) assay was employed, based on the redox status of microbial cells (Herman et al., 2024). An aliquot of 20 μL of a 0.02% (w/v) AB solution was added to each well and incubated at 37°C for 30 minutes. Following incubation, the absorbance was recorded at 570 nm using a microplate reader (Infinite F50 Model, Tecan, AUS). Color changes in the wells were evaluated: pink indicated microbial cell viability, while blue signified microbial cell death. The AB solution was aliquoted and stored at −80°C to

maintain stability and was brought to room temperature before use (Da Silva et al., 2022, 2024).

For MBC and MFC determination, viable cell counts were obtained from samples that showed no visible growth after incubation at 37°C for 24 hours and the colony-forming units (CFU) were counted and expressed as CFU/mL (Peralta et al., 2015, 2016, 2018; Da Silva et al., 2022, 2024). The lowest concentration that prevented the growth of bacterial or yeast colonies on antifungal- or antibiotic-free media was defined as the MBC or MFC, respectively. Each assay was performed in triplicate, and the mean percentage reduction in metabolic activity was used to confirm the MIC.

Controls included growth controls, SN and sterility controls. Strain viability and medium sterility were monitored concurrently to ensure the reliability of the results. Antibiotic or antifungal solution (CIP and AmB) were used as positive controls, dissolved in DMSO (1% v/v) to enhance solubility and stability. Activities were classified as bactericidal (MBC/MIC ≤ 4) or bacteriostatic (MBC/MIC > 4), and as fungicidal (MFC/MIC ≤ 4) or fungistatic (MFC/MIC > 4) based on these ratios (Arce Miranda et al., 2011; Angel Villegas et al., 2015; Da Silva et al., 2022, 2024).

2.5 Time-kill curves

A time-kill curve assay was performed using at MIC and higher concentrations and cell densities for each sample were determined by performing colony counts. This involved diluting the samples in PBS (pH 7.2 ± 0.1), plating them on TSA Petri dishes for bacteria and SDA for *Candida* species, and enumerating colony-forming units (CFU) to estimate viable cell counts, with a detection limit of 100 CFU/mL. To ensure reliability and reproducibility, each assay was performed in triplicate. Positive controls included CIP for *E. coli* and *S. aureus* and AmB for *C. albicans* and *C. tropicalis* were included. A negative control, referred to as the growth control, was also included, where microbial cells were incubated without ZnNPs for the same duration (Da Silva et al., 2021; Yakoup et al., 2024).

2.6 Antimicrobials susceptibility assay in biofilms

Based on the method described by O'Toole and Kolter (1998), mature biofilm formation was quantified using CV staining in 96-well polystyrene microtiter plates (O'Toole and Kolter, 1998; Peralta et al., 2015, 2016, 2018; Da Silva et al., 2021, 2022, 2024). Biofilms of each studied species were prepared by adding 100 µL of a suspension standardized to 1.0 McFarland in each well of flat-bottomed 96-well microtiter plates. To allow mature biofilm formation, after a 90-minute cell adhesion period, the wells were gently washed three times with sterile PBS (pH 7.2 ± 0.1). Then, TSB (200 µL) was added to each well, and the plates were incubated at 37°C for 24 hours (Peralta et al., 2015, 2016, 2018; Da Silva et al., 2021, 2022, 2024). Different concentrations of ZnNPs, including sub-MIC level (1/2 MIC), the MIC, and supra-MIC levels (5×, 10×, 25×, 50× and 100× MIC), were added to wells containing mature biofilms. The samples were then incubated at 37°C for 24 hours. After the incubation time, the supernatant was collected for ROS, RNI, and antioxidants quantification assays, and the wells were rinsed three times with PBS and air-dried for 24 hours (Peralta et al., 2015, 2016, 2018; Da Silva et al., 2021, 2022, 2024).

Biofilms were stained with 200 µL of 1% (w/v) CV solution per well for 5 minutes. After staining, the CV solution was removed, and the wells were washed three times with 300 µL of PBS pH 7.2 ± 0.1. For the quantification of mature biofilm, CV was extracted with 200 µL of an ethanol/glacial acetone solution for 5 minutes (70:30, v/v).

Absorbance was measured spectrophotometrically at 595 nm using a microplate reader (Infinite F50 Model, Tecan, AUS). The biofilm biomass unit (BBU) was arbitrarily defined as 1 BBU = 0.1 optical density $(OD)_{595nm}$. Untreated biofilms were considered positive controls for mature biofilm formation, and the OD of the control wells was subtracted from that of all tested wells. Each strain was tested in three independent experiments conducted on different days to ensure reproducibility (Peralta et al., 2016; Da Silva et al., 2021, 2022).

Sessile Minimum Inhibitory Concentration (SMIC50 and SMIC80) for ZnNPs was determined based on a 50% and 80% reduction in absorbance of mature biofilm biomass following treatment with the NPs, compared to untreated control biofilms formed under identical conditions.

The percentage of biofilm reduction was calculated using the following equation (Arce Miranda et al., 2011; Angel Villegas et al., 2015; Peralta et al., 2015, 2016, 2018; Da Silva et al., 2021, 2022, 2024):

$$Reduction\ (\%) = \frac{BBU\ \ untreated\ -BBU\ \ treated}{BBU\ \ untreated}\ x\ 100$$

2.7 Minimal biofilm eradication concentration

The minimal biofilm eradication concentration (MBEC) was determined by the cultivable sessile cells of mature biofilms after exposure to the ZnNPs using plate counting (CFU/mL), 24 hours of incubation at 37°C. The MBEC50 represents a 50% reduction in viable sessile cells, while the MBEC80 represents an 80% reduction in viable sessile cells of mature biofilm. To resuspend and homogenize the sessile cells, the microplate was sonicated for 1 minute at 40 kHz. Subsequently, 100 µL of sterile PBS previously diluted in serial dilution in PBS were seeded onto a TSA or SDA plate and incubated for 24-48 h at 37°C. The MBEC determined by the AB assay was defined as the reduction of mature biofilm biomass by ≤50% or 80% following the addition of AB. The sessile "Live cells" correspond to the measurement obtained from AB staining, and "Total biofilm" is determined based on the biomass (sessile cells and extracellular matrix) measurement from CV staining (Peralta et al., 2015, 2016, 2018; Da Silva et al., 2021, 2022, 2024; Herman et al., 2024):

The percentage of viability was calculated using the following equation:

$$Viability\ (\%) = \frac{AB\ or\ CFU\ (Live\ Cells)}{BBU\ (Live\ Cells + Dead\ Cells + EPS)}\ x\ 100$$

2.8 Quantification of oxidative and nitrosative stress

ROS production was quantified spectrophotometrically (Baronetti et al., 2011; Arce Miranda et al., 2021). In brief, 100 µL of supernatant separated was incubated with 100 µL of NBT for 30 minutes at 37°C, and the absorbance was measured at 540 nm using a microplate reader (Arce Miranda et al., 2011, 2021; Baronetti et al., 2011; Angel Villegas et al., 2015; Peralta et al., 2018, 2015, 2016; Miranda et al., 2019; Quinteros et al., 2021b, 2021a; Da Silva et al., 2021, 2022, 2024).

The production of RNI was assessed indirectly using the Griess reaction, which quantifies its stable degradation products, nitrate and nitrite. For this assay, 50 µL of supernatant was mixed with 200 µL of Griess reagent, consisting of sulfanilamide (1.5% in 1 N HCl) and N-1-naphthyl ethylene diaminedihydrochloride (0.13% in sterile distilled water). Absorbance was recorded at 540 nm. Sodium nitrite (1 mM) was used as the standard, and a calibration curve was constructed in the range of 100–0.05 mM (Arce Miranda et al., 2011; Baronetti et al., 2013; Angel Villegas et al., 2015; Da Silva et al., 2021; Haddi et al., 2024).

2.9 Total oxidative stress response

The determination of the OSR, enzymatic and non-enzymatic systems, was assessed using the Ferric Reducing Antioxidant Power (FRAP) assay. Microbial suspensions were incubated with 2,4,6-tripyridyl-1,3,5-triazine (TPTZ) in 40 mM HCl, 0.125 mL of 5.4 mg/mL $FeCl_3$Æ6H_2O plus 1.25 mL of 300 mM acetate buffer (pH 3.6). The production of ferrous tripyridyltriazine (Fe^{2+}-TPTZ) complex was evaluated at 595 nm. The FRAP values were calculated using a $FeSO_4$ calibration curve (Arce Miranda et al., 2011; Angel Villegas et al., 2015; Peralta et al., 2015, 2016, 2018; Da Silva et al., 2021, 2022, 2024; Quinteros et al., 2021b, 2021a).

2.10 Statistical analysis

Statistical analysis was conducted using triplicate groups, and each experiment was repeated three times (n = 9). The data are presented as means ± standard deviation. ANOVA was used for analysis, followed by the Student-Newman-Keuls test for multiple comparisons, with *p < 0.1 and ** p < 0.01 for differences compared to untreated biofilms. #p <0.01 differences considered significant for comparisons of ZnNPs and the antimicrobial controls (CIP and AmB) or SMIC and MBEC. Graphical statistical analysis was carried out using GraphPad Prism 6.0 and Microsoft Excel.

3 Results

3.1 Susceptibility of planktonic bacteria and yeast to ZnNPs

The disk diffusion method is one of the oldest techniques used to evaluate the antimicrobial activity of novel compounds. This method assesses the efficacy of a compound by measuring the diameter of the inhibition zone, which reflects its antimicrobial susceptibility against the tested microorganism (Kourmouli et al., 2018). In this study, the antimicrobial activity of biogenic ZnNPs was evaluated using the Kirby-Bauer disk diffusion method against planktonic bacterial and yeast cells, specifically *E. coli* ATCC 25922, *S. aureus* ATCC 29213, *C. albicans* SC 5314, and *C. tropicalis* NCPF 3111. All tested microorganisms exhibited inhibition halos, confirming the antimicrobial activity of ZnNPs. Figures 1A–D illustrate the inhibition zones (halos), while Table 1 provides quantitative data on inhibition diameters in millimeters (mm), ranging from -18.76 ± 1.00 mm to 28.74 ± 1.74 mm. Wells containing CIP served as positive controls for bacterial species, while AmB was used for yeast. Negative controls, including SN and $ZnSO_4$, showed no inhibition halos. The ZnNPs exhibited significant antibacterial activity, with inhibition zone diameters of 28.74 ± 1.74 mm for *S. aureus* and 21.04 ± 0.34 mm for *E. coli*. In contrast, the antifungal activity was lower, as indicated by the inhibition zone of -18.76 mm for *C. albicans* and 26.110 ± 0.86 for *C. tropicalis*.

Based on the PIDG values, which reflect the strength of antimicrobial activity in relation to established antimicrobial agents used in treatments. All tested bacteria and yeasts were found to be susceptible to the biogenic ZnNPs. Higher PIDG values correspond to greater antimicrobial activity. Higher PIDG values correspond to greater antimicrobial activity. However, the negative PIDG values observed indicate that the antimicrobial activity of the ZnNPs was generally weaker than that of the positive control. In this study, the positive control was the reference antimicrobial drug, while the negative control represented the baseline with no antimicrobial effect. Therefore, negative PIDG values mean that ZnNPs showed lower antimicrobial activity compared to the reference drug but still exhibited inhibitory effect. The antimicrobial activity of ZnNPs was comparatively weaker than that of the antimicrobial control, as indicated by negative PIDG values. A comparative analysis demonstrated that planktonic bacterial cells were generally more susceptible to ZnNPs than planktonic yeast cells, with *S. aureus* exhibiting the highest susceptibility (-12.75) and *C. albicans* the lowest (-50.18) (Table 1).

The MIC, MBC and MFC were determined using the standard micro broth dilution method on planktonic bacteria and yeast cells treated with varying concentrations of ZnNPs (Clinical and Laboratory Standards Institute, 2017, 2020). The use of AB facilitated the visualization of MIC values for both bacterial and fungal strains (Herman et al., 2024). Table 2 presents the quantitative antibacterial and antifungal activity data. The MIC for *S. aureus* and *E. coli* was determined to be 200 µg/mL and 100

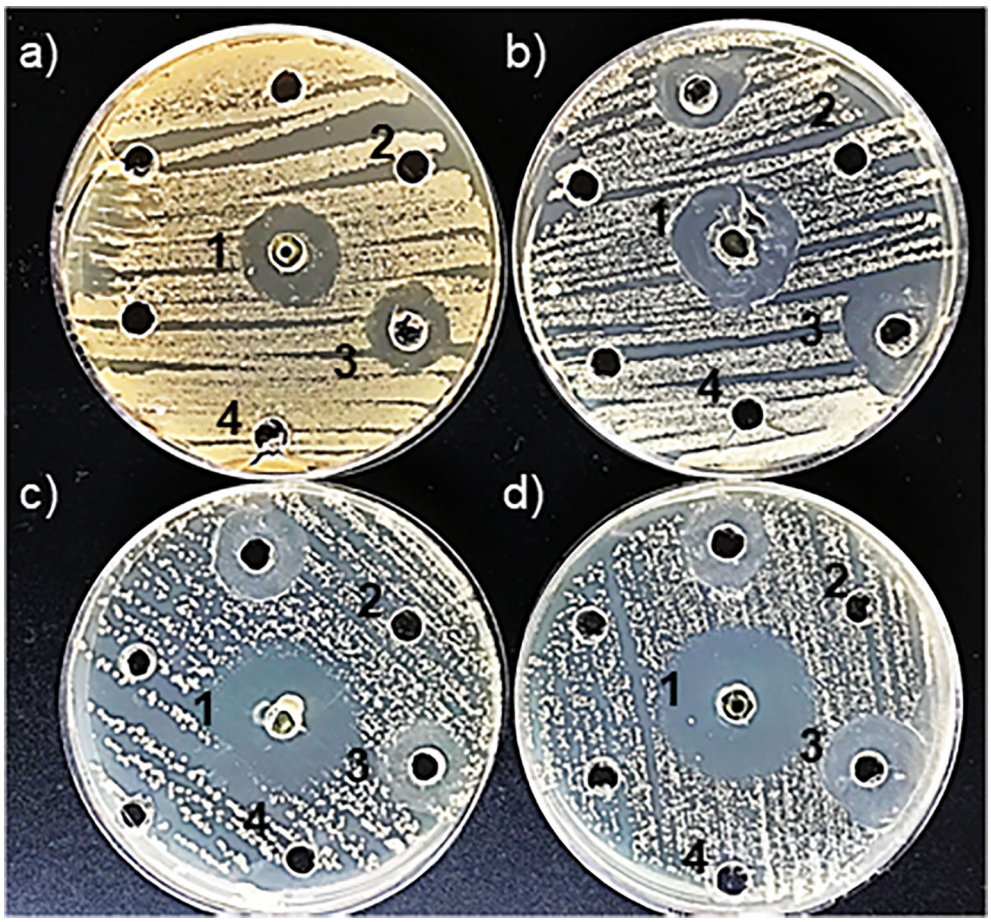

FIGURE 1
Detection of antimicrobial susceptibility using the Kirby-Bauer disk diffusion method by ZnNPs. **(a)** Inhibition halos produced for *E coli*, **(b)** *S. aureus*, **(c)** *C. albicans*, and **(d)** *C. tropicalis*. (1) Positive control: CIP for *E coli* and *S. aureus*; AmB for *C. albicans* and *C tropicalis*. (2) ZnNPs; (3) SN; (4) $ZnSO_4$. Each assay was conducted with three independent determinations, each performed in duplicate.

μg/mL, respectively, while the MBC for both bacterial strains was 200 μg/mL.

The MIC and MFC values for planktonic yeast cells were determined to evaluate their susceptibility to ZnNPs. Both *C. albicans* and *C. tropicalis* reached fungicidal endpoints at 200 μg/mL, which is within the normal range for susceptible strains. However, the MFC for *C. albicans* was 400 μg/mL, whereas for *C. tropicalis*, it was 200 μg/mL.

Additionally, the MBC/MIC and MFC/MIC ratios were calculated to determine the microbicidal efficacy of the ZnNPs. The final column of Table 2 provides the interpretation (INTPN) of the correlation between MIC and MBC values for bacteria, as well as MIC and MFC values for yeast strains. ZnNPs demonstrated effective bactericidal and fungicidal activity, with a ratio ≤ 4.

3.2 Time-kill assay for evaluating antimicrobial activity of ZnNPs

As illustrated in Figure 2, time-kill curves were constructed to evaluate microbial death overtime at MIC concentrations and above (data not shown). The normal growth curve of each microorganism cultured under untreated conditions, represented by the blue lines, demonstrated a substantial increase in growth over time. In contrast, the growth profiles of ZnNP-treated microorganisms (green lines) showed significant deviations from the untreated controls (**p <0.01). The strongest growth-inhibitory response, indicated by the greatest reduction in viable cells, was observed with ZnNPs treatment.

Specifically, *S. aureus* exhibited the highest rate of cell death, with a marked decline in viability observed after 12 hours (Figure 2A, green line, **p < 0.01). In contrast, *E. coli* maintained consistent viability before 24, followed by a significant reduction in viable cells (Figure 2B, green line, **p < 0.01). Similarly, the growth profiles of ZnNPs-treated *C. albicans* (Figure 2C, green line) and *C. tropicalis* (Figure 2D, green line) were significantly altered compared to the untreated controls (**p <0.01). The most substantial inhibitory effect was observed after 12 hours, as indicated by the greatest depletion of viable yeast cells, and more market between 24 and 48 h. Positive controls, represented by the red line in Figure 2, included CIP for *E. coli* and *S. aureus*, and AmB for *C. albicans* and *C. tropicalis*. Differences between ZnNPs and the

TABLE 1 Inhibition zone diameters and PIDG of ZnNPs against different pathogens.

Strains	Inhibition zone diameters (mm)				PIDG (%)
	Positive control	ZnNPs	$ZnSO_4$	SN	
E. coli ATCC 25922	25.90 ± 0.55	21.04 ± 0.34	–	–	-18.76
S. aureus ATCC 29213	32.94 ± 0.24	28.74 ± 1.74	–	–	-12.75
C. albicans SC 5314	39.90 ± 1.13	19.88 ± 1.00	–	–	-50.18
C. tropicalis NCPF 3111	41.20 ± 0.90	26.10 ± 0.86	–	–	-36.65

Percentage inhibition of diameter growth (PIDG), millimeters (mm), biogenic ZnNPs, biosynthesis supernatant (SN).
The PIDG (%) was calculated to assess the antimicrobial activity of the ZnNPs in comparison to the positive control. Positive control: Ciprofloxacin (for *E. coli* and *S. aureus*) and Amphotericin B (for *C. albicans* and *C. tropicalis*); (-) indicates the absence of inhibition zones. All data were the means obtained from three sets of tests carried out in duplicates.

antimicrobial controls (CIP and AmB) are shown in each panel ($^{\#}p<0.01$).

3.3 Total microbial biofilm biomass susceptibility to ZnNPs

Biofilm formation is a pathogenic mechanism employed by bacteria and fungi, contributing to the complications associated with infections caused by these pathogens. Total mature biofilms of both bacteria and yeasts were subjected to serial dilutions at upper and lower MIC levels. In Figure 3, the bar graph represents the total mature biofilm biomass (including sessile cells and extracellular matrix) quantified by crystal violet (CV) staining after antibiofilm activity assays, while the overlaid lines indicate the corresponding percentage of reduction (%R) relative to the untreated biofilms. The results demonstrated that ZnNPs effectively disrupted established mature biofilms of all tested pathogenic strains. *S. aureus* was identified as the strongest biofilm producer, showing greater susceptibility to the antibiofilm effects of ZnNPs compared to untreated controls ($^{**}p < 0.01$). The SMIC50 value was determined to be 200 µg/mL, which was equal to both the MIC and MBC values. The SMIC80 value was achieved at 5 times this value (Figure 3A). Less antibiofilm activity was observed for *E. coli*, where the SMIC50 value was equivalent to the MIC value, however, the SMIC80 value was not achieved, even at concentrations up to 100 times the MIC (Figure 3B, $^{**}p < 0.01$).

TABLE 2 Quantitative data from MIC and MBC assays of ZnNPs against planktonic bacterial and fungal cells.

Strains	Planktonic cells			
	MIC	MBC	MBC/MIC	INTPN
S. aureus ATCC 29213	200	200	1	Bactericide
E. coli ATCC 25922	100	200	2	Bactericide
	MIC	MFC	MFC/MIC	INTPN
C. albicans SC 5314	200	400	2	Fungicide
C. tropicalis NCPF 3111	200	200	1	Fungicide

MIC, minimum inhibitory concentration; MBC, minimum bactericidal concentration; MFC, minimum fungicidal concentration; INTPN, interpretation.
All MIC and MFC data are expressed in terms of µg/mL for ZnNPs. Ciprofloxacin: *E. coli* ATCC 25922: MIC 0.012 µg/mL, MBC 0.12 µg/mL; and *S. aureus* ATCC 29213: MIC 0.25 µg/mL, MBC 2 µg/mL. Amphotericin B: *C. albicans* SC 5314: MIC and MFC 0.25 µg/mL; and *C. tropicalis* NCPF 311: MIC and MFC 0.5 µg/mL.

Regarding the antibiofilm activity of ZnNPs on sessile yeast cells, the SMIC50 value for *C. albicans* was 10 times the MIC (2000 µg/mL). Nevertheless, the SMIC80 threshold was not reached, even when the concentration was increased up to 100-fold above the MIC (Figure 4A, $^{**}p < 0.01$). In the case of *C. tropicalis* exhibited greater sensitivity, achieving the SMIC50 at the same concentration as the MIC (200 µg/mL), indicating higher susceptibility. In contrast, at concentrations 100 times the MIC, the SMIC80 was hardly achieved (Figure 4B, $^{**}p < 0.01$).

Cell viability, assessed through the metabolic activity of microorganisms via aerobic respiration, was determined using resazurin or AB assays. The resazurin method offers a lower detection limit than the OD method, making it well-suited for detecting early metabolic damage induced by ZnNPs. ZnNPs, however, displayed significantly higher microbicidal effects. As shown in Figure 5, ZnNPs had an early and significant impact on the metabolic activity of bacterial and yeast cells, resulting in a lower percentage of cell viability across all studied strains. MBEC50 values were achieved for all tested strains. CFU determination via agar plating, widely regarded as the gold standard for biofilm quantification, proved to be more sensitive in our analysis, further confirming reduced cell viability. Additionally, MBEC80 values were successfully achieved for all strains, highlighting the robust efficacy of ZnNPs. In contrast, neither $ZnSO_4$ nor SN exhibited microbicidal activity, demonstrating that the metal precursor alone lacked antimicrobial efficacy against the tested organisms. Supplementary material 4 evaluates the synergistic effect of ZnNPs in combination with CIP against *S. aureus* and *E. coli*, as well as with AmB against *C. albicans* and *C. tropicalis*. The percentage of viable cells (% viability) was determined by enumerating colony-forming units and resazurin-resorufin (AB) assay (Supplementary Figure S4).

3.4 Cellular stress metabolites and OSR in mature biofilms incubated with ZnNPs

Oxidative stress was investigated as a potential mechanism of action for ZnNPs on mature biofilms. The production of oxidative metabolites, including ROS and RNI, as well as the OSR (measured via the FRAP assay), were evaluated following treatment with ZnNPs at SMIC50, SMIC80, and 100× MIC levels, as was explained above. ZnNPs treatment resulted in a significant increase in ROS, RNI, and OSR enzymatic activity at SMIC50

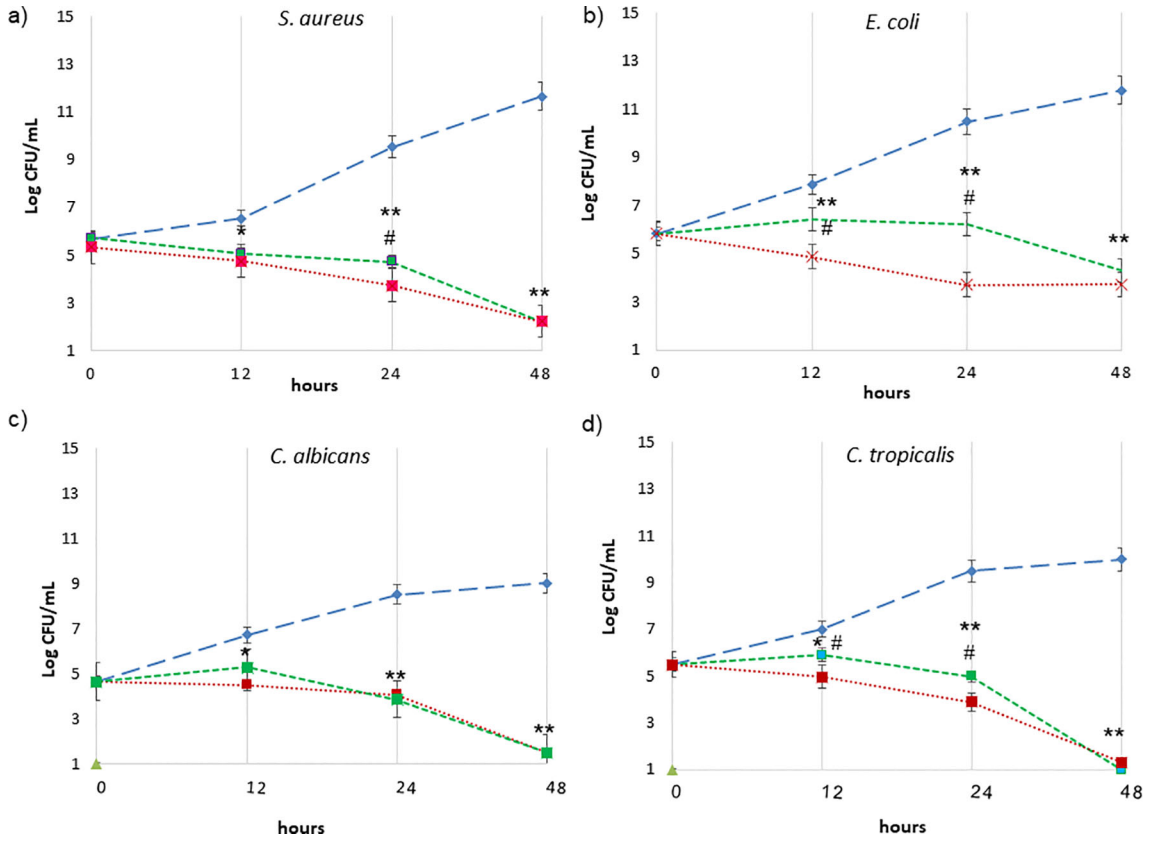

FIGURE 2
Time-kill curves expressed as $\log_{10}$ CFU/mL versus incubation time. ZnNPs at the MIC concentrations are represented by the green lines as follows: **(a)** *S. aureus*, **(b)** *E. coli*, **(c)** *C. albicans*, and **(d)** *C tropicalis*. The growth control, without ZnNPs, is depicted in blue light. The positive control is shown in red: CIP (for *E coli* and *S. aureus*) and AmB (for *C. albicans* and *C. tropicalis*). Data are presented as the mean ± SD from three independent determinations performed in triplicate. *denotes statistical significance at $p < 0.1$ for differences between ZnNPs and untreated controls; **$p < 0.01$ for more significant differences compared with untreated controls. #$p < 0.01$ differences are considered significant for comparisons of ZnNPs and the antimicrobial controls (CIP and AmB).

levels. Figure 6A shows that ROS levels increased in a concentration-dependent manner compared to untreated biofilms (*$p < 0.01$). Additionally, a differential effect was observed, with higher ROS production at SMIC80 or 100× MIC levels compared to SMIC50 levels across the four strains tested ($^{\#}p < 0.01$). RNI generation (Figure 6B) showed the greatest accumulation at SMIC80 or 100× MIC levels compared to untreated controls (*$p < 0.01$), these levels exceeding those of ROS relative to their respective untreated levels. The enzymatic and non-enzymatic antioxidant components were analyzed as indicators of the biofilm's protective mechanisms against oxidative stress. FRAP levels increased following ZnNPs treatment, with the highest increments observed at SMIC50 and comparatively lower levels at SMIC80, possibly due to increased OSR. Treatment resulted in statistically significant differences compared to untreated biofilms. Overall, these results suggest that biofilm growth was predominantly affected by the accumulation of ROS and RNI. *S. aureus* exhibited the highest ROS and RNI levels. The oxidative stress response was more pronounced at SMIC80, indicating a differential stimulation of sessile cells under ZnNPs treatment.

4 Discussion

In recent years, pathogens' increasing persistence and resistance to antimicrobial agents have underscored the urgent need to develop novel antimicrobial agents and innovative strategies (Vitiello et al., 2023; WHO, 2024). Studies estimate that biofilms contribute to approximately 65% of microbial infections and are associated with 78.2% of human chronic infections (Malone et al., 2017; Paraje, 2023; Coenye et al., 2024). As a result, the scientific community has increasingly prioritized the development of antibiofilm strategies. In this context, traditional antimicrobial drugs are widely recognized as having limited efficacy against biofilms, primarily due to intrinsic and extrinsic resistance mechanisms that exacerbate treatment challenges (Sharma et al., 2023; Coenye et al., 2024). These limitations have driven the exploration of innovative approaches, particularly in biomedical science, with nanotechnology-based solutions garnering significant interest.

Numerous studies have highlighted the significant potential of metal and metal oxide nanoparticles in combating microbial

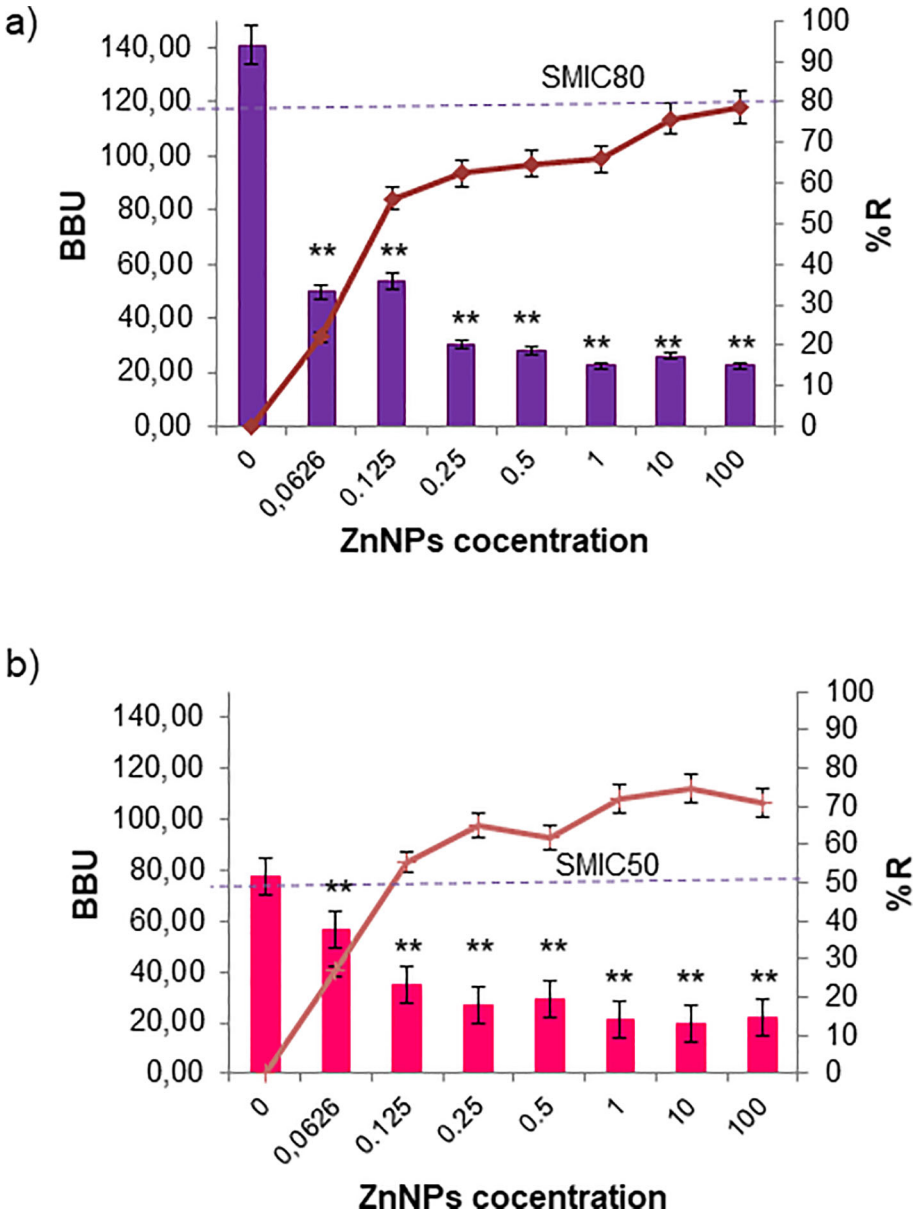

FIGURE 3
Sessile minimum inhibitory concentration (SMIC50 and SMIC80) for ZnNPs on total bacterial biofilms. **(a)** Mature biofilms of *S. aureus* and **(b)** *E. coli* were exposed to serial dilutions of ZnNPs at concentrations above and below the MIC. CV staining was used to quantify biofilm biomass units (BBUs, bars) and the percentage of biofilm reduction (%R, dotted lines). SMIC50 and SMIC80 are shown for each condition, indicating 50% and 80% reductions, respectively. All experiments were performed in triplicate, with three independent replicates, and the numerical data are presented as means ± standard deviation. Statistical significance is denoted by **p < 0.01 for differences compared to untreated biofilms.

resistance. NPs such as gold (Au), silver (Ag), and titanium (Ti) have demonstrated remarkable efficacy against planktonic cells (Crespo et al., 2016; Da Silva et al., 2022, 2024; Arora et al., 2024; Yakoup et al., 2024). However, their application in eradicating sessile cells within biofilms remains underexplored, emphasizing the need for further research to harness their full potential in addressing biofilm-associated infections effectively. In this regard, ZnNPs have received comparatively less attention, underscoring the need for deeper investigation into their antibiofilm properties. One notable advantage of ZnNPs is that they have been generally recognized as safe by the U.S. Food and Drug Administration (Yousef and Danial, 2012). Studies in the literature mainly address the effects of ZnNPs obtained through chemical synthesis (Applerot et al., 2012; Dwivedi et al., 2014; Lee et al., 2014; Kadiyala et al., 2018; Jasim et al., 2020; Bianchini Fulindi et al., 2023) and plant biological synthesis (Agarwal et al., 2018; Lahiri et al., 2022; Velsankar et al., 2022). Those regarding the effects of ZnNPs obtained through microorganism biosynthesis are more scarce, in particular about ZnNPs obtained with *P. aeruginosa* (Barsainya and Pratap Singh, 2018; Abdo et al., 2021). Thus, limited studies have performed comprehensive evaluations of their antimicrobial activity against both planktonic and sessile cells, or across

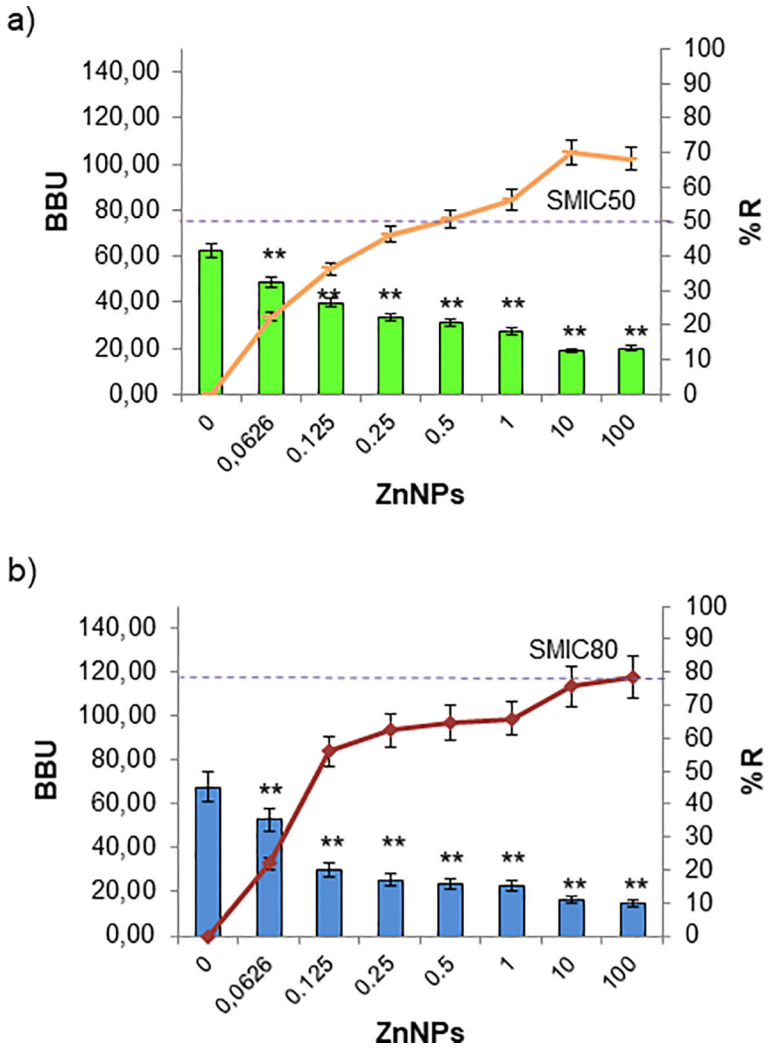

FIGURE 4
Sessile minimum inhibitory concentration (SMIC50 and SMIC80) for ZnNPs on total fungal biofilms. CV staining was used to quantify biofilm biomass units (BBUs, bars) and the percentage of biofilm reduction (%, dotted lines) for **(a)** *C. albicans* and **(b)** *C. tropicalis* exposed to serial dilutions of ZnNPs at concentrations above and below the MIC. SMIC for 50% and 80% reductions (SMIC50 and SMIC80) in sessile fungal cells are indicated for each strain. All experiments were performed in triplicate, with three independent replicates, and the numerical data are presented as means ± standard deviation. Statistical significance is denoted by **p < 0.01 for differences compared to untreated biofilms.

pathogenic bacteria and fungi. This is especially relevant for green-synthesized ZnNPs, which present a promising avenue for addressing biofilm-associated infections.

The disk diffusion method was employed to evaluate the antimicrobial activity of ZnNPs by measuring the diameters of the inhibition zones, which reflect the antimicrobial susceptibility of the tested microorganisms (Kourmouli et al., 2018; Ihsan et al., 2023). In this sense, by agar diffusion technique demonstrated high efficacy against pathogenic Gram-positive bacteria and Gram-negative bacteria (Hossain, 2024). Their activity has also been reported against fungal phytopathogens such as *Rhizoctonia solani*, *Fusarium* spp., and *Penicillium* spp (Barsainya and Pratap Singh, 2018). However, no further studies have evaluated the sensitivity of planktonic versus sessile biofilm cells to ZnNPs. In this study, we demonstrate that biogenic ZnNPs exhibit potent antimicrobial effects against Gram-positive and Gram-negative bacteria, as well as yeasts, in both planktonic and biofilm forms. Additionally, the inhibition zone data were used to calculate the PIDG values (Himratul-Aznita et al., 2011). A positive PIDG value indicates that the antimicrobial activity is stronger than that of the positive control. Although ZnNPs demonstrated significant antibacterial activity, their PIDG values were negative when compared to the positive controls. Among the tested microorganisms, *S. aureus* exhibited the highest PIDG values, indicating the greatest antimicrobial activity, followed by *E. coli*, *C. tropicalis*, and *C. albicans*, which displayed the lowest activity relative to their respective positive controls. According to other authors, Gram-negative bacteria exhibit greater resistance to ZnNPs because the lipopolysaccharides in their cell walls hinder ZnNP adhesion and internalization (Yu et al., 2014; Abdo et al., 2021).

The broth microdilution method was also utilized to assess the antibacterial activity of biogenic Zn NPs, with MIC/MBC and MIC/

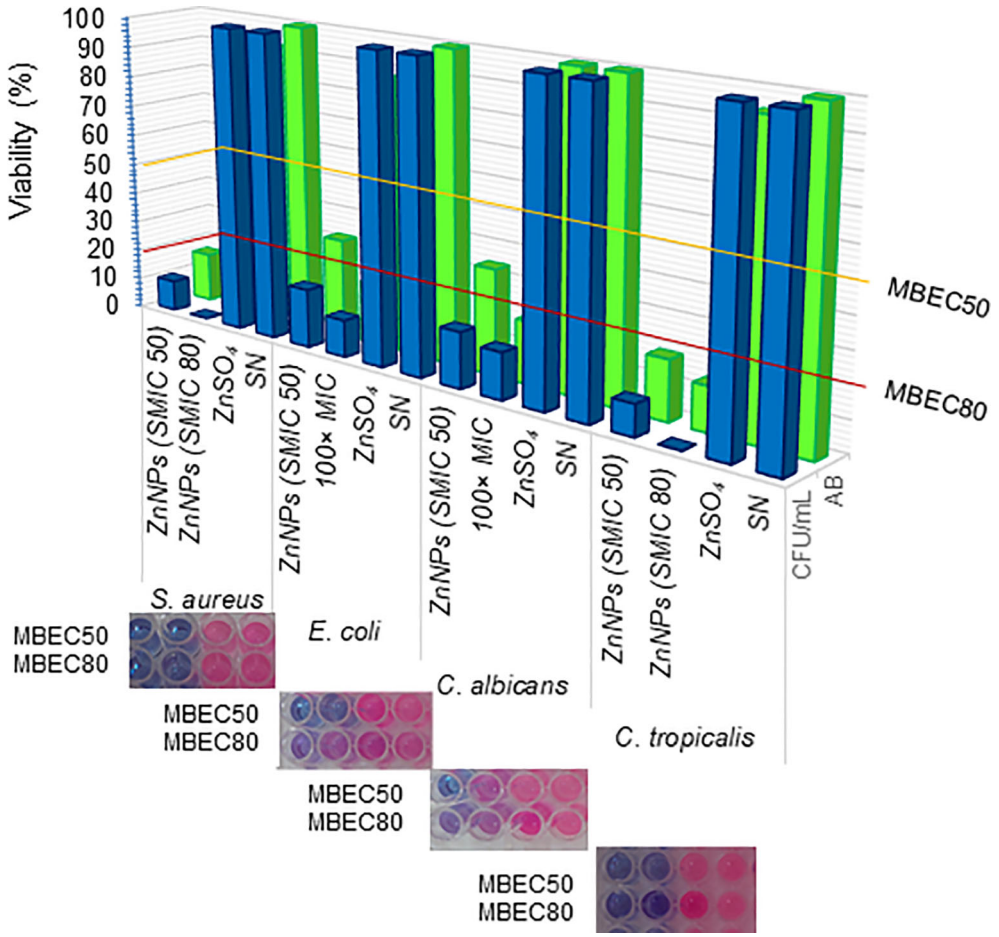

FIGURE 5
Determination of minimal biofilm eradication concentration (MBEC). Effects of ZnNPs. The metabolic activity of sessile cells was assessed via aerobic respiration following exposure to ZnNPs using resazurin (AB) assays (blue bars and upper panel images). The viability of sessile cells was further quantified through CFU/mL determination by agar plating (green bars). $ZnSO_4$ and SN were included as controls. Data are presented as means ± standard deviation (SD from three independent experiments, each performed in triplicate.

MFC results confirming their bactericidal and fungicidal properties. The time-kill kinetics assay quantitatively assesses the antimicrobial activity of an agent over time, focusing on its effects across different microbial growth phases (Chen et al., 2022; Yakoup et al., 2024). This method can determine the bactericidal or fungicidal activity of an agent, defined by a reduction exceeding 3 $\log_{10}$ in CFUs, equivalent to a 99.9% eradication of the initial inoculum. The results confirmed the "cidal" effect of ZnNPs, demonstrating significant antimicrobial activity against both bacterial and fungal strains within 48 hours, with significant deviations compared to untreated controls (**$p < 0.01$). A particularly strong effect was observed on *S. aureus* during both the exponential and stationary growth phases (**$p < 0.01$). In contrast, *E. coli* showed effects during the stationary phase, particularly before 24 hours. For both *Candida* species, the antimicrobial action occurred during the exponential phase, with marked depletion observed between 24 and 48 hours (**$p < 0.01$).

Similar to our findings, previously reported studies have demonstrated that ZnNPs effectively inhibit the growth of *S. aureus* planktonic cells, inducing morphological alterations, shape distortions, and a reduction in enterotoxin A, an important virulence factor (El-Masry et al., 2022). Others have emphasized the attachment of ZnO particles to bacterial membranes and the subsequent toxic effects. Specifically, ZnO^{-1}, which has a greater surface area, offered a higher availability of zinc atoms, further enhancing bacterial toxicity. The adhesion of ZnO to bacterial membranes induced physical damage, as revealed by research on *S. aureus* and *P. aeruginosa* (Ann et al., 2014). These findings highlight the impact of ZnNPs on cell wall morphology and integrity, suggesting their potential to disrupt normal cellular structure and, consequently, their functionality. Beyond direct contact, ZnNPs also exhibit antibacterial activity via numerous mechanisms like the membrane disruption, DNA damage, enzyme inactivation, and mitochondrial damage, as broadly discussed in this Review (Huq et al., 2023). Earlier research indicates that the interactions with membrane proteins play a significant role in bacterial inactivation, rather than direct physical interactions alone (Zhang et al., 2010).

Other studies have evaluated the antimicrobial efficacy of AgNPs, ZnONPs, and TiO_2NPs against *Salmonella typhimurium*,

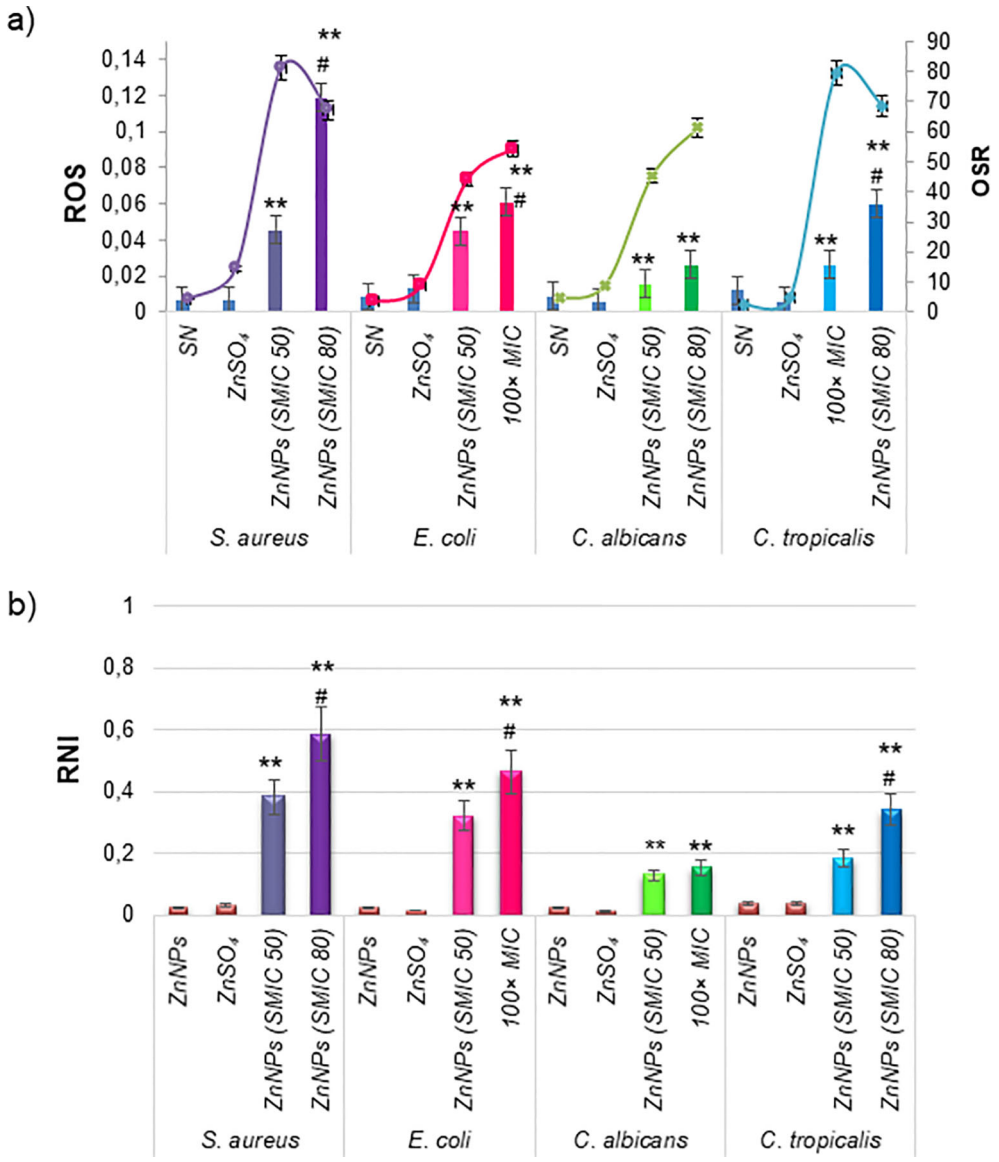

FIGURE 6
Cellular stress metabolites and OSR in total mature biofilms incubated with ZnNPs. **(a)** Levels of ROS (bars) and OSR results from the FRAP assay (lines). **(b)** Generation of RNI. $ZnSO_4$ and SN were included as controls and did not exhibit cellular stress activity. All experiments were conducted in triplicate across three independent experiments, with numerical data presented as means ± standard deviation. Statistical significance is denoted by **p < 0.01 for differences compared to untreated biofilms. Additionally, #p < 0.01 between ZnNPs at SMIC50 and SMIC80.

Brucella abortus, and *C. albicans*, suggesting that nanoparticle solutions exhibit both fungicidal and bactericidal effects on the tested microorganisms (Kareem et al., 2021). Ahmadpour Kermani et al. further demonstrated that TiO_2NPs and ZnONPs possess antifungal activity against five pathogenic *Candida* species, inhibiting the growth of all tested strains. However, consistent with our results, their antifungal properties were significantly less effective compared to AmB (Ahmadpour Kermani et al., 2021). Abdo et al. reported that the biogenic ZnONPs were concentration-dependent, consistent with our findings. They demonstrated high efficacy against pathogenic Gram-positive bacteria (*S. aureus* and *Bacillus subtilis*), Gram-negative bacteria (*E. coli* and *P. aeruginosa*), and unicellular fungi (*C. albicans*). However, they documented relatively smaller inhibition zones for both Gram-positive and Gram-negative bacteria, as well as fungi (Abdo et al., 2021). In contrast, our results indicate a larger halo of inhibition, suggesting enhanced antimicrobial efficacy against planktonic cells. Moreover, a recent report highlighted that eco-friendly synthesized ZnONPs exhibit greater antimicrobial efficacy against Gram-positive bacteria (*Micrococcus luteus*, *S. aureus*, *Bacillus subtilis*) compared to Gram-negative bacteria (*Agrobacterium tumefaciens*, *Salmonella setubal*, *Enterobacter aerogenes*). These authors emphasize the necessity for further research to elucidate the precise mechanisms underlying the action of these NPs and their broader applications in the medical field (Noor et al., 2024). Our study contributes significantly to this growing body of knowledge by addressing these aspects and

providing valuable insights into the antimicrobial properties of green-synthesized ZnNPs and their potential use in medical applications. However, we recognize some limitations, particularly considering that these are *in vitro* studies. For future toxicity studies in human cellular lines, we are considering the inclusion of additional controls.

In contrast to planktonic bacteria, biofilms offer a significant survival advantage to microbial communities. These biofilms are complex microbial communities embedded in a 3D extracellular matrix, primarily composed of polysaccharides, with lesser amounts of proteins, extracellular DNA, lipids, and cellular debris (Paraje, 2023; Sharma et al., 2023; Coenye et al., 2024). They are characterized by strong adhesive capacity and persistent cell population (Da Silva et al., 2021, 2024). Biofilms is a major challenge in modern medicine, as most existing antimicrobial agents are designed to target free-floating microbial cells (Zhao et al., 2023). Currently, there is no standard method for evaluating the efficacy of new antibiofilm drugs (Hossain, 2024). In this study, we utilized a combination of methodologies—the CV assay, resazurin-based method, and CFU plate counting—to evaluate the antibiofilm activity of biogenic ZnNPs on mature biofilms. The CV assay's main limitation is its measurement of total biofilm biomass (BBU), as it stains all components of the biofilm, including live and dead bacteria, as well as the extracellular matrix. Nonetheless, this assay is unable to identify viable bacteria as distinct from non-viable ones (Sharma et al., 2023; Coenye et al., 2024). Viability and vitality assays are critical for assessing the effectiveness of novel therapeutic approaches, with stain-based methods offering speed and objectivity. To address the limitations of the CV assay, we employed two additional cell viability assays. The first was a resazurin-based method, which evaluates cellular metabolic activity by assessing the redox status of microbial cells (Herman et al., 2024). The second method was CFU counting, which is considered the gold standard for determining viable sessile cells by disrupting the total mature biofilm through sonication (Da Silva et al., 2021, 2022, 2024). The combination of these three methodologies provides a broader perspective on the antibiofilm effects of ZnNPs, enabling a more comprehensive assessment of their antimicrobial action. By integrating biofilm biomass measurements and viability assays, we demonstrated that ZnNPs exert significant effects on biofilms formed by both bacteria and fungi. Additionally, we were able to determine important parameters to characterize their action, specifically the SMIC and the MBEC. While the MIC is an important parameter for planktonic cells, the determination of the SMIC is particularly relevant for agents that can inhibit sessile cells, which may be used to design effective antibiofilm therapies. Sessile cells constitute only 5–30% of the volume in mature biofilms, with the remaining volume consisting of the extracellular matrix (Sharma et al., 2023; Coenye et al., 2024). The results obtained in this study, as evaluated by the CV assay, suggest that the extracellular matrix present in the biofilm significantly disrupts the total biofilm when treated with ZnNPs. In addition to determining the SMIC at 50% and 80%, we assessed the MBEC for mature biofilms using both resazurin-based staining and CFU counts. These results reflect the number of viable cells remaining after treatment and demonstrate the effective eradication of mature biofilm formation by various microbial species.

Another important aspect is that by different methods it was confirmed that $ZnSO_4$ and SN did not exhibit inhibition zones or microbicidal activity, indicating that the metal precursor alone lacked antimicrobial efficacy against the tested organisms. In contrast, the biogenic ZnNPs displayed significantly higher microbicidal effects. Different reports have been postulated that the biomolecules stabilizing the NPs and forming their corona also play a role in their antimicrobial effects (Nandhini et al., 2024). These corona components can interact with the microbial cell membrane, followed by internalization and contributing to the control of biofilm-forming microbial pathogens (Kundu et al., 2014; Sass et al., 2018). In addition, siderophores can chelate iron and other metals essential for microbial survival. If siderophores form part of the corona, metal chelation may further aid in biofilm control. In this sense, it has been reported that iron denial produced by pyoverdine was the main mechanism by which pyoverdine inhibited *A. fumigatus* biofilm (Roberts et al., 2024). *Pseudomonas aeruginosa* was selected for this studies due to its well-documented ability to biosynthesize various metallic nanoparticles. This bacterium employs versatile metabolic pathways and secretes biomolecules such as reductase enzymes, proteins, and extracellular polysaccharides, which not only facilitate the bioreduction of metal ions but also serve as natural capping and stabilizing agents for the nanoparticles. These biological molecules adsorbed on the nanoparticle surface give rise to what is known as the nanoparticle corona—a dynamic layer of biomolecules that plays a crucial role in determining nanoparticle characteristics such as colloidal stability, surface charge, aggregation behavior, and biological interactions. In the case of biosynthesized nanoparticles, the corona often includes varying proportions of carbohydrates, proteins, and aliphatic compounds, which can influence their antimicrobial properties, biocompatibility, and functional behavior in environmental and biomedical applications (Alamdari et al., 2022; Ali et al., 2024).

Most research has focused on the antimicrobial properties of ZnNPs, primarily attributed to the generation of ROS, which is the most widely studied and accepted mechanism underlying the antibacterial activity of ZnO. ROS include highly reactive ionic species and free radicals, such as superoxide anion, hydroperoxyl radical, hydrogen peroxide, and hydroxyl radical. These species can damage DNA, lipids, proteins, and cell membranes, ultimately triggering cell death (Yousef and Danial, 2012; Peralta et al., 2018). However, limited studies have explored the effects of RNI and the resulting imbalance on bacteria and yeast (Arce Miranda et al., 2011; Baronetti et al., 2011; Angel Villegas et al., 2015; Da Silva et al., 2021; Quinteros et al., 2021a). In this study, we determined the toxicity mechanism of ZnNPs, demonstrating potent antibacterial, antifungal, and antibiofilm activities mediated by the generation of both ROS and RNI. The results indicate a disturbance in the prooxidant/antioxidant balance, favoring the overproduction of ROS and RNI. Biofilms treated with ZnNPs displayed an ability to respond to the stress generated during treatment when exposed to the SMIC50. However, at the SMIC80, this imbalance was more

pronounced due to the excessive production of free radicals and an insufficient OSR. Higher levels of ROS and RNS accumulation inside of biofilm were observed, resulting in a significant oxidative imbalance.

The RNI, particularly nitric oxide (NO), were identified as the main contributors to the prooxidant/antioxidant balance within biofilms (Sirelkhatim et al., 2015). Due to its small size and neutral charge, NO is able to diffuse freely through the channels and voids of mature biofilms (Arce Miranda et al., 2011; Da Silva et al., 2022, 2024). Inside the biofilm, NO reacts with metals and other radicals to generate additional RNI that can interact with various biofilm components, including the outer cell wall-embedded proteins, which are among the primary targets (Mirhosseini et al., 2019; Costa-Orlandi et al., 2021; Oliveira et al., 2023). This process was concentration-dependent and the accumulation of RNI within biofilms can destabilize the matrix by interacting with polysaccharides and eDNA, resulting in oxidative damage, such as DNA cleavage. Previously, we reported that NO is an effective antibiofilm agent in *S. aureus* with the ability to disperse biofilm-associated microorganisms, penetrate the matrix, and disrupt biofilm structure (Arce Miranda et al., 2011; Angel Villegas et al., 2015; Da Silva et al., 2021). *In vitro* studies have shown c-di-GMP is understood to be regulated by endogenously produced NO during the late stages of biofilm development as a means to induce biofilm dispersal. This NO-mediated dispersal mechanism is conserved across various species, including *P. aeruginosa*, *S. aureus*, *E. coli*, *Fusobacterium nucleatum*, and *Vibrio cholerae* (Altammar, 2023; Burlec et al., 2023; Oliveira et al., 2023; Piluk et al., 2024; Nguyen et al., 2025).

At present, researchers are increasingly focusing on NPs composed of metals and metal oxides as innovative antimicrobial agents. These NPs possess unique physical and chemical properties, including small size, high surface area-to-volume ratio, distinctive surface chemistry, and the ability to effectively penetrate biofilms (Ann et al., 2014; Arora et al., 2024; Yakoup et al., 2024). ZnNPs, in particular, have received significant attention as a promising class of antibacterial agents. This interest arises from their remarkable physicochemical properties and enhanced surface area (Kadiyala et al., 2018; Noor et al., 2024). Zinc, an essential trace element in the metabolism of plants, humans, and animals, plays a critical role in human physiology. It also contributes to ecological sustainability, owing to its solubility, low toxicity, and biodegradability (Krol et al., 2017; Kalaba et al., 2024). Moreover, zinc can promote biofilm dispersal by disrupting cellular balance. In addition to these advantages, ZnNPs are cost-effective and commercially viable, making them suitable for a wide range of applications. Their unique properties position them as highly favorable candidates for both industrial and biomedical purposes (Zhang et al., 2010; Sirelkhatim et al., 2015; Mirhosseini et al., 2019; Costa-Orlandi et al., 2021; Altammar, 2023; Burlec et al., 2023; Oliveira et al., 2023; Noor et al., 2024; Piluk et al., 2024; Nguyen et al., 2025). Despite the promising properties of these ZnNPs, some limitations of this study should be noted. *In vitro* models do not consider the environmental factors of the host and other biotic signals occurring *in vivo* (Lebeaux et al., 2013), that may influence both the stability and the activity of the nanoparticle (Mba and Nweze, 2021).

5 Conclusion

This study demonstrates the antibacterial, antifungal, and antibiofilm activity of biologically synthesized ZnNPs from *P. aeruginosa*, emphasizing their effectiveness against both planktonic and sessile forms of the tested microorganisms. Our findings represent the first comprehensive analysis of the multifunctional antimicrobial properties of these eco-friendly ZnNPs, including microbial toxicity mechanisms triggered by the induction of ROS and RNI, with a disturbance in the prooxidant/antioxidant balance. This research contributes to a deeper understanding of their potential in managing biofilm-associated infections. The clinical relevance of ZnNPs is highlighted by their potential to inform effective strategies for eradicating biofilms, particularly in light of the increasing prevalence of biofilm-related complications among at-risk patients. Their properties render ZnNPs highly valuable for treating infections. This suggests their versatility for various applications in the biomedical field, including the development of new antimicrobial agents, with implications for healthcare, agriculture, and various industries.

Data availability statement

The datasets presented in this article are not readily available. Requests to access the datasets should be directed to gabrielaparaje@gmail.com.

Author contributions

EDLV: Conceptualization, Formal Analysis, Investigation, Methodology, Validation, Writing – original draft. KFCA: Formal Analysis, Methodology, Writing – original draft, Supervision. PSB: Formal Analysis, Methodology, Writing – original draft, Investigation. MMT: Formal Analysis, Methodology, Data curation, Investigation, Writing – original draft. IMH: Investigation, Methodology, Writing – original draft. MGP: Formal Analysis, Investigation, Methodology, Conceptualization, Data curation, Funding acquisition, Project administration, Resources, Supervision, Validation, Visualization, Writing – original draft, Writing – review & editing. NG: Conceptualization, Data curation, Formal Analysis, Funding acquisition, Methodology, Project administration, Resources, Supervision, Validation, Visualization, Writing – original draft, Writing – review & editing.

Funding

The author(s) declare that financial support was received for the research and/or publication of this article. This work received support through grants to MGP from Secretaría de Ciencia y Tecnología (SeCyT-UNC), Proyectos de Investigacion Plurianuales (PIP -CONICET), and Fondo para la Investigacion

Cientıfica y Tecnologica (FONCyT) of Argentina and NG from Universidad Nacional del Comahue (04/U030) and FONCyT.

Acknowledgments

EDLV is a PhD fellow of CONICET. MGP and NG are members of the Scientific and Technological Researcher Career (CIC - CONICET).

Conflict of interest

The authors declare that the research was conducted in the absence of any commercial or financial relationships that could be construed as a potential conflict of interest.

MGP declares that she was an editorial board member of Frontiers at the time of submission. This had no influence on the peer review process or the final decision.

Generative AI statement

The author(s) declare that no Generative AI was used in the creation of this manuscript.

Publisher's note

Supplementary material

The Supplementary Material for this article can be found online at: https://www.frontiersin.org/articles/10.3389/fcimb.2025.1545119/full#supplementary-material

SUPPLEMENTARY FIGURE 2
ZnNPs biosynthesis and characterization. **(a)** UV–vis spectra of biosynthesized ZnNPs by *P. aeruginosa* culture. **(b)** Zeta potential of the biosynthesized ZnNPs. **(c)** Representative TEM image of the biosynthesized ZnNPs. **(c)** Representative SEM images of ZnNPs.

SUPPLEMENTARY FIGURE 3
Characterization and analysis of capping. **(a)** FT-IR spectrum of ZnNPs biosynthesized by P. *aeruginosa*. **(b)** SDS-PAGE silver staining, line 1: supernatant; line 2: ZnNPs sample. The arrows show protein bands. **(c)** Fluorescence spectrum of ZnNPs.

SUPPLEMENTARY FIGURE 4
Study of synergistic antimicrobial activity. Synergistic effect of ZnNPs in combination with CIP against *S. aureus* and *E. coli*, as well as with Amb against *C. albicans* and *C. tropicalis*. The percentage of viable cells (% viability) was determined using colony-forming units per mL (CFU.mL^{-1}, grey bars) and resazurin (AB) assays (blue bars). The numerical data correspond to the relative values (treated/untreated ratio). All experiments were conducted in triplicate across three independent experiments, with numerical data presented as means ± standard deviation. Statistical significance is indicated as follows: $*p < 0.01$ for differences compared to untreated biofilms and $\# p < 0.01$ for significant differences between treatments with antibiotics (CIP) or antifungal (Amb) and ZnNPs.

References

Abdo, A. M., Fouda, A., Eid, A. M., Fahmy, N. M., Elsayed, A. M., Khalil, A. M. A., et al. (2021). Green synthesis of zinc oxide nanoparticles (ZnO-NPs) by *Pseudomonas aeruginosa* and their activity against pathogenic microbes and common house mosquito, *Culex pipiens*. *Materials (Basel).* 14, 6983. doi: 10.3390/ma14226983

Agarwal, H., Menon, S., Venkat Kumar, S., and Rajeshkumar, S. (2018). Mechanistic study on antibacterial action of zinc oxide nanoparticles synthesized using green route. *Chem. Biol. Interact.* 286, 60–70. doi: 10.1016/j.cbi.2018.03.008

Ahmadpour Kermani, S., Salari, S., and Ghasemi Nejad Almani, P. (2021). Comparison of antifungal and cytotoxicity activities of titanium dioxide and zinc oxide nanoparticles with amphotericin B against different *Candida* species: *In vitro* evaluation. *J. Clin. Lab. Anal.* 35, 1–8. doi: 10.1002/jcla.23577

Alamdari, S., Mirzaee, O., Nasiri Jahroodi, F., Tafreshi, M. J., Ghamsari, M. S., Shik, S. S., et al. (2022). Green synthesis of multifunctional ZnO/chitosan nanocomposite film using wild *Mentha pulegium* extract for packaging applications. *Surf Interfaces.* 34, 102349. doi: 10.1016/j.surfin.2022.102349

Ali, Z. H., Abdulazeem, L., Kadhim, W. A., Kzar, M. H., and Al-Sareji, O. J. (2024). Application of green silver nano-particles as anti-bacterial and photo-catalytic degradation of azo dye in wastewater. *Sci. Rep.* 14, 31593. doi: 10.1038/s41598-024-76090-w

Altammar, K. A. (2023). A review on nanoparticles: characteristics, synthesis, applications, and challenges. *Front. Microbiol.* 14. doi: 10.3389/fmicb.2023.1155622

Angel Villegas, N., Baronetti, J., Albesa, I., Etcheverrıa, A., Becerra, M. C., Padola, N. L., et al. (2015). Effect of antibiotics on cellular stress generated in Shiga toxin-producing *Escherichia coli* O157:H7 and non-O157 biofilms. *Toxicol. Vitr.* 29, 1692–1700. doi: 10.1016/j.tiv.2015.06.025

Ann, L. C., Mahmud, S., Bakhori, S. K. M., Sirelkhatim, A., Mohamad, D., Hasan, H., et al. (2014). Antibacterial responses of zinc oxide structures against *Staphylococcus aureus*, *Pseudomonas aeruginosa* and *Streptococcus pyogenes*. *Ceram. Int.* 40, 2993–3001. doi: 10.1016/j.ceramint.2013.10.008

Applerot, G., Lellouche, J., Perkas, N., Nitzan, Y., Gedanken, A., and Banin, E. (2012). ZnO nanoparticle-coated surfaces inhibit bacterial biofilm formation and increase antibiotic susceptibility. *RSC Adv.* 2, 2314. doi: 10.1039/c2ra00602b

Arce Miranda, J. E., Baronetti, J. L., and Paraje, M. G. (2021). Host–pathogen interaction between macrophage co-cultures with *Staphylococcus aureus* biofilms. *Eur. J. Clin. Microbiol. Infect. Dis.* 40, 2563–2574. doi: 10.1007/s10096-021-04306-2

Arce Miranda, J. E., Sotomayor, C. E., Albesa, I., and Paraje, M. G. (2011). Oxidative and nitrosative stress in *Staphylococcus aureus* biofilm. *FEMS Microbiol. Lett.* 315, 23–29. doi: 10.1111/j.1574-6968.2010.02164.x

Arora, A., Lashani, E., and Turner, R. J. (2024). Bacterial synthesis of metal nanoparticles as antimicrobials. *Microb. Biotechnol.* 17, e14549. doi: 10.1111/1751-7915.14549

Baronetti, J. L., Villegas, N. A., Aiassa, V., Paraje, M. G., and Albesa, I. (2013). Hemolysin from *Escherichia coli* induces oxidative stress in blood. *Toxicon* 70, 15–20. doi: 10.1016/j.toxicon.2013.03.014

Baronetti, J. L., Villegas, N. A., Paraje, M. G., and Albesa, I. (2011). Nitric oxide-mediated apoptosis in rat macrophages subjected to Shiga toxin 2 from *Escherichia coli*. *Microbiol. Immunol.* 55, 231–238. doi: 10.1111/j.1348-0421.2011.00310.x

Barsainya, M., and Pratap Singh, D. (2018). Green synthesis of zinc oxide nanoparticles by *Pseudomonas aeruginosa* and their broad-spectrum antimicrobial effects. *J. Pure Appl. Microbiol.* 12, 2123–2134. doi: 10.22207/JPAM.12.4.50

Bianchini Fulindi, R., Domingues Rodrigues, J., Lemos Barbosa, T. W., Goncalves Garcia, A. D., de Almeida La Porta, F., Pratavieira, S., et al. (2023). Zinc-based nanoparticles reduce bacterial biofilm formation. *Microbiol. Spectr.* 11, e0483122. doi: 10.1128/spectrum.04831-22

Borehalli Mayegowda, S., Roy, A., N. G, M., Pandit, S., Alghamdi, S., Almehmadi, M., et al. (2023). Eco-friendly synthesized nanoparticles as antimicrobial agents: an updated review. *Front. Cell. Infect. Microbiol.* 13. doi: 10.3389/fcimb.2023.1224778

Burlec, A. F., Corciova, A., Boev, M., Batir-Marin, D., Mircea, C., Cioanca, O., et al. (2023). Current overview of metal nanoparticles' synthesis, characterization, and biomedical applications, with a focus on silver and gold nanoparticles. *Pharmaceuticals* 16, 1410. doi: 10.3390/ph16101410

Chen, H., Yang, N., Yu, L., Li, J., Zhang, H., Zheng, Y., et al. (2022). Synergistic microbicidal effect of AUR and PEITC against *Staphylococcus aureus* skin infection. *Front. Cell. Infect. Microbiol.* (Wayne, PA: CLSI Clinical and Laboratory Standards Institute) 12. doi: 10.3389/fcimb.2022.927289

Clinical and Laboratory Standards Institute (2017). *M27 Reference method for broth dilution antifungal susceptibility testing of yeast. 4th Edn* (Wayne, PA: CLSI Clinical and Laboratory Standards Institute).

Clinical and Laboratory Standards Institute (2018). *Performance standards for antimicrobial disk susceptibility tests. 13th Edn* (Wayne, PA: CLSI standard M02 Clinical and Laboratory Standards Institute).

Clinical and Laboratory Standards Institute (2020). *Performance standards for antimicrobial susceptibility testing. 30th Edn* (Wayne, PA: CLSI supplement M100. Clinical and Laboratory Standards Institute).

Coenye, T., Ahonen, M., Anderson, S., Camara, M., Chundi, P., Fields, M., et al. (2024). Global challenges and microbial biofilms: Identification of priority questions in biofilm research, innovation and policy. *Biofilm* 8, 100210. doi: 10.1016/j.bioflm.2024.100210

Costa, M. I., Sarmento-Ribeiro, A. B., and Goncalves, A. C. (2023). Zinc: from biological functions to therapeutic potential. *Int. J. Mol. Sci.* 24, 4822. doi: 10.3390/ijms24054822

Costa-Orlandi, C. B., Martinez, L. R., Bila, N. M., Friedman, J. M., Friedman, A. J., Mendes-Giannini, M. J. S., et al. (2021). Nitric oxide-releasing nanoparticles are similar to efinaconazole in their capacity to eradicate *Trichophyton rubrum* biofilms. *Front. Cell. Infect. Microbiol.* 11. doi: 10.3389/fcimb.2021.684150

Crespo, K. A., Baronetti, J. L., Quinteros, M. A., Paez, P. L., and Paraje, M. G. (2016). Intra- and extracellular biosynthesis and characterization of iron nanoparticles from prokaryotic microorganisms with anticoagulant activity. *Pharm. Res.* 34, 591–598. doi: 10.1007/s11095-016-2084-0

Da Silva, M. A., Andrada, K. F. C., Torales, M. M., Hughes, I. M., Pez, P., Garcıa-Martınez, J. C., et al. (2024). Synergistic activity of gold nanoparticles with amphotericin B on persister cells of *Candida tropicalis* biofilms. *J. Nanobiotechnology* 22, 1–12. doi: 10.1186/S12951-024-02415-6/FIGURES/6

Da Silva, M. A., Baronetti, J. L., Paez, P. L., and Paraje, M. G. (2021). Oxidative imbalance in *Candida tropicalis* biofilms and its relation with persister cells. *Front. Microbiol.* 11. doi: 10.3389/fmicb.2020.598834

Da Silva, M. A., Garcıa-Martınez, J. C., Paez, P. L., and Paraje, M. G. (2022). Fungicidal and antibiofilm activities of gold nanoparticles on *Candida tropicalis*. *Nanomedicine (Lond).* 17, 1663–1676. doi: 10.2217/NNM-2022-0087

Dwivedi, S., Wahab, R., Khan, F., Mishra, Y. K., Musarrat, J., and Al-Khedhairy, A. A. (2014). Reactive Oxygen species mediated bacterial biofilm inhibition via zinc oxide nanoparticles and their statistical determination. *PloS One* 9, e111289. doi: 10.1371/journal.pone.0111289

El-Masry, R. M., Talat, D., Hassoubah, S. A., Zabermawi, N. M., Eleiwa, N. Z., Sherif, R. M., et al. (2022). Evaluation of the antimicrobial activity of ZnO nanoparticles against enterotoxigenic *Staphylococcus aureus*. *Life* 12, 1662. doi: 10.3390/life12101662

Haddi, R., El Kharraz, A. M., and Kerroumi, M. I. (2024). Green synthesis of zinc oxide nanoparticles using *Pistacia lentiscus L.* leaf extract and evaluating their antioxidant and antibacterial properties. *Nano Biomed. Eng.* 16, 232–247. doi: 10.26599/NBE.2024.9290056

Herman, T. S., da Silva Goersch, C., Bocca, A. L., and Fernandes, L. (2024). Resazurin to determine the minimum inhibitory concentration on antifungal susceptibility assays for *Fonsecaea* sp. using a modified EUCAST protocol. *Braz. J. Microbiol.* 55, 1349–1357. doi: 10.1007/s42770-024-01293-2

Himratul-Aznita, W. H., Mohd-Al-Faisal, N., and Fathilah, A. R. (2011). Determination of the percentage inhibition of diameter growth (PIDG) of piper betle crude aqueous extract against oral *Candida* species. *J. Med. Plants Res.* 5, 878–884. doi: 10.5897/JMPR.9000441

Hossain, T. J. (2024). Methods for screening and evaluation of antimicrobial activity: A review of protocols, advantages, and limitations. *Eur. J. Microbiol. Immunol.* 14, 97–115. doi: 10.1556/1886.2024.00035

Huq, A., Apu, A. I., Ashrafudoulla,, Rahman, M., Parvez, A. K., Balusamy, S. R., et al. (2023). Bioactive ZnO nanoparticles: biosynthesis, characterization and potential antimicrobial applications. *Pharmaceutics* 15, 2634. doi: 10.3390/pharmaceutics15112634

Ihsan, M., Din, I. U., Alam, K., Munir, I., Mohamed, H. I., and Khan, F. (2023). Green fabrication, characterization of zinc oxide nanoparticles using plant extract of *Momordica charantia* and *Curcuma zedoaria* and their antibacterial and antioxidant activities. *Appl. Biochem. Biotechnol.* 195, 3546–3565. doi: 10.1007/s12010-022-04309-5

Jasim, N. A., Al-Gasha'a, F. A., Al-Marjani, M. F., Al-Rahal, A. H., Abid, H. A., Al-Kadhmi, N. A., et al. (2020). ZnO nanoparticles inhibit growth and biofilm formation of vancomycin-resistant *S. aureus* (VRSA). *Biocatal. Agric. Biotechnol.* 29, 101745. doi: 10.1016/j.bcab.2020.101745

Jesudason, T. (2024). WHO publishes updated list of bacterial priority pathogens. *Lancet Microbe* 5, 100940. doi: 10.1016/j.lanmic.2024.07.003

Kadiyala, U., Turali-Emre, E. S., Bahng, J. H., Kotov, N. A., Scott Vanepps, J., and VanEpps, J. S. (2018). Unexpected insights into antibacterial activity of zinc oxide nanoparticles against methicillin resistant *Staphylococcus aureus* (MRSA). *Nanoscale* 10, 4927–4939. doi: 10.1039/C7NR08499D

Kalaba, M. H., El-Sherbiny, G. M., Ewais, E. A., Darwesh, O. M., and Moghannem, S. A. (2024). Green synthesis of zinc oxide nanoparticles (ZnO-NPs) by *Streptomyces baarnensis* and its active metabolite (Ka): a promising combination against multidrug-resistant ESKAPE pathogens and cytotoxicity. *BMC Microbiol.* 24, 254. doi: 10.1186/s12866-024-03392-4

Kareem, P. A., Salh, K. K., and Ali, F. A. (2021). ZnO, TiO2 and Ag nanoparticles impact against some species of pathogenic bacteria and yeast. *Cell. Mol. Biol.* 67, 24–34. doi: 10.14715/cmb/2021.67.3.4

Kourmouli, A., Valenti, M., van Rijn, E., Beaumont, H. J. E., Kalantzi, O. I., Schmidt-Ott, A., et al. (2018). Can disc diffusion susceptibility tests assess the antimicrobial activity of engineered nanoparticles? *J. Nanoparticle Res.* 20, 1–6. doi: 10.1007/S11051-018-4152-3/FIGURES/4

Krol, A., Pomastowski, P., Rafinska, K., Railean-Plugaru, V., and Buszewski, B. (2017). Zinc oxide nanoparticles: Synthesis, antiseptic activity and toxicity mechanism. *Adv. Colloid Interface Sci.* 249, 37–52. doi: 10.1016/J.CIS.2017.07.033

Kulkarni, D., Sherkar, R., Shirsathe, C., Sonwane, R., Varpe, N., Shelke, S., et al. (2023). Biofabrication of nanoparticles: sources, synthesis, and biomedical applications. *Front. Bioeng. Biotechnol.* 11. doi: 10.3389/fbioe.2023.1159193

Kundu, D., Hazra, C., Chatterjee, A., Chaudhari, A., and Mishra, S. (2014). Extracellular biosynthesis of zinc oxide nanoparticles using *Rhodococcus pyridinivorans* NT2: Multifunctional textile finishing, biosafety evaluation and *in vitro* drug delivery in colon carcinoma. *J. Photochem. Photobiol. B Biol.* 140, 194–204. doi: 10.1016/j.jphotobiol.2014.08.001

Lahiri, D., Ray, R. R., Sarkar, T., Upadhye, V. J., Ghosh, S., Pandit, S., et al. (2022). Anti-biofilm efficacy of green-synthesized ZnO nanoparticles on oral biofilm: *In vitro* and in silico study. *Front. Microbiol.* 13. doi: 10.3389/fmicb.2022.939390

Lebeaux, D., Chauhan, A., Rendueles, O., and Beloin, C. (2013). From *in vitro* to *in vivo* models of bacterial biofilm-related infections. *Pathogens* 2, 288–356. doi: 10.3390/pathogens2020288

Lee, J. H. J.-H., Kim, Y.-G. G., Cho, M. H., and Lee, J. H. J.-H. (2014). ZnO nanoparticles inhibit *Pseudomonas aeruginosa* biofilm formation and virulence factor production. *Microbiol. Res.* 169, 888–896. doi: 10.1016/j.micres.2014.05.005

Malone, M., Bjarnsholt, T., McBain, A. J., James, G. A., Stoodley, P., Leaper, D., et al. (2017). The prevalence of biofilms in chronic wounds: a systematic review and meta-analysis of published data. *J. Wound Care* 26, 20–25. doi: 10.12968/jowc.2017.26.1.20

Masoudi, M., Mashreghi, M., Zenhari, A., and Mashreghi, A. (2024). Combinational antimicrobial activity of biogenic TiO2 NP/ZnO NPs nanoantibiotics and amoxicillin-clavulanic acid against MDR-pathogens. *Int. J. Pharm.* 652, 123821. doi: 10.1016/j.ijpharm.2024.123821

Mba, I. E., and Nweze, E. I. (2021). Nanoparticles as therapeutic options for treating multidrug-resistant bacteria: research progress, challenges, and prospects. *World J. Microbiol. Biotechnol.* 37, 108. doi: 10.1007/s11274-021-03070-x

Miranda, J. E. A., Baronetti, J. L., Sotomayor, C. E., and Paraje, M. G. (2019). Oxidative and nitrosative stress responses during macrophage-*Candida albicans* biofilm interaction. *Med. Mycol.* 57, 101–113. doi: 10.1093/mmy/myx143

Mirhosseini, F., Amiri, M., Daneshkazemi, A., Zandi, H., and Javadi, Z. S. (2019). Antimicrobial effect of different sizes of nano zinc oxide on oral microorganisms. *Front. Dent.* 16, 105–112. doi: 10.18502/fid.v16i2.1361

Nandhini, J., Karthikeyan, E., and Rajeshkumar, S. (2024). Green synthesis of zinc oxide nanoparticles: Eco-friendly advancements for biomedical marvels. *Resour. Chem. Mater.* 3, 294–316. doi: 10.1016/j.recm.2024.05.001

Nguyen, H. S., Nguyen, V. H., Nguyen, T. B., Luong, T. T., and Vu, N. T. (2025). Biologically synthesized Fe0-based nanoparticles and their application trends as catalysts in the treatment of chlorinated organic compounds: a review. *Environ. Sci. Nano.* 12, 1767–1788. doi: 10.1039/D4EN00843J

Noor, H., Ayub, A., Dilshad, E., Afsar, T., Razak, S., Husain, F. M., et al. (2024). Assessment of *Bryophyllum pinnatum* mediated Ag and ZnO nanoparticles as efficient antimicrobial and cytotoxic agent. *Sci. Rep.* 14, 22200. doi: 10.1038/s41598-024-73092-6

O'Toole, G. A., and Kolter, R. (1998). Initiation of biofilm formation in *Pseudomonas fluorescens* WCS365 proceeds via multiple, convergent signalling pathways: A genetic analysis. *Mol. Microbiol.* 28, 449–461. doi: 10.1046/j.1365-2958.1998.00797.x

Okaiyeto, K., Gigliobianco, M. R., and Di Martino, P. (2024). Biogenic zinc oxide nanoparticles as a promising antibacterial agent: synthesis and characterization. *Int. J. Mol. Sci.* 25, 9500. doi: 10.3390/ijms25179500

Oliveira, A. S., Saraiva, L. M., and Carvalho, S. M. (2023). *Staphylococcus epidermidis* biofilms undergo metabolic and matrix remodeling under nitrosative stress. *Front. Cell. Infect. Microbiol.* 13. doi: 10.3389/fcimb.2023.1200923

Paraje, M. G. (2023). From the magic bullet to nanotechnology: nanoantimicrobials as therapeutics to fight multidrug-resistant microorganisms. *Rev. Argent. Microbiol.* 55, 204–205. doi: 10.1016/j.ram.2023.08.001

Peralta, M. A., Da Silva, M. A., Ortega, M. G., Cabrera, J. L., and Paraje, M. G. (2015). Antifungal activity of a prenylated flavonoid from *Dalea elegans* against *Candida albicans* biofilms. *Phytomedicine* 22, 975–980. doi: 10.1016/j.phymed.2015.07.003

Peralta, M., da Silva, M., Ortega, M., Cabrera, J., and Paraje, M. (2016). Usnic Acid activity on oxidative and nitrosative stress of azole-resistant *Candida albicans* biofilm. *Planta Med.* 83, 326–333. doi: 10.1055/s-0042-116442

Peralta, M. A., Ortega, M. G., Cabrera, J. L., and Paraje, M. G. (2018). The antioxidant activity of a prenyl flavonoid alters its antifungal toxicity on *Candida albicans* biofilms. *Food Chem. Toxicol.* 114, 285–291. doi: 10.1016/j.fct.2018.02.042

Pierce, C. G., Uppuluri, P., Tristan, A. R., Wormley, F. L., Mowat, E., Ramage, G., et al. (2008). A simple and reproducible 96-well plate-based method for the formation of fungal biofilms and its application to antifungal susceptibility testing. *Nat. Protoc.* 3, 1494–1500. doi: 10.1038/NPORT.2008.141

Piluk, T., Faccio, G., Letsiou, S., Liang, R., and Freire-Gormaly, M. (2024). A critical review investigating the use of nanoparticles in cosmetic skin products. *Environ. Sci. Nano* 11, 3674–3692. doi: 10.1039/D4EN00489B

Quinteros, M. A., Galera, I. L. D., Tolosa, J., Garcıa-Martınez, J. C., Paez, P. L., and Paraje, M. G. (2021a). Novel antifungal activity of oligostyrylbenzenes compounds on *Candida tropicalis* biofilms. *Med. Mycol.* 59, 244–252. doi: 10.1093/mmy/myaa046

Quinteros, M. A., Tolosa, J., Garcıa-Martınez, J. C., Paez, P. L., and Paraje, M. G. (2021b). Synergic activity of oligostyrylbenzenes with amphotericin B against *Candida tropicalis* biofilms. *Yeast* 38, 634–645. doi: 10.1002/yea.3672

Rasheed, R., Uzair, B., Raza, A., Binsuwaidan, R., and Alshammari, N. (2024). Fungus-mediated synthesis of Se-BiO-CuO multimetallic nanoparticles as a potential alternative antimicrobial against ESBL-producing *Escherichia coli* of veterinary origin. *Front. Cell. Infect. Microbiol.* 14. doi: 10.3389/fcimb.2024.1301351

Roberts, J. M., Milo, S., and Metcalf, D. G. (2024). Harnessing the power of our immune system: the antimicrobial and antibiofilm properties of nitric oxide. *Microorganisms* 12, 2543. doi: 10.3390/microorganisms12122543

Sass, G., Nazik, H., Penner, J., Shah, H., Ansari, S. R., Clemons, K. V., et al. (2018). Studies of *Pseudomonas aeruginosa* mutants indicate pyoverdine as the central factor in inhibition of *Aspergillus fumigatus* biofilm. *J. Bacteriol.* 200, 1–24. doi: 10.1128/JB.00345-17

Sharma, S., Mohler, J., Mahajan, S. D., Schwartz, S. A., Bruggemann, L., and Aalinkeel, R. (2023). Microbial biofilm: a review on formation, infection, antibiotic resistance, control measures, and innovative treatment. *Microorganisms* 11, 1614. doi: 10.3390/microorganisms11061614

Sirelkhatim, A., Mahmud, S., Seeni, A., Kaus, N. H. M., Ann, L. C., Bakhori, S. K. M., et al. (2015). Review on zinc oxide nanoparticles: Antibacterial activity and toxicity mechanism. *Nano-Micro Lett.* 7, 219–242. doi: 10.1007/S40820-015-0040-X/FIGURES/4

Velsankar, K., Venkatesan, A., Muthumari, P., Suganya, S., Mohandoss, S., and Sudhahar, S. (2022). Green inspired synthesis of ZnO nanoparticles and its characterizations with biofilm, antioxidant, anti-inflammatory, and anti-diabetic activities. *J. Mol. Struct.* 1255, 132420. doi: 10.1016/j.molstruc.2022.132420

Vitiello, A., Sabbatucci, M., Boccellino, M., Ponzo, A., Langella, R., and Zovi, A. (2023). Therapeutic and unconventional strategies to contrast antimicrobial resistance: a literature review. *Discov. Med.* 35, 750. doi: 10.24976/Discov.Med.202335178.70

WHO (2024). *Bacterial priority pathogens list 2024: bacterial pathogens of public health importance to guide research, development and strategies to prevent and control antimicrobial resistance* (Geneva: World Health Organization).

Yakoup, A. Y., Kamel, A. G., Elbermawy, Y., Abdelsattar, A. S., and El-Shibiny, A. (2024). Characterization, antibacterial, and cytotoxic activities of silver nanoparticles using the whole biofilm layer as a macromolecule in biosynthesis. *Sci. Rep.* 14, 364. doi: 10.1038/s41598-023-50548-9

Yousef, J. M., and Danial, E. N. (2012). *In Vitro* antibacterial activity and minimum inhibitory concentration of zinc oxide and nano-particle zinc oxide against pathogenic strains. *Int. J. Heal. Sci.* 2, 38–42. doi: 10.5923/j.health.20120204.04

Yu, J., Zhang, W., Li, Y., Wang, G., Yang, L., Jin, J., et al. (2014). Synthesis, characterization, antimicrobial activity and mechanism of a novel hydroxyapatite whisker/nano zinc oxide biomaterial. *Biomed. Mater.* 10, 15001. doi: 10.1088/1748-6041/10/1/015001

Zhang, L., Jiang, Y., Ding, Y., Daskalakis, N., Jeuken, L., Povey, M., et al. (2010). Mechanistic investigation into antibacterial behaviour of suspensions of ZnO nanoparticles against *E. coli*. *J. Nanoparticle Res.* 12, 1625–1636. doi: 10.1007/s11051-009-9711-1

Zhao, A., Sun, J., and Liu, Y. (2023). Understanding bacterial biofilms: From definition to treatment strategies. *Front. Cell. Infect. Microbiol.* 13. doi: 10.3389/fcimb.2023.1137947

Frontiers in
Cellular and Infection Microbiology

Investigates how microorganisms interact with their hosts

Explores bacteria, fungi, parasites, viruses, endosymbionts, prions and all microbial pathogens as well as the microbiota and its effect on health and disease in various hosts.

Discover the latest Research Topics

See more →

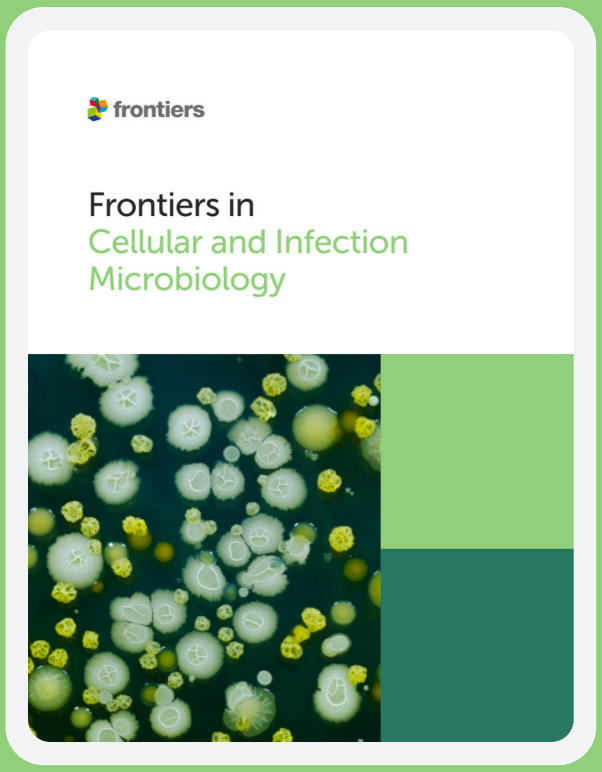

Frontiers

Avenue du Tribunal-Fédéral 34
1005 Lausanne, Switzerland
frontiersin.org

Contact us

+41 (0)21 510 17 00
frontiersin.org/about/contact